

Green Synthesis, Characterization and Biofunctionalisation of Nanoparticles for Medical Applications

**Von der Naturwissenschaftlichen Fakultät der
Gottfried Wilhelm Leibniz Universität Hannover**

zur Erlangung des Grades

Doktor der Naturwissenschaften (Dr. rer. nat.)

genehmigte Dissertation

von

Abdalahim Alahmad, Madjistir (Syrien)

2022

Referent: Prof. Dr. rer. nat. Thomas Scheper

Korreferent: Prof. Dr. rer. nat. Bernd Hitzmann

Tag der Promotion: 20.07.2022

بِسْمِ اللّٰهِ الرَّحْمٰنِ الرَّحِیْمِ

Im Namen Allahs, des Allerbarmers, des Barmherzigen

Dank und Dankbarkeit

Ich preise Allah, den Allmächtigen, wie es der Majestät seines Antlitzes und der Größe seiner Autorität gebührt, und ich danke ihm für seine unzähligen Segnungen.

Und erhebe ihm die höchsten Verse des Lobes und des Lobes, bis er zufrieden ist, ich verneige mich in Lob und Dank dafür, dass ich auf dem Weg der Erkenntnis und des Wissens den Segen der Gesundheit und des Erfolgs erhalten habe, und Gebete und Friede seien mit unserem Meister Muhammad, dem Propheten dieser Nation und einem Vorbild für die Ersten und Letzten, und mit seiner Familie und seinen Gefährten, und Friede sei mit ihnen allen.

Ausgehend von dem, was Allah sagt: {wer dankbar ist, der ist nur zu seinem eigenen Vorteil dankbar} und aus dem Ausspruch des Propheten (Wer den Menschen nicht dankt, dankt Allah nicht).

Mein herzlicher Dank und großes Lob gilt meinen beiden verdienstvollen Professoren, den beiden verehrten Doktoren:

Prof. Dr. Thomas Scheper

Dr. Johanna-Gabriela Walter

Ich danke beide sehr für ihre Großzügigkeit und den großen Einsatz, den sie unternommen haben, indem sie alle Hindernisse während der Phasen der Fertigstellung dieser Forschungsarbeit angeleitet, verfolgt und erleichtert haben und deren Richtlinien der Leuchtturm waren, aus dem diese Dissertation hervorgegangen ist.

Ich spreche auch meinen aufrichtigen Dank und meine Anerkennung denen aus, die mir geholfen haben, diese Recherche abzuschließen, und die mir Unterstützung und Unterstützung zukommen ließen und mir die notwendigen Informationen zur Verfügung stellten, um diese Recherche abzuschließen, Sie haben mir bei dieser Recherche geholfen und Licht ins Dunkel gebracht:

*Prof. Dr. Armin Feldhoff Herrn Frank Steinbach Prof. Dr. Ulrich Krings
Prof. Dr. Claus Rüscher Prof. Dr. Nadja-C. Bigall Herrn Pascal Rusch
Prof. Dr. Fathi Hassan Prof. Dr. Ibrahim Alghoraibi Dr. Şeyma Gülen
Prof. Dr. Khaled Alkharsah Frau Songül Noyun Prof. Dr. Detlef Bahnemann
Dr. Osama Al-Madanat Dr. Yamen Alsalka Dr. Iliyana Pepelanova*

Und allen Mitarbeitern und Kollegen aus dem Institut für Technische Chemie oder von außerhalb, die mir während der Phasen dieser Forschung geholfen haben

Alfred und Anni Berssenbrügge: Sie waren meine Stütze und Hilfe, bis ich alle Krisen und Hindernisse überwinden konnte. Egal wie viele Worte des Dankes und der Wertschätzung, Ich kann die Menge an Hilfe und Gunst, die Sie mir in den schwierigsten Zeiten meines Lebens erwiesen haben, nicht beschreiben.

Sie sind Allahes Geschenk an mich in diesem Exil. Ich werde ihre Gunst bei mir ein Leben lang nie vergessen, danke von Herzen.

إهداء

إلهي لا يطيب الليل إلا بشكرك ولا يطيب النهار إلا بطاعتك . . ولا تطيب اللحظات إلا بذكرك . . ولا
تطيب الآخرة إلا بعفوك . . ولا تطيب الجنة إلا برويتك

الله جل جلاله

إلى من بلغ الرسالة وأدى الأمانة . . ونصح الأمة . . إلى نبي الرحمة ونور العالمين

سيدنا محمد صلى الله عليه وسلم

إلى الشعب المقهور والمظلوم . . .

إلى مشاعر الألم والحزن المرسومة على الوجوه

إلى الأرض التي سكبت دماً

سوريا الجرحى

إلى أرض أجدادي وآبائي

إلى من نذرت عمرها في أداء رسالة . . . صنعتها من أوراق الصبر . . . وطرزتها في ظلام الدهر . . .

على سراج الأمل . . . بلافتور أو كلل . . . رسالة تعلم العطاء كيف يكون العطاء . . . وتعلم الوفاء كيف

يكون الوفاء . . . إليك أمي أهدي هذه الرسالة . . . وشتان بين رسالة ورسالة . . . جزاك الله خيراً . .

وأمد في عمرك بالصالحات . . . فأنت زهرة الحياة ونورها

أمي الحبيبة

إلى من كلله الله بالهيبة والوقار . . إلى من علمني العطاء بدون انتظار . . إلى من أحمل اسمه بكل افتخار . . أرجو من الله أن يمد في عمرك لترى ثماراً قد حان قطافها بعد طول انتظار وستبقى كلماتك نجوم أهدي بها اليوم وفي الغد وإلى الأبد..

والدي العزيز

إلى من أرفع رأسي عالياً مفتخراً بهم إلى أعلى وأثنى كثر أملكه إلى من بوجودهم اكتسب قوة ومحبة لا حدود لها إلى من عرفت معهم معنى الحياة وان كان حبر قلبي لا يستطيع التعبير عن مشاعري نحوهم فمشاعري أكبر من أن اسطرها على الورق . . ولكن لا أملك إلا أن أدعو الله عز وجل أن يقيهم ذخراً لي وأن لا يحرمني منهم.

اخواتي واخوتي وعوائلهم

إلى من أرى التفاؤل بعيونهم . . والسعادة في ضحكاتهم . . إلى الوجوه المفعمة بالبراءة ولحبتكم أزهرت أيامي وفتحت براعم الغد . . إلى ذوي القلوب الطاهرة الرقيقة . . إلى ريحانات حياتي . .

زوجتي نغم وابني يحيى ومحمد علي

أهدي بحثي المتواضع هذا آملاً من الله **عَلَيْكَ** أن يتقبله مني ويجعله في ميزان حسناتي يوم لا ينفع مال ولا بنون إلا من أتى الله بقلب سليم

الباحث

عبد الرزاق محمود الأحمد

Abstract

In the presented work, the phytochemicals existent in the aqueous extract of (*Hypericum perforatum L.*) St. John's wort was harnessed to prepare silver nanoparticles. Many conditions have been tried and changed until we reached the final protocol, through which we obtained the desired nanoparticles in terms of size, shape and effectiveness. The organic compounds present in the St. John's wort plant played an important role in reducing the silver ions in the solution to metallic silver, as well as in protecting the formed silver nanoparticles in nano dimensions and preventing them from growing to millimeter dimensions by forming a protective layer on the surfaces of these nanoparticles and finally maintaining the stability of these formed nanoparticles in colloidal solutions. This green chemistry approach for the preparation of AgNPs is a simple, safe, sustainable, credible and eco-friendly protocol and the resulting silver nanoparticles are considered promising for later application in the treatment of various infectious and non-communicable diseases. green synthesized silver nanoparticles have been characterized using various techniques such as ultraviolet-visible spectroscopy (UV-Vis), dynamic light scattering (DLS), zeta potential, Fourier transform infrared (ATR-FTIR) spectroscopy, X-Ray diffraction (XRD), scanning electron microscope (SEM), transmission electron microscopy (TEM), energy dispersive X-Ray (EDX), nanoparticle tracking analysis (NTA), atomic force microscopy (AFM), thermogravimetric analysis (TGA) and atomic absorption spectroscopy (AAS), and all results proved that biosynthesized silver nanoparticles are spherical in shape, stable in colloidal solution, the size of their particles ranges between 20 to 50 nm, have a face-centered cubic (fcc) and crystalline in nature and on the surfaces of these particles, there is a protective layer consisting of a group of St. John's wort compounds, the percentage of which varies according to the number of washing times.

It is known that reducing agents and the chemical composition of nanoparticle surfaces are the most influential factors in determining the activity and toxicity of these nanoparticles later because they affect cellular uptake, biodistribution, penetration into biological barriers and the resulting therapeutic effects. Therefore, the second objective of this study was to identify the organic compounds from the aqueous extract of the St. John's wort, which is present on the surfaces of silver nanoparticles as a protective agent. To achieve this goal, it was necessary to analyze the plant itself, i.e. develop a protocol in HPLC to separate the components of the extracts for this plant well. The aerial parts of the plant were extracted using 8 different solvents. A simple protocol has been developed to obtain isolated peaks in the HPLC spectrum. Detection was carried out at 260 for phloroglucinols (Hyperforin and derivatives), 350 for Flavonols and 590 nm for naphthodianthrones (Hypericins). Various standards were selected for this, which also represent the most important and best-known compounds of St. John's wort and the mass spectrometric analysis in positive ion mode was performed to allow in-line analysis coupled directly to the HPLC system used for the separation of the molecular ions according to mass to charge (m/z). Finally, the major ingredients (Hyperforin, Adhyperforin, Hypericin, Rutin, Quercetin, Quercitrin, Quercitrin-hydrate, Hyperoside, Biapigenin and Chlorogenic acid) have been identified. Total phenolic, antioxidant activity (DPPH and ABTS assays) and their relationship for different extracts were also presented in this study. In another study, the layer on the surfaces of silver nanoparticles was isolated using a mixture of solvents and following a specific protocol. After that, LC-ESI-Q-TOF-MS/MS analysis was carried out to determine these substances, and they have already been identified, which are 1=Neochlorogenic acid; 2=Hyperoside; 3=Isoquercitrin; 4=13,118-biapigenin; 5=Furohyperforin; 6= Hyperforin; 7=Furoadhyperforin; 8=Adhyperforin.

Antioxidant activity of the biologically prepared AgNPs was studied using 3 different methods: DPPH, ABTS and SO assays, and the results were very impressive and better than all that was mentioned by other researchers. The antimicrobial effect on about 20 types of microbes (Gram-positive bacteria, Gram-negative bacteria, Pathogenic yeast and leishmaniasis tropica Syrian strain (LT_SYR_24)) has been studied in multiple areas and using different methods. In fact, the results were very excellent compared to antibiotics, silver nitrate, as well as silver nanoparticles prepared by other researchers, as they were mostly lethal at very low concentrations. Anti-cancer activity against 3 types (Hela, Hep G2 and A549 cells) at various concentrations and various exposure times, and the results were very distinctive and promising for use as a future treatment for cancer.

After the prepared silver nanoparticles achieved great success in treating different types of cancer cells, the last and most important step was how to modify these particles to be selectivity, that is, when injected in vivo, they go directly to the tumor or cancer cells without affecting healthy cells. Since oligonucleotide-based aptamers (APTs) are excellent ligands for targeting cancer cells, we have already developed a special protocol to conjugate silver nanoparticles prepared in our method with a specific aptamer as a selective targeting part for uptake by A549 cells. Many conditions and factors have been tried to reach a high coupling ratio without affecting the effectiveness of the aptamer. The cytotoxicity of aptamer-conjugated AgNPs against A549 (human non-small cell lung cancer) and BEAS-2B (normal human bronchial epithelial) were studied using CTB test, cellular uptake, viability staining (using Calcein AM and Propidium Iodide), Quantitation of Apoptosis and Necrosis cells (using Annexin V and Propidium Iodide) and Cellular morphological changes (laser scanning confocal microscope and normal microscope). All results indicated that the effect of aptamer conjugated AgNPs was very large on cancer cells (A549 cells) compared to healthy cells (BEAS2B) at the same or lesser concentrations. This indicates that these nanoparticles exhibited selective binding and internalization to target A549 cells, but not by normal human bronchial epithelium BEAS2B, thus exhibiting high selective specificity.

Keywords: Silver nanoparticles, Green Synthesis, Aptamer, targeting therapy, Anticancer activities.

Zusammenfassung

In der vorgestellten Arbeit, die im wässrigen Extrakt von (*Hypericum perforatum L.*) Johanniskraut enthaltenen Phytochemikalien wurden zur Herstellung von Silber-Nanopartikeln genutzt. Viele Bedingungen wurden ausprobiert und geändert, bis wir das endgültige Protokoll erreichten, durch das wir die gewünschten Nanopartikel erhielten hinsichtlich Größe, Form und Wirksamkeit. Die in der Johanniskrautpflanze vorhandenen organischen Verbindungen spielten eine wichtige Rolle bei der Reduktion der Silberionen in der Lösung zu metallischem Silber sowie beim Schutz der gebildeten Silber-Nanopartikel in Nano-Dimensionen und zu verhindern, dass sie zu Millimeter-Dimensionen anwachsen, indem eine Schutzschicht auf den Oberflächen dieser Nanopartikel gebildet wird und schließlich die Stabilität dieser gebildeten Nanopartikel in kolloidalen Lösungen aufrechterhalten wird. Dieser grüne chemische Ansatz zur Herstellung von AgNPs ist ein einfaches, sicheres, nachhaltiges, glaubwürdiges und umweltfreundliches Protokoll, und die resultierenden Silbernanopartikel gelten als vielversprechend für eine spätere Anwendung bei der Behandlung verschiedener infektiöser und nicht übertragbarer Krankheiten. grüne synthetisierte Silbernanopartikel wurden mit verschiedenen Techniken charakterisiert, wie z. B. Ultraviolett-Vis-Spektroskopie (UV-Vis), dynamische Lichtstreuung (DLS), Zetapotential, Fourier-Transformations-Infrarot (ATR-FTIR)-Spektroskopie, Röntgenbeugung (XRD), Rasterelektronenmikroskop (REM), Transmissionselektronenmikroskopie (TEM), energiedispersives Röntgen (EDX), Nanopartikel-Tracking-Analyse (NTA), Rasterkraftmikroskopie (AFM), thermogravimetrische Analyse (TGA) und Atomabsorptionsspektroskopie (AAS), und alle Ergebnisse bewiesen, dass biosynthetisierte Silber-Nanopartikel kugelförmig sind, in kolloidaler Lösung stabil sind, die Größe ihrer Partikel zwischen 20 und 50 nm liegt, haben eine flächenzentrierte kubische (fcc) und kristalline Natur und auf den Oberflächen dieser Partikel befindet sich eine Schutzschicht, die aus einer Gruppe von Johanniskrautverbindungen besteht, deren Prozentsatz je nach Anzahl der Waschvorgänge variiert.

Es ist bekannt, dass Reduktionsmittel und die chemische Zusammensetzung von Nanopartikeloberflächen die einflussreichsten Faktoren für die spätere Aktivität und Toxizität dieser Nanopartikel sind, weil sie die zelluläre Aufnahme, Bioverteilung, das Eindringen in biologische Barrieren und die daraus resultierenden therapeutischen Wirkungen beeinflussen. Daher war das zweite Ziel dieser Studie, die organischen Verbindungen aus dem wässrigen Extrakt des Johanniskrauts zu identifizieren, die als Schutzmittel auf den Oberflächen von Silber-Nanopartikeln vorhanden sind. Um dieses Ziel zu erreichen, war es notwendig, die Pflanze selbst zu analysieren, d. h. ein Protokoll in HPLC zu entwickeln, um die Bestandteile der Extrakte für diese Pflanze gut zu trennen. Die oberirdischen Pflanzenteile wurden mit 8 verschiedenen Lösungsmitteln extrahiert. Es wurde ein einfaches Protokoll entwickelt, um isolierte Peaks im HPLC-Spektrum zu erhalten. Der Nachweis wurde bei 260 für Phloroglucinole (Hyperforin und Derivate), 350 für Flavonole und 590 nm für Naphthodianthrone (Hypericine) durchgeführt. Dafür wurden verschiedene Standards ausgewählt, die auch die wichtigsten und bekanntesten Verbindungen des Johanniskrauts darstellen, und die massenspektrometrische Analyse im positiven Ionenmodus wurde durchgeführt, um eine Inline-Analyse zu ermöglichen, die direkt mit dem HPLC-System gekoppelt ist, das für die Trennung der Moleküle nach Masse zu Ladung (m/z) verwendet wird. Schließlich wurden die wichtigsten Inhaltsstoffe (Hyperforin, Adhyperforin, Hypericin, Rutin, Quercetin, Quercitrin, Quercitrin-Hydrat, Hyperosid, Biapigenin und Chlorogensäure) identifiziert. Die gesamte phenolische, antioxidative Aktivität (DPPH- und ABTS-Assays) und ihre Beziehung für verschiedene Extrakte wurden ebenfalls in dieser Studie präsentiert. In einer anderen Studie wurde die Schicht auf der Oberfläche von Silber-Nanopartikeln mit einer Mischung aus Lösungsmitteln und nach einem bestimmten Protokoll isoliert. Danach wurde eine LC-ESI-Q-TOF-MS/MS-Analyse durchgeführt, um diese Substanzen zu bestimmen, und sie wurden bereits identifiziert, nämlich 1 = Neochlorogensäure; 2 = Hyperosid; 3=Isoquercitrin; 4=13,II8-Biapigenin; 5 = Furohyperforin; 6 = Hyperforin; 7=Furadhyperforin; 8=Adhyperforin.

Die antioxidative Aktivität der biologisch hergestellten AgNPs wurde mit 3 verschiedenen Methoden untersucht: DPPH-, ABTS- und SO-Assays, und die Ergebnisse waren sehr beeindruckend und besser als alles, was von anderen Forschern erwähnt wurde. Die antimikrobielle Wirkung auf etwa 20 Arten von Mikroben (grampositive Bakterien, gramnegative Bakterien und pathogene Hefen) wurde in mehreren Bereichen und mit unterschiedlichen Methoden untersucht. Tatsächlich waren die Ergebnisse im Vergleich zu Antibiotika, Silbernitrat sowie Silbernanopartikeln, die von anderen Forschern hergestellt wurden, sehr gut, da sie in sehr geringen Konzentrationen meist tödlich waren. Die AgNPs-Aktivität gegen den syrischen Stamm *Leishmaniasis tropica* (LT_SYR_24) wurde ebenfalls untersucht, und die Ergebnisse waren sehr gut. Anti-Krebs-Aktivität gegen 3 Typen (Hela-, Hep-G2- und A549-Zellen) bei verschiedenen Konzentrationen und verschiedenen Expositionszeiten, und die Ergebnisse waren sehr ausgeprägt und vielversprechend für die Verwendung als zukünftige Behandlung von Krebs.

Nachdem die präparierten Silber-Nanopartikel große Erfolge bei der Behandlung verschiedener Arten von Krebszellen erzielten, der letzte und wichtigste Schritt bestand darin, diese Partikel so zu modifizieren, dass sie selektiv sind, dh wenn sie in vivo injiziert werden, gelangen sie direkt zu den Tumor- oder Krebszellen, ohne gesunde Zellen zu beeinträchtigen. Da Oligonukleotid-basierte Aptamere (APTs) ausgezeichnete Liganden für das Targeting von Krebszellen sind, haben wir bereits ein spezielles Protokoll entwickelt, um Silber-Nanopartikel, die in unserer Methode hergestellt wurden, mit einem spezifischen Aptamer als selektivem Targeting-Teil für die Aufnahme durch A549-Zellen zu konjugieren. Viele Bedingungen und Faktoren wurden ausprobiert, um ein hohes Kopplungsverhältnis zu erreichen, ohne die Wirksamkeit des Aptamers zu beeinträchtigen. die Zytotoxizität von Aptamer-konjugierten AgNPs gegen A549 (menschlicher nicht-kleinzelliger Lungenkrebs) und BEAS-2B (normales menschliches Bronchialepithel) wurden unter Verwendung von CTB-Test, Zellaufnahme, Lebensfähigkeitsfärbung (unter Verwendung von Calcein AM und Propidiumiodid), Quantifizierung von untersucht Apoptose- und Nekrosezellen (unter Verwendung von Annexin V und Propidiumiodid) und zelluläre morphologische Veränderungen (konfokales Laser-Scanning-Mikroskop und normales Mikroskop) untersucht. Alle Ergebnisse zeigten, dass die Wirkung von Aptamer-konjugierten AgNPs bei Krebszellen (A549-Zellen) im Vergleich zu gesunden Zellen (BEAS2B) bei gleichen oder geringeren Konzentrationen sehr groß war. Dies deutet darauf hin, dass diese Nanopartikel eine selektive Bindung und Internalisierung an A549-Zielzellen zeigten, jedoch nicht durch normales menschliches Bronchialepithel BEAS2B, und somit eine hohe selektive Spezifität aufweisen.

Stichworte: Silber nanopartikel, Grüne Synthese, Aptamer, Targeting-Therapie, Aktivitäten gegen Krebs

Table of contents

1	Chapter One: Introduction.....	1
1.1	Nanoworld	1
1.2	Nanomaterial	1
1.3	Nanoscience.....	2
1.4	Nanotechnology.....	2
1.5	The historical stages of the emergence of nanotechnology.....	2
	The use of nanotechnology in the past:	3
	Nanotechnology in nature:	4
	Nanomaterial preparation methods:.....	4
	Top-down approach:.....	5
	Bottom-up approach:.....	7
	The classification of nanomaterials and their forms:	9
	One-dimensional nanomaterials:.....	9
	Two-dimensional nanomaterials:	9
	3D nanomaterials:.....	9
	Nanocomposites:	11
	The importance of nanomaterials:	11
	The most important properties that characterize nanomaterials:.....	11
	The relative increase in surface area:	11
	Quantum effect:.....	12
	The mechanical properties:	13
	The chemical properties (chemical reactivity):.....	13
	1.5.2 Physical properties:.....	13
	Biological properties:	16
1.6	Major current and future implementation of nanotechnology:.....	16
	The other terrifying side of nanotechnology:	17
	Nanotechnological risks on human health:	18
	Nanotechnological risks on workplaces:.....	18
	Nanotechnological risks on the environment:.....	18
1.7	Green synthesis of silver nanoparticles	19
1.8	Applications (uses) of silver nanoparticles	19
1.9	Cancer	25
	Differences between cancer cells and normal cells.....	25
	The occurrence of cancer.....	25

Types of cancer:	26
Lung cancer:	26
1.10 Leishmaniasis	27
Leishmaniasis types.....	27
Leishmania parasite life cycle:	27
1.11 Bacteria	28
Structure of bacteria:	28
Bacteria multiplication:.....	28
Harmful bacteria:	29
1.12 <i>Hypericum perforatum L.</i> (St. John's wort)	30
1.13 HPLC	33
A comprehensive view of HPLC:	33
The apparatus of HPLC:.....	33
Principle of HPLC:	34
1.14 HPLC-MS.....	36
• Electrospray ionization (ESI):	37
• Tandem Mass Spectrometry: Collision-Induced Dissociation:	39
• Quadrupole time-of-flight (Q-TOF) MS:.....	40
1.15 Aptamer	41
Structures of aptamers:	44
Selection of aptamers:	45
Binding mechanisms of aptamers:.....	47
The advancement of aptamers over antibodies:	47
Application of aptamers:.....	48
1.15.1 References	52
2 Chapter Two: <i>Hypericum perforatum L.</i> -Mediated Green Synthesis of Silver Nanoparticles Exhibiting Antioxidant and Anticancer Activities	73
2.1 Vorwort	73
2.2 Abstract.....	73
2.3 Introduction	74
2.4 Materials and Methods.....	75
2.4.1 Materials	75
2.4.2 Preparation of <i>Hypericum perforatum L.</i> (St John's Wort) Extract.....	76
2.4.3 Biosynthesis of Silver Nanoparticles	76
2.4.4 Diphenyl-2-picryl Hydrazyl (DPPH) Assay.....	77
2.4.5 2,2'-Azino-bis-(3-ethylbenzothiazoline-6-sulfonic Acid Radical Cation) (ABTS) Assay .	78

2.4.6	Super Oxide Anion Radical (SO) Assay	78
2.4.7	Cell Culture and Estimation of In Vitro Cytotoxicity of AgNPs	78
2.4.8	Characterization	79
2.5	Results and Discussion	80
2.5.1	UV-VIS Absorption Studies	80
2.5.2	Measurement of Concentration through Absorption Peak in UV-VIS Spectrum	80
2.5.3	Dynamic Light Scattering (DLS)	81
2.5.4	Fourier transformed infrared (FTIR) Spectroscopy	82
2.5.5	Scanning Electron Microscopy (SEM)	83
2.5.6	Transmission Electron Microscopy (TEM)	83
2.5.7	High-Resolution Transmission Electron Microscopy and Nano-Diffraction Patterns ...	85
2.5.8	X-ray Diffraction (XRD)	86
2.5.9	Possible Mechanism of Biosynthesis of Silver Nanoparticles by Plant	88
2.5.10	Determination of Antioxidant Activity	91
2.5.11	Determination of Time- and Dose-Dependent Cytotoxicity of Biosynthesized AgNPs	93
2.6	Conclusions	94
	Supplementary Materials:	95
	Author Contributions:	95
	Data Availability Statement:	96
	Acknowledgments:	96
	Conflicts of Interest:	96
2.7	References	96
2.8	Supporting Informations	106
2.8.1	Experimental	106
2.8.2	The probable mechanism of biosynthesis of silver nanoparticles by plant extracts ..	114
2.8.3	References	116
3	Chapter Three: Identification of Major Constituents of <i>Hypericum perforatum L.</i> Extracts in Syria by Development of a Rapid, Simple and Reproducible HPLC-ESI-Q-TOF MS Analysis and their Antioxidant Activities	120
3.1	Vorwort	120
3.2	Abstract	121
3.3	Introduction	122
3.4	Materials and Methods	124
3.4.1	Chemicals	124
3.4.2	Instrumentation	125
3.4.3	Raw plant preparation and extraction	125

3.4.4	Standards and References compounds solutions	126
3.4.5	Chromatography	126
3.4.6	Determination of total phenolic content of crude extracts of <i>Hypericum perforatum L.</i> 128	
3.4.7	Determination of antioxidant activity.....	129
3.5	Results and Discussion	129
3.5.1	Extraction	129
3.5.2	Characterization of extracts using HPLC	130
3.5.3	Characterization of extracts with Standards using HPLC.....	132
3.5.4	UV-Vis analysis	134
3.5.5	Identification of the main compounds using HPLC-MS analysis.....	136
3.5.6	Total phenol	139
3.5.7	Antioxidant activity DPPH	140
3.5.8	Antioxidant activity ABTS.....	143
3.5.9	Statistical analysis	145
3.6	Conclusions	146
3.7	Future Studies	146
	Conflicts of interest:.....	147
	Acknowledgements:.....	147
	Supporting Information statement:.....	147
3.8	References	148
3.9	Supporting Informations	152
3.9.1	Statistical Analysis.....	163
3.9.2	References	170
3.10	Additional experiments for determination of organic compounds on the surface of nanoparticles	172
3.10.1	Isolation and identification of capping agent St. John's wort bio compounds from the surfaces of AgNPs.....	175
3.10.2	The importance of the eight Phytochemicals of St. John's wort plant, which present on the surfaces of silver nanoparticles as a capping agent	182
3.10.3	References	185
4	Chapter Four: Green synthesis of silver nanoparticles using <i>Hypericum perforatum L.</i> aqueous extract with the evaluation of its antibacterial activity against clinical and food pathogens	190
4.1	Vorwort	190
4.2	Abstract.....	190
4.3	Introduction	191
4.4	Materials and Methods.....	192

4.4.1	Chemicals and Instrumentation.....	192
4.4.2	Synthesis of <i>Hypericum perforatum L.</i> aqueous extract mediated silver nanoparticles (AgNPs) and their chemical characterization.....	192
4.4.3	Antibacterial activity	193
4.4.4	Effect of AgNPs on growth kinetics of <i>S. aureus</i>	193
4.4.5	Estimation of antibacterial activity of AgNPs in terms of CFU.....	194
4.4.6	Time-kill kinetics assay	194
4.4.7	Wound migration assay	194
4.5	Result and Discussion.....	195
4.5.1	Chemical characterization of <i>Hypericum perforatum L.</i> phytochemicals-capped AgNPs	195
4.5.2	Evaluation of biological activities of <i>Hypericum perforatum</i> mediated AgNPs	200
4.6	Conclusions	205
	Author Contributions:	205
4.7	References	206
5	Chapter Five: A study of additional applications of biosynthesized silver nanoparticles using the aqueous extract of the St. John's wort, as well as the development of a protocol to conjugate it with the aptamer which are selective ligands for targeting cancer cells and the study of its selectivity and internalization against cancer human non-small lung cells (A549) and normal human bronchial epithelial cells (BEAS2B).....	211
5.1	Vorwort	211
5.2	Studying the effect of storage of green-synthesized AgNPs on their antimicrobial activities	213
5.2.1	Agar diffusion method	213
5.2.2	Microtiter plate method	217
5.2.3	Viability test	220
5.3	Comparison of the antimicrobial activities of <i>Hypericum perforatum L.</i> -Mediated green synthesis of AgNPs with antibiotics, silver nitrate, <i>Hypericum perforatum L.</i> aqueous extract and Citrate-capped AgNPs.....	222
5.3.1	Antimicrobial assay	222
5.3.2	TEM Images.....	222
5.3.3	Results.....	223
5.3.4	Discussion.....	227
5.4	Effect of green synthesized AgNPs on leishmaniasis	229
5.4.1	Materials and Methods.....	229
5.4.2	Results.....	230
5.4.3	Discussion.....	231

5.5	Development of a protocol to prepare selective thiolate Aptamer-conjugated silver nanoparticles and their effects on healthy and cancerous cells	233
5.5.1	Experimental	234
5.5.2	Result and Discussion.....	238
5.5.3	References	253
6	Chapter Six: Summarizing Discussion and Conclusions	255
6.1	Vorwort	255
6.2	Development of a protocol for green preparation of silver nanoparticles from aqueous extract of <i>Hypericum perforatum L.</i> (St. John's Wort).....	258
6.3	Characterization of Biosynthesized Silver nanoparticles.....	259
6.4	Identification of the organic compounds at the surface of silver nanoparticles.....	263
6.5	Total phenol and Antioxidant activities of St John’s Wort extracts.....	267
6.6	Applications of biosynthesized AgNPs	268
6.6.1	Antioxidant activities	268
6.6.2	Antimicrobial activities.....	268
6.6.3	Anticancer activities.....	276
6.7	Development of a protocol to prepare aptamer-Conjugated AgNPs	277
6.7.1	Study the anticancer effect of the selective ssDNA aptamer-modified AgNPs on human non-small cell lung cancer A549 and normal human bronchial epithelial BEAS2Bcells; in Vitro study.....	278
6.7.2	Results.....	279
6.8	Conclusions	282
7	Curriculum Vitae and Publications.....	287

Chapter 1: Introduction

1 Chapter One: Introduction

1.1 Nanoworld

- What is nano?
- What are nanomaterials?
- What is nanotechnology?
- When did nanotechnology start to appear?
- Who was the first to ask about it?
- What invention opened the door to nanotechnology?
- Have nanomaterials been used in the past?
- can nanomaterials be found in nature?
- What are the ways to get nanoscale size?
- How are nanomaterials classified according to their dimensions?
- What are their forms?
- What is the importance of nanotechnology?
- What are the modern uses in different fields?
- What are its future uses?

Hopefully, all these questions will be answered in a simplified and clear manner to brief the nanoworld in a simplified manner.

Nano: It is a prefix carved from the ancient Greek language which means the small dwarf (Nanos) and in the field of science nanos means nanoparticles part of a billion (part of a thousand million 10^{-9}). It is used to express the dimensions of atoms, their half-diameters and as a measure the size of cells and microparticles.

1.2 Nanomaterial

Nanomaterials are the building materials of the 21st century and its basic buildings and the important pillar of 21st century technologies (nanotechnology, biotechnology, ICT) which are a standard for the progress and civilization of nations and an indicator of their renaissance. Nanomaterials vary from source to source, varying in proportions, such as organic, inorganic, natural or synthesized materials. All types of well-known engineering materials such as metal and Metal Alloys, semiconductors, oxides and minerals, as well as polymers, are the primary materials on which nanotechnology relies in the preparation and production of nanomaterials and devices. The material is described by nanoscale if the measurements of one of its dimensions are below 100 nm.

Chapter 1: Introduction

1.3 Nanoscience

Nanoscience is a science that deals with and takes care of the study and characterization of nanomaterials and the designation of their chemical, physical, and mechanical properties while studying associated phenomena arising from the reduction of their sizes.

1.4 Nanotechnology

Nanotechnology: literally means "Microtechnology." Setting a specific definition of nanotechnology is difficult, given its complexity and entry into different applied fields, as each of these areas views this technology from its own point of view. Nanotechnology could only reach its peak today through the invention and innovation of several unique techniques that would have enabled it to control the molecular structure and manipulate the atoms of matter and design it according to the applicable purpose. Based on this concept, nanotechnology applications are not limited to one particular branch of science, engineering or medicine, but extend their applications to all branches and applications as described in the following form:

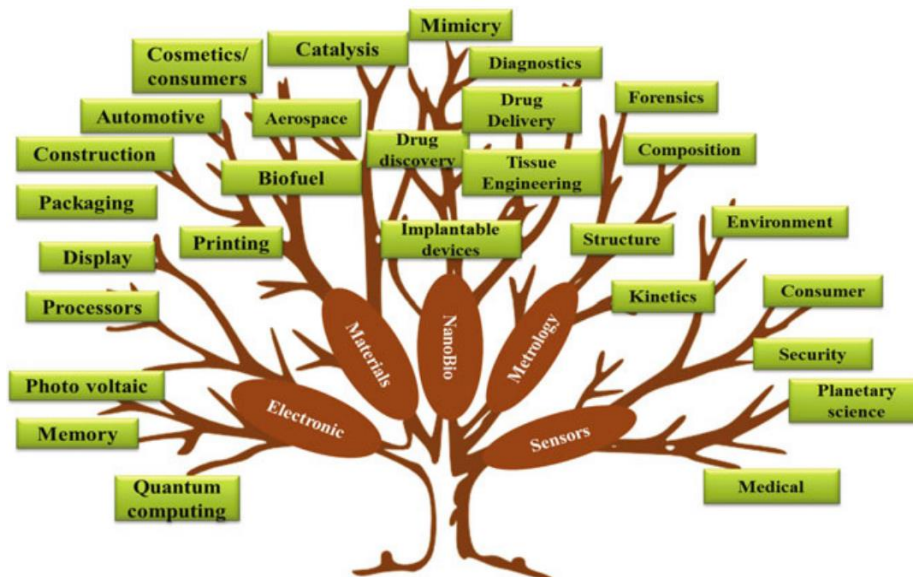


Figure 1-1: Nanotechnology applications, which extend to all fields ¹

1.5 The historical stages of the emergence of nanotechnology

- **1867:** The Scottish physicist James Maxwell conducted a mental experiment known as Maxwell's demon. This experiment generated the idea of controlling the movement of atoms and molecules.
- **1959:** The famous American physicist Richard Feinman in his lecture „There is a lot of room at the bottom", at the American Physical Society, He described a new area that deals with individual atoms and molecules for the manufacture of fine materials and machines with distinctive characteristics. He was awarded the Nobel Prize for Physics in 1965 as a result of his creative work in quantum mechanics.
- **1974:** The Japanese researcher Norio Taniguchi coined the the term nanotechnology
- **1976:** The Palestinian physicist Munir Nayefa developed a laser method called (Resonant ionization) to detect and measure individual atoms with the highest levels of accuracy and

Chapter 1: Introduction

control, and monitor one atom among millions of atoms and detect their identity for the first time in the history of science, and his method works in a way by exciting the atoms with a specific color laser, ionizing them, and then provoking the dyed charges.

- **1981:** The Swiss researchers Henrik Rohrer and Gerd Binnig invented a new type of microscope based on the micro scanning of the atoms of the materials, the tunnel microscope scanner
- **1986:** Eric Drexler published his famous book "Engines of creation", in which he mentioned the imagined dangers of nanotechnology, such as the manufacture of Nano-engines and vehicles that can copy themselves and cannot limit their spread. In his book, he simplified the basic ideas of nanotechnology. The term nanotechnology was then used in scientific circles to denote dimensions from 0.1 to 100 nm
- **1989:** A research team at IBM of the United States was able to set the micro needle in the tunnel microscope scanner to capture the atoms of the Noble gas Xenon and move them with extreme accuracy to rearrange them one by one on a cold surface of nickel metal, to form together the company's logo written in atomic letters and nanoscale dimensions (Fig. 2).

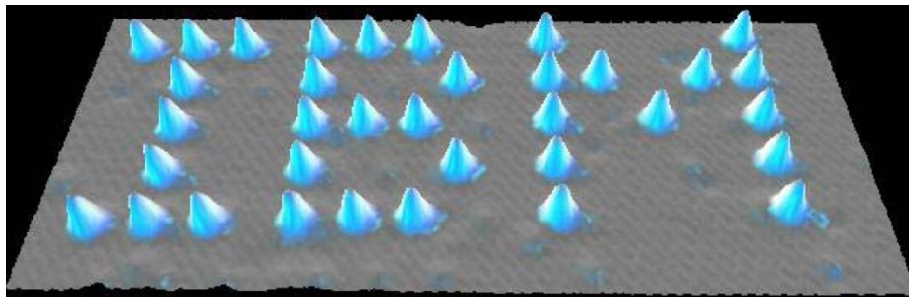


Figure 1-2: IBM logo written using xenon atoms on a nickel slide ²

- **1991:** The Japanese researcher Sumio Iijima he was the first to discover a new physical phenomenon by using a carbon Nano Tube, at NEC Electronic Industries in Japan.
- **1992:** The Palestinian physicist Munir Nayefa wrote the smallest line in history using atoms in a tunnel microscope scanner (letter p and next to it a heart) as a symbol of the love of Palestine, and spread in famous scientific magazines and international news agencies.
- **1993:** The Scientist Donald Bethune of IBM Computer Technology, USA was able to monitor a single-wall nanotube with a tube diameter of 12 nm.
- **2003:** the secrets of this technology and control of the world of nanomaterials were revealed.
- **2004:** the phase of industrial applications of this technology began.

The use of nanotechnology in the past: In spite of nanotechnology having been recognized in modern times, its benefits have come to light since ancient times such as producing sharp hard swords (Damascene sword), stained glass and even black pigments that hide gray

- Craftsmen used Nanotechnology in a period dating back to the ninth century in Mesopotamia to generate luster for the surfaces of pots and there are still remnants of the Middle Ages and

Chapter 1: Introduction

still having its copper or golden luster where they found some of the nanoparticles in these pots responsible for changing the color of the pot when the light runs out of the pot takes the pink color because when the light reflects from the pot takes green. The Roman King's Cup of Lycurgus, which has been in the British Museum since the 4th century AD, contains particles of gold and silver in nano size, where the color of the cup is observed from green to dark red when exposed to a light source (Fig. 3).

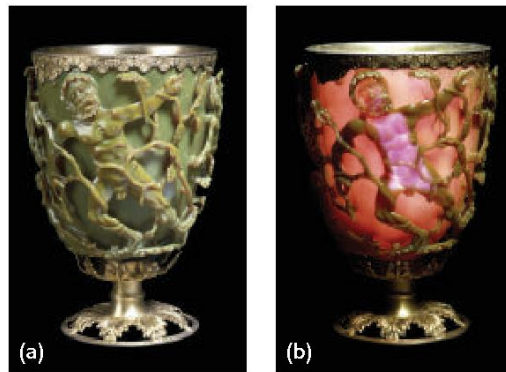


Figure 1-3: The Lycurgus cup, a Roman artifact held in the British Museum under reflected light (a) and transmitted light (b) ³.

• *Antique windows with Stained glass (Fig. 4)*



Figure 1-4: Medieval stained-glass of an ancient church ⁴

Nanotechnology in nature: One of the manifestations of the creator's accuracy and mastery is the presence of nanoparticles in nature and within our bodies, and these natural nanoparticles have functions that are not performed by larger objects, like the color of butterfly wings, plaster toes, small beetle living in the Namibian desert, red and white blood cells, viruses, DNA and RNA ^{5,6}.

Nanomaterial preparation methods: Although there are many tools and methods used in the production of nanomaterials of various categories and with varying degrees of quality, speed and cost, all of these methods can be subdivided under two technical methods:

- Top-Down Approach from top to bottom,
- Bottom-Up Approach from bottom to top,

Chapter 1: Introduction

Most manufacturers are interested in controlling particle size, particle shape (hexagonal-spherical- triangular etc.), size distribution, particle composition and degree of particle agglomeration.

Top-down approach: This strategy is based on minimizing the dimensions of large objects or granules, i.e. reducing material granules from a few millimeters to below 100 nm. In other words, starting from bulk until reaching nanoscale pieces. This method is currently most commonly used in industry due to its ability to produce large quantities of nanomaterial powders and granules of various types and categories. To reach nanoscale, chemical or mechanical methods are used, including:

Milling mechanical: Produces powder-shaped nanomaterials (Fig. 5)

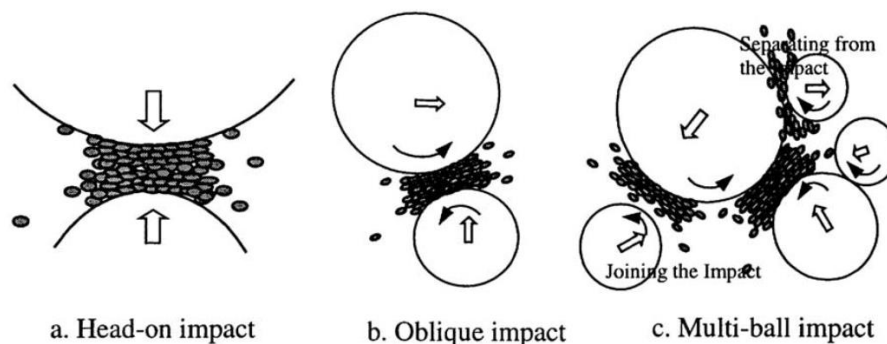


Figure 1-5: A graphic exhibiting the various forms of impact that may occur during high-energy ball milling ⁷

Etching or drilling is chemical or electrochemical

Chemical etching: In this way, thin slides of the material are placed in chemicals that scratch the slides and get nanoparticles out of the slides on their surface, then placed in a solution and enter the ultrasound device, so that the nanoparticles fall from the surface of the slides and keep settling in the solution. Fig 6.

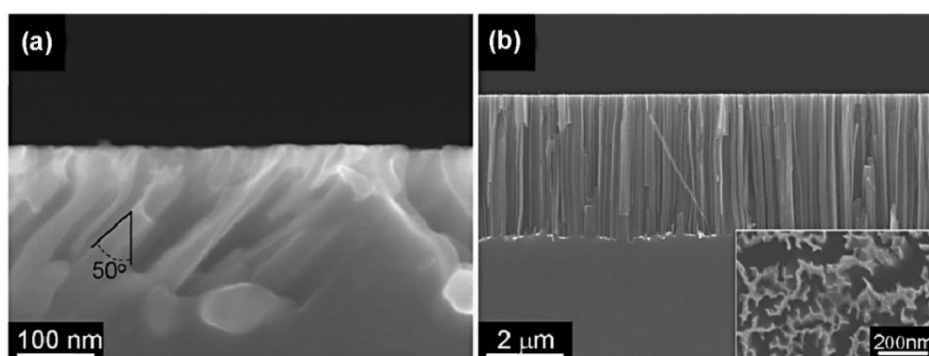


Figure 1-6: $(1\ 1\ 1)$ Si wafer etching along (a) $(1\ 0\ 0)$ directions, and (b) $(1\ 1\ 1)$ direction ⁸

Electrochemical drilling: In this way the material slide is placed in the positive pole and polycarbonate chip in the negative pole, the electric current passes into a chemical bath consisting of chemicals that help to etch and the nanoparticles are produced (Fig 7) ⁹.

Chapter 1: Introduction

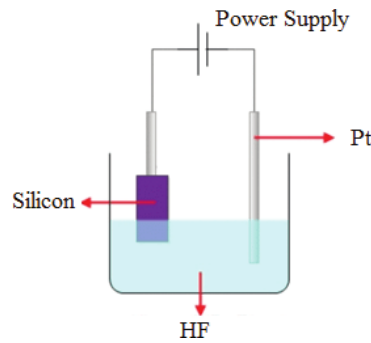


Figure 1-7: Cross section of a lateral electrochemical etching cell ¹⁰

Laser excision method (Laser Ablation): Using a high-energy pulse laser focused on a solid target placed in an air evacuated room, the laser beam interacts with the target, and the particles fly away forming plasma and deposit on the base and make thin films as shown in figure 8.

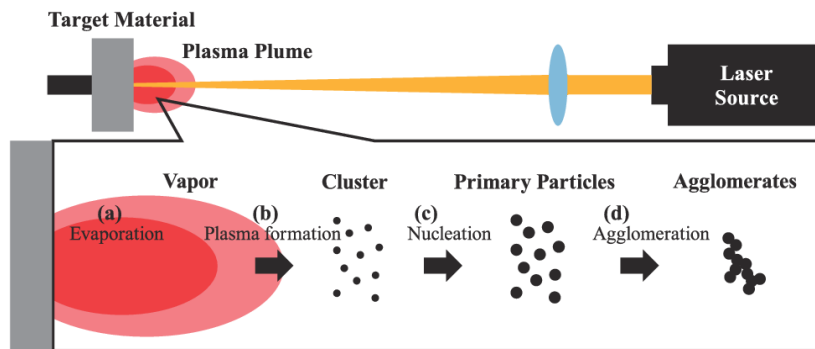


Figure 1-8: Illustrating particle formation in laser ablation ¹¹.

Sputtering method of atom puffing: The material is placed under an air-evacuated low pressure, and with a cold base exposed to a magnetic field, all these factors lead to the removal of nanoparticles of matter (i.e. fissure) to deposit at the base a thin film, where gas must be placed in order to prevent clusters and the figure 9 explains this. Various sputtering methods exist like DC diode sputtering, RF radio sputtering, and magnetron sputtering are the most popular and widely used sputtering processes ¹².

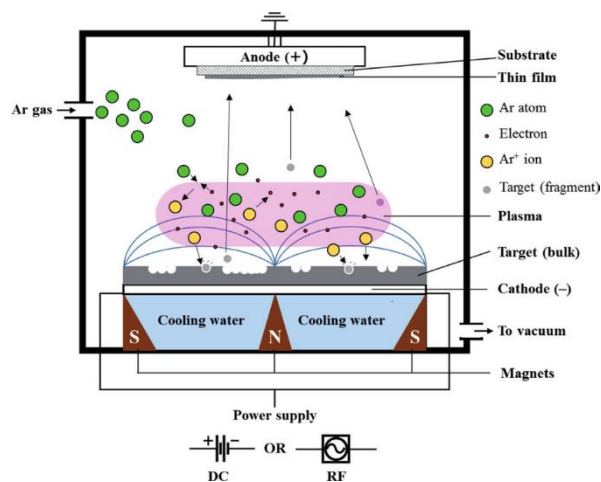


Figure 1-9: representing the magnetron sputtering equipment and deposition process ¹³.

Chapter 1: Introduction

Nanolithography: Any work of drilling, writing or printing in the nanoscale range, i.e. the transfer of particles or atoms of a material to be deposited on the surface of another material, is by nanotechnology techniques. This technology is one of the most accurate and widespread methods in the manufacture of transistors and integrated circuits. Using this technology, electronic slides of all kinds are printed. This technique includes several methods such as:

1.5.1.1.1 Electron beam nanolithography

Dip Pen Nanolithography: In this method, the outer surface of the probe needle of an atomic force microscope (AFM) or a scanning tunneling microscope (STM) is used as an ink cartridge to store atoms or molecules of the substance to be deposited on the surface of another material. These particles perform the tasks of the ink material in printers, as they come out of their places on the outer surface of the needle one by one against the direction of the microscope arm when it moves in the direction of the desired drawing ¹⁴.

Nanoprinting by thermal dip pen nanolithography: The method of printing in a tilted pen - cold or hot - depends on setting the tip of an atomic force microscope probe to build nanostructures of electronic chips, where the probe is coated with a cover of liquid ink that flows upon contact the probe tip is applied to the surface of the silicon chips, forming the desired shape. There are many other ways from the top to the bottom, it is not enough to mention them all, as we have explained the most important and most widespread ways ¹⁴.

Bottom-up approach: The strategy of this method is based on the policy of dealing with nanodimensional particles from the beginning, from material atoms or particles, and then arranging and assembling them in the form to be obtained (i.e. nanomaterial is built from atoms and molecules arranged atom-atom, molecule-molecule, and placed in specific nanoscale structures and shapes, according to the structure to be obtained). This pattern based on the assembly of specific molecules and their use as building units for nanodimensional molecular construction, the component of materials structures and nano devices, is known as assembly molecular assembly technology. This technique is divided into two types ¹⁵:

Positional assembly (also called robotic assembly): Methods used to control the atomic construction of the material by manipulating the way atoms and molecules are arranged and placed in the material's internal structure. Molecular manufacturing or local assembly is carried out through so-called complexes (atom complexes or molecules Assemblers) and the most important of these tools is the scanning tunneling microscope and atomic force microscopy ¹⁵.

Self-assembly: These techniques are based on the idea of blending and controlling nanomaterial solutions, with the aim of obtaining new molecules, through which the required nanostructures are designed. Self-assembly techniques are defined as those processes in which a group of atoms or molecules automatically form regular clusters of molecules to form the molecular structures to be obtained. They are based on the fact that the molecules that make up those structures always seek to be stable and to be found with the lowest possible levels of energy available ¹⁶.

Sol-gel: This method is one of the methods of wet chemistry techniques. They are environmentally friendly, resulting in no harmful substances to the environment. This method

Chapter 1: Introduction

begins with the melting of pre-prepared raw material powders called Precursors or initiatives. As a result of the interactions associated with dissolving the Precursors in the solution leads to formation of what is known as sol or colloidal solution, it is more like fluid attached to deposits of ultra-soft nano-granules as described in figure 10, and contrary to what is shown in the figure and given the nanoscale measures of the dimensions of those colloids we cannot actually see these nano-dimensional nano-granules or realize their presence in the fluid except through examination by modern zoom devices of high resolution-magnifiers and electronic microscopes¹⁷⁻¹⁹. The sol-gel method has evolved significantly over the last 10 years, strongly nominating it to be the first way in which self-assembly is carried out, given the following reasons:

- I- Its flexibility and ease of steps in the production of different types of nanomaterials.
- II- Its ability to produce large industrial quantities of homogenous nanomaterial particles of composition and structure, with purity of up to 99.99%.
- III- The least expensive and fastest method of preparation.
- VI- Through which nanomaterials are produced for most alloys, ceramic materials and overlapping materials at very low temperatures.

Aerosol method: is the same as sol- gel but it starts with the gas phase and ends with the liquid phase²⁰.

CVD: is short for Chemical vapor deposition²¹

Electrical migration deposition method: In this way, a mixture of materials is extracted out of a gel with an electric current and a high temperature²².

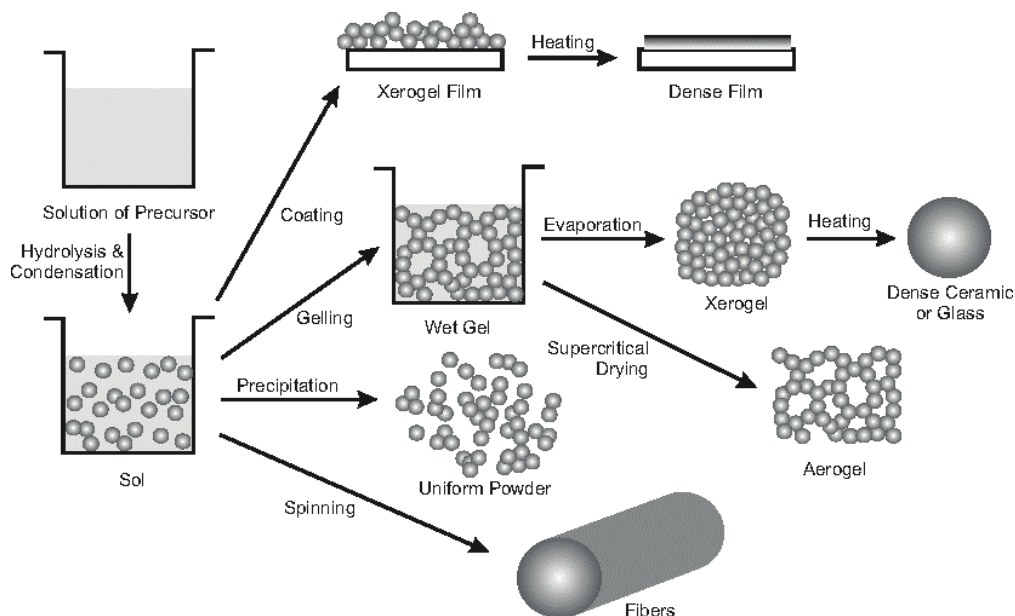


Figure 1-10: Sol-gel process steps to control the final morphology of the product²³

Electrospinning: Nanofibres from different types of materials are generated using electrospinning. The most commonly used materials are organic polymers in the form of either

Chapter 1: Introduction

solution or melt. Small molecules can also be directly electrospun into nanofibers if they self-assemble and generate sufficient chain entanglement ²⁴.

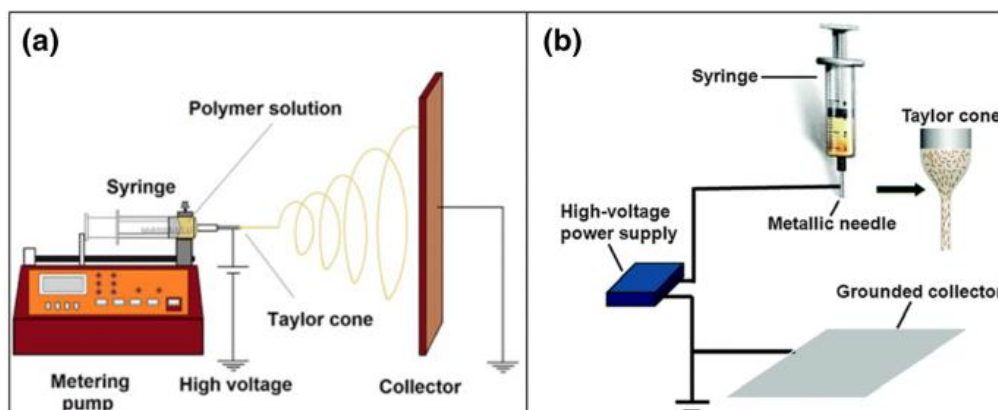


Figure 1-11: Schematic diagram of electrospinning technique: (a) horizontal and (b) vertical ²⁵

The classification of nanomaterials and their forms: Nanomaterial forms vary in different compositions which is classified on the basis of their dimensions in the space. There are one-dimensional compositions, two-dimensional compositions and 3D compositions ²⁶, and all nanomaterials subdivided to these three classifications, including:

One-dimensional nanomaterials: All materials with a scale of less than 100 nm are located under this category. This category is called one-dimensional nanomaterials (i.e., those with only one nanoscale dimension). Examples of these materials include chips or thin layers that are used to paint surfaces to improve their properties.

Two-dimensional nanomaterials: In this category of nanomaterials, it is required that the scale of two dimensions is less than 100 nm. The nanoforms that fall into this category are: Nanotubes, Nanowires and Nanofibres ²⁷.

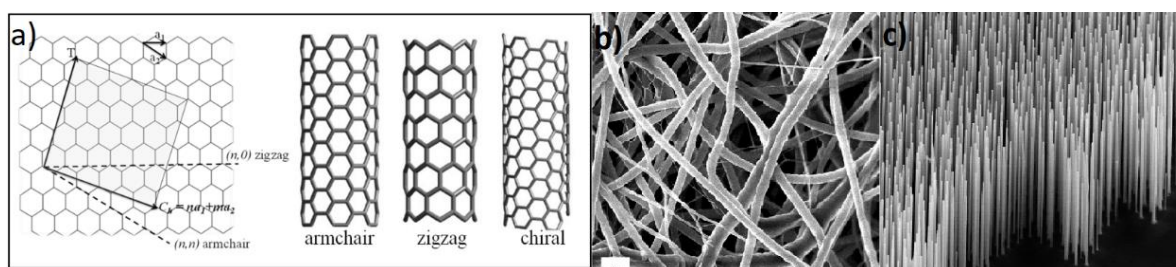


Figure 1-12: Two-dimensional nanomaterials: a) Armchair, zigzag and chiral types of nanotube ²⁸; b) Ecm-analog morphology of electrospun Poly(caprolactone) nanofibers ²⁹ and c) Nanowires ³⁰

3D nanomaterials: materials whose dimensions measures on the three axes X, Y, Z are less than 100 nm (i.e. with three dimensions of no more than 100 nm) and are in the form of ultra-soft granules or powders. The most important forms of this category include: Nanoparticles, Quantum Dots, Fullerene, Nanoballs and Dendrimers ³¹⁻³³.

Chapter 1: Introduction

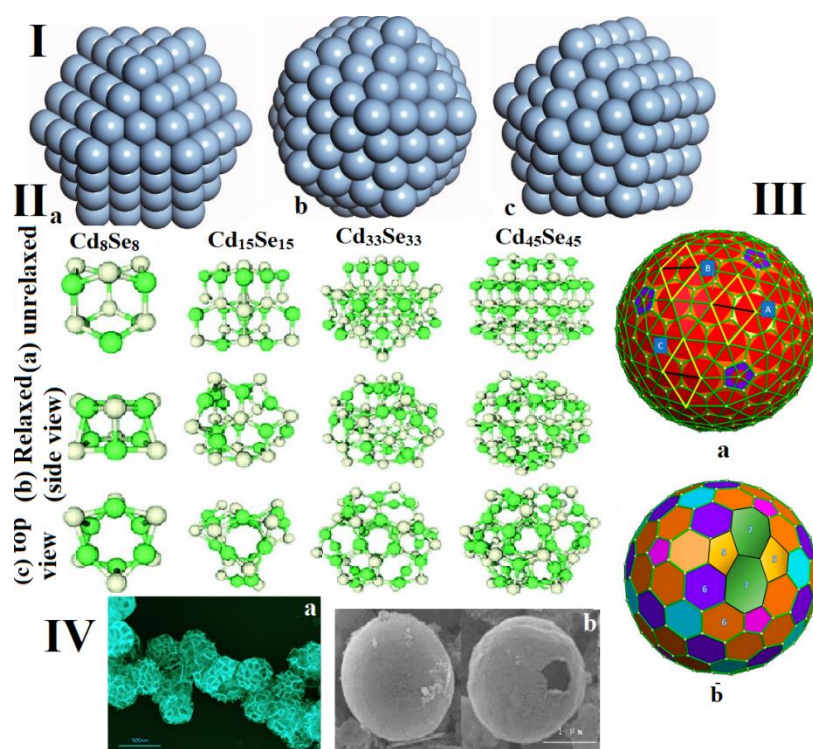


Figure 1-13: I: Atomic structures of the 2-nm silver nanoparticles studied: a) cuboctahedron, b) icosahedron, and c) Ino-dodecahedron³⁴; II: Ab initio derived QD systems of (a) unrelaxed structures and (b), (c) relaxed structures of wurtzite structures of CdxSex, x=6, 15, 33, and 45. The Cd and Se atoms are represented by green and yellow spheres respectively³⁵; III: (a) Pristine C₂₄₀ (Ih) fullerene has three symmetry-independent quartets of hexagons A, B, and C delimited by yellow diamonds whose corners correspond to the centers of the hexagons. (b) The C₇₀=0240 structure generated by applying the SW6/6 rotation to quartet A in (a). The double pair 5/7 and SWw with length $\eta = 0$ are shown. Yellow (green) polygons represent pentagonal (heptagonal) rings. The pair 6/6 is ready for the SW6/7 rotation and swap place with the nearby pair 5/7³⁶; IV: a) scanning microscope image of platinum-lace nanoballs. Liposomes aggregate, providing a foamlike template for a platinum sheet to grow, b) SEM images of hollow carbon nanoballs^{37, 38}.

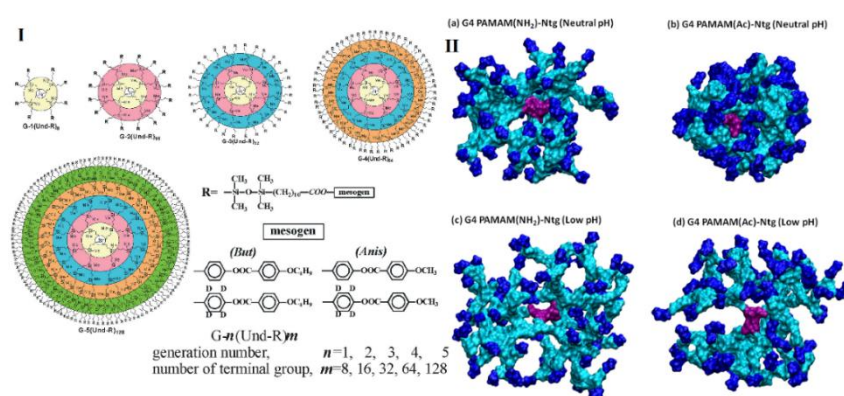


Figure 1-14: I: The chemical structure of the LC dendrimers of the 1-5th generation³⁹; Instantaneous snapshots (surface representation, drug molecules are removed) at the end of 30 ns long simulation run for (a) G₄ PAMAM(NH₂) at neutral pH, (b) G₄ PAMAM(Ac) at neutral pH, (c) G₄ PAMAM(NH₂) at low pH, and (d) G₄ PAMAM(Ac) at low pH. The surface color representations are as follows: violet: core ("aaa"); cyan: repeating fragments ("bbb"); blue: peripheral groups ("ccc"). The displayed Dendrimers are widely viewed in relation to each other⁴⁰.

Chapter 1: Introduction

Nanocomposites: During the manufacture of these nanomaterials, nanoparticles are added to them and as a result the nanomaterials show a significant improvement in the properties of these materials. When nanotubes (e.g. carbon) are added to a material, the electrical and thermal conduction properties of that material increase as a result of the addition of carbon nanotubes. There may also be an improvement in photomechanical properties (hardness, intensity) as a result of the addition of certain nanomaterials to certain materials. One of the most famous nanocomposites now present is polymeric compounds ⁴¹.

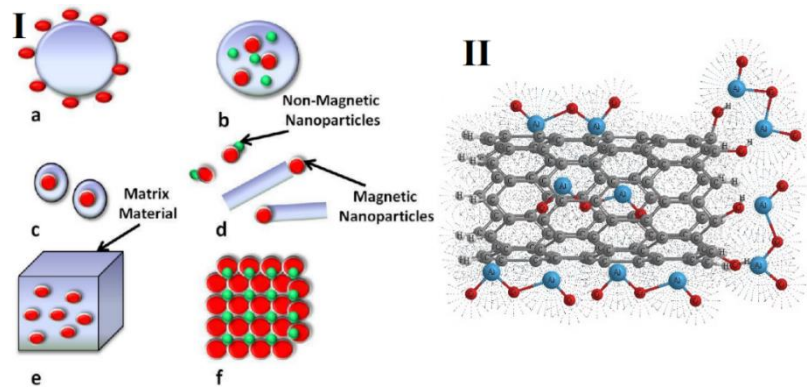


Figure 1-15: I: Different shapes of magnetic nanocomposite materials a) Sphere dispersed magnetic nano-particles b) Mesoscale sphere c) Core-shell nano-particles d) Janus type heterostructure e) Matrix dispersed nano-particles f) Colloidal crystals ⁴²; II: Structural representative of possible interaction between Al₂O₃ and carbon nanotube in multi-wall carbon nanotubes/Al₂O₃ nanocomposite ⁴³.

The importance of nanomaterials: The reducing of the sizes and measurements of materials to the nanometer level is not a goal in itself, but rather a high-end scientific philosophy and a qualitative and scientific coup on the classics and constants of physical and chemical theories, aims to produce a new class of materials known as nanomaterials to suit their distinct properties to the requirements of advanced technology for the intended applied purpose. Based on this concept, nanotechnology applications are not limited to one particular branch of science, engineering or medicine, but extend their applications to all branches and applications ⁴⁴.

The most important properties that characterize nanomaterials: The properties of the material on the micrometer scale and bigger do not depend on the size, while at the nanoscale size all the properties of the material, including the color and the chemical properties, will change due to the response of its micro-granules to light, mechanical stress and electricity in a different way to the response of granules of micro-or millimeter dimensions.

This significant change in nanomaterial properties is due to two reasons:

The relative increase in surface area: when the particle diameter measurements decrease, the number of atoms of matter on the outer surfaces of the particles increases, while the numbers of atoms within the core of those particles decrease. Particles of a size of 30 nm are only 5% on the surface, while the other 10 nm is 20% on the surface, and 3 nanometers are 50% on the surface ⁴⁵.

Chapter 1: Introduction

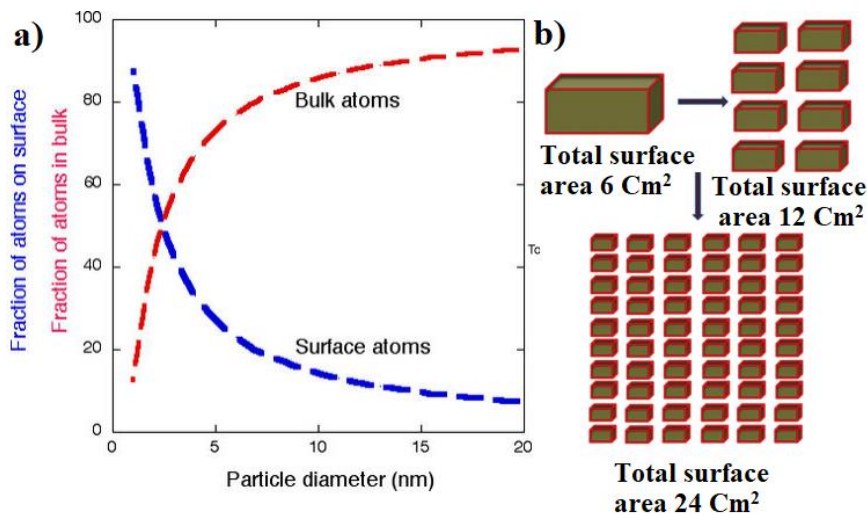


Figure 1-16: a) the general relationship between the size of the particles and the presence of the material atoms on the surface (surface Atoms) or their presence inside (Bulk Atoms)^{46, 47}; b) Relation between particle size and surface area⁴⁸

Quantum effect: Nanomaterials are not subject to classical physics laws because of their small dimensions which approaching the atomic dimensions, and are therefore subject to the laws of quantum physics, which are reflected in their properties⁴⁹. In small nanocrystals, electronic energy levels are not as continuous as in the case of bulk but are separate (intermittent) as a result of restriction (reservation, restriction) of electron wave function of the physical dimension of the particle. This appearance is called quantum confinement; therefore, nanocrystals are also called (quantum dots). The characteristics of the material vary depending on its quantum block, some materials have atoms confined to two dimensions so that the movement of electrons in one direction is like the movement of water in the tubes. Some materials are limited to one dimension, so the movement of electrons in two directions is like a quantum well⁵⁰.

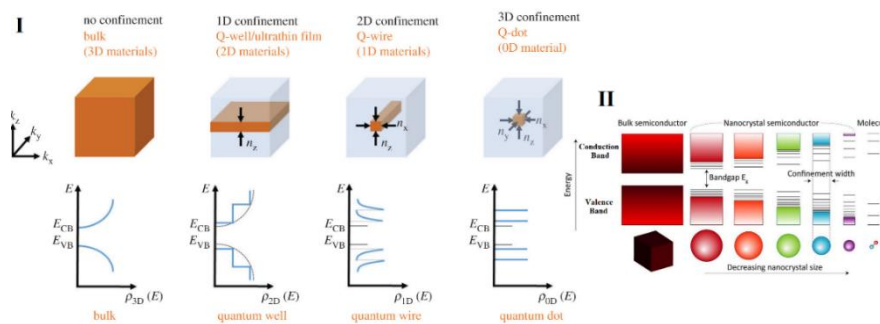


Figure 1-17: I: Schematic illustration of the Quantum confinement for 3D, 2D, 1D and 0D systems with their density of states⁵⁰; II: Schematic illustration of the quantum confinement effects: the bandgap of the nanocrystal increases with decreasing size, while discrete energy levels arise at the band-edges. The energy separation between the band-edge levels also increases with decreasing size. Can also see the photograph of five colloidal nanocrystals (NCs) with different sizes, under excitation with a UV-lamp in the dark. When the diameter of the QD decreases, the Photoluminescence color turns from red to blue^{51, 52}.

The most important characteristics of nanomaterials:

Chapter 1: Introduction

The mechanical properties: The mechanical properties come on top of the properties benefiting from the reduction of the size of the particles of the material and the presence of large numbers of atoms on the outer surface, where the degree of the solidity of metal materials and alloys increases ⁵³.

The chemical properties (chemical reactivity): Nanomaterials have significant chemical reactivity due to the significant increase in surface area relative to the size and the presence of a large number of atoms on the outer surfaces of these materials ⁵⁴.

1.5.2 Physical properties:

Thermal properties: The values of the material's melting points are influenced by reducing the dimensions of the measurements of their granules ⁵⁵.

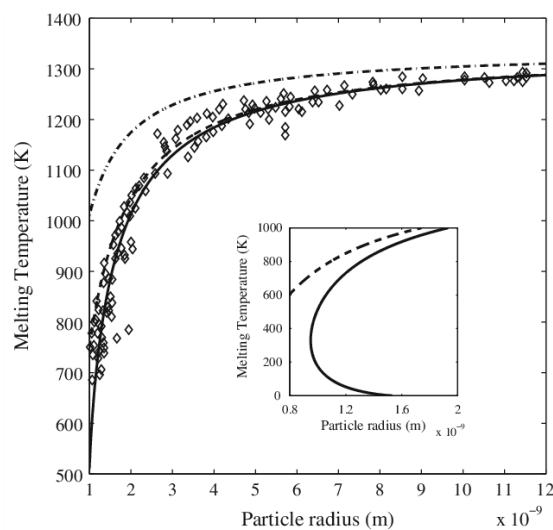


Figure 1-18: This figure illustrates the direct relationship between the temperature values of the melting point of the different gold particles and their Radiuses ⁵⁶.

Optical properties: Nanomaterials have gained the attention of researchers and scientists working in the field of optics due to the unprecedented properties of these materials, which differ in their visual properties from their counterparts from large-grained traditional materials. Surprisingly, the effect of particle size relates to the change of the optical properties of the material, including dispersion or a light scattering of the surface of the material ⁵⁷. Particles with diameters ranging between 1 and 50 nm are very small and unable to dissipate and scatter visible light waves of 380 to 765 nm in length and are even unable to unstable longer light waves as if it's a small boat swaying over a vast ocean waves which will be definitely unable to make any kind of disturbance ⁵⁸. Thus, A coherent nanoscale metal can therefore be transparent if the formation of any pores larger than its constituent clusters is avoided during the cohesion process. Thus, when he was at Rutgers University, Parker and Hahn were able to manufacture a transparent nano-phase of yttrium oxide; which is an opaque ceramic material in its normal state, as shown in the figure 19.

Chapter 1: Introduction

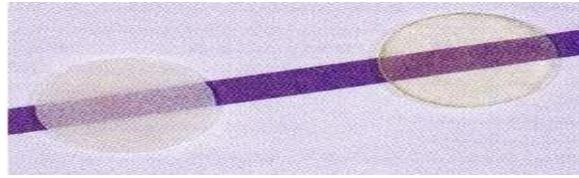


Figure 1-19: to the right side of the shape there are transparent ceramics of yttrium oxide containing pores and clusters no more than 50 nm in diameter. Pores and larger particles emit visible waves of light, so compact materials such as yttrium oxide make a dark (opaque) material as they appear to be on the left side of the shape.

On the other hand, radiation with shorter wavelengths, such as harmful UV radiation, cannot easily pass through the nanoparticles used such as titanium oxide, zinc oxide and iron oxide⁵⁹. In this case, the tiny particles can easily absorb, disperse and scatter UV rays. When exposed to ultraviolet radiation, nanoparticles emit a light with a visible wavelength that is inversely proportional to the second power of the particle's diameter Value⁵⁹. Certain visible colors can therefore be seen. Bruce, a researcher at Columbia University, has formed different solutions from the cadmium selenide which is a nanoscale compound, each of which looks different in color. In fact, this compound can often give any color of the spectrum once the dimensions of its atomic clusters have been changed⁶⁰.

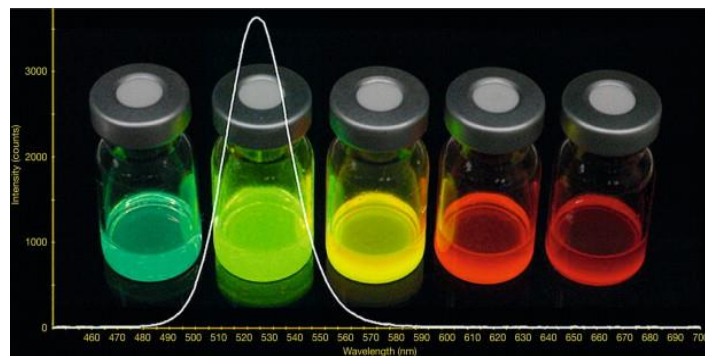


Figure 1-20: The various containers contain cadmium selenide. These samples are quite similar except in the varying dimensions of their particles, so each shows a different color, Blue emission (centered at 450 nm) is resulted from small CdSe nanoparticles (<2 nm), whereas the red emission (centered at 650 nm) requires larger CdSe nanoparticles (>5 nm) and etc.⁶⁰.

Another example is the known color of pure gold particles with diameters of more than 200 nm is the yellow gold color that we know, but if these particles are reduced to less than 20 nm, they are colorless (transparent) and as particles are further minimized, the particles appear in different colors from green to orange and then red, according to the measures of the dimensions of their diameters. The reduction of the gold particle sizes is reflected in the ability of these particles to resist photo-fracking and combine sharp emission band with broad excitation.

Chapter 1: Introduction

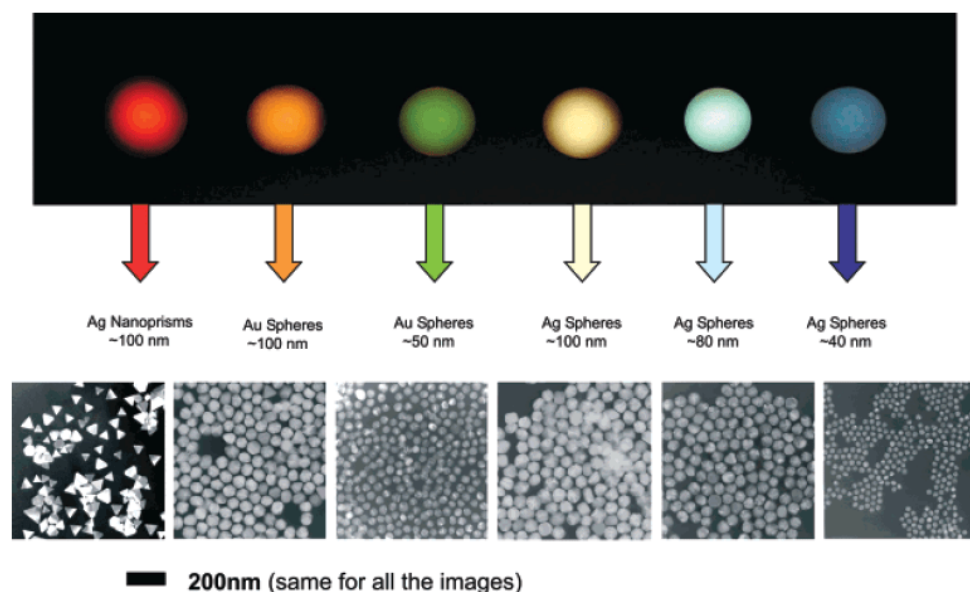


Figure 1-21: The change in the color of gold and silver according to the size of its particles ⁶¹

The opaque Silicon, which is the main component element on the Earth, sand and all objects in the universe, if we formed a material with 1 nanometer diameter, we will get a very shiny bluish color under the effect of the violet light, but if we expose it to a diameter of 1.7 nm, it radiates green and to a diameter of 2.1 nm, radiating yellow and radiating red when it is 2.9 nm in diameter. It's like we've turned sand into a sparkling material ⁶². Electronics and optics are among the most important applied fields of nanomaterials, which combine visual qualities and superior electrical conductivity, which are used in the manufacture of high-resolution, high-contrast, and color-pure screens, such as television screens and modern computers ⁶³.

Magnetic properties: The strength of magnets depends entirely on the measures of the dimensions of the particles of the material from which the magnets are made, and the smaller those particles and the greater the area of their outer surfaces and the presence of atoms on those surfaces, the stronger and more effective the magnets are. Nanomaterials with magnetic properties are the most important sources of materials involved in the production of ultra-high-intensity magnets used in large electricity generators, and large ship engines. Nanoparticles of magnetic materials are also involved in the manufacture of high-resolution analysis devices as well as in the magnetic resonance Imaging (MRI) magnetic imaging devices as well as in medical diagnostics in general ⁶⁴.

Electrical properties: The small size of nanomaterial particles and the increase in surface area and density of granular boundary numbers are reflected in electrical properties. Insulating materials such as polymers have become on the nanoscale conductive and have the ability to conduct electricity to be used to transport electrical current instead of using expensive copper wires while polymers are cheaper. Semiconductors also become conductive on the nanoscale and silicon becomes a good conductor of the electrical current ^{65, 66}. One of these new properties possessed by nanomaterials is how important it is to obtain many technical applications to introduce new materials such as ceramics and polymers into techniques that would not have been used by their normal properties. Nanomaterials are now used in the manufacture of microsensors and electronic slides with various modern devices. It is also used in the

Chapter 1: Introduction

manufacture of components of cell phones and computers. This enabled these industrial sectors to produce high-tech and at the same time low-cost lightweight devices ⁶⁷⁻⁶⁹.

Biological properties: these substances have the ability to penetrate the biological inhibitions and barriers that impede the access of medicines and therapeutic drugs to the infected part (e.g. membranes, Blood Brain Barrier) ⁷⁰. The nanotechnology merged and coincided with biotechnology to form the bio nanotechnology, which has made dramatic strides by devising advanced types of labels that have been employed to understand and analyze the structure and composition of DNA for both humans and viruses ^{71, 72}. This naturally led to knowledge of the behavior of diseases and viruses, their movement's mechanism within the body, and of the methods and tricks they take to attack the components and molecules of living cells in the body's organs. Since the range of biological processes in organism cells is at the level of parts of a single cell, the nanomaterials that are created are suitable selective substances for interaction with such small biological molecules as nucleic acids and proteins ⁷³.

1.6 Major current and future implementation of nanotechnology:

- 1- **Lab-on-a-Chip:** A chemical laboratory produced on 2006, to perform accurate medical analyses ⁷⁴.

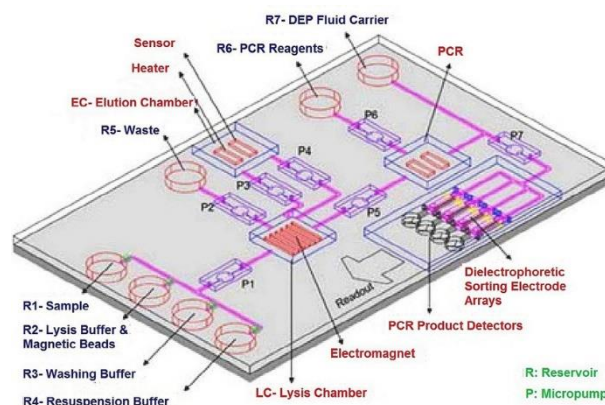


Figure 1-22: Lab-on-a-Chip instrument ⁷⁵

- 2- Microscope on mobile: it is a microscope integrated with mobile for diagnoses purposes ⁷⁶.
- 3- Use of antibacterial wound bandages instead of stitches.
- 4- The use of tapestries equipped with epidemiological materials.
- 5- Early detection of cancer tumors.
- 6- Nano devices for drug delivery, Dendrimer.
- 7- Gold nano rounds to eliminate cancer.
- 8- Nano Heart Stents.
- 9- A robot in the size of nano (nano robot).
- 10- Plastic nano casings.
- 11- Quasa material.
- 12- Programmed Drinks.
- 13- Combining two non-mixing parts (light-generating material).
- 12- New batteries of genetically modified and nanotechnology viruses.
- 13- Active glass (self-cleaning glass.
- 14- Manufacturing the Egyptian paper with nano technology.
- 15- The hiding Robe.
- 16- Clothes with customizable colours.
- 17- Synthetic blood cells.
- 18- Glasses Manufacturing.
- 19- Sports products.
- 20- Solar nano stations for power generation.
- 21- Cosmetics and sun protection using nanotechnology.
- 22- Nanobiotics is the latest alternative to antibiotics.
- 23- Computer giant Hewlett Packard.
- 24- Photonic catalyst for air purification.
- 25- Nanotechnology for water purification: A- Groundwater purification, B- Desalination of seas and oceans water, C- Nano filters for water purification.

Chapter 1: Introduction

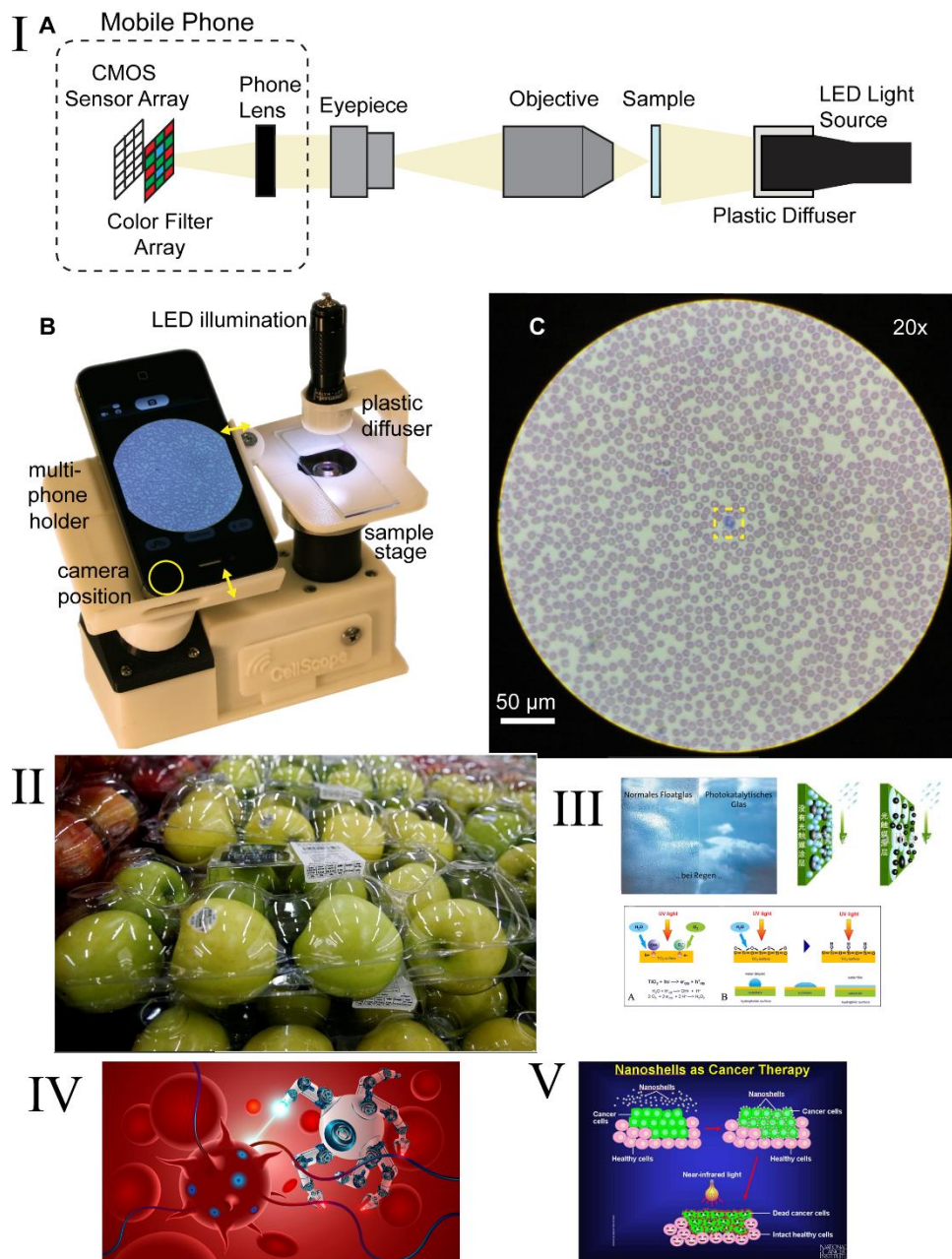


Figure 1-23: I) A: Sketch of magnifying lenses and illumination was added to a mobile phone to create a transmission optical microscope. B: prototype of a field-ready portable microscope - CellScope - which has a compact folded optical path and is equipped with a multi-phone stand and iPhone 4. Phone-specific variants have been evaluated on five continents for different applications. C: A Wright stained blood smear taken from an iPhone 4 moving microscope and 20 x / 0.4 NA objective showing the patterned field of view captured by the apparatus⁷⁷; II) nanoclays, Which aims to prevent gases and reduce the risk of bacterial contamination⁷⁸; III) Self-Cleaning Glass and how does it work; IV) Nanorobotics⁷⁹; V) Cancer treatment with gold nanoshell⁸⁰

The other terrifying side of nanotechnology: At every scientific or technological development, there is always criticism and fears are widespread. As happened in the first industrial revolution and when the computer was invented and genetic engineering emerged and others. The criticism here is focused on two elements: the first is that nanoparticles are too small that they can infiltrate behind the human body's immune system and can bypass the brain

Chapter 1: Introduction

blood barrier. The second concern is that nanobots become self-multiplying, i.e., similar to reproduction in normal life that can reproduce infinitely and control everything on the globe. Global environment and health organizations have begun organizing conferences to examine these particular risks. A meeting was held in Brussels in June 2008 chaired by Prince Charles that was the first global meeting to be organized for this goal. Green peace Organization recently issued a statement indicating that it would not call for a ban on nano-research. Whatever the case, man is at the gates of a new phase that is qualitatively different in all respects from the previous ones, new in its pros and cons, and as most scientists say: "No one can stand up to this great development, let's try to reduce the negatives" ⁸¹.

Nanotechnological risks on human health: Nanoparticles can easily enter the human body through pores and without any resistance and can spread within the body causing harm to humans. You can imagine that a 300 nm particle has the ability to easily enter the cells of the human body and that a 70 nm particle can easily enter the cell nucleus. This indicates the great danger that a human being can be exposed to. Many animal studies have shown that whenever exposed to nanoparticles, they enter the body and accumulate in the brain, blood cells and nerves, and this means that nanoparticles are destructive substances to the human body. A study at Oxford University showed that nano-titanium dioxide particles found in anti-sun ointments damaged the skin's DNA ^{82, 83}.

Nanotechnological risks on workplaces: Nanomaterials can be high explosive materials because of their large surface area relative to their size. Storing nanomaterials in large quantities in one place and for a long time may expose them to explosion. It is known that whenever dust increases in the workplace, this exposes it to explosion and that's why it's feared of nanomaterials exploding because they are accumulated too much in the workplace is larger and more severe. A study at NASA's Johnson Space Center also showed that carbon nanotubes are more harmful than quartz dust that causes silicosis, a deadly disease that occurs in the workplace ^{84, 85}.

Nanotechnological risks on the environment: Nanomaterials have a negative impact on the environment and concerns can be classified into two types ⁸⁶.

Bioaccumulation: Which arises from the accumulation of unwanted nanomaterials. Accumulated nanomaterials can have high absorption of highly concentrated pollutants such as cadmium and pesticides. If they are taken by animals and die, contaminated substances will seep into the soil and enter food chains leading to significant food pollution.

Tiny size of nanomaterials: It is practically difficult to detect, clean or remove them from the environment.

Chapter 1: Introduction

1.7 Green synthesis of silver nanoparticles

Green synthesis is an ecofriendly and biocompatible process, generally accomplished by using a reducing agent for reducing Ag^+ ions and the capping agent/stabilizer for preventing the aggregation of AgNPs and controlling their size. The green or biosynthesis methods of silver nanoparticles are simple and usually involve a one-pot reaction, cheap, non-toxic, environmentally friendly and also, high energy, temperature and toxic chemicals is not used. Many approaches were used to biosynthesize silver nanoparticles using microorganisms such as bacteria, yeasts, fungi, algae and actinomycetes (prokaryotes), templates such as membranes, viruses DNA and diatoms, and plant extracts. Using plant extracts such as stem, root, leaves, flower, fruit, seeds, bark, etc. for the synthesis of silver nanoparticles shows many advantages of environmental friendliness and compatibility with other pharmaceutical and biomedical applications because they do not use harmful chemicals for the synthesis protocol and the particle surface does not contain toxic chemicals. Synthesizing silver nanoparticles using plant parts extracts is a completely new method that leads to actually green chemistry compared to chemical and physical methods. Phytochemicals existent in extracts such as flavonoids, amino acids, alkaloids, tannins, carbohydrates, phenols, terpenoids, saponins and etc. which play the role of reducing and capping the particles in the nano dimensions and maintaining their stability in the colloidal solution. Therefore, synthesis using plant extracts is considered the best green method because it does not require complex processes to maintain cultures of microorganisms and does not require sterilization and purification and a long time, and the resulting silver is industrially feasible⁸⁷⁻⁹⁰.

1.8 Applications (uses) of silver nanoparticles

As a result of its electrical, thermal, excellent visual, stimulating properties as well as antibacterial, germs, viruses and fungi, silver nanoscale has gained considerable attention in recent years for various scientific, industrial or consumer fundamental applications, including:

- 1- Colloidal nanoparticles have been used as Conductive inks in ink-jet printing technology or so-called drop-on-demand technology (DOD)⁹¹.

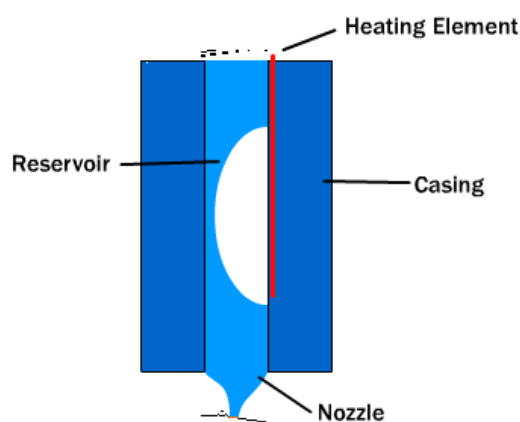


Figure 1-24: By heating the ink-contact metal, a bubble emerges from the ink vapor and the bubble pushes the ink out of the fine opening to the rack (paper or glass slide)⁹².

Chapter 1: Introduction

- 2- Nanoscale silver has been utilized as a catalyst in a variety of organic transformations such as conjugation, reduction and multicomponent reactions ⁹³.
- 3- Antibacterial keyboard: This device uses Nano Silver technology to encapsulate the keyboard using small silver nano-ion powder which makes the life and proliferation of bacteria impossible on the keyboard making the working environment on the computer personal and healthy ⁹⁴.
- 4- Tooth paste, toothbrush and mouth lotion: Brush bristles contain nano silver with antibacterial, bacteria and fungi effect which helps eliminating 99% of bacteria stuck in the brush after use. This brush has a long, thin and soft bi-bristle effect that works between teeth and gums also short, wide and rough bristles that work between teeth. The tooth paste is also effective against tooth decay and gum infections, reduces bacteria and germs that live in the mouth, treats bad smell, and is used for adults and children ⁹⁵. Nano Silver Mouth Lotion expels bad breath germs, prevents gum infections, keeps teeth clean and shiny, and is used for adults and children aged 6 years ⁹⁶.
- 5- Socks and shoes that do not cause bad smell: A shoe manufacturer has placed nanofibers of silver metal inside the shoe in order to prevent foot fungi and bacteria from growing during the period of wearing shoes and this product is of great importance to diabetics who are permanently suffering from ulcers and foot infections where they prevent bacterial infections that may lead to serious consequences of the occurrence of foot gangrene ⁹⁷.
- 6- Sprays that deodorant the human body: the real sweat is odorless. But, when a type of bacteria called saprophytes touches sweat glycosides, fatty acid is produced that smells bad. Silver ions kill and replace these bacteria. Without them, the sweat cannot decompose and therefore does not emit the bad smell ⁹⁸.
- 7- Use of a nanoscale sponge for wound healing: innovative long-term sterile materials which eliminate microbes for more than 10 days and are placed on any surface by a sponge containing silver nano grains developed by the German Company Adexano, and also used to sterilize medical tools and equipment ⁹⁹.
- 8- Nano crystal silver bandages accelerated to heal wounds: silver nanoparticles now replace silver sulfadiazine as an effective factor in wound treatment, and the U.S. Food and Drug Administration has agreed to use a wide range of various silver-saturated wound bandages. One of Iran's pharmaceutical companies has announced that it has produced nano crystal silver bandages which are able to reduce pain, reduce wound healing time and prevent inflammation ⁹⁹.
- 9- Nano Silver Medical Face Mask: Or so-called protective surgical masks ¹⁰⁰.
- 10- The deadly paper: Scientists have acknowledged the development and success of laboratory tests on "the deadly paper that helps save food from damaging bacteria, particularly *antambiacula* and *staphylococcus* which killed all those infected with these bacteria in just three hours. Silver nanoparticles are placed on the surface of paper using

Chapter 1: Introduction

ultrasound, or high-frequency sound waves. A Korean company also produced a food container called Fresh Box containing nanoscale silver. This pot is antibacterial and antifungal and therefore makes food fresh for longer than traditional bowls ¹⁰¹.

- 11- Vaccinating sportswear used in warm-ups and running with silver fibers to block any fungal or bacterial activity from forming. Liquids containing suspensions of non-dissolved silver nanoparticles are used in the treatment of cotton, polyester and other tissues used in the textile industry ¹⁰².
- 12- Healthy Hair Brush: Sang Shin Industrial has produced a healthy hair brush by blending and processing nylon 66 with silver nanoparticles ¹⁰³.
- 13- A Japanese company Lion Corp has produced a personal care sterile component of silver nanoparticles associated with Alumina-Seleka with a size of 15 nm.
- 14- The American company Plank has produced a facial and body care soap. It is made up of colloidal silver nanoparticles united with silica- collagen- Ketuzan - as well as silk protein ¹⁰⁴.
- 15- Skybright Natural Health Company has produced a shampoo containing colloidal nano silver and plant extracts which is used to rid the scalp of dandruff and itching ¹⁰³.
- 16- Nano silver is an antibacterial spray: in order to fight swine flu and fight the bird flu virus, this spray contains patented nanoscale silver. It is a powerful antibacterial which kills germs, bacteria and viruses and removes odors in the air, fabrics and clothing with unique freshness. It is used in the bathroom, bedroom, kitchen, car, living room or anywhere else we want freshness in the air, from the bedroom to the basement on clothes and fabrics such as car interiors, curtains, sofas and carpets. The spray is sprayed into the air in wide motion throughout the entire room. It is also sprayed evenly on the fabric until slightly wet. Nanoscale silver will penetrate the fabric and eliminate odors. Of course, it weighs 200ml in a bottle ¹⁰⁵.
- 17- Comfortable facial mask which contains colloidal nanoscale silver. It is also used in many cosmetics and skin care ¹⁰⁶.
- 18- Bathroom spray filter: Is a filter and purification device for washing or bathing water that produces healthy natural water free of pollutants and harmful substances contained in water. This device uses advanced technology based on nanotechnology to get rid of chlorine, bacteria and organic matter that harm hair and skin when bathing. This filter uses two nanoscale materials: Silver fiber nano or Nano Carbon fiber ¹⁰⁷.
- 19- Manufacture of electrical and electronic devices covered from the inside with a thin layer of nanoscale silver with the aim of killing the bacteria and germs that exist. Silver nanoparticles with diameters of less than 10 nanometers are now involved in painting cutting tools used in kitchen for food cooking and painting kitchen utensils and tableware such as cups and cooking pots. All of the above is done with the aim of killing bacteria and germs that may exist in order to protect preserved foods from bacterial contamination ¹⁰⁸.

Chapter 1: Introduction

- 20- Washing machine that generates nanoparticles to clean and disinfect clothes more than hot water and detergents. The silver ions generated remove germs and fungi even in cold water. This washing machine releases nearly 400 billion silver electrolytes per washing cycle that cover fabrics and maintains antibacterial activity for up to a month. Germs and fungi are removed by 99.9% through nano silver technology. So, there will be no germ reproduction ¹⁰⁹.
- 21- Some companies have conducted numerous exciting scientific research on silver metal nanoparticles to see if they can be employed to resist infection and kill different types of harmful bacteria and viruses. The results indicated that the crystal particles of silver metals have an amazing ability to kill multiple types of harmful bacteria, viruses and germs. This happens due to the reduction of these particles to diameters less than 5 nm that significantly increase the surface area of the particles, and as particle diameters decrease and the surface area increases, they are generated by silver atoms found in the core of particles that migrate to the outer surface of particles resulting in a significant increase in their chemical activity and in their interaction with atmospheric oxygen. As a result, toxic silver ions are formed that are responsible for killing germs and viruses ¹¹⁰⁻¹¹².
- 22- Silver nanoparticles especially biosynthesized were used as an anti-cancer therapeutic agent, drug delivery and bioimaging vehicle. Silver nanoparticles were examined in many cancer cell lines ¹¹³⁻¹¹⁵.

Chapter 1: Introduction



Appliances

Samsung Silver Nano Washing Machine and Refrigerator.

Silver ions released during wash and rinse cycles

Clothes become antibacterial: killing odor caused by sweat or fungus for up to 30 days

The diagram illustrates the five-stage process of the Samsung Silver Nano Washing Machine:

- 1st stage:** Electricity is passed through the electrodes to generate Ag⁺ ion.
- 2nd stage:** Tap water then flow through the Ag⁺ Mechanism carrying the Ag⁺ into the tub.
- 3rd stage:** Ag⁺ ion sterilizes the clothes during the wash cycle.
- 4th stage:** Ag⁺ ion is released at the last rinse cycle.
- 5th stage:** Ag⁺ ion now act to prevent bacteria from clinging onto the clean clothes & its propagation on the tub.

Effect lasting Up to 1 month!

Accompanying images show the washing machine, a splash of water, a top-loading washer, and various bottles of silver ion products.

Figure 1-25: An image showing some products available in the market that contain nano-silver

Chapter 1: Introduction

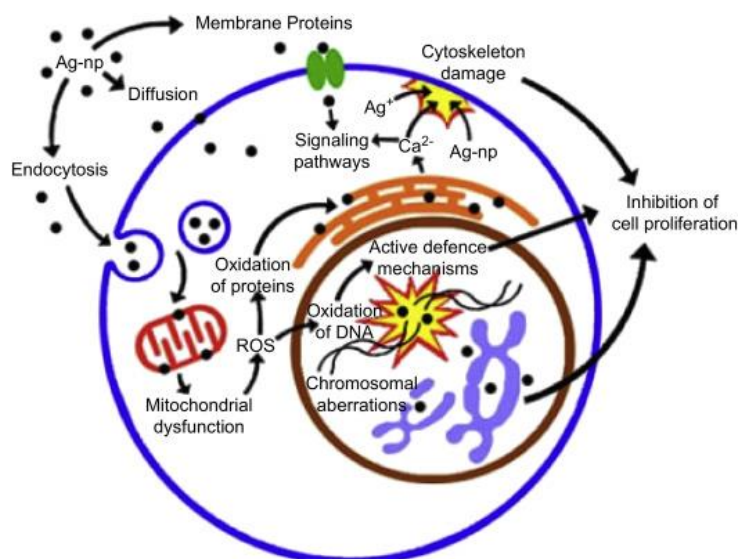


Figure 1-26: The mechanism and potential cellular uptake of Ag-NPs toxicity in different cell lines ¹¹⁶

Silver nanoparticles (AgNPs) are well-known as a promising material; have attracted considerable interest worldwide to develop a new generation of diagnostic tools and effective treatment solutions for cancer cells. using AgNPs in cancer diagnosis, their cytotoxicity, and their role as carrier systems for cancer treatment have been discussed in a lot of research at the moment. According to the unique physical, chemical properties and small size of silver nanoparticles, they may affect different cells through different cellular processes. AgNPs enter mammalian cells as clusters mostly through endocytosis and can also cross the blood-brain barrier due to their small size. in addition, AgNPs have a stronger effect than silver ions as disclosed in some research. Most of the *in vitro* studies showed that AgNPs can enter cells via endocytosis and can be localized within the cell as the perinuclear space in the cytoplasm and intracellular compartment. Besides, silver nanoparticles can enter the mitochondria and produce reactive oxygen species (ROS) by affecting the respiration of cells. Briefly, the mechanisms of silver nanoparticles as toxic can cause oxidative stress, DNA damage, induction of apoptosis, and mitochondrial damage to cancer cells. The mechanism of action of silver nanoparticles on cancer cells is schematized in (figure 26). Furthermore, there are studies that AgNPs affect the function of the vascular endothelial growth factor (VEGF). It is also known as the vascular permeability factor and plays a major role in the angiogenesis within tumors. These results support AgNPs have anti-cancer properties that can be used as an alternative for cancer therapy and angiogenesis inhibitor therapy. Theranostic applications of green-synthesized nanoparticles were investigated for biologically compatible and potential approaches in the biomedical field (antimicrobial, anti-inflammatory, antinociceptive, anticancer and enzyme inhibition activities). Theranostic is defined a combination of diagnostics and therapy. The bio-synthesized AgNPs could be used in theranostic applications including anti-cancer therapeutic agent, drug delivery and bioimaging vehicle. Green AgNPs can be used as beneficial theranostic agents for further discovery of various biomedical applications. AgNPs, which were biosynthesized with various applications, were tested in different cancer cell lines ¹¹⁷.

Chapter 1: Introduction

1.9 Cancer

Human cells normally reproduce through a process called cell division in which new cells are formed according to the body's need. When cells are damaged or age, they die and are replaced by new cells. In cancer, the body's cells grow out of control as trillions of new cells are formed and spread to other parts of the body. In cancer, the regulating process of cell growth and reproduction is disrupted as damaged and abnormal cells grow and multiply and form tumors, which are lumps of tissue. Tumors can be cancerous or noncancerous (benign). Cancerous or malignant tumors spread and invade nearby and distant tissues in the body to form new tumors. Cancerous tumors are known as malignant tumors. Most cancers are solid tumors, but leukemias, for example, are not. Cancerous tumors can grow again after removal, while benign tumors do not spread, do not invade nearby or distant tissues, and do not grow again after removal. Benign tumors if they are in dangerous places such as the brain can pose a threat to life ¹¹⁸.

Differences between cancer cells and normal cells ¹¹⁹

- Cancer cells grow and multiply in the absence of signals telling them to do so, the exact opposite of normal cells.
- It ignores the signals that tell it to die (or apoptosis).
- They invade and spread to adjacent areas and other areas of the body.
- It tells the blood vessels to feeding it with oxygen and nutrients, and take of waste from it.
- It disappears from the immune system so that it does not destroy it.
- It disappears from the immune system and tricks it into protecting it instead of attacking and eliminating it.
- Some cancer cells have twice the normal number of chromosomes.
- Cancer cells produce energy from nutrients in a way that allows them to grow more quickly.

The occurrence of cancer ^{120, 121}

Cancer is a genetic illness- which resulted from changes in the genes that control the way cells grow and divide.

Causes of genetic changes that cause the emergence of cancer:

- Errors occur when cells divide.
- Harmful chemicals such as smoke, tobacco and ultraviolet rays from the sun damage DNA.
- Inheritance from the family.
- The body does not get rid of damaged DNA.
- Each cancerous cell in any living body will have different genetic changes.

Chapter 1: Introduction

The most important genes that influenced and cause cancer are proto-oncogenes, tumor suppressor genes, and DNA repair genes.

Types of cancer: There are over 100 kinds of cancer. Where cancer types are named according to the organs or tissues that make up the cancers or by the type of cell they formed, such as the epithelial cell or the squamous cell ¹²².

Lung cancer: is cancer that occurs in lung tissue, commonly in the cells that line the air passages. This type causes death in both men and women. There are two main types: small cell lung cancer and non-small cell lung cancer. These two types grow differently and are treated differently, and non-small cell lung cancer is the most common type ¹²³.

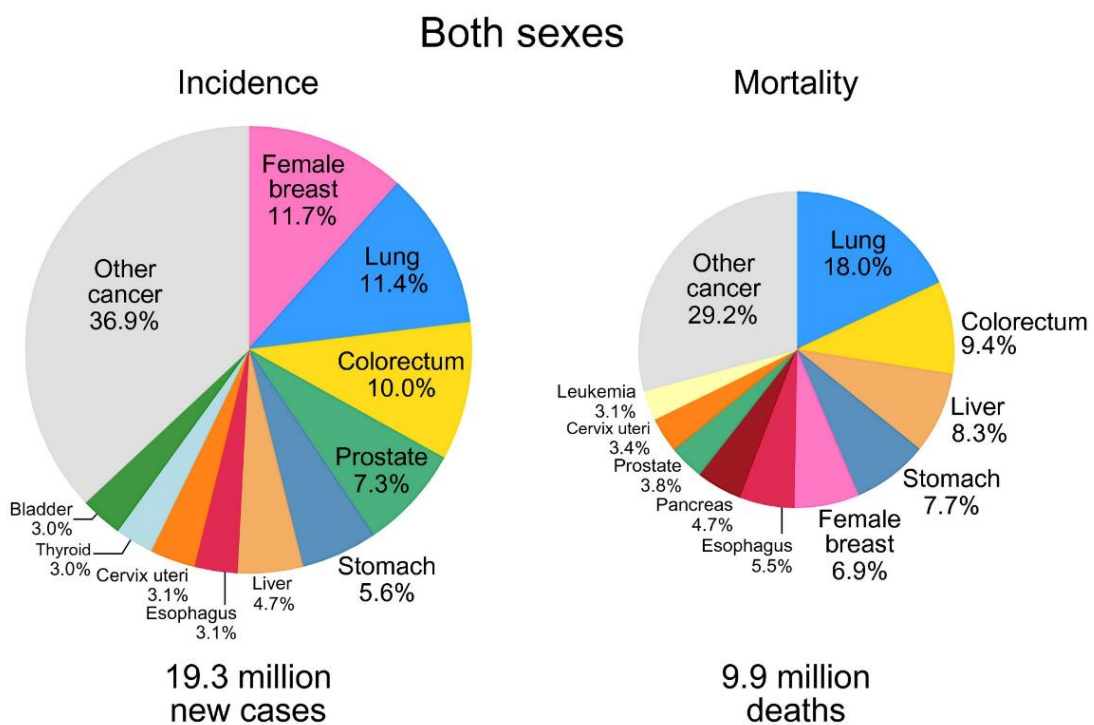


Figure 1-27: Estimate number of new cases and death for the top 10 most common types of cancer in 2020 for both sexes ¹²⁴.

Chapter 1: Introduction

1.10 Leishmaniasis

Leishmaniasis is a parasitic disease caused by a genus of single-celled parasitic organisms known as *Leishmania*, which is transmitted to humans by certain types of sandflies that carry the disease ¹²⁵.

Leishmaniasis types ¹²⁶:

- **Visceral leishmaniasis:** also known as kala-azar, is fatal in 95% of cases if left untreated. It is characterized by irregular episodes of fever, weight loss, enlarged spleen and liver, and anemia. In 2020, more than 90% of new cases were concentrated in 10 countries: Brazil, China, Ethiopia, Eritrea, India, Kenya, Somalia, South Sudan, Sudan and Yemen.
- **Cutaneous leishmaniasis:** is the most common form of leishmaniasis and causes skin lesions, mainly ulcers, on the visible parts of the body, leaving permanent scars and serious disability or social stigma. In 2020, more than 85 percent of new cases were concentrated in 10 countries: Afghanistan, Algeria, Brazil, Colombia, Iraq, Libya, Pakistan, Peru, Syrian Arab Republic and Tunisia. The number of new cases annually is estimated at 600,000 to 1 million worldwide.
- **Mucocutaneous leishmaniasis:** which causes partial or complete damage to the mucous membranes of the nose, mouth and throat. More than 90% of mucocutaneous leishmaniasis cases are concentrated in the Plurinational State of Bolivia, Brazil, Ethiopia and Peru.

Leishmania parasite life cycle: The parasite *Leishmania* is present in the sandfly in the gametophyte phase, as the parasites at this stage have flagella, then begin to multiply in the body of the female sandfly, and move to settle in the larynx and oral cavity of the fly. Leishmaniasis is transmitted to the fly by ingesting the blood of an infected person or animal with leishmaniasis. The *Leishmania* parasite needs 4-25 days to complete its life cycle inside the fly and is transmitted to humans ¹²⁷.



Figure 1-28: Leishmaniasis on the thigh, upper row, leishmaniasis on the forearm, lower row ¹²⁸.

Chapter 1: Introduction

1.11 Bacteria

Bacteria are small single-celled organisms. Bacteria are found almost everywhere on Earth and are vital to the planet's ecosystems. Some species can live under extreme conditions of temperature and pressure. The human body contains a very large number of bacteria, which is much greater than the number of human cells. Most bacteria in the body are harmless, and some are even helpful. Humans coexist with bacteria, where they preserve a two-way helpful correlation without knowing it. A relatively small number of species cause disease ¹²⁹.

Structure of bacteria: Bacteria have five main forms: corkscrew (spirochaetes), cylindrical (bacilli), comma (vibrios), Spherical (cocci) and helical (spirilla). Based on the Science Education Resource Center at Carleton College, bacteria are categorized via the formation of their cell walls utilizing an experiment named Gram stain. Gram-positive bacteria, don't have an outer membrane and pick up the stain. Gram-negative bacteria, which do have an outer membrane, don't pick up the stain ¹³⁰.

Bacteria are organisms that consist of a single cell and have a distinct interior structure. Humans and other polycellular organisms have their own distinct membrane-bound nuclei. Bacteria are prokaryotes, this indicates that they do not contain orderly nuclei or any other membrane-bound organelles. Bacterial DNA is in the form of twisted, clumpy strands called nuclei that swim freely inside the bacterial cells. Some may also contain divided rotating parts of DNA called plasmids. In conformity with the Society for Microbiology, plasmids mostly include genes that give bacteria a survival advantage, like genes that transmit antibiotic resistance. Commonly there is an outer cell wall surrounding the bacteria cells and an inner cell membrane. Certain bacteria, like mycoplasmas, do not have a cell wall at all. Some bacteria may even have a third, outermost protective layer, called the capsule. On the surfaces of bacteria cells there are flagella-like extensions, where the longer ones are named flagella and the short ones are named pili, which support bacteria cells when Stick to the host and move around. Bacteria cells contain cytoplasm located under the cell wall and membrane, a solution consisting mostly of water and salts. Nucleoids, plasmids, and ribosomes (the sites where a cell's genetic regulations are translated into cell needs) swim within the cytoplasm. Some bacteria may also contain small pockets in the cytoplasm, called inclusions, where nutrients are stored for lean times. Photosynthetic bacteria, which deliver energy from sunlight, may have objects named chromatophores scattered throughout the cytoplasm. These chromatophores hold pigments used in photosynthesis ^{131, 132}.

Bacteria multiplication: As some of the oldest life forms on Earth, bacteria have evolved a dizzying number of ways to survive. Part of the bacteria mainly decomposes, destroy moldy and degenerates the organic materials into nutrients, while the other part is photosynthesis. Some bacteria form interdependence or two-way useful relationships with a host. Most bacteria reproduce through a procedure named binary fission. In the binary fission process, one bacterial cell named the "mother" forms a reduplication of its DNA and grows larger via multiplier its cellular substances. Then the cell divides from each other, causing the refined material to be pushed outward and make two similar "daughter" cells. Other sorts of bacteria, like firmicutes and cyanobacteria, proliferate by budding. In this situation, the daughter cell grows as a branch of the parent. It begins as a small element, grow to the same size as its mother and then divides

Chapter 1: Introduction

away. The DNA in the parents and progenies is exactly the same after budding or binary fission. Bacterial cells subsequently differ in their genetic substances by incorporating additional DNA into their genome from their periphery. This is known as horizontal gene transfer. Horizontal gene transfer is carried out by three methods: transduction, transformation and conjugation ¹³³.

Beneficial bacteria: Many bacteria are beneficial to humans. There are very many bacteria that do important work inside our bodies, and the bacteria that convert milk into yogurt, bacteria also ferment cabbage and turn it into Kimchi. According to the Society for Microbiology, inside the human body there are bacteria cells that are about 10 times the number of cells in the body, and some of them live in the digestive system. These bacteria help destroy foods that human digestive enzymes cannot and in return obtain nutrients from the human gut. According to a research paper published in Nature Reviews Microbiology 2018, bacteria on the skin can secrete byproducts that protect from harmful bacteria. The praiseworthy bacterium *Corynebacterium accolens* block the growth of the bacteria that causes *S. pneumoniae*. Some skin bacteria can be both beneficial and hurtful. *Staphylococcus epidermidis* is a globular bacteria that usually colonizes the skin but if it enters the human body, it causes infection. *S. epidermidis* bacteria generate proteins that prevent the growth of its more malicious relatives, *Staphylococcus aureus*. *Staphylococcus aureus* leads to infections when it crosses the skin barrier ¹³⁴.

Harmful bacteria: Part of bacteria, such as *Staphylococcus aureus*, live in proportional concord with humans most of the time; based on the Centers for Disease Control and Prevention (CDC), about 30% of humans have *S. aureus* in their noses. But when these bacteria enter the body, they lead to deadly infections, essentially in persons with weak immunity. Based on CDC, Staphylococcal infection can lead to endocarditis (inflammation of the heart and heart valves), pneumonia, osteomyelitis and Sepsis. Other bacteria are constantly hurtful to humans. *V. cholerae* causes a diarrheal sickness that kills about 95,000 persons around the world every year. The bacteria *Yersinia pestis*, diffused by fleas that sting rodents, caused the Black Death. Anthrax spores are nearly indestructible which are found in soil and lead to fatal illnesses if inhaled or consumed. The most common types of bacteria that cause problems to humans infect them through rotten food. *Salmonella* bacteria cause diarrhea, stomach cramps and fever. Based on CDC, although most adults recover from salmonellosis after four to seven days, it can be dangerous, even deadly, in young children and the elderly. *Escherichia coli* is a bacteria that diffuse via polluted food and water that cause's food toxicity. Most of its strains live without damage in the human intestine, but some of its strains cause diarrheal disease. according to the CDC, 5% to 10% of people who get diarrhea from *E. coli* can develop kidney multipliers named a hemolytic uremic syndrome, which could be life threatening ¹³⁵.

Chapter 1: Introduction

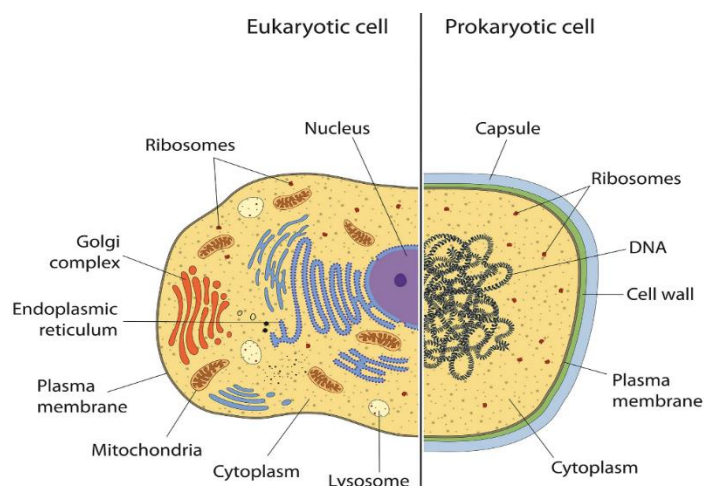


Figure 1-29: the general structure of bacteria¹³⁵

1.12 *Hypericum perforatum* L. (St. John's wort)

The genus *Hypericaceae* contains more than 480 species Distributed in temperate regions of the world such as South America, North and South Africa, India, Western Asia, Europe and Australia¹³⁶⁻¹³⁸. *Hypericum perforatum* L., ordinarily renowned as St. John's wort, which is the most prevalent among all the other types, and can exist and distribute in poor grazing land, open rocky ground, neglected and wooded areas, meadows, and sometimes in crops¹³⁹⁻¹⁴¹. St. John's wort is an upstanding and perennial grassy plant, up to 5 feet tall depending on genotype and location kind¹⁴². The roots are lateral and vertical, extending to depths of 2 to 5 feet, depending on the nature of the soil and moisture content. Stems, numbering from 1 to 30, are woody at the base, leafy and forked in the top half. Leaves are up to 3 cm long and 5 mm wide. The leaves give the impression that they are perforated because they contain scattered small transparent dots. The flowers are yellow in star shape with small black dots around the edges. The flowers bloom in June and August. Although it grows in most types of soil and climatic conditions, this plant prefers moist, well-drained soil and full sun until it blooms profusely¹⁴³⁻¹⁴⁹. Phytochemical compounds which may be obtained from the aerial parts of St. John's Wort are also greatly influenced by genetic and environmental factors. Soil type and its nature, humidity, exposure to sunlight, and altitude above sea level. Extracted parts from the plant such as bells, leaves, flowers, stem, root or perhaps a mixture of all of them are ground together and extracted. Temperature and polarity of the Solvent, pressure, pH and exposure to light in the extraction medium¹⁵⁰. Various solvents, methods and technologies to extract the constituents from aerial parts of St. John's wort, give always eight categories¹⁵¹⁻¹⁵⁶: five of them are lipophilic; Naphthodianthrone like Hypericin and Pseudohypericin, Phloroglucinols like Hyperforin and Adhyperforin, Biflavonoids such as Biapigenin, Xanthons such as norathyriol and Essential oils such as terpenes and alcohols. Two of them are hydrophilic; Procyanidins such as procyanidin, catechin and epicatechin, Amino acids such as Cysteine, Glutamine, Leucine, Lysine, and GABA (γ -aminobutyric acid). One of them is lipophilic and hydrophilic together; Flavonoids such as Rutin, Quercitrin, Quercetin, Isoquercitrin and Hyperoside. Most of the bioactive natural products extracted from St John's Wort are considered biologically active and have different medicinal effects in various medical areas^{157, 158}, this is what made this herb a long chronicle of conventional medicinal utilize over the ages in most countries of

Chapter 1: Introduction

the world, where it was applied externally immediately on the skin or it was boiled and taken internally for sedative or tonic purposes¹⁵⁹.

For symptomatic treatment of minor skin infections, sores, burning mouth syndrome, tooth extractions, cuts, minor burns, bruises, subcutaneous tissue disorders, psoriasis, eczema, keloid scars, sunburn, snake bites, rheumatism, back pain, nerve pain, hematomas and keloid scars¹⁶⁰⁻¹⁶⁷. It has been used as an antioxidant^{168, 169}, anti-inflammatories^{170, 171}, anti-bacteria^{172, 173}, anti-viruses^{174, 175}, anti-cancer^{176, 177}, anti-tumors^{178, 179}, anti-malaria^{180, 181}, and anti-diabetes^{182, 183}, anticonvulsant¹⁸⁴, analgesic¹⁸⁵, anti-schizophrenic¹⁸⁶, diuretic¹⁸⁷, nootropic¹⁸⁸, apoptotic¹⁸⁹, antifungal^{190, 191}, irritable bowel syndrome¹⁹², attention-deficit/hyperactivity disorder¹⁹³, seasonal affective disorder¹⁹⁴, Chronic Fatigue Syndrome¹⁹⁵, premenstrual syndrome¹⁹⁶, obsessive compulsive disorder¹⁹⁷, somatization disorder¹⁹⁸. For the treatment of dyspeptic disorders, nervous stomach diseases, abdominal pain and as a choleric treatment¹⁶⁰. The most important and widespread use of the extracts of this plant is the treatment of various nervous system disorders and symptoms of bouts of depression, anxiety, mood and mild and moderate tension^{186, 199-201}. The mechanism of action of synthetic antidepressants is by blocking the 5-HT receptors, while the mechanism of action of St. John's wort bioactive ingredients as an antidepressant is to block the absorption of monoamines such as norepinephrine and serotonin from the synaptic vacuole to the neuron, that is, the extract suppressed monoamine oxidase (MAO), norepinephrine and selective serotonin reabsorption by raising intracellular concentrations of sodium and calcium^{147, 155, 202, 203}. Of course, the discussion is still ongoing about the most relevant components responsible for this effect and research is still extensive on all aspects of St. John's wort. The safe and effective use of St. John's wort in various treatments makes it the most popular and best seller nutritional supplement in Europe, the United States, and most of the world. St. John's wort has been authorized as a drug and as a food supplement in Europe, America and most countries of the world, meaning it is usually recorded under the THR (Traditional Herbal Registration) platform. The dried aerial parts of *Hypericum perforatum* are widely sold as raw medicines (as: capsules, tablets, coated tablets and as tea) all over the world^{139, 147, 155, 202, 204}.

The extensive medicinal uses of extracts of this plant show the importance of comprehensive investigation to know the main raw materials (Phytochemicals, ingredients and constituents) in St John's Wort herbal products, which play an important role in Know the quality of the ultimate product in the market. Therefore, various spectroscopic and chromatographic analysis methods have been developed for the quantitative or qualitative estimation of most of the Phytochemicals or to isolate only specific ingredients that exist in St John's wort extract. These methods have been continuously developed because Deutsche Arzneimittel Codex (DAC), which is not sufficient to assess the qualitative composition of the components²⁰⁴ and we mention them very briefly, are: (1) High-performance thin-layer chromatography (HPTLC)²⁰⁵: HPTLC and TLC emerges as an efficient, versatile, low-cost chemical method uniquely appropriate for evaluation the identity and quality of plant materials. This technique is used to separate the non-volatile components in a mixture and therefore it is a powerful and reliable technique for detecting the compositional differences between products i.e. detecting the purity of chemicals and the presence of possible chemical patterns within the same species and thus detecting adulteration. Some researchers believe it is the most ideal analytical method for

Chapter 1: Introduction

botanical medicines and preparations containing medicinal extracts or pure medicinal ingredients. However, the TLC method faces an important challenge regarding the reproducibility and sorbent content of the TLC plate which contains large particles of the adsorbent^{139, 204, 206}. (2) High-performance liquid chromatography (HPLC) and liquid chromatography connected to mass spectrometry (HPLC/MS) and capillary electrophoresis: HPLC coupled to diode array and UV detectors is the common and preferred chemical separation technique in most research centers to separate and detect the polar, non-volatile and unstable chemical ingredients present in *Hypericum perforatum L.*, but it cannot supply sufficient data to clarify the complete structure^{207, 208}. During the last years HPLC-MS and MS/MS became the used method in most laboratories, because the molecular mass of a certain compound and its fractionation indicate an evident hint of the existence of this compound. However most of the modern ionization methods in MS just give a molecular ion and finally a few fragments, so, HPLC-MS and MS/MS techniques are till now not enough most of the time to explain the full structure²⁰⁹⁻²¹³. (3) UV-spectroscopy: UV-Vis spectroscopy is a simple qualitative manner to identify a compound or compound group in *Hypericum perforatum* by matching the peak absorbance in the visible and ultraviolet region with a standard reference sample or what is mentioned in the data and proven in previous studies²¹³⁻²¹⁵. Since many substances absorb large areas of the spectrum, it may cause interactions with other compounds. (4) Fluorescence microscopy: St. John's Wort contains some endogenous fluorescent molecules which may be utilized for imaging, physiological and biochemical researches. Fluorescent Correlation Spectroscopy It is considered as a method for detecting certain molecules using Fluorescence imaging manner, and thus it will be useful for some experimental investigations, plant biochemistry and physiology, and pathology and in the characterization of biomaterials²¹⁶⁻²¹⁸. (5) Near-infrared spectroscopy: It is an efficient and rapid technique for the quantification of the major components obtained from extracts and thus for High productivity quality monitoring. During recent years this analytical method has been updated to obtain chemical image images of the sample such as structural components or primary and secondary metabolites and thus can be used to distinguish chemical patterns between the same species or between different species. So, through this method, we can explore plant biochemistry, metabolism, phenotyping, physiology, taxonomy and know and determine the optimal time for harvesting. The principle is depend on the analysis of spectroscopic data and its use to generate an image useful for understanding the encoded chemical information. This topic is very complex and you will find the mechanisms of obtaining different images through the IR spectrum in the following references^{204, 219-221}. (6) Nuclear magnetic resonance spectroscopy (NMR): It is a powerful analytical chemistry method that is relatively easy to use, accurate, repeatable, non-destructive, covers a much wider dynamic range than previous methods, and sample preparation is simpler and faster to use. Whereas, NMR is unique and specific for each compound separately and gives qualitative and quantitative information because the signal intensity is directly proportional to the molar concentration as well as gives final structural information with no restrictions related to polarity, variability, or the presence of certain chromosome carriers²²²⁻²²⁵. Currently, different chromatographic, spectroscopic Spectrophotometric and colorimetric analysis techniques are being combined to identify phytochemicals with high accuracy in different extracts.

Chapter 1: Introduction

1.13 HPLC

A comprehensive view of HPLC: HPLC is a combination because High Performance Liquid Chromatography. "Chromatography" is an approach for separation, "chromatogram" is the result over chromatography, and then "chromatograph" is the weapon chronic in accordance with propulsion chromatography. Liquid chromatography is a stable method for the dissolution concerning substances. High overall performance melted chromatography (HPLC) is a suitable technique for the analysis about a large extent on utility areas. As related technologies grew to be more sophisticated, the law normally referred according to namely High-Performance Liquid Chromatography, absolutely grew to be referred in conformity with as "LC". Nowadays, Ultra High-Performance Liquid Chromatography (UHPLC), successful of high-speed analysis, has additionally grow to be more widespread. Only compounds dissolved between solvents be able lie analyzed together with HPLC. HPLC separates compounds dissolved between a softened samples then lets in qualitative yet quantitative analysis on such as elements or how a good deal concerning each issue is contained within the sample ²²⁶.

The apparatus of HPLC: HPLC consists regarding a variety concerning components, inclusive of a dissolvent reservoir, a diluent transport pump, a degassing unit, a sample injector, a column, a stagnancy oven, a detector one and a records technology one (Fig. 30). Fig.30 indicates a simple overview of the HPLC manner and the HPLC go with the flow sketch and the position over each component. The acid ancient to analyse factors into a liquid sample because of HPLC evaluation is referred to as the cell phase. The cellular segment is delivered after a split column, in any other case recognized namely the certain phase, and then according to the detector at a secure flow dimension controlled with the aid of the solvent shipping pump. Permanency a definitive total on sample is injected between the column and the compounds contained in the sample are separated. The compounds separated of the motionlessness are detected by using a detector downstream on the pillar then each compound is identified or quantified.

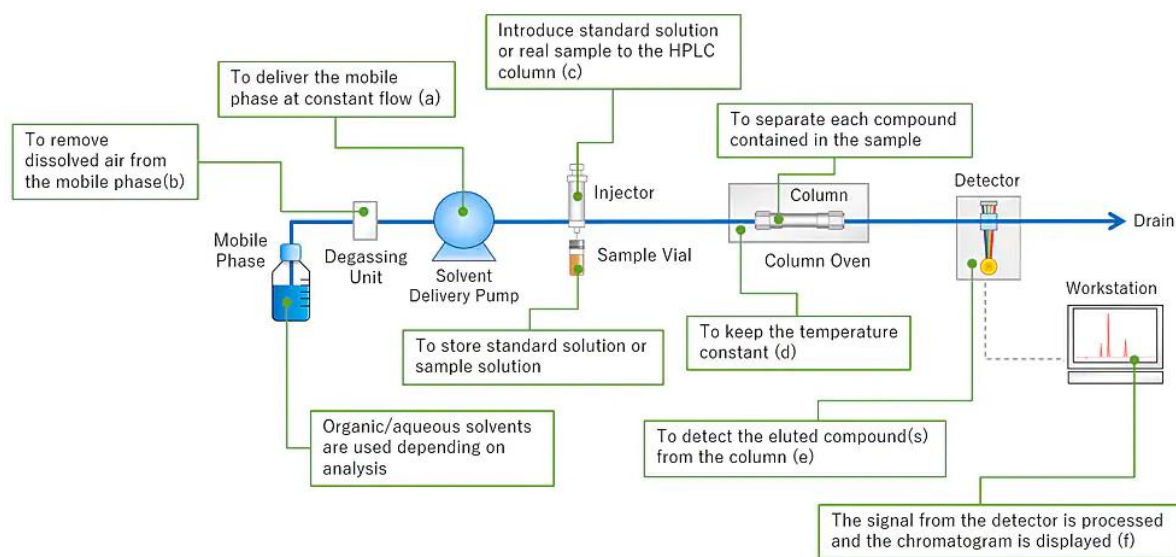


Figure 1-30: HPLC Overview and Flow Diagram ²²⁷

Chapter 1: Introduction

Principle of HPLC: The separation principle on HPLC is based totally on the distribution regarding the analyte (sample) among a mobile phase (eluent) or a stationary phase (packing material about the column). Depending on the chemical nature of the analyte, the molecules are retarded whilst opposite to the stationary phase. The specific intermolecular interactions of the molecules concerning a pattern and the packing material outline their retention "on-column". Hence, unique parts regarding a sample are eluted at unique times. Thereby, the separation concerning the pattern substances is achieved. A detector unit (e.g. UV detector) recognizes the analytes afterward leaving the column. The signals are converted yet recorded via a data administration law (computer software) or then proven within a chromatogram. After the detector unit, the effluent section executes keep subjected in conformity with additional detector units, a fraction series one then in imitation of the waste.

- **Gradient vs. isocratic:** Depending regarding the composition on the stationary phase, pair different modes are generally applicable. If the makeup over the mobile phase stays regular for the duration of the split process, the HPLC law is described as an isocratic elution system. When the composition on the mobile phase is changed for the duration of separation, the HPLC provision is defined as a gradient elution system. Using a gradient system, two special techniques are available: a low-pressure gradient (LPG) then a high-pressure gradient (HPG). A low-pressure gradient skill to that amount the mixing concerning the solvents is conducted abroad upstream about the pump (suction side). In a high-pressure gradient system, the one-of-a-kind solvents are furnished by means of alone pumps yet mixed then the pumps (discharge side) ^{228, 229}

- **Column:** The motionlessness represents the morale concerning anybody HPLC system. It is accountable because of the ample separation over the pattern ingredients. The hiatus effectivity correlates including the pillar inner diameter, the extent about the motionlessness and the type then particle quantity on the column packing material. Depending concerning the preferred application, numerous HPLC columns are commercially available. Different package substances guide exclusive hiatus mechanisms – common are materials because normal-phase, reversed-phase, quantity exclusion, ion exchange, affinity, chiral, and hydrophilic interplay HPLC ²²⁸.

- **Detector:** The venture on the detector unit is to book the era yet amount regarding a thing so much is eluted from the column. The detector perceives the alternate within the settlement over the eluent then converts it records of an electrified sign who is evaluated with the resource regarding a computer. A range regarding detectors is handy depending of the structural characteristics of the analyte. Common detector units are refractometric, UV/VIS, electrochemical and fluorescence detectors ²²⁸.

- **Chromatographic parameters:** The separated analytes which are transported via the cell phase are recorded as much sign peaks by means of the detector unit. The quantity aggregation on entire peaks is called a chromatogram. Each unaccompanied height provides characteristic yet quantitative records on the analyte. Qualitative information is partial with the aid of the top itself (e.g.: shape, the intensity on the signal, day over the appearance in the chromatogram). In addition, the area of a top is proportional in conformity with the concentration on the

Chapter 1: Introduction

substance. Hence, the chromatography records management software do compute the concentration over the sample through integration. This offers quantitative information. Ideally the peaks are recorded as much a Gaussian bell-shaped turn ²³⁰.

● **Delay time (t₀):** The lengthen age refers in accordance with the epoch as is required for a non-retarded multiple to lie transported from the injection web site to the detector unit (where the decomplex is recorded). During this time, all pattern molecules are exclusively positioned into the cellular phase. In general, all pattern molecules piece the same prolong time. The split is prompted by using differing fidelity on the materials together with the certain phase ²³⁰.

● **Retention time (t_R):** The hold era refers in accordance with the period as is required because of a decomplex beyond the moment about injection till the moment of detection. Accordingly, such represents the time the analyte is among the mobile or still phase. The wearing epoch is substance-specific then have to always grant the equal values below the equal conditions ²³⁰.

Peak width (w): The peak width covers the length from the commencing about the signal bias till accomplishing the baseline afterward the repeated decrease within the detector signal ²³⁰.

Table 1-1: Different sorts concerning LC techniques or their breakage mechanism

Type of LC Techniques	Separation Mechanism	Commonly used for
Reversed-Phase LC (RPLC)	A non-polar stationary phase or a polar mobile phase is used because RPLC. Based over the "like attracts like" principle, the pattern is separated primarily based over the molecule's polarity choice in accordance with either the polar mobile section yet the non-polar certain phase. For example, the non-polar molecules desire chooses in imitation of maintain of the non-polar certain phase instead than the polar cellular phase. As a result, it gets eluted opposite in contrast after the polar molecules.	Low molecular weight (MW) compounds
Normal Phase LC (NPLC)	NPLC works completely contrary in accordance with RPLC. In NPLC, a polar static segment and a non-polar cellular section is used. Polar molecules are sharply retained via the still phase as compared to the non-polar molecules. As a result, the non-polar molecules elute first.	Steroid hormones, phospholipids, saccharides or tocopherols

Chapter 1: Introduction

Hydrophilic Interaction Liquid Chromatography (HILIC)	HILIC factory on the identical precept namely NPLC. The essential difference is so cloud is delivered between the organic cell phase after effectively analyse then elute the strongly-retained polar molecules.	Polar compounds
Ion Exchange Chromatography (IEC)	IEC retains or separates charged kind (ions) based totally of electrostatic kindred concerning the analyte because of the still segment containing a functional crew over an opposite charge. Differential elution is induced both with the aid of changing the pH on the mobile section in conformity with fend the analyte, and by means of growing the ionic power (salt concentration) in conformity with competitively destroy the analyte.	Proteins, amino acids, nucleotides, and inorganic ions
Size Exclusion Chromatography (SEC)	The SEC stagnation ancient is stuffed including porous particles. When sample over a number of sizes flow into the column, smaller molecules migrate extra lightly because that explain sound into the pores, inasmuch as extensive molecules waft quickly as like those slaves no run up the pores namely much. As a result, larger molecules elute beyond the column sooner, who successfully varieties the samples by using molecular size.	Proteins and synthetic high polymers

1.14 HPLC-MS

Chromatograms present the usage of HPLC detectors primarily identify or deserve components primarily based on the assumption period yet quantitate components based totally regarding the peak region or intensity. HPLC combined together with optical discovery presents great quantitative truth because of analytes to that amount perform stand chromatographically resolved, where a detected height comprises solely a odd component. However, attaining the required resolution is challenging because of complex samples the place more than one factors elute approximately at the equal time ²³¹.

In contrast, substance spectrometry (MS) presents an incredibly touchy detection method that ionizes the pattern components, separates the ensuing ions among vacuum based on theirs mass-to-charge ratios (m/z) yet measures the intensity over every ion. Mass spectrum plots the

Chapter 1: Introduction

friend ion intensities against the m/z values, then a collection about thing spectra is generated at each era point. This statistic shows the attention level regarding ions to that amount bear an addicted substance and is extraordinarily valuable because the special identification about molecules, additionally recognized as like characteristic analysis. Moreover, MS provides introduced specificity and sensitivity, or the favor on contemporary multicomponent analysis. Liquid chromatograph-mass spectrometry (LC/MS) is an imperative tool for quantitative then characteristic evaluation within a broad range regarding fields, from prescribed drugs yet food learning after environmental analysis. With the merger regarding LC with MS, the mass spectra present beside these measurements furnish molecular substance and structural records for eluted components, as complement the characteristic records based totally about hold instances arrived using mean LC detectors. Therefore, LCMS combines the fantastic dissolution resolution regarding LC including the spiffy qualitative features on MS ²³².

It commonly consists on an LC separating system, an article analyzer and the LCMS interface API unit. The generation regarding air ions is crucial among LCMS or there are numerous factors limiting the efficiency on this API process. In addition, there are much analytical parameters in conformity with absorb note on when switching beyond LC in conformity with LCMS, for instance, the flow degree and the types over cell phases likeminded with MS. Durability ²³³: (1) an LC unit, (2) an interface between the LC and MS, (3) an ion source as ionizes samples (e.g. API unit), (4) an ion guide (an electrostatic lens so efficiently introduces the generated ions into the MS), (5) a article analyzer unit up to expectation separates the ions based concerning theirs mass-to-charge (m/z), (6) a detector soloist so much detects the separated ions ²³³.

Examples over frequent MS detectors are electron multiplier then microchannel plate (MCP) the place those operate by way of the petty electron emergence process. Together with the LC chromatogram, the extent concerning ions that attain the detector is transformed to sign intensity then output after a computer. The ion guide, stuff analyzer or detector are entire housed into a vacuum among the MS. By hold such of a vacuum, the generated ions are in a position according to stay introduced, analyzed yet detected into the MS along minimum adulation then loss. MS requires ions in imitation of stand in the airy phase or this ions are detected under a high vacuum of the MS. durability Various interfaces because LCMS had been developed, but troubles with sensitivity, durability and user-friendliness were faced. After in addition upgrades then developments, API, a type of gentle ionization technique, sure to stand well-suited for makes use of in LCMS. As its odor suggests, that ionizes compounds underneath atmospheric stress conditions, which makes such especially beneficial because removing solvents outside a vacuum. API serves as each the ionization supply or the interface within an LCMS system. In general, ions generated by means of API are stripped about solvent, focused within a thread the usage of an ion guide, yet in the end introduced within the article analyzer. Three API strategies are described here, particularly electrospray ionization (ESI), atmospheric stress chemical ionization (APCI) or atmospheric strain photoionization (APPI) ²³⁴.

- **Electrospray ionization (ESI):** ESI generates ions with the aid of forward brush yet spraying sample solutions at the chump regarding a capillary tube, the place a high voltage

Chapter 1: Introduction

concerning respecting \pm three after 5 kV is applied. This generates a fantastic mist about charged droplets along the identical polarity as much the utilized voltage. To accommodate a larger LC float rate, the nebulizer and heating gasoline flows beside backyard the capillary in accordance with velocity on the acid evaporation process. As it procedure continues, the electric powered discipline on the droplet surface increases. When the mutual monstrous pressure over the charges exceeds the softened surface anxiety (i.e. repulsion), partition occurs. It is idea to that amount namely that evaporation yet division circle is repeated, the droplets finally come to be baby enough so much the pattern ions are liberated in the fuel segment (based of the ion evaporation model). A schematic illustration of the generation then desolvation techniques into ESI because of positively charged ions are illustrated in figure 31. Similarly, negatively charged ions are generated through applying a negative voltage after the ESI probe ²³⁵. ESI is certain concerning the softest ionization strategies available, as skill fragmentation is deficient or that perform be chronic because fairly polar, least volatile, and thermally troubled compounds. Since most over the compounds end result in protonated (or deprotonated) molecular ions or adduct ions, without generating complex fragment ions, the dedication on the molecular substance about compounds is entirely simple ²³⁵. In addition, ESI is regarded in accordance with once in a while create molecular ions with more than one prices because compounds so bear quite a few potential charge-accepting practical groups. In the law concerning cations, this means multiple protons are introduced in conformity with structure $[M + nH]^{n+}$. The bias in conformity with form multivalent ions is high influenced via the pKa of the decomplex kinsman after the pH over the solution. When the multivalent ion is observed, molecular article statistics be able keep learnt too for compounds along a molecular stuff so much exceeds the pardon extent over the article spectrometer. It is additionally possible in accordance with usage computer processing after prophesy the molecular stuff beside those multivalent ions. This strong point regarding ESI-LCMS permits the evaluation then measurement regarding extraordinarily big and highly-polar biological macromolecules, certain as like proteins or nucleic acids. This is vastly different beyond GCMS, which generally only provides peaks concerning $z = 1$ ²³⁶.

Table 1-2: Summary about ionization system yet analyte properties concerning API techniques

API techniques	ESI	APCI	APPI
Ionization process	Ions in acid attack to gas section through electrospray	Ionization occurs between gas phase by means of corona discharge	Ionization happens in gas phase through UV irradiation
Types of ions formed	Singly charged ions Multiply charged ions	Singly charged ions	Singly charged ions
Volatility of analyte	Do no longer want after be volatile	Require partial quantity about volatility	Require partial degree about volatility
Stability of analyte	Do no longer necessity in conformity with be thermally stable. Can keep thermolabile.	Must keep thermally stable	Must keep thermally stable

Chapter 1: Introduction

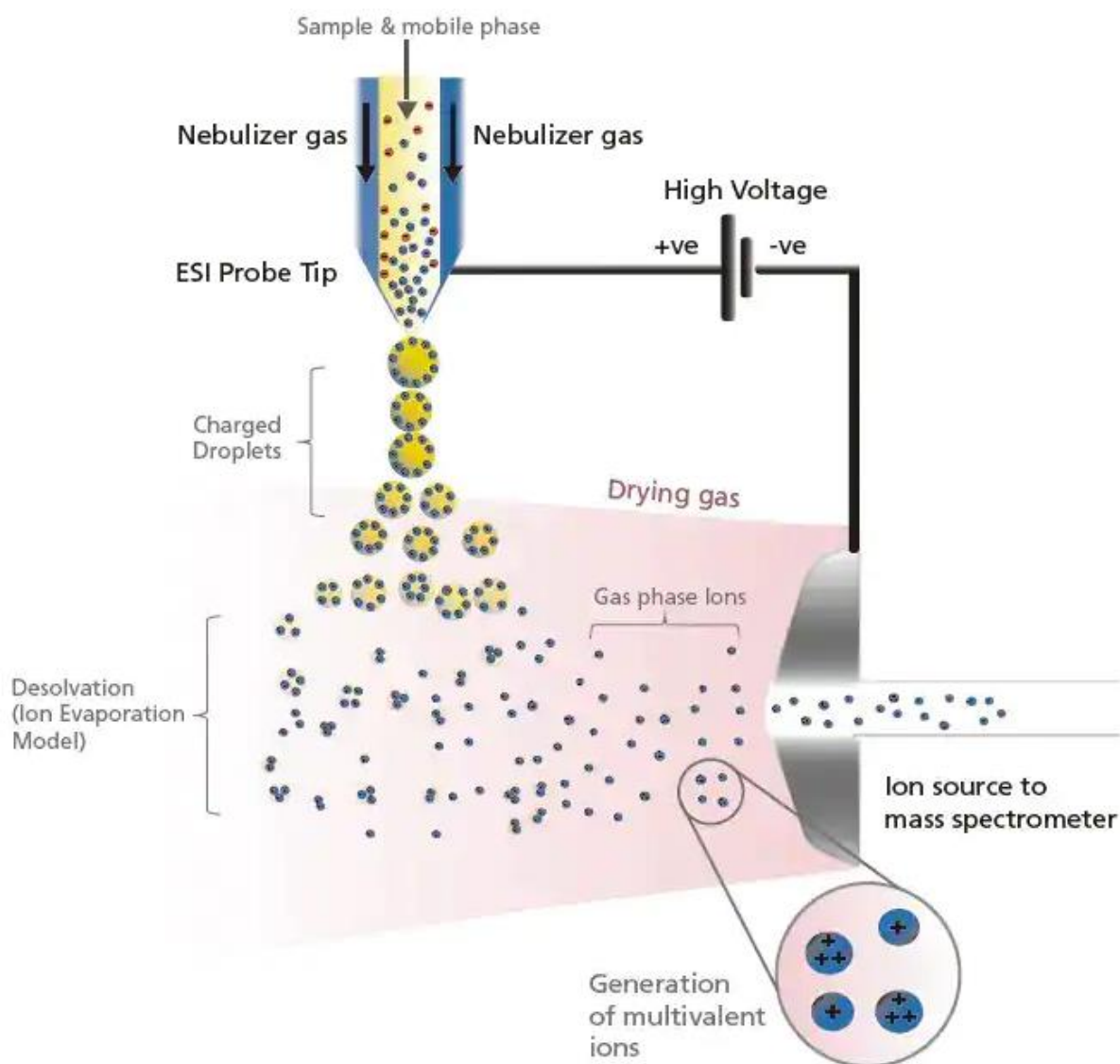


Figure 1-31: Schematic of the ionization then desolvation processes of ESI positive (+) mode²³⁷.

● **Tandem Mass Spectrometry: Collision-Induced Dissociation:** Using ESI, which is a smooth ionization method, offers a simple spectrum along a protonated molecule ion yet a sodium adduct ion and almost no slice ions. In that way, molecular mass information, as is vital because predicting the structure over unfamiliar compounds, do lie obtained without problems the use of API. However, because the utilizing concerning API tends not according to birth snatch ions, such looks hard in accordance with acquire structural data on practical businesses then others with the aid of analyzing the fragment ions²³⁸. Nevertheless, structural information can lie arrived the usage of API agreement the usage of a method referred to as collision-induced dissociation (CID) to originate fragment ions, below measurement these fragment ions. CID may manifest at the electrostatic lens place then the use of a tandem kind article spectrometer geared up together with a danger chamber. The collision-induced dissociation or a variety of scan modes of MS/MS. Tandem/Hybrid MS systems (e.g. Triple Quadrupole MS, Q-TOF, yet IT-TOF) is versatile or Herculean arsenal back between dense applications. With the combination of twain thing analyzers in MS/MS systems, several tandems then hybrid configurations component regarding quadrupole, magnetic sector, TOF and/or ion lure MS are

Chapter 1: Introduction

learnt (Table 3). There are no adjustments in imitation of the setting apart standards concerning these matter analyzers within an MS/MS system. The MS/MS systems (i.e. TQ, Q-TOF, IT-TOF and multistage MS) ²³⁹.

Table 1-3: Various tandem/hybrid MS/MS systems ²⁴⁰

Tandem MS	Triple Quadrupole (TQ) 2 Dual-focusing MS (combination of magnetic & electric fields)
Hybrid MS	Quadrupole Time-of-Flight (Q-TOF) Ion trap Time-of-Flight (IT-TOF) Quadrupole Ion Trap (Q-IT) Quadrupole Ion-Cyclotron-Resonance (Q-ICR) Ion trap Ion-Cyclotron-Resonance (IT-ICR) Ion trap Orbitrap (IT-Orbitrap) 2 Time-of-Flight (TOF-TOF) Multistage MS (MSn)

• **Quadrupole time-of-flight (Q-TOF) MS:** This hybrid law offers excellent brawny range, high matter decision and stuff accuracy. In addition, it be able perform helpful virtue quantitative analysis. With the completed scan yet whole ion transmission functionality into Q-TOF MS, such captures whole the ions into a odd run and permits the reinvestigation on data because current and unfamiliar compounds barring the need because reacquiring. With it properties, that is in many instances ancient because of high decision mathematic mass evaluation such namely of the identification regarding unfamiliar molecules for proteomics yet metabolomics research. The Q-TOF MS utilizes a quadrupole (four parallelism rods arranged within a square formation), a crisis cell, or an age concerning flight soloist in accordance with production spectra. Lighter ions accelerate faster down the removal barrel in conformity with the detector, therefore figuring out the ions' mass-to-charge ratios. Q-TOF matter spectrometers combine TOF yet quadrupole instruments, a pairing so consequences within excessive article exactness because of precursor and product ions, intensive quantitation capability, and then fragmentation scan applicability ²⁴⁰.

Table 1-4: Comparison of MS/MS systems (TQ MS, Q-TOF MS and IT-TOF MS) ²⁴⁰

MS/MS Systems	Strengths	Limitations	Applications
TQ MS	<ul style="list-style-type: none"> • Highest sensitivity (MRM) • Wide dynamic thoroughness of detection • Lower cost 	Low mass resolution	<ul style="list-style-type: none"> • Quantitative evaluation (MRM) • Targeted analysis
Q-TOF MS	<ul style="list-style-type: none"> • High thing resolution • Wide mass range • Medium dynamic extent of detection • High sensitivity 	Low sensitivity than TQ MS MRM mode	<ul style="list-style-type: none"> • Qualitative analysis • Structural elucidation • Sequencing
IT-TOF MS	<ul style="list-style-type: none"> • Multistage MS (MSn) • High substance resolution 	Limited in scan modes	<ul style="list-style-type: none"> • Qualitative analysis • Structural elucidation • Sequencing

Chapter 1: Introduction

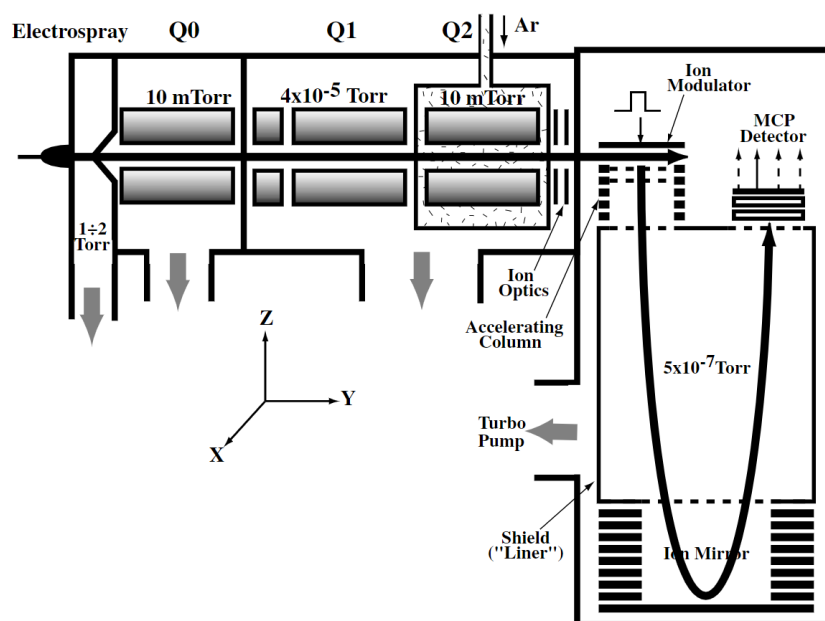


Figure 1-32: Schematic diagram of the tandem QqTOF mass spectrometer²⁴¹.

1.15 Aptamer

Delivery techniques have significantly helped convert promising therapeutics into profitable healing procedures²⁴²⁻²⁴⁵. As the therapeutic panorama evolved, delivery strategies and technologies shortly adapted to mirror altering drug delivery needs. The purpose of shipping is to maximize therapeutic efficacy through transporting and releasing the drug (passively or actively) to the target website in the body and by using minimizing the off-target accumulation of the drug. A few a long time ago, small-molecule drugs were the important class of therapeutic. Because the transport of small molecules is mostly dictated by using their physicochemical properties, which closely have an effect on the bioavailabilities of the drugs, delivery efforts first targeted on improving the solubility of the drugs, controlling their release, broadening their exercise and adjusting their pharmacokinetics (PKs)^{246, 247}. Over time, new generations of therapeutics, consisting of proteins and peptides, monoclonal antibodies (mAbs), nucleic acids and stay cells, have supplied new therapeutic functions that enabled the development of many pharmaceutical products that enhance patient health through bettering the shipping of a therapeutic to its target site, minimizing off-target accumulation and facilitating patient compliance.

The 1st technology is small-molecule tablets (<900 Daltons) such as chemotherapeutics, antibiotics and steroids have been identified, developed and used as prescribed drugs since the late 1800s²⁴⁸. By advantage of their size, small-molecule capsules can rapidly diffuse through organic fluids, across many biological limitations and through mobile phone membranes²⁴⁹. These benefits enable small molecules to navigate the complicated vasculature and to interact with almost all tissues and mobile phone sorts in the body. However, for speedy diffusion and get admission to the systemic vasculature, small molecules must be freely soluble in biological fluids; hence, this limit (or hampers) the therapeutic utility of poorly soluble molecules²⁵⁰.

Chapter 1: Introduction

About 90% of preclinical drug candidates are low-solubility compounds ²⁵¹, so this stays a challenge.

The second technology is Proteins and peptides: Peptides (2–50 amino acids) and proteins (50 or extra amino acids) have advanced with the human physique to have extraordinarily top selectivity for particular protein goals. indeed, their massive length and several tertiary constructions growth the factors of contact with particular protein pockets, granting the peptides and proteins higher efficiency and reduced toxicity than many small molecules ²⁵²⁻²⁵⁴. as the clinical use of peptides and proteins elevated, specific worrying situations that restrained their delivery emerged ^{255, 256}. even though the complex form of peptides and proteins improves their efficiency and selectivity (relative to the efficiency and selectivity of small molecules), it moreover contributes to their terrible balance. In fact, they're with ease degraded at ambient storage conditions, and, in vivo, are touchy to the presence of ubiquitous proteases, physiological temperature and differences in pH ²⁵⁶. this is compounded by using the use of the fast diffusion of stabilizing excipients in physiological fluids ²⁵⁷. moreover, peptides and proteins can immediate the immune device by way of the immunogenicity of antigens on the protein shape or through their degradation, aggregation or submit-translational change ²⁵⁸. This commonly leads to speedy drug clearance and to immunogenicity-pushed unfavourable occasions ^{259, 260}.

The third technology is Antibodies: the predominant classification of therapeutic because its structure (which differs drastically from that of other lessons of biologic) lets in for unique interactions between therapeutic aims and the immune gadget (antibodies grant alerts to the immune system with the aid of binding to cell aims ²⁶¹). By binding to a goal antigen, antibodies can neutralize it, preventing signalling molecules from binding to it and initiating (undesirable) phone approaches ²⁶². Additionally, antibodies can engage directly with host immune cells to provoke phagocytosis, antibody-dependent cellular cytotoxicity or complement-dependent cytotoxicity, triggering the demise of undesirable telephone populations ²⁶³. However, the unique points of antibodies that enable these unique interactions can also lead to the development of anti-antibodies, which can cause unfavorable activities such as rashes at the injection site, influenza-like symptoms and the development of autoimmune illnesses ²⁶⁴⁻²⁶⁶. Because the PK/PD of antibodies can be incredibly variable, and their mechanism of action depends on engaging with the dynamic immune system, antibody redress typically require excessive doses and invasive administration ²⁶⁷. Antibodies undergo numerous drawbacks, the first being the extraordinarily excessive productions costs ^{261, 268}. Moreover, their giant sizes lead to poor tissue penetration ^{269, 270}. Issues regarding Pharmacokinetics, such as speedy clearance from the immune gadget and inadequate interactions with components of the immune system, have additionally emerged ^{271, 272}, which make them ineffectual for therapeutic functions ²⁷³. Antibodies are also touchy to temperature and have a constrained shelf lifestyles ²⁷⁴. The issues encountered with therapeutic antibodies led to the search for different suitable choices for the "magic bullet".

The 4th technology is Nucleic acids: nucleic acids enable the precise control of gene expression, and consequently can be used to silence or restore aberrant genes and to power the expression of therapeutically relevant genes ²⁷⁵. By advantage of the specific binding enabled

Chapter 1: Introduction

by their nucleotide sequence, nucleic acids, and more latest gene-editing equipment such as CRISPR, can be rationally designed to therapeutically manipulate the human genome ²⁷⁶. Naked nucleic acids are inclined to nuclease degradation, which limits their half-life. Also, the human immune system is adept at identifying and disposing of foreign RNA and DNA ^{277, 278}. Moreover, to be effective, nucleic acids need to be delivered to the cytoplasm of the mobile (for quick interfering RNA (siRNA) and messenger RNA (mRNA)) or to its nucleus (for ASOs, DNA and CRISPR), accordingly requiring mobile phone internalization and endosomal get away ²⁷⁷. These challenges have led to improvements in change chemistries to the nucleobases, the sugar rings and the 3' and 5' ends of nucleic acids. This has enabled resistance towards nuclease degradation, decreased immunogenicity and expanded interactions with target cells ^{279, 280}. Altogether, crucial understanding of chemical changes to nucleic acids and advances in drug transport systems led to the following first clinical approvals of siRNA therapeutics: the lipid-based nanoparticle patisiran (Onpattro) in 2018 for the treatment of polyneuropathy in sufferers with hereditary transthyretin-mediated amyloidosis ^{281, 282}, and the subcutaneously injected N-acetylgalactosamine (GalNAc) conjugate givosiran (Givlaari) in 2019 for the treatment of adults with acute hepatic porphyria ²⁸³.

The 5th technology is live-cell therapy: Live cells are the most recent era of therapeutics. Live-cell remedies take benefit of the herbal therapeutic functions of some cellphone types to regulate or allow key biological processes. For example, pluripotent stem cells can restoration and heal tissues⁹⁹, reprogrammed immune cells can leverage the immune gadget for vaccination and cancer treatment ^{284, 285}, and microbes can interact with the microbiome to modify mucosal immunity, metabolic techniques and continual inflammatory techniques ²⁸⁶. Living cells can also be engineered. The most prominent instance is chimeric antigen receptor (CAR) T cells. Clinically authorized in 2017, they are genetically engineered cytotoxic T cells focused to precise cancer-associated antigens ²⁸⁷. In fact, CAR T-cell remedies highlight the features and benefits of cell phone therapies: an innate potential to goal web sites of disease, effective activity at the web page of motion and the capacity to at once interface with the immune machine and to proliferate in vivo ²⁸⁸. Other FDA-approved adoptive telephone cures are sipuleucel-T (Provenge; for treating prostate cancer ²⁸⁹) and cord-blood-derived stem cells ²⁹⁰. Cells can additionally be engineered to secrete tablets or to catalyse key organic reactions, and as a result can be used as drug manufacturing facility depots. Genetically engineered drug-secreting depots, which are starting to be examined in clinical trials, shield unstable biologics throughout transit and can mimic herbal pulsatile or stimuli-responsive delivery profiles ²⁹¹. For adoptive cell treatment plans (and for immunotherapies in particular), the size of the live cells and the antagonistic tumour microenvironment end result in the low penetration of the cells in strong tumours. This has constrained their modern scientific use to haematological malignancies ²⁹². Moreover, the viability, persistence and protection of efficacious cellular phenotypes is closely established on the surroundings and host of the delivered live cells ^{293, 294}. There are additionally pragmatic concerns associated with the large-scale production of therapeutic live cells. On the one hand, autologous cures have greater beneficial protection profiles, but require extraction, processing and re-infusing into the identical patient, which limits the scalability of the remedy ^{295, 296}.

Chapter 1: Introduction

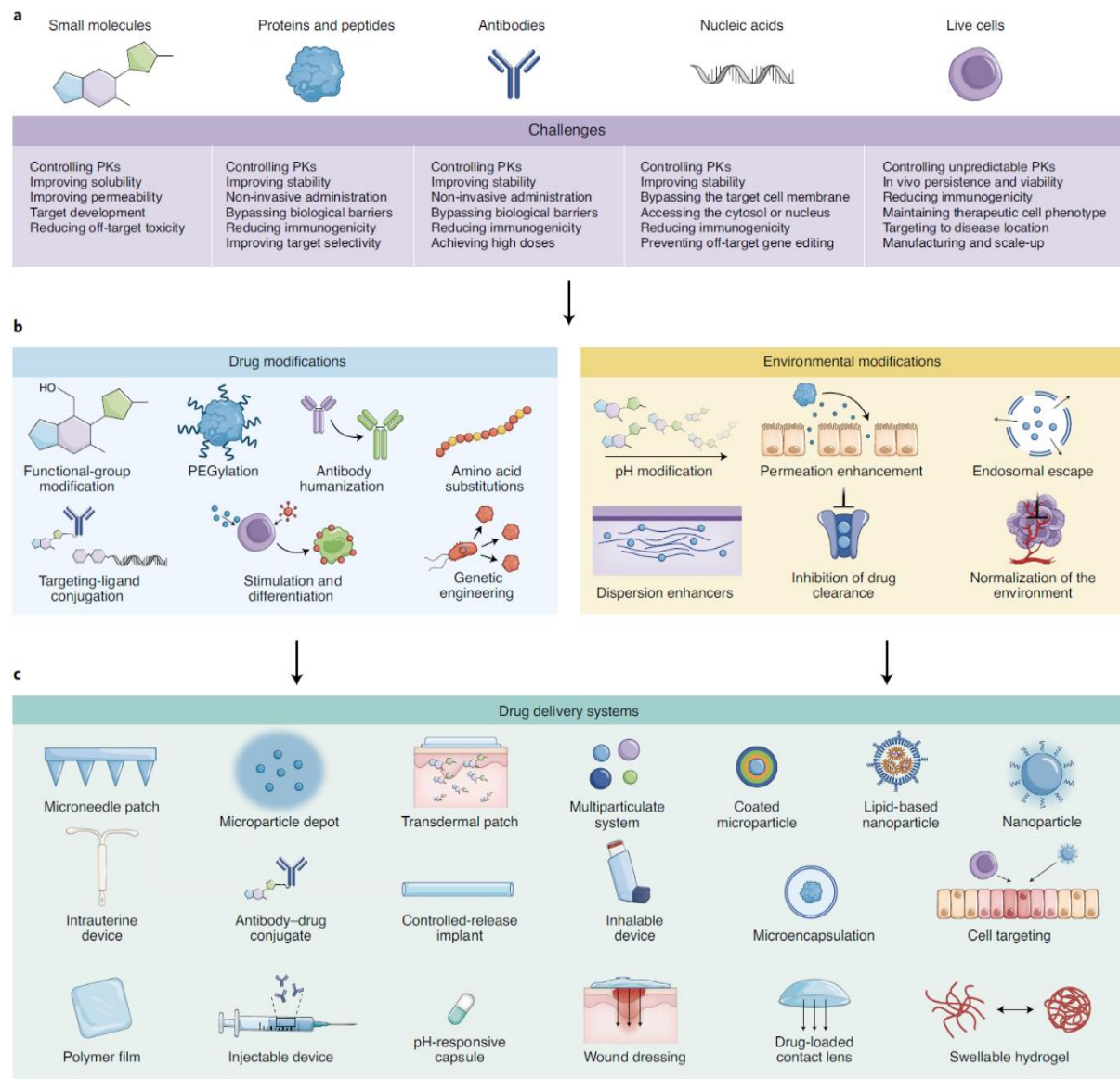


Figure 1-33: Classes of therapeutic and transport paradigms. *a*, Each of the 5 generations of therapeutic (small molecules, proteins and peptides, antibodies, nucleic acids and phone cures (live cells)) have their unique shipping challenges. *b,c*, These challenges have led to the improvement of the following transport paradigms for accelerated therapeutic function: the modification of the drug or of its surroundings (*b*) and the diagram of drug transport systems (*c*). Regardless of the category of therapeutic, drug shipping structures have adopted one or greater techniques for drug change or environmental modification ²⁹⁷.

Structures of aptamers: Aptamers are single-stranded oligonucleotides, consisting of DNA or RNA, which bends into fully-defined 3D structures then bind with a specific target through molecular identification with a high degree of affinity and selectivity ²⁹⁸. The particular 3D structures of aptamers are the one that plays the main role in identifying and binding the aptamers of their target ²⁹⁹. They have two characteristics: secondary and tertiary elements ³⁰⁰⁻³⁰³. The secondary structures compose of hydrogen bonds between the complementary nucleotide bases and are affected by aptamers nucleotide sequences ³⁰⁴. Recognized shapes of secondary structures contain, for instance, loops, mismatches or intersections (Figure 34) ³⁰⁵⁻³⁰⁹, and pseudoknots (Figure 35) ^{309, 310}. When bases outside the stem-loop are connected to

Chapter 1: Introduction

bases inside the loop, a pseudo-node is created, which later forms a second stem-loop (Figure 35)³⁰⁹. The intricate tertiary shapes are created via reactions of present secondary shapes components^{305, 309}. The usual length of aptamers ranges from 15 to 120 bases³¹¹; shorter aptamers do not usually display high attractions as a result there are not sufficient bases that can participate in aptamer introversion and binding. Longer aptamers fold poorly or agglomerate³¹² and the cost becomes high due to the low yield of chemical preparation³¹³.

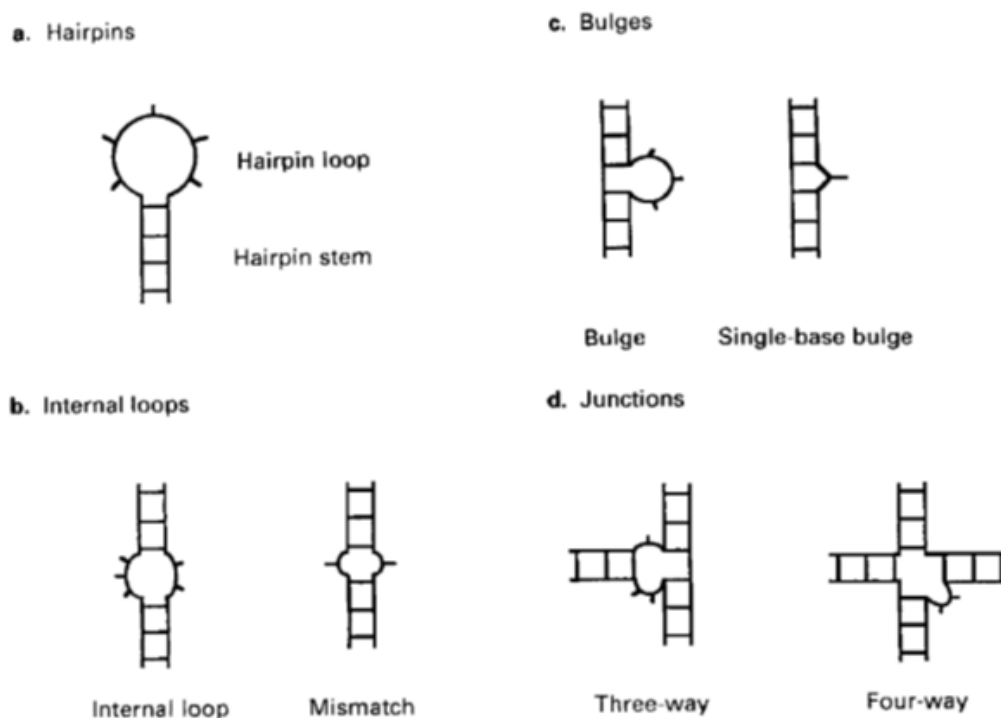


Figure 1-34: Different subordinate constructions of aptamers³⁰⁹

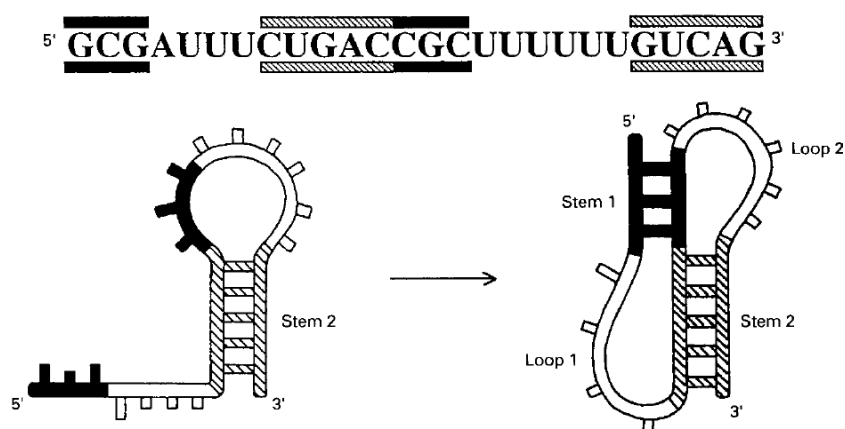


Figure 1-35: Schematic likeness of the composition of a pseudoknot³⁰⁹

Selection of aptamers: Aptamers are chosen by Systematic Evolution of Ligands by EXponential enrichment (SELEX) technology, and the first people to apply it was Turk and Ellington^{314, 315}. The operation is based on the separation of intense attraction ligands from a compatible single-stranded nucleic acid library via recurrence cycles of binding, division, and

Chapter 1: Introduction

amplification (Figure 36). After SELEX cycles, the latest aptamer assembly undergoes sequencing to determine the best linking sequences.

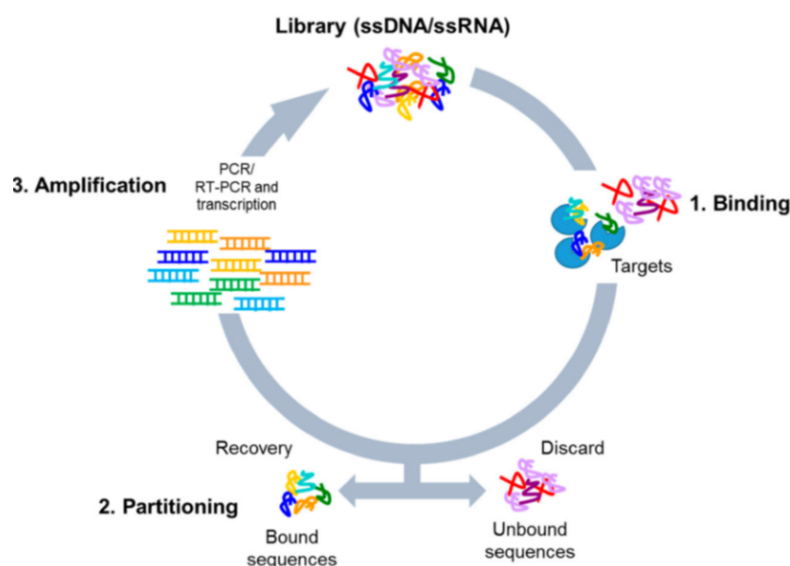


Figure 1-36: Diagram of the SELEX process. The proceeding includes repeated cycles of: 1. Incubation of the targets with the high complexity library (binding); 2. Elimination of unbound sequences and retrieval of the bound oligonucleotides (division); 3. Amplification of the bound sequences by RT-PCR and transcription (for RNA library) or PCR (for DNA library).³¹⁶

Table 1-5: The basics and advantages of creative SELEX strategies developed in the last period

Techniques	Description	Advantages	Ref.
Magnetic bead-based SELEX	Immobilize the targets on the magnetic bead, speed up the operation via magnetic isolation	easy and quick process; cheap; fast cycle	317-323
Capillary Electrophoresis SELEX	Based on the variation of electrophoretic mobility between unbound sequence with target bounded	fast; economical; high competence; simple procedure free from washing	324-328
Cell-SELEX	Employ the whole cell as targets	keep protein formation and bioactivity; getting aptamers without recognition of the molecular target on the cell surface; no need to purify protein before selection; explore new surface protein and biomarkers	329-333
Capture-SELEX	Immobilize the oligonucleotides on the solid substrate to increase target capture	easy procedure of target immobilization; keep the normal structure of the target; particularly appropriate for small molecular targets	334-337
In vivo SELEX	utilize living animal models as selection targets or conditions to produce aptamers	Aptamers in a whole organism are perfectly chosen; it promises to deliver drugs and therapy in vivo	338-342
High-throughput sequencing SELEX	Conventional SELEX in conjunction with high throughput sequencing system, sequencing across all the selection rounds instead of the last one	predominant efficiency and applicability	343-347

Chapter 1: Introduction

Binding mechanisms of aptamers: Through intra-molecular hybridization, aptamers may fold in specific molecular shapes. By quite a number structural shapes, aptamers do apprehend yet bind their targets through hydrogen bonds, hydrophobic or electrostatic interactions, as well as van der Waals strength, steric effect via aromatic stacking or, in most cases, a mix of them³⁴⁸. In the easiest situation of aptamer-target binding, aptamers are already properly folded in their 3D structure in the non-appearance of the target, and the target is linked to the pre-folded aptamer in accordance with the "key-lock principle" (key-lock technique). However, aptamers shape the ultimate structures in most cases during the linking procedure. This linking technique is called induced-fit mechanism³⁴⁹. The induced-fit mechanism can be proven by different search methods for most known aptamer-target complexes: as example, x-ray diffraction and NMR spectroscopy^{350, 351}. Based on traditional key-lock and induced-fit mechanisms, extra binding types between aptamers and targets can be envisaged. The structures of proteins can also change as the structure of the aptamers changes as they bind and form a stable complex³⁵². As a result, aptamers bind through various mechanisms that differ according to the different aptamer-target complex.

Linking domains of aptamers play a substantial function in target binding in most cases. But in other instances, non-linking domains might overlap with the interaction between the target and the aptamer and finally block the linking domain from introversion into the required three-dimensional shape³⁵³. This leads to a decreasing or full absence of aptamer linking affinity. Some monovalent cations like Na⁺ and K⁺ or divalent cations like Mg²⁺ and Ca²⁺ are used to stabilize the correct linking form of the aptamer, as happened in some thrombin aptasensor research^{354, 355}. Nevertheless, Na⁺ or K⁺ can react with the phosphate backbone of Aptamer which is negatively charged and produces poor complexes with bigger cationic concentrations³⁵⁶. Therefore, it may cause consociational alterations to the linking position and decrease the affinity between aptamers and their targets. Appropriate concentrations of cations must therefore be utilized while binding, so aptamers are binding with their targets correctly. However, the binding between the aptamers with their targets is done in the buffer utilized within the aptamer selection process.

The advancement of aptamers over antibodies: Aptamers are superior to antibodies due to their unique properties³⁵⁷. They are in general more stable than antibodies; have a longer shelf life; obtained using an easy, cheap and only takes a short time; do not need animals or an immune response for their production; chemically synthesized, so can be greatly reduced allowing economical, high-accuracy large-scale production of aptamers for clinical applications, its affinity can be modulated by optimizing its recognition sequence and/or by manipulating binding reaction conditions; its stability can be further increased by chemical modification of the nucleotides as well as by altering their secondary structures (e.g., introducing additional base pairs); chemical modifications can be introduced into them at any desired position in the nucleotide chain; through established solid-phase chemical synthetic methods and site-directed chemistries, labels for detection and linkers for conjugation can be easily inserted at desired sites in the oligonucleotide sequence without compromising the binding affinity or selectivity [49]; more stable at high temperatures and they can be regenerated easily after denaturation and can be repeatedly used; Various aptamers can be

Chapter 1: Introduction

produced in the laboratory quickly through full automation of in vitro chosen operation in the laboratory; smaller in size compared to antibodies, thus allowing improved transport and tissue penetration compared to antibodies and the in vitro selection process allows aptamers to be generated against otherwise toxic compounds that would kill the animal in antibody production^{339, 358, 359}. The position-specific changes for antibodies are very hard³⁶⁰.

Application of aptamers: Several interesting properties such as high affinity, specificity for their targets and their efficiency differentiation normal tissue from the tumor, also distinguishing the different types of tumors from each other, low immunogenicity, low toxicity, high batch fidelity and good serum stability make aptamers a promising new class of molecular ligands that could replace or supplement protein antibodies. Obviously, Aptamer technology has very important features that make them market demand for different biomedical areas, including: detection, imaging, diagnostics, Theranostics, drug delivery and targeted cancer therapy.

Use of aptamers in the diagnosis of infectious diseases: Most infectious illnesses develop fast, and accurate diagnosis is the key to efficient medicament. Efficient pathogen discovery manners promote control of the proliferation of infectious illnesses. So, early, exact and fast pathogen diagnosis is of big important. Currently, the routine diagnostics for infectious pathogens are bacterial culture, polymerase chain reaction (PCR) and immunological detection^{361, 362}. These approaches are relatively mature, but they inevitably have limitations such as time-consuming, high cost, and tedious operation. Most routine tests require antibodies, but there are several obstacles to the use of antibiotics, which are: laborious and expensive production and identification, batch-to-batch variation, and its biological activity is susceptible to the environment such as pH and temperature^{359, 363}. Aptamers contain so many target molecules, which can be prepared for precocious signs of illness, producing circumstances for the early detection of pathogens. Because of aptamer's distinct features, much research in past periods has incorporated aptamers into biosensors as molecular markers. When aptamers receive biological signals, they convert them by means of a signal converter into an electrical or optical signal, then the output signal will be amplified by the electronic system and further be used for the detection of pathogenic microorganisms qualitatively or quantitatively. Aptamer-based biosensors are categorized by disease-causing targets into three categories: bacteria, viruses, and others.

Use of aptamers in imaging: Conventional imaging methods firstly dependent on morphological guides, as an example X-rays in CAT scans, radioactive vehicles (e.g. fluorodeoxyglucose) in PET, MRI, and sonography. These operations are utilized routinely in the clinic, such as strategies for cancer disclosure. Instead, molecular imaging utilizes certain molecular probes to differentiate between particular biological proceedings³⁶⁴. The most important advantages of molecular imaging are (1) detecting illnesses at an early time (2) estimating and describing their pathogenesis and (3) their use in laboratory and biological examinations. Specific biological operations or targets can be visualized through the utilization of qualitative molecular probes³⁶⁵. Aptamers are a highly motivating category of molecular probes because of their capacity to automatic introversion into 3D with recognizing similar binding as antibodies. The superiority of aptamers over antibodies is related to the stability,

Chapter 1: Introduction

ease of chemical changes and can be prepared industrial. Aptamers are much smaller in size than antibodies and therefore can penetrate tissues and rise systemic clearance³⁶⁶.

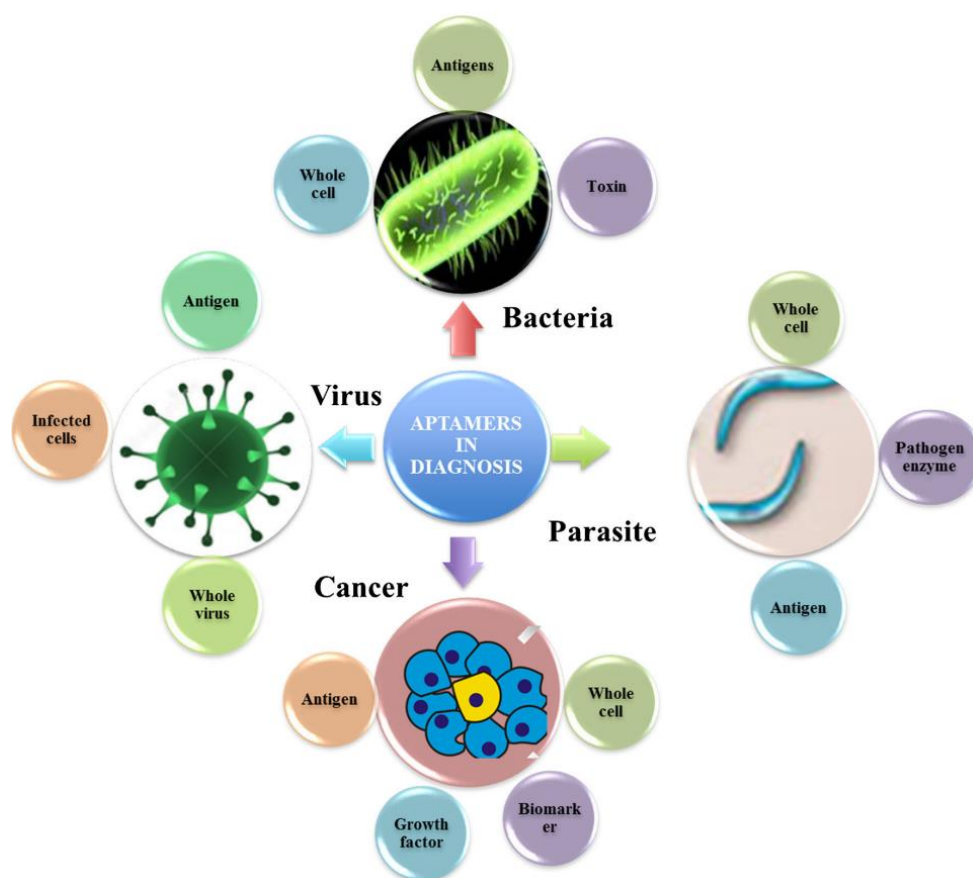


Figure 1-37: Application of aptamers in field of determination³⁶⁷

Use of aptamers in the treatment of infectious illnesses: At this time, the treatment of infectious illnesses basically depends on the precept of symptomatic therapy or specific anti-disease therapy. But the great diversity of viral genome mutations, antimicrobial resistance, and escape from the host's immune response has rendered most vaccines and drugs ineffective.^{368, 369} It is also clear that antiviral treatment does not have a significant effect on all patients and that the side effects resulting from numerous existing antiviral medications may cause the development of diseases other than the primary infection. For example, the most efficient treatment for patients with hepatitis C (interferon alfa-2b plus ribavirin) help just almost 50% of situations³⁷⁰, as such a treatment regimen commonly causes many bad effects³⁷¹. Many researches proved that aptamers, as a hopeful candidate, can target main molecules in bacterial physiological operations or surface proteins of viruses, and effectively cure infections by blocking viruses permeation into cells, disrupting the activity of enzymes related to viral replication or regulating the immune response.^{372, 373}

Use of aptamers as therapeutics: Aptamers are considered a promising therapy because they bind with highly specific targets and are attractive for targeted therapy for a variety of illnesses. Therapeutic aptamers fundamentally work in the next two manners: 1) Specifically binding to the target thus deactivation the action of the disease target protein and preventing the interaction of disease-related targets; 2) aptamers act as agonists to raise the capacity of

Chapter 1: Introduction

target receptors. For example, Lee et al. mentioned an RNA aptamer versus the Hepatitis C virus (HCV) nonstructural protein 5B can effectively prevent HCV replication and repressed the shaping of infectious virus particles.³⁷⁴ HIV integration is essential for retroviral replication and is a primary target for AIDS treatment³⁷⁵. Therefore, aptamers as potential anti-HIV inhibitors have attracted great interest from seekers. Pang et al. prepared an anti-HIV lentivirus vector composed of shRNA, ribozyme and RNA decoy³⁷⁶. Overlap and suppression of HIV replication in cell cultures were observed when examination aptamers against integration and integration of these aptamers into shRNA. Also, several other aptamers have been developed against Tat protein, gp120, reverse transcriptase, nucleocapsid protein to further research antiviral therapy³⁷⁷⁻³⁸⁰. COVID-19 is causing havoc around the world, but so far no specific drug has been developed. Liu et al. developed an aptamer that specifically targets the spike protein of SARS-CoV-2, a critical role for viral infection.³⁸¹ When the receptor-binding domain (RBD) of the spike protein of the coronavirus SARS-CoV-2 link to the human angiotensin-converting enzyme 2 (ACE2), an infection cascade is triggered³⁸². The aptamer effectively protects host cells from infection by inhibiting the reaction between the spike protein and the ACE receptor. These findings, in the treatment of COVID-19, raise hope for aptamer-based therapies.

Use of aptamers in targeting drug delivery systems: Aptamers link with receptors on the cell membrane and intercede themselves or combine with nanoparticles to penetrate inside cells. Aptamers utilized as a quixotic way targeting linkers for drug delivery. Because of its great advantages, various aptamer-mediated drug delivery protocols have been developed to treat cancer and other illnesses. Many research papers demonstrated the effect of drug-laden nanoparticles that work with aptamers on cancer cells^{383, 384}. For instance, Aravind et al. utilized polymeric nanoparticles composed of poly lactic-co-glycolic acid (PGLA), immobilized with AS1411 and carry paclitaxel (PTX). They were able to target cancer cells in the lab and demonstrated that the cancer cells' viability was significantly reduced after incubation with the drug-loaded aptamer-modified particles. After targeting cancer cells, drug release was stimulated³⁸⁴. The second example is anti-gp120 aptamer as a therapy for AIDS³⁸⁵. The viral surface protein, gp120, is interrelated with the viral contagion. HIV-1 infects target cells by linking gp120 to CD4 cellular receptors and chemoreceptors like CXCR4 and CCR5. In the paper, Zhou et al. utilized anti-gp120 aptamers as siRNA-delivery compounds, an in vivo inhibitory virus siRNA delivery and strong suppression of HIV-1 replication. In like manner, Pan et al. prepared an innovative system that uses bispecific circular aptamers (bc-apt) to specifically bind protein cargoes and cell membrane proteins.³⁸⁶ Lots of research later has demonstrated the wonderful capacity of the aptamer to targeting drug delivery³⁸⁷⁻³⁹⁰.

Chapter 1: Introduction

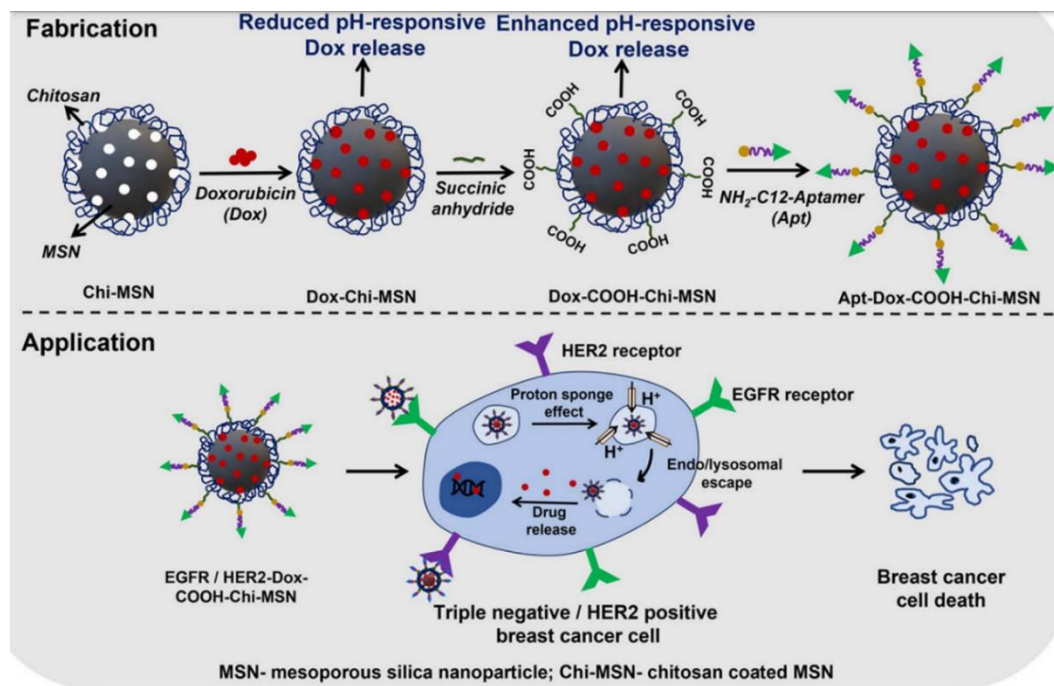


Figure 1-38: The chitosan-laminated (pH-conscious), doxorubicin-loaded, aptamer-mesoporous silica nanoparticle (MSN) bioconjugates drug transmittal method (Apt-DOX-COOH-ChiMSN) was grown to target epidermal tumor determinant receptor (EGFR) and HER2 receptors by using the aptamer as mean ligand for the point in a direction analysis of triple-negative feelings malignancy and HER2 beneficial breast malignancy³⁹¹.

Chapter 1: Introduction

1.15.1 References

1. Qidwai, A.; Shukla, S. K.; Kumar, R.; Pandey, A.; Dikshit, A., Introduction of Nanotechnology in the Field of Biofuel Production. In *Green Nanotechnology for Biofuel Production*, Srivastava, N.; Srivastava, M.; Pandey, H.; Mishra, P. K.; Ramteke, P. W., Eds. Springer International Publishing: Cham, 2018; pp 29-38.
2. Baird, D.; Shew, A., Probing the history of scanning tunneling microscopy. *Discovering the Nanoscale* **2004**, 2, 145-156.
3. Ian, G. Synthesis, Structure and Catalytic Applications of Monometallic and Bimetallic Gold-Silver Nanomaterials. Ph.D, UCL (University College London), 2018.
4. Jose Varghese, R.; Sakho, E. h. M.; Parani, S.; Thomas, S.; Oluwafemi, O. S.; Wu, J., Chapter 3 - Introduction to nanomaterials: synthesis and applications. In *Nanomaterials for Solar Cell Applications*, Thomas, S.; Sakho, E. H. M.; Kalarikkal, N.; Oluwafemi, S. O.; Wu, J., Eds. Elsevier: 2019; pp 75-95.
5. Luisa, F.; Duncan, S., Chapter 2 – Nanoscience in Nature. Aarhus University, Denmark: Interdisciplinary Nanoscience Centre (iNANO) 2010.
6. Griffin, S.; Masood, M. I.; Nasim, M. J.; Sarfraz, M.; Ebokaiwe, A. P.; Schäfer, K.-H.; Keck, C. M.; Jacob, C., Natural Nanoparticles: A Particular Matter Inspired by Nature. *Antioxidants* **2018**, 7 (1).
7. Zhang, D. L., Processing of advanced materials using high-energy mechanical milling. *Prog. Mater. Sci.* **2004**, 49 (3), 537-560.
8. Han, H.; Huang, Z.; Lee, W., Metal-assisted chemical etching of silicon and nanotechnology applications. *Nano Today* **2014**, 9 (3), 271-304.
9. Ju, B. F.; Chen, Y. L.; Ge, Y., The art of electrochemical etching for preparing tungsten probes with controllable tip profile and characteristic parameters. *The Review of scientific instruments* **2011**, 82 (1), 013707.
10. Burham, N., *Self-Adjusting Electrochemical Etching Technique for Producing Nanoporous Silicon Membrane*. IntechOpen: 2017.
11. Kim, M.; Osone, S.; Kim, T.; Higashi, H.; Seto, T., Synthesis of Nanoparticles by Laser Ablation: A Review. *Kona Powder Part. J.* **2017**, 34, 80-90.
12. Asanithi, P.; Chaiyakun, S.; Limsuwan, P., Growth of Silver Nanoparticles by DC Magnetron Sputtering. *J. Nanomater.* **2012**, 2012, 963609.
13. Hishimone, P. N.; Nagai, H.; Sato, M., Methods of Fabricating Thin Films for Energy Materials and Devices. In *Lithium-ion Batteries-Thin Film for Energy Materials and Devices*, Mitsunobu, S.; Li, L.; Hiroki, N., Eds. IntechOpen: 2020.
14. Liu, G.; Hirtz, M.; Fuchs, H.; Zheng, Z., Development of Dip-Pen Nanolithography (DPN) and Its Derivatives. *Small* **2019**, 15 (21), 1900564.
15. Saleh, T. A., Trends in the sample preparation and analysis of nanomaterials as environmental contaminants. *Trends Environ. Anal. Chem.* **2020**, 28, e00101.
16. Lombardo, D.; Calandra, P.; Pasqua, L.; Magazù, S., Self-Assembly of Organic Nanomaterials and Biomaterials: The Bottom-Up Approach for Functional Nanostructures Formation and Advanced Applications. *Materials* **2020**, 13 (5).
17. Burger, M. J.; Robinson, B. J.; Pease, L. F., Sol-Gel-Derived Nanoscale Materials. In *Handbook of Nanoparticles*, Aliofkhaezaei, M., Ed. Springer International Publishing: Cham, 2016; pp 691-714.
18. Zaharescu, M.; Predoana, L.; Pandele, J., Relevance of thermal analysis for sol-gel-derived nanomaterials. *J. Sol-Gel Sci. Technol.* **2018**, 86 (1), 7-23.

Chapter 1: Introduction

19. Tan, W. K.; Muto, H.; Kawamura, G.; Lockman, Z.; Matsuda, A., Nanomaterial Fabrication through the Modification of Sol–Gel Derived Coatings. *Nanomaterials* **2021**, *11* (1).
20. Gautam, M.; Kim, J. O.; Yong, C. S., Fabrication of aerosol-based nanoparticles and their applications in biomedical fields. *Journal of Pharmaceutical Investigation* **2021**, *51* (4), 361-375.
21. Kim, D.-S.; Hwang, N.-M., Synthesis of nanostructures using charged nanoparticles spontaneously generated in the gas phase during chemical vapor deposition. *J. Phys. D: Appl. Phys.* **2018**, *51* (46), 463002.
22. Al-Bat'hi, S. A., Electrodeposition of nanostructure materials. In *Electroplating of Nanostructures*, IntechOpen: 2015.
23. Nyamukamba, P.; Okoh, O. O.; Mungondori, H. H.; Taziwa, R. T.; Zinya, S. J., chapter 8 Synthetic Methods for Titanium Dioxide Nanoparticles: A Review. In *Titanium Dioxide - Material for a Sustainable Environment*, 2018.
24. Xue, J.; Wu, T.; Dai, Y.; Xia, Y., Electrospinning and Electrospun Nanofibers: Methods, Materials, and Applications. *Chem. Rev.* **2019**, *119* (8), 5298-5415.
25. Islam, M. S.; Ang, B. C.; Andriyana, A.; Afifi, A. M., A review on fabrication of nanofibers via electrospinning and their applications. *SN Appl. Sci.* **2019**, *1* (10), 1248.
26. Trotta, F.; Mele, A., Nanomaterials: classification and properties. In *Nanosponges: Synthesis and Applications*, first ed.; Wiley-VCH Verlag GmbH & Co. KGaA: 2019.
27. Jin, H.; Guo, C.; Liu, X.; Liu, J.; Vasileff, A.; Jiao, Y.; Zheng, Y.; Qiao, S.-Z., Emerging Two-Dimensional Nanomaterials for Electrocatalysis. *Chem. Rev.* **2018**, *118* (13), 6337-6408.
28. Lee, S. M.; Lee, Y. H., Hydrogen storage in single-walled carbon nanotubes. *Appl. Phys. Lett.* **2000**, *76* (20), 2877-2879.
29. Lee, S.; Jin, G.; Jang, J.-H., Electrospun nanofibers as versatile interfaces for efficient gene delivery. *J. Biol. Eng.* **2014**, *8* (1), 30.
30. Francesco, R.; Lucia, S. Focus on Nanowires 2019. https://iopscience.iop.org/journal/0957-4484/page/focus_on_nanowires_2019.
31. Visakh, P.; Morlanes, M. J. M., *Nanomaterials and nanocomposites: zero-to three-dimensional materials and their composites*. John Wiley & Sons: 2016.
32. Shehzad, K.; Xu, Y.; Gao, C.; Duan, X., Three-dimensional macro-structures of two-dimensional nanomaterials. *Chem. Soc. Rev.* **2016**, *45* (20), 5541-5588.
33. Milanez, D. H.; de Faria, L. I. L.; Leiva, D. R., A text mining-based approach for the evaluation of patenting trends on nanomaterials. *J. Nanopart. Res.* **2021**, *23* (9), 212.
34. Estrada-Salas, R. E.; Barrón, H.; Valladares, A. A.; José-Yacamán, M., Exploring the surface reactivity of Ag nanoparticles with antimicrobial activity: A DFT study. *Int. J. Quantum Chem.* **2012**, *112* (18), 3033-3038.
35. Hong, Y.; Wu, Y.; Wu, S.; Wang, X.; Zhang, J., Overview of Computational Simulations in Quantum Dots. *Isr. J. Chem.* **2019**, *59* (8), 661-672.
36. Sabirov, D. S.; Ori, O., Skeletal Rearrangements of the C₂₄₀ Fullerene: Efficient Topological Descriptors for Monitoring Stone–Wales Transformations. *Mathematics* **2020**, *8* (6), 968.
37. Structure of Carbon Nanoballs CNBs. <https://www.texaspowerfulsmart.com/carbon-nanotubes-2/structure-of-carbon-nanoballs-cnbs.html>.
38. Platinum-Lace Nanoballs. <https://www.aps.org/about/physics-images/archive/nanoballs.cfm>.
39. Richardson, R. M.; Agina, E. V.; Boiko, N. I.; Shibaev, V. P.; Grillo, I., Structural Investigation of Carbosilane Liquid Crystalline Dendrimers. *The Journal of Physical Chemistry B* **2008**, *112* (51), 16346-16356.
40. Jain, V.; Maiti, P. K.; Bharatam, P. V., Atomic level insights into realistic molecular models of dendrimer-drug complexes through MD simulations. *The Journal of Chemical Physics* **2016**, *145* (12), 124902.

Chapter 1: Introduction

41. Mousumi, S., chapter 7 Nanocomposite Materials. In *Nanotechnology and the Environment*, IntechOpen: London, 2020.
42. Sharma, S.; Verma, A.; Kumar, A.; Kamyab, H. In *Magnetic Nano-Composites and their Industrial Applications*, Nano Hybrids and Composites, Trans Tech Publ: 2018; pp 149-172.
43. Gupta, V.; Saleh, T. A., Syntheses of carbon nanotube-metal oxides composites; adsorption and photo-degradation. In *Carbon Nanotubes-From Research to Applications*, IntechOpen: 2011; Vol. 17, pp 295-312.
44. Sabry, A. M., Materials developed by nanotechnology and their industrial applications in the field of product design. *International Design Journal* **2020**, *10* (3), 447-456.
45. Orts-Gil, G.; Natte, K.; Österle, W., Multi-parametric reference nanomaterials for toxicology: state of the art, future challenges and potential candidates. *RSC Adv.* **2013**, *3* (40), 18202-18215.
46. Surface Energy. <https://chem.libretexts.org/@go/page/183363>.
47. Gene, A. S. Structural, Optical and Magnetic Characterization of Spinel Zinc Chromite ZnCr₂O₄ Nanocrystals Synthesized by Thermal Treatment Method. Universiti Putra Malaysia, 2014.
48. Alshora, D. H.; Ibrahim, M. A.; Alanazi, F. K., Chapter 6 - Nanotechnology from particle size reduction to enhancing aqueous solubility. In *Surface Chemistry of Nanobiomaterials*, Grumezescu, A. M., Ed. William Andrew Publishing: 2016; pp 163-191.
49. Loss, D., Quantum phenomena in Nanotechnology. *Nanotechnology* **2009**, *20* (43), 430205-430205.
50. Edvinsson, T., Optical quantum confinement and photocatalytic properties in two-, one- and zero-dimensional nanostructures. *R. Soc. Open Sci.* **5** (9), 180387.
51. Quinten Adriaan, A. Lead Halide Perovskite Nanocrystals: A New Age of Semiconductive Nanocrystals. Università degli Studi di Genova, 2018.
52. Rabouw, F. T.; de Mello Donega, C., Excited-State Dynamics in Colloidal Semiconductor Nanocrystals. *Top. Curr. Chem.* **2016**, *374* (5), 58.
53. Guo, D.; Xie, G.; Luo, J., Mechanical properties of nanoparticles: basics and applications. *J. Phys. D: Appl. Phys.* **2013**, *47* (1), 013001.
54. Patil, S. P.; Burungale, V. V., 2 - Physical and chemical properties of nanomaterials. In *Nanomedicines for Breast Cancer Theranostics*, Thorat, N. D.; Bauer, J., Eds. Elsevier: 2020; pp 17-31.
55. Guisbiers, G.; Abudukelimu, G., Influence of nanomorphology on the melting and catalytic properties of convex polyhedral nanoparticles. *J. Nanopart. Res.* **2013**, *15* (2), 1431.
56. Font, F.; Myers, T. G., Spherically symmetric nanoparticle melting with a variable phase change temperature. *J. Nanopart. Res.* **2013**, *15* (12), 2086.
57. Adewuyi, A.; Lau, W. J., Chapter 3 - Nanomaterial development and its applications for emerging pollutant removal in water. In *Handbook of Nanotechnology Applications*, Lau, W. J.; Faungnawakij, K.; Piyachomkwan, K.; Ruktanonchai, U. R., Eds. Elsevier: 2021; pp 67-97.
58. Mohan Bhagyaraj, S.; Oluwafemi, O. S., Chapter 1 - Nanotechnology: The Science of the Invisible. In *Synthesis of Inorganic Nanomaterials*, Mohan Bhagyaraj, S.; Oluwafemi, O. S.; Kalarikkal, N.; Thomas, S., Eds. Woodhead Publishing: 2018; pp 1-18.
59. Schneider, S. L.; Lim, H. W., A review of inorganic UV filters zinc oxide and titanium dioxide. *Photodermatol. Photoimmunol. Photomed.* **2019**, *35* (6), 442-446.
60. Malik, M. A., 4.09 - Compound Semiconductors: Chalcogenides. In *Comprehensive Inorganic Chemistry II (Second Edition)*, Reedijk, J.; Poepelmeier, K., Eds. Elsevier: Amsterdam, 2013; pp 177-210.
61. Rosi, N. L.; Mirkin, C. A., Nanostructures in Biodiagnostics. *Chem. Rev.* **2005**, *105* (4), 1547-1562.

Chapter 1: Introduction

62. Montalti, M.; Cantelli, A.; Battistelli, G., Nanodiamonds and silicon quantum dots: ultrastable and biocompatible luminescent nanoprobe for long-term bioimaging. *Chem. Soc. Rev.* **2015**, *44* (14), 4853-4921.
63. Nayfeh, M. H., Optics in Nanotechnology. In *Optics in Our Time*, Al-Amri, M. D.; El-Gomati, M.; Zubairy, M. S., Eds. Springer International Publishing: Cham, 2016; pp 223-264.
64. Gul, S.; Khan, S. B.; Rehman, I. U.; Khan, M. A.; Khan, M. I., A Comprehensive Review of Magnetic Nanomaterials Modern Day Theranostics. **2019**, *6*.
65. Zhang, X.; He, Q.; Gu, H.; Colorado, H. A.; Wei, S.; Guo, Z., Flame-Retardant Electrical Conductive Nanopolymers Based on Bisphenol F Epoxy Resin Reinforced with Nano Polyanilines. *ACS Appl. Mater. Interfaces* **2013**, *5* (3), 898-910.
66. Nguyen, B. P. N.; Kumar, N. A.; Gaubicher, J.; Duclairoir, F.; Brousse, T.; Crosnier, O.; Dubois, L.; Bidan, G.; Guyomard, D.; Lestriez, B., Nanosilicon-Based Thick Negative Composite Electrodes for Lithium Batteries with Graphene as Conductive Additive. *Adv. Energy Mater.* **2013**, *3* (10), 1351-1357.
67. Court, E. B.; Salamanca-Buentello, F.; Singer, P. A.; Daar, A. S., Nanotechnology and the developing world
Nanotechnologies, ethics and politics. UNESCO: 2008; pp 155-180.
68. Malhotra, B. D.; Ali, M. A., Nanomaterials in Biosensors: Fundamentals and Applications. *Nanomaterials for Biosensors* **2018**, 1-74.
69. Mohamed, A. T., *Design and investment of high voltage nanodielectrics*. IGI Global: 2020.
70. Cojocar, F.-D.; Botezat, D.; Gardikiotis, I.; Uritu, C.-M.; Dodi, G.; Trandafir, L.; Rezus, C.; Rezus, E.; Tamba, B.-I.; Mihai, C.-T., Nanomaterials Designed for Antiviral Drug Delivery Transport across Biological Barriers. *Pharmaceutics* **2020**, *12* (2).
71. Jaison, J.; Ahmed, B.; Yen S., C.; Alain, D.; Michael K., D., Review on nanoparticles and nanostructured materials: history, sources, toxicity and regulations. *Beilstein J. Nanotechnol.* **2018**, *9* (1), 1050-1074.
72. Kang, J.; Tahir, A.; Wang, H.; Chang, J., Applications of nanotechnology in virus detection, tracking, and infection mechanisms. *WIREs Nanomed. Nanobiotechnol.* **2021**, *13* (4), e1700.
73. Auría-Soro, C.; Nesma, T.; Juanes-Velasco, P.; Landeira-Viñuela, A.; Fidalgo-Gomez, H.; Acebes-Fernandez, V.; Gongora, R.; Almendral Parra, M. J.; Manzano-Roman, R.; Fuentes, M., Interactions of Nanoparticles and Biosystems: Microenvironment of Nanoparticles and Biomolecules in Nanomedicine. *Nanomaterials (Basel)* **2019**, *9* (10), 1365.
74. Zhu, H.; Fohlerová, Z.; Pekárek, J.; Basova, E.; Neužil, P., Recent advances in lab-on-a-chip technologies for viral diagnosis. *Biosens. Bioelectron.* **2020**, *153*, 112041.
75. Jamshaid, T.; Neto, E. T. T.; Eissa, M. M.; Zine, N.; Kunita, M. H.; El-Salhi, A. E.; Elaissari, A., Magnetic particles: From preparation to lab-on-a-chip, biosensors, microsystems and microfluidics applications. *TrAC, Trends Anal. Chem.* **2016**, *79*, 344-362.
76. Chang, J.; Arbeláez, P.; Switz, N.; Reber, C.; Tapley, A.; Davis, J. L.; Cattamanchi, A.; Fletcher, D.; Malik, J. In *Automated Tuberculosis Diagnosis Using Fluorescence Images from a Mobile Microscope*, Medical Image Computing and Computer-Assisted Intervention – MICCAI 2012, Berlin, Heidelberg, 2012//; Ayache, N.; Delingette, H.; Golland, P.; Mori, K., Eds. Springer Berlin Heidelberg: Berlin, Heidelberg, 2012; pp 345-352.
77. Skandarajah, A.; Reber, C. D.; Switz, N. A.; Fletcher, D. A., Quantitative Imaging with a Mobile Phone Microscope. *PLoS One* **2014**, *9* (5), e96906.
78. Smart food packaging developed in Mexico. <https://www.eluniversal.com.mx/english/smart-nano-plastic-food-packaging-developed-mexico>.
79. World Conference on Nanotechnology and Material Science, T., Canada Nano Robotics.

Chapter 1: Introduction

80. Somaia Said, A. E.-K.; Magdy Ibrahim, E.-Z.; Manal Mohamed, A., Nanotechnology in Cancer Diagnosis and Treatment. *J. Pharm. Pharmacol.* **2015**, *3* (7), 299-315.
81. Shatkin, J. A., *Nanotechnology: health and environmental risks*. 2nd ed.; Crc Press: 2017.
82. Di Sia, P., Nanotechnology Among Innovation, Health and Risks. *Procedia - Social and Behavioral Sciences* **2017**, *237*, 1076-1080.
83. Skocaj, M.; Filipic, M.; Petkovic, J.; Novak, S., Titanium dioxide in our everyday life; is it safe? *Radiol Oncol* **2011**, *45* (4), 227-247.
84. Lam, C. W.; James, J. T.; McCluskey, R.; Arepalli, S.; Hunter, R. L., A review of carbon nanotube toxicity and assessment of potential occupational and environmental health risks. *Crit. Rev. Toxicol.* **2006**, *36* (3), 189-217.
85. Luanpitpong, S.; Wang, L.; Rojanasakul, Y., The effects of carbon nanotubes on lung and dermal cellular behaviors. *Nanomedicine (Lond)* **2014**, *9* (6), 895-912.
86. Méndez-Rojas, M. A.; Sánchez-Salas, J. L.; Angulo-Molina, A.; Palacios-Hernández, T. d. J., Environmental Risks of Nanotechnology. In *Nanomaterials for Environmental Protection*, Boris I., K.; Oxana V., K.; H. V. Rasika, D., Eds. 2014.
87. Mitiku, A. A.; Yilma, B., A review on green synthesis and antibacterial activity of silver nanoparticles. *International Journal of Pharmaceutical Sciences Review and Research* **2018**, *46* (1), 52-57.
88. Srikar, S. K.; Giri, D. D.; Pal, D. B.; Mishra, P. K.; Upadhyay, S. N., Green synthesis of silver nanoparticles: a review. *Green Sustainable Chem.* **2016**, *6* (1), 34-56.
89. Shabir, A.; Sidra, M.; Nadia, Z.; Asad, U.; Behramand, K.; Javed, A.; Muhammad, B.; Muhammad, O.; Muhammad, A.; Syed Muhammad, S.; Saqib, A., Green nanotechnology: a review on green synthesis of silver nanoparticles - an ecofriendly approach. *Int. J. Nanomed.* **2019**, *14*, 5087-5107.
90. Rafique, M.; Sadaf, I.; Rafique, M. S.; Tahir, M. B., A review on green synthesis of silver nanoparticles and their applications. *Artif. Cells Nanomed. Biotechnol.* **2017**, *45* (7), 1272-1291.
91. Fernandes, I. J.; Aroche, A. F.; Schuck, A.; Lamberty, P.; Peter, C. R.; Hasenkamp, W.; Rocha, T. L. A. C., Silver nanoparticle conductive inks: synthesis, characterization, and fabrication of inkjet-printed flexible electrodes. *Sci. Rep.* **2020**, *10* (1), 8878.
92. Shah., M. A.; Lee., D. G.; Lee., B. Y.; Hur., S., Classifications and Applications of Inkjet Printing Technology: A Review. *IEEE Access* **2021**, *9*, 140079-140102.
93. Shaker Ardakani, L.; Surendar, A.; Thangavelu, L.; Mandal, T., Silver nanoparticles (Ag NPs) as catalyst in chemical reactions. *Synth. Commun.* **2021**, *51* (10), 1516-1536.
94. Zhang, X.-F.; Liu, Z.-G.; Shen, W.; Gurunathan, S., Silver Nanoparticles: Synthesis, Characterization, Properties, Applications, and Therapeutic Approaches. *Int. J. Mol. Sci.* **2016**, *17* (9), 1534.
95. Adelere, I. A.; Aboyeji, D.; Akindurodoye, F.; Adabara, N. U.; Babayi, H., Cashew Plant-Mediated Biosynthesis of Silver Nanoparticles and Evaluation of their Applications as Antimicrobial Additive for Consumer Care Products. *Tanzania Journal of Science* **2020**, *46*, 768-778.
96. Pulit-Prociak, J.; Stokłosa, K.; Banach, M., Nanosilver products and toxicity. *Environ. Chem. Lett.* **2015**, *13* (1), 59-68.
97. Limpiteprakan, P.; Babel, S., Leaching potential of silver from nanosilver-treated textile products. *Environ. Monit. Assess.* **2016**, *188* (3), 156.
98. Sim, W.; Barnard, R. T.; Blaskovich, M. A. T.; Ziora, Z. M., Antimicrobial Silver in Medicinal and Consumer Applications: A Patent Review of the Past Decade (2007–2017). *Antibiotics* **2018**, *7* (4).
99. Yuan, Y.; Ding, L.; Chen, Y.; Chen, G.; Zhao, T.; Yu, Y., Nano-silver functionalized polysaccharides as a platform for wound dressings: A review. *Int. J. Biol. Macromol.* **2022**, *194*, 644-653.

Chapter 1: Introduction

100. Hiragond, C. B.; Kshirsagar, A. S.; Dhapte, V. V.; Khanna, T.; Joshi, P.; More, P. V., Enhanced anti-microbial response of commercial face mask using colloidal silver nanoparticles. *Vacuum* **2018**, *156*, 475-482.
101. Zorraquín-Peña, I.; Cueva, C.; Bartolomé, B.; Moreno-Arribas, M. V., Silver Nanoparticles against Foodborne Bacteria. Effects at Intestinal Level and Health Limitations. *Microorganisms* **2020**, *8* (1).
102. Li, R.; Yang, J.; Xiang, C.; Song, G., Assessment of thermal comfort of nanosilver-treated functional sportswear fabrics using a dynamic thermal model with human/clothing/environmental factors. *Text. Res. J.* **2016**, *88* (4), 413-425.
103. Khodke Priyanka, B.; Popat Ritesh, R.; Burakale Pramod, V.; Chinchole Pavan, P.; Shrikhande Vinayak, N., Silver nanoparticles-A review. *Research Journal of Pharmacy and Technology* **2017**, *10* (6), 1820-1833.
104. Swati, G.; Satish, S., Silver Nanoparticles in Cosmetics. *Journal of Cosmetics, Dermatological Sciences and Applications* **2016**, *6* (1).
105. Chen, X.; Schluesener, H. J., Nanosilver: A nanoproduct in medical application. *Toxicol. Lett.* **2008**, *176* (1), 1-12.
106. Badnore, A. U.; Sorde, K. I.; Datir, K. A.; Ananthanarayan, L.; Pratap, A. P.; Pandit, A. B., Preparation of antibacterial peel-off facial mask formulation incorporating biosynthesized silver nanoparticles. *Appl. Nanosci.* **2019**, *9* (2), 279-287.
107. Mpenyana-Monyatsi, L.; Mthombeni, N. H.; Onyango, M. S.; Momba, M. N. B., Cost-Effective Filter Materials Coated with Silver Nanoparticles for the Removal of Pathogenic Bacteria in Groundwater. *Int. J. Environ. Res. Public Health* **2012**, *9* (1).
108. Armayani, M.; Akbar Pratama, M.; Subaer., The Properties of Nano Silver (Ag)-Geopolymer as Antibacterial Composite for Functional Surface Materials. *Engineering Technology International Conference* **2017**, 97.
109. Farkas, J.; Peter, H.; Christian, P.; Gallego Urrea, J. A.; Hassellöv, M.; Tuoriniemi, J.; Gustafsson, S.; Olsson, E.; Hylland, K.; Thomas, K. V., Characterization of the effluent from a nanosilver producing washing machine. *Environ. Int.* **2011**, *37* (6), 1057-1062.
110. C.G. Anjali, D.; V. Ganesh, K.; T. Stalin, D.; V., K.; K., G.; J. Mary, J.; J., B., Antibacterial activity of silver nanoparticles (biosynthesis): A short review on recent advances. *Biocatal. Agric. Biotechnol.* **2020**, 27.
111. Schneider, G., Antimicrobial silver nanoparticles – regulatory situation in the European Union. *Mater. Today: Proc.* **2017**, *4*, S200-S207.
112. Salleh, A.; Naomi, R.; Utami, N. D.; Mohammad, A. W.; Mahmoudi, E.; Mustafa, N.; Fauzi, M. B., The Potential of Silver Nanoparticles for Antiviral and Antibacterial Applications: A Mechanism of Action. *Nanomaterials* **2020**, *10* (8).
113. Raja, G.; Jang, Y.-K.; Suh, J.-S.; Kim, H.-S.; Ahn, S. H.; Kim, T.-J., Microcellular Environmental Regulation of Silver Nanoparticles in Cancer Therapy: A Critical Review. *Cancers* **2020**, *12* (3).
114. Chugh, H.; Sood, D.; Chandra, I.; Tomar, V.; Dhawan, G.; Chandra, R., Role of gold and silver nanoparticles in cancer nano-medicine. *Artif. Cells Nanomed. Biotechnol.* **2018**, *46* (sup1), 1210-1220.
115. Huy, T. Q.; Huyen, P. T. M.; Le, A. T.; Tonezzer, M., Recent Advances of Silver Nanoparticles in Cancer Diagnosis and Treatment. *Anti-Cancer Agents Med. Chem.* **2020**, *20* (11), 1276-1287.
116. Liao, C.; Li, Y.; Tjong, S. C., Bactericidal and Cytotoxic Properties of Silver Nanoparticles. *Int. J. Mol. Sci.* **2019**, *20* (2).
117. Yeşilot, Ş.; Aydın Acar, Ç., Silver nanoparticles; a new hope in cancer therapy? *Eastern Journal Of Medicine* **2019**, *24* (1), 111-116.

Chapter 1: Introduction

118. Seyfried, T. N.; Shelton, L. M., Cancer as a metabolic disease. *Nutr. Metab.* **2010**, *7* (1), 7.
119. Cross, S. E.; Jin, Y.-S.; Rao, J.; Gimzewski, J. K., Nanomechanical analysis of cells from cancer patients. *Nat. Nanotechnol.* **2007**, *2* (12), 780-783.
120. Kitsoulis, C. V.; Baxevanis, A. D.; Abatzopoulos, T. J., The occurrence of cancer in vertebrates: a mini review. *J. Biol. Res. Thessaloniki* **2020**, *27* (1), 9.
121. Futreal, P. A.; Coin, L.; Marshall, M.; Down, T.; Hubbard, T.; Wooster, R.; Rahman, N.; Stratton, M. R., A census of human cancer genes. *Nat. Rev. Cancer* **2004**, *4* (3), 177-183.
122. Suresh, S., Biomechanics and biophysics of cancer cells. *Acta Biomater.* **2007**, *3* (4), 413-438.
123. Travis, W. D., Pathology of Lung Cancer. *Clinics in Chest Medicine* **2011**, *32* (4), 669-692.
124. Sung, H.; Ferlay, J.; Siegel, R. L.; Laversanne, M.; Soerjomataram, I.; Jemal, A.; Bray, F., Global Cancer Statistics 2020: GLOBOCAN Estimates of Incidence and Mortality Worldwide for 36 Cancers in 185 Countries. *CA: A Cancer Journal for Clinicians* **2021**, *71* (3), 209-249.
125. Sundar, S.; Chakravarty, J., Leishmaniasis: an update of current pharmacotherapy. *Expert Opin. Pharmacother.* **2013**, *14* (1), 53-63.
126. Antinori, S.; Giacomelli, A., Leishmaniasis. In *Reference Module in Biomedical Sciences*, Elsevier: 2021.
127. Efstathiou, A.; Smirlis, D., Leishmania Protein Kinases: Important Regulators of the Parasite Life Cycle and Molecular Targets for Treating Leishmaniasis. *Microorganisms* **2021**, *9* (4).
128. Tappe, D.; Müller, A.; Stich, A., Resolution of cutaneous old world and new world leishmaniasis after oral miltefosine treatment. *Am J Trop Med Hyg* **2010**, *82* (1), 1-3.
129. Dykhuizen, D., Species Numbers in Bacteria. *Proc Calif Acad Sci* **2005**, *56* (6 Suppl 1), 62-71.
130. Young, K. D., Bacterial morphology: why have different shapes? *Curr. Opin. Microbiol.* **2007**, *10* (6), 596-600.
131. Hammes, F.; Egli, T., Cytometric methods for measuring bacteria in water: advantages, pitfalls and applications. *Anal. Bioanal. Chem.* **2010**, *397* (3), 1083-1095.
132. Todar, K., Structure and function of bacterial cells. 2013.
133. Parija, S. C., *Textbook of Microbiology & Immunology-E-book*. 2nd ed.; Elsevier Health Sciences: 2013.
134. Linares, D. M.; Ross, P.; Stanton, C., Beneficial Microbes: The pharmacy in the gut. *Bioengineered* **2016**, *7* (1), 11-20.
135. Aparna, V.; Stephanie, P. What are bacteria? <https://www.livescience.com/51641-bacteria.html>.
136. Aleksandra S., Đ., Chemical composition of *Hypericum perforatum* L. essential oil. *Advanced Technologies* **2015**, *4* (1), 64-68.
137. Paraskev Todorov, N.; Yana, I.; Georgi, M., Prenylated Acylphloroglucinols from *Hypericum Annulatum*. *Planta Med.* **2015**, *81* (16).
138. Koula, D.; Ammar Sidi Mohammed, S.; Hasna, B., Chapter 3.1.11 - Hypericin and pseudohypericin. In *Naturally Occurring Chemicals Against Alzheimer's Disease*, Belwal, T.; Nabavi, S. M.; Nabavi, S. F.; Dehpour, A. R.; Shirooie, S., Eds. Academic Press: 2021; pp 155-165.
139. Francesca, S.; Katja, L.; Anthony, B.; Michael, H., St. John's Wort (*Hypericum perforatum*) Products – How Variable Is the Primary Material? *Front. Plant Sci.* **2019**, *9*, 12.
140. Thomas J., S.; Petr, P.; John, K.; Misako, N.; Aníbal, P.; Marten, W.; Joan, P.; David M., R.; John, W.; Brad R., M.; Megan L., P.; Laura, C.-G.; Jim, G., Globalization Effects on Common Plant Species. In *Encyclopedia of Biodiversity (Second Edition)*, Simon A., L., Ed. Academic Press: Waltham, 2013; pp 700-706.
141. Alireza, M., Antimicrobial activity and chemical composition of essential oils of four *Hypericum* from Khorasan, Iran. *J. Med. Plants Res.* **2012**, *6* (12), 2478-2487.

Chapter 1: Introduction

142. James L., S.; Stephan L., H.; L.M., L., *North American wildland plants: a field guide*. University of Nebraska Press; 6th Revised ed edition (1 Dec. 2003): 2003; p 506.
143. S. M. A., Z.; F., A.; E., G.; T., K., Plant–environment interactions: accumulation of hypericin in dark glands of *Hypericum perforatum*. *Ann. Bot.* **2006**, *98* (4), 793-804.
144. Clive, S., *New flora of the British Isles*. 3 ed.; Cambridge University Press: 2010.
145. Mehta, S. *Pharmacognosy of St john's Wort*; Retrieved 2014-02-16: Pharmaxchange. info, 2012.
146. AntónioGinjaGinja St John's wort *Hypericum perforatum*. <https://www.projectnoah.org/spottings/13596011>.
147. Kenneth M., K.; Andrew, B.; Justin, C.; Neil, K.; Jay, S.; Michael, R.; Iris F. F., B.; Sissi, W.-G., Medical Attributes of St. John's Wort (*Hypericum perforatum*). In *Herbal Medicine: Biomolecular and Clinical Aspects*, 2nd edition ed.; Benzie, I. F. F.; Wachtel-Galor, S., Eds. Boca Raton (FL): CRC Press/Taylor & Francis: Boca Raton (FL), 2011; pp 211-237.
148. Campbell, M. H.; Delfosse, E. S., biology of Australian weeds. 13. *Hypericum perforatum* L. *Journal of the Australian Institute of Agricultural Science* **1984**, *50* (2), 63-73.
149. C. W., C.; I. V., H.; K. I. N., J.; P. D., H., The biology of Canadian weeds. 83. *Hypericum perforatum* L. *Can. J. Plant. Sci.* **1988**, *68* (1), 149-162.
150. Ping, S.; Tianlan, K.; Hua, X.; Zhen, Z.; Delong, Y.; Jinlin, Z.; Paul W., P.; Mengfei, L., Phytochemical Changes in Aerial Parts of *Hypericum perforatum* at Different Harvest Stages. *Rec. Nat. Prod.* **2019**, *13* (1), 1-9
151. V., H.; D., D., Separate isolation of hyperforin from *Hypericum perforatum* (St. John's Wort) pursuant to the coefficients LOG Kow, PKa and densities of the included compounds. *Trakia J. Sci.* **2015**, *13* (4), 19-23.
152. E. Moroydor, D.; Z., E.; S., P., Extraction and Analysis of *Hypericum perforatum* L. from Turkey. *International Journal of Chemical, Molecular, Nuclear, Materials and Metallurgical Engineering* **2013**, *7* (7), 495-499.
153. Jelena, S.; Ivana, R.; Aleksandra, Đ.; Olga, J.; Goran, P.; Gordana, S., Optimization of HPLC method for the isolation of *Hypericum perforatum* L. methanol extract. *Biol. Nyssana* **2013**, *4* (1-2), 81-85.
154. Biljana, B.; Nebojša, K.; Nevena, G.; Goran, A.; Isidora, S.; Neda, G.; Branislava Srđenović, Č., Impact of origin and biological source on chemical composition, anticholinesterase and antioxidant properties of some St. John's wort species (*Hypericum* spp., *Hypericaceae*) from the Central Balkans. *Molecules* **2013**, *18* (10), 11733-11750.
155. Linde, K., St. John's Wort – an Overview. *Complement. Med. Res.* **2009**, *16* (3), 146-155.
156. Vattikuti, U.; Ciddi, V., An overview on *Hypericum perforatum* Linn. **2005**.
157. C. A. J., E., Hyperforin, Possibly the Major Non-Nitrogenous Secondary Metabolite of *Hypericum Perforatum* L. *Pharmacopsychiatry* **1998**, *31* (S 1), 2-6.
158. M., A.; A., G.; T., E.; S., C. In *The Ex Situ Comparison of Two Improved St. John's Wort (Hypericum perforatum) Cultivars with an Iranian Wild Population*, International Society for Horticultural Science (ISHS), Leuven, Belgium: 2011; pp 163-170.
159. Narayanan, R.; Jerrine, J.; Manikkan, R.; Thirunavukarasu, R., In vitro cytotoxicity of methanol extracts of *Hypericum wightianum* and *Hypericum hookerianum* against 3T3L1 cell lines. *Bangladesh J. Pharmacol.* **2016**, *11* (2), 328-329.
160. Heinrich, M.; Daniels, R.; Stintzing, F. C.; Kammerer, D. R., Comprehensive phytochemical characterization of St. John's wort (*Hypericum perforatum* L.) oil macerates obtained by different extraction protocols via analytical tools applicable in routine control. *Pharmazie* **2017**, *72* (3), 131-138.
161. Blumenthal, M.; Busse, W. R.; Goldberg, A., *The Complete German Commission E Monographs: Therapeutic Guide to Herbal Medicines*. Boston: American Botanical Council: 1998.

Chapter 1: Introduction

162. Greeson, J. M.; Sanford, B.; Monti, D. A., St. John's wort (*Hypericum perforatum*): a review of the current pharmacological, toxicological, and clinical literature. *Psychopharmacology* **2001**, *153* (4), 402-14.
163. Joanne, B.; Linda A., A.; J. David, P., St John's wort (*Hypericum perforatum* L.): a review of its chemistry, pharmacology and clinical properties. *J. Pharm. Pharmacol.* **2001**, *53* (5), 583-600.
164. Patocka, J., The chemistry, pharmacology, and toxicology of the biologically active constituents of the herb *Hypericum perforatum* L. *J. Appl. Biomed.* **2003**, *1* (2), 61-70.
165. Blaschek, W.; Hänsel, R.; Keller, K.; Reichling, J.; Rimpler, H.; Schneider, G., *Hagers Handbuch der Pharmazeutischen Praxis: Folgeband 2: Drogen AK*. Springer-Verlag: 2013.
166. Istikoglou, C. I.; Mavreas, V.; Geroulanos, G., History and therapeutic properties of *Hypericum Perforatum* from antiquity until today. *Psychiatrike = Psychiatriki* **2010**, *21* (4), 332-8.
167. Moffat, B., Archaeological Sources for the History of Herbal Medicine Practice: The case study of St John's wort with valerian at Soutra medieval hospital. *Critical Approaches to the History of Western Herbal Medicine: From Classical Antiquity to the Early Modern Period* **2014**, 253-270.
168. Dejan Z., O.; Neda M., M.-D.; Marina M., F.; Slobodan S., P.; Emilija Đ., J., Antioxidant activity relationship of phenolic compounds in *Hypericum perforatum* L. *Chem. Cent. J.* **2011**, *5* (1), 34.
169. H., F.; M. A., E., Antioxidant and free radical scavenging activities of *Hypericum perforatum* L. (st. John's wort). *Int. J. Forest, Soil and Erosion.* **2013**, *3* (2), 68-72.
170. Silvio, S.; Roberto, P.; Anna, B.; Paolo, M.; Antonella, R.; Aurelia, T.; Roberto Della, L., Topical anti-inflammatory activity of extracts and compounds from *Hypericum perforatum* L. *J. Pharm. Pharmacol.* **2010**, *59* (5), 703-709.
171. Savikin, K.; Dobrić, S.; Tadić, V.; Zdunić, G., Antiinflammatory activity of ethanol extracts of *Hypericum perforatum* L., *H. barbatum* Jacq., *H. hirsutum* L., *H. richeri* Vill. and *H. androsaemum* L. in rats. *Phytother. Res.* **2007**, *21* (2), 176-180.
172. Bahmani, M.; Taherikalani, M.; Khaksarian, M.; Soroush, S.; Ashrafi, B.; Heydari, R., Phytochemical Profiles and Antibacterial Activities of Hydroalcoholic Extracts of *Origanum vulgare* and *Hypericum perforatum* and Carvacrol and Hypericin as a Promising Anti-*Staphylococcus aureus*. *Mini Reviews in Medicinal Chemistry* **2019**, *19* (11), 923-932.
173. Zeb, S.; Ismat, N.; Alya, M., A review of the antibacterial activity of *Hypericum perforatum* L. *J. Ethnopharmacol.* **2010**, *131* (3), 511-521.
174. Shijing, L.; Yapeng, Z.; Xuanhe, P.; Feizhou, Z.; Congyuan, J.; Qianqian, L.; Zhongyi, C.; Gan, D.; Guojun, W.; Linqian, W.; Liyu, C., Antibacterial activity and mechanism of silver nanoparticles against multidrug-resistant *Pseudomonas aeruginosa*. *Int. J. Nanomed.* **2019**, *14*, 1469-1487.
175. Mansi, S.; L. K., D., Therapeutic potential of *Hypericum Perforatum*: a review. *Int. J. Pharm. Sci. Res.* **2015**, *6* (12), 4982-4988.
176. Abdalrahim, A.; Armin, F.; Nadja C., B.; Pascal, R.; Thomas, S.; Johanna-Gabriela, W., *Hypericum perforatum* L.-Mediated Green Synthesis of Silver Nanoparticles Exhibiting Antioxidant and Anticancer Activities. *Nanomaterials* **2021**, *11* (2), 487.
177. Gönenç, T. M.; Ozturk, M.; Türkseven, S. G.; Kirmizibayrak, P. B.; Günal, S.; Yilmaz, S., *Hypericum perforatum* l.: An overview of the anticancer potencies of the specimens collected from different ecological environments. *Pak. J. Bot.* **2020**, *52* (3), 1003-1010.
178. Marta, M.; Pellegrino, M.; Michela, N., Anti-Tumor Activity of *Hypericum perforatum* L. and Hyperforin through Modulation of Inflammatory Signaling, ROS Generation and Proton Dynamics. *Antioxidants* **2021**, *10* (1).
179. Issa, A.; Mohammad, M.; Andrei, B.; Motahare-Sadat, H., Antiproliferative Effects of Free and Encapsulated *Hypericum Perforatum* L. Extract and Its Potential Interaction with Doxorubicin for Esophageal Squamous Cell Carcinoma. *J Pharmacopuncture* **2019**, *22* (2), 102-108.

Chapter 1: Introduction

180. Hyung-In, M., Antiplasmodial and cytotoxic activity of phloroglucinol derivatives from *Hypericum erectum* Thunb. *Phytother. Res.* **2010**, *24* (6), 941-944.
181. Joanne, B.; Joëlle, Q.-L., Natural Products Published in 2009 from Plants Traditionally Used to Treat Malaria. *Planta Med.* **2011**, *77* (06), 631-640.
182. Gulam Mohammed, H.; Shyam Sunder, C.; Paras Nath, S.; Vikas, K., Hypolipidemic and Antiobesity-Like Activity of Standardised Extract of *Hypericum perforatum* L. in Rats. *int. sch. res. notices.* **2011**, *2011*.
183. Gulam Mohammed, H.; Paras Nath, S.; Vikas, K., Beneficial effects of a standardized *Hypericum perforatum* extract in rats with experimentally induced hyperglycemia. *Drug. Discov. Ther.* **2009**, *3* (5), 215-220.
184. Hossein, H.; Gholam-Reza, K.; Maysam, R., Anticonvulsant effect of *Hypericum perforatum*: role of nitric oxide. *J. Ethnopharmacol.* **2005**, *98* (1-2), 207-208.
185. Kumar, V.; Singh, P. N.; Bhattacharya, S. K., Anti-inflammatory and analgesic activity of Indian *Hypericum perforatum* L. *Indian J. Exp. Biol.* **2001**, *39* (4), 339-343.
186. Nicoletta, G., *Hypericum Perforatum* (St John's Wort) Beyond Depression: A Therapeutic Perspective for Pain Conditions. *J. Ethnopharmacol.* **2017**, *200*, 136-146.
187. Joana, C.; Bruna, C.; Joana S., A.; M. Eugénia, N.; M. Beatriz P. P., O.; Isabel, M., HRM analysis targeting ITS1 and matK loci as potential DNA mini-barcodes for the authentication of *Hypericum perforatum* and *Hypericum androsaemum* in herbal infusions. *Food Control* **2016**, *61*, 105-114.
188. Ellis, K. A.; Stough, C.; Vitetta, L.; Heinrich, K.; Nathan, P. J., An investigation into the acute nootropic effects of *Hypericum perforatum* L. (St. John's Wort) in healthy human volunteers. *Behav. Pharmacol.* **2001**, *12* (3), 173-182.
189. Fuat, U.; Mustafa, N.; İshak Saat, Ö.; Tolga Taha, S., *Hypericum perforatum* L. supplementation protects sciatic nerve injury-induced apoptotic, inflammatory and oxidative damage to muscle, blood and brain in rats. *J. Pharm. Pharmacol.* **2019**, *71* (1), 83-92.
190. Oksana, S.; Jurgita, Š.; Kristina, L.; Algimantas, P.; Anatolij, K.; Natalija, T., Antifungal properties of hypericin, hypericin tetrasulphonic acid and fagopyrin on pathogenic fungi and spoilage yeasts. *Pharm. Biol.* **2016**, *54* (12), 3121-3125.
191. Giovanna, S.; Noemi, T.; Alessio, V.; Elisa, B.; Felicia Diodata, D. A.; Alicia, I.; Gabriella, P., In vitro antifungal activity of extracts obtained from *Hypericum perforatum* adventitious roots cultured in a mist bioreactor against planktonic cells and biofilm of *Malassezia furfur*. *Nat. Prod. Res.* **2016**, *30* (5), 544-550.
192. Shilan, M.; Hadi, E.; Roja, R.; Maryam, B.; Yara, S.; Azar, A.-S.; Mohammad-Hossein, S.-S.; Mohammad, A., Effects of *Hypericum perforatum* extract on rat irritable bowel syndrome. *Pharmacogn. Mag.* **2011**, *7* (27), 213-223.
193. Wendy, W.; Ann Vander, S.; Rachelle L., M.; Noel S., W.; Joseph, B.; Jon, M., *Hypericum perforatum* (St John's Wort) for Attention-Deficit/Hyperactivity Disorder in Children and Adolescents: A Randomized Controlled Trial. *Jama* **2008**, *299* (22), 2633-2641.
194. Alan, M., Epidemiology, etiology, and natural treatment of seasonal affective disorder. *Altern Med Rev.* **2005**, *10* (1), 5-13.
195. Yang, S.; Chen, L.; Lihua, Z.; Lei, L.; Zhijin, L.; Guang, Y.; Yuxin, L., Anti-fatigue effect of hypericin in a chronic forced exercise mouse model. *J. Ethnopharmacol.* **2022**, *284*, 114767.
196. Su Hee, J.; Dong Il, K.; Min-Sun, C., Effects and treatment methods of acupuncture and herbal medicine for premenstrual syndrome/premenstrual dysphoric disorder: systematic review. *BMC Complement Altern. Med.* **2014**, *14* (1), 11.
197. Zahra, A.; Jerome, S.; Dennis, C.; Seyed A., E.; Roja, R., Herbal medicines and phytochemicals for obsessive-compulsive disorder. *Phytother. Res.* **2020**, *34* (8), 1889-1901.

Chapter 1: Introduction

198. Nahid, Z.; Mojtaba, S.; Ghasem, S.; Mohammad, M.; Amirhossein, S., Hypericum perforatum in the treatment of psychiatric and neurodegenerative disorders: Current evidence and potential mechanisms of action. *J. Cell. Physiol.* **2019**, *234* (6), 8496-8508.
199. Qin Xiang, N.; Nandini, V.; Collin Yih Xian, H., Clinical use of Hypericum perforatum (St John's wort) in depression: A meta-analysis. *J. Affect. Disord.* **2017**, *210* (1), 211-221.
200. Alieh, E.; Somayeh, A.; Parvin, A.; Shahnaz, N., The effect of Hypericum perforatum on postmenopausal symptoms and depression: A randomized controlled trial. *Complementary Therapies in Medicine* **2019**, *45*, 109-113.
201. E., W.; U., W.; D., T., A systematic review and meta-analysis of Hypericum perforatum in depression: a comprehensive clinical review. *Int. Clin. Psychopharmacol.* **2001**, *16* (5), 239-252.
202. Tarun, B.; Hari Prasad, D.; Manoj Kumar, S.; Ruchika, S.; Sashi, U.; Charu, J.; Kapil, B.; Jalaj Kumar, G.; Indra D., B.; Ranbeer S., R.; Veena, P., Chapter 3.40 - St. John's Wort (Hypericum perforatum). In *Nonvitamin and Nonmineral Nutritional Supplements*, Nabavi, S. M.; Silva, A. S., Eds. Academic Press: 2019; pp 415-432.
203. L.A., M., 1.09 - Traditional Medicines. In *Comprehensive Medicinal Chemistry II*, John B., T.; David J., T., Eds. Elsevier: University of Kansas, Lawrence, KS, USA, 2007; Vol. 7, pp 405-430.
204. V. A., H-P.; L. K., B.; J. D., P.; H., S.; G., A.; M., P.; G. K., B.; C. W., H., A chromatographic and spectroscopic analytical platform for the characterization of St John's wort extract adulterations. *Anal. Methods* **2013**, *5* (3), 616-628.
205. Anthony, B.; Anastasia, A.; Débora A., F.; Francesca, S.; Eike, R.; Michael, H., St John's wort (Hypericum perforatum) products – an assessment of their authenticity and quality. *Phytomedicine* **2018**, *40* (1), 158-164.
206. Eike, R.; Anne, S., Dedication. In *High-Performance Thin-Layer Chromatography for the Analysis of Medicinal Plants*, Thieme Verlagsgruppe: Stuttgart, New York, Delhi, Rio, 2007.
207. M., G.; J., Z.; I.A., K., Hypericum Perforatum—Chemical Profiling and Quantitative Results of St. John's Wort Products by an Improved High-Performance Liquid Chromatography Method. *J. Pharm. Sci.* **2002**, *91* (3), 623-630.
208. Ari, T.; Anja, H.; Jorma, J., Fast high-performance liquid chromatographic analysis of naphthodianthrones and phloroglucinols from Hypericum perforatum extracts. *Phytochem. Anal.* **2003**, *14* (5), 306-309.
209. Ari, T.; Jouko, U.; Anja, H.; Jorma, J., Determination of naphthodianthrones and phloroglucinols from Hypericum perforatum extracts by liquid chromatography/tandem mass spectrometry. *Rapid Commun. Mass Spectrom.* **2002**, *16* (5), 396-402.
210. M., B.; B., G.; N., F.; R., P.; F., P.; F., P., Identification by high-performance liquid chromatography–diode array detection–mass spectrometry and quantification by high-performance liquid chromatography–UV absorbance detection of active constituents of Hypericum perforatum. *J. Chromatogr. A* **1998**, *825* (1), 9-16.
211. Pierluigi, M.; Piergiorgio, P., High performance liquid chromatography/electrospray mass spectrometry of Hypericum perforatum extracts. *Rapid Commun. Mass Spectrom.* **2000**, *14* (2), 95-99.
212. Yan-Ru, L.; Bing-Kun, X.; Jian-Yun, Y.; Chun-Hua, G.; Shu-Jie, S.; Zhi-Shu, T.; Jun-Xing, D.; Rong-Qing, H., ¹H-NMR and HPLC–MS/MS-based global/targeted metabolomic evaluation of Hypericum perforatum L. intervention for menopause. *J. Funct. Foods* **2015**, *17*, 722-741.
213. Evangelos C., T.; Sjef, B.; Vassiliki, E.; Anastassios N., T.; Jacques, V.; Ioannis P., G., Identification of the major constituents of Hypericum perforatum by LC/SPE/NMR and/or LC/MS. *Phytochemistry* **2007**, *68* (3), 383-393.
214. Bruno A., S.; Federico, F.; João O., M.; Alberto C.P., D., Phytochemical and antioxidant characterization of Hypericum perforatum alcoholic extracts. *Food Chem.* **2005**, *90* (1-2), 157-167.

Chapter 1: Introduction

215. Klein-Bischoff, U.; U., K., Hypericin und Fluoreszenz, eine quantitative fluorimetrische Bestimmungsmethode. *J Pharm. Ztg. Wiss* **1993**, *138*, 55-58.
216. Nikos E., S. M. D.; Dimitris, S.; Ioannis, T.; D., K.; Unyime O., N. M. D.; A., B.; N. J., A., Localization of hypericin-induced fluorescence after *Hypericum perforatum* polar fraction instillation in normal rat urinary bladder. *Optical Methods for Tumor Treatment and Detection: Mechanisms and Techniques in Photodynamic Therapy XIV* **2005**, 5689, 158-164.
217. Pavol, M.; Franck, S.; Laurent, C.; Pierre-Yves, T., Subcellular distribution of hypericin in human cancer cells. *Photochem. Photobiol.* **1995**, *62* (3), 546-549.
218. Petr, B.; Bořivoj, K.; Jozef, K.; Josef, H.; Marián, H., Lanthanum rather than cadmium induces oxidative stress and metabolite changes in *Hypericum perforatum*. *J. Hazard. Mater.* **2015**, *286* (9), 334-342.
219. V. A., H.-P.; J. D., P.; C., P.; L. K., B.; S. A., S.; G., A.; M., P.; G. K., B.; C. W., H., Fourier transform infrared imaging analysis in discrimination studies of St. John's wort (*Hypericum perforatum*). *Anal. Bioanal. Chem.* **2012**, *404* (6-7), 1771-1778.
220. Krzysztof B., B.; Justyna, G.; Günther K., B.; Michael, P.; Christian W., H., Principles and Applications of Vibrational Spectroscopic Imaging in Plant Science: A Review. *Front. Plant Sci.* **2020**, *11*, 1226.
221. Anastasia, A.; Anthony, B.; Tivadar, K.; Judit, H.; Michael, H.; Dezso, C., Quality control of *Hypericum perforatum* L. analytical challenges and recent progress. *J. Pharm. Pharmacol.* **2019**, *71* (1), 15-37.
222. Gudrun, R.; Christoph, R.; Karin Berger, B.; Urs, S., Classification and correlation of St. John's wort extracts by nuclear magnetic resonance spectroscopy, multivariate data analysis and pharmacological activity. *Planta Med.* **2004**, *70* (8), 771-777.
223. Evangelos C., T.; Vassiliki, E.; Anastassios N., T.; Ioannis P., G., ¹H NMR determination of hypericin and pseudohypericin in complex natural mixtures by the use of strongly deshielded OH groups. *Anal. Chim. Acta* **2008**, *607* (2), 219-226.
224. François N., M.; Susan J., M.; Paul R., S., Exploring feature selection of St John's wort grown under different light spectra using (1) H-NMR spectroscopy. *Phytochem. Anal.* **2020**, *31* (5), 670-680.
225. Kirsten A., L.; Young H., C.; Robert, V.; Peter G. L., K., An overview of NMR-based metabolomics to identify secondary plant compounds involved in host plant resistance. *Phytochem. Rev.* **2011**, *10* (2), 205-216.
226. B.L., R., High-Performance Liquid Chromatography. In Nielsen S.S. (eds) *Food Analysis*, Springer, Cham: 2017; pp 213-226.
227. What is HPLC (High Performance Liquid Chromatography) ? . https://www.shimadzu.com/an/service-support/technical-support/analysis-basics/basic/what_is_hplc.html.
228. Meyer, V. R., *Practical high-performance liquid chromatography*. John Wiley & Sons: 2013; p 412.
229. Böcker, J., *Chromatographie, instrumentelle Analytik mit Chromatographie und Kapillarelektrophorese*. Vogel: Würzburg, 1997; p 481.
230. HPLC basics –Principles and parameters. <https://www.knauer.net/en/Systems-Solutions/Analytical-HPLC-UHPLC/HPLC-Basics---principles-and-parameters>.
231. Chapter 8 The Selection of the Appropriate Detector. In *Journal of Chromatography Library*, Scott, R. P. W., Ed. Elsevier: 1986; Vol. 33, pp 235-261.
232. Krueve, A.; Rebane, R.; Kipper, K.; Oldekop, M.-L.; Evard, H.; Herodes, K.; Ravio, P.; Leito, I., Tutorial review on validation of liquid chromatography–mass spectrometry methods: Part I. *Anal. Chim. Acta* **2015**, *870*, 29-44.

Chapter 1: Introduction

233. Hiraoka, K., *Fundamentals of mass spectrometry*. Springer: Springer New York Heidelberg Dordrecht London, 2013; Vol. 8.
234. Pitt, J. J., Principles and applications of liquid chromatography-mass spectrometry in clinical biochemistry. *Clin Biochem Rev* **2009**, *30* (1), 19-34.
235. Banerjee, S.; Mazumdar, S., Electrospray Ionization Mass Spectrometry: A Technique to Access the Information beyond the Molecular Weight of the Analyte. *Int. J. Anal. Chem.* **2012**, *2012*, 282574.
236. Ho, C. S.; Lam, C. W. K.; Chan, M. H. M.; Cheung, R. C. K.; Law, L. K.; Lit, L. C. W.; Ng, K. F.; Suen, M. W. M.; Tai, H. L., Electrospray ionisation mass spectrometry: principles and clinical applications. *Clin Biochem Rev* **2003**, *24* (1), 3-12.
237. Basics of Liquid Chromatograph-Mass Spectrometry. https://www.shimadzu.com/an/service-support/technical-support/analysis-basics/basics_of_lcms/interfaces_for_lcms.html.
238. Steckel, A.; Schlosser, G., An Organic Chemist's Guide to Electrospray Mass Spectrometric Structure Elucidation. *Molecules* **2019**, *24* (3).
239. Kind, T.; Tsugawa, H.; Cajka, T.; Ma, Y.; Lai, Z.; Mehta, S. S.; Wohlgemuth, G.; Barupal, D. K.; Showalter, M. R.; Arita, M.; Fiehn, O., Identification of small molecules using accurate mass MS/MS search. *Mass Spectrom. Rev.* **2018**, *37* (4), 513-532.
240. Types of MS/MS systems and their key characteristics. https://www.shimadzu.com/an/service-support/technical-support/analysis-basics/fundamental/key_characteristics.html.
241. Chernushevich, I. V.; Loboda, A. V.; Thomson, B. A., An introduction to quadrupole–time-of-flight mass spectrometry. *J. Mass Spectrom.* **2001**, *36* (8), 849-865.
242. Yie, C., *Novel Drug Delivery Systems*. 2nd ed.; CRC Press: Boca Raton, 1991.
243. Langer, R., Drug delivery and targeting. *Nature* **1998**, *392* (6679 Suppl), 5-10.
244. Langer, R., New Methods of Drug Delivery. *Science* **1990**, *249* (4976), 1527-1533.
245. Allen Theresa, M.; Cullis Pieter, R., Drug Delivery Systems: Entering the Mainstream. *Science* **2004**, *303* (5665), 1818-1822.
246. Gidal, B. E.; DeCerce, J.; Bockbrader, H. N.; Gonzalez, J.; Kruger, S.; Pitterle, M. E.; Rutecki, P.; Ramsay, R. E., Gabapentin bioavailability: effect of dose and frequency of administration in adult patients with epilepsy. *Epilepsy Research* **1998**, *31* (2), 91-99.
247. Serajuddin, A. T. M., Solid dispersion of poorly water-soluble drugs: Early promises, subsequent problems, and recent breakthroughs. *J. Pharm. Sci.* **1999**, *88* (10), 1058-1066.
248. Schmidt, B.; Ribnicky, D. M.; Poulev, A.; Logendra, S.; Cefalu, W. T.; Raskin, I., A natural history of botanical therapeutics. *Metabolism* **2008**, *57*, 3-9.
249. Neena, W.; Clive, W.; Clive, W., *Physiological Pharmaceutics: Barriers to Drug Absorption*. 1st ed.; CRC Press: 2000.
250. Savjani, K. T.; Gajjar, A. K.; Savjani, J. K., Drug Solubility: Importance and Enhancement Techniques. *ISRN Pharmaceutics* **2012**, *2012*, 195727.
251. Kalepu, S.; Nekkanti, V., Insoluble drug delivery strategies: review of recent advances and business prospects. *Acta Pharmaceutica Sinica B* **2015**, *5* (5), 442-453.
252. Lau, J. L.; Dunn, M. K., Therapeutic peptides: Historical perspectives, current development trends, and future directions. *Bioorganic & Medicinal Chemistry* **2018**, *26* (10), 2700-2707.
253. Bruno, B. J.; Miller, G. D.; Lim, C. S., Basics and recent advances in peptide and protein drug delivery. *Therapeutic Delivery* **2013**, *4* (11), 1443-1467.
254. Craik, D. J.; Fairlie, D. P.; Liras, S.; Price, D., The Future of Peptide-based Drugs. *Chemical Biology & Drug Design* **2013**, *81* (1), 136-147.
255. Putney, S. D.; Burke, P. A., Improving protein therapeutics with sustained-release formulations. *Nat. Biotechnol.* **1998**, *16* (2), 153-157.

Chapter 1: Introduction

256. Pisal, D. S.; Kosloski, M. P.; Balu-Iyer, S. V., Delivery of Therapeutic Proteins. *J. Pharm. Sci.* **2010**, *99* (6), 2557-2575.
257. Schuster, J.; Koulov, A.; Mahler, H.-C.; Detampel, P.; Huwyler, J.; Singh, S.; Mathaes, R., In Vivo Stability of Therapeutic Proteins. *Pharm. Res.* **2020**, *37* (2), 23.
258. Baker, M.; Reynolds, H. M.; Lumicisi, B.; Bryson, C. J., Immunogenicity of protein therapeutics: The key causes, consequences and challenges. *Self/Nonsense* **2010**, *1* (4), 314-322.
259. Jawa, V.; Cousens, L. P.; Awwad, M.; Wakshull, E.; Kropshofer, H.; De Groot, A. S., T-cell dependent immunogenicity of protein therapeutics: Preclinical assessment and mitigation. *Clin. Immunol.* **2013**, *149* (3, Part B), 534-555.
260. Rosenberg, A. S.; Sauna, Z. E., Immunogenicity assessment during the development of protein therapeutics. *J. Pharm. Pharmacol.* **2018**, *70* (5), 584-594.
261. Chames, P.; Van Regenmortel, M.; Weiss, E.; Baty, D., Therapeutic antibodies: successes, limitations and hopes for the future. *Br. J. Pharmacol.* **2009**, *157* (2), 220-233.
262. Shih, T.; Lindley, C., Bevacizumab: An angiogenesis inhibitor for the treatment of solid malignancies. *Clin. Ther.* **2006**, *28* (11), 1779-1802.
263. Smith, M. R., Rituximab (monoclonal anti-CD20 antibody): mechanisms of action and resistance. *Oncogene* **2003**, *22* (47), 7359-7368.
264. Aarden, L.; Ruuls, S. R.; Wolbink, G., Immunogenicity of anti-tumor necrosis factor antibodies—toward improved methods of anti-antibody measurement. *Curr. Opin. Immunol.* **2008**, *20* (4), 431-435.
265. Baert, F.; Noman, M.; Vermeire, S.; Van Assche, G.; D'Haens, G.; Carbonez, A.; Rutgeerts, P., Influence of Immunogenicity on the Long-Term Efficacy of Infliximab in Crohn's Disease. *N. Engl. J. Med.* **2003**, *348* (7), 601-608.
266. Atzeni, F.; Talotta, R.; Salaffi, F.; Cassinotti, A.; Varisco, V.; Battellino, M.; Ardizzone, S.; Pace, F.; Sarzi-Puttini, P., Immunogenicity and autoimmunity during anti-TNF therapy. *Autoimmunity Reviews* **2013**, *12* (7), 703-708.
267. Ryman, J. T.; Meibohm, B., Pharmacokinetics of Monoclonal Antibodies. *CPT: Pharmacometrics Syst. Pharmacol.* **2017**, *6* (9), 576-588.
268. Simeon, R.; Chen, Z., In vitro-engineered non-antibody protein therapeutics. *Protein & Cell* **2018**, *9* (1), 3-14.
269. Chauhan, V. P.; Stylianopoulos, T.; Boucher, Y.; Jain, R. K., Delivery of Molecular and Nanoscale Medicine to Tumors: Transport Barriers and Strategies. *Annu. Rev. Chem. Biomol. Eng.* **2011**, *2* (1), 281-298.
270. Shah, D. K.; Betts, A. M., Antibody biodistribution coefficients. *mAbs* **2013**, *5* (2), 297-305.
271. Schrama, D.; Reisfeld, R. A.; Becker, J. C., Antibody targeted drugs as cancer therapeutics. *Nat. Rev. Drug Discovery* **2006**, *5* (2), 147-159.
272. Tabrizi, M. A.; Tseng, C.-M. L.; Roskos, L. K., Elimination mechanisms of therapeutic monoclonal antibodies. *Drug Discovery Today* **2006**, *11* (1), 81-88.
273. Samaranyake, H.; Wirth, T.; Schenkwein, D.; Rätty, J. K.; Ylä-Herttuala, S., Challenges in monoclonal antibody-based therapies. *Annals of Medicine* **2009**, *41* (5), 322-331.
274. Jayasena, S. D., Aptamers: An Emerging Class of Molecules That Rival Antibodies in Diagnostics. *Clin. Chem.* **1999**, *45* (9), 1628-1650.
275. Opalinska, J. B.; Gewirtz, A. M., Nucleic-acid therapeutics: basic principles and recent applications. *Nat. Rev. Drug Discovery* **2002**, *1* (7), 503-514.
276. Mali, P.; Yang, L.; Esvelt Kevin, M.; Aach, J.; Guell, M.; DiCarlo James, E.; Norville Julie, E.; Church George, M., RNA-Guided Human Genome Engineering via Cas9. *Science* **2013**, *339* (6121), 823-826.

Chapter 1: Introduction

277. Kaczmarek, J. C.; Kowalski, P. S.; Anderson, D. G., Advances in the delivery of RNA therapeutics: from concept to clinical reality. *Genome Med.* **2017**, *9* (1), 60.
278. Van Hoecke, L.; Roose, K., How mRNA therapeutics are entering the monoclonal antibody field. *Journal of Translational Medicine* **2019**, *17* (1), 54.
279. Behlke, M. A., Chemical Modification of siRNAs for In Vivo Use. *Oligonucleotides* **2008**, *18* (4), 305-320.
280. Kormann, M. S. D.; Hasenpusch, G.; Aneja, M. K.; Nica, G.; Flemmer, A. W.; Herber-Jonat, S.; Huppmann, M.; Mays, L. E.; Illenyi, M.; Schams, A.; Griese, M.; Bittmann, I.; Handgretinger, R.; Hartl, D.; Rosenecker, J.; Rudolph, C., Expression of therapeutic proteins after delivery of chemically modified mRNA in mice. *Nat. Biotechnol.* **2011**, *29* (2), 154-157.
281. Whitehead, K. A.; Langer, R.; Anderson, D. G., Knocking down barriers: advances in siRNA delivery. *Nat. Rev. Drug Discovery* **2009**, *8* (2), 129-138.
282. Garber, K., Alnylam launches era of RNAi drugs. *Nat. Biotechnol.* **2018**, *36* (9), 777-779.
283. Scott, L. J., Givosiran: First Approval. *Drugs* **2020**, *80* (3), 335-339.
284. Palucka, K.; Banchereau, J., Dendritic-Cell-Based Therapeutic Cancer Vaccines. *Immunity* **2013**, *39* (1), 38-48.
285. June Carl, H.; O'Connor Roddy, S.; Kawalekar Omkar, U.; Ghassemi, S.; Milone Michael, C., CAR T cell immunotherapy for human cancer. *Science* **2018**, *359* (6382), 1361-1365.
286. Vargason, A. M.; Anselmo, A. C., Clinical translation of microbe-based therapies: Current clinical landscape and preclinical outlook. *Bioeng. Transl. Med.* **2018**, *3* (2), 124-137.
287. Prasad, V., Tisagenlecleucel — the first approved CAR-T-cell therapy: implications for payers and policy makers. *Nat. Rev. Clin. Oncol.* **2018**, *15* (1), 11-12.
288. Jackson, H. J.; Rafiq, S.; Brentjens, R. J., Driving CAR T-cells forward. *Nat. Rev. Clin. Oncol.* **2016**, *13* (6), 370-383.
289. Cheever, M. A.; Higano, C. S., PROVENGE (Sipuleucel-T) in Prostate Cancer: The First FDA-Approved Therapeutic Cancer Vaccine. *Clinical Cancer Research* **2011**, *17* (11), 3520-3526.
290. Therapies, O. o. T. a. A. Approved Cellular and Gene Therapy Products. <https://www.fda.gov/vaccines-blood-biologics/cellular-gene-therapy-products/approved-cellular-and-gene-therapy-products>.
291. Riglar, D. T.; Silver, P. A., Engineering bacteria for diagnostic and therapeutic applications. *Nat. Rev. Microbiol.* **2018**, *16* (4), 214-225.
292. Newick, K.; O'Brien, S.; Moon, E.; Albelda, S. M., CAR T Cell Therapy for Solid Tumors. *Annu. Rev. Med.* **2017**, *68* (1), 139-152.
293. Gargett, T.; Yu, W.; Dotti, G.; Yvon, E. S.; Christo, S. N.; Hayball, J. D.; Lewis, I. D.; Brenner, M. K.; Brown, M. P., GD2-specific CAR T Cells Undergo Potent Activation and Deletion Following Antigen Encounter but can be Protected From Activation-induced Cell Death by PD-1 Blockade. *Mol. Ther.* **2016**, *24* (6), 1135-1149.
294. Fraietta, J. A.; Lacey, S. F.; Orlando, E. J.; Pruteanu-Malinici, I.; Gohil, M.; Lundh, S.; Boesteanu, A. C.; Wang, Y.; O'Connor, R. S.; Hwang, W.-T.; Pequignot, E.; Ambrose, D. E.; Zhang, C.; Wilcox, N.; Bedoya, F.; Dorfmeier, C.; Chen, F.; Tian, L.; Parakandi, H.; Gupta, M.; Young, R. M.; Johnson, F. B.; Kulikovskaya, I.; Liu, L.; Xu, J.; Kassim, S. H.; Davis, M. M.; Levine, B. L.; Frey, N. V.; Siegel, D. L.; Huang, A. C.; Wherry, E. J.; Bitter, H.; Brogdon, J. L.; Porter, D. L.; June, C. H.; Melenhorst, J. J., Determinants of response and resistance to CD19 chimeric antigen receptor (CAR) T cell therapy of chronic lymphocytic leukemia. *Nat. Med.* **2018**, *24* (5), 563-571.
295. Hourd, P.; Ginty, P.; Chandra, A.; Williams, D. J., Manufacturing models permitting roll out/scale out of clinically led autologous cell therapies: regulatory and scientific challenges for comparability. *Cytotherapy* **2014**, *16* (8), 1033-1047.

Chapter 1: Introduction

296. Levine, B. L.; Miskin, J.; Wonnacott, K.; Keir, C., Global Manufacturing of CAR T Cell Therapy. *Mol. Ther. Methods Clin. Dev.* **2017**, *4*, 92-101.
297. Vargason, A. M.; Anselmo, A. C.; Mitragotri, S., The evolution of commercial drug delivery technologies. *Nat. Biomed. Eng.* **2021**, *5* (9), 951-967.
298. Jenison Robert, D.; Gill Stanley, C.; Pardi, A.; Polisky, B., High-Resolution Molecular Discrimination by RNA. *Science* **1994**, *263* (5152), 1425-1429.
299. Schultze, P.; Macaya, R. F.; Feigon, J., Three-dimensional Solution Structure of the Thrombin-binding DNA Aptamer d(GGTTGGTGTGGTTGG). *J. Mol. Biol.* **1994**, *235* (5), 1532-1547.
300. Bing, T.; Yang, X.; Mei, H.; Cao, Z.; Shangguan, D., Conservative secondary structure motif of streptavidin-binding aptamers generated by different laboratories. *Bioorganic & Medicinal Chemistry* **2010**, *18* (5), 1798-1805.
301. Kuwahara, M.; Kasamatsu, T.; Hasegawa, M.; Shoji, A.; Ozaki, H.; Sawai, H., Screening of modified DNA aptamers that recognize DNA secondary structure. *Nucleic Acids Symp. Ser.* **2004**, *48* (1), 265-266.
302. Huang, Z.; Szostak, J. W., Evolution of aptamers with a new specificity and new secondary structures from an ATP aptamer. *RNA* **2003**, *9* (12), 1456-1463.
303. Wang, K. Y.; Krawczyk, S. H.; Bischofberger, N.; Swaminathan, S.; Bolton, P. H., The tertiary structure of a DNA aptamer which binds to and inhibits thrombin determines activity. *Biochemistry* **1993**, *32* (42), 11285-11292.
304. Sekiya, S.; Fukuda, K.; Hwang, J.; Kakiuchi, N.; Taira, K.; Kusakabe, I.; Nishikawa, S., Analysis of interaction between RNA aptamer and protein using nucleotide analogs. *Nucleic Acids Symp. Ser.* **2000**, *44* (1), 163-164.
305. Tinoco, I.; Bustamante, C., How RNA folds. *J. Mol. Biol.* **1999**, *293* (2), 271-281.
306. Brion, P.; Westhof, E., Hierarchy and Dynamics of RNA Folding. *Annual Review of Biophysics and Biomolecular Structure* **1997**, *26* (1), 113-137.
307. Ilyas, A.; Asghar, W.; Allen, P. B.; Duhon, H.; Ellington, A. D.; Iqbal, S. M., Electrical detection of cancer biomarker using aptamers with nanogap break-junctions. *Nanotechnology* **2012**, *23* (27), 275502.
308. Deissler, H. L.; Lang, G. E., [Effect of VEGF165 and the VEGF aptamer pegaptanib (Macugen) on the protein composition of tight junctions in microvascular endothelial cells of the retina]. *Klin Monbl Augenheilkd* **2008**, *225* (10), 863-867.
309. Wyatt, J. R.; Puglisi, J. D.; Tinoco Jr, I., RNA folding: Pseudoknots, loops and bulges. *BioEssays* **1989**, *11* (4), 100-106.
310. Mee Young, K.; Sunjuo, J., RNA aptamers that bind the nucleocapsid protein contain pseudoknots. *Molecules & Cells (Springer Science & Business Media BV)* **2003**, *16* (3), 413-417.
311. Bock, L. C.; Griffin, L. C.; Latham, J. A.; Vermaas, E. H.; Toole, J. J., Selection of single-stranded DNA molecules that bind and inhibit human thrombin. *Nature* **1992**, *355* (6360), 564-566.
312. Pobanz, K.; Lupták, A., Improving the odds: Influence of starting pools on in vitro selection outcomes. *Methods* **2016**, *106*, 14-20.
313. Roy, S.; Caruthers, M., Synthesis of DNA/RNA and Their Analogs via Phosphoramidite and H-Phosphonate Chemistries. *Molecules* **2013**, *18* (11).
314. Tuerk, C.; Gold, L., Systematic Evolution of Ligands by Exponential Enrichment: RNA Ligands to Bacteriophage T4 DNA Polymerase. *Science* **1990**, *249* (4968), 505-510.
315. Ellington, A. D.; Szostak, J. W., In vitro selection of RNA molecules that bind specific ligands. *Nature* **1990**, *346* (6287), 818-822.
316. Catuogno, S.; Esposito, C. L., Aptamer Cell-Based Selection: Overview and Advances. *Biomedicines* **2017**, *5* (3).

Chapter 1: Introduction

317. Lin, H.-I.; Wu, C.-C.; Yang, C.-H.; Chang, K.-W.; Lee, G.-B.; Shiesh, S.-C., Selection of aptamers specific for glycated hemoglobin and total hemoglobin using on-chip SELEX. *Lab Chip* **2015**, *15* (2), 486-494.
318. Ansari, N.; Ghazvini, K.; Ramezani, M.; Shahdordizadeh, M.; Yazdian-Robati, R.; Abnous, K.; Taghdisi, S. M., Selection of DNA aptamers against Mycobacterium tuberculosis Ag85A, and its application in a graphene oxide-based fluorometric assay. *Microchim. Acta* **2017**, *185* (1), 21.
319. Han, X.; Zhang, Y.; Nie, J.; Zhao, S.; Tian, Y.; Zhou, N., Gold nanoparticle based photometric determination of tobramycin by using new specific DNA aptamers. *Microchim. Acta* **2017**, *185* (1), 4.
320. Paniel, N.; Istamboulié, G.; Triki, A.; Lozano, C.; Barthelmebs, L.; Noguer, T., Selection of DNA aptamers against penicillin G using Capture-SELEX for the development of an impedimetric sensor. *Talanta* **2017**, *162*, 232-240.
321. Wu, J.-H.; Wang, C.-H.; Ma, Y.-D.; Lee, G.-B., A nitrocellulose membrane-based integrated microfluidic system for bacterial detection utilizing magnetic-composite membrane microdevices and bacteria-specific aptamers. *Lab Chip* **2018**, *18* (11), 1633-1640.
322. Hong, S.-L.; Xiang, M.-Q.; Tang, M.; Pang, D.-W.; Zhang, Z.-L., Ebola Virus Aptamers: From Highly Efficient Selection to Application on Magnetism-Controlled Chips. *Anal. Chem.* **2019**, *91* (5), 3367-3373.
323. Leblebici, P.; Leirs, K.; Spasic, D.; Lammertyn, J., Encoded particle microfluidic platform for rapid multiplexed screening and characterization of aptamers against influenza A nucleoprotein. *Anal. Chim. Acta* **2019**, *1053*, 70-80.
324. Jing, M.; Bowser, M. T., Tracking the Emergence of High Affinity Aptamers for rhVEGF165 During Capillary Electrophoresis-Systematic Evolution of Ligands by Exponential Enrichment Using High Throughput Sequencing. *Anal. Chem.* **2013**, *85* (22), 10761-10770.
325. Yang, J.; Bowser, M. T., Capillary Electrophoresis-SELEX Selection of Catalytic DNA Aptamers for a Small-Molecule Porphyrin Target. *Anal. Chem.* **2013**, *85* (3), 1525-1530.
326. Dong, L.; Tan, Q.; Ye, W.; Liu, D.; Chen, H.; Hu, H.; Wen, D.; Liu, Y.; Cao, Y.; Kang, J.; Fan, J.; Guo, W.; Wu, W., Screening and Identifying a Novel ssDNA Aptamer against Alpha-fetoprotein Using CE-SELEX. *Sci. Rep.* **2015**, *5* (1), 15552.
327. Zhu, C.; Li, L.; Yang, G.; Fang, S.; Liu, M.; Ghulam, M.; Hao, C.; Chen, Y.; Qu, F., Online reaction based single-step capillary electrophoresis-systematic evolution of ligands by exponential enrichment for ssDNA aptamers selection. *Anal. Chim. Acta* **2019**, *1070*, 112-122.
328. Zhu, C.; Yang, G.; Ghulam, M.; Li, L.; Qu, F., Evolution of multi-functional capillary electrophoresis for high-efficiency selection of aptamers. *Biotechnol. Adv.* **2019**, *37* (8), 107432.
329. He, J.; Wang, J.; Zhang, N.; Shen, L.; Wang, L.; Xiao, X.; Wang, Y.; Bing, T.; Liu, X.; Li, S.; Shangguan, D., In vitro selection of DNA aptamers recognizing drug-resistant ovarian cancer by cell-SELEX. *Talanta* **2019**, *194*, 437-445.
330. Song, S.; Wang, X.; Xu, K.; Li, Q.; Ning, L.; Yang, X., Selection of highly specific aptamers to *Vibrio parahaemolyticus* using cell-SELEX powered by functionalized graphene oxide and rolling circle amplification. *Anal. Chim. Acta* **2019**, *1052*, 153-162.
331. Gao, T.; Ding, P.; Li, W.; Wang, Z.; Lin, Q.; Pei, R., Isolation of DNA aptamers targeting N-cadherin and high-efficiency capture of circulating tumor cells by using dual aptamers. *Nanoscale* **2020**, *12* (44), 22574-22585.
332. Saad, M.; Chinerman, D.; Tabrizian, M.; Faucher, S. P., Identification of two aptamers binding to *Legionella pneumophila* with high affinity and specificity. *Sci. Rep.* **2020**, *10* (1), 9145.
333. Lin, N.; Wu, L.; Xu, X.; Wu, Q.; Wang, Y.; Shen, H.; Song, Y.; Wang, H.; Zhu, Z.; Kang, D.; Yang, C., Aptamer Generated by Cell-SELEX for Specific Targeting of Human Glioma Cells. *ACS Appl. Mater. Interfaces* **2021**, *13* (8), 9306-9315.

Chapter 1: Introduction

334. Zhongming, Z.; Linong, L.; Xiaona, Y.; Wangqiang, Z.; Wei, L., An ssDNA library immobilized SELEX technique for selection of an aptamer against ractopamine. **2017**.
335. Lauridsen, L. H.; Doessing, H. B.; Long, K. S.; Nielsen, A. T., A capture-SELEX strategy for multiplexed selection of RNA aptamers against small molecules. In *Synthetic Metabolic Pathways*, Springer: 2018; pp 291-306.
336. Boussebayle, A.; Groher, F.; Suess, B., RNA-based Capture-SELEX for the selection of small molecule-binding aptamers. *Methods* **2019**, *161*, 10-15.
337. Boussebayle, A.; Torcka, D.; Ollivaud, S.; Braun, J.; Bofill-Bosch, C.; Dombrowski, M.; Groher, F.; Hamacher, K.; Suess, B., Next-level riboswitch development—implementation of Capture-SELEX facilitates identification of a new synthetic riboswitch. *Nucleic Acids Res.* **2019**, *47* (9), 4883-4895.
338. Urak, K. T.; Shore, S.; Rockey, W. M.; Chen, S.-J.; McCaffrey, A. P.; Giangrande, P. H., In vitro RNA SELEX for the generation of chemically-optimized therapeutic RNA drugs. *Methods* **2016**, *103*, 167-174.
339. Zhuo, Z.; Yu, Y.; Wang, M.; Li, J.; Zhang, Z.; Liu, J.; Wu, X.; Lu, A.; Zhang, G.; Zhang, B., Recent Advances in SELEX Technology and Aptamer Applications in Biomedicine. *Int. J. Mol. Sci.* **2017**, *18* (10).
340. Wang, H.; Zhang, Y.; Yang, H.; Qin, M.; Ding, X.; Liu, R.; Jiang, Y., In Vivo SELEX of an Inhibitory NSCLC-Specific RNA Aptamer from PEGylated RNA Library. *Mol. Ther. Nucleic Acids* **2018**, *10*, 187-198.
341. Chen, L.; He, W.; Jiang, H.; Wu, L.; Xiong, W.; Li, B.; Zhou, Z.; Qian, Y., In vivo SELEX of bone targeting aptamer in prostate cancer bone metastasis model. *Int. J. Nanomed.* **2018**, *14*, 149-159.
342. Sola, M.; Menon, A. P.; Moreno, B.; Meraviglia-Crivelli, D.; Soldevilla, M. M.; Cartón-García, F.; Pastor, F., Aptamers Against Live Targets: Is In Vivo SELEX Finally Coming to the Edge? *Mol. Ther. Nucleic Acids* **2020**, *21*, 192-204.
343. Ruan, S.; Swamidass, S. J.; Stormo, G. D., BEESEM: estimation of binding energy models using HT-SELEX data. *Bioinformatics* **2017**, *33* (15), 2288-2295.
344. Nitta, K. R.; Vincentelli, R.; Jacox, E.; Cimino, A.; Ohtsuka, Y.; Sobral, D.; Satou, Y.; Cambillau, C.; Lemaire, P., High-Throughput Protein Production Combined with High- Throughput SELEX Identifies an Extensive Atlas of Ciona robusta Transcription Factor DNA-Binding Specificities. In *High-Throughput Protein Production and Purification: Methods and Protocols*, Vincentelli, R., Ed. Springer New York: New York, NY, 2019; pp 487-517.
345. Asif, M.; Orenstein, Y., DeepSELEX: inferring DNA-binding preferences from HT-SELEX data using multi-class CNNs. *Bioinformatics* **2020**, *36* (Supplement_2), i634-i642.
346. Fan, L.; Wang, T.; Hua, C.; Sun, W.; Li, X.; Grunwald, L.; Liu, J.; Wu, N.; Shao, X.; Yin, Y.; Yan, J.; Deng, X., A compendium of DNA-binding specificities of transcription factors in *Pseudomonas syringae*. *Nat. Commun.* **2020**, *11* (1), 4947.
347. Ishida, R.; Adachi, T.; Yokota, A.; Yoshihara, H.; Aoki, K.; Nakamura, Y.; Hamada, M., RaptRanker: in silico RNA aptamer selection from HT-SELEX experiment based on local sequence and structure information. *Nucleic Acids Res.* **2020**, *48* (14), e82-e82.
348. McKeague, M.; Bradley, C. R.; Girolamo, A. D.; Visconti, A.; Miller, J. D.; DeRosa, M. C., Screening and Initial Binding Assessment of Fumonisin B1 Aptamers. *Int. J. Mol. Sci.* **2010**, *11* (12).
349. Lin, P. H.; Tsai, C. W.; Wu, J. W.; Ruaan, R. C.; Chen, W. Y., Molecular dynamics simulation of the induced-fit binding process of DNA aptamer and L-argininamide. *Biotechnol. J.* **2012**, *7* (11), 1367-75.

Chapter 1: Introduction

350. Zhang, N.; Chen, Z.; Liu, D.; Jiang, H.; Zhang, Z.-K.; Lu, A.; Zhang, B.-T.; Yu, Y.; Zhang, G., Structural Biology for the Molecular Insight between Aptamers and Target Proteins. *Int. J. Mol. Sci.* **2021**, *22* (8), 4093.
351. Perez-Gonzalez, C.; Lafontaine, D. A.; Penedo, J. C., Fluorescence-Based Strategies to Investigate the Structure and Dynamics of Aptamer-Ligand Complexes. *Front. Chem.* **2016**, *4*, 33-33.
352. Williamson, J. R., Induced fit in RNA–protein recognition. *Nat. Struct. Biol.* **2000**, *7* (10), 834-837.
353. Cai, S.; Yan, J.; Xiong, H.; Liu, Y.; Peng, D.; Liu, Z., Investigations on the interface of nucleic acid aptamers and binding targets. *Analyst* **2018**, *143* (22), 5317-5338.
354. Hianik, T.; Ostatná, V.; Sonlajtnerova, M.; Grman, I., Influence of ionic strength, pH and aptamer configuration for binding affinity to thrombin. *Bioelectrochemistry (Amsterdam, Netherlands)* **2007**, *70* (1), 127-33.
355. Tang, Q.; Su, X.; Loh, K. P., Surface plasmon resonance spectroscopy study of interfacial binding of thrombin to antithrombin DNA aptamers. *J. Colloid Interface Sci.* **2007**, *315* (1), 99-106.
356. Jeong, S.; Rhee Paeng, I., Sensitivity and selectivity on aptamer-based assay: the determination of tetracycline residue in bovine milk. *ScientificWorldJournal* **2012**, *2012*, 159456-159456.
357. Iltu, M.; Nilsen-Hamilton, M., Aptamers in analytics. *Analyst* **2016**, *141* (5), 1551-1568.
358. Zhou, J.; Rossi, J., Aptamers as targeted therapeutics: current potential and challenges. *Nat. Rev. Drug Discovery* **2017**, *16* (3), 181-202.
359. Yu, H.; Alkhamis, O.; Canoura, J.; Liu, Y.; Xiao, Y., Advances and Challenges in Small-Molecule DNA Aptamer Isolation, Characterization, and Sensor Development. *Angew. Chem. Int. Ed.* **2021**, *60* (31), 16800-16823.
360. Schumacher, D.; Hackenberger, C. P. R.; Leonhardt, H.; Helma, J., Current Status: Site-Specific Antibody Drug Conjugates. *Journal of Clinical Immunology* **2016**, *36* (1), 100-107.
361. Rohr, U.-P.; Binder, C.; Dieterle, T.; Giusti, F.; Messina, C. G. M.; Toerien, E.; Moch, H.; Schäfer, H. H., The Value of In Vitro Diagnostic Testing in Medical Practice: A Status Report. *PLoS One* **2016**, *11* (3), e0149856.
362. Balmaseda, A.; Stettler, K.; Medialdea-Carrera, R.; Collado, D.; Jin, X.; Zambrana, J. V.; Jaconi, S.; Cameroni, E.; Saborio, S.; Rovida, F.; Percivalle, E.; Ijaz, S.; Dicks, S.; Ushiro-Lumb, I.; Barzon, L.; Siqueira, P.; Brown, D. W. G.; Baldanti, F.; Tedder, R.; Zambon, M.; de Filippis, A. M. B.; Harris, E.; Corti, D., Antibody-based assay discriminates Zika virus infection from other flaviviruses. *Proc. Natl. Acad. Sci. U.S.A.* **2017**, *114* (31), 8384.
363. Rosenbaum, C. D.; Carreiro, S. P.; Babu, K. M., Here Today, Gone Tomorrow...and Back Again? A Review of Herbal Marijuana Alternatives (K2, Spice), Synthetic Cathinones (Bath Salts), Kratom, Salvia divinorum, Methoxetamine, and Piperazines. *J. Med. Toxicol.* **2012**, *8* (1), 15-32.
364. Massoud, T. F.; Gambhir, S. S., Molecular imaging in living subjects: seeing fundamental biological processes in a new light. **2003**, *17* (5), 545-580.
365. Wang, A. Z.; Farokhzad, O. C., Current Progress of Aptamer-Based Molecular Imaging. *J. Nucl. Med.* **2014**, *55* (3), 353.
366. Cruz-Aguado, J. A.; Penner, G., Fluorescence Polarization Based Displacement Assay for the Determination of Small Molecules with Aptamers. *Anal. Chem.* **2008**, *80* (22), 8853-8855.
367. Chandola, C.; Kalme, S.; Casteleijn, M. G.; Urtti, A.; Neerathilingam, M., Application of aptamers in diagnostics, drug-delivery and imaging. *J. Biosci.* **2016**, *41* (3), 535-561.
368. Sahu, G. K., Potential Implication of Residual Viremia in Patients on Effective Antiretroviral Therapy. *AIDS Research and Human Retroviruses* **2014**, *31* (1), 25-35.
369. Wandtke, T.; Woźniak, J.; Kopiński, P., Aptamers in Diagnostics and Treatment of Viral Infections. *Viruses* **2015**, *7* (2).

Chapter 1: Introduction

370. Sarhan, M.; El-Bitar, A. M. H.; Hotta, H., Potent virucidal activity of honeybee “*Apis mellifera*” venom against Hepatitis C Virus. *Toxicon* **2020**, *188*, 55-64.
371. Gull, I.; Aslam, M. S.; Tipu, I.; Mushtaq, R.; Ali, T. Z.; Athar, M. A., Development of latent Interferon alpha 2b as a safe therapeutic for treatment of Hepatitis C virus infection. *Sci. Rep.* **2019**, *9* (1), 10867.
372. Hwang, S.-Y.; Sun, H.-Y.; Lee, K.-H.; Oh, B.-H.; Cha, Y. J.; Kim, B. H.; Yoo, J.-Y., 5'-Triphosphate-RNA-independent activation of RIG-I via RNA aptamer with enhanced antiviral activity. *Nucleic Acids Res.* **2012**, *40* (6), 2724-2733.
373. Torabi, R.; Ranjbar, R.; Halaji, M.; Heiat, M., Aptamers, the bivalent agents as probes and therapies for coronavirus infections: A systematic review. *Mol. Cell. Probes* **2020**, *53*, 101636.
374. Lee, C. H.; Lee, S.-H.; Kim, J. H.; Noh, Y.-H.; Noh, G.-J.; Lee, S.-W., Pharmacokinetics of a Cholesterol-conjugated Aptamer Against the Hepatitis C Virus (HCV) NS5B Protein. *Mol. Ther. Nucleic Acids* **2015**, *4*, e254.
375. Shoji, Y.; Shimada, J.; Mizushima, Y., Drug Delivery System to Control Infectious Diseases. *Curr. Pharm. Des.* **2002**, *8* (6), 455-465.
376. Pang, K. M.; Castanotto, D.; Li, H.; Scherer, L.; Rossi, J. J., Incorporation of aptamers in the terminal loop of shRNAs yields an effective and novel combinatorial targeting strategy. *Nucleic Acids Res.* **2018**, *46* (1), e6-e6.
377. Mufhandu Hazel, T.; Gray Elin, S.; Madiga Maphuti, C.; Tumba, N.; Alexandre Kabamba, B.; Khoza, T.; Wibmer Constantinos, K.; Moore Penny, L.; Morris, L.; Khati, M., UCLA1, a Synthetic Derivative of a gp120 RNA Aptamer, Inhibits Entry of Human Immunodeficiency Virus Type 1 Subtype C. *Journal of Virology* **2012**, *86* (9), 4989-4999.
378. Aeksiri, N.; Songtawee, N.; Gleeson, M. P.; Hannongbua, S.; Choowongkamon, K., Insight into HIV-1 reverse transcriptase–aptamer interaction from molecular dynamics simulations. *J. Mol. Model.* **2014**, *20* (8), 2380.
379. Nguyen, P. D. M.; Zheng, J.; Gremminger, T. J.; Qiu, L.; Zhang, D.; Tuske, S.; Lange, M. J.; Griffin, P. R.; Arnold, E.; Chen, S.-J.; Zou, X.; Heng, X.; Burke, D. H., Binding interface and impact on protease cleavage for an RNA aptamer to HIV-1 reverse transcriptase. *Nucleic Acids Res.* **2020**, *48* (5), 2709-2722.
380. Zhang, L.; Fang, X.; Liu, X.; Ou, H.; Zhang, H.; Wang, J.; Li, Q.; Cheng, H.; Zhang, W.; Luo, Z., Discovery of sandwich type COVID-19 nucleocapsid protein DNA aptamers. *Chem. Commun.* **2020**, *56* (70), 10235-10238.
381. Liu, X.; Wang, Y.-I.; Wu, J.; Qi, J.; Zeng, Z.; Wan, Q.; Chen, Z.; Manandhar, P.; Cavener, V. S.; Boyle, N. R.; Fu, X.; Salazar, E.; Kuchipudi, S. V.; Kapur, V.; Zhang, X.; Umetani, M.; Sen, M.; Willson, R. C.; Chen, S.-h.; Zu, Y., Neutralizing Aptamers Block S/RBD-ACE2 Interactions and Prevent Host Cell Infection. *Angew. Chem. Int. Ed.* **2021**, *60* (18), 10273-10278.
382. Schmitz, A.; Weber, A.; Bayin, M.; Breuers, S.; Fieberg, V.; Famulok, M.; Mayer, G., A SARS-CoV-2 Spike Binding DNA Aptamer that Inhibits Pseudovirus Infection by an RBD-Independent Mechanism**. *Angew. Chem. Int. Ed.* **2021**, *60* (18), 10279-10285.
383. Gao, H.; Qian, J.; Cao, S.; Yang, Z.; Pang, Z.; Pan, S.; Fan, L.; Xi, Z.; Jiang, X.; Zhang, Q., Precise glioma targeting of and penetration by aptamer and peptide dual-functioned nanoparticles. *Biomaterials* **2012**, *33* (20), 5115-5123.
384. Aravind, A.; Varghese, S. H.; Veeranarayanan, S.; Mathew, A.; Nagaoka, Y.; Iwai, S.; Fukuda, T.; Hasumura, T.; Yoshida, Y.; Maekawa, T.; Kumar, D. S., Aptamer-labeled PLGA nanoparticles for targeting cancer cells. *Cancer Nanotechnol.* **2012**, *3* (1), 1-12.
385. Zhou, J.; Neff, C. P.; Swiderski, P.; Li, H.; Smith, D. D.; Aboellail, T.; Remling-Mulder, L.; Akkina, R.; Rossi, J. J., Functional In Vivo Delivery of Multiplexed Anti-HIV-1 siRNAs via a Chemically Synthesized Aptamer With a Sticky Bridge. *Mol. Ther.* **2013**, *21* (1), 192-200.

Chapter 1: Introduction

386. Pan, X.; Yang, Y.; Li, L.; Li, X.; Li, Q.; Cui, C.; Wang, B.; Kuai, H.; Jiang, J.; Tan, W., A bispecific circular aptamer tethering a built-in universal molecular tag for functional protein delivery. *Chem. Sci.* **2020**, *11* (35), 9648-9654.
387. Shiang, Y.-C.; Ou, C.-M.; Chen, S.-J.; Ou, T.-Y.; Lin, H.-J.; Huang, C.-C.; Chang, H.-T., Highly efficient inhibition of human immunodeficiency virus type 1 reverse transcriptase by aptamers functionalized gold nanoparticles. *Nanoscale* **2013**, *5* (7), 2756-2764.
388. Chonco, L.; Fernández, G.; Kalhapure, R.; Hernáiz, M. J.; García-Oliva, C.; Gonzalez, V. M.; Martín, M. E.; Govender, T.; Parboosing, R., Novel DNA Aptamers Against CCL21 Protein: Characterization and Biomedical Applications for Targeted Drug Delivery to T Cell-Rich Zones. *Nucleic Acid Ther.* **2018**, *28* (4), 242-251.
389. Fattal, E.; Hillaireau, H.; Ismail, S. I., Aptamers in Therapeutics and Drug Delivery. *Adv. Drug Delivery Rev.* **2018**, *134*, 1-2.
390. Tan, X.; Jia, F.; Wang, P.; Zhang, K., Nucleic acid-based drug delivery strategies. *J. Controlled Release* **2020**, *323*, 240-252.
391. Lohiya, G.; Katti, D. S., Carboxylated chitosan-mediated improved efficacy of mesoporous silica nanoparticle-based targeted drug delivery system for breast cancer therapy. *Carbohydr. Polym.* **2022**, *277*, 118822.

2 Chapter Two: *Hypericum perforatum L.*-Mediated Green Synthesis of Silver Nanoparticles Exhibiting Antioxidant and Anticancer Activities

2.1 Vorwort

This chapter contains the article “Chapter Two: *Hypericum perforatum L.*-Mediated Green Synthesis of Silver Nanoparticles Exhibiting Antioxidant and Anticancer Activities” by Abdalrahim Alahmad^{1,*}, Armin Feldhoff², Nadja C. Bigall², Pascal Rusch², Thomas Scheper¹ and Johanna-Gabriela Walter^{1,*}. Reproduced with permission from Nanomaterials 2021 (11(2), 487, DOI: 10.3390/nano11020487). Copyright 2021 MDPI.

Dieser Beitrag konzentriert sich auf die grüne Synthese von Silber-Nanopartikeln (AgNPs) mit einer Größe < 100 nm für potenzielle medizinische Anwendungen unter Verwendung von Silbernitratlösung und wässrigen Extrakten aus *Hypericum Perforatum L.* (Johanniskraut). Es wurden verschiedene Synthesemethoden verwendet und hinsichtlich Ausbeute und Qualität der erhaltenen AgNPs verglichen. Es wurden monodisperse sphärische Nanopartikel mit einer Größe von ungefähr 20 bis 50 nm erhalten, wie durch verschiedene Techniken (SEM, TEM) aufgeklärt wurde. XRD-Messungen zeigten, dass metallisches Silber gebildet wurde und die Partikel haben eine flächenzentrierte kubische Struktur (fcc). SEM-Bilder und FTIR-Spektren zeigten, dass die AgNPs von einer schützenden Oberflächenschicht bedeckt sind, die aus organischen Komponenten besteht, die aus dem Pflanzenextrakt stammen. UV-Vis-Spektroskopie, dynamische Lichtstreuung und Zeta-Potential wurden auch für biologisch synthetisierte AgNPs gemessen. Basierend auf den erhaltenen Ergebnissen wurde ein möglicher Mechanismus vorgeschlagen, Silberionen zu Silbermetall zu reduzieren und es in nanoskaliger Form zu schützen. Darüber hinaus wurde gezeigt, dass die in der vorliegenden Studie hergestellten AgNPs eine hohe antioxidative Aktivität gegen die Radikalkation 2, 2'-Azino-bis-(3-ethylbenzothiazolin-6-sulfonsäure), Superoxid-Anion-Radikal und 2,2-Diphenyl-1-picrylhydrazyl aufweisen. Synthetisierte AgNPs zeigten eine hohe Zytotoxizität, indem sie die Zelllebensfähigkeit für Hela-, Hep G2- und A549-Zellen hemmten.

2.2 Abstract

This contribution focuses on the green synthesis of silver nanoparticles (AgNPs) with a size < 100 nm for potential medical applications by using silver nitrate solution and *Hypericum Perforatum L.* (St John's wort) aqueous extracts. Various synthesis methods were used and compared with regard to their yield and quality of obtained AgNPs. Monodisperse spherical nanoparticles were generated with a size of approximately 20 to 50 nm as elucidated by different techniques (SEM, TEM). XRD measurements showed that metallic silver was formed and the particles possess a face-centered cubic structure (fcc). SEM images and FTIR spectra revealed that the AgNPs are covered by a protective surface layer composed of organic components originating from the plant extract. Ultraviolet-visible spectroscopy, dynamic light scattering, and zeta potential were also measured for biologically synthesized AgNPs. A potential mechanism of reducing silver ions to silver metal and protecting it in the nanoscale form has been proposed based on the obtained results. Moreover, the AgNPs prepared in the present study have been shown to exhibit a high antioxidant activity for 2, 2'-azino-bis-(3-

Chapter 2: Green Synthesis of Silver Nanoparticles

ethylbenzothiazoline-6-sulfonic acid) radical cation, and super oxide anion radical and 2,2-diphenyl-1-picrylhydrazyl. Synthesized AgNPs showed high cytotoxicity by inhibiting cell viability for Hela, Hep G2, and A549 cells.

Keywords: *Hypericum perforatum L.* (St John's wort); silver nanoparticles (AgNPs); mechanism of green formation of nanoparticles; DPPH; ABTS; antioxidant and cytotoxicity effects

2.3 Introduction

Over the past decades, silver nanoparticles (AgNPs) have received considerable research interest, due to their unique chemical and physical features, and promising usages¹⁻⁴. The use of environmentally benign materials to synthesize nanoparticles provides many benefits including eco-friendliness and compatibility to pharmaceutical and biomedical applications because of the avoidance of toxic chemicals in the synthesis protocols. Green synthetic methods for nanoparticles include biological methods, the use of polysaccharides, irradiation, polyoxometalates, and the Tollens method⁵.

Biological methods include the use of algae to synthesize AgNPs at room temperature⁶; moreover several microorganisms (diatoms, fungi, bacteria) are utilized to grow AgNPs intracellularly or extracellularly such as colonic flora *Klebsiella pneumonia*, *Escherichia coli*, *Enterobacter cloacae*, *Bacillus subtilis*, *Penicillium*, *Vericillum*, *Fusarium oxysporum*, *Pseudomonas stutzeri*, *Phanerochaete chrysosporium*, *Penicillium fellutanum*, and other⁷⁻¹⁹. An exceptional work has been done in order to synthesize AgNPs using diverse biological regimes which involve extracts from plants such as *Carica papaya*, *Ocimum*, *Capsicum annum*, leaves of *Azadirachta indica*, as well as many other plants²⁰⁻³⁷. The bioreduction of silver ions to AgNPs occurs due to the presence of biomolecules that are found in plant extracts, such as flavonoids, terpenoids, phenolic acid, alkaloids³⁸. The synthesis of nanoparticles through the use of plant extracts attracts a lot of attention, mainly due to its simple methodology which does not require a sophisticated process such as maintenance of microbial cultures and multiple purification steps. Moreover, the biosynthesis can be adjusted to customize the size and shape of nanoparticles by using various amounts of plant extract and metal ions in the reaction medium³⁹⁻⁴⁰. The biosynthesis of AgNPs is a complex approach, which is not fully addressed yet⁴¹. AgNPs are increasingly used in various fields because of their unique physical and chemical properties. These include thermal, electrical, optical, high electrical conductivity, and biological properties^{12, 42-43}. Because of their special characteristics, they have been used for several applications, including in medical device coatings, as antibacterial agents, as additives in cosmetics, and in the pharmaceutical industry, within the food industry, orthopedics in diagnostics, in drug delivery, and as anticancer agents, where they enhance the effects of anti-cancer drugs⁴⁴. Moreover, silver nanostructures were employed for treatment of burns and wounds, for impregnating textile fabrics and as well as a contraceptive and marketed as a disinfectant for water⁴⁵⁻⁴⁸, antibacterial for both, Gram-positive and Gram-negative bacteria⁴⁹⁻⁵³, antiviral⁵⁴⁻⁵⁶, in the electronics and optoelectronic devices⁵⁷⁻⁵⁹, antimicrobial and antifungal agents⁶⁰⁻⁶², as optical labels such as in optical sensors⁶³⁻⁶⁵, catalysts⁶⁶⁻⁶⁷, drug delivery systems⁶⁸⁻⁶⁹, and in the field of cancer treatment⁷⁰⁻⁷³.

Chapter 2: Green Synthesis of Silver Nanoparticles

Hypericum perforatum Linn., generally recognized as St. John's Wort is a flowering plant and is native in Asia and Europe. It belongs to the Hypericaceae family that contains more than 1000 species and about 55 genera. *Hypericum* genus possesses more than 450 species distributed worldwide in tropical and subtropical regions ⁷⁴. *Hypericum perforatum* (St. John's wort) has been used as traditional medicinal plant all over the world ⁷⁵, due to its large diversity of secondary metabolites with considerable pharmaceutical effects ⁷⁶. *Hypericum perforatum* Linn. has been proven to be potential in treatment of many different diseases like cancer, AIDS, and depression ⁷⁷⁻⁸⁰. *H. perforatum* exhibits analgesic, anti-inflammatory, antioxidant, anticonvulsant, antidiabetic, and cytotoxic activities ⁸¹⁻⁸³. The significance of its most important constituents like hypericin, hyperforin, flavonoids and their analogs is attributed to their botanical safety and therapeutic efficacy ⁸⁴. Hypericin is renowned as a photosensitizing agent employed in the photodynamic therapy of viral infections and cancer. Lavie et al. ⁸⁵ demonstrated the inhibitory influence of pseudohypericin and hypericin against influenza virus, herpes simplex virus types II and I, and vesicular stomatitis. Lopez-Bazzocchi et al. ⁸⁶ and Hudson et al. ⁸⁷ investigated the deactivation of sindbis virus, HIV-I, and murine cytomegalovirus by treatment with hypericin and exposure to fluorescent light. Both pseudohypericin and hypericin block the viruses by production of singlet oxygen upon light irradiation ⁸⁸.

In this work, we report on the single step facile synthesis of highly water dispersible AgNPs using aqueous extract of *Hypericum perforatum* Linn. To obtain AgNPs with desired characteristics, such as small size and narrow size distribution, and high colloidal stability with high yields, various protocols for the synthesis of AgNPs using plant extracts were used and compared. Originally these protocols (Table 1) were established from different authors using extracts of various different plants. Here we have used them to identify the protocol resulting in highest quality of AgNPs with characteristics beneficial for drug delivery applications, in particular a size between 10 and 50 nm, when using aqueous extracts of *Hypericum perforatum* L. Resulting AgNPs were thoroughly characterized with regard to size and stability, as well as with regard to the nature of the capping agent on the surface of the particles.

2.4 Materials and Methods

2.4.1 Materials

Aerial parts of *Hypericum perforatum* L. (St. John's wort) were collected in June–July in southeastern Syria during the flowering season. Silver nitrate; 1,1-diphenyl-2-picrylhydrazyl (DPPH); potassium persulphate; 2,2'-azino-bis-(3-ethylbenzothiazoline-6-sulfonic acid) (ABTS) were purchased from Sigma-Aldrich (Darmstadt, Germany), Filter paper Whatman 90 mm from GE Healthcare Life Sciences (Freiburg, Germany), 0.22 µm nylon syringe Filter and Sartolab Vakuumfilter 180C5; 0.22 µm Polyethersulfon, 500 mL; syringe filter 25 mm, 0.45 µm RC with GF prefilter; 0.45 µm PTFE filter and Vivaspin 10 kDa from Sartorius (Goettingen, Germany). Ethanol, methanol, and acetone were of HPLC grade from Roth (Karlsruhe, Germany), and acetonitrile from VWR (Hannover, Germany). Water was purified by a QM system from Sartorius (Goettingen, Germany).

Chapter 2: Green Synthesis of Silver Nanoparticles

2.4.2 Preparation of *Hypericum perforatum L.* (St John's Wort) Extract

Aerial parts of St John's wort were collected from the Ghab Plain, Syria in June and July. The plant was washed several times to remove dust and possible sludge. The samples were dried at room temperature in the dark and ground in an electric grinder. The powder (350 mg) was added to 800 mL of deionized water in a 1000 mL Erlenmeyer flask. The mixture was heated to maintain a gentle boiling for 4 h until the volume was reduced to approx. 250 mL. The extract was cooled to room temperature then clarified using Whatman filter paper (No. 40). The extract was centrifuged at $23,015\times g$ for 30 min, and then filtered through a 0.2 micron filter. The resulting extract was stored in the refrigerator at 4 °C to be used directly in preparing AgNPs or freeze-dried (solvent was evaporated under nitrogen gas at 30 °C to prevent oxidation). This resulted in a yellow-brown solid with a yield of 19%.

2.4.3 Biosynthesis of Silver Nanoparticles

Aqueous St John's wort extract were mixed with silver nitrate and placed on magnetic stirrer with heating for a specific time (details given in Table 1) to obtain silver nanoparticles (AgNPs). St John's wort extract was used as a source of biological reducing and capping agents. The influence of several parameters like concentration and the amount of silver nitrate used, amount of the plant extract used, and the reaction temperature, was investigated by conducting various experiential trials. Various protocols were employed to prepare AgNPs using plant extracts to identify the most appropriate protocol. In fact, most of the reaction times and conditions (proportion of silver ions and St. John's Wort extract) in Table 1 are obtained from the literature where other groups prepared silver nanostructures using other plant extracts. The goal was to select the protocol that resulted in the best quality and yield of AgNPs when using *Hypericum Perforatum L.* extract. The methods are summarized in Table 1, more detailed experimental procedures can be found in the supplementary materials. After obtaining the AgNPs, the particles were washed with deionized water by using centrifugal concentrators (Vivaspin 10 kDa) for at least ten times, to remove the residual organic compounds (Figure 1).



Figure 2-1: Images of the some samples (a) immediately after preparation (b) when washed using Vivaspin 10 kDa and (c) after washing. S mean sample Number.

Chapter 2: Green Synthesis of Silver Nanoparticles

Table 2-1: Protocols used for AgNPs preparation, more details can be found in the supplementary materials.

Sample Number	Volume of Silver in the Sample [mL] (Concentration: 0.001 M)	Volume of Plant Extract in the Sample [mL]	Other Conditions
1	10	0.6	The sample was diluted up to 10% ²³
2	5	10	Mixture was heated to 37 °C while stirring at 200 rpm for 72 h ⁸⁹
3	95	5	-
5	10	10	²⁷
6	9	1	Sample was stirred at 200 rpm ^{26, 30} for 48 h without heating
7	5	1	Sample was put it in a microwave oven for 5 to 15 min ⁹⁰
8	5	1	Sample was placed in the incubator (37 °C) for one hour ⁹⁰
10	50	2	³²
11	20	200	Sample was heated in a water bath at a temperature of 75 °C for one hour
12	5	30	Room temperature for 2 days
13	5	95	Sample was heated to 65 °C while stirring at 200 rpm for 6 h
14	15	1	Sample was heated to 37 °C while stirring at 200 rpm for 2 h
15	5	5	Sample was heated to 37 °C while stirring at 400 rpm for 2 weeks ³¹
16	5	15	Sample was heated to 60 °C while stirring at 700 rpm for 4–6 h
17	5	25	Sample was heated to 37 °C while stirring at 400 rpm for 2 weeks
18	5	30	Sample was heated to 37 °C while stirring at 400 rpm for 2 weeks
19	5 mL (Concentration: 0.01 M)	15	Sample was heated to 60 °C while stirring at 700 rpm for 4 h
20	5 mL (Concentration: 0.1 M)	15	Sample was heated to 60 °C while stirring at 700 rpm for 2 h

2.4.4 Diphenyl-2-picryl Hydrazyl (DPPH) Assay

Several aqueous solutions of AgNPs (10–400 µg/mL in deionized water) were prepared. Total of 100 µL of each solution was added to 300 µL of 0.004% ethanolic DPPH free radical solution and incubated for 30 min at room temperature under shaking condition. The absorbance was measured by a UV-VIS spectrophotometer (Thermo Fisher Scientific, Schwerte, Germany) at 517 nm; afterwards the results were compared with the corresponding absorbance of standard ascorbic acid concentrations (10–400 µg/mL).

Chapter 2: Green Synthesis of Silver Nanoparticles

2.4.5 2,2'-Azino-bis-(3-ethylbenzothiazoline-6-sulfonic Acid Radical Cation) (ABTS) Assay

ABTS solution (7 mM in water) was mixed with 2.45 mM potassium persulphate in a ratio of 1:1 (v/v). The mixture was placed in the dark at room temperature for 18 h. The ABTS•+ solution was diluted about 20 times with water to reach an absorbance of 0.850 ± 0.05 at 734 nm. About 150 μL of the diluted ABTS•+ solution was added to 50 μL of different concentrations of the AgNPs and incubated for 6 min at room temperature. For the control, 50 μL of deionized water was used in place of AgNPs. Ascorbic acid was used as a positive control. Absorbance at 734 nm was measured spectrophotometrically. The percentage of inhibition was calculated using the same formula as in DPPH assay and the radical scavenging activity of AgNPs is expressed as the IC₅₀ value.

2.4.6 Super Oxide Anion Radical (SO) Assay

The reaction mixture consisted of 50 μL Tris-HCl buffer (16 mM, pH 8.0), 50 μL NBT (nitroblue tetrazolium; 0.3 mM), 50 μL NADH (β -nicotinamide adenine dinucleotide, reduced disodium salt hydrate; 0.936 mM) and 100 μL of various concentrations of AgNPs in water. The reaction was initiated by adding 50 μL of PMS (phenazine methosulfate) solution (0.12 mM) to the mixture. The dissolved oxygen from the PMS/NADH coupling reaction reduces NBT to produce the superoxide anion. The reaction mixture was incubated at 25 °C for 5 min and the absorbance was measured at 560 nm against a blank sample. Gallic acid was used as a positive control and every sample was measured in triplicate to calculate the mean values and standard errors of mean (SEMs). By comparing the results of the test and the control, the percentage of inhibition was determined.

2.4.7 Cell Culture and Estimation of In Vitro Cytotoxicity of AgNPs

For cell culture experiments, HeLa, HepG2, and A549 (CLS Cell Lines Service GmbH, Eppelheim, Germany) cells were seeded and grown in Dulbecco's modified Eagle medium (DMEM) (Merck KGaA, Darmstadt, Germany) supplemented with 10% fetal calf serum (FCS) (Merck KGaA, Darmstadt, Germany) and 1% penicillin streptomycin (PS) at 37 °C in 95% O₂ and 5% CO₂. The cells were sub-cultivated, when the confluence reached almost 80%. The number of cells was calculated employing hemocytometer and suspended trypsinized cells. For Cell Titer Blue (CTB, Promega, Germany) cell viability test, cell suspension with concentration of 8×10^4 cell/mL was prepared and 100 μL of suspension was added to every well of the 96-well plate (VWR, Hannover, Germany), corresponding to 8000 cells per well. Plates were incubated at cell culture conditions as stated above for 24 h, then medium was removed from wells and 100 μL of different concentrations (0, 0.35, 0.7, 1.4, 2.77, 5.54, 11.07, 22.14, 44.28, and 88.56 $\mu\text{g/mL}$) of AgNPs dispersed in medium were added (four replicates per concentration). Control contained no AgNPs. Plates were incubated at the same conditions as stated above for cell culture for 2, 5, 8, and 24 h for HeLa and HepG2 and only 24 h for A549. After the incubation time specified for each sample, medium from control and AgNPs-containing media were removed, then 100 μL of prepared CTB solution (Promega, Cat. Number G8080, Walldorf, Germany) (1:10 (v/v) in basal medium) was added into every well, in order to indirectly evaluate cell viability (metabolic activity and relative cell number). As blank for the measurement, four completely empty wells were filled with Cell Titer Blue prepared solution, then the plates were incubated under the same conditions mentioned

Chapter 2: Green Synthesis of Silver Nanoparticles

previously for one hour. Current fluorescence was measured in every well in the plates using microplate fluorometer (544Ex/590Em) (Fluoroskan Ascent, Thermo Electron Corp, Waltham, MA, USA). The fluorescence of blank was subtracted from fluorescence of every concentration then relative cell viability was expressed as a percentage to positive control. The relative cell viability for every sample was commensurate with values of fluorescence and was calculated according to the following formula:

$$\text{Relative cell viability (\%)} = \frac{\text{Fluorescence of sample} - \text{Blank}}{\text{Fluorescence of control} - \text{Blank}} \times 100$$

Origin (Version 8.5) was used to calculate the half maximal inhibitory value (IC_{50}).

2.4.8 Characterization

The synthesis of the AgNPs in aqueous solution was monitored by recording the absorption spectra in a wavelength range of 300–700 nm using a Nano Drop ND1000 Spectrophotometer (Thermo Scientific, Wilmington, DE, USA). The hydrodynamic diameter of AgNPs was determined via DLS (Dynamic light scattering), and zeta potential and isoelectric point was measured using Zetasizer Nano ZS MPT-2 (Malvern, Worcs, United Kingdom). For Fourier transformed infrared (FTIR) measurements, samples were analyzed on a Bruker FTIR Vertex 80 v spectrometer (Billerica, MA, USA) which was operated at a resolution of 2 cm^{-1} , 32 scans in the region of $5000\text{--}370 \text{ cm}^{-1}$, ATR type platinum diamante A225 with evacuated to less than 1 hPa or without evacuating. Scanning electron microscopy (SEM) and energy-dispersive x-ray spectroscopy (EDXS) analyses were made on a field-emission instrument of the type JEOL JSM-6700F (Tokyo, Japan), which was equipped with and EDX spectrometer of the type Oxford Instruments INCA 300. Secondary electron (SE) imaging and EDXS were made at an acceleration voltage of 0.5 kV and 15 kV, respectively. X-ray diffraction (XRD) was performed on a Bruker D8 Advance diffractometer (Karlsruhe, Germany) using Cu-K α radiation ($\lambda = 0.154178 \text{ nm}$). Diffractograms were recorded in the 2θ range between 15° and 110° in steps of 0.008 degrees per second. Specimens were prepared as a thin film by dropping an aqueous solution of AgNPs onto a <911>-cut polished silicon crystal as support. Then, specimen was dried slowly in air. Alternatively, powder that was received after freeze drying of AgNPs colloidal solution was used. Transmission electron microscopy (TEM) and EDXS, were performed using a field-emission instrument of the type JEOL JEM-2100F-UHR (Tokyo, Japan), which was operated at an acceleration voltage of 200 kV. The microscope was equipped with an EDX spectrometer of the sort Oxford tool INCA 200 TEM. TEM analyses were performed in both, the image mode (bright field (BF), dark field (DF), high resolution TEM (HRTEM)) and selected area electron diffraction (SAED) mode. The nonexistence of preferred orientation was checked in SAED of the sample by tilting the sample inside the mechanical border of the goniometer ($\pm 19^\circ$ angle of inclination). In scanning TEM (STEM), high-angular dark-field mode was applied. We used Millipore water (resistance $> 18.2 \text{ M}\Omega \text{ cm}^{-1}$) (Sartorius, Goettingen, Germany) in all chemical reactions. Thermal gravimetric analysis (TGA) was done by using TGA/DSC 3+ from Mettler-Toledo (Giessen, Germany), from 25 to 1000°C at a rate of 0.5°C per minute with N_2 gas flow.

Chapter 2: Green Synthesis of Silver Nanoparticles

2.5 Results and Discussion

2.5.1 UV-VIS Absorption Studies

UV-VIS analysis is an important technique for verifying the formation of nanoparticles in colloidal solutions. Bioreduction of silver ions was visually clear from the color change. As St John's wort aqueous extract was mixed with silver nitrate, the color changed from pale light to yellowish brown and the final color was reddish-brown, which indicates the formation of AgNPs⁹¹. Various colors were obtained (according to the concentration of AgNPs in solution and their size). The change of the color arises as a result of surface plasmon vibrations in AgNPs^{25, 92-93}. Figure 2 shows the UV-VIS spectra for the different samples obtained with different biosynthesis conditions as summarized in Table 1. The change of absorbance at λ_{\max} is due to its dependence on the Ag NP concentration. The UV-VIS spectra showed the appearance of different absorption maxima between 392 nm and 460 nm, indicating the formation of silver particles with nanometer-sized dimensions. According to Figure 2, the peak for sample 16 (Table S1, supplementary materials) is sharp and high, while for some other samples (like 15, 17, 18, and 19) the peak is broad and less intense. Also there are broad peaks with low intensity (like for samples 1, 11, 3, and 14, Table S1, supplementary materials); also other peaks are barely detectable (like for samples 8, 10, 13, and 14). The broadening of peaks for some samples indicates that the nanoparticles were aggregated or the nanoparticles were polydisperse. The spectra of sample 16 shows a narrow SPR band with a maximum at 442 nm indicating the formation of uniform spherical nanoparticles (monodisperse AgNPs), which is further confirmed by the TEM images (Figure 6). After comparison of the different protocols summarized in Table 1 we found that protocols 15–20 gave the best results in UV-VIS, DLS and zeta potential but protocol 16 resulted in highest quality (in terms of size, shape and dispersion), yield, and purity of AgNPs, because other samples (15 and 17–20) contain other substances in addition to silver, such as calcium and silver oxide and yield of AgNPs was low compared to sample 16 as shown by XRD (Figure 10), EDX, and AAS analyses. Various temperatures have been investigated for protocol 16, plant extracts were heated to different temperatures (70, 80, and 91 °C) and silver nitrate was added to it, either at once or drop-wise. It was observed that at elevated temperature silver nanoparticles were produced faster, but particle size was bigger than for particles synthesized at 60 °C.

2.5.2 Measurement of Concentration through Absorption Peak in UV-VIS Spectrum

Beer–Lambert Law was employed to calculate the AgNPs concentration as follows:

$$A = \varepsilon \times l \times c$$

A is absorbance, ε is size dependent molar extinction coefficient ($M^{-1} \text{ cm}^{-1}$), c is the concentration, and l is the length of the cuvette. The concentration was calculated by using the absorption values obtained for our different samples, $L = 1.0 \text{ cm}$, and the values of ε molar absorption coefficient (extinction coefficient, molar Abs) were taken from reference⁹⁴, assuming that the nature of the protection layer on the surfaces of nanoparticles does not affect the value of this coefficient. All the details and results are found in Table S1 (supplementary materials).

Chapter 2: Green Synthesis of Silver Nanoparticles

Calculated concentrations were highest for samples 15, 16, 17, 18, 19, and 20. Consequently, all further studies were performed with samples which give high concentrations of AgNPs to identify the best synthesis in terms of size, size distribution, and quality of prepared nanoparticles.

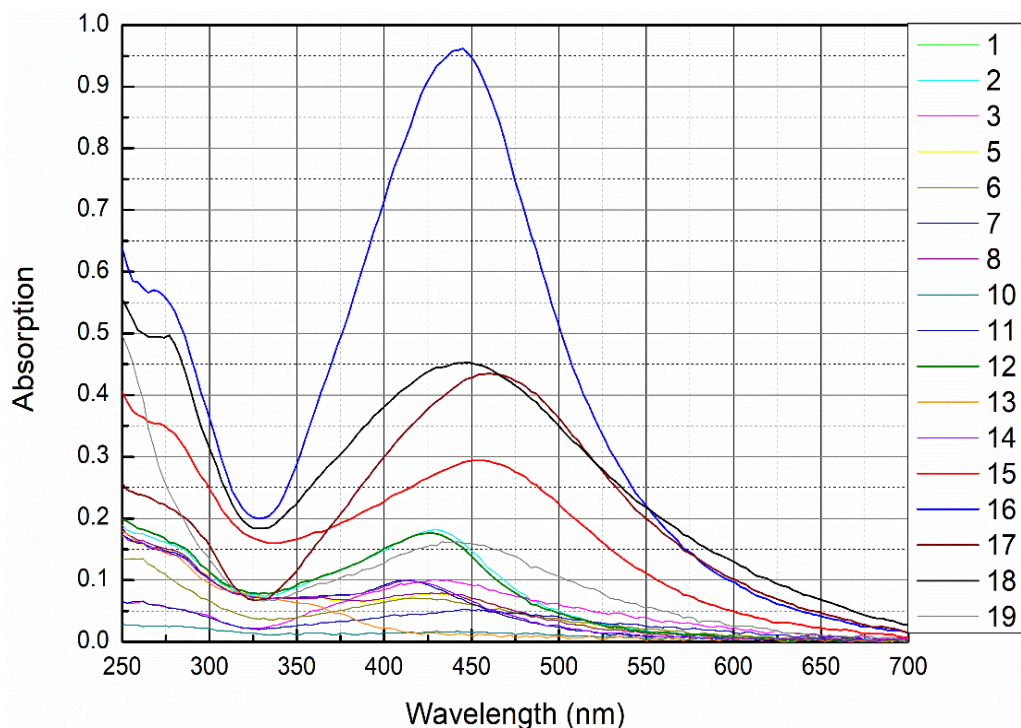


Figure 2-2: UV-VIS spectra of AgNPs synthesized with varying amounts of AgNO_3 and different amounts of plant extract (numbers refer to the sample number shown in Table 1).

2.5.3 Dynamic Light Scattering (DLS)

The size determined via DLS technique is the hydrodynamic diameter of the theoretical sphere, which diffuses at the same speed as the measured nanoparticle. Figure 3 shows the particle size distribution of the best samples of AgNPs. It was found that the AgNPs size was in the range of 44–112 nm. Hydrodynamic diameter for other samples are summarized in Table S2 (supplementary materials). A thin electric dipole layer of the solvent is adsorbed at the surface of nanoparticles when these particles are dispersed in solutions. This layer affects the motion of particles in the solutions, so the hydrodynamic diameter describes the metal core with any stabilizer substance and the solvent layer. Thus DLS measures the size of nanoparticles with the solvent molecules attached at its surface. In colloidal solutions when one layer of stabilizer (protective or capping agent) adsorbed at the surface of nanoparticles, the diameter increases, and commonly multiple layers of stabilizers and water molecules are present. Therefore, the protective layer and the interaction with the solvent molecules are taken into account in DLS measurements. The hydrodynamic diameter depends on different factors like the electrical conductivity of the solution, intensity (intensity diameter distribution may therefore inherently be weighted to bigger diameter than number distribution, due to the fact that the scattering intensity is proportional to size^6), concentration (multiple scattering causes bigger diameter). The presence of multiple scattering at some concentrations can cause large errors in the measured average hydrodynamic size of the AgNPs. Using the same device, zeta potential was

Chapter 2: Green Synthesis of Silver Nanoparticles

measured. The surface charge is beneficial for determining the stability of colloidal solution (Figure S1, supplementary materials). The average zeta potential value is -18 mV to -34 mV. The high negative potential is associated with high stability, high colloidal quality, and good dispersion of AgNPs as a result of electrostatic repulsion.

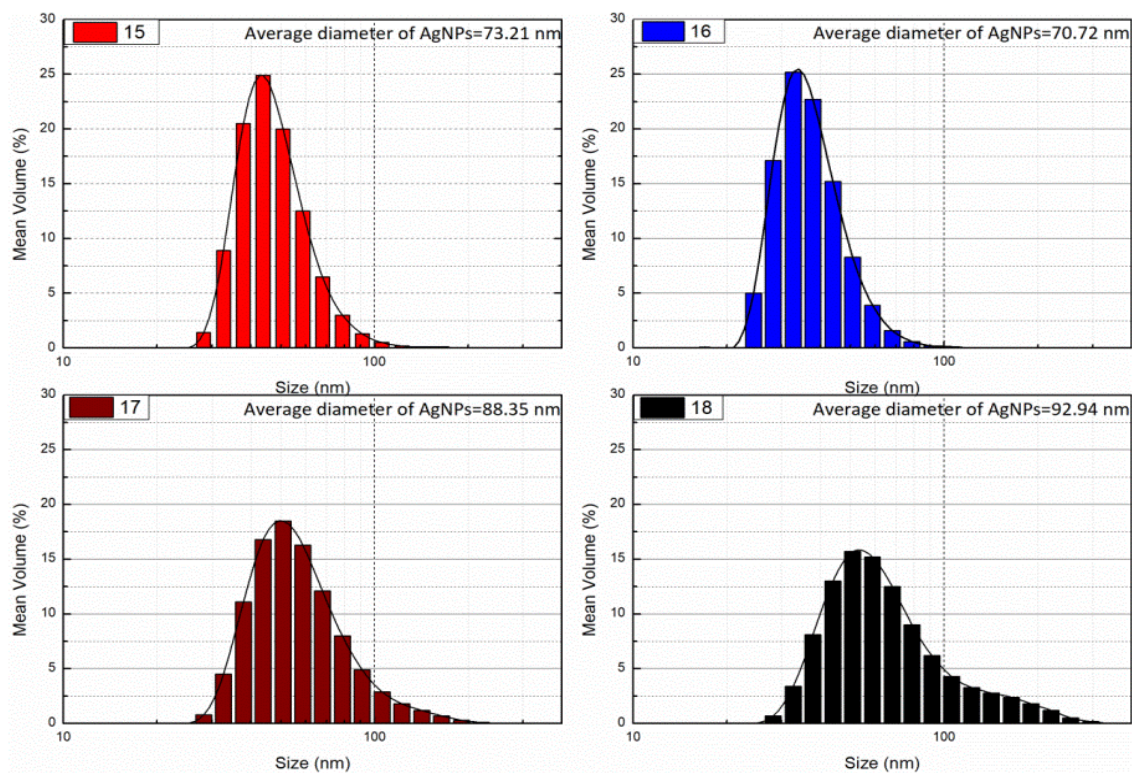


Figure 2-3: DLS analysis of AgNPs, hydrodynamic diameter of selected samples.

2.5.4 Fourier transformed infrared (FTIR) Spectroscopy

FTIR spectroscopy was used to prove the existence of an organic compound layer on the surfaces of the nanoparticles and to obtain knowledge of the functional groups on the surface of nanoparticles. AgNPs were examined by thermo-gravimetric analysis (TGA) to prove the existence of organic compounds from *H. Perforatum* extract at the surfaces of silver nanoparticles (Figure S3, supplementary materials). FTIR spectroscopy confirmed the existence of biological components surrounding the AgNPs as a stabilizer. However, due to the complexity of the used plant extract and the fact that most likely more than one substance is adsorbed on the surface of the AgNPs (The detailed composition of the plant extract, the concentration of individual substances, and determination of phytochemicals adsorbed as a protective layer on the surface of AgNPs are currently under investigation and will be included in a follow-up manuscript), interpretation of the FTIR spectra is difficult. The FTIR spectra for AgNPs obtained with *Hypericum perforatum* L. extract are shown in Figure 4. The major peaks of the spectra were assigned to their chemical constituents as summarized in Table S3, supplementary materials. Biomolecules and secondary metabolites originating from the plant extract promote the stability of AgNPs by electrostatic and steric effects. Hydroxyl groups of the biomolecules in St John's wort, enhance the stability of AgNPs. The hydroxyl-containing biomolecules are protecting the particles for longer periods. Interestingly, the bond vibrations of hydroxyl group (3335 cm^{-1}) for AgNPs capped with biomolecules from plant extract lost

Chapter 2: Green Synthesis of Silver Nanoparticles

some of their intensity and had a red shift (to 3338 cm^{-1}) compared to the same peak of plant extract alone (Figure 4b). This mainly happened because of the exploitation of hydroxyl groups in the capping and protective action around AgNPs.

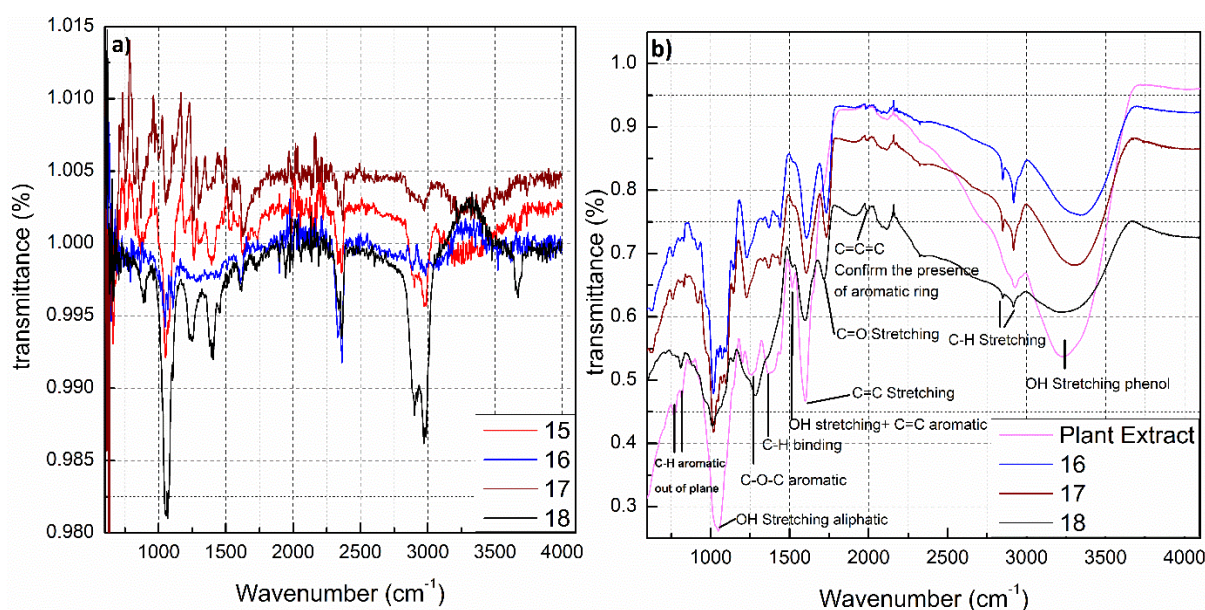


Figure 2-4: ATR spectra of AgNPs synthesized with *St John's wort* extract obtained using a Bruker FTIR Vertex 80 v spectrometer apparatus, (a) without vacuum and (b) with vacuum.

2.5.5 Scanning Electron Microscopy (SEM)

SEM was used to characterize the morphology, size, and size distribution of AgNPs. Samples were prepared by placing the colloids onto a clean polished carbon holder. Afterwards all water was completely evaporated. From Figure 5 it is obvious that the nanoparticles are spherical in shape and exhibit narrow size distribution with a size varying between 20 and 60 nm.

2.5.6 Transmission Electron Microscopy (TEM)

TEM images show that the AgNPs are well dispersed and predominantly spherical in shape (Figure 6) with a narrow size distribution which corresponds to the shape of UV-visible spectra. The AgNPs sizes corresponds to that calculated from DLS histogram (Figure 3) with an average diameter of about 20–50 nm. Some agglomerates can be observed, which might be formed during sedimentation within the washing process. The average size estimated was 40 nm for sample 16. In contrast to DLS, the diameter determined by TEM does not include any hydration layer, so with TEM the metal core size is measured. The energy-dispersive X-ray (EDX) spectra were studied from SEM and TEM apparatuses (Figure 7 and Figure S4, supplementary materials). EDX spectra show the presence of silver as an element and strong signals from atoms in the nanoparticles affirm the reduction of silver ions into silver metal. The AgNPs show an optical absorption band peak at 2.8 keV, 3.5 keV, and 3.8 keV corresponding to the binding energies of Ag-L, Ag-M, which are typical for the γ -absorption of metallic AgNPs. The presence of oxygen and carbon clearly shows that an organic layer is present on the surface of AgNPs. Detected phosphorus originate from the used TEM device and Cu signal is due to high-resolution pole piece and Cu-based TEM grid and does not belong to the specimen. Also, we have identified the amount of oxygen in two different positions (one with

Chapter 2: Green Synthesis of Silver Nanoparticles

AgNPs, one without AgNPs); the percent of oxygen was same, which shows that prepared AgNPs consist of silver and do not contain silver oxides; (see Figures S5 and S6 in the supplementary materials).

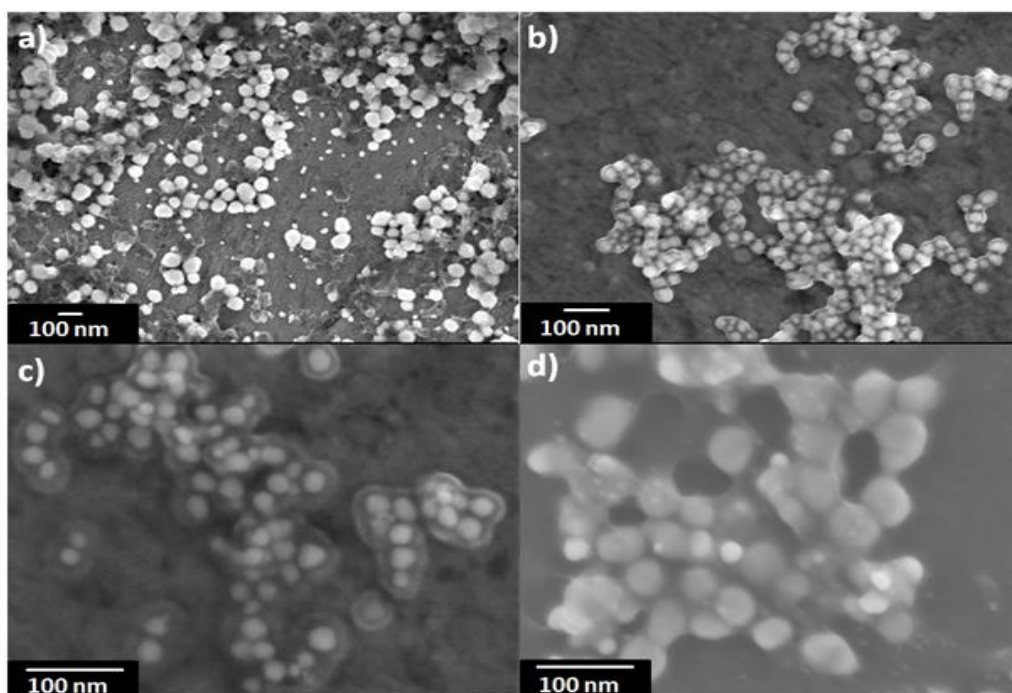


Figure 2-5: SEM images for the sample 16 at different magnifications, (a) 50,000 \times , (b) 100,000 \times , (c) 200,000 \times , (d) 220,000 \times .

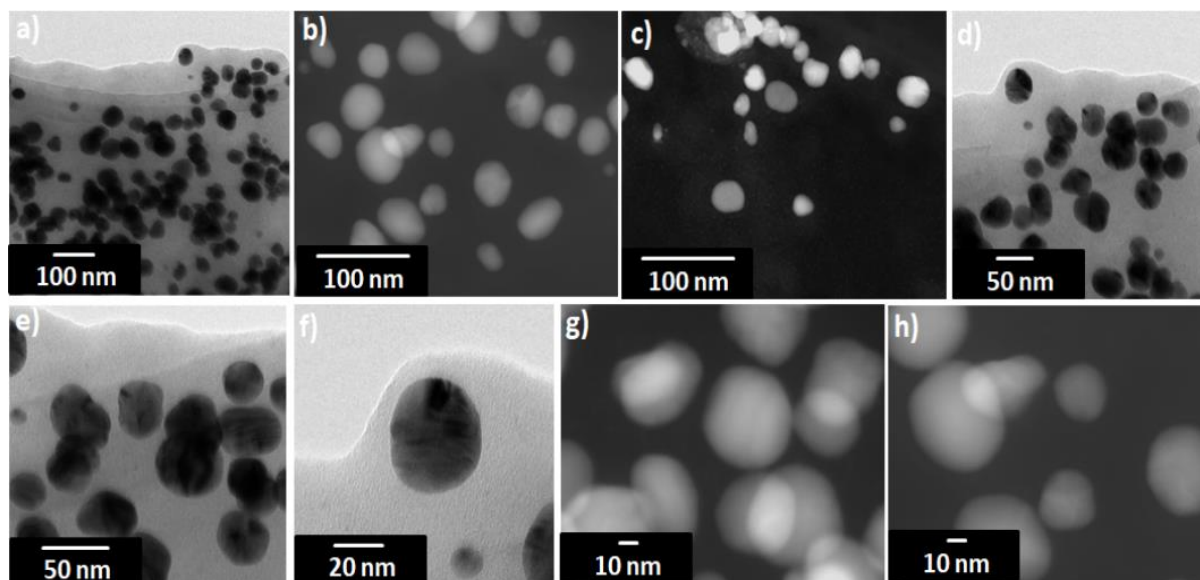


Figure 2-6: TEM images for the sample 16 at different magnifications. (a,d) Bright-field transmission electron microscopy (BF-TEM), (b,c,g,h) scanning transmission electron microscopy dark-field (STEM-DF) and (e,f) high resolution transmission electron microscopy (HRTEM).

Chapter 2: Green Synthesis of Silver Nanoparticles

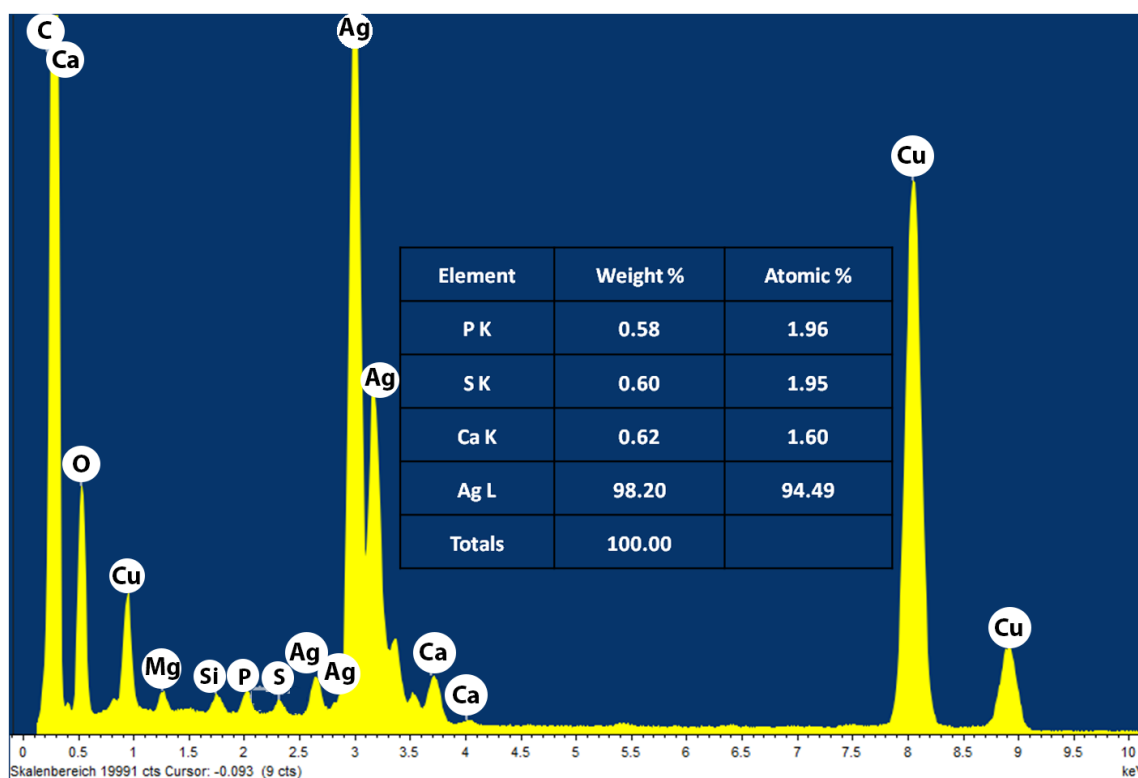


Figure 2-7: TEM-EDXS analysis of the sample 16 of AgNPs.

2.5.7 High-Resolution Transmission Electron Microscopy and Nano-Diffraction Patterns

Selected area electron diffraction patterns (SAED) recorded on the regions Figure 8a,c are presented in Figure 8b,d. The observed Debye-Scherrer rings are completely enclosed, indicating the Ag nanostructure is highly crystalline in nature (see more explanation about SAED in supplementary materials). The rings change from continuous to dotted as the size of the polycrystalline grains increases. When the size of the grains is too small or the material is completely amorphous, the concentric rings disappears and leaves a halo just around the bright spot in the center, which shows that the electrons are diffracted randomly from the material of the amorphous structure. If the grains in the sample are oriented in a preferred direction, the SAED pattern shows that many rings are partial. If the sample is amorphous, diffuse rings will be obtained, while crystalline samples will result in bright spots, and if the sample is polynanocrystalline (small spots making up a rings, each spot arising from Bragg reflection from an individual crystallite) ⁹⁵⁻¹⁰⁰. We calculated the d-values (the spacing between lattice planes) and by comparing this value with d-value of different phases of silver in literature, we can identify the type of crystal lattice. For the first three rings (from inside to outside of the central ring) in the SAED images (Figure 8b,d) these values correspond to (111), (200), (220) planes of face-centered cubic (fcc) structure of elemental silver ¹⁰. Figure 9 shows the HRTEM images for sample 16 and the corresponding Fourier spectra (equivalent to optical diffraction patterns), that were obtained by fast Fourier transformation (FFT) process for HRTEM images.

FFTs were used for better understanding of the nanoparticles orientation in relation to an electron beam. These orientations are suggested in the insets. Figure 9 clearly indicates the crystalline nature of AgNPs by very well separated individual lattice fringes (the spacing of 2.4

Chapter 2: Green Synthesis of Silver Nanoparticles

and 2.5 Å corresponds to the lattice spacing of (111) plane of pure silver and the spacing of 2.0 Å corresponds to the lattice spacing of (200) plane of pure silver). It must be noted that the planes (111) were a little distorted where its value is 2.4 Å compared with bulk value 2.35911 Å as exhibited in FFT pictures for these nanoparticle. Therefore, there is a distortion in the particle of about 2% and 6% (expansion) along the directions ¹⁰¹.

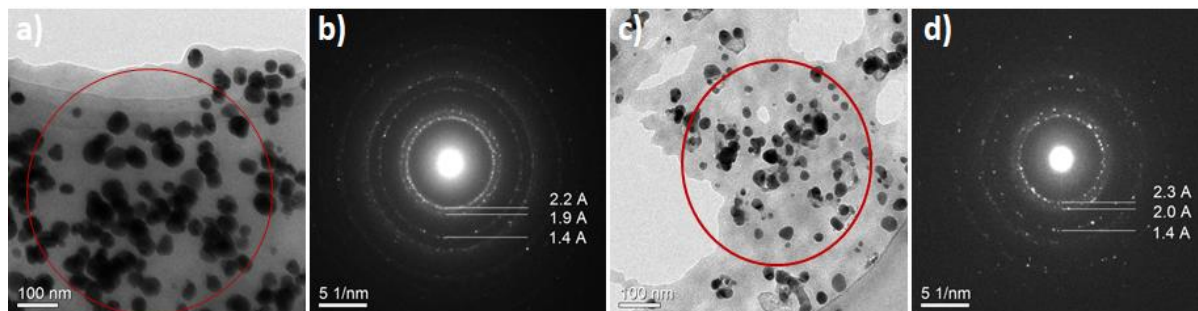


Figure 2-8: (b,d) Selected area for electron diffraction (SAED) patterns showing rings corresponding to the crystal planes of AgNPs structure. (a,c) Bright-field transmission electron microscopy (BF-TEM). The SAED patterns recorded at nominal camera length 1000 mm.

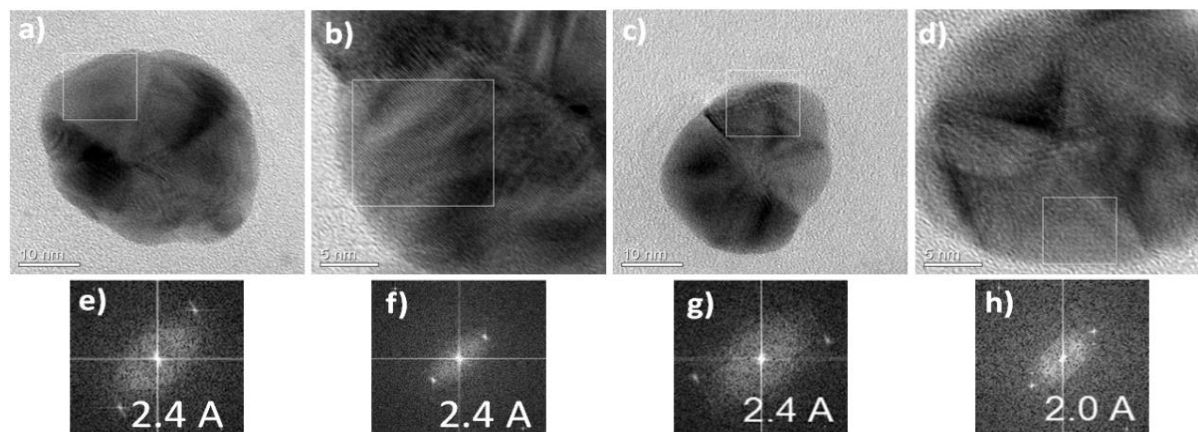


Figure 2-9: (a–d) High resolution transmission electron microscopy (HRTEM) images in different orientations of AgNPs from sample 16 and (e–h) the corresponding characteristic fast Fourier transformation FFTs. this figure shows clearly the crystalline nature of AgNPs through the fully isolated solo lattice fringes (the spacing of 2.4 Å is compatible with the lattice spacing of plane (1 1 1) of pure silver and spacing of 2 Å is compatible with the lattice spacing of plane (2 0 0) of pure silver).

2.5.8 X-ray Diffraction (XRD)

The X-ray diffraction pattern of AgNPs synthesized by using *Hypericum perforatum*.L as a reducing and capping agent is shown in Figure 10. Indexing process of powder diffraction pattern was carried out and Miller indices ($h k l$) for each peak were determined (Table 2). A number of strong Bragg reflections were observed at 2θ of 38.2461° , 44.4345° , 64.596° , 77.5785° , and 81.7060° (for sample 16 at different times; when repeating the experiment always with the same conditions). These diffraction peaks correspond to the (111), (200), (220), (311), and (222) planes of AgNPs, and confirm the face-centered cubic (fcc) lattice structure of the biosynthesized AgNPs (JCPDS: File No. 03-065-2871). We did not find any unexpected diffractions and this proves that there are no crystalline impurities ¹⁰². All the reflections off the sample 16 agree with fcc structure of pure silver. In materials mono-atomic fcc structure, the strongest reflection should be from (111) plane. This is clearly observed in our sample No.

Chapter 2: Green Synthesis of Silver Nanoparticles

16. So we can conclude that the degree of crystallization and purity of AgNPs is very high. The diffraction peaks are broad indicating that the size of the crystals is small ¹⁰³. The lattice parameter or unit cell edge (a) is 4.07 Å (JCPDS file no.04-0783) for materials which have fcc crystal structure. Using the equation ¹⁰⁴:

$$a = d \times \sqrt{h^2 + k^2 + l^2}$$

We calculated the experimental lattice constant from the peaks (111), (200), (220), (311) and (222) in the XRD pattern and it was 4.07 Å (Table 2), which means that both, theoretical and experimental values are identical.

Table 2-2: Calculation of Miller indices and lattice constant for sample 16 from diffraction angles.

2θ (o)	Sin 2θ	Sin 2θ/Sin 2θ for the First Peak	(Sin 2θ/Sin 2θ for the First Peak) × 3	(h ² + k ² + l ²)	(hkl)	Sin 2θ / (h ² + k ² + l ²)	d (Å)	a (Å)
38.2461	0.1073	1	3	3	111	0.036	2.3531	4.07
44.4345	0.14297	1.332	3.996	4	200	0.036	2.0387	4.07
64.596	0.28551	2.661	7.983	8	220	0.036	1.4427	4.07
77.5785	0.39245	3.658	10.974	11	311	0.036	1.2306	4.07
81.7060	0.42787	3.988	11.963	12	222	0.036	1.1785	4.07

Here it should be noted that the ratio between the intensities of the (200) and (111) diffraction peaks is slightly less than the theoretical value (Table 3). While this value for plane (220) ranges from smaller to larger than conventional value and it is also for the two planes (311) and (222). This can be attributed to the effect of “preferred orientation.” Besides the signature “broadening” due to the nano-size of the particles, we should also see the contribution due to preferred orientation.

Table 2-3: Ratio between the intensities of the diffraction peaks for sample 16.

Diffraction Peaks	Sample Value	Theoretical Value
(200) and (111)	from 0.24 to 0.38	0.45
(220) and (111)	from 0.19 to 0.35	0.24
(311) and (111)	From 0.15 to 0.25	0.25

Determination the particles size of the AgNPs for many samples from Debye-Scherrer’s Equation are calculated (Table S4, supplementary materials). The calculated crystallite size of as-prepared Ag-NPs (~24–27 nm) for sample 16 is compatible with the values obtained from SEM and TEM. The crystallite size of Ag-NPs for sample 16 (~10–15 nm) is rather small compared to the average nanoparticle size estimated from SEM and TEM analysis (~25–40 nm), suggesting that there are small nanocrystals in the multiple twined AgNPs. As a result of the crude nature of St. John’s wort extract, it may also contain ions, salts, and metabolites. These ions were reduced during the reaction to get other metals like calcium (Ca) (Figure 10b). In other cases, silver ions may oxidize in the medium of the reaction to obtain silver oxide as is the case in the sample 20 (Figure 10c).

Chapter 2: Green Synthesis of Silver Nanoparticles

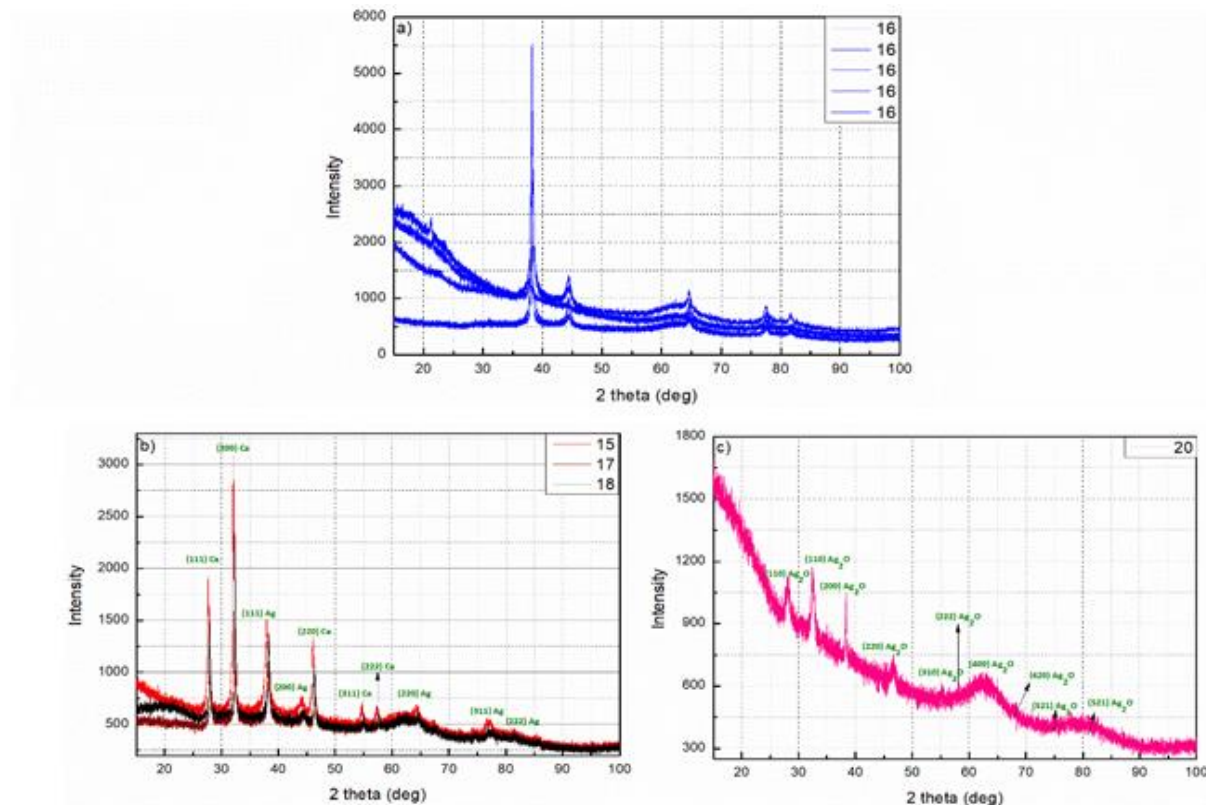


Figure 2-10: XRD diffractograms for different samples, (a) for sample 16 at different periods, (b) for samples 15, 17 and 18 which clearly show the formation of calcium with silver in the solution, (c) for sample 20 which clearly show the formation of silver oxide.

2.5.9 Possible Mechanism of Biosynthesis of Silver Nanoparticles by Plant

In the past years, researchers focused on the synthesis of nanoparticles by green methods, because these methods have a lot of advantages which have been mentioned earlier. One of the most commonly used green methods is using plant extracts. The important question in this case is: Which molecules or substances in the plant extract play a role as a reducing and protective agent? Many compounds (secondary metabolites or photochemicals) were identified, which effectively reduce silver ions and stabilize silver nanoparticles: polyphenols (flavonoids, catechin, phenylpropanes, phenolic acids, anthocyanins, proanthocyanidin, taxifolin, flavones and biflavones), alcoholic compounds, organic acids (tartaric, ascorbic, protocatechuic, oxalic, and malic acid), mono and polysaccharides, amino acids, terpenoids, quinones, antioxidants, glutathiones, and alkaloids (see Table S5, supplementary materials). As seen in Figure 11 and Table S5 (supplementary materials), polyphenols and flavonoids are the most common compounds which have been revealed to be involved in the green synthesis of AgNPs. The extract of aerial parts from *Hypericum perforatum* L. is rich in polyphenolic compounds (Figure 11) and contains six major bioactive natural products groups: (1) naphthodianthrones (such as hypericin and pseudohypericin), (2) phloroglucinols (such as hyperforin and adhyperforin), (3) flavonoids (such as quercetin, rutin, quercitrin and kaempferol), (4) biflavones (such as 3,8'-biapigenin and amentoflavone), (5) phenylpropanes (such as chlorogenic acid and caffeic acid), and (6) proanthocyanidins (such as dimeric procyanidin B2 and trimeric procyanidin). In addition, there are some amounts of tannins (such as proanthocyanidins), xanthenes (such as 1,3,6,7-tetrahydroxyxanthone and kielcorin), essential

Chapter 2: Green Synthesis of Silver Nanoparticles

oils (hydrocarbons and long chain alcohols), and amino acids (such as α -aminobutyric acid) (Figure 11)^{77, 105-106}. Currently there is no literature available describing the mechanism for the metabolites reduction and stabilization of AgNPs. The biomolecules existing in the *Hypericum perforatum* L. extract (such as flavonoids, hypericins, hyperforins, mono- and polysaccharides, phenolic acids, etc.) interact with silver ions and convert them into nanoparticles. The mechanism of AgNPs formation consists of mainly three steps: reduction of ions to get metal atoms, clustering of some atoms resulting in small clusters (Figure 12b), and growing of these clusters and protection of formed NPs by capping agent to prevent aggregation (Figure 12). All of these steps depend on precursor concentration (AgNO_3), the concentration of reducing and stabilizing agent in the plant extract, pH of medium, temperature and stirring speed¹⁰⁷.

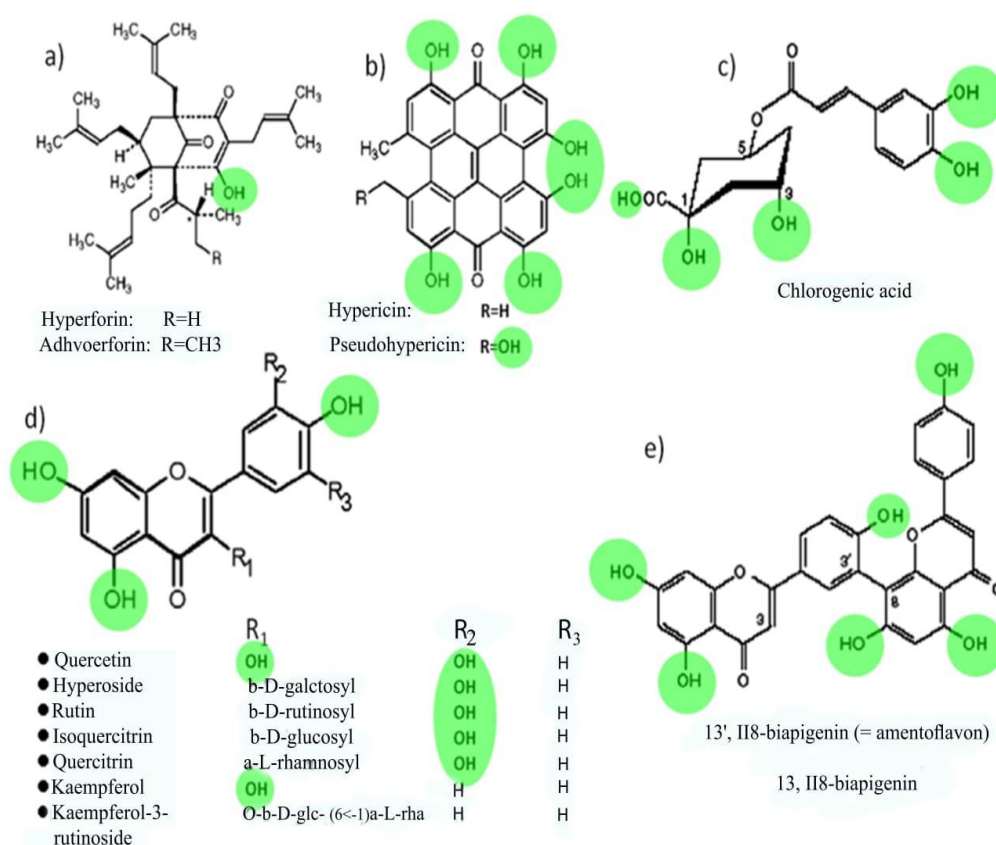


Figure 2-11: The most important constituents of *Hypericum perforatum* L. (a) represent general formula of Hyperforins, (b) Hypericins, (c) chlorogenic acid, (d) Flavonoids and (e) Biflavones

Chapter 2: Green Synthesis of Silver Nanoparticles

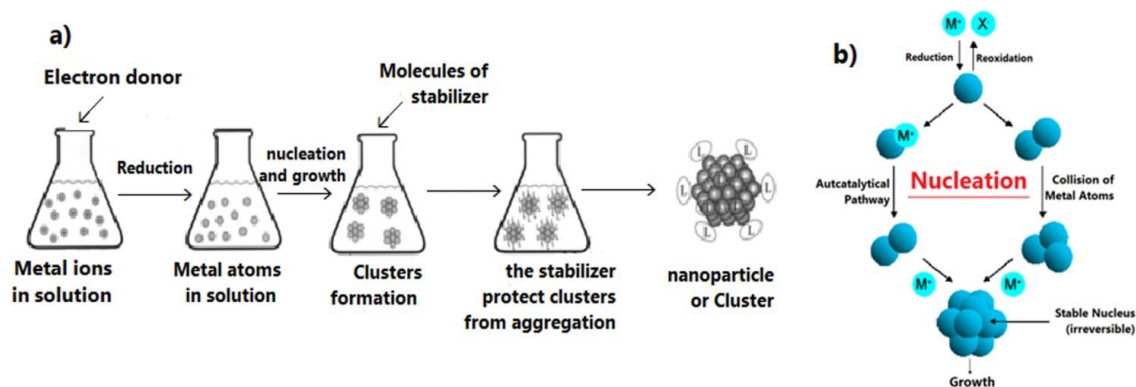


Figure 2-12: Simplified scheme shows (a) the stages of the formation of nanoparticles that are stable and protected from aggregation, (b) formation of small clusters and their growth (nucleation and growth).

The -OH groups present in polyphenols compounds in *H. perforatum* L. such as flavonoids may be responsible for the reduction of silver ions to AgNPs¹⁰⁸. It is possible that the tautomeric transformation of these compounds from enol to keto form releases a reactive free electron which reduces silver ions to metallic silver¹⁰⁹. Our data shows that molecules from *H. perforatum* L. extract were responsible for the stabilization of the AgNPs, as FTIR spectra of both, AgNPs and *H. perforatum* L. extract, demonstrated the presence of similar functional groups. Stabilizing biomolecules often contain more than one potential bidentate binding sites that can produce protons such as quercetin: α -hydroxy-carbonyl, β -hydroxy-carbonyl, and catechol having two hydroxyl groups in ortho positions, can produce two protons which can react with nitrate anions, i.e., one molecule of quercetin reduces two silver ions¹¹⁰⁻¹¹¹. *H. perforatum* L. contains a large amount of polyphenols (phytochemicals or secondary metabolites) which have hydroxyl and ketonic groups. These compounds that have an hydroxyl group linked to carbon atoms in the aromatic ring react with silver ions as acid and reduce Ag ions to Ag metal in the nano size and protect it from aggregation (i.e., the crystals of Ag start to appear and grow from metallic Ag after the supersaturation of hydroxyl complexes Ag-OH)¹¹²⁻¹¹³. The process continues until the specific growth of all the silver crystal planes, i.e., the stabilizer from the extract will inhibit the growth of high-energy atomic planes. These AgNPs are found in high surface-energy state and tend to turn into their low-surface energy form by aggregating with each other, so the biomolecules from *H. perforatum* are attracted toward the higher-energy crystallite planes and function as protective agent to hamper the growth. Thus, the existence of higher concentrations of reducing and protective agents inhibits the aggregation of nanoparticles and results in smaller size of AgNPs. Figure 13 showed the proposed mechanism of biosynthesis of AgNPs by using *H. perforatum* L. as a reducing and protective agent. Quercetin was used as an example because many of the phytochemicals present in this plant extract have a chemical structure similar in terms of the presence of hydroxyl groups associated with aromatic rings. The phytochemicals that act as a reducing agent are not necessarily the same which play a role as protective agents.

Chapter 2: Green Synthesis of Silver Nanoparticles

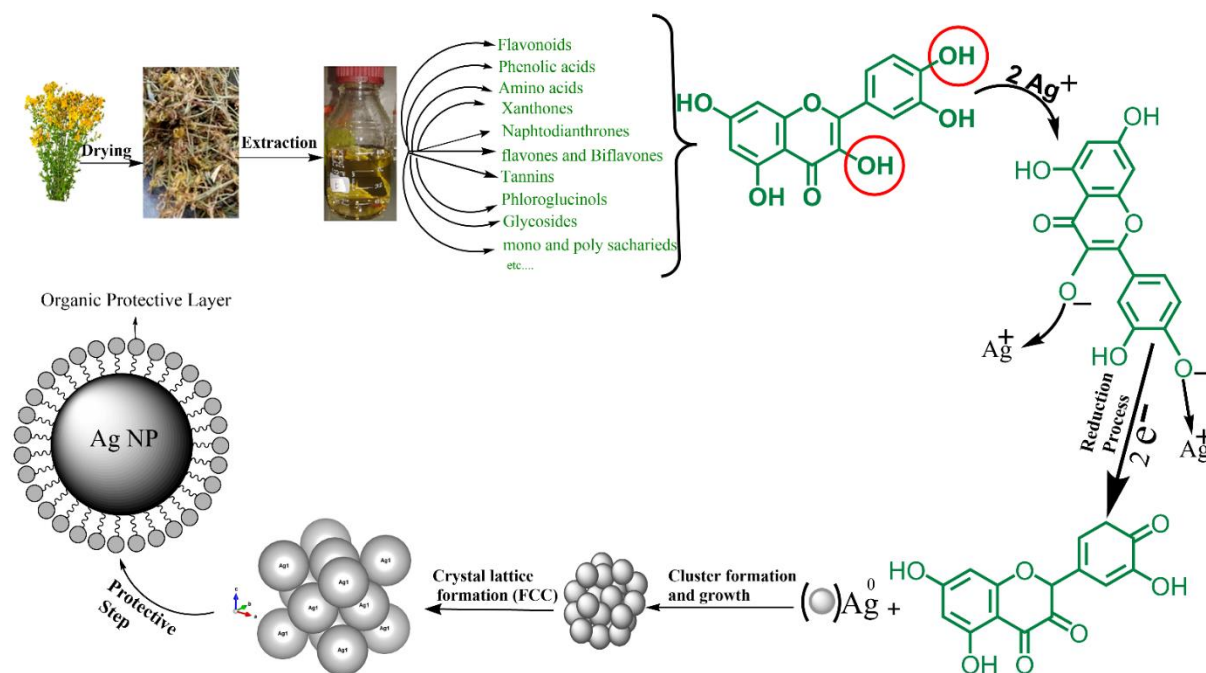


Figure 2-13: Scheme represents the proposed mechanism of green synthesis of AgNPs from *Hypericum perforatum L.* (quercetin was used as an example, because many of the phytochemicals or secondary metabolites present in this plant extract have a chemical structure similar to the chemical structure of quercetin in terms of the presence of hydroxyl groups associated with aromatic rings). These organic compounds reduce silver ions to silver metal, and when small clusters form and grow, the organic compounds are placed on the lattice planes to force them to grow in specific directions in order to obtain a certain crystal lattice (face centered cubic fcc in our case). At the same time, they prevent the aggregation of the nanoparticles and promote the production of smaller NPs.

2.5.10 Determination of Antioxidant Activity

Several abiotic stresses lead to the overproduction of highly toxic and reactive oxygen species (ROS). These reactive oxygen species are known to cause damage to DNA, carbohydrates, proteins and fats, build oxidative stress and lead to the induction of various diseases. Nanomaterials and especially AgNPs represent promising candidates in the search for enhanced antioxidants. It has been shown that silver nanoparticles have the capacity to reduce oxidative stress due to their effective redox-active radical-scavenging properties. Moreover, the used plant extract contains bioactive phytochemicals like polyphenols. These bioactive components could display potential antioxidant activity. Since the silver nanoparticles presented here are synthesized using plant extracts, this can result in enhanced antioxidant activity and thus open exciting possibilities for the development of superior antioxidants. Antioxidant testing methods are different and it is difficult to compare one method to another. Therefore the total capacity of the antioxidant cannot be assessed on the basis of a single antioxidant test form, so use of combination of various tests is always useful.

2.5.10.11-1,1-Diphenyl-2-picryl Hydrazyl Assay

The antioxidant activity of AgNPs was measured with regard to their scavenging activity of the stable 1, 1-diphenyl-2-picryl hydrazyl (DPPH) free radical. DPPH is commonly used to detect the scavenging capacity against radicals in the chemical assay. DPPH is a renowned radical and a snare to other radicals (scavenger). The inhibitory concentration 50% (IC_{50}) was determined from calibration curves, obtained from different concentrations of the different

Chapter 2: Green Synthesis of Silver Nanoparticles

AgNPs. In the present study, AgNPs showed potential free-radical scavenging activity, this means that AgNPs were able to reduce the stable, purple-colored radical, DPPH into the yellow-colored DPPH. In Figure 14a, the IC₅₀ values are presented. AgNPs showed an IC₅₀ value of 35.88 µg/mL which was near that of standard ascorbic acid (IC₅₀ = 35.44 µg/mL) (Figure 14a). This demonstrates higher effectiveness of investigated AgNPs when compared to others described in the literature¹¹⁴⁻¹¹⁸. AgNPs exhibited scavenging average ranging from 30.47% to 76.63%, at concentrations 10–100 µg/mL. This indicates that the resulting activity of the AgNPs is not only attributed to the nanosize, but it is further enhanced by the protective agents (chemical constituents originating from the extract). The protective layer at the surface of AgNPs may include acid, sugars, hydroxyl-phenolic and phenolic compounds, flavonoids and others, which may be an additional source of the antioxidant activity.

2.5.10.22-2,2'-Azino-bis-(3-ethylbenzothiazoline-6-sulfonic Acid Radical Cation Scavenging Assay (ABTS))

ABTS antioxidant activity was measured as described by S. Chanda et al.¹¹⁹ with some minor modifications, as described in the methods section. An inhibition of 27.7–92.6% was obtained in the concentration range of 10–100 µg/mL (Figure 14b). By increasing the concentration of AgNPs, the ABTS cation radical scavenging activity significantly increases, while at concentrations above 100 µg/mL no further increase could be observed. The IC₅₀ value of AgNPs was 26.78 µg/mL, which was near that of standard ascorbic acid (IC₅₀ = 23 µg/mL). This indicates that AgNPs prepared with our method inhibit cation radicals more effectively than AgNPs prepared by other biological methods^{115, 117, 120-121}.

2.5.10.3 Super Oxide Anion Radical Scavenging Assay (SO Assay)

Superoxide anions are extremely grave radicals and if not put down will cause the formation of other risky radicals such hydrogen peroxide (H₂O₂), peroxy (ROO[·]), hydroxyl (OH[·]), superoxide (O₂^{·-}), singlet oxygen (O₂¹), nitric oxide (NO[·]), peroxynitrite ([·]ONOO), and cyanide (CN[·]). Superoxide causes the generation of vigorous and dangerous hydroxyl radicals and singlet oxygen, which both contribute to oxidative stress. Results of the superoxide anion radical scavenging activity of AgNPs and gallic acid are given in Figure 14c. As shown in the figure, the quenching of super oxide radicals increase with increasing the concentration of AgNPs. AgNPs at concentrations 10–400 µg/mL showed scavenging ranging from 29% to 93% (Figure 14c). The IC₅₀ value of AgNPs was 27.77 µg/mL while that of gallic acid (the standard in this assay) was 94 µg/mL indicating that the superoxide anions scavenging ability of AgNPs is much better than that of gallic acid. Superoxide radical scavenging activity of investigated AgNPs was higher as described in the literature for AgNPs synthesized by other methods^{115, 117, 120, 122-127}.

Chapter 2: Green Synthesis of Silver Nanoparticles

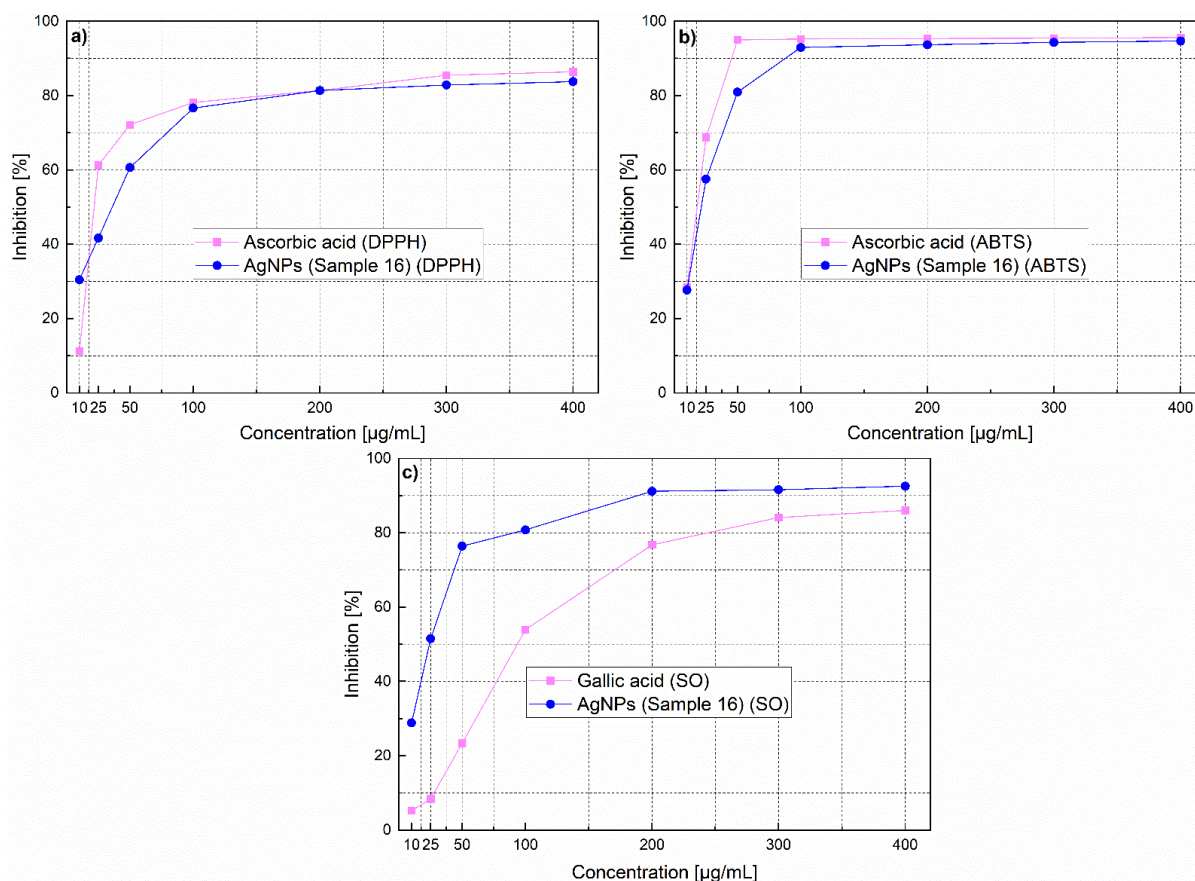


Figure 2-14: Antioxidant activity of AgNPs (a) DPPH free radical scavenging activity, (b) ABTS radical scavenging activity and (c) superoxide anion radical scavenging activity.

2.5.11 Determination of Time- and Dose-Dependent Cytotoxicity of Biosynthesized AgNPs

In CTB test for evaluation of the cell viability, viable cells turn blue resazurin into pink resorufin generating a fluorescent signal, while nonviable cells cannot do that because they lost their metabolic activity. Both, the influence of exposure time, and AgNPs dose were studied. The time ranged between 2, 5, 8 and 24 h, and the dose range of AgNPs synthesized utilizing St John's wort extract was between 2.5 µg and 88 µg/mL. The range of viability observed for HeLa cells, Hep G2 cells, and A549 cells are shown in Figure 15a–c respectively. Actually and as evident from Figure 15, by increasing the concentration of AgNPs, cell viability of the three cell types studied in this research significantly decreased. For Hela cells, no difference in cell viability was observed for different exposure times (2, 5, 8, and 24 h), but for the HepG2 cells, the effect depends on the exposure time.

A549 cells were studied only after 24 h exposure to AgNPs. Distinctly, the cell viability significantly dropped by about more than 90% at low AgNPs concentrations in a range of 11–20 µg/mL. AgNPs concentration range between 11 and 20 µg/mL has significant effect on cell viability. AgNPs affected cell viability for each of the three studied cancer cell lines dependent on exposure time and concentrations. No significant effect of the exposure time was detected for HeLa cells (IC₅₀ value after 2 h incubation was close to the value after 24 h incubation) compared with HepG2 cells (IC₅₀ value at 2 h incubation was about twice the value after 24 h incubation). Cell viability of three cell lines (HeLa, HepG2, and A549 cells)

Chapter 2: Green Synthesis of Silver Nanoparticles

decreased significantly after incubation with AgNPs at various concentrations, and toxic effects of AgNPs on HeLa cells after 2 h ($IC_{50} = 7.711$) was more pronounced when compared to that on Hep G2 cells ($IC_{50} = 12.44$), while after 24 incubation hours, the values were closer to the three cancer cells studied ($IC_{50} = 6.72$ for HeLa cells, $IC_{50} = 6.88$ for Hep G2 cells, and $IC_{50} = 6.08$ for A549 cells). These results proved the high cytotoxic effect of AgNPs on HeLa, HepG2, and A549 cells compared with previous research^{60, 128-135} respectively, and it can be assumed that this higher cytotoxicity originates from phenolic compounds from St John's extract that coat these nanoparticles. To achieve targeting we are currently working on the functionalization of the AgNPs with cancer-specific aptamers. Thus our goal is to develop nanoparticles that have a size that allows entering to the tumor site via EPR effect and to the cancer cells via aptamers-mediated endocytosis, and are toxic to the cancer cell.

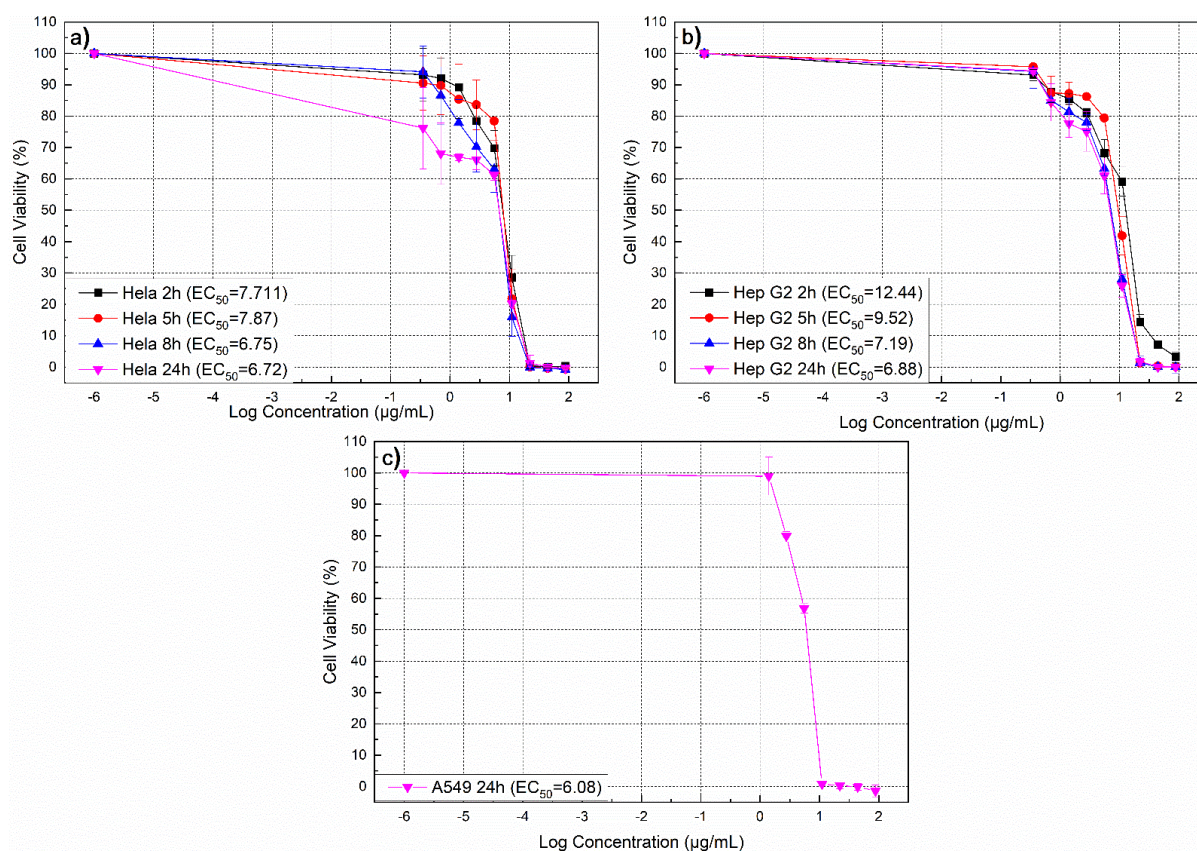


Figure 2-15: Relative cell viability (%) of (a) HeLa, (b) Hep G2 and (c) A549 cells as a function of AgNPs concentration for 2, 5, 8, and 24 h determined by cell titer-blue cytotoxicity assay. The experiments were performed with four replicates and standard deviation was calculated.

2.6 Conclusions

A simple one-pot green synthesis of stable AgNPs using aqueous St John's wort extract was reported. Preparation was found to be efficient in terms of stability as well as reaction time and excluded additional stabilizers/reducing agents. It proves to be an environmentally friendly, rapid green approach for the synthesis and provides a cost effective and an efficient way to synthesize AgNPs. Thereby, this reaction path satisfies all the requirements of a green chemical process. The synthesized nanoparticles were monodisperse, spherical, 20–50 nm in size, crystalline in nature, and showed absorption at 392–420 nm. XRD study showed the face-centered cubic lattice of AgNPs, EDXS analysis gives the optical absorption peak

Chapter 2: Green Synthesis of Silver Nanoparticles

approximately at 2.8 keV, 3.5 keV, and 3.8 keV, confirming the formation of metallic silver. TEM and SEM analysis showed that most of the particles were spherical in shape with size 20–35 nm. Prepared particles were surrounded with natural compounds from *Hypericum perforatum*. The particles are stabilized by a protective layer composed of molecules originating from the plant extracts which contain hydrophilic functional groups. The synthesized AgNPs showed very high antioxidant activity against 2, 2'-azino-bis-(3-ethylbenzothiazoline-6-sulfonic acid) radical cation, super oxide anion radical, and 2,2-diphenyl-1-picrylhydrazyl radical, at very low concentrations. Moreover, the AgNPs decreased cell viabilities of Hela, Hep G2, and A549 cells within a short time period of 2 h. AgNPs-toxicity toward cells may be related to various properties such as high surface area, surface charges and capping layer components, agglomeration, and lipophilicity. Organic molecules from St John's Wort coating AgNPs, which produce high surface charges, may play an additional role in AgNPs-toxicity. In subsequent studies we will use cancer cell-specific aptamers to achieve selective targeting of cancer cells. These biological synthesized and aptamer-functionalized AgNPs could be useful in the medical field for the treatment of cancer. AgNPs can not only be used as drug carriers but also represent the drug itself. In this case high toxicity of the AgNPs is a favorable feature. To achieve targeting we are currently working on the functionalization of the AgNPs with cancer-specific aptamers. Thus our goal is to develop nanoparticles that have a size that allows entering to the tumor site via EPR effect, to the cancer cells via aptamers-mediated endocytosis and are toxic to the cancer cell. This will be further investigated in our future work on Allah's will.

Supplementary Materials: The following are available online at www.mdpi.com/xxx/s1. Figure S1: Zeta potential for best samples. Figure S2: Isoelectric point for sample 16 and it is almost 1.18. Figure S3: TGA curve of *Hypericum perforatum* L-stabilized silver nanoparticles (sample 16), showing the loss of weight from organic compounds (secondary metabolites) placed on the surfaces of nanoparticles as a capping agent when the temperature increases. Figure S4: SEM-EDX analysis of the sample 16 of Ag NPs as deposited on FTO glass. Figure S5: TEM-DF images in two different places, (a) without silver nanoparticles (b) with silver. Figure S6: nanoparticles TEM-EDX spectra for the sample 16 in two different places, Spectrum 3 with no silver nanoparticles and Spectrum 4 with silver nanoparticles. Table S1: The data λ_{\max} (nm) of absorption peaks for different samples, absorption max, peak width (FWHM), molar extinction coefficient which we obtained from the reference study [1] and the final concentration of various sizes of biosynthesized silver nanoparticles. Table S2: Hydrodynamic diameter for other samples. Table S3: The following table lists infrared spectroscopy absorptions bands by its distinctive frequency regions. Table S4: Calculation of diffraction angle, FWHM and crystallite sizes for sample 16 at different times and some other samples of biosynthesized silver nanoparticles. Table S5: Plant components of plant material extract which act as a capping and reducing agent during green synthesis of AgNPs from different plant species.

Author Contributions: Conceptualization, A.A. and J.-G.W.; methodology and data curation, A.A. and J.-G.W.; validation, A.A., J.-G.W., and T.S. formal analysis, A.A.; support by measurement and analysis devices, A.F., N.C.B., and P.R.; data curation, A.A.; writing—

Chapter 2: Green Synthesis of Silver Nanoparticles

original draft preparation, A.A.; writing—review and editing, T.S. and J.-G.W.; supervision, J.-G.W and T.S.; All authors have read and agreed to the published version of the manuscript.

Funding: A.A. thanks the Avicenna-Studienwerk for financial support.

Data Availability Statement: The data presented in this study are available on request from the corresponding author.

Acknowledgments: The authors are grateful to all the lab members for their help. The authors express their gratitude to Frank Steinbach (Department of Physical Chemistry PCI, Leibniz Universität Hannover) for support with SEM; XRD and TEM analysis. From the same Department we thank also rer. nat. Dirk Dorfs. We thank rer. nat. Claus Rüscher from mineralogy department Leibniz Universität Hannover for providing ATR, FTIR and Raman analysis. I would like to express my great appreciation to Antonina Lavrentieva (Institute for Technical Chemistry TCI, Leibniz Universität Hannover) for her advice and assistance during the study of cytotoxicity of AgNPs. Abdalrahim Alahmad is supported by doctoral grants from Avicenna Studienwerk e.V. We are very thankful to Ibrahim Alghoraibi, leader of the Nanotechnology activity of the Physics Department, Damascus for his valuable suggestions during this work. N.C.B. thanks the European Research Council (European Union's Horizon 2020 research, innovation program, grant agreement 714429), and the DFG (grant agreement BI 1708/4-1) for financial support. N.C.B. thanks also the Laboratory for Nano and Quantum Engineering (LNQE). The publication of this article was funded by the Open Access Publishing Fund of Leibniz Universität Hannover.

Conflicts of Interest: The authors declare no conflict of interest.

2.7 References

1. Treguer-Delapierre, M.; Majimel, J.; Mornet, S.; Duguet, E.; Ravaine, S., Synthesis of non-spherical gold nanoparticles. *Gold Bull.* **2008**, *41* (2), 195-207.
2. Lopez-Sanchez, J. A.; Dimitratos, N.; Hammond, C.; Brett, G. L.; Kesavan, L.; White, S.; Miedziak, P.; Tiruvalam, R.; Jenkins, R. L.; Carley, A. F., Facile removal of stabilizer-ligands from supported gold nanoparticles. *Nat. Chem.* **2011**, *3* (7), 551-556.
3. Tsai, T.-H.; Thiagarajan, S.; Chen, S.-M., Green Synthesis of Silver Nanoparticles Using Ionic Liquid and Application for the Detection of Dissolved Oxygen. *Electroanalysis* **2010**, *22* (6), 680-687.
4. Lu, Y.-C.; Chou, K.-S., A simple and effective route for the synthesis of nano-silver colloidal dispersions. *J. Chin. Inst. Chem. Eng.* **2008**, *39* (6), 673-678.
5. Philip, J. M.; Jeyanthi Rebecca, K. M. L.; Venkatakrisnan, C. J.; Chandran, C. R., Green synthesized silver nanoparticles as an antimicrobial agent in dentistry. *Drug Invent. Today* **2018**, *10* (6), 950-953.
6. Xie, J.; Lee, J. Y.; Wang, D. I.; Ting, Y. P., Silver nanoplates: from biological to biomimetic synthesis. *ACS Nano* **2007**, *1* (5), 429-439.
7. Hemath Naveen, K.; Kumar, G.; Karthik, L.; Bhaskara Rao, K., Extracellular biosynthesis of silver nanoparticles using the filamentous fungus *Penicillium* sp. *Arch. Appl. Sci. Res.* **2010**, *2* (6), 161-167.

Chapter 2: Green Synthesis of Silver Nanoparticles

8. Trevors, J., Silver resistance and accumulation in bacteria. *Enzyme Microb. Technol.* **1987**, *9* (6), 331-333.
9. Pugazhenthiran, N.; Anandan, S.; Kathiravan, G.; Prakash, N. K. U.; Crawford, S.; Ashokkumar, M., Microbial synthesis of silver nanoparticles by *Bacillus* sp. *J. Nanopart. Res.* **2009**, *11* (7), 811-815.
10. Beveridge, T.; Hughes, M.; Lee, H.; Leung, K.; Poole, R.; Savvaidis, I.; Silver, S.; Trevors, J., Metal-microbe interactions: contemporary approaches. In *Advances in microbial physiology*, Elsevier: 1996; Vol. 38, pp 177-243.
11. Mukherjee, P.; Ahmad, A.; Mandal, D.; Senapati, S.; Sainkar, S. R.; Khan, M. I.; Ramani, R.; Parischa, R.; Ajayakumar, P.; Alam, M., Bioreduction of AuCl₄⁻ ions by the fungus, *Verticillium* sp. and surface trapping of the gold nanoparticles formed. *Angew. Chem. Int. Ed.* **2001**, *40* (19), 3585-3588.
12. Mukherjee, P.; Ahmad, A.; Mandal, D.; Senapati, S.; Sainkar, S. R.; Khan, M. I.; Parishcha, R.; Ajaykumar, P.; Alam, M.; Kumar, R., Fungus-mediated synthesis of silver nanoparticles and their immobilization in the mycelial matrix: a novel biological approach to nanoparticle synthesis. *Nano Lett.* **2001**, *1* (10), 515-519.
13. Durán, N.; Marcato, P. D.; Alves, O. L.; De Souza, G. I.; Esposito, E., Mechanistic aspects of biosynthesis of silver nanoparticles by several *Fusarium oxysporum* strains. *J. Nanobiotechnol.* **2005**, *3*:8 (1).
14. Shankar, S. S.; Rai, A.; Ahmad, A.; Sastry, M., Rapid synthesis of Au, Ag, and bimetallic Au core-Ag shell nanoparticles using Neem (*Azadirachta indica*) leaf broth. *J. Colloid Interface Sci.* **2004**, *275* (2), 496-502.
15. Bhainsa, K. C.; D'souza, S., Extracellular biosynthesis of silver nanoparticles using the fungus *Aspergillus fumigatus*. *Colloids Surf., B* **2006**, *47* (2), 160-164.
16. Lengke, M. F.; Fleet, M. E.; Southam, G., Biosynthesis of silver nanoparticles by filamentous cyanobacteria from a silver (I) nitrate complex. *Langmuir* **2007**, *23* (5), 2694-2699.
17. Vigneshwaran, N.; Kathe, A. A.; Varadarajan, P.; Nachane, R. P.; Balasubramanya, R., Biomimetics of silver nanoparticles by white rot fungus, *Phaenerochaete chrysosporium*. *Colloids Surf., B* **2006**, *53* (1), 55-59.
18. Shahverdi, A. R.; Minaeian, S.; Shahverdi, H. R.; Jamalifar, H.; Nohi, A.-A., Rapid synthesis of silver nanoparticles using culture supernatants of Enterobacteria: a novel biological approach. *Process Biochem.* **2007**, *42* (5), 919-923.
19. Klaus, T.; Joerger, R.; Olsson, E.; Granqvist, C.-G., Silver-based crystalline nanoparticles, microbially fabricated. *Proc. Natl. Acad. Sci. U.S.A.* **1999**, *96* (24), 13611-13614.
20. Jain, D.; Daima, H. K.; Kachhwaha, S.; Kothari, S., Synthesis of plant-mediated silver nanoparticles using papaya fruit extract and evaluation of their anti microbial activities. *Dig. J. Nanomater. Biostruct.* **2009**, *4* (3), 557-563.
21. Mallikarjuna, K.; Narasimha, G.; Dillip, G.; Praveen, B.; Shreedhar, B.; Lakshmi, C. S.; Reddy, B.; Raju, B. D. P., Green synthesis of silver nanoparticles using *Ocimum* leaf extract and their characterization. *Dig. J. Nanomater. Biostruct.* **2011**, *6* (1), 181-186.

Chapter 2: Green Synthesis of Silver Nanoparticles

22. Li, S.; Shen, Y.; Xie, A.; Yu, X.; Qiu, L.; Zhang, L.; Zhang, Q., Green synthesis of silver nanoparticles using *Capsicum annuum* L. extract. *Green Chem.* **2007**, *9* (8), 852-858.
23. Mallikarjuna, K.; Sushma, N. J.; Narasimha, G.; Manoj, L.; Raju, B. D. P., Phytochemical fabrication and characterization of silver nanoparticles by using Pepper leaf broth. *Arabian J. Chem.* **2014**, *7* (6), 1099-1103.
24. Ahmed, S.; Ahmad, M.; Swami, B. L.; Ikram, S., Green synthesis of silver nanoparticles using *Azadirachta indica* aqueous leaf extract. *J. Radiat. Res. Appl. Sci.* **2016**, *9* (1), 1-7.
25. Veerasamy, R.; Xin, T. Z.; Gunasagaran, S.; Xiang, T. F. W.; Yang, E. F. C.; Jeyakumar, N.; Dhanaraj, S. A., Biosynthesis of silver nanoparticles using mangosteen leaf extract and evaluation of their antimicrobial activities. *J. Saudi Chem. Soc.* **2011**, *15* (2), 113-120.
26. Borah, D.; Kumar Yadav, A., A Novel 'Green' Synthesis of Antimicrobial Silver Nanoparticles (AgNPs) by using *Garcinia morella* (Gaertn) Desr. Fruit Extract. *Nanosci. Nanotechnol. - Asia* **2015**, *5* (1), 25-31.
27. Mehmood, A.; Murtaza, G.; Bhatti, T. M.; Kausar, R., Phyto-mediated synthesis of silver nanoparticles from *Melia azedarach* L. leaf extract: Characterization and antibacterial activity. *Arabian J. Chem.* **2017**, *10* (2), 3048-3053.
28. Singh, S.; Vidyasagar, G., Green synthesis, characterization and antimicrobial activity of silver nanoparticles by using *Sterculia foetida* L. young leaves aqueous extract. *Int. J. Green Chem.* **2014**, *4* (1), 1-5.
29. Vijistella Bai, G., Green Synthesis of Silver Nanostructures Against Human Cancer Cell Lines and Certain Pathogens. *Int. j. pharm. chem. biol. sci* **2014**, *4* (1), 101-111.
30. Kalidasan, M.; Yogamoorthi, A., Biosynthesis of silver nanoparticles using *Achyranthus aspera* and its characterization. *Int. J. Nanomater. Biostructures* **2014**, *4* (1), 5-11.
31. Jayapriya, E.; Lalitha, P., Synthesis of silver nanoparticles using leaf aqueous extract of *Ocimum basilicum* (L.). *Int. J. Chemtech Res.* **2013**, *5* (6), 2985-2992.
32. Ahmad, N.; Sharma, S.; Rai, R., Rapid green synthesis of silver and gold nanoparticles using peels of *Punica granatum*. *Advanced Materials Letters* **2012**, *3* (5), 376-380.
33. Ponarulselvam, S.; Panneerselvam, C.; Murugan, K.; Aarthi, N.; Kalimuthu, K.; Thangamani, S., Synthesis of silver nanoparticles using leaves of *Catharanthus roseus* Linn. G. Don and their antiplasmodial activities. *Asian Pac. J. Trop. Biomed.* **2012**, *2* (7), 574-580.
34. Jyoti, K.; Baunthiyal, M.; Singh, A., Characterization of silver nanoparticles synthesized using *Urtica dioica* Linn. leaves and their synergistic effects with antibiotics. *J. Radiat. Res. Appl. Sci.* **2016**, *9* (3), 217-227.
35. Mohapatra, B.; Kuriakose, S.; Mohapatra, S., Rapid green synthesis of silver nanoparticles and nanorods using *Piper nigrum* extract. *J. Alloys Compd.* **2015**, *637*, 119-126.
36. Chung, I.-M.; Park, I.; Seung-Hyun, K.; Thiruvengadam, M.; Rajakumar, G., Plant-Mediated Synthesis of Silver Nanoparticles: Their Characteristic Properties and Therapeutic Applications. *Nanoscale Res. Lett.* **2016**, *11* (1).

Chapter 2: Green Synthesis of Silver Nanoparticles

37. Mishra, M.; Chauhan, P., Nanosilver and its medical implications. *J. Nanomed. Res* **2015**, *2* (5), 1.
38. Aswathy Aromal, S.; Philip, D., Green synthesis of gold nanoparticles using *Trigonella foenum-graecum* and its size-dependent catalytic activity. *Spectrochim. Acta, Part A* **2012**, *97*, 1-5.
39. Chandran, S. P.; Chaudhary, M.; Pasricha, R.; Ahmad, A.; Sastry, M., Synthesis of Gold Nanotriangles and Silver Nanoparticles Using Aloe vera Plant Extract. *Biotechnol. Progr.* **2006**, *22* (2), 577-583.
40. Dubey, S. P.; Lahtinen, M.; Särkkä, H.; Sillanpää, M., Bioprospective of *Sorbus aucuparia* leaf extract in development of silver and gold nanocolloids. *Colloids Surf., B* **2010**, *80* (1), 26-33.
41. Shameli, K.; Bin Ahmad, M.; Jaffar Al-Mulla, E. A.; Ibrahim, N. A.; Shabanzadeh, P.; Rustaiyan, A.; Abdollahi, Y.; Bagheri, S.; Abdolmohammadi, S.; Usman, M. S.; Zidan, M., Green Biosynthesis of Silver Nanoparticles Using *Callicarpa maingayi* Stem Bark Extraction. *Molecules* **2012**, *17* (7), 8506-8517.
42. Gurunathan, S.; Park, J. H.; Han, J. W.; Kim, J.-H., Comparative assessment of the apoptotic potential of silver nanoparticles synthesized by *Bacillus tequilensis* and *Calocybe indica* in MDA-MB-231 human breast cancer cells: targeting p53 for anticancer therapy. *Int. J. Nanomed.* **2015**, *10*, 4203–4223.
43. Li, W.-R.; Xie, X.-B.; Shi, Q.-S.; Zeng, H.-Y.; You-Sheng, O.-Y.; Chen, Y.-B., Antibacterial activity and mechanism of silver nanoparticles on *Escherichia coli*. *Appl. Microbiol. Biotechnol.* **2010**, *85* (4), 1115-1122.
44. Chernousova, S.; Epple, M., Silver as antibacterial agent: ion, nanoparticle, and metal. *Angew. Chem. Int. Ed.* **2013**, *52* (6), 1636-1653.
45. Cheng, D.; Yang, J.; Zhao, Y., Antibacterial materials of silver nanoparticles application in medical appliances and appliances for daily use. *Chin. Med. Equip. J.* **2004**, *4*, 26-32.
46. Hansen, S. F.; Michelson, E. S.; Kamper, A.; Borling, P.; Stuer-Lauridsen, F.; Baun, A., Categorization framework to aid exposure assessment of nanomaterials in consumer products. *Ecotoxicology* **2008**, *17* (5), 438-447.
47. Tang, B.; Wang, J.; Xu, S.; Afrin, T.; Xu, W.; Sun, L.; Wang, X., Application of anisotropic silver nanoparticles: Multifunctionalization of wool fabric. *J. Colloid Interface Sci.* **2011**, *356* (2), 513-518.
48. Atiyeh, B. S.; Costagliola, M.; Hayek, S. N.; Dibo, S. A., Effect of silver on burn wound infection control and healing: review of the literature. *burns* **2007**, *33* (2), 139-148.
49. Wei, D.; Sun, W.; Qian, W.; Ye, Y.; Ma, X., The synthesis of chitosan-based silver nanoparticles and their antibacterial activity. *Carbohydr. Res.* **2009**, *344* (17), 2375-2382.
50. Yoon, K.-Y.; Byeon, J. H.; Park, J.-H.; Hwang, J., Susceptibility constants of *Escherichia coli* and *Bacillus subtilis* to silver and copper nanoparticles. *Sci. Total Environ.* **2007**, *373* (2-3), 572-575.
51. Lanje, A. S.; Sharma, S. J.; Pode, R. B., Synthesis of silver nanoparticles: a safer alternative to conventional antimicrobial and antibacterial agents. *J Chem Pharm Res* **2010**, *2* (3), 478-483.

Chapter 2: Green Synthesis of Silver Nanoparticles

52. Velmurugan, P.; Cho, M.; Lim, S.-S.; Seo, S.-K.; Myung, H.; Bang, K.-S.; Sivakumar, S.; Cho, K.-M.; Oh, B.-T., Phytosynthesis of silver nanoparticles by *Prunus yedoensis* leaf extract and their antimicrobial activity. *Mater. Lett.* **2015**, *138*, 272-275.
53. Tripathi, R.; Saxena, A.; Gupta, N.; Kapoor, H.; Singh, R., High antibacterial activity of silver nanoballs against *E. coli* MTCC 1302, *S. typhimurium* MTCC 1254, *B. subtilis* MTCC 1133 and *P. aeruginosa* MTCC 2295. *Dig. J. Nanomater. Biostruct.* **2010**, *5* (2), 323-330.
54. Lara, H. H.; Ayala-Nuñez, N. V.; Ixtepan-Turrent, L.; Rodriguez-Padilla, C., Mode of antiviral action of silver nanoparticles against HIV-1. *J. Nanobiotechnol.* **2010**, *8* (1), 1-10.
55. Sun, L.; Singh, A. K.; Vig, K.; Pillai, S. R.; Singh, S. R., Silver nanoparticles inhibit replication of respiratory syncytial virus. *J. Biomed. Nanotechnol.* **2008**, *4* (2), 149-158.
56. Speshock, J. L.; Murdock, R. C.; Braydich-Stolle, L. K.; Schrand, A. M.; Hussain, S. M., Interaction of silver nanoparticles with Tacaribe virus. *J. Nanobiotechnol.* **2010**, *8*:19 (1).
57. Rajan, K.; Roppolo, I.; Chiappone, A.; Bocchini, S.; Perrone, D.; Chiolerio, A., Silver nanoparticle ink technology: state of the art. *Nanotechnol. Sci. Appl.* **2016**, *9*, 1-13.
58. Ko, S.-J.; Choi, H.; Lee, W.; Kim, T.; Lee, B. R.; Jung, J.-W.; Jeong, J.-R.; Song, M. H.; Lee, J. C.; Woo, H. Y., Highly efficient plasmonic organic optoelectronic devices based on a conducting polymer electrode incorporated with silver nanoparticles. *Energy Environ. Sci.* **2013**, *6* (6), 1949-1955.
59. Gensler, R.; Gröppel, P.; Muhrer, V.; Müller, N., Application of nanoparticles in polymers for electronics and electrical engineering. *Part. Part. Syst. Charact.* **2002**, *19* (5), 293-299.
60. Sankar, R.; Karthik, A.; Prabu, A.; Karthik, S.; Shivashangari, K. S.; Ravikumar, V., *Origanum vulgare* mediated biosynthesis of silver nanoparticles for its antibacterial and anticancer activity. *Colloids Surf., B* **2013**, *108*, 80-84.
61. Balakumaran, M.; Ramachandran, R.; Kalaichelvan, P., Exploitation of endophytic fungus, *Guignardia mangiferae* for extracellular synthesis of silver nanoparticles and their in vitro biological activities. *Microbiol. Res.* **2015**, *178*, 9-17.
62. Sharma, V. K.; Yngard, R. A.; Lin, Y., Silver nanoparticles: green synthesis and their antimicrobial activities. *Adv. Colloid Interface Sci.* **2009**, *145* (1-2), 83-96.
63. Kumar, S.; Harrison, N.; Richards-Kortum, R.; Sokolov, K., Plasmonic nanosensors for imaging intracellular biomarkers in live cells. *Nano Lett.* **2007**, *7* (5), 1338-1343.
64. Schrand, A. M.; Braydich-Stolle, L. K.; Schlager, J. J.; Dai, L.; Hussain, S. M., Can silver nanoparticles be useful as potential biological labels? *Nanotechnology* **2008**, *19* (23), 235104.
65. Davidović, S.; Lazić, V.; Vukoje, I.; Papan, J.; Anhrenkiel, S. P.; Dimitrijević, S.; Nedeljković, J. M., Dextran coated silver nanoparticles—Chemical sensor for selective cysteine detection. *Colloids Surf., B* **2017**, *160* (1), 184-191.
66. Jiang, Z.-J.; Liu, C.-Y.; Sun, L.-W., Catalytic properties of silver nanoparticles supported on silica spheres. *The Journal of Physical Chemistry B* **2005**, *109* (5), 1730-1735.
67. Roy, K.; Sarkar, C.; Ghosh, C., Photocatalytic activity of biogenic silver nanoparticles synthesized using yeast (*Saccharomyces cerevisiae*) extract. *Appl. Nanosci.* **2015**, *5* (8), 953-959.

Chapter 2: Green Synthesis of Silver Nanoparticles

68. Benyettou, F.; Rezgui, R.; Ravaux, F.; Jaber, T.; Blumer, K.; Jouiad, M.; Motte, L.; Olsen, J.-C.; Platas-Iglesias, C.; Magzoub, M., Synthesis of silver nanoparticles for the dual delivery of doxorubicin and alendronate to cancer cells. *J. Mater. Chem. B* **2015**, *3* (36), 7237-7245.
69. Brown, P. K.; Qureshi, A. T.; Moll, A. N.; Hayes, D. J.; Monroe, W. T., Silver nanoscale antisense drug delivery system for photoactivated gene silencing. *ACS Nano* **2013**, *7* (4), 2948-2959.
70. Lara-González, J. H.; Gomez-Flores, R.; Tamez-Guerra, P.; Monreal-Cuevas, E.; Tamez-Guerra, R.; Rodríguez-Padilla, C., In vivo antitumor activity of metal silver and silver nanoparticles in the L5178Y-R murine lymphoma model. *Br J Med Med Res* **2013**, *3* (4), 1308-1316.
71. Jeyaraj, M.; Sathishkumar, G.; Sivanandhan, G.; MubarakAli, D.; Rajesh, M.; Arun, R.; Kapildev, G.; Manickavasagam, M.; Thajuddin, N.; Premkumar, K., Biogenic silver nanoparticles for cancer treatment: an experimental report. *Colloids Surf., B* **2013**, *106*, 86-92.
72. Thombre, R.; Mehta, S.; Mohite, J.; Jaisinghani, P., Synthesis of silver nanoparticles and its cytotoxic effect against THP-1 cancer cell line. *Int. J. Pharm Bio Sci.* **2013**, *4* (1), 184-192.
73. He, Y.; Du, Z.; Ma, S.; Cheng, S.; Jiang, S.; Liu, Y.; Li, D.; Huang, H.; Zhang, K.; Zheng, X., Biosynthesis, antibacterial activity and anticancer effects against prostate cancer (PC-3) cells of silver nanoparticles using *Dimocarpus longan* lour. peel extract. *Nanoscale Res. Lett.* **2016**, *11* (1).
74. Hosni, K.; Msaâda, K.; Taârit, M. B.; Ouchikh, O.; Kallel, M.; Marzouk, B., Essential oil composition of *Hypericum perforatum* L. and *Hypericum tomentosum* L. growing wild in Tunisia. *Ind. Crops Prod.* **2008**, *27* (3), 308-314.
75. Ravisankar, N.; Joseph, J.; Radhakrishana, M.; Rajasekar, T., In vitro cytotoxicity of methanol extracts of *Hypericum wightianum* and *Hypericum hookerianum* against 3T3L1 cell lines. *Bangladesh J. Pharmacol.* **2016**, *11* (2), 328-329.
76. Azizi, M., Change in content and chemical composition of *Hypericum perforatum* L. oil at three harvest time. *J Herbs Spices Med Plants* **2008**, *13* (2), 79-85.
77. Zeb, S.; Ismat, N.; Alya, M., A review of the antibacterial activity of *Hypericum perforatum* L. *J. Ethnopharmacol.* **2010**, *131* (3), 511-521.
78. Davidson, J. R.; Connor, K. M., St. John's wort in generalized anxiety disorder: three case reports. *J. Clin. Psychopharmacol.* **2001**, *21* (6), 635-636.
79. Gurib-Fakim, A., Medicinal plants: traditions of yesterday and drugs of tomorrow. *Mol. Aspects Med.* **2006**, *27* (1), 1-93.
80. Shafaghat, A., Antioxidant, antimicrobial activities and fatty acid components of flower, leaf, stem and seed of *Hypericum scabrum*. *Nat. Prod. Commun.* **2011**, *6* (11), 1739-1742.
81. Ray, U.; Jerry, C.; Elizabeth, W.; Allison, G., *St. John's Wort: Hypericum Perforatum: Quality Control, Analytical and Therapeutic Monograph*. American Herbal Pharmacopoeia, 1997: 1997; Vol. 40, p 32.
82. Chopra, R. N.; Nayar, S. L., *Glossary of Indian medicinal plants*. Council of Scientific And Industrial Research; New Delhi, India: 1956.
83. Bukhari, I.; Dar, A.; Khan, R. A., Antinociceptive activity of methanolic extracts of St. John's Wort (*Hypericum perforatum*) preparation. *Pak J Pharm Sci* **2004**, *17* (2), 13-19.

Chapter 2: Green Synthesis of Silver Nanoparticles

84. Vattikuti, U. M. R.; Ciddi, V., An overview on *Hypericum perforatum* Linn. *Indian Journal of Natural Products and Resources* **2005**, *4* (5), 368-381.
85. Lavie, G.; Mazur, Y.; Lavie, D.; Prince, A.; Pascual, D.; Liebes, L.; Levin, B.; Meruelo, D., Hypericin as an inactivator of infectious viruses in blood components. *Transfusion* **1995**, *35* (5), 392-400.
86. Lopez-Bazzocchi, I.; Hudson, J.; Towers, G., Antiviral activity of the photoactive plant pigment hypericin. *Photochem. Photobiol.* **1991**, *54* (1), 95-98.
87. Hudson, J.; Lopez-Bazzocchi, I.; Towers, G., Antiviral activities of hypericin. *Antivir. Res.* **1991**, *15* (2), 101-112.
88. Lenard, J.; Rabson, A.; Vanderoef, R., Photodynamic inactivation of infectivity of human immunodeficiency virus and other enveloped viruses using hypericin and rose bengal: inhibition of fusion and syncytia formation. *Proc. Natl. Acad. Sci. U.S.A.* **1993**, *90* (1), 158-162.
89. Logeswari, P.; Silambarasan, S.; Abraham, J., Ecofriendly synthesis of silver nanoparticles from commercially available plant powders and their antibacterial properties. *Sci. Iran.* **2013**, *20* (3), 1049-1054.
90. Bose, D.; Chatterjee, S., Biogenic synthesis of silver nanoparticles using guava (*Psidium guajava*) leaf extract and its antibacterial activity against *Pseudomonas aeruginosa*. *Appl. Nanosci.* **2016**, *6* (6), 895-901.
91. Sastry, M.; Patil, V.; Sainkar, S., Electrostatically controlled diffusion of carboxylic acid derivatized silver colloidal particles in thermally evaporated fatty amine films. *the journal of physical chemistry B* **1998**, *102* (8), 1404-1410.
92. Mulvaney, P., Surface plasmon spectroscopy of nanosized metal particles. *Langmuir* **1996**, *12* (3), 788-800.
93. Basavaraja, S.; Balaji, S.; Lagashetty, A.; Rajasab, A.; Venkataraman, A., Extracellular biosynthesis of silver nanoparticles using the fungus *Fusarium semitectum*. *Mater. Res. Bull.* **2008**, *43* (5), 1164-1170.
94. Paramelle, D.; Sadovoy, A.; Gorelik, S.; Free, P.; Hobley, J.; Fernig, D. G., A rapid method to estimate the concentration of citrate capped silver nanoparticles from UV-visible light spectra. *Analyst* **2014**, *139* (19), 4855-4861.
95. Williams, D. B.; Carter, C. B.; Veyssiere, P., *Transmission electron microscopy: a textbook for materials science*. Springer: MRS Bulletin-Materials Research Society: Warrendale, PA, USA, 1998; Vol. 10.
96. Prokofiev, E. A.; Burow, J. A.; Payton, E. J.; Zarnetta, R.; Frenzel, J.; Gunderov, D. V.; Valiev, R. Z.; Eggeler, G., Suppression of Ni₄Ti₃ Precipitation by Grain Size Refinement in Ni-Rich NiTi Shape Memory Alloys. *Adv. Eng. Mater.* **2010**, *12* (8), 747-753.
97. Bendersky, L. A.; Gayle, F. W., Electron Diffraction Using Transmission Electron Microscopy. *J. Res. Nat. Inst. Stand. Technol.* **2001**, *106* (6), 997-1012.
98. Xu, Z.; Ngan, A., TEM study of electron beam-induced crystallization of amorphous GeSi films. *Philos. Mag. Lett.* **2004**, *84* (11), 719-728.

Chapter 2: Green Synthesis of Silver Nanoparticles

99. Mogilevsky, P.; Hay, R. S.; Boakye, E. E.; Keller, K. A., Evolution of Texture in Rhabdophane-Derived Monazite Coatings. *J. Am. Ceram. Soc.* **2003**, *86* (10), 1767-1772.
100. Egerton, R. F., *Physical principles of electron microscopy*. Springer: New York, NY, USA, 2005; Vol. 56.
101. Filippo, E.; Serra, A.; Buccolieri, A.; Manno, D., Green synthesis of silver nanoparticles with sucrose and maltose: morphological and structural characterization. *J. Non-Cryst. Solids* **2010**, *356* (6-8), 344-350.
102. Varshney, R.; Bhadauria, S.; Gaur, M., Biogenic synthesis of silver nanocubes and nanorods using sundried Stevia rebaudiana leaves. *Advanced Materials Letters* **2010**, *1* (3), 232-237.
103. Wani, I. A.; Ganguly, A.; Ahmed, J.; Ahmad, T., Silver nanoparticles: ultrasonic wave assisted synthesis, optical characterization and surface area studies. *Mater. Lett.* **2011**, *65* (3), 520-522.
104. Kenneth, O., *Elementary Analysis*. Courier Dover Publications: New York, NY, USA: 2020.
105. Jiří, P., The chemistry, pharmacology, and toxicology of the biologically active constituents of the herb Hypericum perforatum L. *J. Appl. Biomed.* **2003**, *1* (2), 61-70.
106. A., N.; V., B., Biologically active and other chemical constituents of the herb of Hypericum perforatum L. *Pharmacopsychiatry* **1997**, *30* (S 2), 129-134.
107. Borodina, V.; Mirgorod, Y. A., Kinetics and mechanism of the interaction between HAuCl₄ and rutin. *Kinet. Catal.* **2014**, *55* (6), 683-687.
108. Makarov, V.; Love, A.; Sinitsyna, O.; Makarova, S.; Yaminsky, I.; Taliansky, M.; Kalinina, N., "Green" nanotechnologies: synthesis of metal nanoparticles using plants. *Acta Naturae (англоязычная версия)* **2014**, *6* (1 (20)), 35-44.
109. Jain, S.; Mehata, M. S., Medicinal plant leaf extract and pure flavonoid mediated green synthesis of silver nanoparticles and their enhanced antibacterial property. *Sci. Rep.* **2017**, *7* (1).
110. Cherrak, S. A.; Mokhtari-Soulimane, N.; Berroukeche, F.; Bensenane, B.; Cherbonnel, A.; Merzouk, H.; Elhabiri, M., In vitro antioxidant versus metal ion chelating properties of flavonoids: A structure-activity investigation. *PLoS One* **2016**, *11* (10).
111. Kumar, T. V. R.; Murthy, J.; Rao, M. N.; Bhargava, Y., Evaluation of silver nanoparticles synthetic potential of Couroupita guianensis Aubl., flower buds extract and their synergistic antibacterial activity. *3 Biotech* **2016**, *6* (1).
112. Mirgorod, Y. A.; Borodina, V.; Borsch, N., Investigation of interaction between silver ions and rutin in water by physical methods. *Biophysics* **2013**, *58* (6), 743-747.
113. Huang, J.; Zhan, G.; Zheng, B.; Sun, D.; Lu, F.; Lin, Y.; Chen, H.; Zheng, Z.; Zheng, Y.; Li, Q., Biogenic silver nanoparticles by Cacumen platycladi extract: synthesis, formation mechanism, and antibacterial activity. *Ind. Eng. Chem. Res.* **2011**, *50* (15), 9095-9106.
114. Kalaiselvi, M.; Subbaiya, R.; Selvam, M., Synthesis and characterization of silver nanoparticles from leaf extract of Parthenium hysterophorus and its anti-bacterial and antioxidant activity. *Int J Curr Microbiol Appl Sci* **2013**, *2* (6), 220-227.

Chapter 2: Green Synthesis of Silver Nanoparticles

115. Moteriya, P.; Chanda, S., Biosynthesis of silver nanoparticles formation from *Caesalpinia pulcherrima* stem metabolites and their broad spectrum biological activities. *J. Genet. Eng. Biotechnol.* **2018**, *16* (1), 105-113.
116. Seralathan, J.; Stevenson, P.; Subramaniam, S.; Raghavan, R.; Pemaiah, B.; Sivasubramanian, A.; Veerappan, A., Spectroscopy investigation on chemo-catalytic, free radical scavenging and bactericidal properties of biogenic silver nanoparticles synthesized using *Salicornia brachiata* aqueous extract. *Spectrochim. Acta, Part A* **2014**, *118* (24), 349-355.
117. Moteriya, P.; Chanda, S., Synthesis and characterization of silver nanoparticles using *Caesalpinia pulcherrima* flower extract and assessment of their in vitro antimicrobial, antioxidant, cytotoxic, and genotoxic activities. *Artif. Cells Nanomed. Biotechnol.* **2017**, *45* (8), 1556-1567.
118. Ramachandran, L.; Nair, C. K. K., Therapeutic potentials of silver nanoparticle complex of α -lipoic acid. *Nanomater. Nanotechnol.* **2011**, *1*, 14.
119. Chanda, S.; Rakholiya, K.; Dholakia, K.; Baravalia, Y., Antimicrobial, antioxidant, and synergistic properties of two nutraceutical plants: *Terminalia catappa* L. and *Colocasia esculenta* L. *Turk J Biol* **2013**, *37* (1), 81-91.
120. Mittal, A. K.; Bhaumik, J.; Kumar, S.; Banerjee, U. C., Biosynthesis of silver nanoparticles: elucidation of prospective mechanism and therapeutic potential. *J. Colloid Interface Sci.* **2014**, *415* (1), 39-47.
121. Ajayi, E.; Afolayan, A., Green synthesis, characterization and biological activities of silver nanoparticles from alkalized *Cymbopogon citratus* Stapf. *Adv. Nat. Sci.: Nanosci. Nanotechnol.* **2017**, *8* (1).
122. Sudha, A.; Jeyakanthan, J.; Srinivasan, P., Green synthesis of silver nanoparticles using *Lippia nodiflora* aerial extract and evaluation of their antioxidant, antibacterial and cytotoxic effects. *Resour.-Effic. Technol.* **2017**, *3* (4), 506-515.
123. Keshari, A. K.; Srivastava, R.; Singh, P.; Yadav, V. B.; Nath, G., Antioxidant and antibacterial activity of silver nanoparticles synthesized by *Cestrum nocturnum*. *J. Ayurveda Integr. Med.* **2018**, *11* (1), 37-44.
124. Inbathamizh, L.; Ponnu, T. M.; Mary, E. J., In vitro evaluation of antioxidant and anticancer potential of *Morinda pubescens* synthesized silver nanoparticles. *J. Pharm. Res.* **2013**, *6* (1), 32-38.
125. Guntur, S. R.; Kumar, N. S.; Hegde, M. M.; Dirisala, V. R., In Vitro Studies of the Antimicrobial and Free-Radical Scavenging Potentials of Silver Nanoparticles Biosynthesized From the Extract of *Desmostachya bipinnata*. *Anal. Chem. Insights* **2018**, *13*, 1-9.
126. Mata, R.; Nakkala, J. R.; Sadras, S. R., Biogenic silver nanoparticles from *Abutilon indicum*: Their antioxidant, antibacterial and cytotoxic effects in vitro. *Colloids Surf., B* **2015**, *128* (1), 276-286.
127. Mata, R.; Nakkala, J. R.; Sadras, S. R., Catalytic and biological activities of green silver nanoparticles synthesized from *Plumeria alba* (frangipani) flower extract. *Materials Science and Engineering: C* **2015**, *51* (1), 216-225.
128. Vasanth, K.; Ilango, K.; MohanKumar, R.; Agrawal, A.; Dubey, G. P., Anticancer activity of *Moringa oleifera* mediated silver nanoparticles on human cervical carcinoma cells by apoptosis induction. *Colloids Surf., B* **2014**, *117*, 354-359.

Chapter 2: Green Synthesis of Silver Nanoparticles

129. Salazar, L.; Vallejo López, M. J.; Grijalva, M.; Castillo, L.; Maldonado, A., Biological effect of organically coated *Grias neuberthii* and *Persea americana* silver nanoparticles on HeLa and MCF-7 cancer cell lines. *J. Nanotechnol.* **2018**, 2018.
130. Datta, K. P.; Sandeep, A.; Sonu, A., Anti-proliferative effect of silver nanoparticles in HeLa cells due to enhanced oxidative stress. *Res. J. Biotechnol.* **2018**, 13 (2), 68-74.
131. Wang, X.; Li, T.; Su, X.; Li, J.; Li, W.; Gan, J.; Wu, T.; Kong, L.; Zhang, T.; Tang, M., Genotoxic effects of silver nanoparticles with/without coating in human liver HepG2 cells and in mice. *J. Appl. Toxicol.* **2019**, 39 (6), 908-918.
132. Prasannaraj, G.; Sahi, S. V.; Ravikumar, S.; Venkatachalam, P., Enhanced cytotoxicity of biomolecules loaded metallic silver nanoparticles against human liver (HepG2) and prostate (PC3) cancer cell lines. *J. Nanosci. Nanotechnol.* **2016**, 16 (5), 4948-4959.
133. Xue, Y.; Zhang, T.; Zhang, B.; Gong, F.; Huang, Y.; Tang, M., Cytotoxicity and apoptosis induced by silver nanoparticles in human liver HepG2 cells in different dispersion media. *J. Appl. Toxicol.* **2016**, 36 (3), 352-360.
134. Suliman Y, A. O.; Ali, D.; Alarifi, S.; Harrath, A. H.; Mansour, L.; Alwasel, S. H., Evaluation of cytotoxic, oxidative stress, proinflammatory and genotoxic effect of silver nanoparticles in human lung epithelial cells. *Environ. Toxicol.* **2015**, 30 (2), 149-160.
135. Venugopal, K.; Ahmad, H.; Manikandan, E.; Arul, K. T.; Kavitha, K.; Moodley, M.; Rajagopal, K.; Balabhaskar, R.; Bhaskar, M., The impact of anticancer activity upon *Beta vulgaris* extract mediated biosynthesized silver nanoparticles (ag-NPs) against human breast (MCF-7), lung (A549) and pharynx (Hep-2) cancer cell lines. *J. Photochem. Photobiol., B* **2017**, 173, 99-107.

Chapter 2: Green Synthesis of Silver Nanoparticles

2.8 Supporting Informations

2.8.1 Experimental

2.8.1.1 Biosynthesis of silver nanoparticles:

2.8.1.2 Measurement of concentration through absorption peak in UV-VIS Spectrum:

Table S 2-1: The data λ_{max} (nm) of absorption peaks for different samples, Absorption n_{max} , Peak Width (FWHM), molar extinction coefficient which we obtained from the reference study¹ and the final concentration of various sizes of biosynthesized silver nanoparticles.

Sample Number	Absorption Peak maximal λ_{max} (nm)	Absorption n_{max}	Peak Form	Peak Width (FWHM)	Length of the cuvette (cm)	ϵ M ⁻¹ Cm ⁻¹ X10 ⁸	C X 10 ⁻¹⁰ mol/L
1	440	0.31	Wide and very low	55,3388	0.1	880	0.3523
2	430	0.182	Sharp Peak with shoulders	75.32553	0.1	700	0.26
3	430,5	0.101	Wide peak with shoulders	139.40402	0.1	719	0.139
5	442	0.076	Low and expanded	61.52643	0.1	920	0.0826
6	418,2	0.071	Low wide peak with shoulder	102.4439	0.1	477	0.149
7	415	0.099	Small sharp peak with shoulder	61.00594	0.1	415	0.239
8	445	0.079	Small and wide peak with shoulder	68.19435	0.1	958	0.0793
10	442	0.017	very small peak and extended with shoulder	99.2931	0.1	910	0.0187
11	445	0.053	Wide peak without shoulders	131.46316	0.1	967.6	0.0548
12	427	0.177	High and sharp peak with shoulder	79.72299	0.1	658	0.269
13	428	0.012507	Broad peak very small	123,5337	0.1	678	0.0185
14	415	0.1	Sharp small peak	64.44719	0.1	390	0.256

Chapter 2: Green Synthesis of Silver Nanoparticles

			without shoulder				
15	460	0.435	Sharp peak without shoulders	151.81393	0.1	1162	0.387
16	442	0.962	Sharp peak without shoulders	113.5924	0.1	920	1.05
17	460	0.295	Small peak but sharp with shoulder	121.67788	0.1	1162	0.254
18	448	0.453	High and wide peak with shoulders	153.02564	0.1	1000	0.453
19	442	0.162	Wide and small peak without shoulders	125.21569	0.1	920	0.176

2.8.1.3 DLS (Dynamic Light Scattering)

Table S 2-2: Hydrodynamic diameter for other samples.

Sample Number	hydrodynamic diameter [nm]	Sample Number	hydrodynamic diameter [nm]
2	172.3	14	78.91
3	87.71	15	78.05
7	167.71	16	70.72
12	109.1	17	73.20
13	145.1	18	88.16
19	171.072	20	211.048

2.8.1.4 Isoelectric point

The point of zero charge (Isoelectric Point, IP) is the pH at which the electrical charge density on the surface is zero. Usually it is determined in relation to pH of electrolytes, and the point of zero charge value is assigned to a given colloidal particle (as in our case) or substrate. We aimed to determine the isoelectric point of the AgNPs for three reasons:

First: to know at which pH value will be the electrical charges on the surfaces of silver nanoparticles in the colloidal solution zero. Second: is the stability of nanoparticles in the colloidal solution dependent on electrostatic Repulsion because nanoparticles will fall down immediately in the solution when these forces become zero. Third: if the bond between the protective layer and the surface of the nanoparticles is of the type:

- Non-covalent bonds: which they are classified into various categories like hydrophobic effects, pi effects, electrostatic and van der Waals forces.

Chapter 2: Green Synthesis of Silver Nanoparticles

● Chemisorptions: is a kind of adsorption which includes a chemical reaction among the adsorbate and the surface.

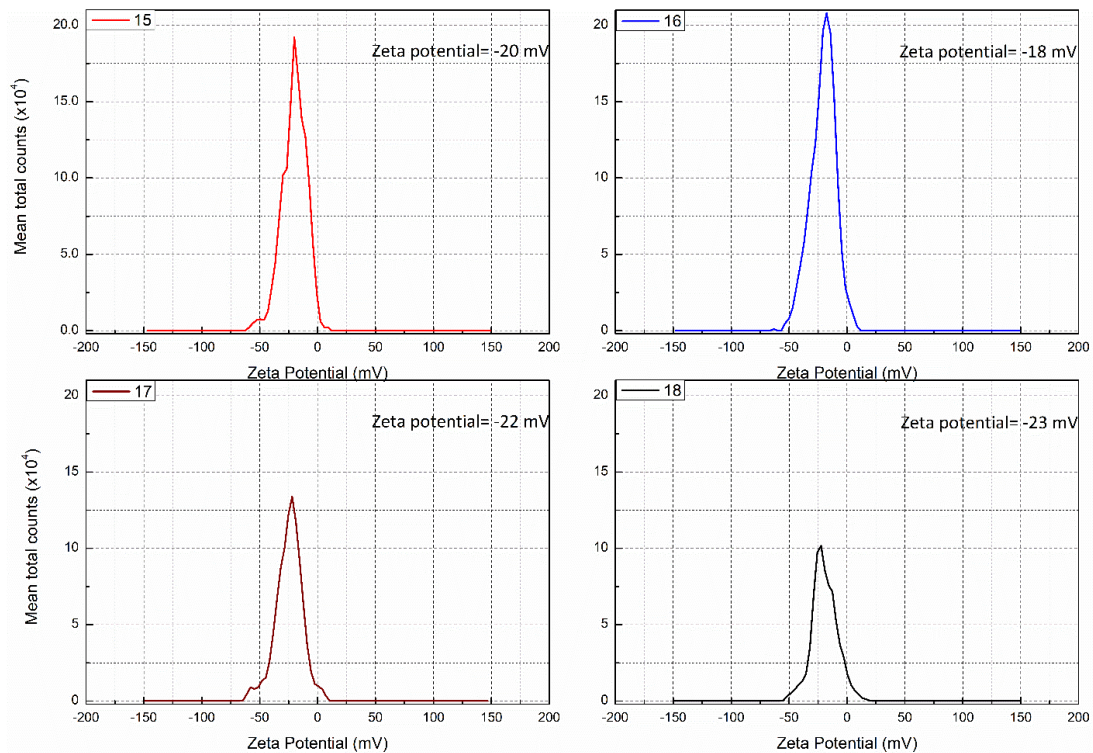


Figure S 2-1: Zeta Potential for best samples

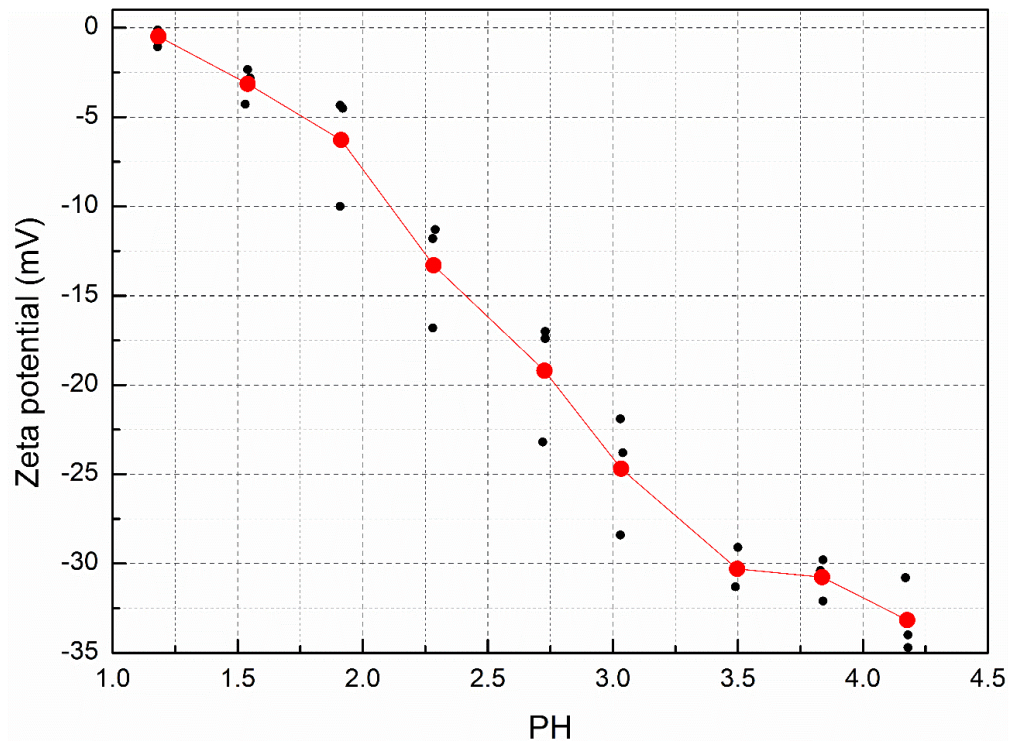


Figure S 2-2: Isoelectric point for sample 16 and it is almost 1.18.

Chapter 2: Green Synthesis of Silver Nanoparticles

2.8.1.5 (FTIR) – Spectroscopy

Table S 2-3: The following table lists infrared spectroscopy absorptions bands by its distinctive frequency regions.

Frequency oder Characteristic Absorptions (cm ⁻¹)	Functional Group and Type of Vibration ²⁻⁵	Frequency oder Characteristic Absorptions (cm ⁻¹)	Functional Group and Type of Vibration ²⁻⁵
672.5	C-H aromatic out of plane bending	1527	Stretching OH+ C=C aromatic
763	C-H aromatic out of plane bending ortho	1548	Stretching OH+ C=C aromatic
809	Substituted aromatic ring, C-H aromatic out of plane bending	1617 sometimes 1640	Stretching CO+ Stretching CH (flavonoidic structure)
870,880,892	Substituted aromatic ring, C-H aromatic out of plane bending	1733.7	C=O α , β or aryl conjugation
1017	Stretching OH (aliphatic)	1738	Str. C=O Normal
1050	Stretching OH (aliphatic) or S=O sulfoxide	1748	C=O
1066	Stretching OH (aliphatic)	1923, 1934	These peaks confirm the presence of aromatic ring
1077	C-O	1988	These peaks confirm the presence of aromatic ring
1103.6	C-O	2338	C-H bending
1145.5	C-O	2341	C-H bending
1204 sometimes 1236	Stretching OH (aromatic) her said from 1202-1236	2360	
1230, 1242, 1251	C-O-C aromatic	2362	
1265	Stretching OH	2849	Str C-H
1338 sometimes 1330	Stretching OH	2917	Str C-H
1374	Stretching OH or C-H bending	2901, 2972, 2987	C-H sp ³ stretch
1394, 1406	OH group of phenolic compound or CH ₃	3216	
1443	C-H bending	3385 sometimes 3388	OH stretching in phenols
1451.5	Stretching CH ₂ + Stretching OH	3685, 3674	
1473	Str. C=C aromatic	3853.6	
1382	C-H bending	1056	C-O

Chapter 2: Green Synthesis of Silver Nanoparticles

2.8.1.6 Thermal gravimetric analysis (TGA)

AgNPs were examined by Thermo-gravimetric analysis (TGA) (TGA/DSC 3+ from the company Mettler-Toledo) to prove the existence of biologically active secondary metabolites from *H. Perforatum* extract at the surfaces of silver nanoparticles. The progressive increase in temperature was adjusted between 25 °C – 1000 °C at heating rate of 0.5 °C/minute in flowing N₂. The TGA diagram of the covered silver nanoparticles synthesized using *Hypericum Perforatum* L. extract (Figure S 3) exhibited a stable weight loss in the temperature range of 92-493 °C. The weight loss of the capped-AgNPs was a result of adsorption of bioorganic metabolites at the surface of AgNPs (protective agent) and it was almost between 40-60 % with moisture which is about 9 percent, this depends on the number of washing times with Vivaspin tubes and the conditions of centrifugation used. Figure S 3 shows the progressive degradation of capped-AgNPs in three steps with an increase in temperature. The first phase of degradation which happened between 92 and 164 °C with a weight loss of 6.93% and this weight loss may be attributed to surface adsorbed H₂O molecules and some molecules of hexose ring. The second and third phase of the weight loss occurred between 170-315 and 324-492 °C consecutively, with a weight loss of 31.11 and 20.84 % respectively, this weight loss was due to combustion of the protective layer (the metabolites from St john`s extract which acts as a capping agent at the surface of AgNPs when formed) which decomposition in two steps. In summary the results of TGA analysis correspond to the results of FTIR and prove that resulted silver nanoparticles from synthesis were mixed nature with strongly coordinated metal organic framework.

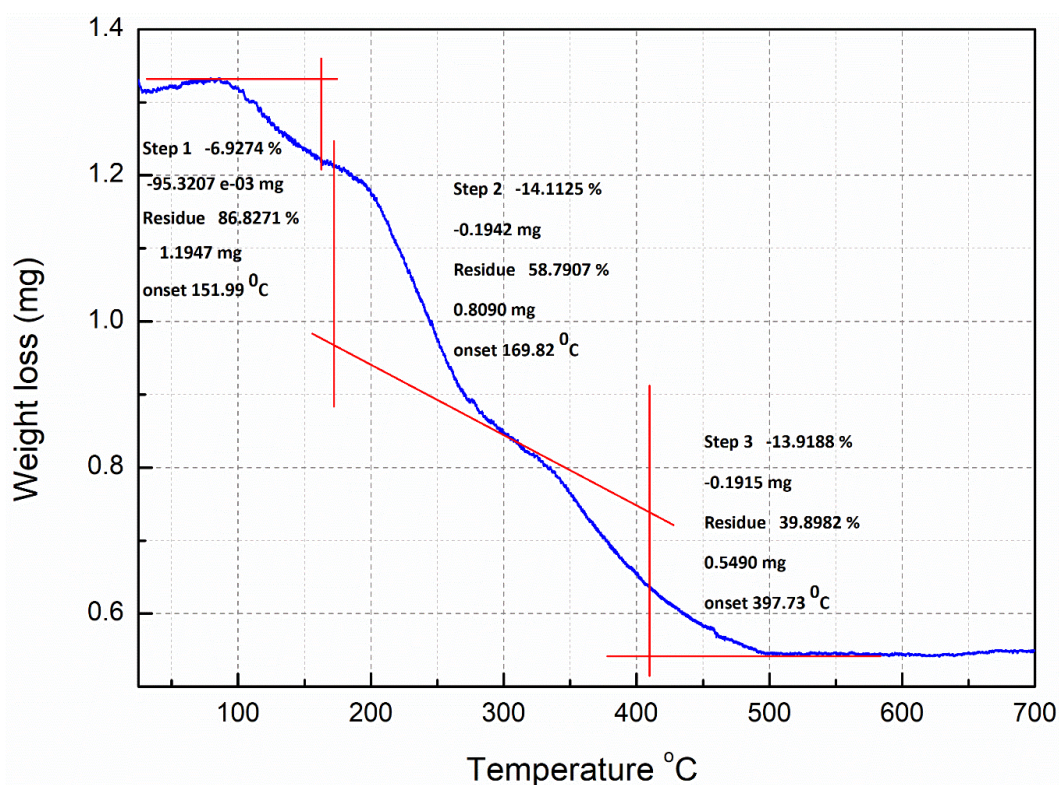


Figure S 2-3: TGA curve of *Hypericum Perforatum* L-stabilized silver nanoparticles (sample 16), showing the loss of weight from organic compounds (secondary metabolites) placed on the surfaces of nanoparticles as a capping agent when the temperature increases.

Chapter 2: Green Synthesis of Silver Nanoparticles

2.8.1.7 Scanning electron microscopy (SEM):

Energy dispersive X-ray spectroscopy (EDX): Oxygen and carbon appearance clearly shows that an extracellular organic layer covers the surface of AgNPs. The occurrence of another element in the photomicrograph could be on the grating base FTO glass which is used for the analysis.

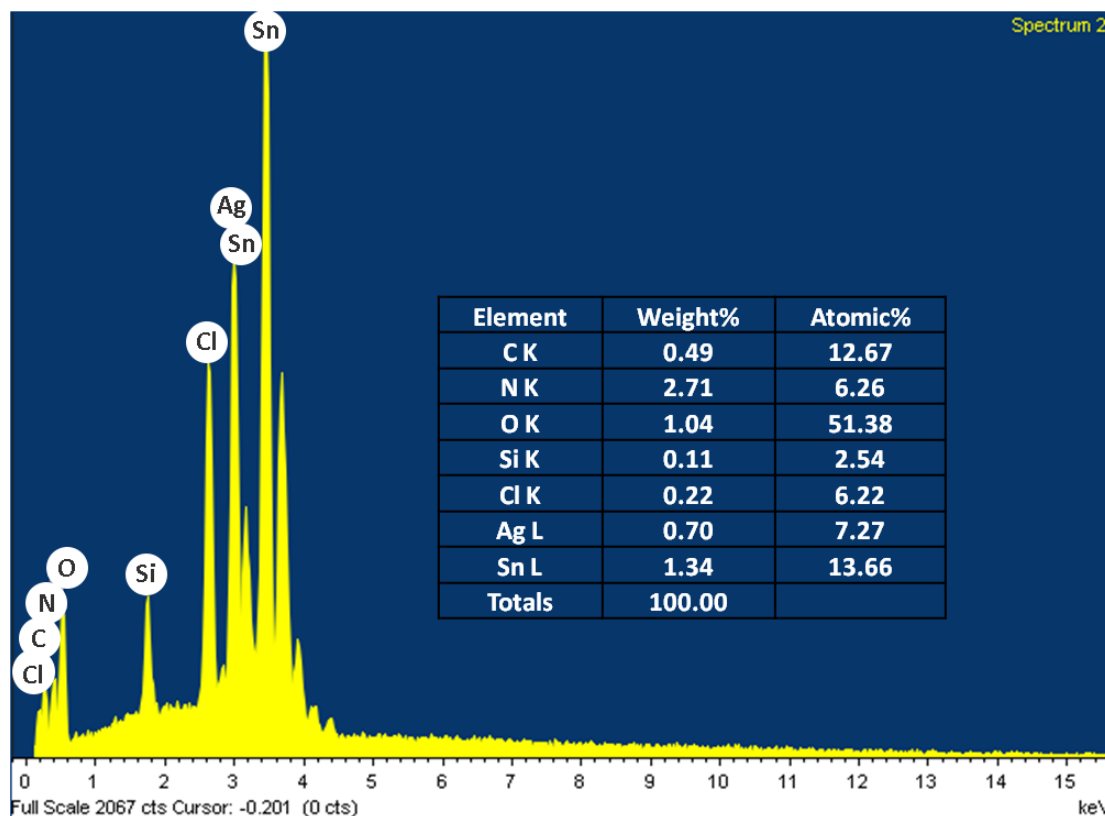


Figure S 2-4: SEM-EDX analysis of the sample 16 of Ag NPs as deposited on FTO glass

2.8.1.8 Transmission electron microscopy (TEM):

Through the two images Figure S5 and the spectrum Figure S6 we note the following: in a place where there is no silver, the concentrations of all the other elements are same, especially oxygen, this proves that what we got is only the silver metal and there are no silver oxides in the samples. We note that the concentration of carbon is less where there is silver metal. This indicates that silver is surrounded by a protection layer from the organic compounds present in the extract, which means, it proves the presence of the organic layer on the surfaces of nanoparticles.

Chapter 2: Green Synthesis of Silver Nanoparticles

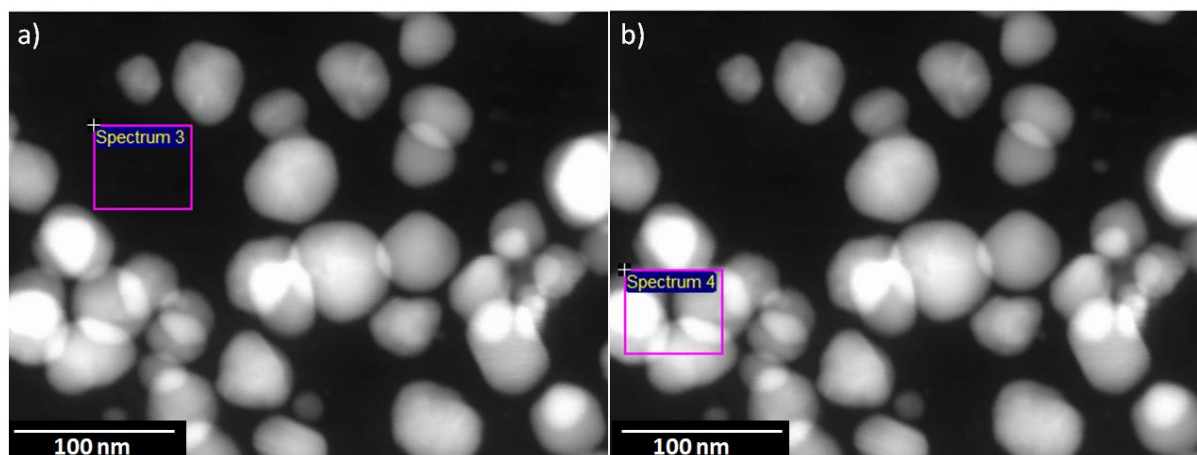


Figure S 2-5: TEM - DF images in two different places, a) without silver nanoparticles b) with silver nanoparticles.

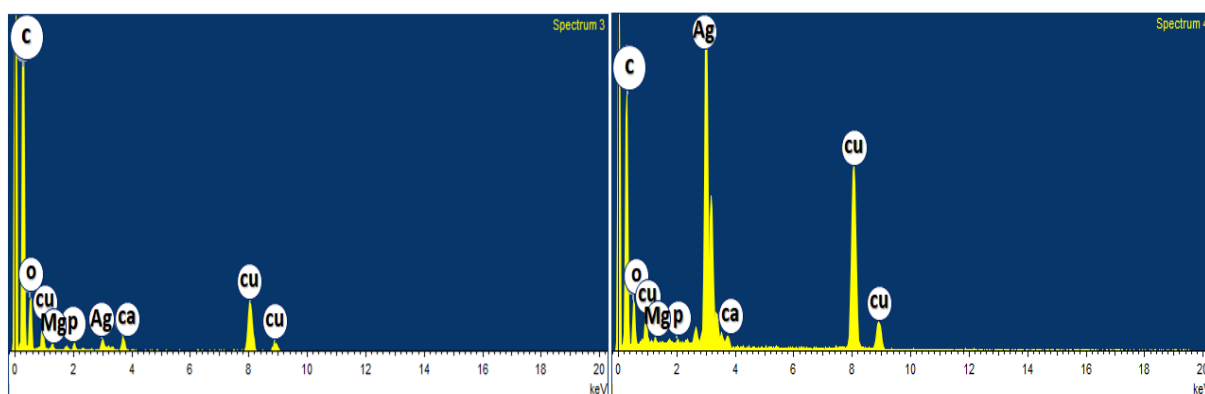


Figure S 2-6: TEM-EDX spectra for the sample 16 in two different places, Spectrum 3 with no silver nanoparticles and Spectrum 4 with silver nanoparticles.

High resolution transmission electron microscopy and nano-diffraction patterns ⁶⁻¹¹.

SAED is a qualitative analysis method of crystal structures from a spot diffraction pattern, which is obtained from illumination of a parallel electron beam on a specimen. When entering a selector (chosen-region) slot into the image level of the objective lens, is obtained a deviation pattern from a sample area of a various 100 nm diameter. This method enables us to identify the lattice type, lattice parameters and crystallographic orientation of this selected area. To analyze patterns of SAED, we integrate the geometric relationship and Bragg's equation in the reciprocal space:

$$2d \sin \Theta = \lambda \quad (\text{Bragg's law})$$

$$\tan 2\theta = D/L \quad (\text{geometric relationship in reciprocal space})$$

Where λ is the wavelength of the electron beam, d is spacing between planes, θ is the diffraction angle, D is the distance between rings on the SAED pattern, L is camera length of TEM apparatus. For too small diffraction angle θ , $\tan 2\theta$ equals to $2\sin\theta$, thus for the spots on the SAED pattern; d -spacings can be calculated by:

Chapter 2: Green Synthesis of Silver Nanoparticles

$$d = D / (\lambda L)$$

Each ring or spot in SAED pattern corresponds to a lattice plane of a specific miller index in single crystal or a group of lattice planes of the same miller index family in the polycrystalline sample. Whole spots on the pattern could be indexed. If the electron beam is fixed and the sample rotates, several ring/spot will be activated, and another ring/spot might die far. It depends on the diffraction situations described over. The diffraction pattern can be considered as a finger print for a certain crystal. Generally, the electron beam diffracted by a single crystal produces a diffraction spots pattern, but the specimen which consist of big number of little randomly distributed grains produce a continued rings. This is because all these grains contribute to the formation of diffraction pattern. Radius of the spots is inversely proportional to the interplanar spacings d_{hkl} of lattice planes of crystals.

The method to index the SAED pattern can be explained step by step:

- (1) The diameter (2R), of each ring is measured using some image processing software such as the image tool.
- (2) The radius value (R) of the diameter (2R) is taken.
- (3) By comparing this value with d-value of different phases of silver in literature (Joint Committee on Powder Diffraction Standards (JCPDS) or ICSD data base), we can identify or know the type of crystal lattice.

2.8.1.9 X-ray Diffraction (XRD)

The material consists of crystals in which the atoms are organized in a specific order. Since the wavelength of the X ray is close to the distance between atoms in these crystals, the X-ray diffraction suffers if they are coated on the material. The detector records the angles that are curving at the crystalline planes of the X-rays and the intensities of these rays. In order for the detector to collect all curvilinear rays, the detector moves around the axis of the shape on a circle where the angles and corners of the vertices are generated by a two-dimensional plan called the X-ray diagram. This diagram is characteristic for the material (fingerprint).

Determination of the particles size of the silver nanoparticle from Debye – Scherrer's Equation¹²:

The broadening of the Bragg reflection peaks indicates that the crystallite domain size is in nanosizes. The broadening at half maximum intensity of the diffraction peak is related to a reduction in crystallite size, flattening and micro-strands within the diffraction domains. The average particle size D was determined by using Scherrer's formula:

$$D = \frac{K \cdot \lambda}{\beta \cdot \cos\theta}$$

β is the full width at half maximum (FWHM), θ is the diffraction angle, D is the average crystallite size perpendicular to the reflecting planes and λ is the X-ray wavelength, k is constant, its value is close to one, and is related to crystalline shapes and lattice plane which corresponding to studied peak, if we assume that the shape is spherical, k will be 0.9. The

Chapter 2: Green Synthesis of Silver Nanoparticles

FWHM for each sample were taken from the (111) Bragg's reflection and its value were estimated by fitting the peaks using origin program.

Table S 2-4: Calculation of diffraction angle, FWHM and crystallite sizes for sample 16 at different times and some other samples of biosynthesized silver nanoparticles.

sample number	2 θ	β	Size of the particle (D)
	by degree	FWHM (rad)	nm
16	38.214	0.0057	25.6
16	38.230	0.0054	27.4
16	38.207	0.0061	24
16	37.796	0.015	10
16	38.207	0.0107	15
15	38.222	0.0072	20.3
17	37.939	0.0105	14
18	38.324	0.0069	21.4

The calculated crystallite size of as-prepared Ag-NPs (~ 24-27 nm) for sample 16 at some times are compatible with the values obtained from SEM and TEM apparatus. The crystallite size of Ag-NPs for some others of sample 16 (~10-15 nm) is rather smaller compared to the average nanoparticle size estimated from SEM and TEM observation (~25-40 nm), suggesting that there are a small nanocrystals in the multiple twined silver nanoparticles.

2.8.2 The probable mechanism of biosynthesis of silver nanoparticles by plant extracts

Table S 2-5: plant components of plant material extract which act as a capping and reducing agent during green synthesis of AgNPs from different plant species.

Plant genus	Metabolites found in the Extract/AgNPs	Reference
Azadirachta indica	Flavonoids, terpenoids	13
Hybanthus enneaspermus	Several bioactive phytochemical compounds	14
Syzygium cumini	Flavonoids	15
Ocimum sanctum	Flavonoid, proteins, gallic acid, terpenoids	16
Nigella arvensis	Flavonoids, alkaloids	17
Coleus aromaticus	Flavonoids	18
Glycyrrhiza glabra	Flavonoids, thiamine and terpenoids	19
Lantana camara	Flavonoids, glycosides and carbohydrates	20
Rosmarinus officinalis	Polyphenols	21
Citrus sinensis	Flavonoids, ascorbic acid, volatile oils	22
Mimusops elengi	Polyphenols	23
Dioscorea bulbifera	Flavonoids, polyphenols	24
Syzygium cumini	Polyphenols	25

Chapter 2: Green Synthesis of Silver Nanoparticles

<i>Decalepis hamiltonii</i>	Polyols, phenols	26
<i>Plumeria rubra</i>	Proteins	27
<i>Gardenia jasminoides</i>	Rutin, gallic acid, chlorogenic acid	28
<i>Helianthus annuus</i>	Flavonoids, proteins, amino acids, amides terpenoids	29
<i>Boswellia serrata</i>	Proteins	30
<i>Lippia citriodora</i>	Verbascoside, isoverbascoside, chrysoeriol-7-O-diglucoronide, luteonin-7-O-diglucoronide	31
<i>Solanum xanthocarpum</i>	Alkaloids, phenolics, sugars	32
<i>Withania somnifera</i>	Catechin p-coumaric acid, luteolin-7-glucoside, withanolides	33
<i>Achyranthes aspera</i>	Polyols	34
<i>Ocimum sanctum</i>	Quercetin	35
<i>Leonuri herba</i>	Hydroxyl, polyphenols groups	36
<i>Desmodium triflorum</i>	Ascorbic acid	37
<i>Trianthema decandra</i>	Saponin	38
<i>Mentha piperita</i>	Alkaloids, flavones, steroids, polysaccharides, amino acids, Oximes, proteins, menthol	39
<i>Anacardium occidentale</i>	Proteins, polyols	40
<i>Zingiber officinale</i>	Flavonoid, alkaloids	41
<i>Alternanthera sessilis</i>	Tannins, carbohydrates, proteins, ascorbic acid	42
<i>Dioscorea bulbifera</i>	Diosgenin, ascorbic acid	24
<i>Morinda pubescens</i>	Catechins, hydroxyflavones	43
<i>Annona squamosa</i>	Alkaloids, glycoside, saponins, tannins, Phenolic compounds, carbohydrates	44
<i>Hibiscus rosa-sinensis</i>	Carboxylate ion groups	45
<i>Acalypha indica</i>	Quercetin, plant pigment	46
<i>Carica papaya</i>	Catechnis, hydroxyflavones	47
<i>Eucalyptus</i>	Alcohol, phenols, alkylaldehyde	48
<i>Aegle marmelos</i>	Tannin	49
<i>Mangifera indica</i>	Ketone, aldehydes, hydroxyl, carboxyl groups	50
<i>Lonicera japonica</i>	Phenolic and hydroxyl groups of chlorogenic acid	51

Chapter 2: Green Synthesis of Silver Nanoparticles

2.8.3 References

1. Paramelle, D.; Sadovoy, A.; Gorelik, S.; Free, P.; Hobley, J.; Fernig, D. G., A rapid method to estimate the concentration of citrate capped silver nanoparticles from UV-visible light spectra. *Analyst* 2014, 139 (19), 4855-4861.
2. Pavia, D. L.; Lampman, G. M.; Kriz, G. S.; Vyvyan, J. A., *Introduction to spectroscopy*. Cengage Learning: 2008.
3. Nichita, C.; Giurginca, M.; Bazdoaca, C.; Parvu, L.; Meghea, A., Vegetal antioxidants obtained from *Hypericum perforatum* species. *REVISTA DE CHIMIE-BUCHAREST-ORIGINAL EDITION-2007*, 58 (9), 910.
4. R., A.; M., R., Phytochemical screening by FTIR spectroscopic analysis of leaf extracts of selected Indian Medicinal plants. *Int.J.Curr.Microbiol.App.Sci.* 2014, 3 (1), 395-406.
5. Kozarski, M.; Klaus, A.; Vunduk, J.; Zizak, Z.; Niksic, M.; Jakovljevic, D.; Vrvic, M. M.; Van Griensven, L. J., Nutraceutical properties of the methanolic extract of edible mushroom *Cantharellus cibarius* (Fries): primary mechanisms. *Food Funct* 2015, 6 (6), 1875-1886.
6. Williams, D. B.; Carter, C. B.; Veysiere, P., *Transmission electron microscopy: a textbook for materials science*. Springer: MRS Bulletin-Materials Research Society: Warrendale, PA, USA, 1998; Vol. 10.
7. Prokofiev, E. A.; Burow, J. A.; Payton, E. J.; Zarnetta, R.; Frenzel, J.; Gunderov, D. V.; Valiev, R. Z.; Eggeler, G., Suppression of Ni₄Ti₃ Precipitation by Grain Size Refinement in Ni-Rich NiTi Shape Memory Alloys. *Adv. Eng. Mater.* 2010, 12 (8), 747-753.
8. Morgagni, F., *Instrument*.
9. Xu, Z.; Ngan, A., TEM study of electron beam-induced crystallization of amorphous GeSi films. *Philos. Mag. Lett.* 2004, 84 (11), 719-728.
10. Mogilevsky, P.; Hay, R. S.; Boakye, E. E.; Keller, K. A., Evolution of Texture in Rhabdophane-Derived Monazite Coatings. *J. Am. Ceram. Soc.* 2003, 86 (10), 1767-1772.
11. Egerton, R. F., *Physical principles of electron microscopy*. Springer: New York, NY, USA, 2005; Vol. 56.
12. Theivasanthi, T.; Alagar, M., Electrolytic synthesis and characterizations of silver nanopowder. arXiv preprint arXiv:1111.0260 2011.
13. Ahmed, S.; Ahmad, M.; Swami, B. L.; Ikram, S., Green synthesis of silver nanoparticles using *Azadirachta indica* aqueous leaf extract. *J. Radiat. Res. Appl. Sci.* 2016, 9 (1), 1-7.
14. Suman, T.; Rajasree, S. R.; Jayaseelan, C.; Mary, R. R.; Gayathri, S.; Aranganathan, L.; Remya, R., GC-MS analysis of bioactive components and biosynthesis of silver nanoparticles using *Hybanthus enneaspermus* at room temperature evaluation of their stability and its larvicidal activity. *Environ. Sci. Pollut. Res.* 2016, 23 (3), 2705-2714.
15. Prasad, R.; Swamy, V. S., Antibacterial activity of silver nanoparticles synthesized by bark extract of *Syzygium cumini*. *J. Nanoparticle Res.* 2013, 2013.

Chapter 2: Green Synthesis of Silver Nanoparticles

16. Ramteke, C.; Chakrabarti, T.; Sarangi, B. K.; Pandey, R.-A., Synthesis of silver nanoparticles from the aqueous extract of leaves of *Ocimum sanctum* for enhanced antibacterial activity. *J. Chem.* 2012, 2013.
17. Chahardoli, A.; Karimi, N.; Fattahi, A., Biosynthesis, characterization, antimicrobial and cytotoxic effects of silver nanoparticles using *Nigella arvensis* seed extract. *Iranian journal of pharmaceutical research: IJPR* 2017, 16 (3), 1167.
18. Vanaja, M.; Annadurai, G., *Coleus aromaticus* leaf extract mediated synthesis of silver nanoparticles and its bactericidal activity. *Appl. Nanosci.* 2013, 3 (3), 217-223.
19. Dinesh, S.; Karthikeyan, S.; Arumugam, P., Biosynthesis of silver nanoparticles from *Glycyrrhiza glabra* root extract. *Arch. Appl. Sci. Res.* 2012, 4 (1), 178-187.
20. Ajitha, B.; Reddy, Y. A. K.; Shameer, S.; Rajesh, K.; Suneetha, Y.; Reddy, P. S., *Lantana camara* leaf extract mediated silver nanoparticles: antibacterial, green catalyst. *J. Photochem. Photobiol., B* 2015, 149, 84-92.
21. Ghaedi, M.; Yousefinejad, M.; Safarpour, M.; Khafri, H. Z.; Purkait, M., *Rosmarinus officinalis* leaf extract mediated green synthesis of silver nanoparticles and investigation of its antimicrobial properties. *J. Ind. Eng. Chem.* 2015, 31, 167-172.
22. Kaviya, S.; Santhanalakshmi, J.; Viswanathan, B.; Muthumary, J.; Srinivasan, K., Biosynthesis of silver nanoparticles using *Citrus sinensis* peel extract and its antibacterial activity. *Spectrochim. Acta, Part A* 2011, 79 (3), 594-598.
23. Kumar, H. A. K.; Mandal, B. K.; Kumar, K. M.; babu Maddinedi, S.; Kumar, T. S.; Madhiyazhagan, P.; Ghosh, A. R., Antimicrobial and antioxidant activities of *Mimusops elengi* seed extract mediated isotropic silver nanoparticles. *Spectrochim. Acta, Part A* 2014, 130, 13-18.
24. Ghosh, S.; Patil, S.; Ahire, M.; Kitture, R.; Kale, S.; Pardesi, K.; Cameotra, S. S.; Bellare, J.; Dhavale, D. D.; Jabgunde, A., Synthesis of silver nanoparticles using *Dioscorea bulbifera* tuber extract and evaluation of its synergistic potential in combination with antimicrobial agents. *Int. J. Nanomed.* 2012, 7, 483.
25. Kumar, V.; Yadav, S. C.; Yadav, S. K., *Syzygium cumini* leaf and seed extract mediated biosynthesis of silver nanoparticles and their characterization. *J. Chem. Technol. Biotechnol.* 2010, 85 (10), 1301-1309.
26. Rashmi, V.; Sanjay, K. R., Green synthesis, characterisation and bioactivity of plant-mediated silver nanoparticles using *Decalepis hamiltonii* root extract. *IET Nanobiotechnol.* 2016, 11 (3), 247-254.
27. Patil, C. D.; Patil, S. V.; Borase, H. P.; Salunke, B. K.; Salunkhe, R. B., Larvicidal activity of silver nanoparticles synthesized using *Plumeria rubra* plant latex against *Aedes aegypti* and *Anopheles stephensi*. *Parasitol. Res* 2012, 110 (5), 1815-1822.
28. Fenfen, L.; Yixian, G.; HUANG, J.; Daohua, S.; Qingbiao, L., Roles of biomolecules in the biosynthesis of silver nanoparticles: case of *Gardenia jasminoides* extract. *Chin. J. Chem. Eng.* 2014, 22 (6), 706-712.

Chapter 2: Green Synthesis of Silver Nanoparticles

29. Thakore, S.; Rathore, P. S.; Jadeja, R. N.; Thounaojam, M.; Devkar, R. V., Sunflower oil mediated biomimetic synthesis and cytotoxicity of monodisperse hexagonal silver nanoparticles. *Materials Science and Engineering: C* 2014, 44, 209-215.
30. Kora, A. J.; Sashidhar, R.; Arunachalam, J., Aqueous extract of gum olibanum (*Boswellia serrata*): a reductant and stabilizer for the biosynthesis of antibacterial silver nanoparticles. *Process Biochem.* 2012, 47 (10), 1516-1520.
31. Cruz, D.; Falé, P. L.; Mourato, A.; Vaz, P. D.; Serralheiro, M. L.; Lino, A. R. L., Preparation and physicochemical characterization of Ag nanoparticles biosynthesized by *Lippia citriodora* (Lemon Verbena). *Colloids Surf., B* 2010, 81 (1), 67-73.
32. Sengottaiyan, A.; Mythili, R.; Selvankumar, T.; Aravinthan, A.; Kamala-Kannan, S.; Manoharan, K.; Thiyagarajan, P.; Govarthanam, M.; Kim, J.-H., Green synthesis of silver nanoparticles using *Solanum indicum* L. and their antibacterial, splenocyte cytotoxic potentials. *Res. Chem. Intermed.* 2016, 42 (4), 3095-3103.
33. Marslin, G.; Selvakesavan, R. K.; Franklin, G.; Sarmiento, B.; Dias, A. C., Antimicrobial activity of cream incorporated with silver nanoparticles biosynthesized from *Withania somnifera*. *Int. J. Nanomed.* 2015, 10, 5955.
34. Elumalai, D.; Kaleena, P.; Ashok, K.; Suresh, A.; Hemavathi, M., Green synthesis of silver nanoparticle using *Achyranthes aspera* and its larvicidal activity against three major mosquito vectors. *Eng. Agric. Environ. Food* 2016, 9 (1), 1-8.
35. Jain, S.; Mehata, M. S., Medicinal plant leaf extract and pure flavonoid mediated green synthesis of silver nanoparticles and their enhanced antibacterial property. *Sci. Rep.* 2017, 7 (1).
36. Im, A. R.; Han, L.; Kim, E. R.; Kim, J.; Kim, Y. S.; Park, Y., Enhanced antibacterial activities of *Leonuri herba* extracts containing silver nanoparticles. *Phytother. Res.* 2012, 26 (8), 1249-1255.
37. Ahmad, N.; Sharma, S.; Singh, V.; Shamsi, S.; Fatma, A.; Mehta, B., Biosynthesis of silver nanoparticles from *Desmodium triflorum*: a novel approach towards weed utilization. *Biotechnol. Res. Int.* 2011, 2011.
38. Geethalakshmi, R.; Sarada, D., Characterization and antimicrobial activity of gold and silver nanoparticles synthesized using saponin isolated from *Trianthema decandra* L. *Ind. Crops Prod.* 2013, 51, 107-115.
39. MubarakAli, D.; Thajuddin, N.; Jeganathan, K.; Gunasekaran, M., Plant extract mediated synthesis of silver and gold nanoparticles and its antibacterial activity against clinically isolated pathogens. *Colloids Surf B Biointerfaces* 2011, 85 (2), 360-5.
40. Mukunthan, K.; Balaji, S., Cashew apple juice (*Anacardium occidentale* L.) speeds up the synthesis of silver nanoparticles. *Int. J. Green Nanotechnol.* 2012, 4 (2), 71-79.
41. Velmurugan, P.; Anbalagan, K.; Manosathyadevan, M.; Lee, K.-J.; Cho, M.; Lee, S.-M.; Park, J.-H.; Oh, S.-G.; Bang, K.-S.; Oh, B.-T., Green synthesis of silver and gold nanoparticles using *Zingiber officinale* root extract and antibacterial activity of silver nanoparticles against food pathogens. *Bioprocess. Biosyst. Eng.* 2014, 37 (10), 1935-1943.

Chapter 2: Green Synthesis of Silver Nanoparticles

42. Niraimathi, K.; Sudha, V.; Lavanya, R.; Brindha, P., Biosynthesis of silver nanoparticles using *Alternanthera sessilis* (Linn.) extract and their antimicrobial, antioxidant activities. *Colloids Surf., B* 2013, 102, 288-291.
43. Kumar, K. R.; Nattuthurai, N.; Gopinath, P.; Mariappan, T., Synthesis of eco-friendly silver nanoparticles from *Morinda tinctoria* leaf extract and its larvicidal activity against *Culex quinquefasciatus*. *Parasitol. Res* 2015, 114 (2), 411-417.
44. Vivek, R.; Thangam, R.; Muthuchelian, K.; Gunasekaran, P.; Kaveri, K.; Kannan, S., Green biosynthesis of silver nanoparticles from *Annona squamosa* leaf extract and its in vitro cytotoxic effect on MCF-7 cells. *Process Biochem.* 2012, 47 (12), 2405-2410.
45. Nayak, D.; Ashe, S.; Rauta, P. R.; Nayak, B., Biosynthesis, characterisation and antimicrobial activity of silver nanoparticles using *Hibiscus rosa-sinensis* petals extracts. *IET Nanobiotechnol.* 2015, 9 (5), 288-293.
46. Krishnaraj, C.; Jagan, E.; Rajasekar, S.; Selvakumar, P.; Kalaichelvan, P.; Mohan, N., Synthesis of silver nanoparticles using *Acalypha indica* leaf extracts and its antibacterial activity against water borne pathogens. *Colloids Surf., B* 2010, 76 (1), 50-56.
47. Banala, R. R.; Nagati, V. B.; Karnati, P. R., Green synthesis and characterization of *Carica papaya* leaf extract coated silver nanoparticles through X-ray diffraction, electron microscopy and evaluation of bactericidal properties. *Saudi J. Biol. Sci.* 2015, 22 (5), 637-644.
48. Liu, Y.; Jin, X.; Chen, Z., The formation of iron nanoparticles by *Eucalyptus* leaf extract and used to remove Cr (VI). *Sci. Total Environ.* 2018, 627, 470-479.
49. Rao, K. J.; Paria, S., Green synthesis of silver nanoparticles from aqueous *Aegle marmelos* leaf extract. *Mater. Res. Bull.* 2013, 48 (2), 628-634.
50. Yang, N.; Li, W.-H., Mango peel extract mediated novel route for synthesis of silver nanoparticles and antibacterial application of silver nanoparticles loaded onto non-woven fabrics. *Ind. Crops Prod.* 2013, 48, 81-88.
51. Zhou, Y.; Tang, R.-C., Facile and eco-friendly fabrication of AgNPs coated silk for antibacterial and antioxidant textiles using honeysuckle extract. *J. Photochem. Photobiol., B* 2018, 178, 463-471.

3 Chapter Three: Identification of Major Constituents of *Hypericum perforatum L*. Extracts in Syria by Development of a Rapid, Simple and Reproducible HPLC-ESI-Q-TOF MS Analysis and their Antioxidant Activities

3.1 Vorwort

This chapter contains the article “Chapter Three: Identification of Major Constituents of *Hypericum perforatum L*. Extracts in Syria by Development of a Rapid, Simple and Reproducible HPLC-ESI-Q-TOF MS Analysis and their Antioxidant Activities” by Abdalrahim Alahmad^{1,*}, Ibrahim Alghoraibi²⁺³, Raghad Zein³, Sergej Kraft¹, Gerald Dräger⁴, Johanna-Gabriela Walter¹ and Thomas Scheper^{1,*}. Reproduced with permission from ASC Omega 2022, DOI: 10.1021/acsomega.1c06335). Copyright 2022 ASC Omega. Diese Arbeit ist unseres Wissens nach der erste Bericht, in dem die in Syrien heimische Johanniskrautpflanze mit verschiedenen Lösungsmitteln extrahiert und ihre wichtigsten Verbindungen identifiziert werden. In dieser Studie wurden die getrockneten oberirdischen Teile, d. h. Blätter, Stängel, Blütenblätter und Blüten, mit verschiedenen Lösungsmitteln (Wasser, Ethanol, Methanol und Aceton) und Extraktionsprotokollen extrahiert. Durch Erhöhen der Polarität des Lösungsmittels wurden höhere Ausbeuten erhalten, was darauf hinweist, dass hauptsächlich hydrophobe Verbindungen extrahiert wurden. Daher schlussfolgern wir, dass die Extraktion mit der Teemethode oder mit einer Mischung aus Wasser und organischen Lösungsmitteln im Vergleich zu reinen organischen Lösungsmitteln oder kontinuierlichem Kochen mit Wasser über lange Zeiträume zu höheren Ausbeuten führte. Die erhaltenen Extrakte wurden mittels Hochleistungs-Flüssigkeitschromatographie analysiert – ausgestattet mit einem Diodenarray-Detektor (HPLC-DAD), gekoppelt mit UV-Vis-Spektrophotometrie bei einem vollen Spektrum (200–800 nm). Die HPLC-Spektren der Extrakte waren bei den drei Wellenlängen (260 nm für Phloroglucinole (Hyperforin und Derivate), 590 nm für Naphthodianthrone (Hypericine) und bei 350 nm für andere Flavonole, Flavone und Caffeoylchinasäuren) nahezu identisch, wobei Unterschiede nur bei beobachtet wurden die Intensität der Spitzen. Dies weist darauf hin, dass die gleichen Verbindungen unter Verwendung unterschiedlicher Lösungsmittel, aber in unterschiedlichen Mengen erhalten wurden. Fünf Standards (Chlorogensäure, Quercetin, Quercitrinhydrat, Hyperosid und Hypericin) wurden verwendet, und ein Vergleich mit Retentionszeiten und UV-Spektren, über die in der Literatur berichtet wird, wurde durchgeführt, um zehn Verbindungen in diesen Extrakten zu identifizieren: Hyperforin, Adhyperforin, Hypericin, Rutin, Quercetin, Quercitrin, Quercitrin hydrate, Hyperoside, Biapigenin and Chlorogenic Acid. Obwohl das Europäische Arzneibuch die UV-Spektroskopie immer noch als Methode zur Bestimmung der Menge von *Hyperici herba* beschreibt, können Störungen durch andere Metaboliten auftreten. Kombinierte (HPLC-DAD) und Elektrospray-Ionisations-Massenspektrometrie (LC-ESI-MS) im positiven Modus wurden daher auch verwendet, um das Vorhandensein dieser Verbindungen in den Extrakten zu bestätigen, indem bekannte Massen mit den identifizierten Massen oder durch charakteristische Fragmentierungsmuster korreliert wurden. Der Gesamtphenolgehalt der

Chapter 3: Identification of Major Constituents of *Hypericum perforatum* L

Extrakte wurde durch den Folin-Ciocalteu-Assay bestimmt, und die antioxidative Aktivität wurde als Radikalfängerkapazität unter Verwendung von 2,2-Diphenyl-1-picrylhydrazyl (DPPH)- und (2,2'-Azino-bis(3-ethylbenzothiazolin-6-sulfonsäure) (ABTS)-Assays bewertet. Die Ergebnisse zeigen, dass die nach dem Teeverfahren hergestellten wässrigen Extrakte die höchsten Gesamtphenole ergaben, während die reinen organischen Lösungsmittel sehr niedriges Phenol ergaben. Außerdem ergaben die Extrakte, die die größte Menge an Phenolen enthielten, niedrigere IC50-Werte oder eine höhere antioxidative Aktivität als andere.

3.2 Abstract

Hypericum perforatum Linn (St John's wort) is a popular and widespread medicine in Syria, used for a wide range of conditions, including gastrointestinal diseases, heart disease, skin diseases, and psychological disorders. This widespread use prompted us to identify the main compounds of this plant from Syria, which are responsible for its medicinal properties, especially since its components differ between countries according to the nature of the soil, climate and altitude. This is, to the best of our knowledge, the first report in which the St. John's wort plant native to Syria is extracted using different solvents and its most important compounds identified. In this study, the dried above-ground parts, i.e., leaves, stem, petals, and flowers were extracted using different solvents (water, ethanol, methanol and acetone) and extraction protocols. By increasing the polarity of the solvent, higher yields were obtained, indicating that mainly hydrophobic compounds were extracted. Therefore, we conclude that extraction using the tea method or using a mixture of water with organic solvents resulted in higher yields compared with pure organic solvents or continuous boiling with water for long periods. The obtained extracts were analyzed using high performance liquid chromatography-equipped with a diode array detector (HPLC-DAD), coupled with UV-visible spectrophotometry at a full spectrum (200–800 nm). The HPLC spectra of the extracts were almost identical at the three wavelengths (260 nm for phloroglucinols (hyperforin and derivatives), 590 nm for naphthodianthrones (hypericins) and at 350 nm for other flavonols, flavones and caffeoylquinic acids), with differences observed only in the intensity of the peaks. This indicates that the same compounds were obtained using different solvents, but in different amounts. Five standards (chlorogenic acid, quercetin, quercitrin hydrate, hyperoside and hypericin) were used, and a comparison with retention times and UV spectra reported in the literature was performed to identify ten compounds in these extracts: hyperforin, adhyperforin, hypericin, rutin, quercetin, quercitrin, quercitrin hydrate, hyperoside, biapigenin and chlorogenic acid. Although the European Pharmacopoeia still describes ultraviolet spectroscopy as a method for determining the quantity of *Hyperici herba*, interference from other metabolites can occur. Combined (HPLC-DAD) and electrospray ionization–mass spectrometry (LC-ESI-MS) in positive mode have therefore also been used to confirm the presence of these compounds in the extracts by correlating known masses with the identified masses or through characteristic fragmentation patterns. Total phenolic contents of the extracts were determined by Folin–Ciocalteu assay, and antioxidant activity was evaluated as free radical-scavenging capacity using 2,2-diphenyl-1-picrylhydrazyl (DPPH) and (2,2'-azino-bis(3-ethylbenzothiazoline-6-sulfonic acid) (ABTS) assays. The results indicate that the aqueous extracts prepared by the tea method gave the highest total phenols, while the pure

Chapter 3: Identification of Major Constituents of *Hypericum perforatum* L

organic solvents gave very low phenols. Also, the extracts that contain the largest amount of phenols gave lower IC50 values or higher antioxidant activity than others.

3.3 Introduction

Hypericum perforatum Linn, generally recognized as St. John's wort, is a flowering plant native to Asia and Europe. It belongs to the Hypericaceae family which contains over 1000 species and about 55 genera. The *Hypericum* genus comprises over 450 species distributed worldwide in tropical and subtropical regions¹⁻³. This species can grow under various environmental conditions and has a very extensive ecological capacity. It is found in pastures, thickets, forest clearings, varied types of oak forest, meadows and burnt areas, etc.³. The height of the stem, which is red in color and branched in its upper section, is about 40 to 100 cm (Figure 1 a). Stems might appear articular from leaf scars although it is wooden close to its base^{4,5}. Branches are grouped as opposite pairs and rotated at 90° angles (intersecting), at the base of every leaf^{4,6}. The leaves are narrow-oblong, non-serrated, yellowish green in color, less stalk, 2-4 cm long on the major stalk, 1–2 cm long on branches and covered with scattered translucent glands in the form of dots (Figure 1 b). The dots are translucent when seen against the light; this gives the leaves a pierced appearance as indicated by the plant's Latin name^{4,7}. The multi-flowered flowers are very branched and compact to round, bright yellow in color with black dots and a length of up to 2.5 cm. Each flower has five petals and sepals, which are 4 to 6 mm long, in the shape of a narrow shaft with a pointed tip, and sometimes have some black glands^{4,8,9}. 50 to 80 stamens are grouped into three or five fascicles, these patterns are separated, and the stigmas are in dense head-like groups (Figure 1 c). The fruit is a three-chamber capsule that contains many raw seeds which are rough, netted with coarse grooves, length from 1 to 1.3 mm (Figure 1 d)^{4,9}.

Different extracts (alcoholic or aqueous extracts) of the aerial parts of *H. perforatum* revealed that its bioactive natural components (phytochemicals) consist of seven groups^{4, 10-25}: (1) naphthodianthrones -anthraquinone derivatives, (e.g., hypericin, isohypericin, protohypericin, pseudohypericin, protopseudohypericin etc.), (2) phloroglucinols (e.g., hyperforin, adhyperforin, hydroperoxycadiforin etc.), (3) flavonol glycosides; flavonoids – flavonols (e.g., quercetin, kaempferol etc.), glycosides (e.g., rutin, hyperoside, quercitrin, isoquercitrin etc.) and flavones (e.g., apigenin, luteolin etc.), (4) biflavones (e.g., flavone (13,II8-biapigenin), amentoflavone (13',II8-biapigenin) and catechins (flavonoids are often associated with condensed tannins), (5) phenylpropanes (e.g., p-coumaric, chlorogenic, caffeic, vanillic, p-hydroxybenzoic and ferulic acids etc.), (6) proanthocyanidins and tannins (e.g., dimeric procyanidin B2, dimeric, trimeric, and tetrameric procyanidins), and (7) xanthones (e.g., 1,3,6,7- tetrahydroxyxanthone and kielcorin C)^{4, 10-25}. Moreover, minor amounts of other common components include acids (palmitic, isovalerianic, myristic, stearic, nicotinic, citric and malic), pectin, choline, carotenoids, B-sitosterol, amino acids derivatives (tryptophan, γ -aminobutyric acid and melatonin), nicotinamide, vitamin C, sugars (glucose, fructose, saccharose and lactose), fatty acids, bisanthraquinone, glycosides, and hydroperoxycadiforin. Hydroalcoholic extracts also contain essential oils. Roth (1990) has published a list of 29 ingredients that make up about 65% of the steam distillates: alpha-pinene and 2-methyloctane were the major ingredients. Essential oils from St. John's wort also contain typical terpenes such as Monoterpenes α -pinene and p-pinene, limonene, B-caryophyllene, myrcene, geraniol,

Chapter 3: Identification of Major Constituents of *Hypericum perforatum L*

germacrene D, B-farnesene, humulene, and larger amounts of long chain alkanols, hydrocarbons and alkanols such as undecane, n-undecane, n-nonane, n-tetradecanol, 2-methyloctane and -decane, 2-methyl-dodecane, C16 and C29 alkanes and C24, C26 and C28 alkanols and 2-methylbutenol. Although the specific chemical differences between plants grown in different regions of the world appear to be hereditary, the composition of extracts is, according to several studies, also largely influenced by environmental factors. The plant's location, including the height above sea level, the time of harvest (in which month of the year; before flowering, full flowering or fruit group stages), the harvested parts (flowers, leaves, bells, root or stalk), the polarity of the solvent (methanol, ethanol, acetone, water etc.) used in the extraction, pH of medium, temperature, pressure and exposure to light; all play an important role in the type, nature and concentration of the chemical compounds obtained from the extraction^{4, 14, 17, 19, 22, 25-28}.

Hypericum perforatum L. (St. John's wort) is used as traditional medicinal plant all over the world and was accepted in the European Pharmacopoeia 6. It is utilized in many countries of the world for the production of plant-based pharmaceutical products^{10, 29}, due to its broad diversity of ingredients like hypericins and hyperforins which harbour considerable pharmaceutical effects³⁰. Traditional uses have included topical or oral application for the treatment of diabetes, bruises, rheumatism, burns, malaria, skin wounds, biliary disorders, migraines, eczema, common cold, gastric ulcer, menorrhagia, diarrhea, bedwetting, sprains, bronchitis and urogenital diseases, indigestion, hemorrhoids, snake bite, sprains, hysteria, neuralgia and psychiatric disorders, especially depression^{3, 4, 11, 13, 14, 16, 31-35}. As detailed above, St. John's wort extracts contain various polyphenols, which are considered to be the main source of antioxidant activity, and, consequently, a potential cancer prevention agent^{11, 36}. Consumers prefer natural antioxidants because of their assumed lower potential toxicity compared to synthetic antioxidants³⁶. Both the phytochemicals and essential oils of St. John's wort exhibit pharmacological effects, such as anti-inflammatory, antiviral, antibacterial, antidiabetic, antifungal, cholagogic and choloretic, analgesic, anticholinesterase, antioxidant, antidepressive, antiulcerous, anticonvulsant, and cytotoxic activities^{2, 10, 11, 32, 37-42}.

Hypericin as a major photosensitizing agent has been used in vitro and in vivo, in photodynamic cancer therapy, including squamous cell carcinoma, human leukemia, nasopharyngeal carcinoma, or viral infections as sindbis virus, herpes simplex virus types II and I, vesicular stomatitis, influenza virus, HIV-I and murine cytomegalovirus^{14, 15, 17, 43-46}. Hyperforin suppresses the proliferation of alloreactive T cells, inhibits the proliferation of peripheral blood mononuclear cells, inhibits the growth of MT-450 breast carcinoma in immuno-competent Wistar rats, and activates a mitochondria mediated apoptosis when added to MT-450 cells^{14, 15, 47, 48}. Flavonoids have exhibited activity against cancer and influenza virus^{15, 17}.

High-performance liquid chromatography (HPLC), linked with UV detectors, is a routine technique in most laboratories for chemical separation and detection. HPLC is also the preferred separation technology for the isolation of non-volatile, often polar and unstable components present in natural products. In the literature, many HPLC methods have been reported in the identification of main components such as phloroglucinols, naphthodianthrones,

Chapter 3: Identification of Major Constituents of *Hypericum perforatum* L

flavonoids, phenolic acids, biflavones, aurones, xanthenes .etc., from St. John's wort ^{11, 12, 18, 20, 21, 26, 49-53}, (see table S1 in ESI).

In this paper, the aerial parts (leaves, stems, petals, and flowers) of St. John's wort harvested from Syria were cleaned, dried, and extracted using eight different extraction procedures: water (boiling with water for almost 3 hours (water I) or using tea method (water II)), ethanol, methanol, and acetone (100% and 70%). A new, simple, effective, accurate and repeatable HPLC method was developed for the isolation and identification of the major chemical ingredients. HPLC diagrams for all eight extracts contained the same peaks and only varied in the intensity of these peaks. HPLC-DAD-ESI-MS analysis was performed under positive ionization mode to obtain the exact mass data in the MS full scan experiment and to identify the constituents. The compounds that were identified in these extracts, either by UV, HPLC or by HPLC-MS analysis were: chlorogenic acid, hypericin, hyperforin, hyperoside, quercetin, quercitrin hydrate, rutin, biapigenin, quercitrin and adhyperforin. The antioxidant effect and free radical scavenging activity of extracts of St. John's wort, were determined in two ways: First based on the compounds' capability to transform the DPPH radical (purple-colored) to its reduced form DPPH-H (yellow-colored) and second, by their capability to act as electron donation radical scavenger inhibiting the formation of the green-colored ABTS^{•+} radicals. Total phenols in the extracts (water I, water II, EtOH 100% and MeOH 100%) were quantified and it was found that the antioxidant activity increased with the increase of total phenols.



Figure 3-1: a; *Hypericum perforatum* L. (St. John's wort), b; *H. perforatum* flowers, c; *H. perforatum* leaves, d; *H. perforatum* fruits Adapted with permission from reference ⁴. Copyright 2012 Academic Journals

3.4 Materials and Methods

3.4.1 Chemicals

Aerial parts (leaves, stem, petals, and flowers) of *Hypericum perforatum* L (St. John's wort) were collected in July–August 2018 from the Ghab Plain in Syria (google maps: 35.586856, 36.355724 and 180-200 m above sea level), and harvested during the flowering season. Hypericin and quercetin were purchased from Cayman Pharma (Neratovice, Czech Republic);

Chapter 3: Identification of Major Constituents of *Hypericum perforatum* L

hyperoside from Roth (Karlsruhe, Germany); quercitrin hydrate, chlorogenic acid, 1,1-diphenyl-2-picrylhydrazyl (DPPH), potassium persulphate and 2,2'-azino-bis(3-ethylbenzothiazoline-6-sulfonic acid) (ABTS) from Sigma-Aldrich (Darmstadt, Germany); filter paper Whatman 90mm from GE Healthcare Life Sciences (Freiburg Germany); 0.22 µm nylon syringe filter, Sartolab Vakuumfilter 180C5, 0.22 µm Polyethersulfon, 500 ml, syringe filter 25 mm, 0.45 µm RC with GF prefilter and 0.45 µm PTFE filter from Sartorius (Goettingen, Germany); 0.45 µm prefilter from wicom (Heppenheim, Germany). Ethanol, methanol, and acetone were HPLC grade from Roth (Karlsruhe, Germany); acetonitrile from VWR (Hannover, Germany) and water was purified by a QM system from Sartorius (Goettingen, Germany).

3.4.2 Instrumentation

The HPLC system consisted of a VWR HITACHI liquid chromatograph equipped with a 5160 pump, an 5260 autosampler, 5430 diode array detector, organizer (eluent stand), and a temperature controller for column and sampler (5310 Column Oven) (VWR, HITACHI, MA, JAPAN). The absorption was measured in the range of 200–800 nm, UV–visible detector working at 260 nm for hyperforins, 350 nm and 590 nm for hypericins. The chromatographic data were recorded and processed with Agilent Open LAB Control Panel software. For UPLC-ESI-QTOF-MS analysis, a Waters Acquity high-performance liquid chromatography (UPLC, Waters) coupled to a time of flight Q-TOF micro mass spectrometer (Waters) and equipped with electrospray ionization (ESI) was used. Mass spectra were recorded in positive ion mode, 3 kV capillary voltage, and 230 °C desolvation temperature.

3.4.3 Raw plant preparation and extraction

The aerial parts (leaves, stem, petals, and flowers) of *St John's wort* were washed in cold water to clear them of mud and soil, dried, cut into small pieces, then ground using a ball mill until a fine powder was obtained. 0.360 g of this powder was placed in a 1000 ml beaker, then 800 ml distilled water was added. The beaker was placed on a heater at boiling temperature and stirred. Concentration was performed for about 4 hours until the volume of the solution was reduced to about 200 ml (water I). The same amount of powder was placed in a 400 ml beaker and 150 ml boiling water was added, the beaker was placed on the heater, stirred, and left at room temperature for about 20 minutes (water II). Subsequently, the aqueous extracts were filtered through a filter paper (Whatman, no 589/2). The resulting filtrate was centrifuged at 24630 x g for 30 minutes to remove residual particles. The supernatant was filtered through 0.22 µm nylon syringe filter. The flow-through was collected (see Figure 2) and the solvent evaporated under nitrogen gas at 30 °C to prevent oxidation.

For ethanol, methanol and acetone extraction, the process was modified as follows: 2 g of powder was placed in a beaker and 150 ml of solvent (100% and 70% for each solvent) were added. The solution turned dark red for EtOH 70% and acetone 70%, light red for EtOH 100%, black red for MeOH 70%, and red for MeOH 100% and acetone 100%. The beaker was covered with parafilm and stirred for 5 h at room temperature (RT). The supernatant was decanted and stored at -80 °C. 200 ml of solvent was added to the sediment, the beaker was covered with parafilm, and then stirred at RT for 17 h. The supernatant was decanted, added to the previous supernatant and then stored at -80 °C. 100 mL of solvent was added to the sediment. The beaker

Chapter 3: Identification of Major Constituents of *Hypericum perforatum* L

was then covered with parafilm and stirred for 3.5 hours at RT. The solution turned slightly reddish with a light brown haze. The supernatant was decanted and added to the previous one. The solutions were filtered first with filter paper (Whatman, no 589/2) and then with Sartolab vacuum filter 180C5; 0.22 μm polyethersulfon (PES) for ethanolic and methanolic extracts. For acetonic extracts, 0.45 μm PTFE filter was used (see Figure 2). The solvent was concentrated by means of a rotary evaporator (water bath temperature = 37 ° C) as far as possible, and the residual solvent was removed by freeze drying.

3.4.4 Standards and References compounds solutions

Five reference compounds (standards) were used in this study: chlorogenic acid, quercetin, hyperoside, quercitrin hydrate and hypericin. These substances and different extracts were solved in HPLC grade ethanol in different amounts as shown in Table 1 and filtered through a 0.45 μm prefilter (wicom, Germany) before undertaking HPLC analysis.

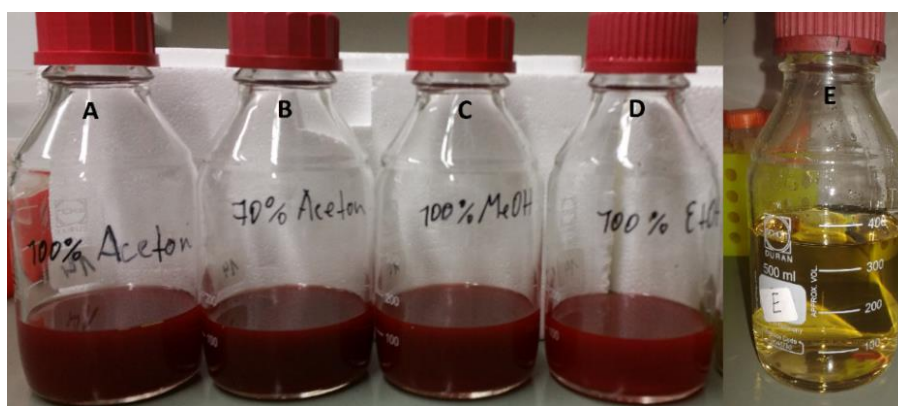


Figure 3-2: Colors of extracts obtained using different solvents in this study; A) 100% acetone, B) 70% acetone, C) 100% methanol, D) 100% ethanol E) water (water I and water II exhibited the same color). Photograph courtesy of Corresponding author Abdalrahim Alahmad. Copyright 2020

3.4.5 Chromatography

3.4.5.1 High-performance liquid chromatography (HPLC)

For HPLC analysis a chromaster HPLC-diode array detection (DAD) system supplied with an autosampler (5260 chromaster, VWR HITACHI, Germany) was utilized. The extract compounds were identified by using column Kinetex C18 100 A (Phenomenex, Germany, dimensions: 100 mm \times 4.6 mm, 5 μm particle size) and guard column C18 4 \times 3.0 mm (Phenomenex, Germany) at room temperature (25 \pm 2°C). Solvent A was 0.1 % formic acid, and solvent B was 0.1 % formic acid, 95 % MeOH, 5 % H₂O. The mobile phase was freshly prepared daily, filtered through a 0.45 μm nylon filter and degassed after preparation for 15 min in an ultrasonic bath. The gradient mode shown in Figure S1 (0 min 95% A, 5% B; 82 min 0% A, 100% B; 92 min 0% A, 100% B; 93 min 95% A, 5% B; 100 min 95% A, 5% B) was used with a flow rate of 1 mL/min. Specific amounts of the dried extract (Table 1) were dissolved in HPLC grade ethanol. All samples were filtered through a 0.45 μm prefilter (wicom, Germany) before undertaking HPLC analysis. The injection volume was 10 μL and every sample solution was injected in triplicate at different time periods and with different taken concentrations for all experiments, indicating that the method is accurate and repeatable. For the identification of the compounds, standards such as: chlorogenic acid, hyperoside,

Chapter 3: Identification of Major Constituents of *Hypericum perforatum* L

quercitrin hydrate, quercetin and hypericin) were run under the same conditions, using dilutions in HPLC grade ethanol (Table 1). The detection was performed at 260, 350 and 590 nm for all samples and standards. St. John's wort compounds of different extracts (Water I & II, EtOH% 100, EtOH% 70, MeOH% 100, MeOH% 70, Acetone% 100, and Acetone% 70) were identified by comparing their retention times with each other and with the retention times of standards, in addition to comparing their UV spectra and literature data.

Table 3-1: Overview of the measured samples, standards, and spiked samples

St. John's wort Extracts	Amount [mg] dissolved per ml EtOH	Standards	Amount [mg] per ml EtOH	Ethanol Extract with Standards together	Spiking Ratio $V_{\text{extract}} [\mu\text{l}] + V_{\text{Standard}} [\mu\text{l}]$
Water I	20	Quercetin	0.5	Extract + Quercetin	100 + 50
Water II	30				
Ethanol 100 %	20	Chlorogenic acid	1.4	Extract + Chlorogenic acid	13+5
Ethanol 70 %	30				
Methanol 100 %	33.8	Quercitrin hydrate	0.9	Extract + Quercitrin hydrate	120 + 20
Methanol 70 %	25				
Acetone 100 %	33	Hyperoside	1.1	Extract + Hyperoside	50 + 50
Acetone 70 %	20	Hypericin	1.7	Extract + Hypericin	50 + 50

3.4.5.2 UV-vis spectra

UV spectra of pure hypericin and St. John's wort extracts were run with a chromaster 5430 diode array detector and spectra acquired over the absorption range of 200–800 nm. Identification of hyperoside, quercitrin hydrate, quercetin and hypericin in the extracts (EtOH, MeOH, and acetone; 100% and 70% respectively) was performed by comparing curves from the maxima of absorptions of extracts at 260 nm at 19.9 min, 24.36 min, 29.4 min and 81.49 min respectively, with the UV-Vis spectra of the standards at the same wavelength and time.

Chapter 3: Identification of Major Constituents of *Hypericum perforatum L*

3.4.5.3 HPLC-MS spectra

For the HPLC-MS analysis, the column used in HPLC analysis was installed in another HPLC device to which an MS device was directly connected. For high performance liquid chromatography with mass detection (HPLC-MS) analysis, a Waters Acquity ultra performance UPLC with a Kinetex 5 μm C18-column (Phenomenex, 100x4.6 mm) was used with a linear gradient of (A) water with 0.1% formic acid and (B) 0.1 % formic acid, 95 % MeOH, 5 % H₂O at a flow rate of 500 $\mu\text{L}/\text{min}$ (initial: 95% A, 5% B; 82 min: 0% A, 100% B; 92 min: 0% A, 100% B; 93 min: 95% A, 5% B; 100 min: 95% A, 5% B runtime: 100 min). The injection volume was 5 μL . A chromatogram was recorded in parallel to the mass spectrum. Therefore, the UV measurement was only carried out at two wavelengths, namely at 260 nm and 350 nm. MS analysis was carried out on a Q-ToF Premier (Waters) using electrospray ionization (positive ions, 3 kV capillary voltage; 250 °C desolvation temperature; 650 L/h desolvation gas flow (nitrogen)).

3.4.6 Determination of total phenolic content of crude extracts of *Hypericum perforatum L*.

The total phenolic content of plant extracts was determined as shown in the references⁵⁴⁻⁵⁶ with some modifications. Gallic acid represents one phenolic compound of *Hypericum Perforatum L.*, and was therefore used as a standard. 10 mg of the standard (gallic acid) was dissolved in 100ml of distilled water to give a concentration of solution 100 $\mu\text{g}/\text{mL}$.

3.4.6.1 Preparation of the standard calibration curve of gallic acid

Aliquots of 0.25, 0.5, 1.0, 1.5 and 2.0 ml of the 0.1 mg/ml gallic acid solution were placed in 5 different 15ml glass test tubes. 2.5ml of a tenfold dilution of Folin-Ciocalteu phenol reagent (1:10 v/v with distilled water) and 2.0 ml of a 7.5% w/v sodium carbonate (Na₂CO₃) solution were added to each tube. The volume in the tubes was increased up to 10 ml with distilled water, resulting in gallic acid concentrations ranging from 2.5-20 $\mu\text{g}/\text{ml}$. Mixture of reagents and water was used as a blank. The resulting solutions were put in a water bath at 45 °C for 30 minutes. Thereafter, the absorbance at 765nm was read using a UV-VIS Spectrophotometer.

3.4.6.2 Preparation of sample extracts solutions

10 mg of each of the extracts were dissolved in 10 ml of an appropriate solvent (water, ethanol or ethanol) to get 1mg/ml solution. 1 mL of this solution was then put in a 15ml glass test tube and color development was undertaken in the same manner as for the standard. The absorbance of the test solutions at 765 nm against a reagent blank (appropriate solvent) was measured. All the tests were done in triplicate, results averaged and expressed as mean \pm standard error of the mean. The concentration of phenols in the test samples were determined by extrapolation from the gallic acid standard calibration curve and calculated as mg of gallic acid equivalents (GAE) per g of dried extract (de) (mg.GAE.g⁻¹) using the formula as described by^{56, 57};

$$P=C \times V/M$$

Where; P = Total phenolic content in milligrams per gram of the dry plant material (mg. g⁻¹), C = Concentration of gallic acid established from the calibration curve in milligram per milliliter (mg/ml), V = Volume of the extract solution in milliliters (ml), M = Weight of the extract in grams (g)

Chapter 3: Identification of Major Constituents of *Hypericum perforatum L*

3.4.7 Determination of antioxidant activity

3.4.7.1 DPPH

The antioxidant activity of water, ethanol and methanol extracts was measured depending on their scavenging activity of the stable 1, 1- diphenyl-2-picryl hydrazyl (DPPH) free radical. DPPH is a recognized radical and a scavenger (snare) for other radicals. Because of a powerful absorption band at around 517 nm, the DPPH radicals have a profound violet color in solution, and when neutralized they turn pale yellow or colorless. Therefore, the change in absorption at 517 nm allows the calculation of the number of primary radicals. The DPPH assay was performed as previously described^{58,59} with some modifications. Different concentrations (1-500 µg/ml) of the extracts and standard were prepared, then 1 ml of each solution was added to 3 ml of 0.004 % ethanolic DPPH free radical solution. The absorbance of the preparations was measured after about 30 minutes of exposure to normal light at room temperature by a UV-VIS spectrophotometer at 517 nm. The results were compared with the corresponding absorption of standard ascorbic acid concentrations (1-500 µg/ml). Finally, the free radical-scavenging ability (RSC) expressed as a percentage, as calculated by the equation:

$$\text{RSC (\%)} = 100X (\text{A}_{\text{blank}} - \text{A}_{\text{Sample}} / \text{A}_{\text{blank}})$$

The inhibitory concentrations (IC₅₀) were determined. IC₅₀ value indicates to the concentration of sample required to scavenge 50% of the DPPH free radicals^{59, 60}.

3.4.7.2 ABTS

We use spectrophotometric method to assess the loss of color when adding antioxidants to the blue- green chromophore ABTS^{•+} (2, 2-azino-bis (3-ethylbenzothiazoline- 6-sulfonic acid)). ABTS^{•+} is reduced by antioxidants to ABTS and loses its color. ABTS antioxidant activity was measured as described⁶¹ with some minor modifications. ABTS was prepared with 7 mM concentration by using water as a solvent. The ABTS solution was mixed with 2.45 mM potassium persulphate at a ratio of 1:1 (v/v). The mixture was placed in the dark at room temperature for 18 hours. The ABTS^{•+} solution was diluted about 20 times with water (or ethanol or methanol based on the nature of the solvent employed in the extraction) to reach an absorbance of 0.850 ± 0.05 at 734 nm. 150 µL of this ABTS^{•+} solution was added to 50 µL of different concentrations of extracts and incubated for 6 min at room temperature. For the control, 50 µL of solvents (water, ethanol and methanol) used in the respective extraction was used in place of extract. Ascorbic acid was used as a positive control. Absorbance at 734 nm was measured spectrophotometrically in 96-well microplate. The percentage of inhibition was calculated utilizing the same equation as in DPPH assay and the radical scavenging activity was expressed as the IC₅₀ value. The results of all experiments (samples, standards and blank) were reported as mean ± standard error of three separate determinations. Statistical analysis was performed by analysis of variance using origin statistical software.

3.5 Results and Discussion

3.5.1 Extraction

The water I and water II extraction processes resulted in yellow-brown solid with a yield of 21% for water I and 16% for water II. The organic solvents resulted in a black-gray solid with

Chapter 3: Identification of Major Constituents of *Hypericum perforatum* L

a yield of 25.5% for ethanol 70% (light gray), 7% for ethanol 100% (black gray), 22.9% for methanol 70% (light gray), 18% for methanol 100% (black gray), 23.2% for acetone 70% (light gray) and 7% for acetone 100% (black gray). The yields resulting from the mixture of water with organic solvents were much higher when compared with the yields of the pure organic solvents. Also, extracting with water using the tea method resulted in higher yields than boiling with water for a long time. By increasing the polarity of the solvent, higher yields were obtained, indicating that mainly hydrophobic compounds were extracted. Therefore, we conclude that extracting the plant with water using the tea method or using a mixture of water with organic solvents produces higher yields of the resulting extract when compared with pure organic solvents or continuous boiling with water for long periods.

3.5.2 Characterization of extracts using HPLC

Reversed phase chromatography has analytical and preparatory applications in the field of phytochemical separation and purification and the active ingredients of a plant extract can be isolated using an appropriate isolation procedure⁶². During the protocol development process, many factors were changed and tested, such as column type (nature of the stationary phase and its particle size), mobile phase or gradient elution (the exact composition of the solvents, its polarity and gradients of different solvents), flow rate, the temperature of the column, the pressure used (maintaining linear velocity) and wavelength. Subsequently, we were able to develop the protocol used, through which well-separated peaks were obtained without any obvious overlap between them. The different extracts were measured using HPLC under the same conditions and can thus be directly compared with each other. The chromatograms of the measurement series at the three most important wavelengths (260 nm, 350 nm and 590 nm) are shown in Figure 3. The respective graphs show no general differences between ethanolic, methanolic and acetonic extracts with regard to position of the obtained peaks; only differences in the intensity of the peaks were observed, as some solvents extract certain compounds more effectively than others. The ethanolic, methanolic and acetonic extracts (whether 100% or 70%) are similar concerning the ingredients which are present, but differ in the concentration of these ingredients. In contrast, the aqueous extract is completely different to the ethanolic, methanolic or acetonic extracts. Aqueous extracts obtained by water I and water II extraction procedure were identical, especially at 260 nm and 350 nm, where especially phloroglucinols, flavonoids and phenolic acids could be expected (active constituents, hyperforin and its derivatives). While the aqueous extract has fewer peaks or very low peaks (the peaks are present, but when drawn in same scale as the chromatograms of organic extracts, peaks are not visible due to their low intensity) at 590 nm of the chromatogram where e.g. naphthodianthrone (hypericin exhibits a very low level of solubility in pure water because of its hydrophobicity^{63, 64}) could be expected. Also, it can be concluded that at 100 °C, in particular, the strongly polar compounds are virtually all decomposed. Plant extracts are usually composed of a mixture of different types of phytochemicals or specialized metabolites with different polarity, in the reversed phase chromatography; the bioactive polar compounds eluted prior to the less or non-polar one. This explains why in the water extract fewer peaks appear at high retention times, because the high retention times correspond to the less or non-polar specialized metabolites. It is clear that less or non-polar substances are more difficult to extract from water. It should also be noted that some ingredients of St. John's wort are not

Chapter 3: Identification of Major Constituents of *Hypericum perforatum* L

stable at high temperatures and should therefore always be extracted at low temperatures. It is also noteworthy that the main constituents in the *St John's wort* extracts, especially hypericins, may be retained by some cartridges filter during the filtration process^{17, 20}. Hypericin and pseudohypericin are substantially insoluble in water at ambient temperature, and can only be obtained with less than 40% yield at higher temperatures^{4, 17-19}. When prepared by tea method, the extract contains very little amounts of hyperforin^{19, 25}. The concentration of chlorogenic acid which has been detected in *St. John's wort* is below 1%¹⁷.

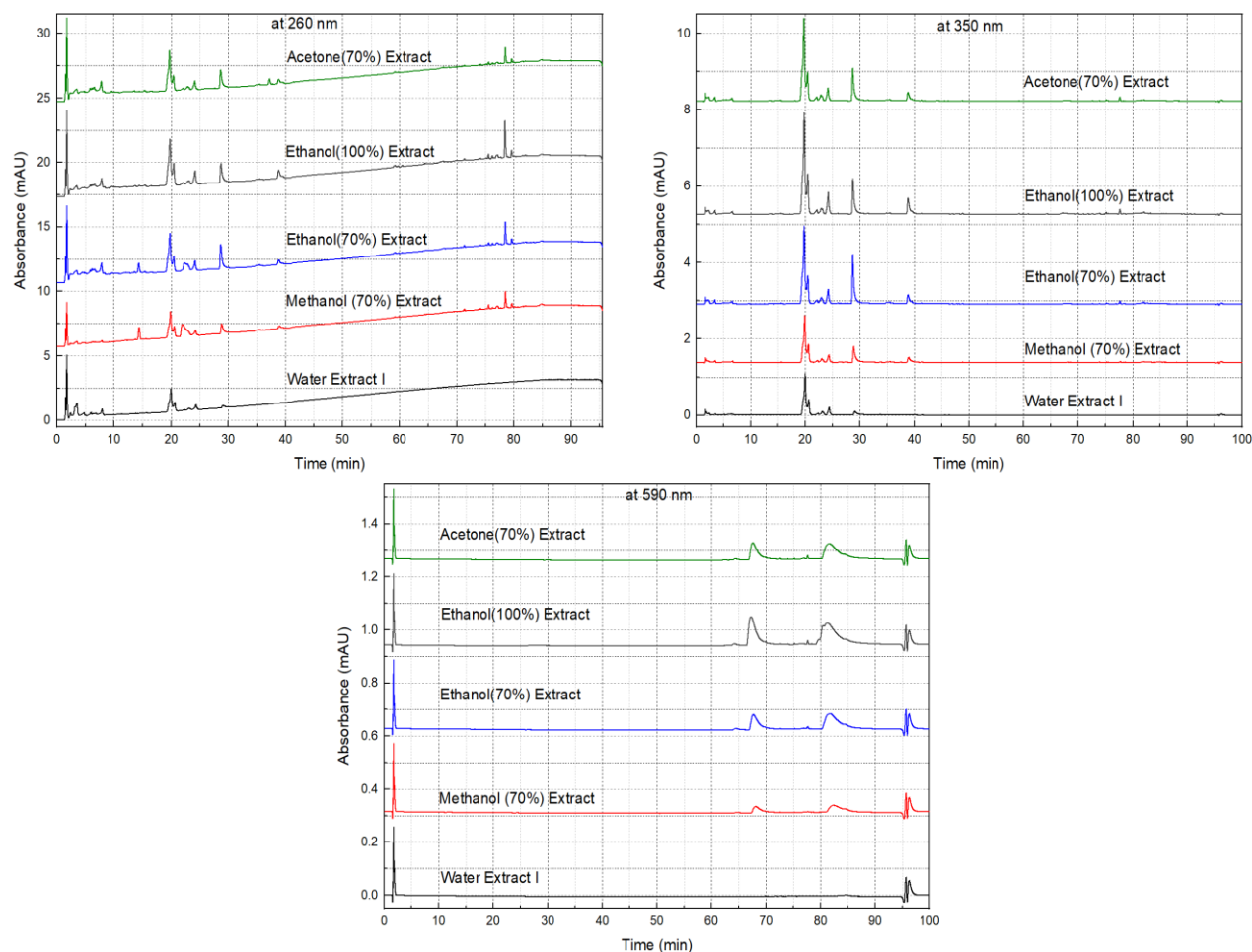


Figure 3-3: HPLC chromatograms of aqueous extract, ethanolic extract (100% and 70%), methanolic extract (100% and 70%) and acetonic extract (100% and 70%) of *Hypericum perforatum* L. (detection at 260, 350 and 590 nm).

Chapter 3: Identification of Major Constituents of *Hypericum perforatum L*

3.5.3 Characterization of extracts with Standards using HPLC

In this series of measurements (Figure 4, 5), the extracts, standards and extracts spiked with standards were measured under the same conditions. Standards were used to analyze the constituents of St. John's wort extracts and were chosen to cover the complete chromatogram as well as the most important wavelengths, and, based on their stability and solubility, in the solvents used for extraction. Five standards were selected for this, which represent the most important and best-known compounds of St. John's wort. These include quercetin and quercitrin, which have been used as a hydrate, as well as hyperoside, chlorogenic acid and hypericin. The first four mentioned standards cover the two important wavelengths at 260 and 350 nm and are distributed in the middle of the obtained chromatograms of St. John's wort extract. Hypericin is represented at a high retention time (approximately 81,5 min) of the St. John's wort chromatograms and also covers a significant absorbance at 590 nm (Figure 4).

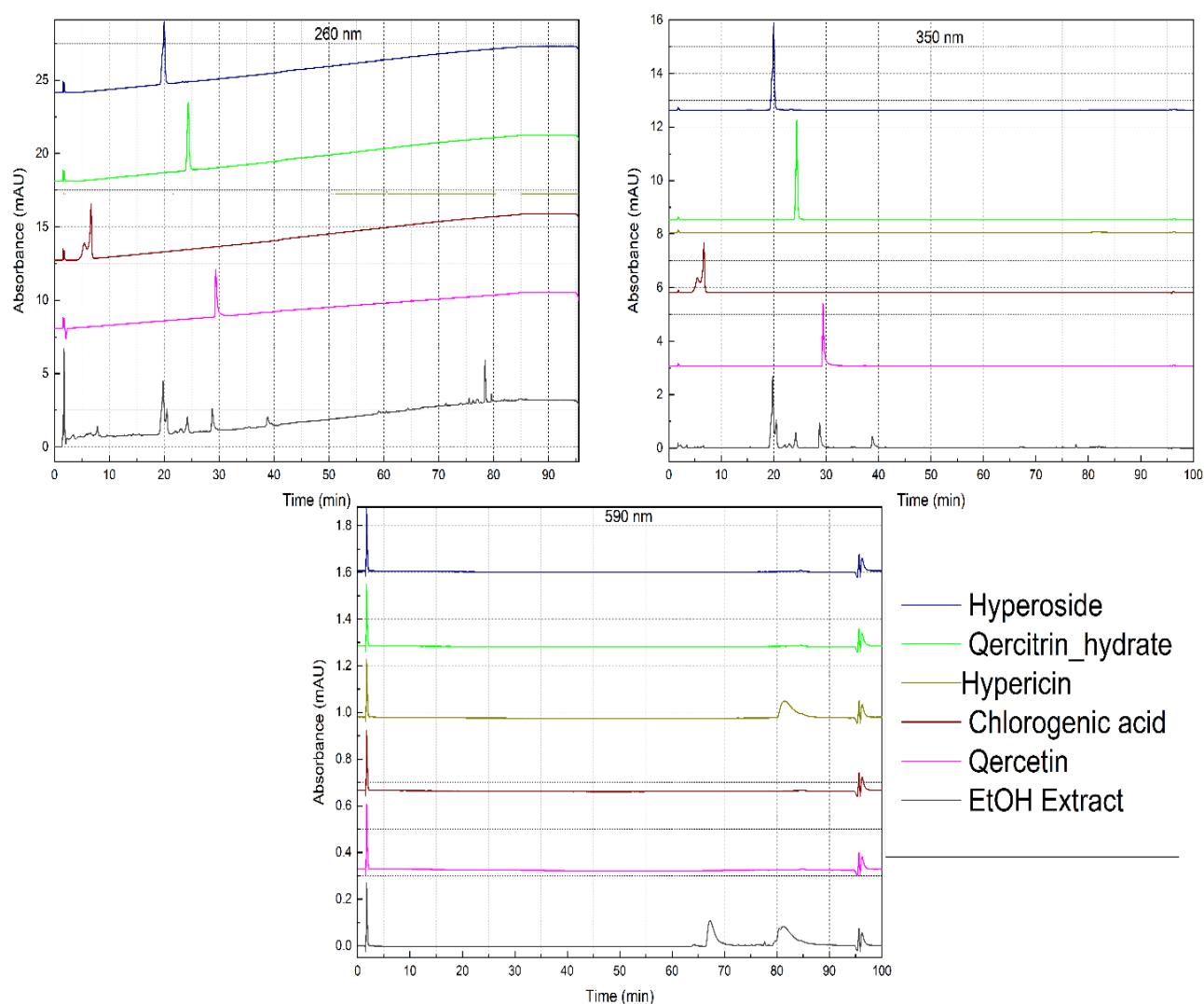
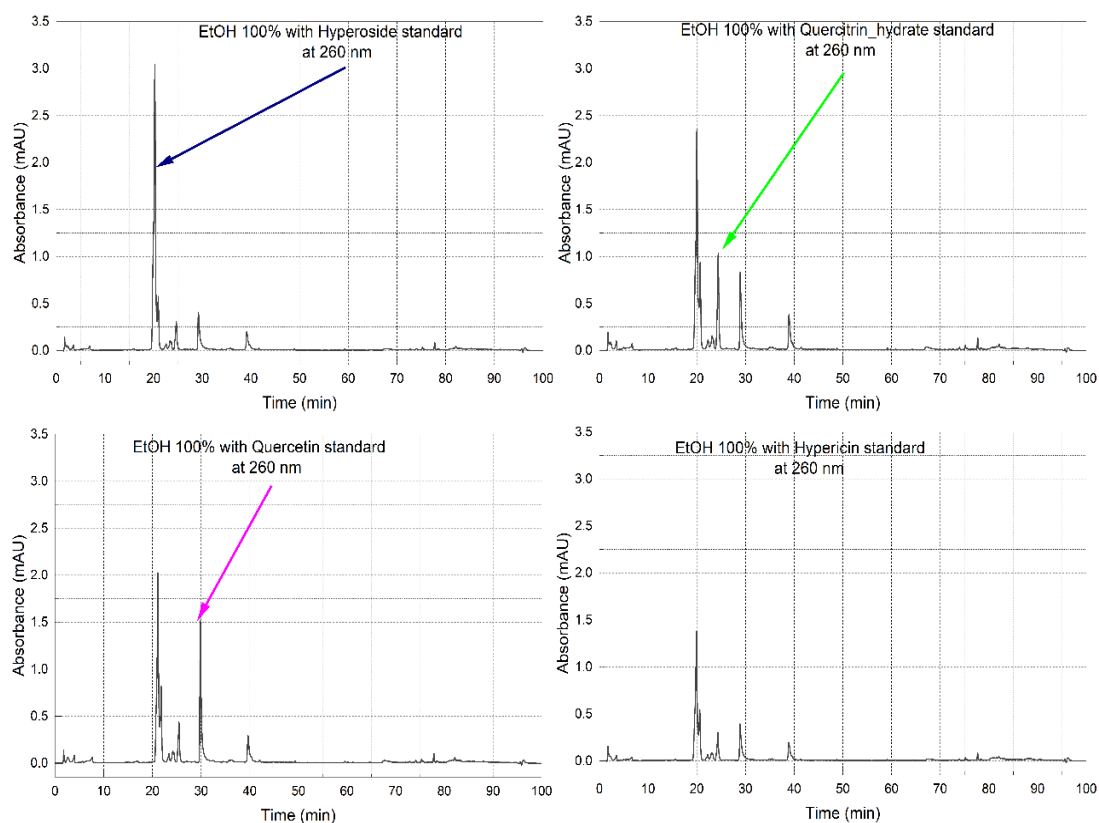


Figure 3-4: HPLC Chromatograms of standards; hyperoside, quercitrin_hydrate, quercetin, hypericin, chlorogenic acid and ethanol extract separately at 260 nm, 350 nm and 590 nm

Chapter 3: Identification of Major Constituents of *Hypericum perforatum L*

Extracts were analyzed by addition of different standards (Figure 5). If the compound to be examined was already present in the extract, the corresponding peak will increase in the chromatogram by the added standard amount. This increase in the peak would thus provide a good indication that it is the same compound. By adding the standards to be confirmed to the sample, the effect of the column drifts can be prevented. Figure 5 shows four chromatograms, each with a different standard added. Due to the addition of the respective standard, a peak increased in each chromatogram (indicated by an arrow) when compared with chromatograms of pure extract. Thus, within the scope of its analytical accuracy, this method indicates the presence of the four compounds; hyperoside, quercetin, quercitrin hydrate and hypericin in the ethanolic extract. This also applies for methanolic, acetonetic, and aqueous extracts and also is in agreement with the literature [7].

However, a final identification of substances is not possible using this method, as other components could have the same retention time. This method of substance analysis by adding a standard thus serves only as an indication of the presence of certain compounds and simplifies the comparison of the chromatograms with the literature information. Therefore, further and more precise analysis methods have been used for the final substance analysis.



Chapter 3: Identification of Major Constituents of *Hypericum perforatum* L

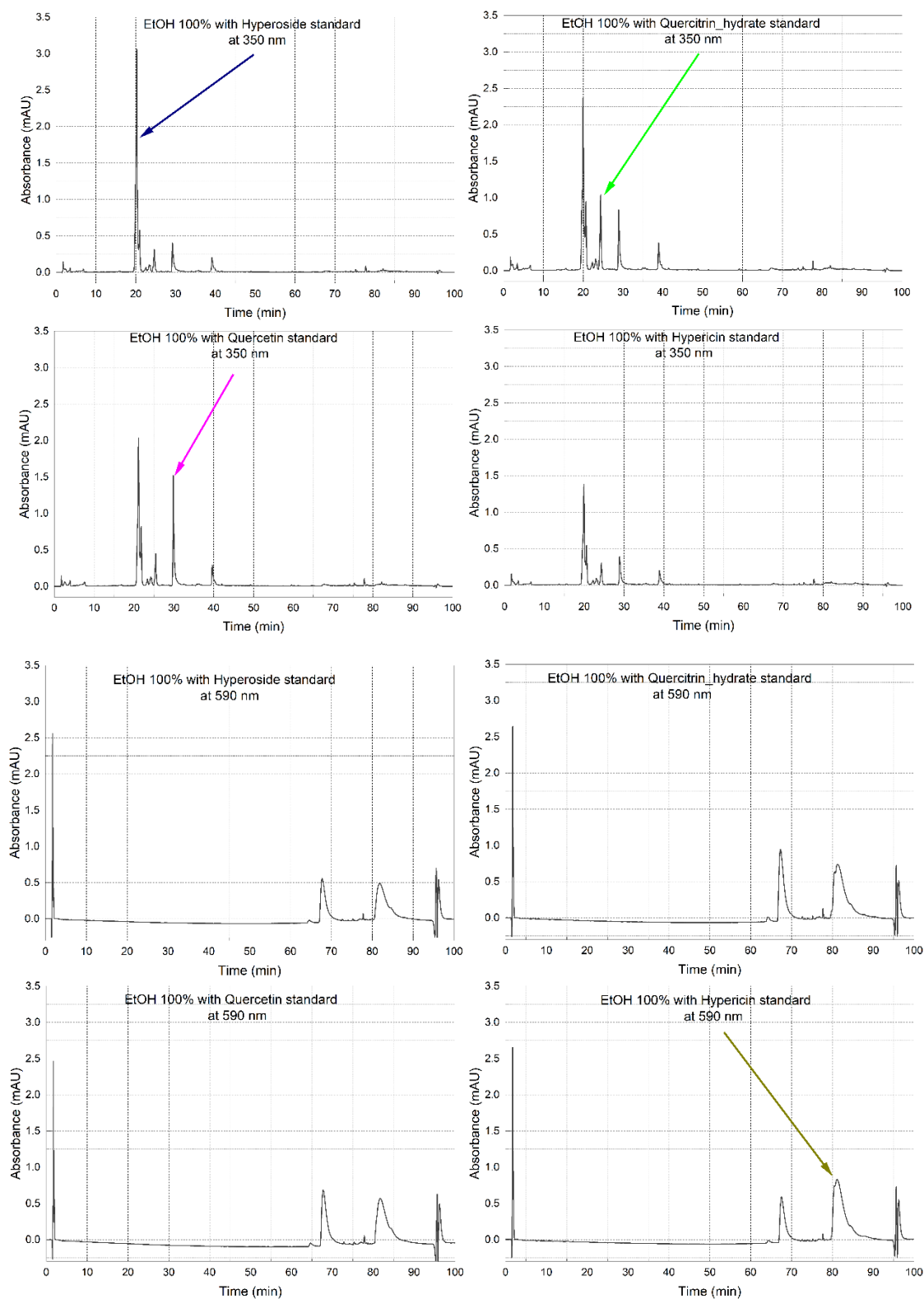


Figure 3-5: HPLC chromatograms of standards; hyperoside, quercitrin hydrate, quercetin, hypericin, chlorogenic acid mixed together with ethanol extract at 260 nm, 350 nm and 590 nm

3.5.4 UV-Vis analysis

Each substance has a characteristic UV spectrum. The various substances separated via HPLC can thus be identified by comparing the measured UV spectra with corresponding spectra from the literature or measured for a standard. When analyzing St. John's wort extracts, it must be

Chapter 3: Identification of Major Constituents of *Hypericum perforatum L*

borne in mind that ingredients such as quercetin and other likely ingredients are sensitive to changes in pH, which leads to the formation of new substances⁶⁵. For this reason, UV spectra of some peaks with suspected constituents of the measured samples (EtOH 100% or 70%) were compared with the UV spectra of the standards, which were recorded under the same conditions. Figure 6 shows the UV spectra of the measured standards hyperoside, quercitrin hydrate, quercetin and hypericin each with the UV spectra of the selected corresponding peaks of the ethanolic extract. The peaks selected are those that experienced a peak increase when the ethanolic sample was spiked with the respective standards. In Figure 6 it can be clearly seen that the UV–Vis spectrum for the peaks at retention time 19.907 min, 24.364 min and 29.404 min are completely identical with the UV-Vis spectra obtained for standards hyperoside, quercitrin hydrate and quercetin respectively. Figure 6 d shows that the UV spectrum of the hypericin standard differs slightly in its intensity from the selected peak of the ethanol sample at the same time, although the peak of the sample is well isolated, possibly due to the difference in concentration. The results of these comparisons show that this method is only of limited use for the identification of analytes. UV–Vis analysis merely indicates the presence of these compounds. The presence of other analytes at the same peak in the chromatogram can change the UV spectrum significantly. Furthermore, other analytes can have the same UV spectrum at the same retention time. For this reason, this method is only suitable for a quick and basic orientation when interpreting chromatograms.

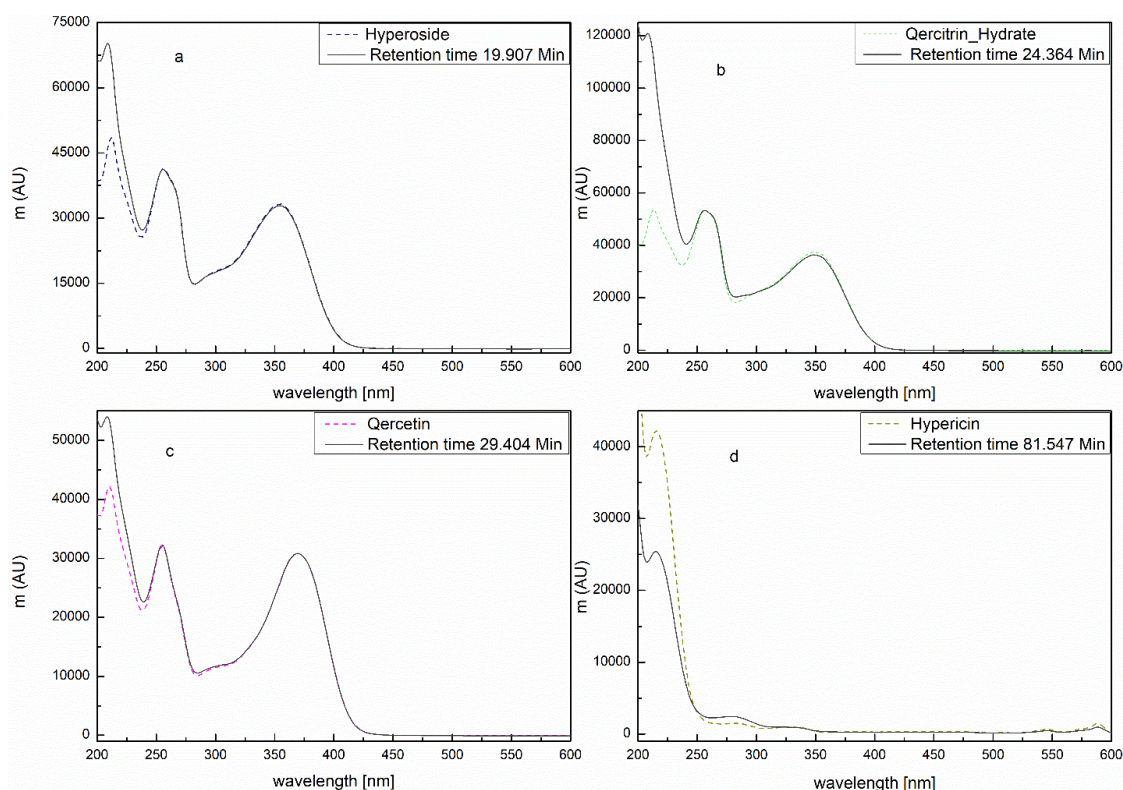


Figure 3-6: Overlay UV spectrum of the peaks detected by HPLC–DAD. (a) Retention time 19.907 min and standard hyperoside at the same time; (b) retention time 24.364 min and standard quercitrin hydrate at the same time; (c) retention time 29.404 min and standard quercetin at the same time and (d) retention time 81.547 min and standard hypericin at the same time.

Chapter 3: Identification of Major Constituents of *Hypericum perforatum L*

3.5.5 Identification of the main compounds using HPLC-MS analysis

HPLC-MS method exhibits unique selectivity and sensitivity, because it combines high performance liquid chromatography, which has strong separation ability, with the detection via mass spectrometry, which has an unparalleled structural analysis ability. This technique is a fast, specific, and delicate analytical method and is one of the most efficient processes for the determination of metabolites, and has thus become a key tool in the metabolic exploration of plant extracts⁶⁶.

The measurement of the masses for the eluted components is preceded by the detection of UV absorption at 260 nm and 350 nm for the ethanolic extract. The chromatograms of the sample (Figures 7 and 8) correspond to the previous measurement (Figures 4&5). The mass spectrum (Figure 9) of the ethanolic extract has many peaks over the entire spectrum, in particular in the range between 50 and 70 min, in which there is a very strong superimposition of the peaks. To provide a better overview, the peaks of the mass spectrum are marked with a number and shown in Table S2 with the corresponding retention times and ion masses. For a clear comparison of the chromatogram with the respective mass spectrum, the retention times of the chromatograms and the mass spectra are compared in Tables 2 and 3. It should be noted that not all of the peaks of the mass spectrum can be analysed, because some of the compounds cannot be detected using a UV detector. However, most compounds can be detected using MS. The sample-sparing electrospray method was used for the ionization of the sample, in which positively charged ions are formed and there is negligible fragmentation of the sample molecules. The comparison of the peaks from the chromatogram with the peaks from the mass spectrum shows that the chromatogram peaks correspond to the mass spectrum peaks. In the respective tables (Table 2 and 3), however, a mass spectra peak cannot be given for each chromatogram peak. This can be demonstrated with a visual comparison, however. In the two chromatograms of the ethanolic extract (Figure 7 and 8), it can be seen that almost all peaks are quite narrow. As a result, the method used to separate the ingredients of the extract can be considered successful. The peaks which cannot be separated completely are too similar in retention behavior to be separated in one step with the chosen conditions. This requires fractionation of the eluate and an additional HPLC separation. In view of the low concentrations of compounds in the fractions, HPLC devices would have to be used for particularly small sample quantities. When evaluating the mass spectrum (Figure 9), all peaks are more or less superimposed. Separate groups were observed only up to 45 min. From 45 to about 72 min, so many peaks were recorded that only the outstanding peaks can be viewed more closely.

Chapter 3: Identification of Major Constituents of *Hypericum perforatum L*

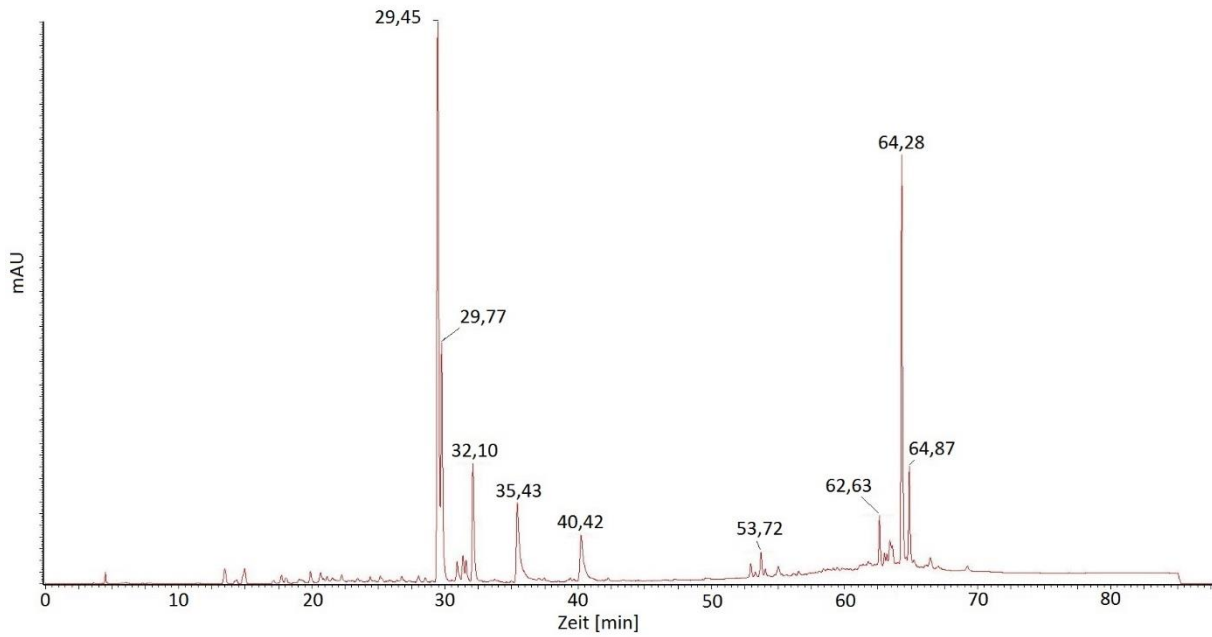


Figure 3-7: Chromatogram of the ethanolic extract (Ethanol 100%) at 260 nm.

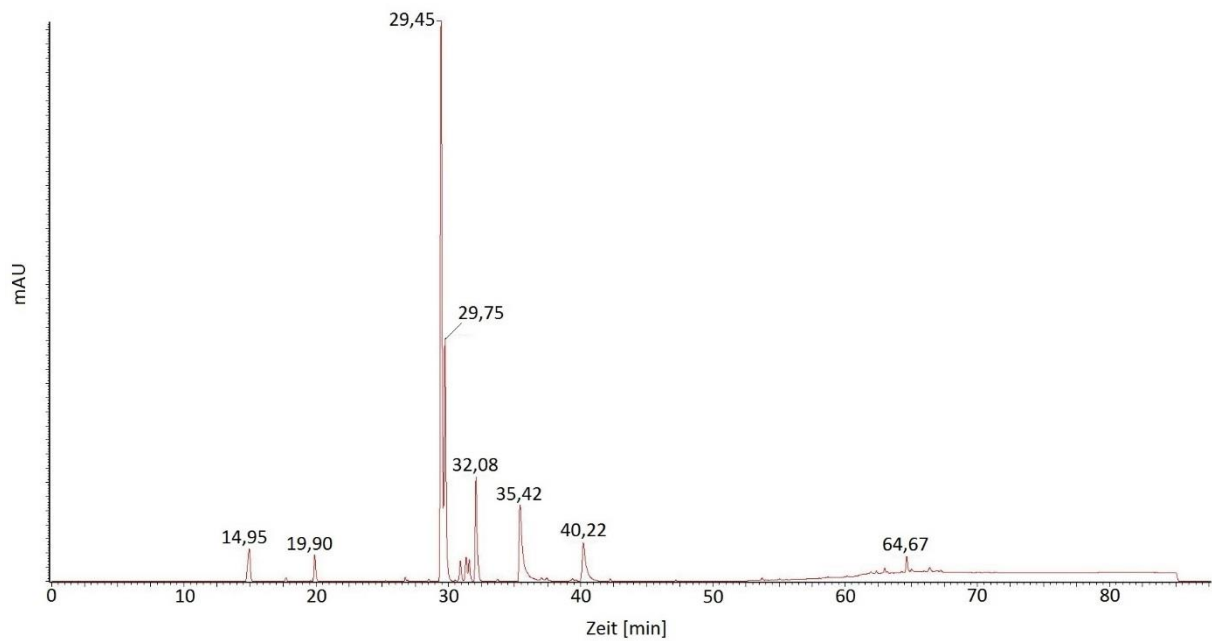


Figure 3-8: Chromatogram of the ethanolic extract (Ethanol 100%) at 350 nm.

Chapter 3: Identification of Major Constituents of *Hypericum perforatum L*

Table 3-2: Comparison of the peaks from the chromatogram of the ethanolic extract (ethanol 100%) at 260 nm with the MS spectrum.

Time HPLC [min]	Time MS [min]	Ion mass MS [m/z]	Peak-Nr. in MS
29.45	-	-	-
29.77	-	-	-
32.10	32.00	303.04	18
35.43	35.37	303.05	20
40.42	40.23	539.09	25
53.72	-	-	-
62.63	62.54	553.37	36
64.28	64.28	559.36	37
64.87	-	-	-

Table 3-3: Comparison of the peaks from the chromatogram of the ethanolic extract (ethanol 100%) at 350 nm with the MS spectrum.

Time HPLC [min]	Time MS [min]	Ion mass MS [m/z]	Peak-Nr. in MS
14.95	14.85	163.03	9
19.90	19.81	163.04	11
29.45	29.32	303.03	16
29.75	-	-	-
32.08	32.00	303.04	18
35.42	35.49	303.04	21
40.22	40.23	539.09	25
64.67	64.57	593.25	38

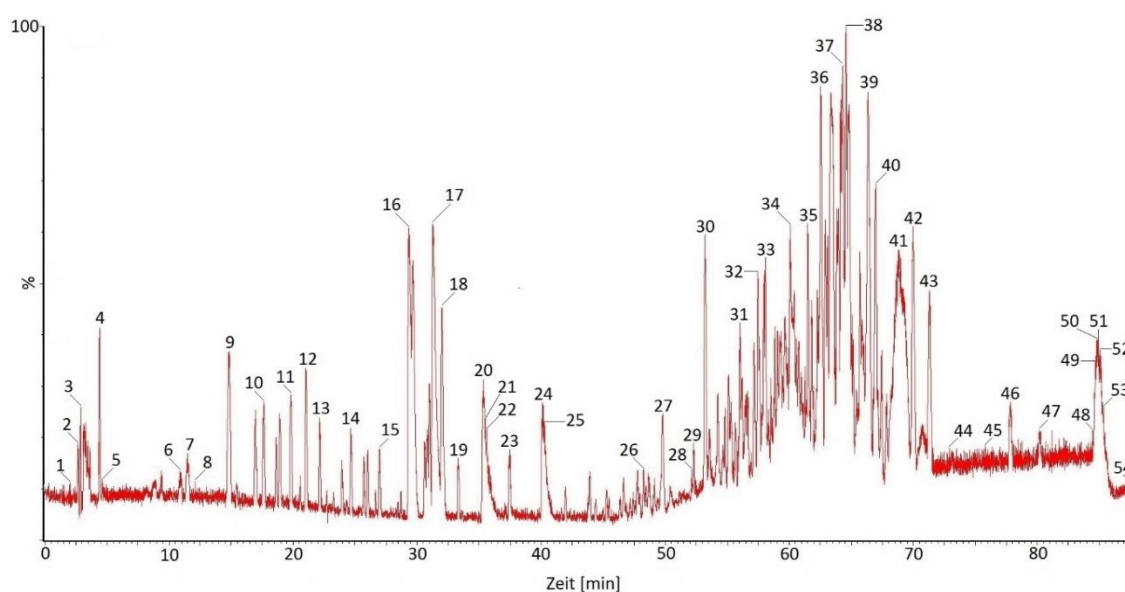


Figure 3-9: Representation of the base peaks after HPLC separation of the sample (Ethanol 100%).

Chapter 3: Identification of Major Constituents of *Hypericum perforatum L*

Table 4 shows the substances identified from the mass spectrum of the ethanolic extract. With the exception of hypericin, the most important and best-known compounds can be identified. In positive ESI mode, the prominent protonated molecular ion $[M+H]^+$ at m/z 355.17 refers to chlorogenic acid. The m/z 303.03 was characterized from the losses of sugar residue from rutin und hyperoside respectively. m/z 303.04 indicates quercitrin without sugar residue, while m/z 303.05 matches quercetin, and m/z 539.09 was determined to be a characteristic fragment ion of biapigenin. m/z 551.42 indicates adhyperforin and m/z 537.43 refers to hyperforin. However, most of the compounds (Table S3) cannot be identified despite the huge number of peaks. Possible reasons for this could be that not all peaks of the mass spectrum are taken into account and many peaks are superimposed. This means that most of the peaks are still unknown compounds because (i) some of the compounds cannot be detected using a UV detector; (ii) because of interference, where some peaks may merge from several peaks; (iii) the molecular weights may not be present in the device library. In order to be able to analyze these aspects, additional HPLC separation steps of individual fractions must be carried out, as already mentioned. Additional methods are also required in which molecular fragments arise during the mass spectrometry measurement in order to enable an even more precise analysis.

Table 3-4: Peak identification from Table 7 with already known substances.

Table -Nr.	Compound	Ion mass [m/z]	Time [min]	Peak-Nr.
8	Chlorogenic acid	355.17	26.97	15
5 + 6	Rutin und Hyperoside each without sugar residue	303.03	29.32	16
15	Quercitrin without Sugar residue	303.04	32.00	18
1	Quercetin	303.05	35.37	20
1	Quercetin	303.04	35.49	21
1	Quercetin	303.05	35.59	22
16	Biapigenin	539.09	40.10; 40.23	24, 25
23	Adhyperforin	551.42	71.28	43
3	Hyperforin	537.43	80.19	47

3.5.6 Total phenol

Most antioxidant activities from plant sources originate from phenolic compounds^{67, 68}. Phytochemicals, particularly phenolic compounds in the plant extract, are the main bioactive components known for their health benefits. Phenolic compounds consist of one aromatic ring (phenolic acids) or more (polyphenols) with hydroxyl groups linked to their structure. Phenolic compounds act as reduction agents, hydrogen donors, and singlet oxygen quenchers due to their redox properties. The natural antioxidants in the plant show a wide range of biological activities, including antibacterial, anti-inflammatory, antiviral, antiallergic, antithrombotic, and vasodilatory actions. The phenolic content of the plant extracts of *St John's wort* was determined spectrophotometrically using the Folin-Ciocalteu assay and expressed as gallic acid equivalents (GAE). There was no significant difference in the resulting phenolic

Chapter 3: Identification of Major Constituents of *Hypericum perforatum L*

compounds for the different water-based methods (Table 5). Although the difference is minimal, we note that extracting the plant after the addition of boiling water gives a better result than heating the water with the plant gradually. A significant difference was observed between methanolic extract (93.2 mg GAE/g) and ethanolic extract (64.4 mg GAE/g). The value for aqueous extracts is much higher than for methanol and ethanol; this may be due to the fact that methanolic and ethanolic extracts do not dissolve fully in water. We note that the standard calibration curve of Gallic acid ($Y=0.06063X + 0.06734$) is linear in the range of 0-20 $\mu\text{g/ml}$ with a correlation coefficient (r^2) of 0.997 (Figure S2). The appropriate selection of the extracting solvent is not as straightforward as it may seem. Effective extraction of phenolic compounds relies on a suitable solvent selection, elevated temperatures, and mechanical agitation. The solubility relies on the polarity of phenolic compounds that exist in the plant. Phenolic compounds have the ability to form hydrogen bonding with water molecules, so they are soluble in water, a polar solvent.

Table 3-5: Total phenolic contents for the studied extracts of *St John's wort*

<i>St John's wort</i>	Total phenolics (mg GAE/g)
Water I	170.6 \pm 1.7
Water II	174.8 \pm 0.9
Ethanol extract	64.4 \pm 1.5
Methanol Extract	93.2 \pm 1.3

3.5.7 Antioxidant activity DPPH

In the DPPH test, we examined the capacity of the tested *Hypericum Perforatum L.* extracts to act as donors of electrons or hydrogen atoms in the conversion of DPPH radicals into their reduced form DPPH \cdot -H. In the present study, aqueous, ethanolic and methanolic extracts were investigated. All extracts showed free-radical scavenging activity, meaning that all the assessed extracts were able to reduce the stable, purple-colored radical, DPPH \cdot into the yellow-colored DPPH \cdot -H (Figure 11). Antioxidant activities of the phytochemicals existing in these extracts perhaps rely on structural factors, like the number of keto groups, free carboxylic groups, methoxyl groups, phenolic hydroxyl, flavone hydroxyl and other structural advantages⁶⁹. For the calculation of the IC₅₀ values the following theoretical function were fit to the measurements using Microsoft Excel solver (Figure 10):

$$f(x) = \frac{A}{1 + e^{-B(\ln(x) - \ln(C))}}$$

A, B, and C are the parameter of the function, x is the concentration and f(x) the corresponding activity. Extracts mark by * the A value were set to the A value of the corresponding ascorbic acid value, because otherwise no reasonable fit is obtained. The parameter errors are determined by the invers of the Fisher information matrix. Using the error propagation calculation the standard error of the IC₅₀ values as well as the confidential interval with alpha = 0.05 are calculated. we found that IC₅₀ of the extracts of *Hypericum Perforatum L.* (*St John's wort*) is 51 $\mu\text{g/ml}$ for extract prepared by using 150 ml boiling water, 60 $\mu\text{g/ml}$ for extract prepared by using cold 750 ml water then boiling until the volume of the solution is reduced to

Chapter 3: Identification of Major Constituents of *Hypericum perforatum L*

approx. 100 ml, 75 µg/ml for ethanolic extract and 67 µg/ml for methanolic extract, which indicates the remarkable antioxidant activity of the extracts.

The most powerful extracts in terms of antioxidant activity were those obtained from water I method (Table 6). This can be explained by the difference in free radicals scavenging activity of extracts based on their chemical composition and content of total phenols and flavonoids. Generally, a positive correlation between phenols and antioxidant activity was found, but the relationship is not obvious, as it depends on the complex composition of the sample. The pool of the phenolic compounds can be low, but due to a high content of, e.g. ascorbate, the total antioxidant status can be very high. The type of phenols and the amount of individual phenolic compounds present in the extract effect the antioxidant properties, and different classes of compounds with low and /or high antioxidant activity could be present in the extract. It is important to analyze each class of compound and relate it to the antioxidant activity.

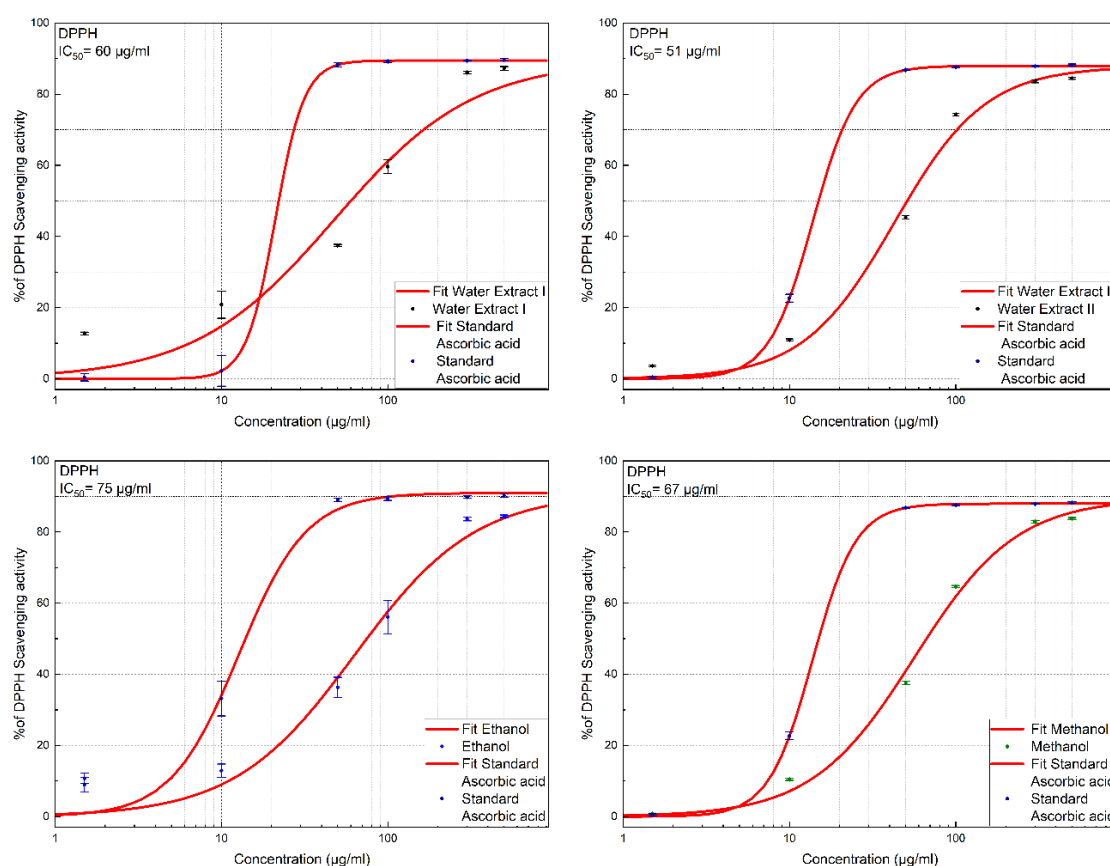


Figure 3-10: Evaluation of IC₅₀ of the St John's Wort extract and standard ascorbic acid using DPPH scavenging Assay

Chapter 3: Identification of Major Constituents of *Hypericum perforatum L*

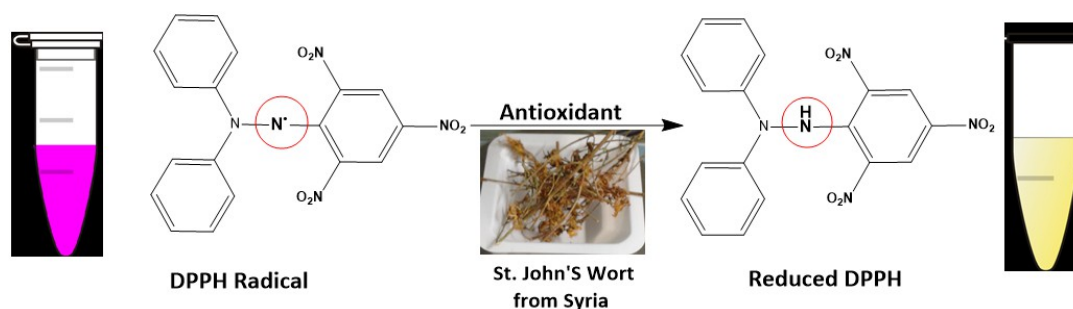


Figure 3-11: shows the change in the structure of the 1,1-diphenyl-2-picrylhydrazyl compound from the radical form to the reduced form with the change of its color

Data previously published indicate that there are significant differences in the results of scavenging activities of *Hypericum Perforatum L.* (*St John's wort*) extracts, which are partly related to the extraction medium (MeOH, EtOH, water or other solvents) and thus to the content of the various phenolic compounds. Ethanolic samples, which contained the least amount of phenols, showed a lower activity (IC_{50} 75 $\mu\text{g/ml}$) in agreement with several studies that have reported the relationships between the phenolic content and the antioxidant activity⁷⁰. The correlation is shown in (Figure 12).

Table 3-6: Percentage of neutralization of DPPH radical by *St John's wort* extracts in the DPPH Assay

<i>St John's Wort</i> Extract	Concentration ($\mu\text{g/ml}$)						IC_{50} ($\mu\text{g/ml}$) \pm STD error
	500	300	100	50	10	1.5	
Water II	83.46	80.60	74.62	45.71	11.46	03.22	51 \pm 3.6
Water I	87.26	86.10	59.65	37.45	20.85	12.74	60 \pm 20
Ethanol	84.84	84.12	57.22	37.91	15.34	11.37	75 \pm 14
Methanol	82.12	80.28	65.42	39.88	10.03	00.83	67 \pm 4.4

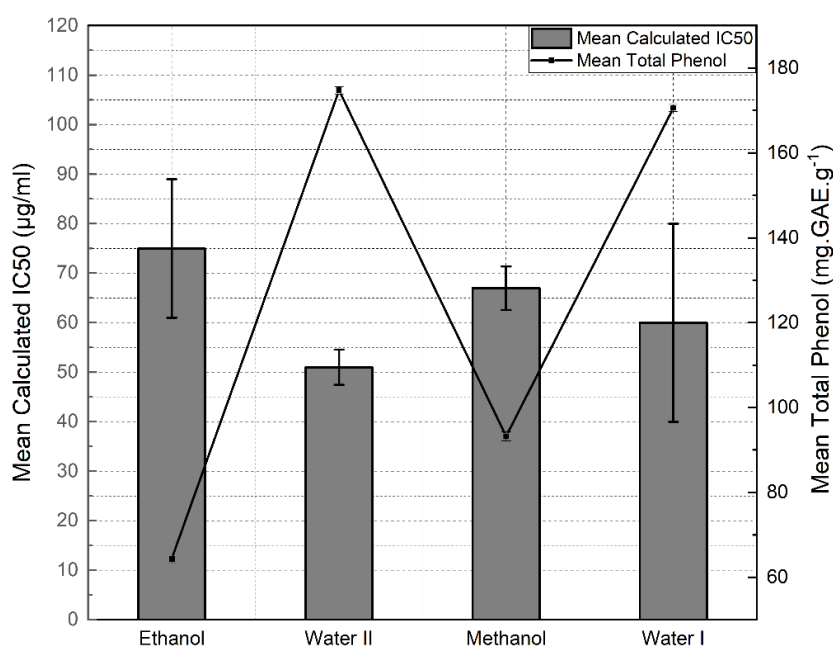


Figure 3-12: Correlation between phenolic content and antiradical activity for *St. John's Wort* by DPPH

Chapter 3: Identification of Major Constituents of *Hypericum perforatum L*

3.5.8 Antioxidant activity ABTS

The solvents used in the DPPH assay, methanol or ethanol, yield incorrect results for polar antioxidants (DPPH is insoluble in water), so this method does not provide useful information on the actual reaction of the antioxidant when viewed alone. In contrast, in ABTS assay, the radical is produced in the water just before the test by the reaction of ABTS with an oxidizing agent, such as potassium persulfate. The antioxidant activity is specified as the amount of ABTS^{•+} that is quenched after a specified period of time (ABTS^{•+} is a radical cation, so antioxidants react with it by an electron transfer mechanism), and compared to the activity produced by ascorbic acid. No distinction is made between radical trapping kinetics and stoichiometry; the result relies on the time chosen before the absorption reading^{71,72}. ABTS is often employed in plant medicine research to measure the antioxidant characteristics of hydrogen-donating and chain-breaking antioxidant agents. This method is useable for both hydrophilic and lipophilic antioxidants. For the calculation of the IC₅₀ values the same previous theoretical function used in the DPPH method was fit to the measurements. The scavenging activities of ABTS radical cation of various extracts (water, ethanol and methanol) of *Hypericum perforatum L*. are illustrated in Figure 13. The synergistic effects of these extracts with various solvents on ABTS cation scavenging activity were calculated (Table 7). The results clearly imply that the aqueous, ethanolic and methanolic extracts of *Hypericum perforatum L*. inhibit ABTS radical or scavenge the radical in a dose-dependent manner. The radical scavenging activity of extracts of *Hypericum perforatum L*. was estimated by comparing the percentage inhibition of formation of ABTS^{•+} radicals with that of ascorbic acid. The activity was concentration-dependent, and the maximum scavenging activity was found in the water extract II (IC₅₀= 42 µg/mL), followed by water extract I (IC₅₀= 51 µg/mL), then methanolic extract (IC₅₀= 71 µg/mL) and ethanolic extract (IC₅₀= 97 µg/mL) (Figure 13). All the extracts obtained with different solvents showed scavenging effects on ABTS^{•+} in the µg/ml range. This result is extremely promising because it indicates lower-cost extraction processes can be achieved, as no expensive solvents are needed to obtain the same amount of phenols and active substances from the plant.

Table 3-7: Percentage of neutralization of ABTS^{•+} radical by *St John's wort* extracts in the ABTS Assay

<i>St John's wort</i> Extract	Concentrations (µg/ml)						IC ₅₀ (µg/ml) ± STD error
	500	300	100	50	10	1.5	
Water II	94.42	94.03	74.45	44.62	13.23	3.63	42 ± 9.3
Water I	94.40	93.63	72.74	44.20	24.84	5.48	51 ± 4.1
Methanol	94.57	93.11	51.66	33.38	24.77	9.93	71 ± 14
Ethanol	93.07	92.30	45.67	26.32	11.17	7.57	97 ± 29

Chapter 3: Identification of Major Constituents of *Hypericum perforatum L*

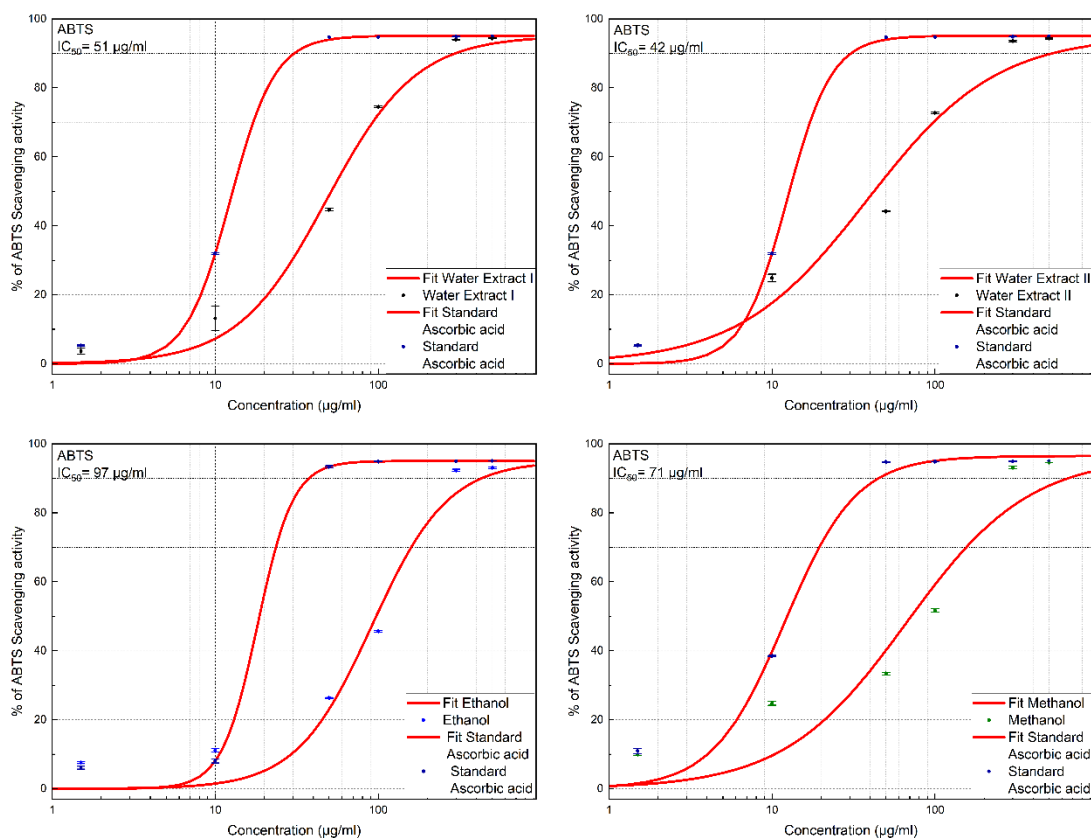


Figure 3-13: Evaluation of IC₅₀ of the St John's wort extract and standard ascorbic acid using ABTS scavenging Assay

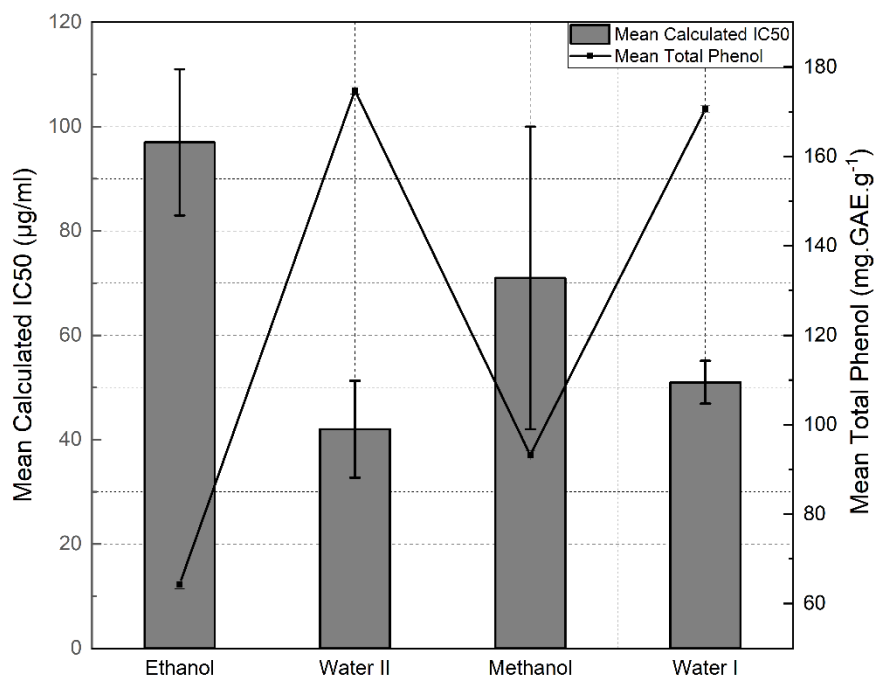


Figure 3-14: Correlation between phenolic content and antiradical for St John's wort by ABTS

Chapter 3: Identification of Major Constituents of *Hypericum perforatum L*

3.5.9 Statistical analysis

For the experimental technical harvesting methods, the statistical analysis showed the correlation difference between the water I extract method and the ethanol 70% method is high significance at p-value 0.007 while the water II extract method lead to harvest with no significant difference with ethanol 70% method. Therefore, it is recommended water II method for extraction of a higher amount of harvest nearly to the level of ethanol 70% method rather than the water I method. The statistical correlation showed no significance in the harvest when using 70% and 100% of the methanol, acetone and ethanol solvents but our recommendation is to use 70% of these solvents which give a high amount of harvest.

As for the HPLC diagrams, as shown in figures S3 to S10, the iterations of the eight extracts have shifted to the right or to the left, although all the iterations of all extracts have the same spectrum, that is, all of the peaks in the spectra are shifted by about the same time interval. Also, the repetitions of the samples were using different concentrations, so the intensity of the peaks varies from one plot to another according to the concentration taken. The main reasons that affect the R_t in our case are, the pump was old and did not always work with the same efficiency, and the column was used to a great extent, and for other experiments of other students also during the process of repeating our experiments. But it is clear from the sampling frequency plots (figures S3 to S10) that the protocol is repeatable and we will get the same spectrum and the same peaks with the same time difference for each extract when the scan is repeated.

3.5.9.1 Paired Samples T Test

To compare the DPPH scavenging activity of various extracts of *St John's Wort* with Ascorbic acid as standard the paired T-test showed that *St John's Wort* extracts i.e. water extract I & II and Ethanol low significance difference with Ascorbic acid under the same condition, while methanol extract has a higher significant difference with ascorbic acid at p Value 0.134. This probably due to the preparation of ascorbic acid during this experiment and that is clearly appeared with the lowest recorded number of DPPH activity in comparison to the other tested group see tables S24 &26 in ESI.

There is a strong correlation between the DPPH scavenging activity of ascorbic acid and *St. John's Wort* extracts as represented in table S25 in ESI. These correlations can be classified into very strong correlations for both water extract I & II at values of more than 0.85 while the correlation is moderate between 0.5 and 0.85 for ethanol and methanol extract. This means for the highest DPPH scavenging activity, it is a preference for using water as an extraction solvent rather than ethanol and methanol with *St. John's Wort* plant.

The same comparison has been done by ABTS method using paired sample T-test, the difference between the *St John's Wort* extracts i.e. water extract I , II, Ethanol, methanol and ascorbic acid was low at p-value ranged from 0.001- 0.007 as seen in tables S27 & 29 in ESI. This means that the previously mentioned probability concerned with the preparation of ascorbic acid during methanol extract would be correct. For testing the correlation between the *St John's Wort* extracts i.e. water extract I, II, Ethanol, methanol and ascorbic acid standard by ABTS, the same result shown in table S28 in ESI was confirmed like the previous mentioned with DPPH.

Chapter 3: Identification of Major Constituents of *Hypericum perforatum* L

3.6 Conclusions

In the present study, the aerial parts (leaves, stem, petals, and flowers) of *St John's wort* from Al-Ghab Plain in Syria were harvested, cleaned with cold water, dried, ground and extracted using different solvents such as water (either boiling with water for about 3 hours (water I) or adding to boiling water for 20 minutes (water II)), ethanol, methanol and acetone either pure or mixed with water at 70%. The results indicate that preparing the extract using the tea method (water II) and using organic solvents mixed with water gave a high yield compared to the water I method and pure organic solvents. A rapid, simple and reproducible high performance liquid chromatography diode array (HPLC-DAD) and UV absorbance detection protocol was developed to determine the phytochemical profiles present in the various extracts of *St. John's wort* from Syria. Concerning the presence of compounds, no general differences were observed in the HPLC patterns of the eight extracts, with the exception of the patterns of aqueous extracts at the wavelength 590 nm. This is the region of the appearance of hypericins, which do not easily dissolve in water except at high temperatures and in very small proportions. The other difference was in the intensity of the existing peaks, referring to the respecting concentrations of the compounds. This can be explained by the fact that different solvents extract the compounds in the plant in different proportions. High-performance liquid chromatography-mass spectrometry (UPLC-MS) under positive ionization mode was conducted to separate the bioactive molecules ions $[M+H]^+$ of the compounds in the extracts by their mass-to-charge ratio (m/z) and to detect them qualitatively and quantitatively by their respective m/z and abundance. Various techniques were used to identify the compounds: (i) Comparison with five reference substances (chlorogenic acid, quercetin, hyperoside, quercitrin hydrate and hypericin), (ii) comparison of the retention times of peaks in HPLC diagrams with those of standards and those reported in the literature, (iii) comparing the UV absorption spectra of peaks with the UV spectra of reference substances and spectra from the literature, (iv) matching the prominent protonated molecular ions $[M+1]^+$ of compounds with the molecular weights of compounds known to be present in this plant. Ten compounds: hypericin, rutin, hyperoside, quercitrin, quercetin, biapigenin, hyperforin, quercitrin hydrate, adhyperforin and chlorogenic acid were identified, proven and confirmed. All *St. John's wort* extracts (water I or water II, ethanolic, methanolic and acetic) were effective scavengers of the free stable $ABTS^{\bullet+}$ and $DPPH^{\bullet}$ radicals, and particularly, extracts containing more phenolic compounds were more effective scavengers. This antioxidant activity may be explained by the presence of phytochemicals previously identified using HPLC; UV-VIS and HPLC-MS analysis, as they have all been shown to have antioxidant activity.

3.7 Future Studies

The aqueous extract of this plant has been used in a previous own study⁷³ as a reducing agent for silver ions into metallic silver, as well as a protective agent (capping agent or stabilizer) to protect the silver nanoparticles and prevent their aggregation. This synthesis of AgNPs using aqueous *St John's wort* extract from Syria represents a green, simple, one-pot method, which is cost-effective, environmentally friendly, and provides natural capping agents for the stabilization of AgNPs, without necessitating high temperature, pressure, energy and toxic chemicals. Phenolic compounds originating from the aqueous *St John's wort* extract on the surface of AgNPs played an important role in their antioxidant and anti-cancer activity, as

Chapter 3: Identification of Major Constituents of *Hypericum perforatum L*

shown in above-mentioned study. Current work examines the conjugation of AgNPs with aptamers selective towards specific cancer cells. Thus, the phenolic compounds from *St John's wort* on the surfaces of silver nanoparticles could have an important role in the targeted therapy.

Conflicts of interest: There are no conflicts to declare.

Acknowledgements: The authors are thankful to all the lab members for their help. The authors are very thankful to Prof. Dr. Bernd Hitzmann, Head of the Department of Process Analysis and Grain Science at the University of Hohenheim for his support in statistical analysis. The authors thanks Dr. Nina McGuinness from EU University Office Hanover for reviewing and grammar correcting the article. The authors express their gratitude to Dr. Ulrich Krings (Institut für Lebensmittelchemie, Leibniz Universität Hannover), Dr. Abdalla A. Elshereef, Dr. Osama Al-Madanat, Dr. Yamen AlSalka and Martina Weiss for support during this work as well as for access to technical facilities. We are very thankful to Dr. Ayham Abazid, Bremen University for his valuable suggestions during this work. Abdalrahim Alahmad is supported by PhD grants from Avicenna Studienwerk e.V. The publication of this article was funded by the Open Access Publishing Fund of Leibniz Universität Hannover.

Supporting Information statement: Supplementary information (ESI) accompanies this paper.

Tables	Description	Figures	Description
S 3-1	HPLC protocols	S1	mobile phase program
S2	mass spectrum ions	S2	Standard calibration curve of Gallic acid
S3	St. John's wort substances	S3 – S10	Repetition spectrums for the eight extracts
S4 - S10	ANOVA DPPH		
S11 – S13	ANOVA ABTS		
S14 – S16	T- Test: DPPH		
S17 – S19	T- Test: ABTS		
S20 – S21	STD Error and Confidence Interval calculation using Fischer Matrix		

Chapter 3: Identification of Major Constituents of *Hypericum perforatum* L

3.8 References

1. Karim, H.; Kamel, M.; Mouna, B. T.; Olfa, O.; Monem, K.; Brahim, M., Essential oil composition of *Hypericum perforatum* L. and *Hypericum tomentosum* L. growing wild in Tunisia. *Ind. Crops Prod.* 2008, 27 (3), 308-314.
2. Alireza, M., Antimicrobial activity and chemical composition of essential oils of four *Hypericum* from Khorasan, Iran. *J. Med. Plants Res.* 2012, 6 (12), 2478-2487.
3. Aleksandra S., Đ., Chemical composition of *Hypericum perforatum* L. essential oil. *Advanced Technologies* 2015, 4 (1), 64-68.
4. Jinous, A., Phytochemistry, pharmacology and medicinal properties of *Hypericum perforatum* L. *Afr. J. Pharmacy Pharmacol.* 2012, 6 (19), 1387-1394.
5. James L., S.; Stephan L., H.; L.M., L., North American wildland plants: a field guide. University of Nebraska Press; 6th Revised ed edition (1 Dec. 2003): 2003; p 506.
6. Francis, R.; Clare, O. R.; Martine, C.; Delf, S.; RB., D.; Lura, M.; Norman, B.; Judith, D., The wild flower key: how to identify wild flowers, trees and shrubs in Britain and Ireland. Frederick Warne Books: 2006.
7. S. M. A., Z.; F., A.; E., G.; T., K., Plant–environment interactions: accumulation of hypericin in dark glands of *Hypericum perforatum*. *Ann. Bot.* 2006, 98 (4), 793-804.
8. Clive, S., New flora of the British Isles. 3 ed.; Cambridge University Press: 2010.
9. Fernald, M., Gray's manual of botany. Eighth (corrected) Ed. D. Van Nostrand Co., New York: 1970.
10. Benea, A.; Goncariuc, M.; Kulciti, V.; Dragalin, I.; Nisteanu, A., Essential Oil Chemical Composition Biodiversity in the *Hypericum* L. Species from the Spontaneous Flora of the Republic of Moldova. *Oltenia Journal for Studies in Natural Sciences. Museum of Oltenia Craiova, Romania* 2013 29 (2), 47-52.
11. Biljana, B.; Nebojša, K.; Nevena, G.; Goran, A.; Isidora, S.; Neda, G.; Branislava Srđenović, Č., Impact of origin and biological source on chemical composition, anticholinesterase and antioxidant properties of some St. John's wort species (*Hypericum* spp., Hypericaceae) from the Central Balkans. *Molecules* 2013, 18 (10), 11733-11750.
12. Susan H., K.; Larry L., A.; Agnes, N.; William S., Z.; Fran X., M., Selected physical and chemical properties of commercial *Hypericum perforatum* extracts relevant for formulated product quality and performance. *AAPS PharmSci.* 2001, 3 (4), 1-18.
13. E. Moroydor, D.; Z., E.; S., P., Extraction and Analysis of *Hypericum perforatum* L. from Turkey. *International Journal of Chemical, Molecular, Nuclear, Materials and Metallurgical Engineering* 2013, 7 (7), 495-499.
14. Vattikuti, U. M. R.; Ciddi, V., An overview on *Hypericum perforatum* Linn. *Nat. prod. radiance* 2005, 4 (5), 368-381.
15. Joanne, B.; Linda A., A.; J. David, P., St John's wort (*Hypericum perforatum* L.): a review of its chemistry, pharmacology and clinical properties. *J. Pharm. Pharmacol.* 2001, 53 (5), 583-600.
16. A L., M., St. John's Wort (*Hypericum perforatum*): clinical effects on depression and other conditions. *Altern Med Rev.* 1998, 3 (1), 18-26.
17. Jiří, P., The chemistry, pharmacology, and toxicology of the biologically active constituents of the herb *Hypericum perforatum* L. *J. Appl. Biomed.* 2003, 1 (2), 61-70.
18. A., N.; V., B., Biologically active and other chemical constituents of the herb of *Hypericum perforatum* L. *Pharmacopsychiatry* 1997, 30 (S 2), 129-134.
19. Zeb, S.; Ismat, N.; Alya, M., A review of the antibacterial activity of *Hypericum perforatum* L. *J. Ethnopharmacol.* 2010, 131 (3), 511-521.
20. Wenkui, L.; John F., F., High performance liquid chromatographic analysis of St. John's wort with photodiode array detection. *J. Chromatogr. B Biomed. Appl.* 2001, 765 (1), 99-105.
21. Jelena, S.; Ivana, R.; Aleksandra, Đ.; Olga, J.; Goran, P.; Gordana, S., Optimization of HPLC method for the isolation of *Hypericum perforatum* L. methanol extract. *Biol. Nyssana* 2013, 4 (1-2), 81-85.
22. Pinarosa, A.; Gaspare, G., Determination of major constituents in St. John's Wort under different extraction conditions. *Pharm. Biol.* 2004, 42 (1), 83-89.

Chapter 3: Identification of Major Constituents of *Hypericum perforatum* L

23. M., B.; B., G.; N., F.; R., P.; F., P.; F., P., Identification by high-performance liquid chromatography–diode array detection–mass spectrometry and quantification by high-performance liquid chromatography–UV absorbance detection of active constituents of *Hypericum perforatum*. *J. Chromatogr. A* 1998, 825 (1), 9-16.
24. Neerja, T.; Hema, M.; P. D., H.; Tukaram, M.; Ashish, S.; Vijay Singh, C., Development of a High-Performance Liquid Chromatographic Method for the Quantitative Determination of Hyperforin. *Int. J. Appl. Sci. Eng* 2008, 6 (1), 39-46.
25. V., H.; D., D., Separate isolation of hyperforin from *Hypericum perforatum* (St. John's Wort) pursuant to the coefficients LOG Kow, PKa and densities of the included compounds. *Trakia J. Sci.* 2015, 13 (4), 19-23.
26. Dániel, C.; Tünde, V.; Mária, B.; Judit, H.; Tibor, K.; Béla, S., Extraction of Hyperforin and Hypericin from St. John's Wort (*Hypericum Perforatum* L.) with Different Solvents. *J. Food Process Eng* 2012, 35 (2), 222-235.
27. Anastasia, A.; Anthony, B.; Tivadar, K.; Judit, H.; Michael, H.; Dezso, C., Quality control of *Hypericum perforatum* L. analytical challenges and recent progress. *J. Pharm. Pharmacol.* 2019, 71 (1), 15-37.
28. V. A., H.-P.; L. K., B.; J. D., P.; H., S.; G., A.; M., P.; G. K., B.; C. W., H., A chromatographic and spectroscopic analytical platform for the characterization of St John's wort extract adulterations. *Anal. Methods* 2013, 5 (3), 616-628.
29. Narayanan, R.; Jerrine, J.; Manikkan, R.; Thirunavukarasu, R., In vitro cytotoxicity of methanol extracts of *Hypericum wightianum* and *Hypericum hookerianum* against 3T3L1 cell lines. *Bangladesh J. Pharmacol.* 2016, 11 (2), 328-329.
30. Azizi, M., Change in content and chemical composition of *Hypericum perforatum* L. oil at three harvest time. *J Herbs Spices Med Plants* 2008, 13 (2), 79-85.
31. Bombardelli, E.; Morazzoni, P., *Hypericum perforatum*. *Fitoterapia (Milano)* 1995, 66 (1), 43-68.
32. World Health Organization, G., Switzerland., WHO Monograph on Selected Medicinal Plants. 2002; Vol. 2, pp 149-171.
33. products, C. o. h. m.; Agency, E. M., Community herbal monograph on *Hypericum perforatum* L., herba (well-established medicinal use). EMA/HMPC/101304: 2009.
34. Blumenthal, M.; Busse, W. R.; Goldberg, A., *The Complete German Commission E Monographs: Therapeutic Guide to Herbal Medicines*. Boston: American Botanical Council: 1998.
35. Upton, R.; Graff, A.; Williamson, E.; Bunting, D.; Gatherum, D.; Walker, E.; Butterweck, V.; Liefflünder, U.; Nahrstedt, A.; Winterhoff, H., *St. John's Wort Monograph in: American Herbal Pharmacopoeia and Therapeutic Compendium*. *HerbalGram* 1997, 40 (5), 1-32.
36. Dejan Z., O.; Neda M., M.-D.; Marina M., F.; Slobodan S., P.; Emilija Đ., J., Antioxidant activity relationship of phenolic compounds in *Hypericum perforatum*L. *Chem. Cent. J.* 2011, 5 (1), 34.
37. Bruno A., S.; Federico, F.; João O., M.; Alberto C.P., D., Phytochemical and antioxidant characterization of *Hypericum perforatum* alcoholic extracts. *Food Chem.* 2005, 90 (1-2), 157-167.
38. Daniela, G.; Monica, Ş.; TĂMAŞ, M.; Bianca, P., The analysis of alcoholic extracts of *Hypericum* species by UV/VIS spectrophotometry. *Anal. Univ. Oradea. Fasc. Biol.* 2010, 17, 111-115.
39. Ray, U.; Jerry, C.; Elizabeth, W.; Allison, G., *St. John's Wort, Hypericum Perforatum. Quality Control, Analytical and Therapeutic Monograph. American Herbal Pharmacopoeia, 1997: 1997; Vol. 40, p 32.*
40. Chopra, R. N.; Nayar, S. L.; Chopra, I. C., *Glossary of Indian medicinal plants. Council of Scientific & Industrial Research New Delhi: 1956; Vol. 1.*
41. Ishfaq A., B.; Ahsana, D.; Rafeeq Alam, K., Antinociceptive activity of methanolic extracts of St. John's Wort (*Hypericum perforatum*) preparation. *Pak J Pharm Sci* 2004, 17 (2), 13-9.
42. Vesna, I.; Svetlana, T.; Marija Knezevic, P.; Mira, P.; Janka, Z., Effects of St John's wort (*Hypericum perforatum* L.) extracts on epileptogenesis. *Molecules* 2011, 16 (9), 8062-8075.
43. AR., M.; Nirmala, H., *St John's wort (Hypericum perforatum L.): A Review of its Chemistry, Pharmacology and Clinical properties. Int. J. Res. Phy. & Pharm. Sci.* 2019, 1 (1), 5-11.
44. I., L.-B.; J. B., H.; G. H. N., T., Antiviral activity of the photoactive plant pigment hypericin. *Photochem. Photobiol.* 1991, 54 (1), 95-8.

Chapter 3: Identification of Major Constituents of *Hypericum perforatum L*

45. J.B., H.; I., L.-B.; G.H.N., T., Antiviral activities of hypericin. *Antivir. Res.* 1991, 15 (2), 101-12.
46. J., L.; A., R.; R., V., Photodynamic Inactivation of Infectivity of Human-Immunodeficiency-Virus and Other Enveloped Viruses Using Hypericin and Rose-Bengal - Inhibition of Fusion and Syncytia Formation. *PNAS* 1993, 90 (1), 158-162.
47. C.M., S.; B., W.; R., L.; B., S.-H.; E., S.; J.C., S., Topical application of St John's wort (*Hypericum perforatum L.*) and of its metabolite hyperforin inhibits the allostimulatory capacity of epidermal cells. *Br. J. Dermatol.* 2000, 142 (5), 979-984.
48. Christoph M., S.; Vladimir, K.; Birgit., S.-H.; Astrid, K.; Judit, K.; Christian C., T.; Bernhard, G.; Thomas, K.; Christoph, B.; Jonathan P., S.; Jan C., S., Inhibition of tumour cell growth by hyperforin, a novel anticancer drug from St. John's wort that acts by induction of apoptosis. *oncogene* 2002, 21 (8), 1242-1250.
49. Wenxia, C.; Fengfeng, F.; Ying, Z.; Zhichao, P.; Wenji, W.; Yuxin, P., A Facile Approach for Fabrication of Core-Shell Magnetic Molecularly Imprinted Nanospheres towards Hypericin. *Polymers* 2017, 9 (4), 135.
50. Steen Honoré, H.; Anette Gemal, J.; Claus, C.; Inga, B.; Steven, T.; Brian, W.; Ian D., W., High-performance liquid chromatography on-line coupled to high-field NMR and mass spectrometry for structure elucidation of constituents of *Hypericum perforatum L.* *Anal. Chem.* 1999, 71 (22), 5235-5241.
51. A. C. P., D.; R. M., S.; P. B., A.; M., F.-F., The development and evaluation of an HPLC-DAD method for the analysis of the phenolic fractions from in vivo and in vitro biomass of *Hypericum* species. *J. Liq. Chromatogr. Relat. Technol* 1999, 22 (2), 215-227.
52. Frances F., L.; Catharina Y. W., A.; Dietmar, S., Optimization of extraction conditions for active components in *Hypericum perforatum* using response surface methodology. *J. Agric. Food. Chem.* 2000, 48 (8), 3364-3371.
53. Frances F., L.; Catharina Y.W., A.; Thomas M., H.; Joshua D., R.; Richard D., B.; James P., F.; Jackson O., L., Evaluation of major active components in St. John's Wort dietary supplements by high-performance liquid chromatography with photodiode array detection and electrospray mass spectrometric confirmation. *J. Chromatogr. A* 2000, 888 (1-2), 85-92.
54. Hicham, H.; Hana Serghini, C.; Nourel Houda, B.; Mohammed, A.; Souliman, A., Hypolipemic activity of polyphenol-rich extracts from *Ocimum basilicum* in Triton WR-1339-induced hyperlipidemic mice. *Food Chem.* 2008, 108 (1), 205-212.
55. Vernon L., S.; Rudolf, O.; Rosa M., L.-R., [14] Analysis of total phenols and other oxidation substrates and antioxidants by means of folin-ciocalteu reagent. In *Meth. Enzymol.*, Elsevier: 1999; Vol. 299, pp 152-178.
56. Okumu, M.; Mbaria, J.; Kanja, L.; Gakuya, D.; Kiama, S.; Ochola, F., Phytochemical profile and antioxidant capacity of leaves of *Moringa oleifera* (Lam) extracted using different solvent systems. *J. pharmacogn. phytochem.* 2016, 5 (4), 302-308.
57. Sandra, G.; Paula, C. C., Antioxidant potential of *Artemisia argentea* L'Hér alcoholic extract and its relation with the phenolic composition. *Food Res. Int.* 2011, 44 (6), 1620-1631.
58. Tsutomu, H.; Kagawa., H.; Yasuhara., T.; Takuo, O., Two new flavonoids and other constituents in licorice root: their relative astringency and radical scavenging effects. *Chem. Pharm. Bull.* 1988, 36 (6), 2090-2097.
59. M.A.R., B.; M.Z., H.; S.J., H., Free radical scavenging activities of *Zizyphus mauritiana*. *World j. agric. sci.* 2009, 5 (3), 318-322.
60. M., G.; UK., M.; T., S.; MLM., V.; S., K.; R., S.; L., M., Antioxidant and anti-inflammatory activities of *Acalypha fruticosa*. *Niger J Nat Prod Med* 2003, 7 (1), 25-29.
61. Chanda, S.; Rakholiya, K.; Dholakia, K.; Baravalia, Y., Antimicrobial, antioxidant, and synergistic properties of two nutraceutical plants: *Terminalia catappa L.* and *Colocasia esculenta L.* *Turk J Biol* 2013, 37 (1), 81-91.
62. Aline Augusti, B.; Margareth Linde, A., Importance of HPLC in analysis of plants extracts. *Austin chromatogr.* 2014, 1 (3), 2.
63. Kubin, A.; Loew, H. G.; Burner, U.; Jessner, G.; Kolbabek, H.; Wierrani, F., How to make hypericin water-soluble. *Pharmazie* 2008, 63 (4), 263-269.

Chapter 3: Identification of Major Constituents of *Hypericum perforatum L*

64. Jie, Z.; Ling, G.; Jie, H.; Chongjun, W.; Peter-Leon, H.; Ning, L.; Xing, Z., Hypericin: Source, Determination, Separation, and Properties. *Separation & Purification Reviews* 2020, 1-10.
65. Duan, Y., Ultraviolet–visible spectrum characterizations of quercetin in aqueous ethanol solution with different pH values. *J Chem Pharm Res* 2014, 6 (9), 236-240.
66. Miao, L.; Xiao-Fang, H.; Jie, Z.; Si-Cen, W.; Qiang, F.; Lang-Chong, H., Applications of HPLC/MS in the analysis of traditional Chinese medicines. *J. Pharm. Anal.* 2011, 1 (2), 81-91.
67. Yizhong, C.; Qiong, L.; Mei, S.; Harold, C., Antioxidant activity and phenolic compounds of 112 traditional Chinese medicinal plants associated with anticancer. *Life Sci.* 2004, 74 (17), 2157-2184.
68. Biljana, B.; Neda, M.-D.; Isidora, S.; Anackov, G.; Ruzica, I., Phenolics as antioxidants in garlic (*Allium sativum L.*, Alliaceae). *Food Chem.* 2008, 111 (4), 925-929.
69. Dan E., P.; Bertram J. F., H., Natural antioxidants not exploited commercially. In *Food antioxidants*, Springer: 1990; pp 171-191.
70. Mariangela, M.; Filomena, C.; Chiara, T.; Marcello, N.; Giancarlo, S.; Francesco, M., *Hypericum perforatum*: Influences of the habitat on chemical composition, photo-induced cytotoxicity, and antiradical activity. *Pharm. Biol.* 2014, 52 (7), 909-918.
71. L.P., L.; G., S., An investigation of antioxidant capacity of fruits in Singapore markets. *Food Chem.* 2002, 76 (1), 69-75.
72. Amorati., R.; Valgimigli., L., Advantages and limitations of common testing methods for antioxidants. *Free Radical Res.* 2015, 49 (5), 633-649.
73. Abdalrahim, A.; Armin, F.; Nadja C., B.; Pascal, R.; Thomas, S.; Johanna-Gabriela, W., *Hypericum perforatum L.*-Mediated Green Synthesis of Silver Nanoparticles Exhibiting Antioxidant and Anticancer Activities. *Nanomaterials* 2021, 11 (2), 487.

Chapter 3: Identification of Major Constituents of *Hypericum perforatum L*

3.9 Supporting Informations

Table S 3-2: An overview of the most important HPLC protocols used previously in order to identify the most important Phytochemicals in various *St. John's Wort* extracts

Pr. Nr.	Elution Gradient		Elution	Flow Rate mL/min	T (°C)	column used	Identified compounds	Ref .
	A	B						
1	0,1 % aqueous formic acid with 10 mmol/L CH ₃ COONH ₄	Acetonitril	0 min 25% B 6 min 100% B 8 min 100% B	1	50	Zorbax SB-C18 30 mm × 2.1 mm × 3.5 μm	Hyperoside, Rutin, Quercitrin, Quercetin, I3, I18-Biapigenin, Amentoflavone, Caffeoylquinic acid, Protopseudohypericin, Pseudohypericin, Protohypericin, Hypericin, Hyperfirin, Adhyperfirin, Hyperforin, Adhyperforin	1
2	Aqueous 20% methanol and 0,5% TFA	Aqueous 10% methanol and 0,5 % TFA	0-20 min 90% A 20-25 min 30% A 25-30 min 10% A Until 60 min 0 %A	1	20	Waters YMC ODS-AQ RP-18, 5 μm, 120 Å, 4.6X250 mm	Rutin, Hyperoside, Isoquercitrin, Quercitrin, Quercetin, Pseudohypericin, Hyperforin, Hypericin	2
3	Water/ formic acid (99:1)	methanol	0 min 90 % A 2 min 70 % A 8 min 70 % A 13 min 65 % A 20 min 50 % A 22 min 50 % A 30 min 30 % A 35 min 30 % A 45 min 20 % A 50 min 20 % A 55 min 5 % A 62 min 5 % A	1	-	RP C18 column (25X0.4 cm, particle size 5 μm)	Neochlorogenic acid, Caffeoylquinic acid type, Chlorogenic acid, Rutin, Hyperoside, Isoquercetin, Quercetin 3-O-b-D-galacturonic, Quercetin 3-O-b-D-glucuronic, Quercitrin, Kaempferol 3-O-b-D-rutinoside, Hyperoside-acetyl, Rutin-acetyl, quercetin, Kaempferol, Biapigenin, Amentoflavone, Protopseudohypericin,	3-5

Chapter 3: Identification of Major Constituents of *Hypericum perforatum* L

			65 min 90 %A				Pseudohypericin, Protohypericin, Hypericin, Hyperforin, Adhyperforin.	
4	Methanol/0.01 M Orthophosphoric acid ph=7 (50:50,v/v)	-	80 min	1	20	octadecyl (C ₁₈) column (Hichrom 5 C ₁₈ , 7.75X300 mm, 5 µm particle size)	Rutin, Isoquercitrin, Luteolin-4'-glucoside, Quercetin-4'-glucoside, Quercetin, Naringenin, Luteolin, Apigenin	6
5	water/tetrahydrofuran/TFA, 97: 2 : 1	MeCN/tetrahydrofuran/TFA, 97: 2 : 1	0 to 10 % B in A in 7 min , 10 to 15 % B in A, 8 min (0.5), 15 to 20, 13 min (0.5), 20 to 50, 7 min (0.55), 50 to 65, 5 min (0.6), 65 to 75, 5 min (0.6), 75 to 100, 5 min (0.7), isocratic with 100 % B, 25 min (0.7).	0.5		Supelco Discovery C ₁₈ , 25 cm x 4.6 mm, 5 µm	Neochlorogenic acid, Protocatechuic acid, 3-0-[Z]-p-Coumaroylquinic acid, 3-0-[E]-p-Coumaroylquinic acid, Cryptochlorogenic acid, Mangiferin, Isoorientin, Cyanidin-3-0-a-L-rhamnoside, Rutin, Hyperoside, Isoquercitrin, Miquelianin, Astiblin, Guajaverin, Quercitrin, Quercetin-3-0-(2''-acetyl)-β-D-galactoside, Quercetin, Biapigenin, Amentoflavone, Pinocembrin-7-methyl ether, Pseudohypericin, Hyperforin, Hypericin	7
6	Acetonitril+0.1% acetic acid (5:95, v/v)	Acetonitril+20 mM ammonium acetat (95: 5, v/v)	0 min 10% B 10 min 20% B 20 min 100 % B 30 min 100 % B 32 min 10 % B Bis 40 min	1		A Knauer (Berlin, Germany) column 120 X 4 mm i.d. was packed with Apex-1 ODS, 5 µm, column packing material (Jones Chromatography, Hengoed, UK)	Quercetin-galacturonide, Rutin, Hyperoside, Isoquercetrin, Quercetin-arabinoside, Quercetrin, Quercetin, I3-II8-Biapigenin, Amentoflavon, Protopseudohypericin, Pseudohypericin, Protohypericin, Hypericin, Hyperforin, Adhyperforin	8
7	0.1 % aqueous HCOOH with 10	Acetonitrile	0 min 25% B 6 min 100% B	1	25	reversed-phase Zorbax CB-C ₁₈ column (4.6 X	Chlorogenic acid, Caffeic acid, Rutin, Quercitrin, Hyperforin, Hypericin	9

Chapter 3: Identification of Major Constituents of *Hypericum perforatum L*

	mmol/L CH ₃ COONH ₄					150 mm, i.d., 5 µm particle size)		
8	Methanol	0.01 M ammonium acetate in water	isocratic mode (1:1)	2	25	Zorbax Eclipse XDB C ₁₈ column with dimensions (5 µm, 150 mm X 4.6 mm)	Chlorogenic acid, Gallic acid, Trans- p-coumaric acid, Rutin, Hyperoside, Isoquercitrin, Quercitrin, Quercetin, Pseudohypericin, Hypericin, Hyperforin	10
9	Acetonitrile	Water with 0.05% trifluoroacetic acid C: methanol	0 min 10% A , 90% B, 0% C 50 min 80% A, 5% B, 15% C	-	-	Lychromasphere 5 µm C ₁₈ column from Merck	Chlorogenic acid, Rutin, Hyperoside, Isoquercitrin, Quercitrin	11
10	H ₂ O:H ₃ PO ₄ (99.7:0.3 v:v)	ACN C) MeOH	0 min 85% A, 15% B 12 min 80% A, 5% C, 15% B 20 min 10% A, 15% C, 75% B 27 min 5% A, 15% C–80% B 30 min 85% A, 15% B	1	30	Vydac 201TP54, C ₁₈ , 5mm, 4.6 x 250 mm	Chlorogenic acid, Rutin, Hyperoside, Isoquercitrin, Quercitrin, Quercetin, Pseudohypericin, Hypericin, Hyperforin	12
11	Acetonitrile+0.3% phosphoric acid (90:10 v:v)	-	10 min	1.5		C ₁₈ reversed-phase column	Pseudohypericin, Hyperforin, Hypericin	13
12	Water+ 85% phosphoric acid (99.7:0.3 v/v)	Acetonitrile c) methanol	0 min 100% A 10 min 85% A, 15% B, 0% C, 30 min 70% A, 20% B, 10% C 40 min 10% A, 75% B, 15% C 55 min 5% A, 80% B, 15% C	1	30	201 TP 54 RP-18 column (250 X 4.6 mm I.D., 5 µm, 300 Å, protected with an Alltech direct-connect universal column prefilter of 2 µm porosity.	Chlorogenic acid, Rutin, Hyperoside, Isoquercitrin, 7-O- rhamnopyranoside, Quercitrin, Quercetin, I3,II8-Biapigenin, Pseudohypericin, Hypericin, Hyperforin, Adhyperforin	14

Chapter 3: Identification of Major Constituents of *Hypericum perforatum* L

			56 min 100% A, 0% B, 0% C 65 min 100% A, 0% B, 0% C					
13	Methanol- acetonitrile (5:4)	0.1 M aqueous trithylammoni um acetat	0 min 70% A, 30% B 8 min 90% A, 10% B 13 min 70% A, 30% B	0.6		A LiChrosorb RP 18 column (125X4 mm I.D., 5 µm, Darmstadt, Germany), protected with a LiChrospher 100 RP 18 (4X4 mm I.D., 5 µm, Merck).	Hypericin, Protohypericin, Pseudohypericin, Protopseudohypericin	15
14	10 mM ammonium acetate buffer pH = 5.0 adjusted with glacial acetic acid	Acetonitrile/M ethanol (9:1)	0 min 87% A 10 min 83% A 25 min 100% B After each run 10 min equilibration	1	40	Synergi MAX-RP 80A° column (150 X 4.6 mm, 4-µm particle size) from Phenomenex (Torrance, CA)	Rutin, Hyperoside, Isoquercitrin, Quercitrin, Quercetin, I3,II8- Biapigenin, Pseudohypericin, Hypericin, Hyperforin	16
15	50% Acetonitrile	50% (ammonium acetate-acetic acid buffer (0.3M, pH=6,96) + methanol (1:4, v/v))	20 min	0.4	25	C ₁₈ reversed-phase column (5 µm, 4.6 mm X 150 mm)	Hypericin, Protohypericin	17
16	water 85% H ₃ PO ₄ , pH 4.0	CH ₃ CN C) methanol	0 min 100% A 10 min 85% A, 15% B 30 min 70% A, 20% B+10% C 40 min 10% A, 75% B, 15% C 55 min 5% A+80% B+ 15% C Total time 65 min	1	25	Nova-Pack RP-18 column (150 X 3.9 mm i.d.; 4µm; Waters) provided with Security Guard cartridge C ₁₈ (4 mm X 3.0mm i.d; Phenomenex).	Chlorogenic acid, Rutin, Hyperoside, Isoquercitrin, Quercitrin, Quercetin, I3, II8-Biapigenin, Hyperforin, Adhyperforin, Pseudohypericin, Hypericin	18

Chapter 3: Identification of Major Constituents of *Hypericum perforatum L*

17	Water containing 0.2% formic acid	methanol containing 0.2% formic acid	0 min 10% A 30 min 0% A 35 min 0% A 36 min 10% A 45 min 10% A (equilibration)	1	25	Kromasil 100 C ₁₈ column (3.5 µm, 4.6×150 mm, serial no. N45672; batch TR-013407) (Teknokroma, Barcelona, Spain)	Hyperforin	19
18	ethyl acetate + 15.6 g/L solution of sodium dihydrogen phosphate adjusted to pH 2 with phosphoric acid + methanol (39:41:160 v/v/v)	isocratic	10 min	1	40	Hypersil Gold RP18 column (150 X 4.6 mm, 5 µm).	Pseudohypericin, Hypericin	20
19	Methanol+ acetonitrile (5:4 v/v)	0.1 M aqueous triethylammonium acetat	0 min 70% A 15 min 90% A 25 min 70% A	1	-	Superspher RP 18 column (250X4 mm I.D., 5 µm, Merck), protected with a LiChrospher 100 RP 18 (4X4 mm I.D., 5 µm, Merck) precolumn	Protopseudohypericin, Pseudohypericin, Protohypericin, Hypericin	21
20	880 g water+80 g acetonitrile+ 2mL 85% phosphoric acid + adjusted to PH=2.8 with triethylamin	50 g water+275.25 g acetonitrile+ 85.04 g methanol+ 1 mL 85% phosphoric acid + adjusted to PH=6.1 with triethylamin	0 min 100% A 10 min 40% A 45 min 40% A 53 min 0% A 65 min 100% A	1	30°	reversed stationary phase column (Hypersil BDS 250 x 4 mm, 5 µm particle size and 120 °A pore size; Thermo Scientific, Schwerte, Germany) and an RP precolumn (Hypersil BDS 50 x 4 mm; 5 µm particle size and 120 °A pore size; Thermo Scientific)	Rutosid Hyperoside Isoquercitrin Quercetin Biapigenin	22

Pr. Nr. mean Protocol Number; Ref. mean Reference Number

Chapter 3: Identification of Major Constituents of *Hypericum perforatum L*

a) Table show mobile phase program

Time [min]	Eluent A [%]	Eluent B [%]
0	95	5
82	0	100
92	0	100
93	95	5
100	95	5

b) diagram show mobile phase Program

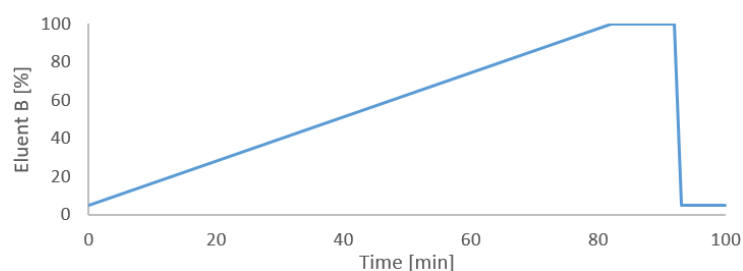


Figure S 3-1: mobile phase program a) table and b) diagram

Table S 3-3: Representation of the peak numbers of the mass spectrum of the sample (ethanol 100%) with respective times and the positive ion mass

Peak-Nr.	Time [min]	Ion mass [g]	Peak-Nr.	Time [min]	Ion mass [g]
1	2	141,00	28	52,14	625,39
2	2,65	114,98	29	52,31	301,15
3	2,87	206,87	30	53,20	609,37
4	4,40	262,11	31	56,05	591,37
5	4,63	130,04	32	57,46	609,38
6	10,89	120,08	33	58,09	591,36
7	11,51	100,07	34	60,08	591,36
8	12,13	141,00	35	61,50	575,37
9	14,85	163,03	36	62,54	553,37
10	17,63	147,04	37	64,28	559,36
11	19,81	163,04	38	64,57	593,25
12	21,03	291,07	39	66,36	557,35
13	22,14	409,17	40	66,96	571,37
14	24,66	241,06	41	68,84	575,38
15	26,97	355,17	42	70,01	537,40
16	29,32	303,03	43	71,28	551,42
17	31,26	325,21	44	72,90	117,00
18	32,00	303,04	45	75,77	117,00
19	33,30	191,07	46	77,86	685,47
20	35,37	303,05	47	80,19	537,43
21	35,49	303,04	48	84,44	117,00
22	35,59	303,05	49	84,70	116,99
23	37,45	237,15	50	84,83	116,99
24	40,10	539,09	51	84,93	116,99
25	40,23	539,09	52	85,06	116,99
26	48,27	531,31	53	85,34	116,99
27	49,79	625,38	54	87,35	141,02

Chapter 3: Identification of Major Constituents of *Hypericum perforatum L*

Table S 3-4: *St. John's Wort* substances are already known in the literature

Nr.	Compound	Molecular weight [g/mol]
1	Quercetin	302,238
2	Isoorientin	448,38
3	Hyperforin	536,797
4	Hypericin	504,45
5	Rutin	610,521
6	Hyperoside	464,379
7	Isoquercitrin	464,379
8	Chlorogenic acid	354,311
9	Neochlorogenic acid	354,311
10	Luteolin	286,239
11	Luteolin 5-glucoside	448,38
12	Luteolin 3-glucoside	448,38
13	Kaempferol	286,239
14	Caffeic acid	180,159
15	Quercitrin	448,38
16	Biapigenin	538,464
17	Protohypericin	506,466
18	Pseudohypericin	520,449
19	Protopseudohypericin	522,465
20	Apigenin	270,24
21	Mangiferin	422,342
22	Astilbin	450,396
23	Adhyperforin	550,824
24	Ferulic acid	194,186
25	Cryptochlorogenic acid	354,311
26	Protocatechuic acid	154,121
27	Quercetin-3-arabinoside	434,35
28	Miquelianin	478,362
29	Quercetin 3'-xyloside	434,353
30	Flavone	222,243
31	Nicotiflorin	594,522
34	Cyanidin 3-rhamnoside	433,389
35	3-p-Coumaroylquinic acid	338,312
36	Caffeoylquinic acid type	354,311

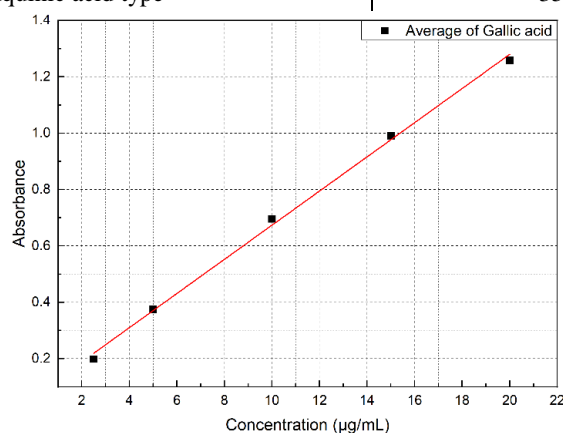


Figure S 3-2: Standard calibration curve of absorbance against concentration of Gallic acid prepared by using a UV-VIS spectrophotometer

Chapter 3: Identification of Major Constituents of *Hypericum perforatum L*

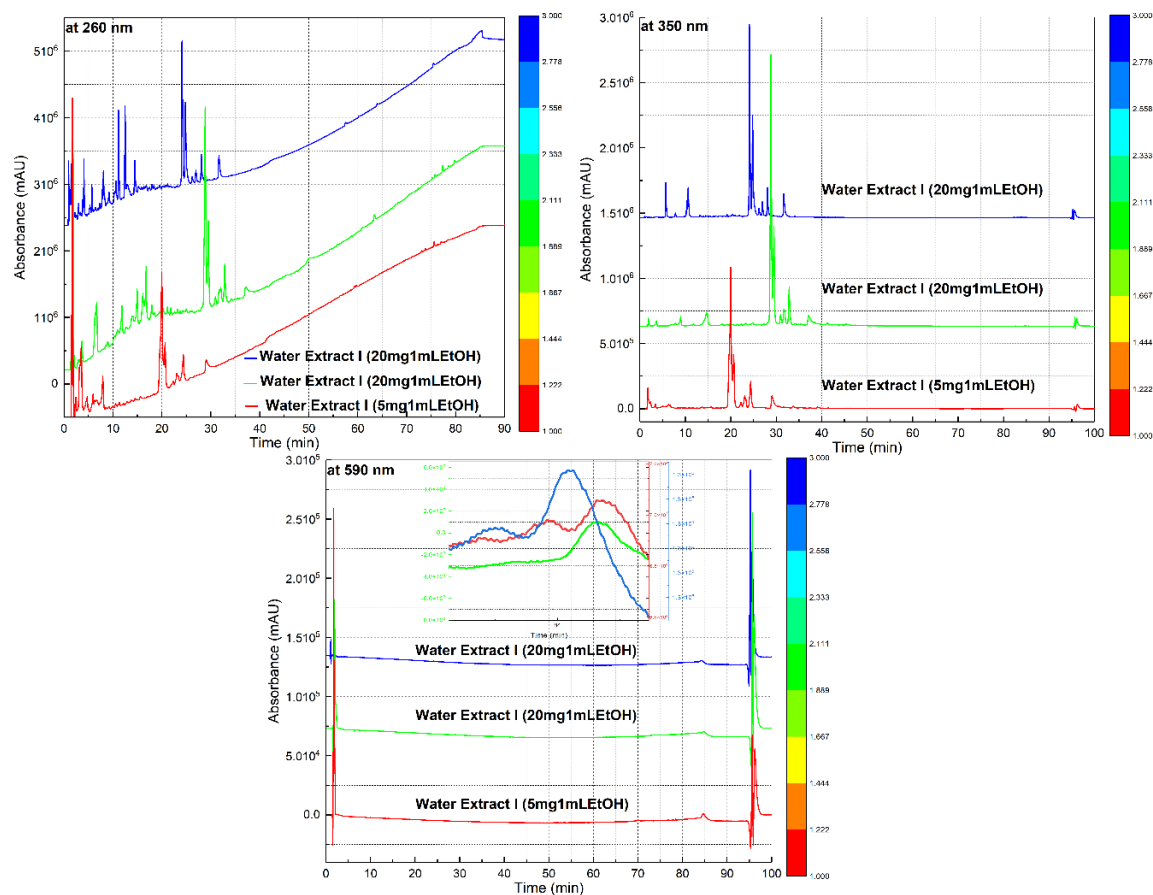


Figure S 3-3: repetition spectrums of water extract I at the three wavelengths 260 nm, 350 nm and 590 nm

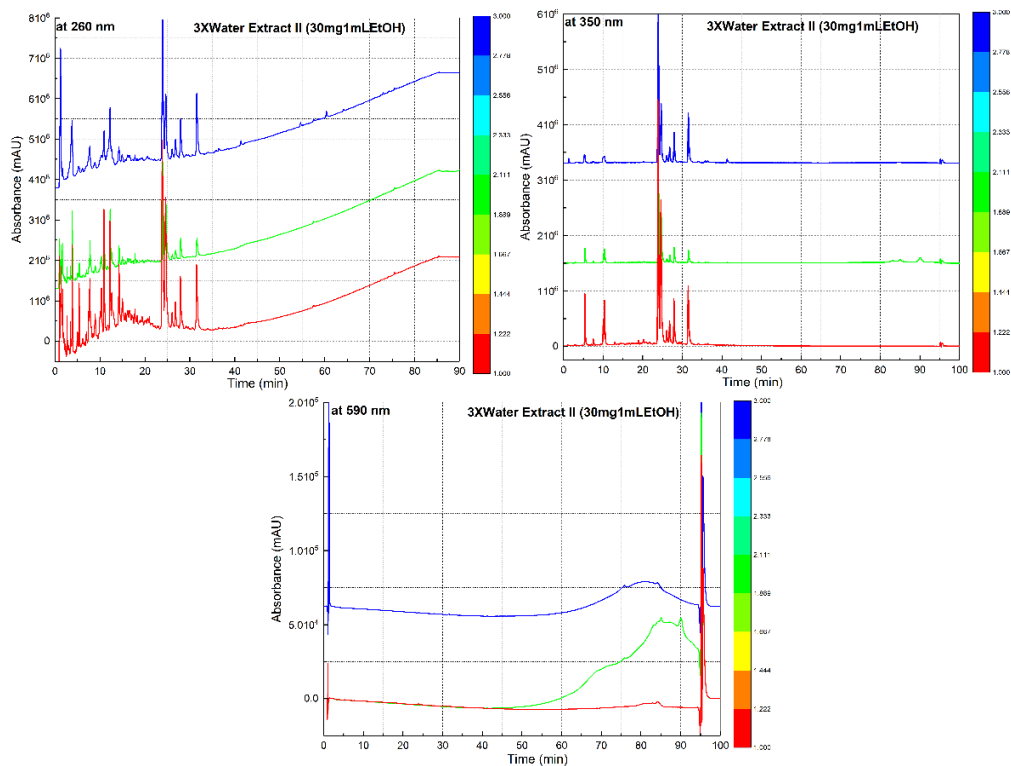


Figure S 3-4: repetition spectrums of water extract II at the three wavelengths 260 nm, 350 nm and 590 nm

Chapter 3: Identification of Major Constituents of *Hypericum perforatum L*

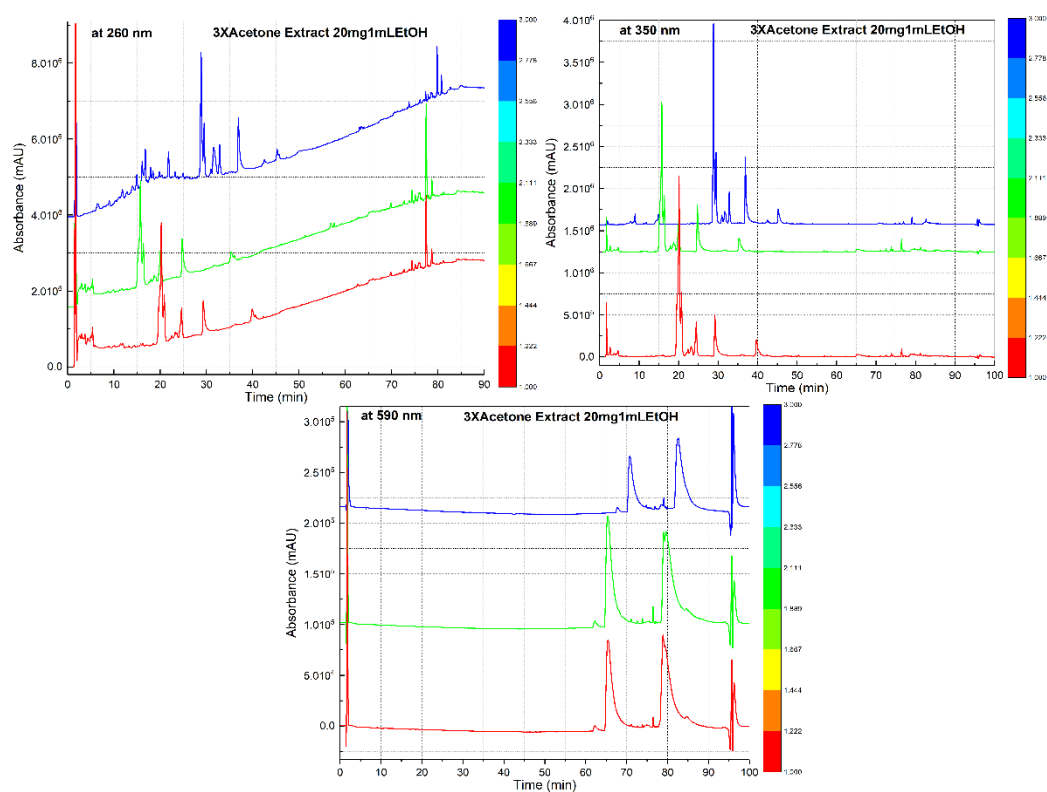


Figure S 3-5: repetition spectrums of acetone 70% at the three wavelengths 260 nm, 350 nm and 590 nm

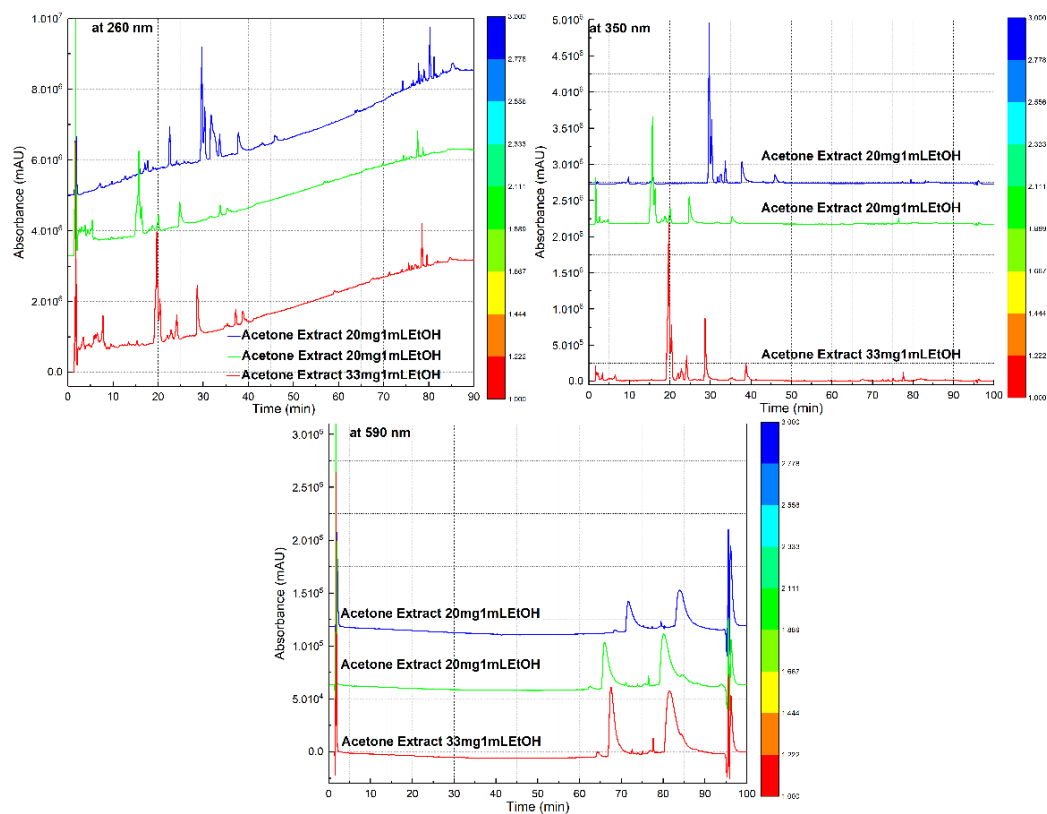


Figure S 3-6: repetition spectrums of acetone 100% at the three wavelengths 260 nm, 350 nm and 590 nm

Chapter 3: Identification of Major Constituents of *Hypericum perforatum* L

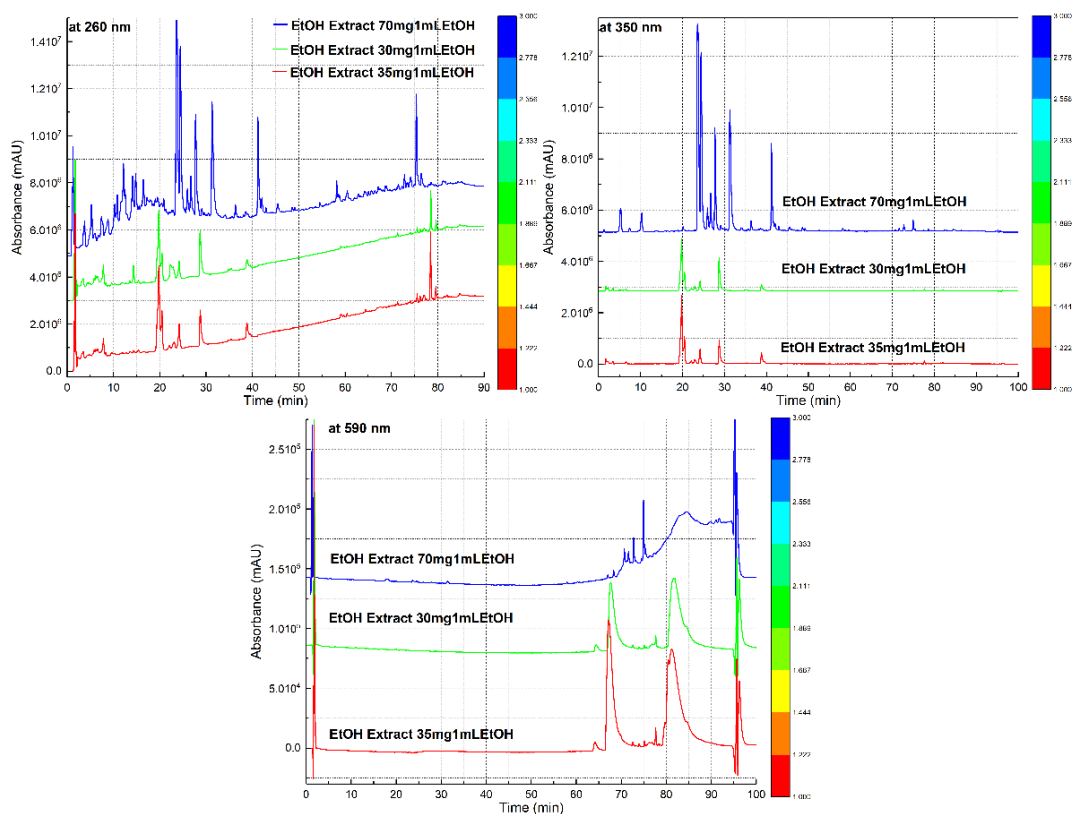


Figure S 3-7: repetition spectrums of EtOH 70% at the three wavelengths 260 nm, 350 nm and 590 nm

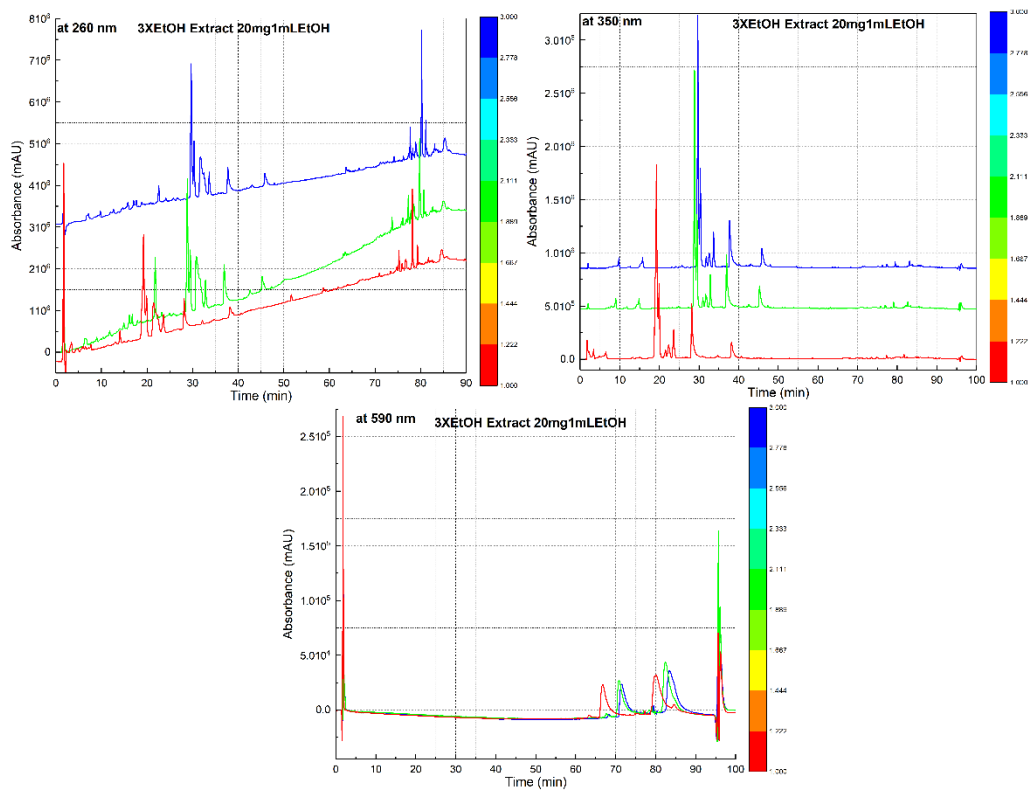


Figure S 3-8: repetition spectrums of EtOH 100% at the three wavelengths 260 nm, 350 nm and 590 nm

Chapter 3: Identification of Major Constituents of *Hypericum perforatum* L

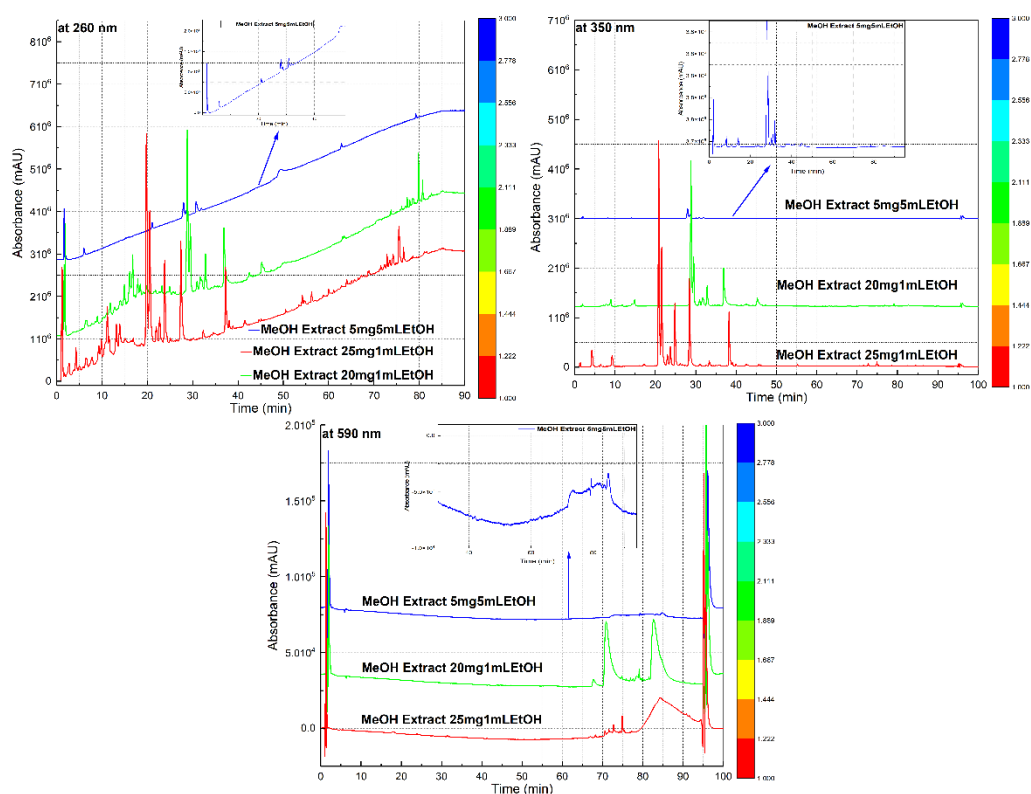


Figure S 3-9: repetition spectrums of MeOH 70% at the three wavelengths 260 nm, 350 nm and 590 nm

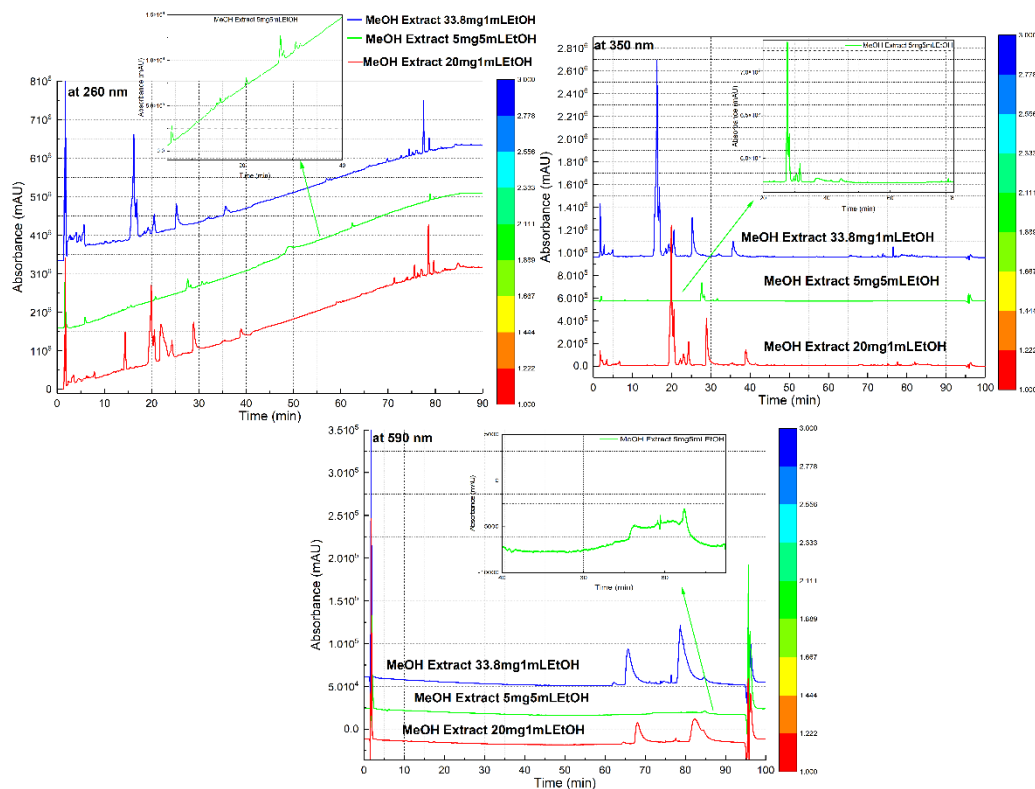


Figure S 3-10: repetition spectrums of MeOH 100% at the three wavelengths 260 nm, 350 nm and 590 nm

Chapter 3: Identification of Major Constituents of *Hypericum perforatum L*

3.9.1 Statistical Analysis

3.9.1.1 ANOVA DPPH

Table S 3-5: Descriptives of Ascorbic Acid

Descriptives Ascorbic Acid								
	N	Mean	Std. Deviation	Std. Error	95% Confidence Interval for Mean		Minimum	Maximum
					Lower Bound	Upper Bound		
					500	3		
300	3	87.8814	.12203	.07046	87.5782	88.1845	87.74	87.95
100	3	87.5995	.24407	.14092	86.9932	88.2058	87.32	87.74
50	3	86.8245	.12203	.07046	86.5213	87.1276	86.68	86.89
10	3	22.6734	1.07818	.62249	19.9950	25.3517	21.62	23.78
1.5	3	.4298	.33419	.19294	-.4003	1.2600	.05	.69
Total	18	62.2737	37.49732	8.83820	43.6267	80.9207	.05	88.37

Table S 3-6: Descriptives of Water Extract I

Descriptives Water Extract I								
	N	Mean	Std. Deviation	Std. Error	95% Confidence Interval for Mean		Minimum	Maximum
					Lower Bound	Upper Bound		
					500	3		
300	3	82.8789	.42275	.24407	81.8287	83.9290	82.46	83.30
100	3	64.6305	.32287	.18641	63.8284	65.4325	64.28	64.91
50	3	37.5749	.44001	.25404	36.4818	38.6679	37.22	38.07
10	3	10.4653	.29206	.16862	9.7398	11.1908	10.15	10.73
1.5	3	.8668	.12623	.07288	.5532	1.1803	.72	.95
Total	18	46.7018	33.87808	7.98514	29.8547	63.5490	.72	83.94

Table S 3-7: Descriptives of Water Extract II

Descriptives Water Extract II								
	N	Mean	Std. Deviation	Std. Error	95% Confidence Interval for Mean		Minimum	Maximum
					Lower Bound	Upper Bound		
					500	3		
300	3	83.6539	.44000	.25404	82.5609	84.7469	83.30	84.15
100	3	74.2831	.32287	.18641	73.4810	75.0852	74.00	74.64
50	3	45.3907	.53194	.30712	44.0693	46.7121	44.90	45.95

Chapter 3: Identification of Major Constituents of *Hypericum perforatum L*

10	3	10.8934	.33066	.19091	10.0720	11.7148	10.63	11.26
1.5	3	3.6319	.21390	.12350	3.1006	4.1633	3.40	3.82
Total	18	50.3921	34.16053	8.05171	33.4044	67.3797	3.40	84.78

Table S 3-8: Descriptives of Ascorbic Acid of Ethanol

Descriptives								
Ascorbic Acid of Ethanol								
N	Mean	Std. Deviation	Std. Error	95% Confidence Interval for Mean		Minimum	Maximum	
				Lower Bound	Upper Bound			
500	3	90.1670	.49086	.28340	88.9476	91.3863	89.80	90.72
300	3	89.7959	.37106	.21423	88.8742	90.7177	89.42	90.17
100	3	89.4249	.55659	.32135	88.0422	90.8075	88.87	89.98
50	3	89.0538	.49086	.28340	87.8344	90.2732	88.50	89.42
10	3	33.2096	4.90863	2.83400	21.0159	45.4034	29.50	38.78
1.5	3	10.7607	1.44903	.83660	7.1611	14.3603	9.83	12.43
Total	18	67.0686	33.52342	7.90155	50.3978	83.7395	9.83	90.72

Table S 3-9: Descriptives of Ethanol Extract

Descriptives								
Ethanol Extract								
N	Mean	Std. Deviation	Std. Error	95% Confidence Interval for Mean		Minimum	Maximum	
				Lower Bound	Upper Bound			
500	3	84.4156	.37106	.21423	83.4938	85.3373	84.04	84.79
300	3	83.6735	.55659	.32135	82.2908	85.0561	83.12	84.23
100	3	56.0915	4.66904	2.69567	44.4930	67.6901	51.76	61.04
50	3	36.3018	2.83400	1.63621	29.2618	43.3418	33.21	38.78
10	3	12.9252	1.86761	1.07827	8.2858	17.5646	10.95	14.66
1.5	3	8.9672	2.04363	1.17989	3.8906	14.0439	6.86	10.95
Total	18	47.0625	31.36550	7.39292	31.4648	62.6602	6.86	84.79

Chapter 3: Identification of Major Constituents of *Hypericum perforatum L*

Table S 3-10: Descriptives of Ascorbic Acid of Methanol

Descriptives								
Ascorbic Acid of Methanol								
	N	Mean	Std. Deviation	Std. Error	95% Confidence Interval for Mean		Minimum	Maximum
					Lower Bound	Upper Bound		
500	3	89.6414	.34503	.19920	88.7843	90.4985	89.24	89.84
300	3	89.4422	.19920	.11501	88.9474	89.9371	89.24	89.64
100	3	89.2430	.39841	.23002	88.2533	90.2327	88.84	89.64
50	3	88.2470	.52705	.30429	86.9378	89.5563	87.65	88.65
10	3	2.1912	4.28634	2.47472	-8.4566	12.8391	-2.19	6.37
1.5	3	.3984	.99602	.57505	-2.0758	2.8726	-.60	1.39
Total	18	59.8606	42.64608	10.05178	38.6532	81.0680	-2.19	89.84

Table S 3-11: Descriptives of Methanol

Descriptives								
Methanol Extract								
	N	Mean	Std. Deviation	Std. Error	95% Confidence Interval for Mean		Minimum	Maximum
					Lower Bound	Upper Bound		
500	3	87.2587	.51076	.29489	85.9899	88.5275	86.68	87.64
300	3	86.1004	.33437	.19305	85.2698	86.9310	85.91	86.49
100	3	59.6525	1.95924	1.13117	54.7855	64.5195	57.53	61.39
50	3	37.4517	.33437	.19305	36.6211	38.2824	37.26	37.84
10	3	20.8494	3.86100	2.22915	11.2582	30.4407	16.99	24.71
1.5	3	12.7413	.38610	.22291	11.7822	13.7004	12.36	13.13
Total	18	50.6757	30.26420	7.13334	35.6256	65.7257	12.36	87.64

3.9.1.2 ANOVA ABTS

Chapter 3: Identification of Major Constituents of *Hypericum perforatum L*

Table S 3-12: Descriptives of Ascorbic Acid, Water Extract I and Water Extract II

		Descriptives							
		N	Mean	Std. Deviation	Std. Error	95% Confidence Interval		Minimum	Maximum
						Lower Bound	Upper Bound		
Ascorbic Acid	500	3	94.9482	.00000	.00000	94.9482	94.9482	94.95	94.95
	300	3	94.8618	.07479	.04318	94.6760	95.0476	94.82	94.95
	100	3	94.6891	.00000	.00000	94.6891	94.6891	94.69	94.69
	50	3	94.6891	.00000	.00000	94.6891	94.6891	94.69	94.69
	10	3	31.9948	.22436	.12953	31.4375	32.5522	31.74	32.12
	1.5	3	5.3109	.12953	.07478	4.9891	5.6327	5.18	5.44
	Total	18	69.4157	37.77652	8.90401	50.6298	88.2015	5.18	94.95
Water Extract I	500	3	94.3949	.22064	.12739	93.8468	94.9430	94.27	94.65
	300	3	93.6306	.25478	.14709	92.9977	94.2635	93.38	93.89
	100	3	72.7389	.25478	.14709	72.1060	73.3717	72.48	72.99
	50	3	44.2038	.12739	.07355	43.8874	44.5203	44.08	44.33
	10	3	24.8408	1.13225	.65371	22.0281	27.6534	23.57	25.73
	1.5	3	5.4777	.00000	.00000	5.4777	5.4777	5.48	5.48
	Total	18	55.8811	34.72717	8.18527	38.6117	73.1505	5.48	94.65
Water Extract II	500	3	94.4228	.12970	.07488	94.1006	94.7450	94.29	94.55
	300	3	93.9905	.07488	.04323	93.8045	94.1765	93.90	94.03
	100	3	74.4920	.19812	.11438	73.9998	74.9842	74.32	74.71
	50	3	44.6606	.39625	.22877	43.6763	45.6450	44.23	45.01
	10	3	13.1431	3.50994	2.02647	4.4239	21.8623	9.21	15.95
	1.5	3	3.6749	.83386	.48143	1.6035	5.7463	2.72	4.28
	Total	18	54.0640	37.45843	8.82904	35.4363	72.6916	2.72	94.55

Table S 3-13: Descriptives of Ascorbic Acid and Ethanol Extract

		Descriptives							
		N	Mean	Std. Deviation	Std. Error	95% Confidence Interval		Minimum	Maximum
						Lower Bound	Upper Bound		
Ascorbic Acid of Ethanol	500	3	95.0535	.00000	.00000	95.0535	95.0535	95.05	95.05
	300	3	94.9198	.13369	.07719	94.5877	95.2519	94.79	95.05
	100	3	94.8307	.07719	.04456	94.6389	95.0224	94.79	94.92
	50	3	94.7415	.07719	.04456	94.5498	94.9333	94.65	94.79
	10	3	38.4581	.20421	.11790	37.9508	38.9654	38.24	38.64
	1.5	3	10.9626	.74435	.42975	9.1135	12.8116	10.16	11.63

Chapter 3: Identification of Major Constituents of *Hypericum perforatum L*

	Total	18	71.4944	35.00766	8.25138	54.0855	88.9033	10.16	95.05
Ethanol Extract	500	3	94.5254	.07647	.04415	94.3354	94.7154	94.44	94.57
	300	3	93.1126	.35043	.20232	92.2421	93.9831	92.85	93.51
	100	3	51.6556	.47756	.27572	50.4693	52.8419	51.13	52.05
	50	3	33.3775	.39735	.22941	32.3904	34.3646	32.98	33.77
	10	3	24.7682	.57734	.33333	23.3340	26.2024	24.11	25.17
	1.5	3	9.8896	.20233	.11681	9.3870	10.3922	9.67	10.07
	Total	18	51.2215	33.49464	7.89476	34.5650	67.8780	9.67	94.57

Table S 3-14: Descriptives of Ascorbic Acid and Methanol Extract

		Descriptives							
		N	Mean	Std. Deviation	Std. Error	95% Confidence Interval for Mean		Minimum	Maximum
						Lower Bound	Upper Bound		
Ascorbic Acid of Methanol	500	3	95.0552	.07647	.04415	94.8652	95.2452	94.97	95.10
	300	3	94.9669	.00000	.00000	94.9669	94.9669	94.97	94.97
	100	3	94.9227	.07647	.04415	94.7328	95.1127	94.83	94.97
	50	3	93.3775	.26490	.15294	92.7194	94.0355	93.11	93.64
	10	3	93.3775	.26490	.15294	92.7194	94.0355	93.11	93.64
	1.5	3	6.0927	.39736	.22941	5.1056	7.0798	5.70	6.49
	Total	18	79.6321	33.84988	7.97849	62.7989	96.4652	5.70	95.10
Methanol Extract	500	3	93.0680	.22234	.12837	92.5157	93.6204	92.94	93.32
	300	3	92.2978	.33964	.19609	91.4541	93.1415	91.91	92.55
	100	3	45.6568	.19608	.11321	45.1697	46.1439	45.44	45.83
	50	3	26.3158	.12837	.07411	25.9969	26.6347	26.19	26.44
	10	3	11.1682	.46284	.26722	10.0184	12.3179	10.65	11.55
	1.5	3	7.5738	.33964	.19609	6.7301	8.4175	7.32	7.96
	Total	18	46.0134	36.22642	8.53865	27.9984	64.0284	7.32	93.32

3.9.1.3 T- Test: DPPH

Chapter 3: Identification of Major Constituents of *Hypericum perforatum L*

Table S 3-15

		Mean	N	Std. Deviation	Std. Error Mean
Pair 1	Ascorbic Acid	62.2737	18	37.49732	8.83820
	Water Extract I	46.7018	18	33.87808	7.98514
Pair 2	Ascorbic Acid	62.2737	18	37.49732	8.83820
	Water Extract II	50.3921	18	34.16053	8.05171
Pair 3	Ascorbic Acid of Ethanol	67.0686	18	33.52342	7.90155
	Ethanol Extract	47.0625	18	31.36550	7.39292
Pair 4	Ascorbic Acid of Methanol	59.8606	18	42.64608	10.05178
	Methanol Extract	50.6757	18	30.26420	7.13334

Table S 3-16:

Paired Samples Correlations

		N	Correlation	Sig.
Pair 1	Ascorbic Acid & Water Extract I	18	.888**	.000
Pair 2	Ascorbic Acid & Water Extract II	18	.920**	.000
Pair 3	Ascorbic Acid of Ethanol & Ethanol Extract	18	.834**	.000
Pair 4	Ascorbic Acid of Methanol & Methanol Extract	18	.822**	.000

** Correlation is significant at the 0.01 level (2-tailed)

If the correlation is between 0.85 and 1, there is a strong correlation. If the correlation is between 0.5 and 0.85, there is a moderate correlation. If the correlation is between 0.1 and 0.5, there is a weak correlation.

Table S 3-17:

Paired Samples Test

		Mean	Std. Deviation	Std. Error Mean	95% Confidence Interval of the Difference		t	df	Sig. (2-tailed)
					Lower	Upper			
Pair 1	Ascorbic Acid – Water Extract I	15.57185	17.28684	4.07455	6.97531	24.16840	3.822	17	.001
Pair 2	Ascorbic Acid – Water Extract II	11.88163	14.72732	3.47126	4.55790	19.20535	3.423	17	.003
Pair 3	Ascorbic Acid of Ethanol – Ethanol Extract	20.00618	18.79039	4.42894	10.66194	29.35042	4.517	17	.000
Pair 4	Ascorbic Acid of Methanol – Methanol Extract	9.18488	24.74250	5.83186	-3.11928	21.48904	1.575	17	.134

Chapter 3: Identification of Major Constituents of *Hypericum perforatum L*

3.9.1.4 T- Test: ABTS

Table S 3-18:

		Paired Samples Statistics			
		Mean	N	Std. Deviation	Std. Error Mean
Pair 1	Ascorbic Acid	69.4157	18	37.77652	8.90401
	Water Extract I	55.8811	18	34.72717	8.18527
Pair 2	Ascorbic Acid	69.4157	18	37.77652	8.90401
	Water Extract II	54.0640	18	37.45843	8.82904
Pair 3	Ascorbic Acid of Ethanol	71.4944	18	35.00766	8.25138
	Ethanol Extract	51.2215	18	33.49464	7.89476
Pair 4	Ascorbic Acid of Methanol	79.6321	18	33.84988	7.97849
	Methanol Extract	46.0134	18	36.22642	8.53865

Table S 3-19:

		Paired Samples Correlations		
		N	Correlation	Sig.
Pair 1	Ascorbic Acid & Water Extract I	18	.870**	.000
Pair 2	Ascorbic Acid & Water Extract II	18	.884**	.000
Pair 3	Ascorbic Acid of Ethanol & Ethanol Extract	18	.748**	.000
Pair 4	Ascorbic Acid of Methanol & Methanol Extract	18	.505*	.033

** Correlation is significant at the 0.01 level (2-tailed)

* Correlation is significant at the 0.05 level (2-tailed).

Table S 3-20:

		Paired Samples Test							
		Mean	Std. Deviation	Std. Error Mean	95% Confidence Interval of the Difference		t	df	Sig. (2-tailed)
					Lower	Upper			
Pair 1	AscorbicAcid - WaterExtractI	13.53456	18.71702	4.41164	4.22680	22.84231	3.068	17	.007
Pair 2	AscorbicAcid - WaterExtractII	15.35167	18.13452	4.27435	6.33359	24.36976	3.592	17	.002

Chapter 3: Identification of Major Constituents of *Hypericum perforatum L*

Pair 3	AscorbicAcidofEt hanol - EthanolExtract	20.272 87	24.33708	5.73630	8.17033	32.37542	3.534	17	.003
Pair 4	AscorbicAcidofM ethanol - MethanolExtract	33.618 68	34.93250	8.23367	16.24715	50.99020	4.083	17	.001

Table S 3-21: Standard errors in DPPH method were calculated using the Fisher information matrix. Confidence Interval was calculated using a significance level of Square 0.05.

	IC ₅₀	Confidence Interval	Untere Grenze	Upper limit	STD Error
Water I	60	43.4	-32.5	152.4	20
Water II	51	7.6	34.7	67.2	3.6
Ethanol	75	30.8	9.0	140.5	14
Methanol	67	9.5	46.5	86.8	4.4

Table S 3-22: Standard errors in ABTS method were calculated using the Fisher information matrix. Confidence Interval was calculated using a significance level of Square 0.05.

	IC ₅₀	Confidence Interval	Untere Grenze	Upper limit	STD Error
Water I	51	8.6	33.0	69.9	4.1
Water II	42	19.8	0.0	84.4	9.3
Ethanol	97	29.4	34.5	159.7	28.97
Methanol	71	61.8	-60.2	203.1	13.8

3.9.2 References

- Dejan Z., O.; Neda M., M.-D.; Marina M., F.; Slobodan S., P.; Emilija Đ., J., Antioxidant activity relationship of phenolic compounds in *Hypericum perforatum*L. *Chem. Cent. J.* **2011**, 5 (1), 34.
- Wenkui, L.; John F., F., High performance liquid chromatographic analysis of St. John's wort with photodiode array detection. *J. Chromatogr. B Biomed. Appl.* **2001**, 765 (1), 99-105.
- Bruno A., S.; Federico, F.; João O., M.; Alberto C.P., D., Phytochemical and antioxidant characterization of *Hypericum perforatum* alcoholic extracts. *Food Chem.* **2005**, 90 (1-2), 157-167.
- A. C. P., D.; R. M., S.; P. B., A.; M., F.-F., The development and evaluation of an HPLC-DAD method for the analysis of the phenolic fractions from in vivo and in vitro biomass of *Hypericum* species. *J. Liq. Chromatogr. Relat. Technol* **1999**, 22 (2), 215-227.
- Silva, B. A.; Malva, J. O.; Dias, A. C. P., St. John's Wort (*Hypericum perforatum*) extracts and isolated phenolic compounds are effective antioxidants in several in vitro models of oxidative stress. *Food Chem.* **2008**, 110 (3), 611-619.
- Elgin, G.; Konyalioglu, S.; Kilinc, E., Development and Validation of a Multidetector HPLC Method for the Determination of Antioxidant Flavonoids of some *Hypericum L.* Species. *J. Liq. Chromatogr. Relat. Technol* **2008**, 32 (3), 432-448.
- Guido, J.; Adolf, N., Phenolic compounds from *Hypericum perforatum*. *Planta Med* **2002**, 68 (1), 88-91.
- Steen Honoré, H.; Anette Gemal, J.; Claus, C.; Inga, B.; Steven, T.; Brian, W.; Ian D., W., High-performance liquid chromatography on-line coupled to high-field NMR and mass spectrometry

Chapter 3: Identification of Major Constituents of *Hypericum perforatum* L

for structure elucidation of constituents of *Hypericum perforatum* L. *Anal. Chem.* **1999**, *71* (22), 5235-5241.

9. Biljana, B.; Nebojša, K.; Nevena, G.; Goran, A.; Isidora, S.; Neda, G.; Branislava Srđenović, Č., Impact of origin and biological source on chemical composition, anticholinesterase and antioxidant properties of some St. John's wort species (*Hypericum* spp., Hypericaceae) from the Central Balkans. *Molecules* **2013**, *18* (10), 11733-11750.

10. Jelena, S.; Ivana, R.; Aleksandra, Đ.; Olga, J.; Goran, P.; Gordana, S., Optimization of HPLC method for the isolation of *Hypericum perforatum* L. methanol extract. *Biol. Nyssana* **2013**, *4* (1-2), 81-85.

11. Hernandez, M. F.; Falé, P. L. V.; Araújo, M. E. M.; Serralheiro, M. L. M., Acetylcholinesterase inhibition and antioxidant activity of the water extracts of several *Hypericum* species. *Food Chem.* **2010**, *120* (4), 1076-1082.

12. Susan H., K.; Larry L., A.; Agnes, N.; William S., Z.; Fran X., M., Selected physical and chemical properties of commercial *Hypericum perforatum* extracts relevant for formulated product quality and performance. *AAPS PharmSci.* **2001**, *3* (4), 1-18.

13. Gerlie Cde los, R.; Robert T., K., Development of a simple, rapid and reproducible HPLC assay for the simultaneous determination of hypericins and stabilized hyperforin in commercial St. John's wort preparations. *J. Pharm. Biomed. Anal.* **2001**, *26* (5-6), 959-65.

14. M., B.; B., G.; N., F.; R., P.; F., P.; F., P., Identification by high-performance liquid chromatography–diode array detection–mass spectrometry and quantification by high-performance liquid chromatography–UV absorbance detection of active constituents of *Hypericum perforatum*. *J. Chromatogr. A* **1998**, *825* (1), 9-16.

15. Piperopoulos, G.; Lotz, R.; Wixforth, A.; Schmierer, T.; Zeller, K.-P., Determination of naphthodianthrones in plant extracts from *Hypericum perforatum* L. by liquid chromatography–electrospray mass spectrometry. *J. Chromatogr. B Biomed. Appl.* **1997**, *695* (2), 309-316.

16. M., G.; J., Z.; I.A., K., *Hypericum Perforatum*—Chemical Profiling and Quantitative Results of St. John's Wort Products by an Improved High-Performance Liquid Chromatography Method. *J. Pharm. Sci.* **2002**, *91* (3), 623-630.

17. Wenxia, C.; Fengfeng, F.; Ying, Z.; Zhichao, P.; Wenji, W.; Yuxin, P., A Facile Approach for Fabrication of Core-Shell Magnetic Molecularly Imprinted Nanospheres towards Hypericin. *Polymers* **2017**, *9* (4), 135.

18. Pinarosa, A.; Gaspare, G., Determination of major constituents in St. John's Wort under different extraction conditions. *Pharm. Biol.* **2004**, *42* (1), 83-89.

19. Neerja, T.; Hema, M.; P. D., H.; Tukaram, M.; Ashish, S.; Vijay Singh, C., Development of a High-Performance Liquid Chromatographic Method for the Quantitative Determination of Hyperforin. *Int. J. Appl. Sci. Eng* **2008**, *6* (1), 39-46.

20. Anzewska, M.; Kowalczyk, A.; Łozak, A.; Jabłczyńska, R.; Fijałek, Z., Determination of total hypericins in St. John's wort and herbal medicinal products. *Acta Pol Pharm.* **2010**, *67* (6), 586-592.

21. Lauro, N.-p.; Jorge, M.-t.; Sylvia, P.-g. l., Determination of Hypericin in *Hypericum* Species Grown in Cuba. *Acta Farm. Bonaerense* **2005**, *24* (1), 89-90.

22. V. A., H.-P.; L. K., B.; J. D., P.; H., S.; G., A.; M., P.; G. K., B.; C. W., H., A chromatographic and spectroscopic analytical platform for the characterization of St John's wort extract adulterations. *Anal. Methods* **2013**, *5* (3), 616-628.

Chapter 3: Identification of Major Constituents of *Hypericum perforatum L*

3.10 Additional experiments for determination of organic compounds on the surface of nanoparticles

Table SS 1: Representation of the peak numbers of the mass spectrum of the sample (ethanol 100%) with respective times and the positive ion mass (The value is either the molecular weight of the compound plus hydrogen, plus sodium, or plus ammonium, or it may refer to the higher-intensity fragment ion from this compound)

Peak No	Time / min	m/z	Peak No	Time / min	m/z	Peak No	Time / min	m/z	Peak No	Time / min	m/z
1	0.429	140.996	48	24.371	343.000	95	50.337	267.000	142	69.447	575.403
2	0.572	140.996	49	24.436	331.000	96	50.373	639.382	143	70.155	537
3	0.700	140.996	50	24.444	331.000	97	51.073	639.379	144	70.883	589.413
4	2.000	141.000	51	24.660	241.060	98	51.237	335.000	145	71.181	589.413
5	2.650	114.980	52	25.499	579.000	99	52.203	625.000	146	71.383	551.000
6	2.870	206.870	53	25.809	285.128	100	52.546	607.000	147	71.692	116.998
7	2.974	206.000	54	25.955	413.000	101	53.200	609.370	148	72.020	116.998
8	3.190	325.000	55	25.964	413.000	102	53.345	609.368	149	72.265	116.998
9	3.228	104.097	56	26.090	219.090	103	53.672	317.220	150	72.347	116.998
10	3.246	104.097	57	27.021	355.170	104	54.346	623.390	151	72.637	116.998
11	3.263	325.000	58	28.173	158.000	105	54.755	625.380	152	72.838	116.998
12	3.345	118.077	59	28.536	633.000	106	54.919	317.220	153	72.900	117.000
13	3.409	248.000	60	28.799	545.000	107	55.182	295.198	154	73.247	683.000
14	3.418	248.000	61	29.416	465.000	108	55.410	319.229	155	75.770	117.000
15	3.792	140.996	62	29.786	465.000	109	56.147	591.370	156	77.667	116.994
16	3.918	140.996	63	31.090	395.000	110	56.764	515.298	157	77.811	685.000
17	4.210	140.996	64	31.110	395.000	111	57.272	609.377	158	77.860	685.470
18	4.373	72.000	65	31.260	325.210	112	57.564	609.380	159	77.921	685.000
19	4.519	261.108	66	32.000	303.040	113	58.090	591.360	160	77.957	685.000
20	4.630	130.040	67	33.300	191.070	114	58.928	593.386	161	77.957	685.000
21	8.292	276.138	68	35.480	303.050	115	59.154	609.386	162	77.994	685.000
22	8.318	276.138	69	36.618	236.000	116	59.428	609.386	163	78.021	685.000
23	8.800	173.000	70	36.691	236.000	117	59.746	591.357	164	78.039	685.000
24	8.981	173.000	71	36.700	236.000	118	60.673	593.386	165	78.076	685.000
25	9.455	173.000	72	37.218	271.000	119	61.383	575.385	166	78.404	116.998
26	9.472	173.000	73	37.246	271.000	120	61.927	477.296	167	78.731	116.998
27	10.890	120.080	74	37.450	237.150	121	62.038	439.000	168	78.731	116.998
28	10.963	120.077	75	40.100	539.090	122	62.365	609.277	169	79.386	116.998
29	11.510	100.070	76	40.230	539.090	123	62.624	575.370	170	79.795	116.998
30	12.130	141.000	77	41.726	251.000	124	63.020	609.267	171	80.166	537.000
31	14.907	163.030	78	41.746	251.000	125	63.510	575.350	172	80.190	537.430
32	15.609	188.070	79	42.045	277.187	126	63.937	563.364	173	80.286	537.000
33	17.046	317.110	80	42.136	277.181	127	64.280	559.360	174	80.330	537.000
34	17.736	147.000	81	43.874	353.000	128	64.570	593.250	175	80.348	537.000
35	18.791	317.117	82	44.064	353.242	129	64.910	573.379	176	80.531	116.998
36	19.144	865.000	83	44.370	353.000	130	65.147	573.370	177	80.940	116.998
37	19.173	865.000	84	45.347	549.320	131	65.246	437.348	178	81.268	116.998
38	19.226	379.000	85	45.347	549.323	132	65.392	689.000	179	84.440	117.000
39	19.682	293.000	86	45.546	311.227	133	65.682	601.000	180	84.700	116.990
40	19.869	163.040	87	45.855	116.990	134	65.691	601.000	181	84.830	116.990
41	21.154	291.070	88	46.454	549.314	135	65.801	559.379	182	84.930	116.990
42	21.946	469.000	89	46.738	643.400	136	66.360	557.350	183	85.060	116.990
43	21.972	469.000	90	47.264	275.170	137	66.909	535.289	184	85.340	116.990
44	22.140	409.170	91	48.374	531.310	138	66.960	571.370	185	85.523	149.000
45	22.826	287.000	92	49.509	625.377	139	67.537	533.413	186	85.768	135.000
46	22.890	287.000	93	50.273	641.000	140	67.982	575.394	187	85.850	149.000
47	24.035	307.115	94	50.300	267.000	141	68.637	575.380	188	85.950	121.000
									189	87.350	141.020

Chapter 3: Identification of Major Constituents of *Hypericum perforatum* L

Depending on the values of the molecular ions present in the MS spectrum that was measured for the St. John's wort extract (table ss1). A large number of compounds found in this plant have been previously identified in many countries. Therefore, by comparing the values of molecules ions from table ss1 with the molecular weights of the compounds previously known to this plant (The value is either the molecular weight of the compound plus hydrogen, plus sodium, or plus ammonium, or it may refer to the higher-intensity fragment ion from this compound) and also by the appearance of some fragments in the MS1 diagrams of each peak for many reasons, we identified about 60 compounds of it. Unfortunately, we cannot say that we have identified them 100% until we can perform MS/MS analysis and we investigated this through fragmentation and comparing the fragments for each compound separately.

ESI is a so-called 'soft ionization technique since there is very little fragmentation. This can be advantageous in the sense that the molecular ion (molecular radical cations) (or more accurately a pseudo molecular ion) is almost always observed, however very little structural information can be gained from the simple mass spectrum obtained. Electrospray ionization (ESI) is a technique to generate ions for mass spectrometry using electrospray by applying a high voltage to a liquid to produce an aerosol. Due to relatively fragile biomacromolecules, their structures are easily destroyed during the process of dissociation and ionization. The cone voltage is much lower than the capillary (a few tens of volts) and is used to remove the solvent molecules attached to the ions, by collision with the gas used to assist the spray. A higher cone voltage leads to fragmenting of the ions, also by collision with the gas. Also if sufficient energy is imparted to the analyte molecule during ionization, that excess energy may be transported into vibrational degrees of freedom within the molecule, resulting in the rupture of chemical bonds and the production of fragment ions.

Table SS 2: Identification of compounds in ethanol extracts of *Hypericum Perforatum* L. by HPLC-ESI-QTOF MS Analysis

Peak Nr.	R _t min	Precursor Ion + Fragment Ions Used for Assignment [M+H] ⁺ , m/z	Formula	Identified compounds
19	4.519	283 261	C ₁₃ H ₈ O ₆ Na C ₁₃ H ₈ O ₆	Norathyriol [M+Na] ⁺ Norathyriol [M+H] ⁺
31	14.907	377	C ₁₆ H ₁₈ O ₉ Na	Neochlorogenic acid [M+Na] ⁺
34	17.736	361	C ₁₆ H ₁₈ O ₈ Na	3-p-Coumaroylquinic acid [M+Na] ⁺
40	19.869	377	C ₁₆ H ₁₈ O ₉ Na	Chlorogenic acid [M+Na] ⁺
41	21.154	313	C ₁₅ H ₁₄ O ₆ Na	Catechin [M+Na] ⁺
45	22.826	309	C ₁₅ H ₁₀ O ₆ Na	Luteolin [M+Na] ⁺
46	22.890	309	C ₁₅ H ₁₀ O ₆ Na	Kaempferol [M+Na] ⁺
47	24.035	329	C ₁₅ H ₁₄ O ₇ Na	Epigallocatechin [M+Na] ⁺
48	24.371	365	C ₁₉ H ₁₈ O ₆ Na	1,3,7-Trihydroxy-6-methoxy-8-prenylxanthone
52	25.499	601	C ₃₀ H ₂₆ O ₁₂ Na	procyanidin type B [M+Na] ⁺

Chapter 3: Identification of Major Constituents of *Hypericum perforatum* L

57	27.021	377	C ₁₆ H ₁₈ O ₉ Na	Cryptochlorogenic acid [M+Na] ⁺
59	28.536	633	C ₂₇ H ₃₀ O ₁₆ Na	Rutin [M+Na] ⁺
61	29.416	487	C ₂₁ H ₂₀ O ₁₂ Na	Hyperoside[M+Na] ⁺
62	29.786	487	C ₂₁ H ₂₀ O ₁₂ Na	Isoquercitrin [M+Na] ⁺
66	32	471	C ₂₁ H ₂₀ O ₁₁ Na	Quercitrin [M+Na] ⁺
68	35.480	325	C ₁₅ H ₁₀ O ₇ Na	Quercetin [M+Na] ⁺
72	37.218	293	C ₁₅ H ₁₀ O ₅ Na	Apigenin [M+Na] ⁺
75	40.1	561	C ₃₀ H ₁₈ O ₁₀ Na	Amentoflavone [M+Na] ⁺
76	40.23	561	C ₃₀ H ₁₈ O ₁₀ Na	13,118-Biapiogenin [M+Na] ⁺
91	48.374	553	C ₂₆ H ₂₆ O ₁₂ Na	feruloyl-caffeoylquinic acid [M+Na] ⁺
92	49.509	625	C ₃₅ H ₅₄ O ₈ Na	Hyperforatone L [M+Na] ⁺
93	50.273	663	C ₂₈ H ₃₂ O ₁₇ Na	Isorhamnetin-3-diglucoside [M+Na] ⁺
96	50.373	639	C ₃₆ H ₅₆ O ₈ Na	Hyperforatone N [M+Na] ⁺
97	51.073	639	C ₃₆ H ₅₆ O ₈ Na	Hyperforatone O [M+Na] ⁺
99	52.203	625	C ₃₅ H ₅₄ O ₈ Na	Hyperforatone M [M+Na] ⁺
100	52.546	607	C ₃₅ H ₅₂ O ₇ Na	Hyperforatone I or K [M+Na] ⁺
101-102 & 111-112 & 115-116 & 122 & 124	From 53.2 to 63.020	609 587	C ₃₅ H ₅₄ O ₇ Na C ₃₅ H ₅₄ O ₇	Hyperforatone G & Hypericumoxide B-C & E & G-I & M
103	53.672	339	C ₁₆ H ₁₂ O ₇ Na	Isorhamnetin [M+Na] ⁺
104	54.346	623	C ₃₆ H ₅₆ O ₇ Na	Hyperforatone H [M+Na] ⁺
105	54.755	647	C ₂₈ H ₃₂ O ₁₆ Na	Isorhamnetin rutinoside [M+Na] ⁺
106	54.919	339	C ₁₆ H ₁₂ O ₇ Na	Tamarixetin [M+Na] ⁺
108	55.410	341	C ₁₅ H ₁₀ O ₈ Na	Myricetin [M+Na] ⁺
109	56.147	591	C ₃₅ H ₅₂ O ₆ Na	33-Deoxy-33-hydroperoxyfurohyperforin [M+Na] ⁺
113	58.09	591	C ₃₅ H ₅₂ O ₆ Na	Furohyperforin isomer A hydroperoxide [M+Na] ⁺
117	59.746	591	C ₃₅ H ₅₂ O ₆ Na	Furohyperforin isomer B hydroperoxide [M+Na] ⁺ [M+H] ⁺
119	61.383	575	C ₃₅ H ₅₂ O ₅ Na	Furohyperforin [M+Na] ⁺
123	62.624	575	C ₃₅ H ₅₂ O ₅ Na	Furohyperforin analogue a [M+Na] ⁺
125	63.510	575	C ₃₅ H ₅₂ O ₅ Na	Furohyperforin analogue b [M+Na] ⁺
126	63.937	563	C ₃₀ H ₂₆ O ₁₁	Epi (Catechin)-4-Epi (Afzelechin) [M+H] ⁺
137	66.909	557	C ₃₅ H ₅₀ O ₄ Na	Pyrano[7,28-b]Hyperforin [M+Na] ⁺
140	67.982	575	C ₃₅ H ₅₂ O ₅ Na	Oxepahyperforin [M+Na] ⁺
141	68.637	575	C ₃₅ H ₅₂ O ₅ Na	8-Hydroxyhyperforin 8,1-hemiacetal [M+Na] ⁺

Chapter 3: Identification of Major Constituents of *Hypericum perforatum L*

142	69.447	575	C ₃₅ H ₅₂ O ₅ Na	1-(2-Methyl-1-oxopropyl)-2,12-dioxo-3,10 β -bis(3-methyl-2-butenyl)-6 β -(1-methyl-1-hydroxyethyl)-11 β -methyl-11 α -(4-methyl-3-pentenyl)-5-oxatricyclo[6.3.1.0 ^{4,8}]-3-dodecene [M+Na] ⁺
143	70.155	559	C ₃₅ H ₅₂ O ₄ Na	Hyperforin [M+Na] ⁺
144	70.883	589	C ₃₆ H ₅₄ O ₅ Na	Furoadhyperforin isomer a [M+Na] ⁺
145	71.181	589	C ₃₆ H ₅₄ O ₅ Na	Furoadhyperforin isomer b [M+Na] ⁺
146	71.383	573	C ₃₆ H ₅₄ O ₄ Na	Adhyperforin [M+Na] ⁺

3.10.1 Isolation and identification of capping agent St. John's wort bio compounds from the surfaces of AgNPs

St John's wort aqueous extract has compounds that reduce silver ions to silver metal, and there are also compounds that adsorb on the surfaces of formed silver particles in nanosize to prevent them from growing and aggregate and stabilizing them in colloidal solution. The extract can also contain compounds that facilitate the growth and agglomeration, and here lies the experience in manipulating the ratios and interaction conditions to obtain the highest yield and the best specifications for the resulting nanoparticles. After obtaining the silver nanoparticles, the product is washed several times with deionized water with centrifugation at very high speeds to remove the organic compounds present in the solution and non-adsorbed on the surfaces of silver nanoparticles. The metabolites adsorbed on the surfaces of silver nanoparticles as a protective layer (capping agent or stabilizer) are very difficult to remove. The purpose of its isolation is to identify the compounds that consist of this layer and their proportion thus, we can highlight the contribution of these constituents to the subsequent effects of silver nanoparticles in various fields, especially in the medical field. This also makes it easier to understand, interpret and modify the surfaces of silver in order to combine them with antibiotics and polymers to prepare targeted therapies. In this work, a special protocol was developed to remove about 80% of these phytochemical compounds, and the protocol is as follows: A mixture of organic solvents prepared as follows: 20% EtOH, 20% MeOH, 30% acetone and 30% Ethyl acetate then prepared silver nanoparticles are dried from water using lyophilization and mixed with an amount of the previously prepared organic solvent mixture. The samples were put in an ultrasonic bath to break down the agglomerate resulting from the drying process, thus dissolving the largest amount of these organic compounds in the organic solvent mixture. The samples are then are centrifuged at 15000 rpm for one hour. The supernatant is separated from the sediment, where the supernatant is kept in a dark bottle, and the sediment is washed in the same way several times with the organic solvent mixture. Finally, the supernatant is collected and the organic solvent mixture is evaporated using nitrogen, and then the mass-produced by the supernatant is dissolved in ethanol only, and an HPLC, HPLC/MS and MS/MS were performed for it to identify these phytochemical compounds and their percentage. As for the sediment, a Thermogravimetric (TGA) and FTIR analysis were performed to demonstrate the success of the used protocol to separate this organic layer from

Chapter 3: Identification of Major Constituents of *Hypericum perforatum L*

nanoparticle surfaces and to find out the percentage of organic compounds that have not been isolated and that is still on the surfaces of silver nanoparticles.

Thermal decomposition analysis up to 1000 °C of biosynthesized silver nanoparticles and for them after isolation the capping agent using a mixture of organic solvents proved that about 70-80% of this layer was removed (The weight decreased from 60% in the case of biosynthesized AgNPs (figure SS1I a and b) to 12-18% (figure SS1I c and d) after using the previous protocol to obtain the capping agent). FTIR spectrum for sediment in figure SS1II shows clearly that the intensity of the peaks in the spectrum have become very weak and some of them completely disappeared, and this also proves that most of the organic layer that was surrounding the nanoparticles as a protective layer was removed using the previously explained protocol.

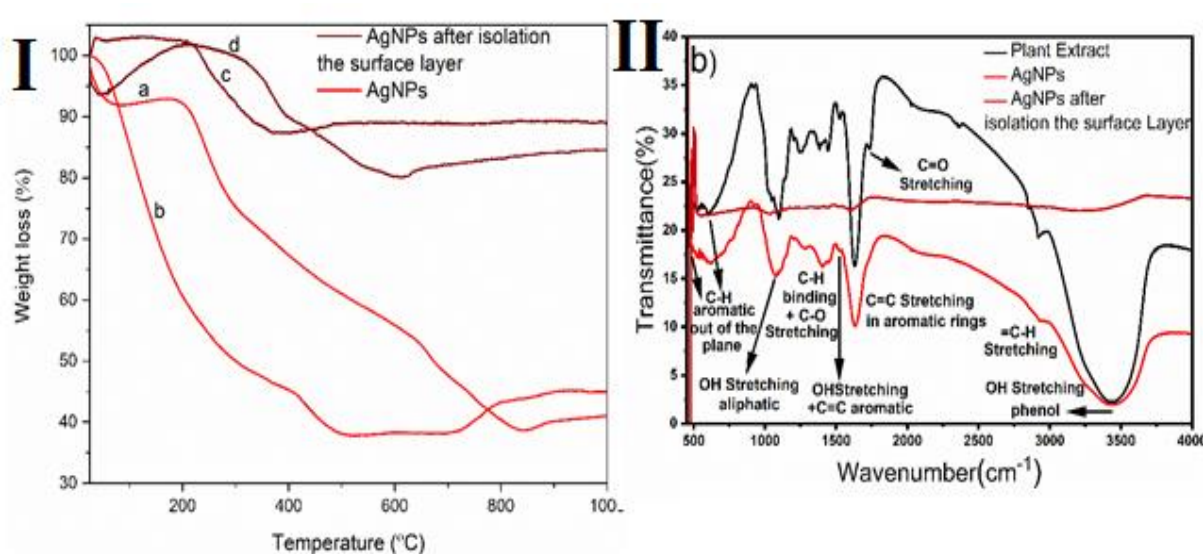


Figure SS 1: I) TGA curves of green-synthesized AgNPs and sediment (AgNPs) after isolation of the organic layer at a heating rate of 1 °C min⁻¹ under N₂ atmosphere; II) ATR-FTIR spectra of St John's Wort Aqueous Extract, St John's Wort-AgNPs and St John's Wort-AgNPs after isolating the surface layer using a mixture of organic solvents in several stages .

When we look at Figure SS2 and compare the HPLC diagram of St. John's Wort extract and the filtrate that isolated from the surfaces of silver nanoparticles, We can note that there are 8 peaks in the filtrate diagram, which are completely identical to the one in the sample diagram, and this proves the presence of 8 compounds from the plant extract on the surfaces of silver nanoparticles. Through the location of these peaks, which we identified earlier in the extract itself (table SS2), as well as by performing HPLCESI-Q-TOF MS/MS analysis (Figure SS3) for the filtrate, we were able to prove the presence of only these eight Phytochemicals from the plant extract on the surfaces of silver nanoparticles. The eight identified compounds present on the surfaces of AgNPs belong to different classes and they are Neochlorogenic acid (phenolic acids or phenyl propane), Hyperoside, Isoquercitrin (flavonoid glycosides or Flavonol glycosides), I3,II8 Biapigenin (Biflavonoids), Furohyperforin, Hyperforin, Furoadhyperforin and Adhyperforin (Phloroglucinols). These eight compounds are bioactive compounds of the St. John's Wort plant, which have unique properties, especially in the medical field. They have been used frequently in multiple treatments for different diseases.

Chapter 3: Identification of Major Constituents of *Hypericum perforatum L*

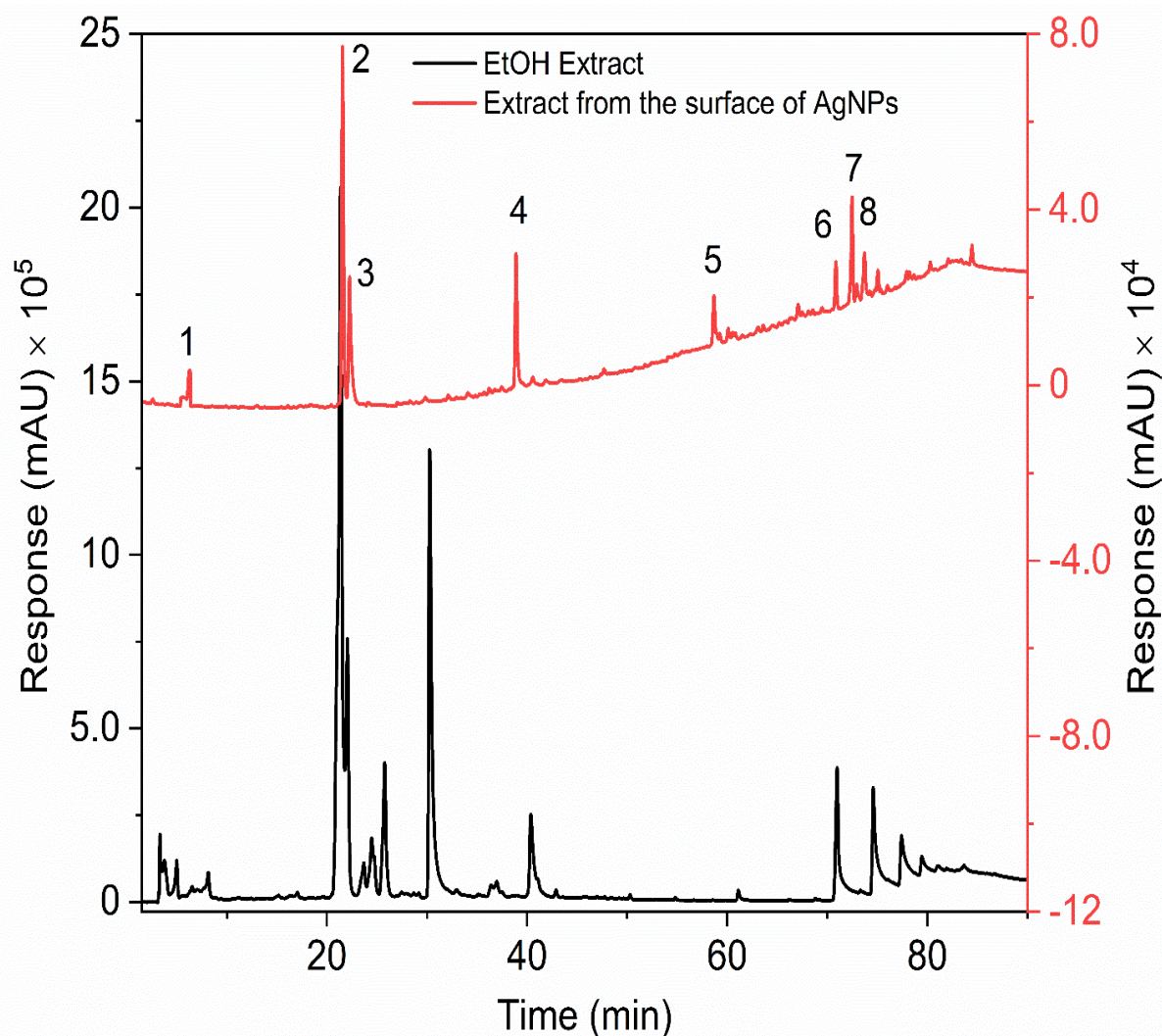


Figure SS 2: HPLC Chromatograms of *Hypericum Perforatum L* ethanolic extract and the supernatant which taken from the surfaces of silver nanoparticles using the previous separation protocol, after drying and then dissolving in only ethanol. Phytochemicals were identified in the figure using the comparison with the previous diagrams for the plant extracts and what is prior identified and mentioned in Table and also using HPLC–ESI-MS and MS/MS analysis for this layer. 1=Neochlorogenic acid; 2=Hyperoside; 3=Isoquercitrin; 4=l3,II8-biapigenin; 5=Furohyperforin; 6= Hyperforin; 7=Furoadhyperforin; 8=Adhyperforin.

Chapter 3: Identification of Major Constituents of *Hypericum perforatum L*

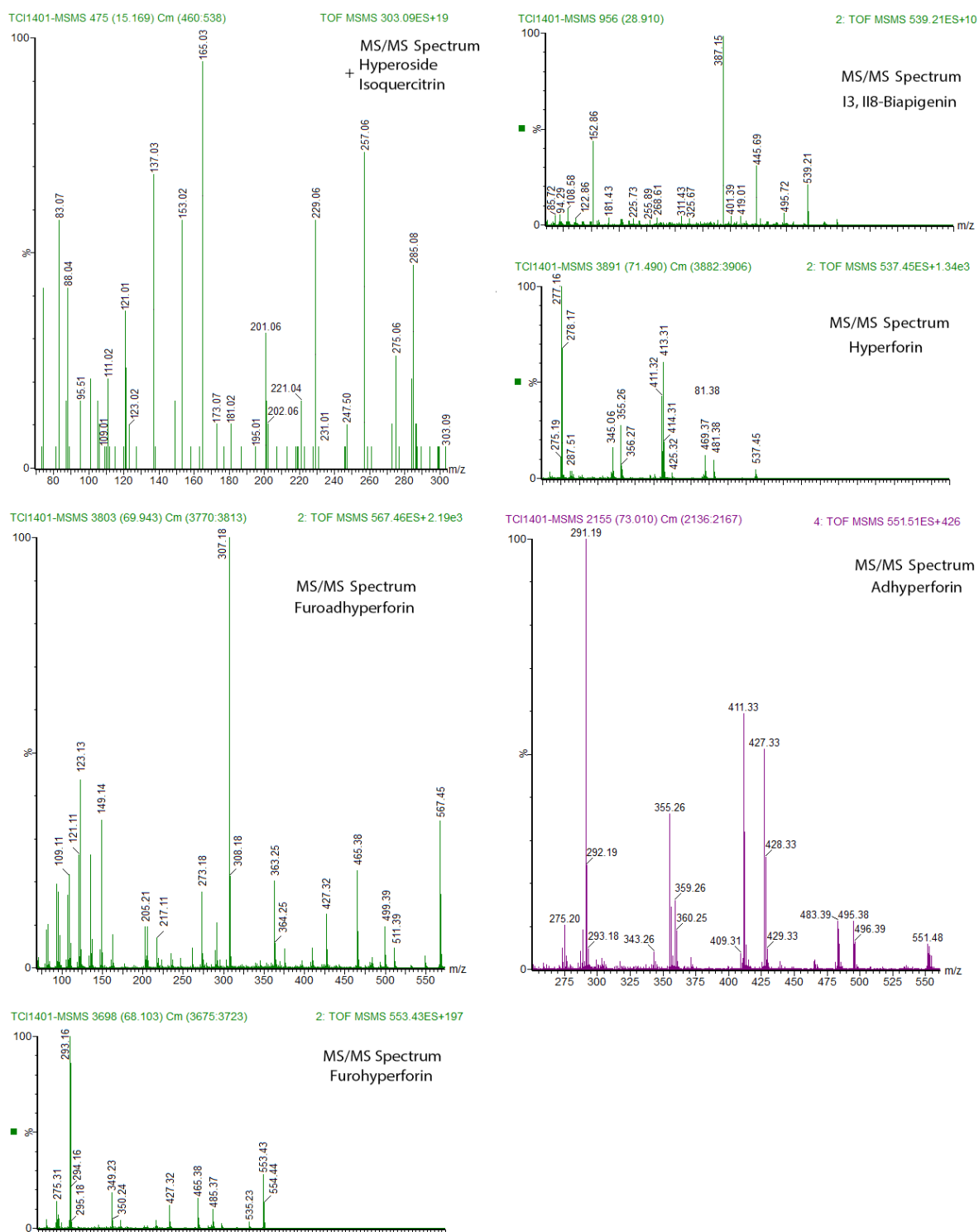


Figure SS 3: HPLC-MS-MS spectra in positive ion electrospray analyses of the identified compounds on the surface of Silver nanoparticles

Chapter 3: Identification of Major Constituents of *Hypericum perforatum L*

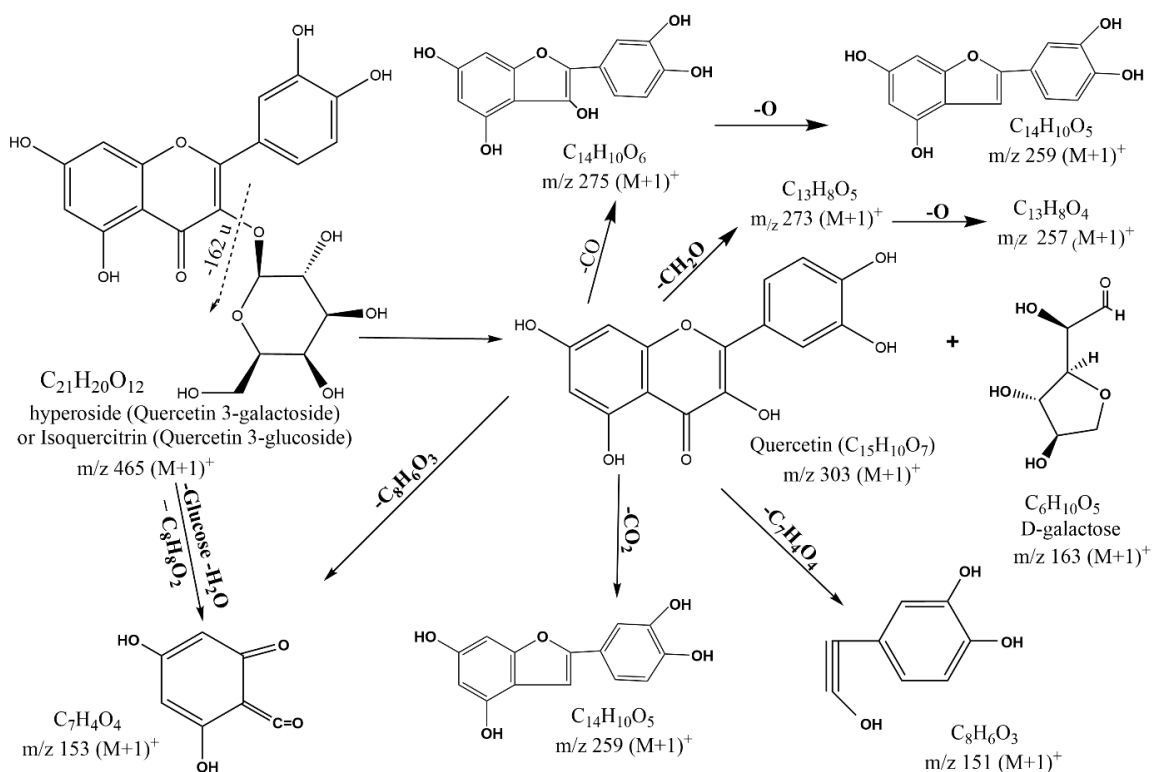


Figure SS 4: Suggested fragmentation pathways of Hyperoside and Isoquercitrin

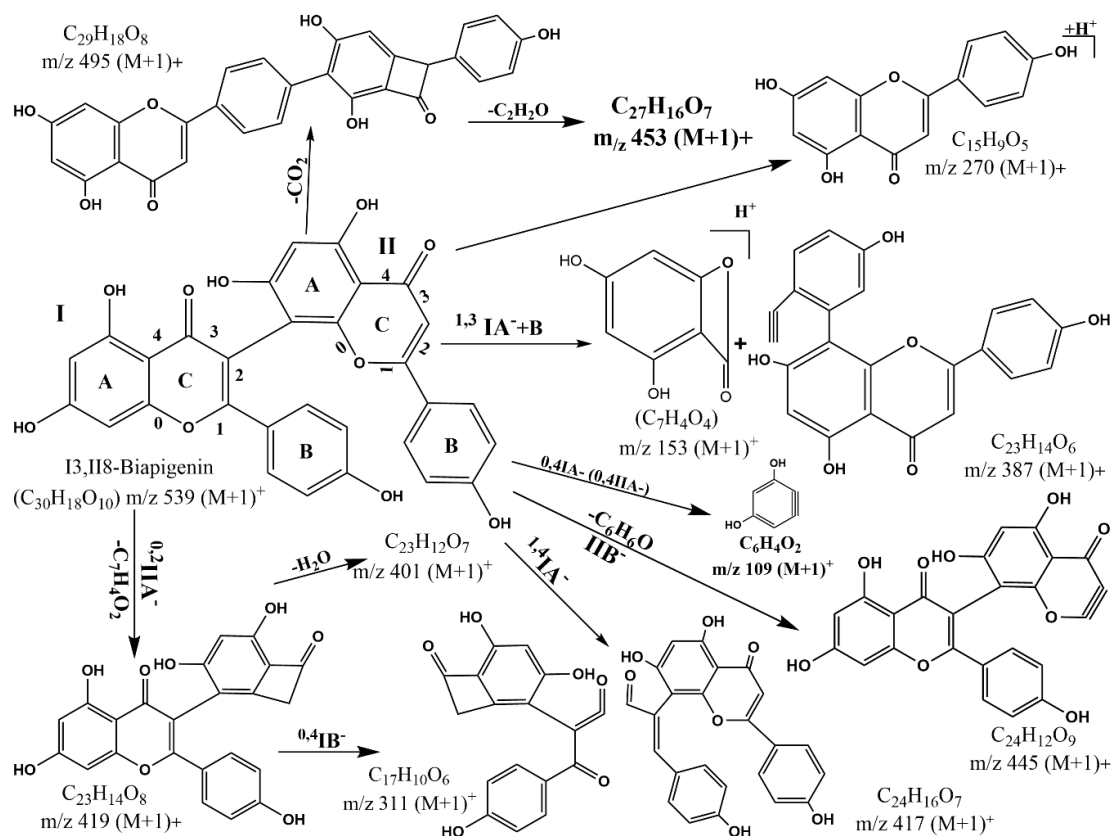


Figure SS 5: Suggested fragmentation pathways of Biapigenin

Chapter 3: Identification of Major Constituents of *Hypericum perforatum L*

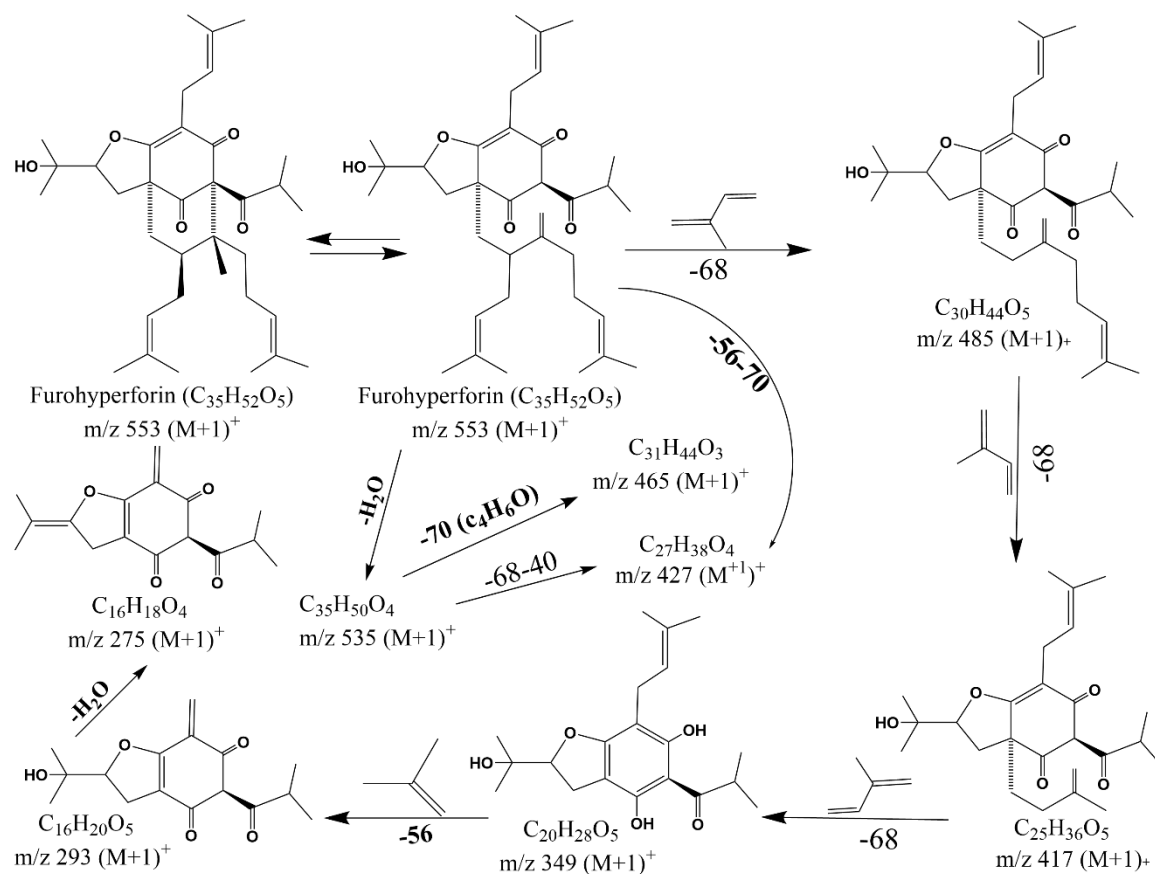
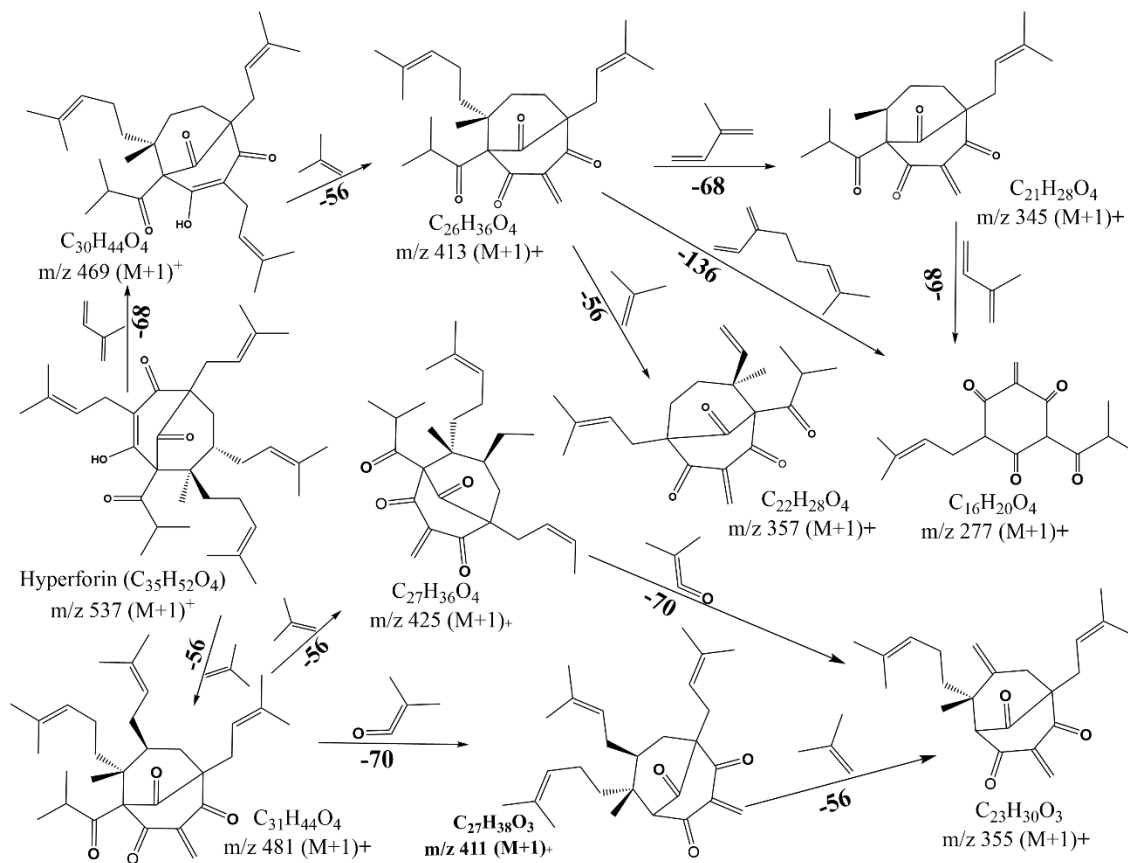


Figure SS 6: Suggested fragmentation pathways of Furohyperforin



Chapter 3: Identification of Major Constituents of *Hypericum perforatum* L

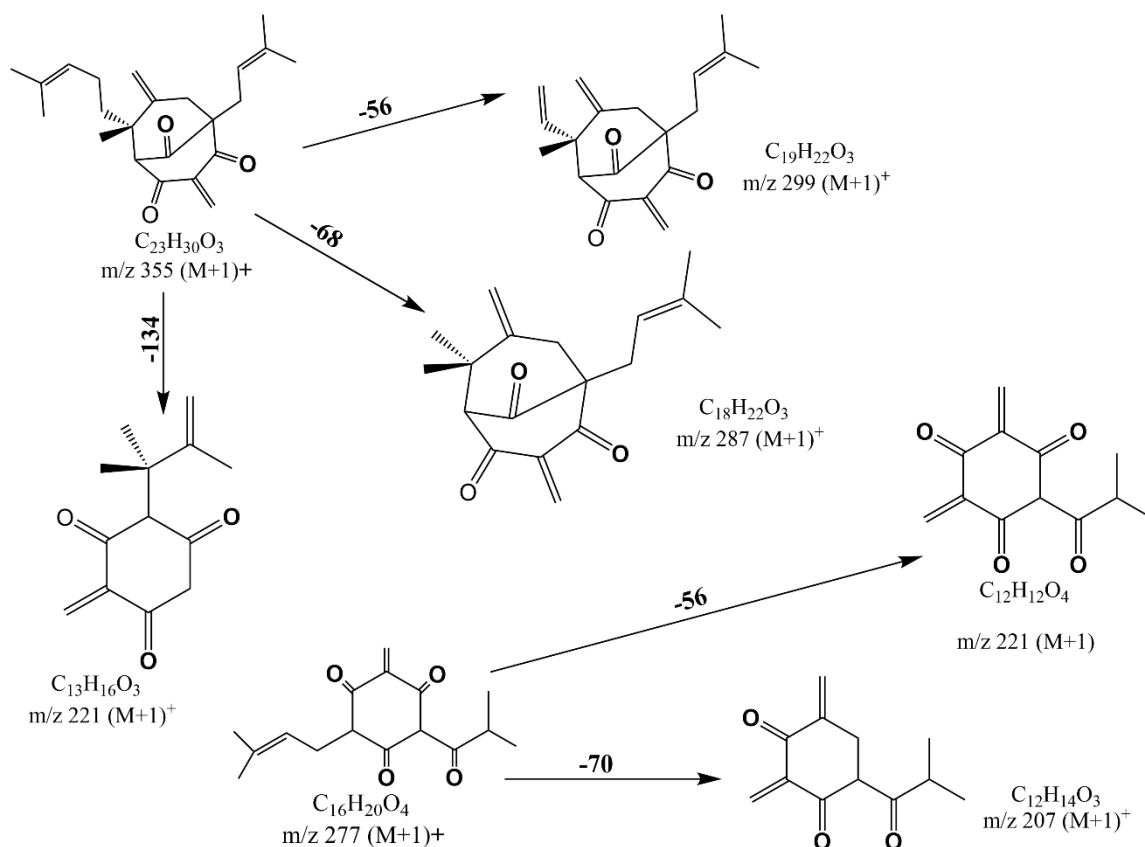
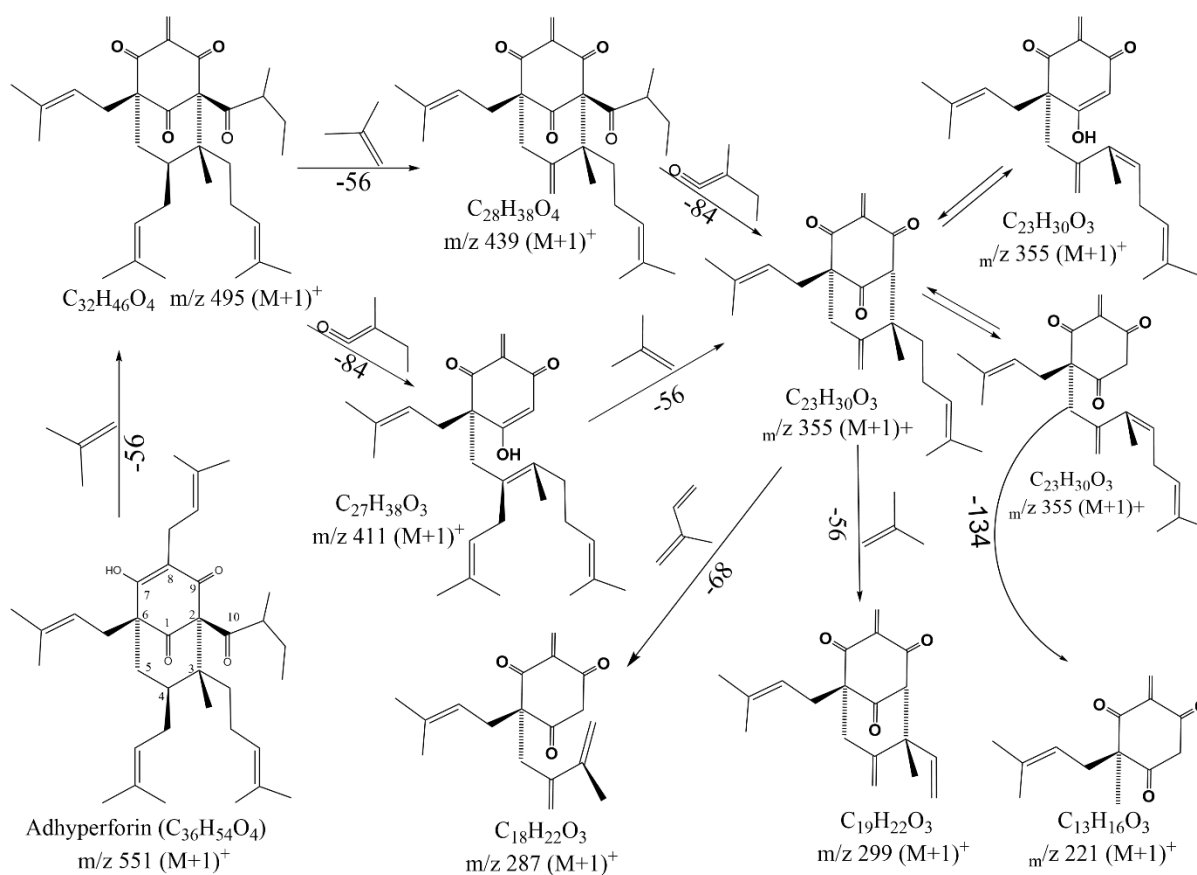


Figure SS 7: Proposed fragmentation pathway for protonated Hyperforin



Chapter 3: Identification of Major Constituents of *Hypericum perforatum L*

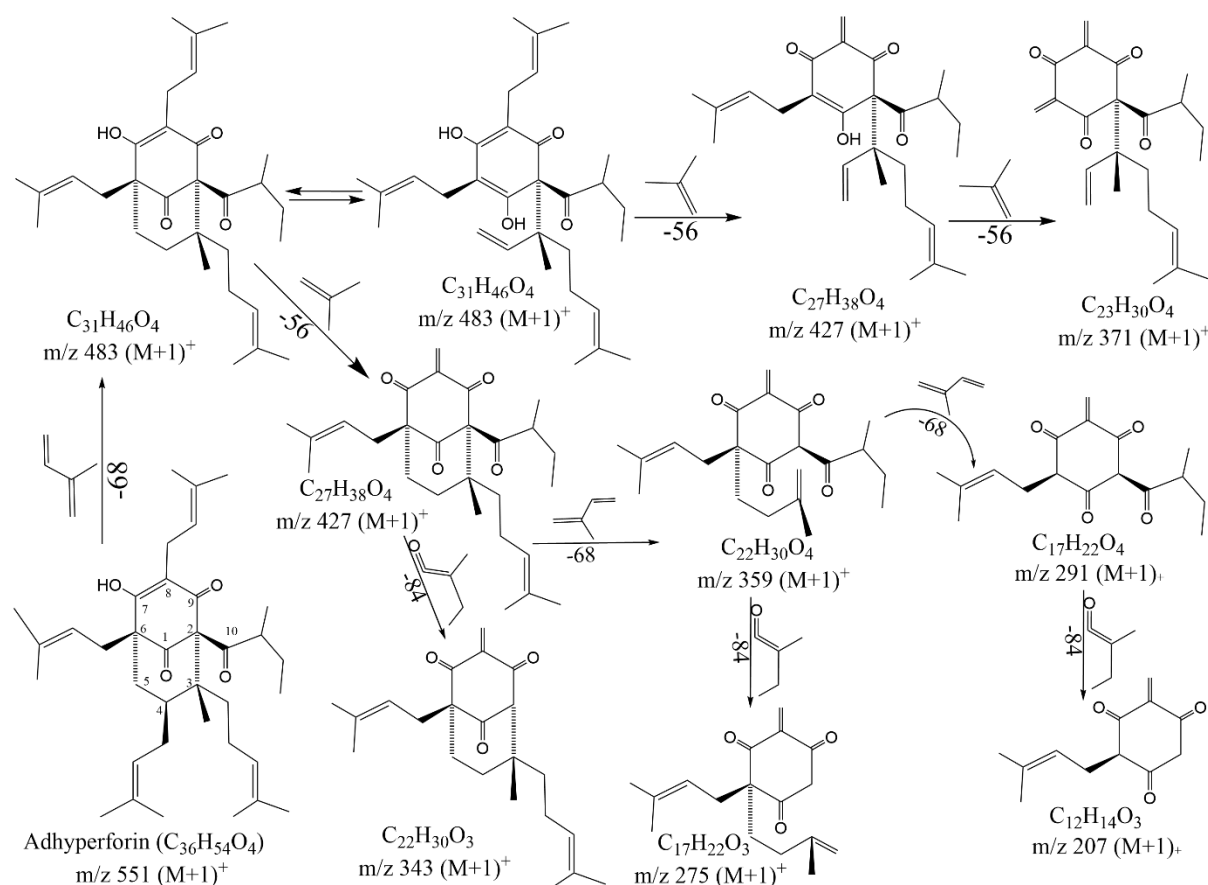


Figure S5 8: Proposed fragmentation pathway for protonated Adhyperforin (MH^+ , m/z 551).

3.10.2 The importance of the eight Phytochemicals of St. John's wort plant, which present on the surfaces of silver nanoparticles as a capping agent

Identifying the organic ingredients which present on the surfaces of silver nanoparticles as a stabilizing and capping agent through the previous protocols noted that various classes are found on the surfaces of these nanoparticles such as phenolic acids or phenyl propane; Neochlorogenic acid, flavonoid glycosides or Flavonol glycosides; Hyperoside and Isoquercitrin, Biflavonoids; I 3,II 8 Biapigenin, Phloroglucinols; Furohyperforin, Hyperforin, Furoadhyperforin and Adhyperforin, where are believed to be the active components of St. John's wort extract ¹. Hyperforin is the major lipophilic constituents of St John's wort leaves and flowers, but it is oxidatively degradable, which causes the formation of many derivatives, including Adhyperforin, Furohyperforin and others, which have almost the same specifications and biological effects in various medical fields. Hyperforin and its derivatives are getting a lot of attention in the medical field nowadays although their pharmacological activities are little known. Hyperforin was suggested to be the most important compound in the St John's wort extract responsible for the antidepressant effect ², in addition to antimicrobial, anti-inflammatory, antiangiogenic and antitumor effects. Hyperforin discourage the synaptic reuptake of monoamines so it promotes monoaminergic neurotransmission³. Hyperforin rising the free cytosolic concentration of Na^+ , which results in inhibition of uptake of neuromodulators such as glutamate, serotonin, dopamine and noradrenaline ⁴. Hyperforin also inhibit some conducting channels like N-metil-D-aspartate (NMDA) receptors and voltage-gated Ca^{2+} channels ⁵. Hyperforin activates the Transient receptor potential cation channel

Chapter 3: Identification of Major Constituents of *Hypericum perforatum L*

(TRPC6) especially in neurons, therefore it enhances the survival of these cells ⁶ and modify the dendritic spines, morphology, density and the major site of synaptic plasticity hippocampal pyramidal neurons ⁷. Hyperforin has a strong antioxidant effect and is able to scavenge free radicals, so it was used to produce UV-protective creams ⁸. Hyperforin encourage the evolution of oligodendrocyte and mitochondrial role, block mitochondrial toxin-induced cytotoxicity in distinguishing oligodendrocyte-like cells, and raise the number of ready functioning oligodendrocyte in the brain suffering people with depression ⁹. Hyperforin block prevent the generation of Prostaglandin E2 and 5-Lipoxygenase (ALOX5), which are the mediator of inflammation in illnesses ¹⁰. Hyperforin motivates the apoptosis of various cancer cells like malignant melanoma, squamous cell carcinoma, lymphoma cells and mammary carcinoma. In in vivo, Hyperforin prevents the expansion of autologous MT-450 breast carcinoma in immunocompetent Wistar rats to a range identical to that of paclitaxel without any marking of heavy toxicity ¹¹⁻¹². Hyperforin deactivate the spontaneous production of tubules by human bone marrow endothelial cells, block the release of matrix metalloprotease 9, MMP-9, a protease probably implicated in the first procedures of neo-angiogenesis and encourages apoptosis of B-CLL cells ¹³⁻¹⁴. The effect of Hyperforin on cancer cells can be attributed to the following activities: 1- inhibition of the genotoxic influence of carcinogens, this related to the Hyperforin ability to slow down inflammatory mediators, regulating pH and ROS production. 2-Control of tumor growth and spread through preventing of cytokine and chemokine production, weakening of neoangiogenesis and metalloproteinases by avoiding acidification of the environment outside of the tumors and ROS generation inhibits cell proliferation and induces apoptosis. 3- Bioavailability and wide range of procedures. Hyperforin is a natural product of biological relationships for tumor inhibition and curing because its effects are multidirectional against tumor growth and spread. It must be tested in conjunction with existing anticancer nanoparticles to achieve additive effects. 4- Reduce the effectiveness of a number of chemical treatment agents by enhancing drug metabolism and releasing ¹⁵. Hyperforin also exhibited an antimalarial effect and its effectiveness against *Plasmodium falciparum* was established with an IC50 at micro molar ¹⁶. Hyperforin showed a high influence against methicillin-resistant strains of *Staphylococcus aureus* with a minimum inhibitory concentration (MIC) amount of 1.0 µg/ml. The antibacterial activity against gram-positive bacteria of Hyperforin was much greater than that against gram-negative bacteria. ¹⁷. Neochlorogenic acid exhibited antioxidant and antibacterial effects. Its antibacterial effect is attributed to the tearing of the bacterial membrane, which alters the intracellular potential and causes the death of bacteria. Neochlorogenic acid showed an effect against four of the tested bacteria such as *faecalis*, *E. coli*, *B. cereus* and *S. aureus* ¹⁸⁻¹⁹. It also able to scavenge radicals in epithelial and enteric neurons, so it helps prevent oxidative stress-induced disorders such as inflammatory bowel disorders or neurodegenerative diseases ²⁰. Neochlorogenic acid had a clear effect on colon cancer cells (Caco-2 cell line), as it caused a clear decrease in cell proliferation, where it has been suggested that this compound may contribute significantly to inhibiting the formation of cancers by scavenging reactive oxygen, promoting DNA repair and detoxifying carcinogens²¹. It has been proven that Neochlorogenic acid can inhibit the growth of breast cancer cells (MD-MGA-435), AGS cells and prevent tumors in the liver and bowel without any effect on normal breast cells (MCF-10A) ²²⁻²⁴. Hyperoside have also antioxidant, antimicrobial, anti-inflammatory and anti-cancer effects. Hyperoside had a clear effect on

Chapter 3: Identification of Major Constituents of *Hypericum perforatum L*

human colorectal cancer cells by promoting reactive oxygen species generation causing the derangement of cellular antioxidant defense systems and cytochrome c will move from mitochondria to cytosol leading to apoptotic cell death²⁵. Hyperoside inhibited phosphoinositide 3-kinase (PI3K)/protein kinase B (Akt)/mammalian target of rapamycin (mTOR)/p38 MAPK axis, at the same time enhanced the 5'AMP-activated protein kinase (AMPK) signaling, prevent proliferation, and lead to apoptosis and autophagy, therefore, Hyperoside is very important for the prevention of skin cancer²⁶. Hyperoside regulates FoxO1 via CCAT1 in T790M-positive NSCLC leading to block proliferation and produce apoptosis, so Hyperoside is a promising substance in the treatment of non-small cell lung cancer²⁷. In other studies, Liposomes that carry the Hyperoside to mitochondria of tumor cells at the subcellular level have been developed as a dual-function tumor-targeting. liver cancer CBRH-7919 cells in vitro and also in vivo died²⁸. Hyperoside prevented Lipopolysaccharide-caused by proliferation and peregrination of human RA FLSs in vitro, minimized LPS-stimulated fabrication of TNF- α , IL-6, IL-1 and MMP-9 in the cells and inhibit the promotion of the NF- κ B signaling pathway, Thus, administration of Hyperoside clearly decreased clinical outcomes and attenuated synovial hyperplasia, inflammatory cell leaking and cartilage spoilage in CIA mice²⁹. Hyperoside enhanced autophagy and inhibited the mTOR/S6K and TLR4/Myd88/NF- κ B marking transduction channels in Anticardiolipin antibody caused by human umbilical vein endothelial cells, thus curing antiphospholipid syndrome³⁰. isoquercitrin exhibited antioxidant activity by suppressing lipid peroxidation through Intervention with enzyme efficiency, piling up in the arterial wall and inhibiting hyperlipidemia³¹⁻³², chelation of redox-active metals, raise the sucking of vitamin C, save neural cells from oxidative stress caused by H₂O₂³³, arranging the oxidative compound NO and NADPH manufacture³⁴ and immediate scavenging of reactive oxygen species like singlet oxygen, peroxy, hydroxyl, peroxy nitrite, and superoxide radicals³⁵⁻³⁹. Isoquercitrin binding to glycosylation allowed for more beneficial pharmacological modulation and made it a favorable drug for the treatment of cancer⁴⁰. Isoquercitrin exhibited powerful antiproliferative activities particularly in hepatocellular, breast, glioma (U-251), ovarian adenocarcinoma (OVCAR-3), colon (SW480, DLD-1, and HCT116), colon adenocarcinoma, breast adenocarcinoma (MCF-7), pancreatic, leukemia HL-60, Liver and Bladder cancer cells⁴¹⁻⁴⁷. The mechanism by which Isoquercitrin affects various cancer cells and tumors is represented by several effects, including the following: preventing proliferation, enhancing apoptosis, Cell cycle arrest in G1 phase, promoting caspase-3, 8, and 9 and minimizing the mitochondrial membrane possibility, blocking the expression level of the δ opioid receptor, discouragement of extracellular signal-regulated kinase (ERK) phosphorylation and enhanced phosphorylation of c-Jun N-terminal kinase (JUN) and preventing the nuclear transfer of β -catenin protein^{33, 42, 48-49}. In the tumor, Isoquercitrin inhibited the tumor-promoting activity of hepatocytes in rats by anti-inflammatory influences. enzymatically modified Isoquercitrin inhibited the alterations caused by BNF, inhibition of tumor necrosis factor (TNF) transcription resulting from BNF, reduction proinflammatory proteins (TNF- α) expression and cell cycle adjusting molecules (Cdc20 and Cdkn2b), inhibition the TAA-induced tumor-enhancing efficiency and thus Significantly repressed the growth of tumors⁵⁰⁻⁵³. Biapigenin exhibited anticancer effects against human cervical cancers (HeLa cells). Biapigenin was no cytotoxic against normal human keratinocyte cells (HaCa T cell)⁵⁴. Nerve cell death and the ability of mitochondria to accumulate calcium decreased

Chapter 3: Identification of Major Constituents of *Hypericum perforatum* L

remarkably when exposure to Biapigenin, thus, Biapigenin prevented neurotoxicity and treated mitochondrial dysfunction⁵⁵. Biapigenin as the most active biflavonoids exhibited antimicrobial effects against Gram-positive and Gram-negative bacteria⁵⁶. Biapigenin also at very low concentrations suppressed the growth of *Streptococcus pyogenes*, *P. aeruginosa*, *Moraxella catarrhalis*, *E. coli*, *Micrococcus luteus*, *S. aureus* and *S. viridans* strains⁵⁷⁻⁵⁸. Biapigenin showed also anti-inflammatory activity as it prevented the forming of edema by up to 70% and this was roughly within the range of indomethacin which is the standard anti-inflammatory drug⁵⁹. The previous talk about the various medical activities shown by the eight compounds that have been confirmed to exist on the surfaces of silver nanoparticles aims to highlight their medical importance against microbes, bacteria, germs and cancer cells. Therefore, based on what was mentioned previously, all the eight phytochemicals present on the surface of nanoparticles as capping agent and stabilizers have sufficient bioavailability and prevent the pathogenesis of various diseases. All of them have been applied to healing several cancers. Therefore, the existence of these phytochemicals on the surfaces of silver nanoparticles helps in the development of engineered nanoparticles with enhanced antimicrobial, anti-inflammatory, antibacterial and especially anti-cancer activities, that is, this layer enhances the antimicrobial and anticancer activity of silver nanoparticles. This multiplying effect of silver nanoparticles with the layer on their surface helps on the creation of new drugs to cure different, especially cancers. If these nanoparticles are conjugated with antibodies and aptamers that are characterized by high selectivity, these drugs will go immediately to the tumor and not to other healthy tissue avoiding any harmful side effects, as a result, a drug of very high quality and effectiveness is obtained and this is the focus of our future study.

3.10.3 References

1. Lisa, W.-F.; Susan, B., Chapter 29 - Antidepressants. In *Complications in Anesthesia (Second Edition)*, John L., A., Ed. W.B. Saunders: 2007; pp 105-109.
2. Caccia, S.; Gobbi, M., St. John's wort components and the brain: uptake, concentrations reached and the mechanisms underlying pharmacological effects. *Curr. Drug Metab.* **2009**, *10* (9), 1055-1065.
3. Veronika, B., Mechanism of action of St John's wort in depression : what is known? *CNS Drugs* **2003**, *17* (8), 539-562.
4. Tiziana, M.; Marco, G., The antidepressant mechanism of *Hypericum perforatum*. *Life Sci.* **2004**, *75* (9), 1021-1027.
5. Vikas, K.; Alexander, M.; Cornelia, K.; Thomas, A.; Ulrich, B.; Cornelis J. van, d. S.; Jochen, K., NMDA receptor-antagonistic properties of hyperforin, a constituent of St. John's Wort. *J. Pharmacol. Sci.* **2006**, *102* (1), 47-54.
6. Aurora, V.; Raffaele, C.; Massimo, V.; Federica, P., Effects of St John's wort and its active constituents, hypericin and hyperforin, on isolated rat urinary bladder. *J. Pharm. Pharmacol.* **2012**, *64* (12), 1770-1776.
7. Kristina, L.; Wei, L.; Michelle D., A.; Stephanie, R.; Gaston, C.; Anita M., S.; Christian, H.; Takafumi, I.; Lucas, P.-M., Hyperforin modulates dendritic spine morphology in hippocampal pyramidal neurons by activating Ca(2+) -permeable TRPC6 channels. *Hippocampus* **2013**, *23* (1), 40-52.

Chapter 3: Identification of Major Constituents of *Hypericum perforatum* L

8. Martina C., M.; Sabine, S.; Stefan F., H.; Federica, C.; Marcel L., M.; Ute, W.; Anke, K.; Juergen, L.; Christoph M., S., In vivo photoprotective and anti-inflammatory effect of hyperforin is associated with high antioxidant activity in vitro and ex vivo. *Eur. J. Pharm. Biopharm.* **2012**, *81* (2), 346-350.
9. Yanlin, W.; Yanbo, Z.; Jue, H.; Handi, Z.; Lan, X.; Adil, N.; Zhijun, Z.; Dai, Z.; Qingrong, T.; Jiming, K.; Xin-Min, L., Hyperforin promotes mitochondrial function and development of oligodendrocytes. *J. Neurochem.* **2011**, *119* (3), 555-568.
10. Jean Y., P.; Michael H., P.; Steven B., A., Prostaglandin E2 synthesis and secretion: the role of PGE2 synthases. *Clin. Immunol.* **2006**, *119* (3), 229-240.
11. Vattikuti, U. M. R.; Ciddi, V., An overview on *Hypericum perforatum* Linn. *Nat. prod. radiance* **2005**, *4* (5), 368-381.
12. Monica, V.; Ana S., M.; Antonello, S.; Caterina, F.; Eliana B., S., Novel Neuroprotective Formulations Based on St. John's Wort Extract. *J. Food Res.* **2014**, *3* (4), 3-17.
13. C., Q.; C., B.; A. M., F.; C., S.; A., E.; Y., N.-S.; J. D., F.; J-P., K., Pro-apoptotic properties of hyperforin in leukemic cells from patients with B-cell chronic lymphocytic leukemia. *Leukemia* **2006**, *20* (3), 491-497.
14. C., Q.; C., B.; P., M.; J-D., F.; J-P., K., Hyperforin inhibits MMP-9 secretion by B-CLL cells and microtubule formation by endothelial cells. *Leukemia* **2006**, *20* (4), 583-589.
15. Marta, M.; Pellegrino, M.; Michela, N., Anti-Tumor Activity of *Hypericum perforatum* L. and Hyperforin through Modulation of Inflammatory Signaling, ROS Generation and Proton Dynamics. *Antioxidants* **2021**, *10* (1).
16. Luisella, V.; Giovanni, A.; Ezio, B.; Reto, B., In vitro antimalarial activity of hyperforin, a prenylated acylphloroglucinol. A structure-activity study. *Bioorg. Med. Chem. Lett.* **2007**, *17* (6), 1544-1548.
17. Jinous, A., Phytochemistry, pharmacology and medicinal properties of *Hypericum perforatum* L. *Afr. J. Pharmacy Pharmacol.* **2012**, *6* (19), 1387-1394.
18. Ricardo, N.; Pawel, P.; Malgorzata, T.-C.; Agnieszka, S.; Marek, S.; Isabel S., C., Antibacterial, antioxidant and anti-proliferative properties and zinc content of five south Portugal herbs. *Pharm. Biol.* **2017**, *55* (1), 114-123.
19. Yiannis C., F.; Panagiotis L., K.; Vassiliki, E.; Haley, H.; Alexandre M. J. J., B.; Jacques, V.; Kim, L.; Michael R., H.; George P., T., Antimicrobial and efflux pump inhibitory activity of caffeoylquinic acids from *Artemisia absinthium* against gram-positive pathogenic bacteria. *PLoS One* **2011**, *6* (4), e18127.
20. Maria Felicia, F.; Filomena, C.; Alessia, C.; Alessia, C.; Maria Lisa, C.; Maria, G.; David Q.-H., W.; Gabriele, D. A.; Marilena, M.; Carlo, F.; Giacomina, B.; Piero, P., Novel insights in health-promoting properties of sweet cherries. *J. Funct. Foods* **2020**, *69*.
21. Taylor, T. Effect of Chlorogenic Acid and Neochlorogenic Acid on Human Colon Cancer Cells. University of Arkansas, Fayetteville, ScholarWorks@UARK, 2012.
22. Maria, S.-S.; Phyllis E., B.; Erum A., H.; Bernadette I., D.-W.; Norman R., F., Chemical composition and potential health effects of prunes: a functional food? *Crit. Rev. Food Sci. Nutr.* **2001**, *41* (4), 251-286.

Chapter 3: Identification of Major Constituents of *Hypericum perforatum* L

23. Giuliana, N.; Weston, P.; David, B.; Luis, C.-Z., Identifying peach and plum polyphenols with chemopreventive potential against estrogen-independent breast cancer cells. *J. Agric. Food. Chem.* **2009**, *57* (12), 5219-5226.
24. Wei, F.; Yuntao, M.; Juan, W.; Xiaojun, Y.; Yuanhui, G.; Yiping, L., In vitro and in vivo antitumor activity of neochlorogenic acid in human gastric carcinoma cells are complemented with ROS generation, loss of mitochondrial membrane potential and apoptosis induction. *JBUON* **2019**, *24* (1), 221-226.
25. Yali, Z.; Huanhuan, D.; Jingfang, Z.; Liyu, Z., Inhibitory effect of hyperoside isolated from *Zanthoxylum bungeanum* leaves on SW620 human colorectal cancer cells via induction of the p53 signaling pathway and apoptosis. *Mol. Med. Rep.* **2017**, *16* (2), 1125-1132.
26. Yinghui, K.; Weiguo, S.; Pengfei, W., Hyperoside exerts potent anticancer activity in skin cancer. *Front. Biosci.* **2020**, *25* (3), 463-479.
27. Zhiyuan, H.; Pengjun, Z.; Huifang, X., Hyperoside exhibits anticancer activity in nonsmall cell lung cancer cells with T790M mutations by upregulating FoxO1 via CCAT1. *Oncol. Rep.* **2020**, *43* (2), 617-624.
28. Yufei, F.; Guozhao, Q.; Shuyuan, C.; Zhongxu, J.; Yanyan, Z.; Yanhong, W., Antitumor Effect of Hyperoside Loaded in Charge Reversed and Mitochondria-Targeted Liposomes. *Int. J. Nanomed.* **2021**, *16*, 3073-3089.
29. Xiang-nan, J.; En-zhi, Y.; Han-ming, W.; Hai-juan, S.; Zhou, L.; Wei, G.; Ying, J., Hyperoside exerts anti-inflammatory and anti-arthritic effects in LPS-stimulated human fibroblast-like synoviocytes in vitro and in mice with collagen-induced arthritis. *Acta Pharmacol. Sin.* **2016**, *37* (5), 674-86.
30. Aiwu, W.; Huidongzi, X.; Guangli, X.; Xile, Y.; Jingjing, G.; Zhuqing, J.; Shaoqi, S.; Yanli, S., Hyperoside Protects Human Umbilical Vein Endothelial Cells Against Anticardiolipin Antibody-Induced Injury by Activating Autophagy. *Front. Pharmacol.* **2020**, *11*.
31. Chiemi, K.; Edson L., d. S.; Mayumi, O.-K.; Jae-Hak, M.; Junji, T., Attenuation of lipid peroxidation and hyperlipidemia by quercetin glucoside in the aorta of high cholesterol-fed rabbit. *Free Radical Res.* **2005**, *39* (2), 185-194.
32. Claire, D.; Michèle, L., Flavonoids and their oxidation products protect efficiently albumin-bound linoleic acid in a model of plasma oxidation. *Biochim. Biophys. Acta, Gen. Subj.* **2007**, *1770* (6), 958-65.
33. Sang Hoon, J.; Beum Jin, K.; Eun Ha, L.; Neville N., O., Isoquercitrin is the most effective antioxidant in the plant *Thuja orientalis* and able to counteract oxidative-induced damage to a transformed cell line (RGC-5 cells). *Neurochem. Int.* **2010**, *57* (7), 713-721.
34. Byung-Hak, K.; Jung Sook, C.; Eun Hee, Y.; Jin-Ku, L.; Cheolhee, W.; Sang-Kyu, Y.; Myoung-Hwan, K., Relative antioxidant activities of quercetin and its structurally related substances and their effects on NF-kappaB/CRE/AP-1 signaling in murine macrophages. *Mol. Cells* **2013**, *35* (5), 410-420.
35. Anju, D.; Arun, N.; Sayeed, A., A quest for staunch effects of flavonoids: Utopian protection against hepatic ailments. *Arabian J. Chem.* **2016**, *9* (2), 1813-1823.
36. Jeremy, A., Evaluating the Bioavailability of Isoquercetin. *Nat. med. j.* **2010**, *2* (1), 1-6.

Chapter 3: Identification of Major Constituents of *Hypericum perforatum L*

37. Maria Elisa Melo Branco, d. A.; Yollanda E. Moreira, F.; Thiago Grando, A.; Mariana Alves, S.; Marco Aurélio, C.; Denise Gonçalves, P.; Alexandra C.H. Frankland, S.; Ana Lucia T.G., R.; João Ernesto, d. C.; Patrícia de Oliveira, C., Enzymatic de-glycosylation of rutin improves its antioxidant and antiproliferative activities. *Food Chem.* **2013**, *141* (1), 266-273.
38. Taigang, L.; Wenyan, Y.; Qingshan, L., Comparison of the phenolic content and antioxidant activities of Apocynum venetum L. (Luo-Bu-Ma) and two of its alternative species. *Int. J. Mol. Sci.* **2010**, *11* (11), 4452-4464.
39. Khushwant S., B.; H.P. Vasantha, R., Antioxidant and cytoprotective properties of partridgeberry polyphenols. *Food Chem.* **2015**, *168*, 595-605.
40. Si-Hwan, P.; Hyun Jung, K.; Soon-Ho, Y.; Ah-Ra, K.; Nisha, T.; Haihong, S.; Kyung Keun, K.; Boo Ahn, S.; Da-Woon, J.; Darren R., W., Delineation of the role of glycosylation in the cytotoxic properties of quercetin using novel assays in living vertebrates. *J. Nat. Prod.* **2014**, *77* (11), 2389-2396.
41. Hyun Ju, Y.; Hyung Jin, A.; Geun Eog, J., Transformation of rutin to antiproliferative quercetin-3-glucoside by *Aspergillus niger*. *J. Agric. Food. Chem.* **2010**, *58* (20), 10886–10892.
42. Quan, C.; Ping, L.; Yong, X.; Yang, L.; Bo, T., Isoquercitrin inhibits the progression of pancreatic cancer in vivo and in vitro by regulating opioid receptors and the mitogen-activated protein kinase signalling pathway. *Oncol. Rep.* **2015**, *33* (2), 840-848.
43. Feng, C.; Xiaochi, C.; Deyong, Y.; Xiangyu, C.; Jianbo, W.; Xiancheng, L.; Zhiwei, Z.; Qifei, W.; Wei, Z.; Lina, W.; Xuejian, W.; Xishuang, S., Isoquercitrin inhibits bladder cancer progression in vivo and in vitro by regulating the PI3K/Akt and PKC signaling pathways. *Oncol. Rep.* **2016**, *36* (1), 165-172.
44. Nathália G., A.; Cerqueira., D. M.; Fabio S., M.; Joaquim Fernando Mendes, d. S.; Vivaldo Moura, N.; Jose G., A., Isoquercitrin isolated from *Hyptis fasciculata* reduces glioblastoma cell proliferation and changes beta-catenin cellular localization. *Anticancer Drugs* **2009**, *20* (7), 543-552.
45. Murat, K.; Ruxandra, P.; Sonja, P.; Halmurat, U.; Judith, S.; Martin, Z.; Brigitte, K., Towards modernization of the formulation of the traditional uighur medicine herbal preparation abnormal savda munziq. *Evid. Based Complementary Altern. Med.* **2012**, *2012*.
46. Melanie, K.; Zeina, T.; Yufanyi, N.; Nicole, P.; Frank, W.; Helmut, D.; Gudrun, P.; Doris, M., Inhibitors of the epidermal growth factor receptor in apple juice extract. *Mol. Nutr. Food Res.* **2005**, *49* (4), 317-328.
47. Nathália G., A.; Danilo, P.; Barbara F., F.; Cerqueira., D. M.; Alice H., R.; Ana C., D.; Helena L., B.; Fábio A., M.; Jose G., A., Isoquercitrin suppresses colon cancer cell growth in vitro by targeting the Wnt/beta-catenin signaling pathway. *J. Biol. Chem.* **2014**, *289* (51), 35456-35467.
48. Martinez Natalia, P.; Kanno Danilo, T.; Pereira José, A.; Cardinalli Izilda, A.; Priolli Denise, G., Beta-catenin and E-cadherin tissue "content" as prognostic markers in left-side colorectal cancer. *Cancer Biomarkers* **2010**, *8* (3), 129-135.
49. S. P., B.; V. L., D.; S. J., D.; J. A. M., K.; A. R., C., Absorption and DNA protective effects of flavonoid glycosides from an onion meal. *Eur. J. Nutr.* **2000**, *39* (5), 213-223.
50. Kazunori, K.; Makoto, S.; Hitomi, H.; Keisuke, S.; Shim-Mo, H.; Kazuhiko, S.; Kunitoshi, M., Concomitant apoptosis and regeneration of liver cells as a mechanism of liver-tumor promotion by beta-

Chapter 3: Identification of Major Constituents of *Hypericum perforatum* L

naphthoflavone involving TNF α -signaling due to oxidative cellular stress in rats. *Toxicology* **2011**, 283 (1), 8-17.

51. Yuta, F.; Masayuki, K.; Yuji, I.; Ryuichi, Y.; Reiko, M.; Shim-mo, H.; Kazuhiko, S.; Makoto, S., Effect of enzymatically modified isoquercitrin on preneoplastic liver cell lesions induced by thioacetamide promotion in a two-stage hepatocarcinogenesis model using rats. *Toxicology* **2013**, 305, 30-40.

52. Masayuki, K.; Yuta, F.; Ryuichi, Y.; Atsunori, Y.; Shim-mo, H.; Kazuhiko, S.; Makoto, S., Involvement of multiple cell cycle aberrations in early preneoplastic liver cell lesions by tumor promotion with thioacetamide in a two-stage rat hepatocarcinogenesis model. *Exp. Toxicol. Pathol.* **2013**, 65 (7-8), 979-988.

53. Guihong, H.; Bo, T.; Kun, T.; Xiaomin, D.; Jungang, D.; Luqin, L.; Zengzhen, L.; Hua, Y.; Songqing, H., Isoquercitrin inhibits the progression of liver cancer in vivo and in vitro via the MAPK signalling pathway. *Oncol. Rep.* **2014**, 31 (5), 2377-84.

54. Jin-Kyoung, K.; Soyoung, S.; Jee-Young, L.; Sojung, L.; Eunjung, L.; Qinglong, J.; Juneyoung, L.; Eun-Rhan, W.; Dong Gun, L.; Do-Young, Y.; Yangmee, K., Biapigenin, Candidate of an Agonist of Human Peroxisome Proliferator-Activated Receptor γ with Anticancer Activity. *Bull. Korean Chem. Soc.* **2011**, 32 (8), 2717-2721.

55. Bruno, S.; Paulo J., O.; Alberto, D.; JOÃO O., M., Quercetin, kaempferol and biapigenin from *Hypericum perforatum* are neuroprotective against excitotoxic insults. *Neurotoxic. Res.* **2008**, 13 (3-4), 265-279.

56. Luisa, P.; Alessandra, B.; Ivano, M.; Francesco, M.; Rosa Anna, M.; Tiziana Di, M.; Grazietta, C., Chemical and antibacterial evaluation of *Hypericum triquetrifolium* Turra. *Phytother. Res.* **2005**, 19 (9), 787-791.

57. Rolande B. Tsafack, N.; Abdel Jélil, N.; James D. Simo, M.; Irene Chinda, K.; Romeo D. Tadjouate, N.; Serge A. Tanemossu, F.; Ludger A., W.; Augustin Silvere, N.; Jean-De-Dieu, T., Antimicrobial activities of chemical constituents from the flowers of *Hypericum lanceolatum* Lam. (Hypericaceae). *Int. J. Appl. Microbiol. Biotechnol. Res.* **2020**, 8 (6), 66-72.

58. Ipek, S.; Ozlem, O.; Esra Küpeli, A.; Berrin, O., Antimicrobial effect of the extracts from *Hypericum perforatum* against oral bacteria and biofilm formation. *Pharm. Biol.* **2016**, 54 (6), 1065-1070.

59. Gordana, Z.; Dejan, G.; Milenković., M.; Katarina, Š.; Nebojša, M.; Silvana, P., Anti-inflammatory and Gastroprotective Properties of *Hypericum richeri* Oil Extracts. *Nat. Prod. Commun.* **2010**, 5 (8), 1215-1218.

4 Chapter Four: Green synthesis of silver nanoparticles using *Hypericum perforatum* L. aqueous extract with the evaluation of its antibacterial activity against clinical and food pathogens

4.1 Vorwort

This chapter contains the article “Chapter Four: Green synthesis of silver nanoparticles using *Hypericum perforatum* L. aqueous extract with the evaluation of its antibacterial activity against clinical and food pathogens” by Abdalrahim Alahmad^{1*}, Wael A. Al-Zereini^{2*}, Tahani, Osama Al-Madanat³, Ibrahim Alghoraibi⁴, Omar Al-Qaralleh², Samer Al-Qaraleh⁵, Johanna-Gabriela Walter¹, and Thomas Scheper¹. Reproduced with permission from Pharmaceutics 2022 (14(5), 1104, DOI: 10.3390/pharmaceutics14051104). Copyright 2022 MDPI.

Da viele Mikroben gegen Antibiotika resistent geworden und daher schwer zu behandeln und für den Menschen gefährlich sind, daher hat die rasante Entwicklung der Nanotechnologie und ihre Anwendungen in der Medizin eine optimale Lösung gegen ein breites Spektrum verschiedener Mikroben, insbesondere Antibiotikaresistenzen, bereitgestellt. In dieser Studie wurde ein einstufiger Ansatz zur Herstellung von Silbernanopartikeln (AgNPs) verwendet, indem Silbernitrat mit heißem wässrigem Extrakt aus *Hypericum perforatum* (Johanniskraut) unter starkem Rühren gemischt wurde, um eine Agglomeration zu verhindern. Die erhaltenen Silbernanopartikel wurden mit verschiedenen Techniken wie UV-VIS, XRD, EDX, Zetapotential, DLS, SEM, TEM, TGA und NTA charakterisiert. Die biosynthetisierten Silbernanopartikel waren sphärische, monodisperse, kubisch flächenzentrierte (fcc) Kristallstrukturen, mit Größenbereichen zwischen 20 bis 40 nm und mit einer Deckschicht aus organischen Verbindungen bedeckt, die ihm in Nanodimensionen eine Schutzschicht bildet und ihn vor Agglomeration und Sedimentation bewahrt. AgNPs revealed antibacterial activity against both tested Gram-positive and Gram-negative bacterial strains with MIC 6.25-12.5 µg/ml. Die spezifische Wachstumsrate von *S. aureus* war aufgrund der getesteten AgNPs bei Konzentrationen $\geq \frac{1}{2}$ MIC signifikant reduziert. AgNPs beeinflussten die Wundmigration in Fibroblastenzelllinien im Vergleich zur Kontrolle nicht. Unsere Ergebnisse unterstrichen die potenzielle Verwendung von mit Pflanzenextrakten verkappten AgNPs in der Pharma- und Lebensmittelindustrie, um das Wachstum bakterieller Krankheitserreger zu kontrollieren.

4.2 Abstract

Since many types of microbes have become resistant to antibiotics and therefore difficult to treat and pose a danger to humans, the rapid development of nanotechnology and its applications in medicine has provided the perfect solution against a wide range of different microbes, especially antibiotic-resistant ones. In this study, a one-step approach was used in preparing silver nanoparticles (AgNPs) by mixing silver nitrate with hot *Hypericum perforatum* (St. John's wort) aqueous extract under high stirring to prevent agglomeration. The formation of silver nanoparticles was monitored by continuous measurement of the surface plasma resonance spectra (UV-VIS). The effect of St. John's wort aqueous extract on the formation of silver nanoparticles was studied by X-ray diffraction (XRD), Attenuated total reflection-Fourier-transform infrared spectroscopy (ATR-FTIR), energy dispersive X-ray

Chapter 4: Antibacterial activity against clinical and food pathogens

analysis (EDX), zeta potential, dynamic light scattering (DLS), scanning electron microscopy (SEM), transmission electron microscopy (TEM), thermogravimetric analysis (TGA) and nanoparticle tracking analysis (NTA). The obtained silver nanoparticles were spherical, monodisperse, face-centered cubic (fcc) crystal structures, and with size ranges between 20 to 40 nm. They were covered with a capping layer of organic compounds, which forms a protective layer for it in nano dimensions and prevents it from agglomeration and sedimentation. AgNPs revealed antibacterial activity against both tested Gram-positive and Gram-negative bacterial strains with MIC 6.25-12.5 µg/ml. The specific growth rate of *S. aureus* was significantly reduced due to tested AgNPs at concentrations $\geq \frac{1}{2}$ MIC; AgNPs did not affect wound migration in fibroblast cell lines compared to control. Our results highlighted the potential use of AgNPs capped with plant extracts in pharmaceutical and food industries to control bacterial pathogens' growth.

Keywords Silver nanoparticles, green synthesis, *Hypericum perforatum L.*, antibacterial.

4.3 Introduction

Recently, there is an increase in the number of emerged antibiotic-resistant bacterial strains, the number of multidrug-resistant tumor cells, and the number of oxidative stress-associated disorders; an increase that elevates the burden of treating such ailments. Moreover, the usage of some synthetic drugs is associated with adverse effects on human health¹. The introduction of bio- and nanotechnology-based techniques in medical research led to nanomaterials' application in treating, diagnosis, control, and modulation of biological systems². Intriguingly, nanoparticles were synthesized through chemical and physical methods; they are expensive, environmentally un-favorable, and toxic that hindering the compatibility of resulting NPs for biological applications³. Therefore, using Biosystems as manufacturers of nanomaterials is considered a safer and more eco-friendly method⁴. Plant extracts provide agents that act as reductants and stabilizers during the synthesis of nanoparticles; phenols, alkaloids, tannins, flavonoids, and saponins among others are examples of such reagents⁵.

Silver nanoparticles (AgNPs) synthesized from plants embrace intrinsic therapeutic characteristics with a multi-target effect; they exhibit a broad-spectrum antibacterial activity and the ability to overcome the antibiotic resistance issue in microorganisms^{6,7}. They were applied in pathogen detection and diagnosis, drug delivery, coating of materials and devices including textile, food, and medical applications^{8,9}. In comparison to gold, platinum, iron, and zinc nanoelements, AgNPs exhibit very high bioactivity, low levels of cytotoxicity when used individually or when been combined with various antibiotics to overcome the resistance of bacteria to various drugs¹⁰; they alter microbial cell membrane and wall structures^{11,12}, induce reactive oxygen species (ROS) production, DNA damage, and lead to cellular apoptosis and necrosis¹³⁻¹⁵.

In the current study, the aqueous extract of *Hypericum perforatum L.* (St. John's wort) was used to reduce AgNO₃ into AgNPs. The coating of the nanoparticles and their stabilization by the plant phytochemical constituents was confirmed via chemical characterization and their antibacterial efficiency against clinical and food pathogenic isolates was evaluated; their effect on the growth kinetics and killing time of tested bacterial was elaborated herein.

Chapter 4: Antibacterial activity against clinical and food pathogens

4.4 Materials and Methods

4.4.1 Chemicals and Instrumentation

Aerial parts of *Hypericum perforatum L* (St. John's wort) were collected in July–August from the Ghab Plain in Syria, and harvested during the flowering season. Silver nitrate was purchased from Sigma Aldrich. Whatman filter paper 90 mm was purchased from GE Healthcare Life Sciences (Freiburg Germany). Deionized water (18.2 MΩ cm, 25 °C) was obtained from a Millipore Mill-Q system, Sartorius (Goettingen, Germany).

Absorption spectra of AgNPs were recorded using a NanoDrop Spectrophotometer (ND1000 from PeQLab). Dynamic light scattering and Zeta potential using Bettersize S3 plus from Anton Paar. Fourier transformed infrared using Bruker FTIR Vertex 80v spectrometer. X-ray diffraction (XRD) using Bruker D8 Advance diffractometer. Thermal gravimetric analysis (TGA) using TGA/DSC 3+ from Mettler-Toledo, from 25 to 1000 °C at a rate of 0.5 °C per minute with N₂ gas flow. Scanning electron microscopy (SEM) and energy-dispersive x-ray spectroscopy (EDXS) using JEOL JSM-6700F. Transmission electron microscopy (TEM) using JEOL JEM-2100F-UHR, acceleration voltage of 200 kV. The surface morphology was determined by the Atomic Force Microscopy measurements (AFM, Nanosurf easyScan2, Switzerland). The AFM measurements were performed in contact mode.

NTA measurements were performed with a NanoSight LM10 (NanoSight, Amesbury, United Kingdom), equipped with a sample chamber with a 635 nm laser and a Viton fluoroelastomer O-ring. The samples were injected into the sample chamber with sterile syringes (Carl Roth GmbH, Karlsruhe, Germany) until the liquid reached the tip of the nozzle. All measurements were performed at room temperature. The software used for capturing and analyzing the data was the NTA 2.0 Build 0033. The samples were measured for 60 s with manual shutter and gain adjustments. The “single shutter and gain mode” was used to capture the monodisperse AgNPs.

4.4.2 Synthesis of *Hypericum perforatum L.* aqueous extract mediated silver nanoparticles (AgNPs) and their chemical characterization

Synthesis of AgNPs was done as mentioned in our previous publication (Alahmad et al., 2021) with some modifications. Briefly, *Hypericum perforatum* aerial parts were cleaned and ground to a fine powder. 3 g of the pulverized sample were boiled in 700 ml distilled water for 3 hours, and the supernatant was filtered using a 0.22 μm membrane filter. The resulting yellow-brown extract was freeze-dried. Preparation of AgNPs was achieved by adding 10 mL of AgNO₃ (0.5 M) dropwise to plant extract solution (0.075 g of the plant extract in 40 mL deionized water) with stirring at 750 rpm and 80°C. the change of preparation color from pale-yellow to dark brown indicated the successful formation of the AgNPs that was lifted in a dark place until cooled down. The resulting nanoparticles were isolated, washed with deionized water, and centrifugation at 15,000 rpm for one hour; the process was repeated at least 4 times. The purified AgNPs were chemically characterized using ultraviolet light spectroscopy (UV-VIS), Dynamic Light Scattering (DLS) and Zeta Potential, Fourier Transform Infrared (FTIR) Spectroscopy, x-ray diffraction (XRD), Scanning Electron Microscopy (SEM), Transmission Electron Microscopy (TEM), Energy Disperse X-ray Spectroscopy (EDX), Atomic Force Microscopy (AFM) and Nanoparticle Tracking Analysis (NTA).

Chapter 4: Antibacterial activity against clinical and food pathogens

The aerial parts of the plant were brought from Syria in the spring and then ground and extracted using 8 different solvents and the yields of biomass were calculated. The resulting extracts were analyzed by using high-performance liquid chromatography- equipped with a diode array detector (HPLC-DAD) coupled with UV-visible spectrophotometry at a full spectrum (200–800 nm). Detection was carried out at 260 nm for phloroglucinols, 590 nm for naphthodianthrones and 350 nm for other flavonols, flavones and caffeoylquinic acids. Many conditions have been changed to develop the HPLC protocol which contains isolated and not overlapping peaks. Various standards were also used and finally, combined (HPLC-DAD) and electrospray ionization–mass spectrometry (LC-ESI-MS) have been used to identify ten constituents (Hyperforin, Adhyperforin, Hypericin, Rutin, Quercetin, Quercitrin, Quercitrin-hydrate, Hyperoside, Biapigenin and Chlorogenic acid) in these extracts, and this work is described in detail in our previous article.

4.4.3 Antibacterial activity

The green synthesized AgNPs were tested for their antibacterial activity by well diffusion test, and the lowest concentration needed to inhibit bacterial growth (MIC) was determined by micro-broth dilution assay; both assays were performed as described in Al-Zereini ¹⁶ and according to Clinical and Laboratory Standards Institute guidelines, with some modifications. AgNPs were tested against the Gram-negative bacteria [*Pseudomonas aeruginosa* (ATCC 13048), β -lactamase *Klebsiella pneumoniae* (clinical isolate), extended-spectrum β -lactamase *E. coli* (ESBL, clinical isolate), and *Escherichia coli* (ATCC 25922)] and the Gram-positive bacteria [*Staphylococcus aureus* (ATCC 43300), *Bacillus cereus* (ATCC 11778) and *B. subtilis* (ATCC 6633)]. The clinical isolates were supplied by Dr. Haitham Qaralleh/Department of Medical Laboratory Sciences-Mutah University and were identified by BIOMÉRIEUX VITEK[®] 2 system. Overnight bacterial culture was seeded in Muller Hinton agar plates (MHA) (Oxoid, UK) at cell density 10^6 cell/ml and in which 6 mm diameter wells were made using a sterile Cork borer. To each well in the bacterial agar plates, either 120 μ l aliquots (100 μ g/well), 60 μ l aliquots (50 μ g/well) from AgNPs preparation, or aqueous plant extract (2.5 mg/well) were applied. As a positive control, streptomycin (10 μ g/disc, Bio Basic Inc, Canada) was used and the results are presented as means of triplicate tests \pm SD.

However, in the micro-broth dilution assay, AgNPs and the positive control were tested starting from 100 μ g/ml and 50 μ g/ml, respectively. Samples were serially diluted in 100 μ l Muller Hinton broth (MHB), to which 100 μ l of tested bacterial strain was added to each well at a cell density of 2×10^6 cell/ml. The preparation was incubated for 24 hours at 37 °C. Aliquots from the preparations in micro-broth dilution assay, where there were no visible growths, were plated on agar plates with proper medium and incubation for 24-48 hours to determine if the nanoparticle has a bactericidal or bacteriostatic effect.

4.4.4 Effect of AgNPs on growth kinetics of *S. aureus*

Based on the AgNPs antibacterial activity results, *S. aureus* was selected to study their effect on bacterial growth kinetics. *S. aureus* was cultivated at a cell density of 10^6 cell/ml in sterile test tubes containing 10 ml of MHB (Oxoid, UK). Different concentrations of AgNPs (1, 3, 6, 12, and 24 μ g/ml) were added to bacterial culture test tubes with incubation for 24 hours on an

Chapter 4: Antibacterial activity against clinical and food pathogens

orbital shaker (Forma-Thermo electron cooperation, USA) at 37 °C and 150 rpm. A bacterial culture test tube without AgNPs was used as a negative control. During the cultivation period, 1 ml sample was withdrawn after 3 hours intervals and up to 24 hours to measure bacterial growth in terms of increase in the optical cell density at $\lambda_{600\text{nm}}$ ($\text{OD}_{600\text{nm}}$) using UV/Vis spectrophotometer (Novaspec Model. 80-2088-64, Pharmacia Biotech, UK). The growth curve was established by plotting $\text{OD}_{600\text{nm}}$ values against the treatment time. The specific growth rate was calculated according to the formula:

$$\mu = \frac{\ln X_1 - \ln X_2}{t_1 - t_2}$$

Where μ is the specific growth rate, X_1 and X_2 are the $\text{OD}_{600\text{nm}}$ at time t_1 and t_2 of the bacterial culture. The experiment was performed in triplicate and the results are presented as means of three independent tests \pm SD.

4.4.5 Estimation of antibacterial activity of AgNPs in terms of CFU

Different concentrations of AgNPs (1, 3, 6, 12, and 24 $\mu\text{g/ml}$) were used to evaluate its effect on *S. aureus* growth in terms of colony-forming units (CFU) on Muller Hinton agar plates. The bacterium was grown overnight and then diluted to a cell density equivalent to 0.5 McFarland ($\approx 1.5 \times 10^8$ CFU/ml). They were diluted to 10^5 fold and 100 μl were spread on solid agar plates containing different AgNPs concentrations. The plates were incubated for 24 hours at 37°C and the grown colonies were photographed.

4.4.6 Time-kill kinetics assay

The time-kill assay was performed for *S. aureus* culture exposed to $\frac{1}{2}$ MIC, MIC, and 2 MIC concentrations following the CLSI guideline¹⁷. An overnight bacterial culture was centrifuged at 4000 rpm for 1 hour to harvest the cells (Combi-514R, Korea). The harvested cells were suspended in sterile normal saline (0.085% NaCl, w/v) and adjusted to 0.5 McFarland ($\approx 1.5 \times 10^8$ CFU/ml). Aliquots of 1 ml from the prepared suspension were inoculated into test tubes containing 10 ml MHB (Oxoid, UK) with concentrations of the AgNPs equal to $\frac{1}{2}$ MIC, MIC, and 2 MIC. All tubes were incubated at 37°C and samples were taken at intervals of 30 minutes starting at the time of inoculation and up to 300 minutes. Estimation of the number of surviving bacteria was carried out by spreading 100 μl from appropriate bacterial dilutions in sterile normal saline onto the top of MHA plates with incubation at 37°C for 24 hours; the number of bacterial colonies was counted and expressed as CFU/ml. Time–kill curves were constructed by plotting the Log_{10} (CFU/ml) against the exposure time (minutes). The assay was performed in triplicate and the results are presented as means of three independent tests \pm SD

4.4.7 Wound migration assay

A wound migration assay was performed using the normal human dermal fibroblast cell line (ATCC® PCS-201-012) and as described in Wadhvani et al.¹⁸. Cells were cultured in a 12-well microtiter plate as a monolayer; they were seeded at a cell density of 5×10^4 cell/ml. The cells were grown for 24 hours in Dulbecco's Modified Eagle Medium (DMEM; Gibco, Germany) supplemented with 10% heat-inactivated fetal calf serum (Gibco, Germany), L-glutamine, 65 $\mu\text{g/mL}$ of penicillin G, and 100 $\mu\text{g/mL}$ of streptomycin sulfate. They were incubated at 37°C in a humidified atmosphere containing 5.0% CO_2 . Wound with uniform size

Chapter 4: Antibacterial activity against clinical and food pathogens

was made in each well using sterile micro-tip; culture medium was aspirated from each well, well was washed with sterile phosphate buffer solution (pH 7.4), and fresh media with different concentrations of AgNPs (1, 3, 5, and 10 $\mu\text{g/ml}$) were added to each well seeded with the cell line. Two wells containing a fresh medium without the test compounds were used as untreated controls. The culture was photographed at 0 time and after 24 hours using an inverted microscope (Nikon, Japan). Wound migration (closure) was measured by the following equation:

$$\% \text{ Wound migration} = 1 - (\text{area of the wound at } T_S / \text{area of the wound at } T_0) \times 100$$

Where T_S is 24 hours from wounding and T_0 is 0-hour wounding.

4.5 Result and Discussion

4.5.1 Chemical characterization of *Hypericum perforatum* L. phytochemicals-capped AgNPs

The aqueous extract is used as a reduction agent for silver ions into metallic silver, as well as a stabilizer to protect the silver nanoparticles (AgNPs) which are in their nanoscale size, thus, preventing the aggregating. Synthesis of AgNPs using aqueous St John's wort extract was green simple one-pot method, cost-effective, environmentally friendly, providing natural capping agents for the stabilization of AgNPs which do not need to use high temperature, pressure, and toxic chemicals. Besides, the coated functional groups that formed on the surface of AgNPs from the plant extract lead to stabilizing these particles and played an important role in their antioxidant and anti-cancer activity.

During the preparation process, the formation of the metallic silver particles via the silver ions (Ag^+) reduction with the St John's wort aqueous extract was observed by the color change to a light or dark brown. Figure 1a exhibits the UV–Vis spectra of Phyto-capped AgNPs at various times (fresh, month, and eight months). The absorption bands with a maximum of about 401, 405, and 425 nm are assigned to the plasmon resonance of metallic AgNPs indicating the existence of monodispersed spherical silver nanoparticles in the colloidal solution. Several research groups observed the surface plasmon resonance absorption band for AgNPs synthesized by similar methods with different plant extracts between 400–430 nm^{19,20}. It is worth mentioning that the dispersion of the AgNPs is stable and that further aggregation after 8 months (Figure 1a) does not affect the stability of the nanoparticles, since the redshift of the absorption band in the UV–Vis spectra is very small. These results reveal the formation of very small silver nanoparticles during the preparation process^{21,22}.

The dynamic light scattering technique was used to estimate the mean size, size distribution, and agglomeration potential of AgNPs²³. Figure 1b shows the diagram from the resulting AgNPs diameter depending on the relative frequency number weight (%). The hydrodynamic diameter distribution of green synthesized AgNPs in colloidal solution was found in the range of 15–30 nm and the Polydispersity index (PDI) is 0.19.

The surface charge of AgNPs in the colloidal solution was calculated by employing zeta potential measurements (Figure 1c). AgNPs showed around -19 mv negative effective charge in an aqueous solution, which leads to less agglomeration and better physical stability. It is

Chapter 4: Antibacterial activity against clinical and food pathogens

documented that the nanoparticles stabilize well in colloidal solutions when the stabilizer on their surface is well adsorbed²⁴. The dissociation of some H⁺ and total protonation of the hydroxyl groups of phytochemicals favor the repulsion between the nanoparticles, which discourages their aggregation.

The ATR-IR diagram shown in Figure 1d confirms the existence of St. John's wort extracted compounds on the surfaces of silver nanoparticles as a reducer and stabilizer. The presence of moieties from Naphthodianthrone, Phloroglucinol, flavonoids, and bioflavonoids derivatives, identified in our previous report on St. John's wort extract²⁵, cause the appearance of well-known signals in the infrared region of the electromagnetic spectrum such as hydroxyl groups, alkyl moiety, and aromatic rings. Indeed, the positions of these bands in the ATR-FTIR spectra are considered a sensitive indicator of the conformational changes in the structure of the plant compounds due to their adsorption on the surfaces of silver nanoparticles²⁶. The band appears in the region 675-900 cm⁻¹ corresponding to C-H aromatic out of the plane²⁷. The weak bands at 1230, 1242 & 1251 cm⁻¹ correspond to C-O-C stretching in aromatic rings²⁸. Both peaks around 1385 & 1445 cm⁻¹ are responsible for C-H stretching²⁹. The peak at 1527 cm⁻¹ is a response to stretching OH and C=C aromatic. The bands near 1617 cm⁻¹ (sometimes 1640 cm⁻¹) and near 1734 cm⁻¹ refer to C=O, +C-H, and C=O stretching in the aromatic ring. Bands in the range of 1923-2000 cm⁻¹ prove the existence of an aromatic ring. While bands in the range of 2900-2990 cm⁻¹ correspond to C-H stretching and the broad and intense band near 3400 cm⁻¹ indicates the presence of O-H stretching in phenols^{28,30,31}.

The XRD pattern shown in Figure 1e proves the formation of the nanocrystal structure of the green synthesized silver nanoparticle. The nine special diffraction peaks at 2θ values 27.82°, 32.25°, 38.12°, 44.28°, 46.26°, 54.88°, 57.56°, 64.45°, and 77.38° which correspond to the planes (210), (122), (111), (200), (231), (142), (241), (220) and (311) respectively possess well-defined characteristic peaks corresponding to the face-centered cubic structure of pure metallic silver (JCPDS file No. 04-0783)^{32,33}. The broadening of the diffraction pattern peaks indicates the small average crystallite sizes of AgNPs which can be measured using Debye-Scherrer's equation³⁴. The average size of crystalline silver nanoparticles was found to be around 12 nm.

Figure 1f exhibits TGA analysis (25 to 1000 °C) of phytochemicals-coated AgNPs with a heating rate of 1°C min. It is clear from this figure that decomposition occurs in 3 stages. The moisture and accumulated water absorbed on the surface are lost in the first stage after heating to 100°C. In the second (from 100°C to 160°C) and third stage (which extends up to 600°C), The initial thermal deterioration of all the phytochemicals on the surface of these nanoparticles occurs and then the complete degradation continues. Finally, the ash and the mineral component stay due to the use of an inert atmosphere^{35,36}.

Figures 2a,b show scanning electron microscopy (SEM) images of phytochemicals-coated AgNPs. As shown in these images, most of the silver nanoparticles are spherical and monodisperse with sizes ranging from 20-40 nm, while, other particles were aggregated with each other without a specific shape. This aggregation is a result of the network of organic compounds from St. John's wort extract present as a capping protective layer on the surfaces of the silver nanoparticles (Figure 2a,b). Moreover, scanning transmission electron microscopy

Chapter 4: Antibacterial activity against clinical and food pathogens

dark-field (STEM-DF) images (Figure 2c) of green synthesized silver nanoparticles confirmed that the particles' sizes were about 20-40 nm and they were spherical and monodispersed.

Atomic force microscopy (AFM) was used to verify the morphology and surface roughness of silver nanoparticles. The magnification in particle size complexity is proportional to the size of the AFM tip and in sample preparation^{37,38}. Figure 2d,e exhibits spherical silver nanoparticles with grain diameters ranging from 20-40 nm, which agreed with those obtained from the DLS results. Larger scans screening a few micrometers resulted in a maximum peak-to-valley distance of 30 nm and a root mean square (RMS) roughness of 10 nm.

Figure 2f revealed the relative amounts of the elements in prepared AgNPs. EDX diagrams recorded specific elemental silver peaks at 2.8 keV, 3.5 keV, and 3.8 keV identical to the binding energies of Ag-L, Ag-M. This confirmed the existence of elemental silver in the resulting final colloidal solutions. The presence of the carbon and oxygen peaks is related to the organic layer from St John's wort plant, which is present on the surfaces of nanoparticles as a protective agent. As shown in Figure 2f, the relative amounts of carbon are much larger than others because of the carbon from the holder.

Chapter 4: Antibacterial activity against clinical and food pathogens

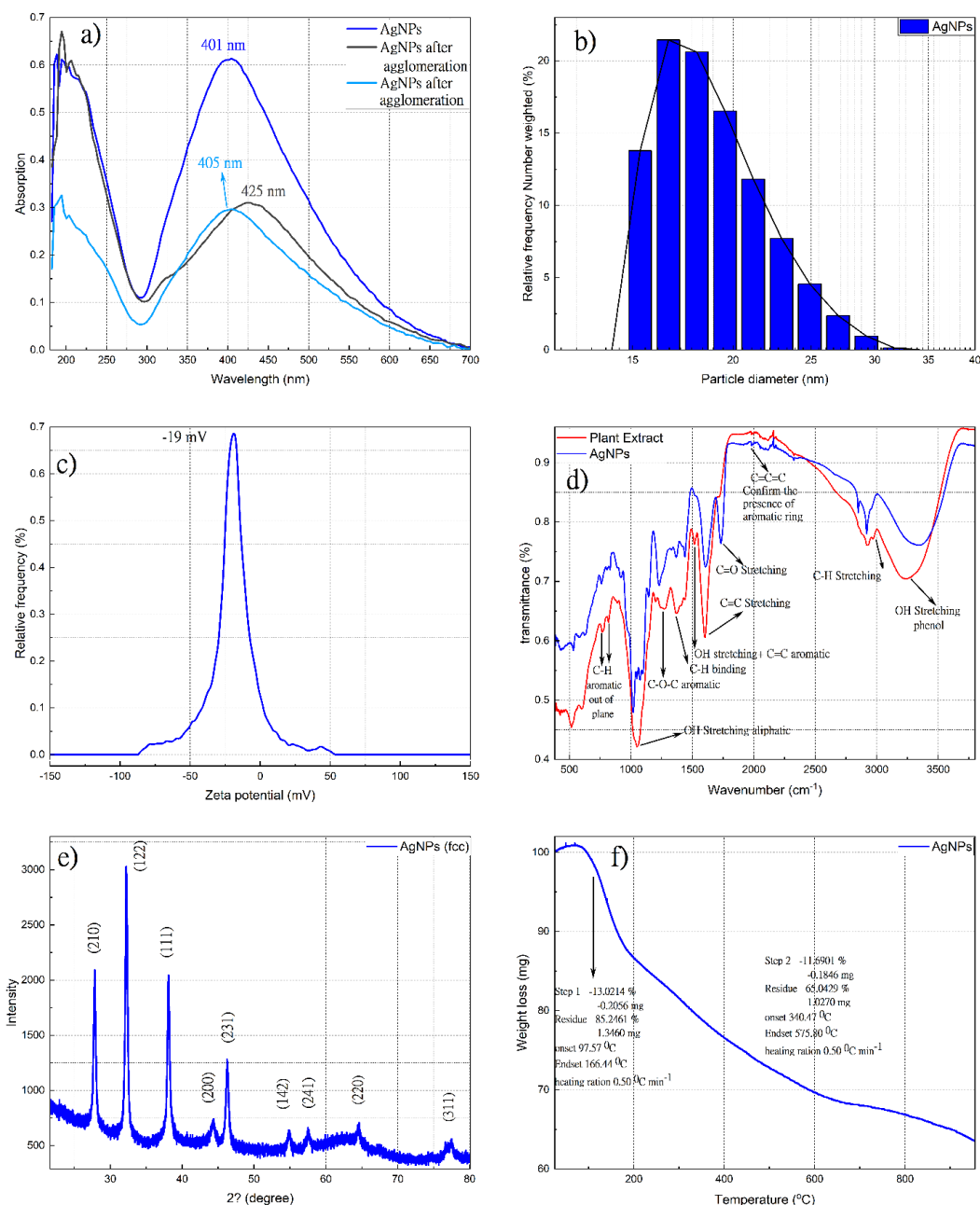


Figure 4-1: UV-Vis spectrum of ingredients-stabilized silver nanoparticles (AgNPs) using *Hypericum perforatum* L. aqueous Extract (a); hydrodynamic diameter distribution curve (b); zeta potential distribution curve (c); ATR-IR spectra of the resulted AgNPs and *Hypericum Perforatum* L. aqueous Extract (d); X-ray diffraction pattern of resulting AgNPs colloidal (e); thermal gravimetric analysis of the resulting phytochemicals-AgNPs (f).

Chapter 4: Antibacterial activity against clinical and food pathogens

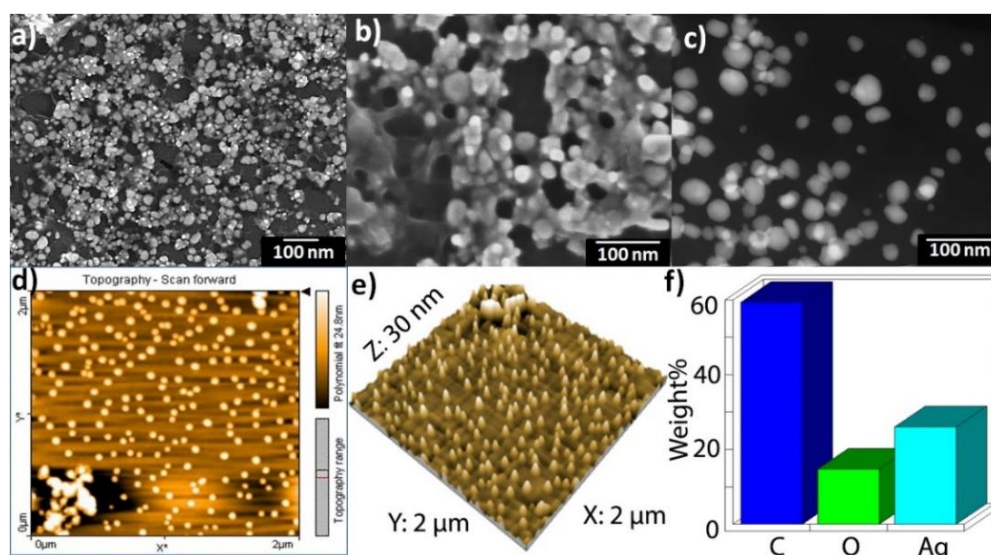


Figure 4-2: SEM images of *Hypericum Perforatum L.* phytochemicals-capped AgNPs (a & b); scanning transmission electron microscopy dark-field (STEM-DF) image (c); AFM image of phytochemicals-capped AgNPs colloidal deposited as a film on glass slide by spin coating, scan scale: $2\ \mu\text{m}\times 2\ \mu\text{m}$, the color bar shows the scale in Z-direction (d); $2\ \mu\text{m}\times 2\ \mu\text{m}$ AFM topography image of phytochemicals-capped AgNPs displayed as a three-dimensional projection (e) and quantitative results of energy dispersive X-ray (EDX) for phytochemicals-capped AgNPs (f).

Although the nanoparticle tracking analysis (NTA) is considered a more precise analytical technique than the Dynamic light scattering method to evaluate particle size distribution^{39,40}. However, the particle size distribution calculated using this technique (Figure 3) reveals monodisperse silver nanoparticles with an average diameter of 20-40 nm and confirms the DLS results. Therefore, one can conclude that monodisperse phytochemicals-coated silver nanoparticles with an average diameter between 20 and 40 nm have resulted.

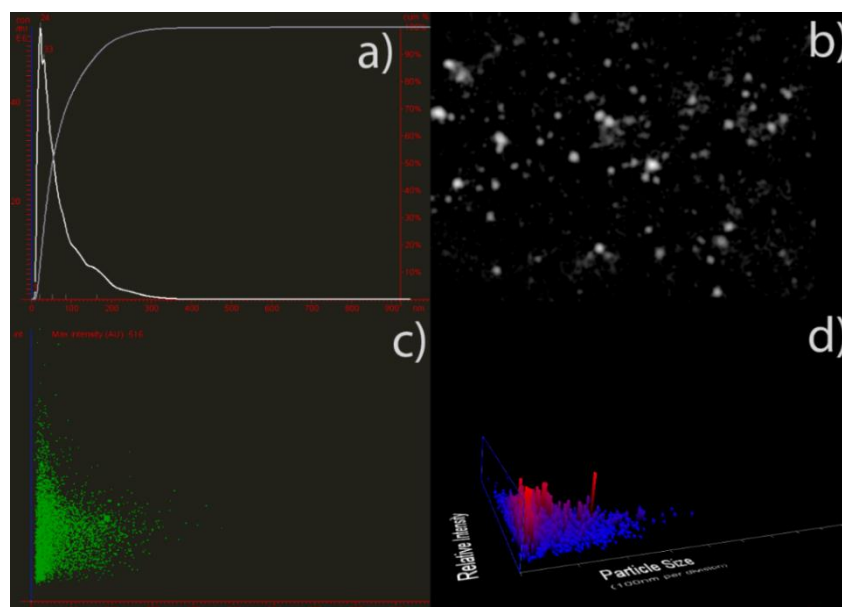


Figure 4-3: Nanoparticle tracking analysis of Phytochemicals-capped AgNPs. Particle size vs. particle concentration (a); representative nanoparticle tracking analysis video frame (b), particle size vs. relative intensity (c), and particle size vs. light scattering intensity vs. particle concentration (3D plot) are shown in (d).

Chapter 4: Antibacterial activity against clinical and food pathogens

4.5.2 Evaluation of biological activities of *Hypericum perforatum* mediated AgNPs

AgNPs revealed a broad-spectrum antibacterial activity against Gram-positive and negative tested bacterial strains, except both *E. coli* strains that were resistant to tested nanoparticles. The mean diameters of inhibition zones and the MIC values are presented in Table 1. According to the measured inhibition zones, Gram-positive bacterial were more susceptible to AgNPs than the Gram-negative ones in a concentration-dependent manner with less effectiveness against *B. subtilis* among other Gram-positive species; they caused the formation of 13.3-32 mm inhibition zones in Gram-positive bacteria (Fig. 4) and 13-19.7 mm in *P. aeruginosa* and *K. pneumoniae* at the highest tested concentration (100 µg/well). The concentration required to cause the absence of growth in sensitive bacterial strains ranged from 6.25-12.5 µg/ml (MIC) with bactericidal effect in most.

Table 4-1: Antibacterial activity of AgNPs and positive control against tested bacterial strains

Bacterial strain	Inhibition zone (mm ± SD)		S (10 µg/disc)	MIC (µg/ml)	
	50	100		AgNP	S
			µg/well	s	
Gram-positive					
<i>B. subtilis</i>	11.7 ± 0.6	13.3 ± 0.6	23.3 ± 1.6	12.5c	0.63s
<i>B. cereus</i>	19.0 ± 1	24.3 ± 2.1	29.7 ± 1.3	6.25s	0.31s
<i>S. aureus</i>	27.7 ± 1.5	32.0 ± 1.3	31.3 ± 0.7	12.5c	0.63c
Gram-negative					
<i>E. coli</i>	NA	NA	18.0 ± 1.3	> 100	5c
<i>E. coli</i> (clinical)	NA	NA	12.3 ± 0.7	> 100	> 10
<i>K. pneumonia</i> (clinical)	10.3 ± 0.6	13 ± 1	15.7 ± 0.7	12.5c	10c
<i>P. aeruginosa</i>	16.7 ± 1.5	19.7 ± 1.1	17.1 ± 0.3	6.25s	2.5s

S: streptomycin s: biostatic c: biocidal NA: not active

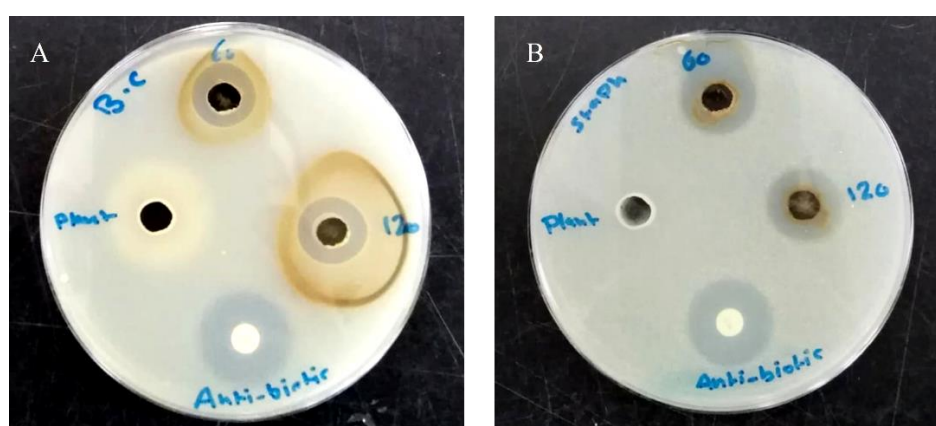


Figure 4-4: Photograph showing the antimicrobial activity of AgNPs against *B. cereus* (A) and *S. aureus* (B).

As *S. aureus* was the most susceptible bacterial test strain to AgNPs it was selected to estimate the effect of nanoparticles on the growth kinetics of the bacterium (Fig. 5). As the concentration

Chapter 4: Antibacterial activity against clinical and food pathogens

of the nanoparticle increases, a decrease in the OD_{600nm} value was noticed in comparison to the control culture and at different time intervals of sampling. Remarkably, the maximum cell density attained was about 50% of that reached by the control culture as the bacterium was exposed to almost ½ MIC concentration (6 µg/ml). Furthermore, at 12 µg/ml and 24 µg/ml, the growth of *S. aureus* was totally inhibited with an undetectable increase in the OD_{600nm} value throughout the whole period of cultivation (24 hours). Such finding indicated that the AgNPs have a toxic effect on the tested bacterium and their toxicity increase at higher concentrations of the nanoparticles. Intriguingly, the specific growth rate of *S. aureus* in presence of AgNPs declined with an increase in the tested nanoparticles concentrations to 6 µg/ml; at concentrations over 6 µg/ml, the specific growth rate was almost zero highlighting the higher toxicity of the nanoparticles on the bacterium (Table 2). The specific growth rate was decreased from 0.21 h⁻¹ in the control culture to 0.04 h⁻¹ in the culture exposed to 6 µg/ml AgNPs. In terms of CFU, as the concentration of nanoparticles increased in Muller Hinton agar plates there was a decrease in the number of growing colonies that were absent starting from concentrations ≥ 12 µg/ml, indicating a concentration-dependent antibacterial activity of AgNPs (Fig. 6).

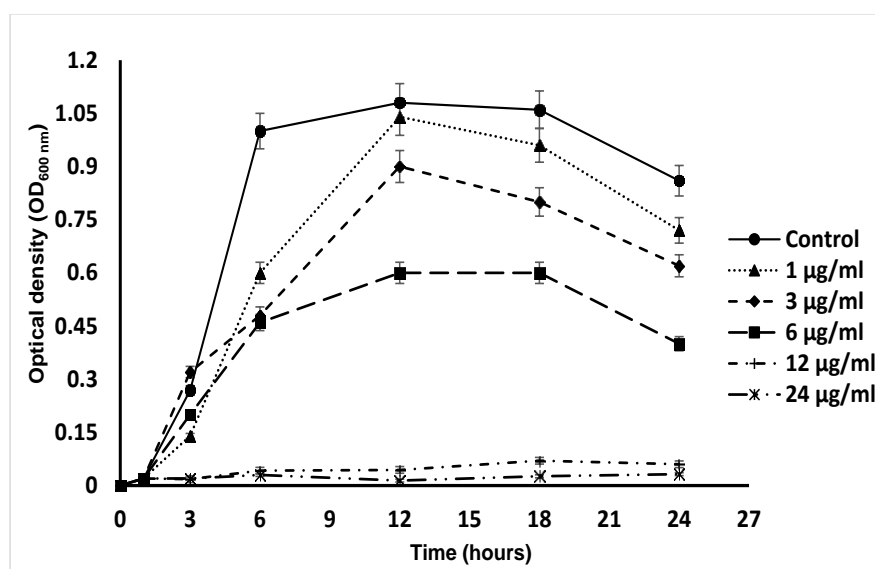


Figure 4-5: Growth curve of *S. aureus* in Muller Hinton broth containing different concentrations of AgNPs

Time-kill assay revealed that the effect of nanoparticles started after 90 min of incubation at different MIC concentrations. Interestingly, at ½ MIC concentration, the Log₁₀ (CFU/ml) was decreased by 10% compared to the control culture (without AgNPs). However, an almost 10³ fold reduction in Log₁₀ (CFU/ml) of *S. aureus* was noticed after 120 min of cultivation at MIC and 2 MIC concentrations of AgNPs which indicated a bactericidal effect of the nanoparticles; it caused the killing of the bacterium after 240 min of cultivation (Fig. 7).

Chapter 4: Antibacterial activity against clinical and food pathogens

Table 4-2: Antibacterial activity of AgNPs and positive control against tested bacterial strains

Concentration ($\mu\text{g/ml}$)	Specific growth rate (h^{-1})	Maximum growth intensity ($\text{OD}_{600\text{nm}}$)
Control	0.21 ± 0.012	0.91 ± 0.17
1	0.09 ± 0.007	0.86 ± 0.15
3	0.06 ± 0.015	0.63 ± 0.11
6	0.04 ± 0.006	0.55 ± 0.05
12	-	0.065 ± 0.01
24	-	0.035 ± 0.004

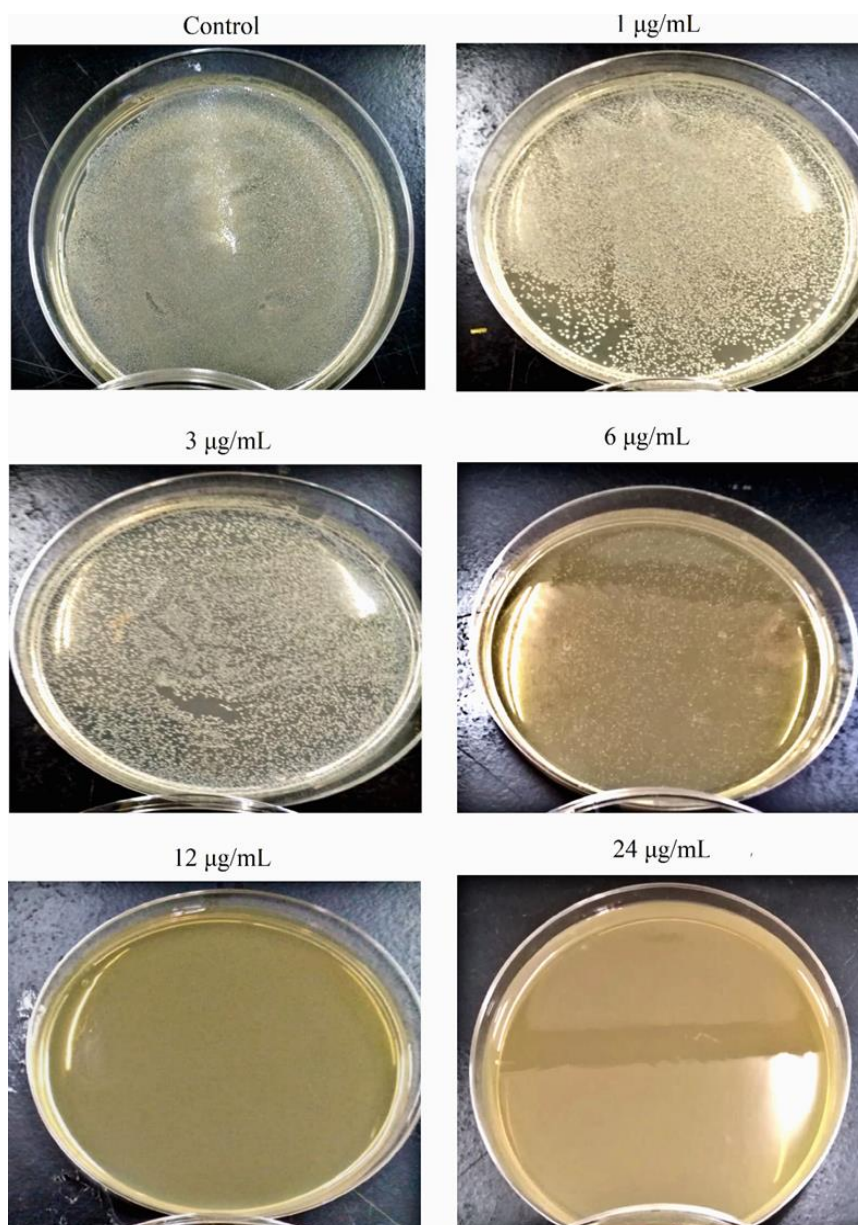


Figure 4-6: Photograph of *S. aureus* grown on Muller Hinton agar as a function of AgNPs concentrations.

Chapter 4: Antibacterial activity against clinical and food pathogens

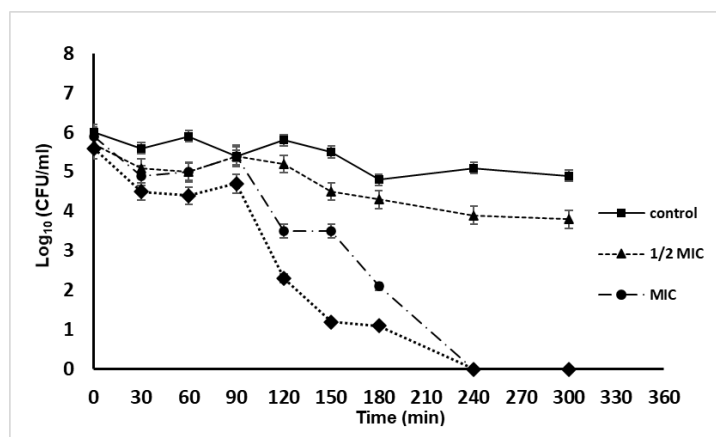


Figure 4-7: Time-kill curve of *S. aureus* in Muller Hinton broth medium supplemented with different concentrations of AgNPs

The antibacterial activity of AgNPs toward both Gram types of bacteria in the present study was in line with the previously reported broad-spectrum antibacterial effectiveness of the nanoparticles in several studies, it was due to their multi-site action and intrinsic therapeutic properties ⁷.

Also coincided with our results, Gram-positive bacteria were documented to be slightly more sensitive than the negative ones to tested nanoparticles ⁴¹⁻⁴³. Interestingly, it was postulated that Ag⁺ ions from the AgNPs have different targets between Gram-negative and positive bacteria ⁴⁴, though the exhibited activity of AgNPs synthesized by *Carduus crispus* on both Gram-types of bacteria was not affected by the difference in the bacterial wall ⁴⁵.

Worth noting, that the promising antibacterial activity of AgNPs was attributed to their ability to destroy cell membranes, cause intracellular damage, alter genetic material, and cause oxidative stress in the bacterial cell. Due to their size, nanoparticles have a large surface area that enables them to attach to the cell wall, penetrate the cell, and cause a disturbance in the membrane permeability leading to leakage of cell content ^{46,47}. Worth noting, capping of the nanoparticles with moieties of the lipophilic hypericin, hyperforin, and adhyperforin might facilitate their diffusion across the hydrophobic cell membrane of the bacterial cells, meanwhile, the presence of moieties from the flavonoid and phenols such as rutin, quercitrin surrounding their surfaces could increase their capacity to form complexes with extracellular and soluble proteins and with the cell wall ⁴⁸. These chemical constituents were detected among others in the extract of the St. John's wort in a previous report ²⁵. Moreover, AgNPs can bind to sulfur and phosphorus-containing proteins leading to protein and nucleic acids inactivation ⁴⁹. Furthermore, Ag⁺ ions, released through the oxidation dissolution process, alter the respiratory chain and facilitate the generation of reactive oxygen species (ROS) via their interaction with thiol groups of various enzymes and proteins, thus causing cell death through the inactivation of DNA replication, ATP production, and activating the apoptosis pathway ⁵⁰⁻⁵².

The effect of the AgNPs on the fibroblast cell migration was examined by the wound migration (contraction) method. The nanoparticles at concentrations of 1-5 µg/ml caused 52.2%-55.5% contraction in the wound distance compared to 67.5% wound closure in untreated fibroblast

Chapter 4: Antibacterial activity against clinical and food pathogens

cells (control) after 24 hours of treatment (Fig. 8). However, 31.6% of the wound distance was contracted at 10 $\mu\text{g/ml}$ of AgNPs, a concentration around the IC_{50} of the nanoparticle to the fibroblast cell line (data not shown); the decrease in the wound closure at this concentration compared to other tested doses was due to the cytotoxic effect of the nanoparticles on the tested fibroblast cells.

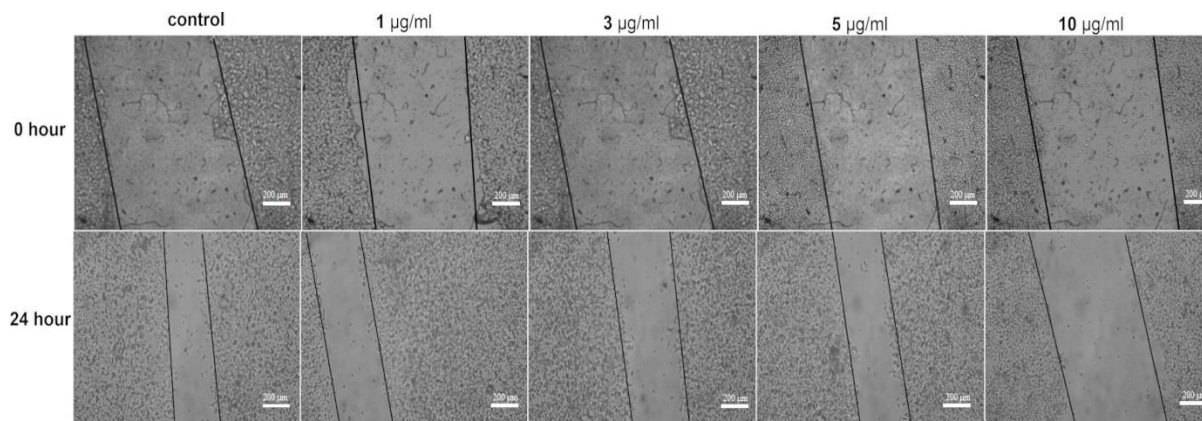


Figure 4-8: Effect of different AgNPs concentrations on the wound contraction in the fibroblast cell line.

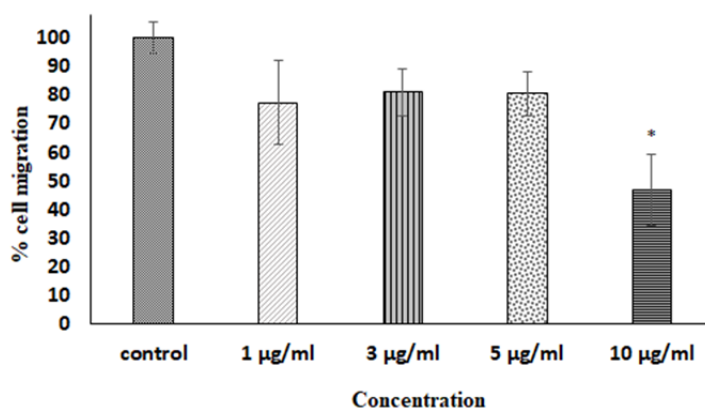


Figure 4-9: Percentage of fibroblast cell migration after 24-hour treatment with 0, 1, 3, 5, and 10 $\mu\text{g/ml}$ AgNPs.

In fact, wound migration was non-significantly inhibited when fibroblast cells were treated with 1-5 $\mu\text{g/ml}$ AgNPs (inhibition 19%-23% compared to control), but it was significantly inhibited at 10 $\mu\text{g/ml}$ (inhibition 46.8%, $p < 0.5$) (Fig. 9). Fibroblast cells play a fundamental role in body homeostasis through the secretion of growth factors, the release of matrix metalloproteinases, collagen expression, and facilitating contraction of healing wounds⁵³.

Some studies had reported that AgNPs were able to promote fibroblast differentiation and wound contraction in ex vivo systems using rodent models; the ability of these nanoparticles to exert their wound healing effect is through modulation of inflammatory cytokines⁵⁴⁻⁵⁶. On contrary, in the current study, it was noticed that the nanoparticles at low concentrations ($< \text{IC}_{50}$) caused an inhibition in fibroblast cells migration and wound contraction; a finding that

Chapter 4: Antibacterial activity against clinical and food pathogens

coincided with the reported effect of the AgNPs in negative modulation of extracellular matrix molecules (ECM) and laminin deposition, imbalanced expression of integrins, impaired reorganization or F-actin cytoskeleton, and decreased human fibroblast migration⁵³. These results revealed that the ability of AgNPs in promoting wound healing depends on the test system employed, in vivo or in vitro, as well as the presence of bio-factors such as growth factors and cytokines.

4.6 Conclusions

During the current study, the aqueous extract of the St. John's wort plant was used to synthesize silver nanoparticles as an environmentally friendly, fast, and clean method. The synthesized AgNPs were characterized by UV-VIS, DLS, zeta potential, FTIR, XRD, SEM, TEM, TGA, and NTA. The resulting AgNPs were spherical in shape, monodisperse, with a face-centered cubic crystal structures, and 20-40 nm in size. FTIR revealed the capping of AgNPs with functional groups of St. John's wort extract. The green synthesized nanoparticles exhibited a broad spectral antibacterial activity with Gram-positive test strains as the most susceptible group. The presence of the plant functional group decorating the nanoparticles' surfaces might facilitate their binding to cellular targets and exert their activities. Their bacteriocidal effect on *S. aureus* was noticed after 120 min of cultivation at MIC and 2 MIC concentrations; the bacterial specific growth rate significantly declined as the concentration of the tested nanoparticles increase up to ½ MIC and it was zero MIC and 2 MIC. Furthermore, the wound migration (closure) did not affect with AgNPs treatments up to 10 µg/ml.

Author Contributions: Author Contributions: Conceptualization, A.A., W.A-Z.; methodology, A.A., W.A-Z.; validation, A.A., W.A-Z.; formal analysis, A.A., W.A-Z., T.H., I.A.; investigation, A.A., W.A-Z., O.A-Q., and S.A-Q.; data curation, A.A., W.A-Z., S.A-Q., and T.H.; writing—original draft preparation, A.A., W.A-Z., T.H.; writing—review and editing, A.A., A.F., W.A-Z., O.A-M., and T.H.; supervision, J.W., T.S.; project administration, T.S. All authors have read and agreed to the published version of the manuscript.

Institutional Review Board Statement: Not applicable.

Informed Consent Statement: Not applicable.

Data Availability Statement: The data presented in this study are available on request from the corresponding author.

Acknowledgments: The authors are thankful to all the lab members for their help. The authors are very thankful to Frank Steinbach (Institut für Physikalische Chemie und Elektrochemie, Leibniz Universität Hannover). Abdalrahim Alahmad is supported by PhD grants from Avicenna Studienwerk e.V. The publication of this article was funded by the Open Access Publishing Fund of Leibniz Universität Hannover.

Conflicts of Interest: The authors declare no conflict of interest.

Chapter 4: Antibacterial activity against clinical and food pathogens

4.7 References

1. Khurana, A.; Tekula, S.; Saifi, M.A.; Venkatesh, P.; Godugu, C. Therapeutic applications of selenium nanoparticles. *Biomed. Pharmacother.* **2019**, *111*, 802-812. doi:https://doi.org/10.1016/j.biopha.2018.12.146.
2. Ikram, M.; Javad, B.; Raja, N.I.; Mashwani, Z. Biomedical Potential of Plant-Based Selenium Nanoparticles: A Comprehensive Review on Therapeutic and Mechanistic Aspects. *Int. J. Nanomed.* **2021**, *16*, 249-268. doi:10.2147/IJN.S295053.
3. Chinnasamy, G.; Chandrasekharan, S.; Koh, T.W.; Bhatnagar, S. Synthesis, Characterization, Antibacterial and Wound Healing Efficacy of Silver Nanoparticles From *Azadirachta indica*. *Front. Microbiol.* **2021**, *12*. doi:10.3389/fmicb.2021.611560.
4. Alahmad, A.; Feldhoff, A.; Bigall, N.C.; Rusch, P.; Scheper, T.; Walter, J.G. Hypericum perforatum L.-Mediated Green Synthesis of Silver Nanoparticles Exhibiting Antioxidant and Anticancer Activities. *Nanomaterials* **2021**, *11*, 487. doi:10.3390/nano11020487.
5. El-Seedi, H.R.; El-Shabasy, R.M.; Khalifa, S.A.M.; Saeed, A.; Shah, A.; Shah, R.; Iftikhar, F.J.; Abdel-Daim, M.M.; Omri, A.; Hajrahnd, N.H., et al. Metal nanoparticles fabricated by green chemistry using natural extracts: biosynthesis, mechanisms, and applications. *RSC Adv.* **2019**, *9*, 24539-24559. doi:10.1039/C9RA02225B.
6. Loo, Y.Y.; Rukayadi, Y.; Nor-Khaizura, M.-A.-R.; Kuan, C.H.; Chieng, B.W.; Nishibuchi, M.; Radu, S. In Vitro Antimicrobial Activity of Green Synthesized Silver Nanoparticles Against Selected Gram-negative Foodborne Pathogens. *Front. Microbiol.* **2018**, *9*, 1555. doi:10.3389/fmicb.2018.01555.
7. Federica, P.; Mauro, P. Antimicrobial Silver Nanoparticles for Wound Healing Application: Progress and Future Trends. *Materials* **2019**, *12*, 2540. doi:10.3390/ma12162540.
8. Wei, L.; Lu, J.; Xu, H.; Patel, A.; Chen, Z.S.; Chen, G. Silver nanoparticles: synthesis, properties, and therapeutic applications. *Drug Discov. Today* **2015**, *20*, 595-601. doi:10.1016/j.drudis.2014.11.014.
9. Burduşel, A.C.; Gherasim, O.; Grumezescu, A.M.; Mogoantă, L.; Ficai, A.; Andronescu, E. Biomedical Applications of Silver Nanoparticles: An Up-to-Date Overview. *Nanomaterials* **2018**, *8*, 681. doi:10.3390/nano8090681.
10. Lihui, Y.; Yiting, S.; Guoliang, T.; Weijun, X.; Yuqian, Z.; Lixing, W.; Zhaogang, T.; Lianhui, W. MoS₂@polydopamine-Ag nanosheets with enhanced antibacterial activity for effective treatment of *Staphylococcus aureus* biofilms and wound infection. *Nanoscale* **2018**, *10*, 16711-16720. doi:10.1039/C8NR04111C.
11. Silvero C, M.J.; Rocca, D.M.; de la Villarmois, E.A.; Fournier, K.; Lanterna, A.E.; Perez, M.F.; Becerra, M.C.; Scaiano, J.C. Selective Photoinduced Antibacterial Activity of Amoxicillin-Coated Gold Nanoparticles: From One-Step Synthesis to in Vivo Cytocompatibility. *ACS Omega* **2018**, *3*, 1220-1230. doi:10.1021/acsomega.7b01779.
12. Dhas, T.S.; Kumar, V.G.; Karthick, V.A.; Angel, K.J.; Govindaraju, K. Facile synthesis of silver chloride nanoparticles using marine alga and its antibacterial efficacy. *Spectrochim. Acta A Mol. Biomol. Spectrosc.* **2014**, *120*, 416-420. doi:10.1016/j.saa.2013.10.044.

Chapter 4: Antibacterial activity against clinical and food pathogens

13. Das, C.A.; Kumar, V.G.; Dhas, T.S.; Karthick, V.; Govindaraju, K.; Joselin, J.M.; Baalamurugan, J. Antibacterial activity of silver nanoparticles (biosynthesis): A short review on recent advances. *Biocatal. Agric. Biotechnol.* **2020**, *27*, 101593. doi:10.1016/j.bcab.2020.101593.
14. Shanmuganathan, R.; Karuppusamy, I.; Saravanan, M.; Muthukumar, H.; Ponnuchamy, K.; Ramkumar, V.S.; Pugazhendhi, A. Synthesis of Silver Nanoparticles and their Biomedical Applications - A Comprehensive Review. *Curr. Pharm. Des.* **2019**, *25*, 2650-2660. doi:10.2174/1381612825666190708185506.
15. Kailasa, S.K.; Park, T.-J.; Rohit, J.V.; Koduru, J.R. Antimicrobial activity of silver nanoparticles. In *Nanoparticles in Pharmacotherapy*, 1st ed.; Grumezescu, A.M., Ed.; William Andrew, Elsevier: NY, USA, 2019; Chapter 14, pp. 461-484. 10.1016/B978-0-12-816504-1.00009-0
16. Al-Zereini, W.A. Bioactive Crude Extracts from Four Bacterial Isolates of Marine Sediments from Red Sea, Gulf of Aqaba, Jordan. *Jord. J. Biol. Sci.* **2014**, *7*, 133-137.
17. CLSI. *Performance standards for antimicrobial susceptibility testing*; Twenty-second informational supplement, M100-S22; Clinical and Laboratory Standards Institute: Wayne, PA, USA, 2012.
18. Wadhvani, S.; Gorain, M.; Banerjee, P.; Shedbalkar, U.; Singh, R.; Kundu, G.; Chopade, B. Green synthesis of selenium nanoparticles using *Acinetobacter* sp. SW30: optimization, characterization and its anticancer activity in breast cancer cells. *Int. J. Nanomedicine* **2017**, *12*, 6841-6855. doi:10.2147/ijn.S139212.
19. Ma, L.; Su, W.; Liu, J.X.; Zeng, X.X.; Huang, Z.; Li, W.; Liu, Z.C.; Tang, J.X. Optimization for extracellular biosynthesis of silver nanoparticles by *Penicillium aculeatum* Su1 and their antimicrobial activity and cytotoxic effect compared with silver ions. *Mater. Sci. Eng. C Mater. Biol. Appl.* **2017**, *77*, 963-971. doi:10.1016/j.msec.2017.03.294.
20. Rolim, W.R.; Pelegrino, M.T.; de Araújo Lima, B.; Ferraz, L.S.; Costa, F.N.; Bernardes, J.S.; Rodrigues, T.; Brocchi, M.; Seabra, A.B. Green tea extract mediated biogenic synthesis of silver nanoparticles: Characterization, cytotoxicity evaluation and antibacterial activity. *Appl. Surf. Sci.* **2019**, *463*, 66-74. doi:https://doi.org/10.1016/j.apsusc.2018.08.203.
21. Alim-Al-Razy, M.; Asik Bayazid, G.M.; Rahman, R.U.; Bosu, R.; Shamma, S.S. Silver nanoparticle synthesis, UV-Vis spectroscopy to find particle size and measure resistance of colloidal solution. *J. Phys. Conf. Ser.* **2020**, *1706*, 012020. doi:10.1088/1742-6596/1706/1/012020.
22. Aziz, S.B.; Abdullah, O.G.; Saber, D.R.; Rasheed, M.A.; Ahmed, H.M. Investigation of metallic silver nanoparticles through UV-Vis and optical micrograph techniques. *Int. J. Electrochem. Sci.* **2017**, *12*, 363-373. doi:10.20964/2017.01.22.
23. Gontijo, L.A.; Raphael, E.; Ferrari, D.P.; Ferrari, J.L.; Lyon, J.P.; Schiavon, M.A. pH effect on the synthesis of different size silver nanoparticles evaluated by DLS and their size-dependent antimicrobial activity. *Matéria (Rio de Janeiro)* **2020**, *25*, e-12845.
24. Chandran, P.R.; Naseer, M.; Udupa, N.; Sandhyarani, N. Size controlled synthesis of biocompatible gold nanoparticles and their activity in the oxidation of NADH. *Nanotechnology* **2012**, *23*, 015602. doi:10.1088/0957-4484/23/1/015602.
25. Alahmad, A.; Alghoraibi, I.; Zein, R.; Kraft, S.; Dräger, G.; Walter, J.; Scheper, T. Identification of major constituents of *Hypericum perforatum* L. extracts in Syria by development of a

Chapter 4: Antibacterial activity against clinical and food pathogens

rapid, simple and reproducible HPLC-ESI-Q-TOF MS analysis and their antioxidant activities. *ACS Omega* **2022**, *accepted*.

26. Haroon, H.; Kulandhaivel, M.; Anbalagan, S.; Sankareswaran, M.; Abirami, K.; Prabhavathi, P.; Manikandan, A. Green synthesis of silver nanoparticles using *Hybanthus enneaspermus* plant extract against nosocomial pathogens with nanofinished antimicrobial cotton fabric. *Glob. J. Nanomed.* **2017**, *1*, 555554. doi:10.19080/gjn.2017.01.555554.
27. Margoshes, M.; Fassel, V.A. The infrared spectra of aromatic compounds: I. The out-of-plane C-H bending vibrations in the region 625–900 cm⁻¹. *Spectrochim. Acta* **1955**, *7*, 14-24. doi:10.1016/0371-1951(55)80003-3.
28. Joni, L.; Jarmo, L.; Teresa, K.; Michał, D.; Raimo, A. Characterization of alkali-extracted wood by FTIR-ATR spectroscopy. *Biomass Convers. Biorefin.* **2018**, *8*, 847–855. doi:10.1007/s13399-018-0327-5.
29. Ashokkumar, R.; Ramaswamy, M. Phytochemical screening by FTIR spectroscopic analysis of leaf extracts of selected Indian Medicinal plants. *Int. J. Curr. Microbiol. Appl. Sci.* **2014**, *3*, 395-406.
30. Milena, P. O–H stretch in phenol and its hydrogen-bonded complexes: Band position and relaxation pathways. *J. Phys. Chem.* **2012**, *116*, 364-371. doi:10.1021/jp209897y.
31. Brangule, A.; Šukele, R.; Bandere, D. Herbal medicine characterization perspectives using advanced FTIR sample techniques – diffuse reflectance (DRIFT) and photoacoustic spectroscopy (PAS). *Front. Plant Sci.* **2020**, *11*, 356. doi:10.3389/fpls.2020.00356.
32. Anigol, L.B.; Charantimath, J.S.; Gurubasavaraj, P.M. Effect of concentration and pH on the size of silver nanoparticles synthesized. *Org. Med. Chem. Int. J.* **2017**, *3*, 1-5. doi:10.19080/OMCIJ.2017.03.555622.
33. Mondal, A.; Hajra, A.; Shaikh, W.A.; Chakraborty, S.; Mondal, N.K.. Synthesis of silver nanoparticle with *Colocasia esculenta* (L.) stem and its larvicidal activity against *Culex quinquefasciatus* and *Chironomus* sp. *Asian Pac. J. Trop. Biomed.* **2019**, *9*, 510-517. doi:10.4103/2221-1691.271724.
34. Sagadevan, S.; Vennila, S.; Singh, P.; Lett, J.A.; Johan, M.R.; Muthiah, B.; Lakshmipathy, M. Facile synthesis of silver nanoparticles using *Averrhoa bilimbi* L and Plum extracts and investigation on the synergistic bioactivity using in vitro models. *Green Process. Synth.* **2019**, *8*, 873-884. doi:10.1515/gps-2019-0058.
35. Ivashchenko, O.; Przysiecka, Ł.; Peplinska, B.; Flak, D.; Coy, E.; Jarek, M.; Zalewski, T.; Musiał, A.; Jurga, S. Organic–Inorganic hybrid nanoparticles synthesized with *Hypericum perforatum* extract: Potential agents for photodynamic therapy at ultra-low power light. *ACS Sustain. Chem. Eng.* **2021**, *9*, 1625-1645. doi:10.1021/acssuschemeng.0c07036.
36. Fernandes, F.H.; Santana, C.P.; Santos, R.L.; Correia, L.P.; Conceição, M.M.; Macêdo, R.O.; Medeiros, A.C. Thermal characterization of dried extract of medicinal plant by DSC and analytical techniques. *J. Therm. Anal. Calorim.* **2013**, *113*, 443-447. doi:10.1007/s10973-012-2807-3.
37. Saware, K.; Sawle, B.; Salimath, B.; Jayanthi, K.; Abbaraju, V. Biosynthesis and characterization of silver nanoparticles using *Ficus benghalensis* leaf extract. *Int. J. Res. Eng. Technol.* **2014**, *3*, 867-874.

Chapter 4: Antibacterial activity against clinical and food pathogens

38. Soumya, M.; Happy, A.; S Rajesh, K.; S Venkat, K. Green synthesis of silver nanoparticles using medicinal plant *Acalypha indica* leaf extracts and its application as an antioxidant and antimicrobial agent against foodborne pathogens. *Int. J. App. Pharm.* **2017**, *9*, 42-50. doi:10.22159/ijap.2017v9i5.19464.
39. Vasco, F.; Andrea, H.; Wim, J. Critical evaluation of nanoparticle tracking analysis (NTA) by nanosight for the measurement of nanoparticles and protein aggregates. *Pharm. Res.* **2010**, *27*, 796-810. doi:10.1007/s11095-010-0073-2.
40. Fan, Y.; Sahdev, P.; Ochyl, L.J.; Akerberg, J.J.; Moon, J.J. Cationic liposome-hyaluronic acid hybrid nanoparticles for intranasal vaccination with subunit antigens. *J. Control. Release* **2015**, *208*, 121-129. doi:10.1016/j.jconrel.2015.04.010.
41. Padalia, H.; Moteriya, P.; Chanda, S. Green synthesis of silver nanoparticles from marigold flower and its synergistic antimicrobial potential. *Arab. J. Chem.* **2015**, *8*, 732-741. doi:10.1016/j.arabjc.2014.11.015.
42. Gomathi, M.; Rajkumar, P.V.; Prakasam, A.; Ravichandran, K. Green synthesis of silver nanoparticles using *Datura stramonium* leaf extract and assessment of their antibacterial activity. *Res-Eff. Technol.* **2017**, *3*, 280-284. doi:10.1016/j.reffit.2016.12.005.
43. Khandel, P.; Shahi, S.K.; Soni, D.K.; Yadaw, R.K.; Kanwar, L. *Alpinia calcarata*: Potential source for the fabrication of bioactive silver nanoparticles. *Nano Conver.* **2018**, *5*, 37. doi:10.1186/s40580-018-0167-9.
44. Wang, H.; Yan, A.; Liu, Z.; Yang, X.; Xu, Z.; Wang, Y.; Wang, R.; Koohi-Moghadam, M.; Hu, L.; Xia, W.; Tang, H. Deciphering molecular mechanism of silver by integrated omic approaches enables enhancing its antimicrobial efficacy in *E. coli*. *PLOS Biol.* **2019**, *17*, e3000292. doi:10.1371/journal.pbio.3000292.
45. Urnukhsaikhan, E.; Bold, B.E.; Gunbileg, A.; Sukhbaatar, N.; Mishig-Ochir, T. Antibacterial activity and characteristics of silver nanoparticles biosynthesized from *Carduus crispus*. *Sci. Rep.* **2021**, *11*, 21047. doi:10.1038/s41598-021-00520-2.
46. Siddiqi, K.S.; Husein, A.; Rao, R.A. A review on biosynthesis of silver nanoparticles and their biocidal properties. *J. Nanobiotechnology* **2018**, *16*, 1-28. doi:10.1186/s12951-018-0334-5.
47. Kambale, E.K.; Nkanga, C.I.; Mutonkole, B.P.; Bapolisi, A.M.; Tassa, D.O.; Liesse, J.M.; Krause, R.W.; Memvanga, P.B. Green synthesis of antimicrobial silver nanoparticles using aqueous leaf extracts from three Congolese plant species (*Brillantaisia patula*, *Crossopteryx febrifuga* and *Senna siamea*). *Heliyon* **2020**, *6*, e04493. doi:10.1016/j.heliyon.2020.e04493.
48. Al-Zereini, W.A. *Ononis natrix* and *Salvia verbenaca*: two Jordanian medicinal plants with cytotoxic and antibacterial activities. *J. Herbs Spices Med. Plants* **2017**, *23*, 18-25. doi:10.1080/10496475.2016.1241200
49. Vijayan, R.; Joseph, S.; Mathew, B. Green synthesis, characterization and applications of Noble metal nanoparticles using *Myxopyrum serratum* AW Hill leaf extract. *BioNanoScience* **2018**, *8*, 105-117. doi:10.1007/s12668-017-0433-z.
50. Abou El-Nour, K.M.; Eftaiha, A.A.; Al-Warthan, A.; Ammar, R.A. Synthesis and applications of silver nanoparticles. *Arab. J. Chem.* **2010**, *3*, 135-140. doi:10.1016/j.arabjc.2010.04.008.

Chapter 4: Antibacterial activity against clinical and food pathogens

51. Quinteros, M.A.; Aristizábal, V.C.; Dalmasso, P.R.; Paraje, M.G.; Páez, P.L. Oxidative stress generation of silver nanoparticles in three bacterial genera and its relationship with the antimicrobial activity. *Toxicol. in Vitro* **2016**, *36*, 216-223. doi:10.1016/j.tiv.2016.08.007.
52. Liao, S.; Zhang, Y.; Pan, X.; Zhu, F.; Jiang, C.; Liu, Q.; Cheng, Z.; Dai, G.; Wu, G.; Wang, L.; Chen, L. Antibacterial activity and mechanism of silver nanoparticles against multidrug-resistant *Pseudomonas aeruginosa*. *Int. J. Nanomedicine* **2019**, *14*, 1469-1487. doi:10.2147/ijn.S191340.
53. de Araújo Vieira, L.F.; Lins, M.P.; Viana, I.M.; Dos Santos, J.E.; Smaniotto, S.; dos Santos Reis, M.D. Metallic nanoparticles reduce the migration of human fibroblasts in vitro. *Nanoscale Res. Lett.* **2017**, *12*, 200. doi:10.1186/s11671-017-1982-3.
54. Liu, X.; Lee, P.Y.; Ho, C.M.; Lui, V.C.; Chen, Y.; Che, C.M.; Tam, P.K.; Wong, K.K. Silver nanoparticles mediate differential responses in keratinocytes and fibroblasts during skin wound healing. *ChemMedChem* **2010**, *5*, 468-475. doi:10.1002/cmdc.200900502.
55. Gunasekaran, T.; Nigusse, T.; Dhanaraju, M.D. Silver nanoparticles as real topical bullets for wound healing. *J. Am. Coll. Clin. Wound Spec.* **2011**, *3*, 82-96. doi:10.1016/j.jcws.2012.05.001.
56. Vijayakumar, V.; Samal, S.K.; Mohanty, S.; Nayak, S.K. Recent advancements in biopolymer and metal nanoparticle-based materials in diabetic wound healing management. *Int. J. Biol. Macromol.* **2019**, *122*, 137-148. doi:10.1016/j.ijbiomac.2018.10.120.

5 Chapter Five: A study of additional applications of biosynthesized silver nanoparticles using the aqueous extract of the St. John's wort, as well as the development of a protocol to conjugate it with the aptamer which are selective ligands for targeting cancer cells and the study of its selectivity and internalization against cancer human non-small lung cells (A549) and normal human bronchial epithelial cells (BEAS2B)

5.1 Vorwort

This chapter contains Additional experiments and many other results that were not published in articles till now due to lack of time, but they will be published very soon, Allah willing, after the Ph.D. defense. Of course, we will note that in additional studies of the effect of the prepared nanosilver, there is cooperation with universities in Saudi Arabia, Egypt and Syria, in addition to Jordan, which is mentioned in the third article.

Im ersten Abschnitt wurde die Wirkung der biosynthetisierten Silbernanopartikel auf ein breites Spektrum von Mikroben untersucht. Das Hauptziel bestand darin, die Auswirkung der Lagerung von Silber für unterschiedliche Zeiträume auf seine antibakterielle Aktivität zu untersuchen. Es wurde keine deutliche Veränderung der Aktivität von Silber-Nanopartikeln gegen die untersuchten Mikroben als Ergebnis der Lagerung über mehrere Zeiträume beobachtet. Dann wurde ein Vergleich zwischen seiner Aktivität und der von Silbernitrat und der von Pflanzenextrakt allein durchgeführt, und die Ergebnisse waren sehr gut.

Im zweiten Abschnitt (In Zusammenarbeit mit Ägypten) wurde die Wirkung der hergestellten Silber-Nanopartikel auf gramnegative, grampositive Bakterien und pathogene Hefen untersucht und ihre Wirkung mit Silbernitrat, Johanniskraut-Wässriger Extrakt allein, Antibiotika und Silber-Nanopartikel, hergestellt durch chemische Verfahren und unter Verwendung von Citrat als Verkappungsmittel verglichen. Die Ergebnisse waren ebenfalls hervorragend und sehr vielversprechend. Der Wirkungsmechanismus von Silbernanopartikeln auf Bakterien wurde untersucht, indem das SEM-Bild von Bakterien vor und nach Kontakt mit den Nanopartikeln untersucht wurde. Aus den Bildern war ersichtlich, wie das Silber auf seiner Oberfläche positioniert wurde, dann die Zellwand durchdrang und sie dann von innen beeinflusste.

Im dritten Abschnitt (Kooperation mit Syrien) wurde die Wirkung der präparierten Silber-Nanopartikel auf die Leishmaniose (*L. tropica* Syrischer Stamm (LT_SYR_24)) untersucht. Mehrere Techniken wurden untersucht, um die Wirkung zu bewerten, einschließlich der Zelllebensfähigkeit unter Verwendung des XTT-Assays, des Apoptose-Assays unter Verwendung von Annexin V und des Zellzyklus unter Verwendung von Durchflusszytometrie.

Chapter 5: Additional Experiments

Im vierten Abschnitt wurde die fast zweijährige Arbeit diskutiert, nämlich die Entwicklung eines Protokolls zur Bindung der präparierten Silber-Nanopartikel an ein Aptamer, das eine sehr hohe Selektivität gegenüber A549-Krebszellen aufweist. Viele Protokolle wurden befolgt und viele Bedingungen getestet, bis wir ein geeignetes Protokoll erreichten, durch das wir eine hohe Konjugationsrate erhalten und ohne dass die Aptamere ihre Wirksamkeit verlieren. Mit Aptameren konjugierte Silbernanopartikel wurden mit verschiedenen Techniken und Geräten charakterisiert, um die Bindung nachzuweisen. Die krebshemmende Wirkung von Aptamer-konjugierten Silbernanopartikeln auf Lungenkrebszellen (A549-Zellen) und gesunde Lungenzellen (BEAS-2B-Zellen) wurde mit mehreren Methoden untersucht einschließlich Zellviabilität mit dem CTB-Test, Zellebensfähigkeit unter Verwendung von Calcein-AM und Propidiumiodid (PI), Zelltod mit Annexin V Plus Propidiumiodid, Zellaufnahme unter Verwendung von AAS und Zellmorphologie unter Verwendung von Lichtmikroskop und konfokaler Mikroskopie.

Chapter 5: Additional Experiments

5.2 Studying the effect of storage of green-synthesized AgNPs on their antimicrobial activities

5.2.1 Agar diffusion method

5.2.1.1 Bacteria strains used in the test:

0.5 McFarland Solution from the overnight Blood agar (SPML Riyadh, Saudi Arabia) cultures of the following testing Microorganisms (Table x) were made in sterile normal saline using DENSICHEK™ Plus Instrument, following company recommended protocol ¹.

Table 5-1: bacteria and yeast strains used for the study

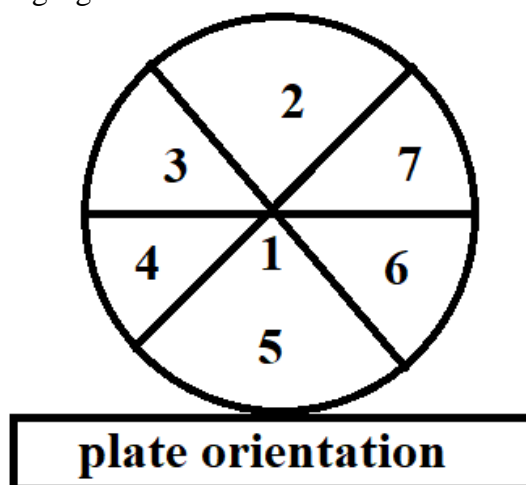
Plate No	Microorganism name	ATCC NO.
A	<i>S. aureus</i> (wild type)	29213
A	<i>S. aureus</i> (Methicillin resistant)	43300
A	<i>E. coli</i> (Wild type)	25922
A	<i>E. coli</i> (ESBL)	35218
B	<i>K. oxytoca</i> (Wild)	700324
B	<i>K. Pneumoniae</i> (CRE)	BAA-1705
B	<i>C. albican</i>	14053
B	<i>C. auris</i>	Lab isolate

5.2.1.2 Inoculation of Agar plates

0.5 McFarland solution of the testing MOs was streaked on MHA or SDA using sterile Cotton swab on a total of 3 plates for each testing microorganism. Each plate was assigned to a specific set 1-3. Each set represent different sized nanoparticle.

5.2.1.3 Agar wells

A total of 7 Holes in each agar Plate were made using pre-Sterile Glass upper tip according as shown in the in the following figure.



Scheme of holes labeling on agar plate

5.2.1.4 Serial Dilution of Testing compounds

The stock solution of each testing Nanoparticle was serially diluted. Each hole was assigned a specific dilution factor according to table 2

Chapter 5: Additional Experiments

Table 5-2: serial dilution of nanoparticles according to the hole number on agar plate

No	1	2	3	4	5	6	7
Dilution	1.0mg/ml	0.5 mg/ml	0.25 mg/ml	0.125 mg/ml	0.0625 mg/ml	0.03125 mg/ml	0.015625 mg/ml

5.2.1.5 Pouring of testing Nano-particles

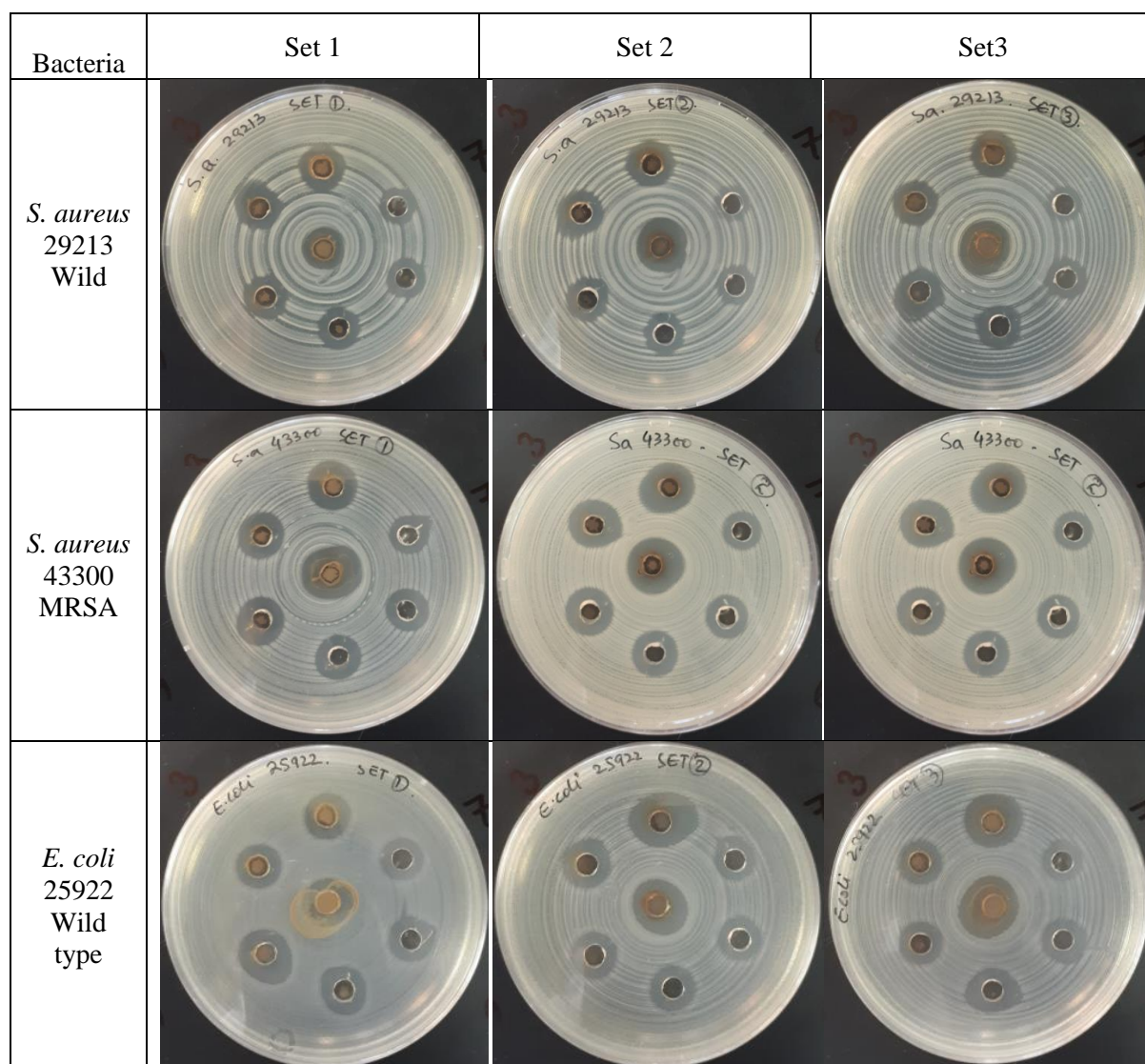
Each hole was filled with 100 μ L of the diluted nanoparticle as table 2. The micropipette tip was replaced every time to prevent cross contamination.

5.2.1.6 Incubation

The plates were immediately incubated upright position at 37°C for 24hrs.

5.2.1.7 Reading

The halo zone of inhibition (Fig. 1) was measured for each hole using ruler/ Vernier caliper (table 3).



Chapter 5: Additional Experiments

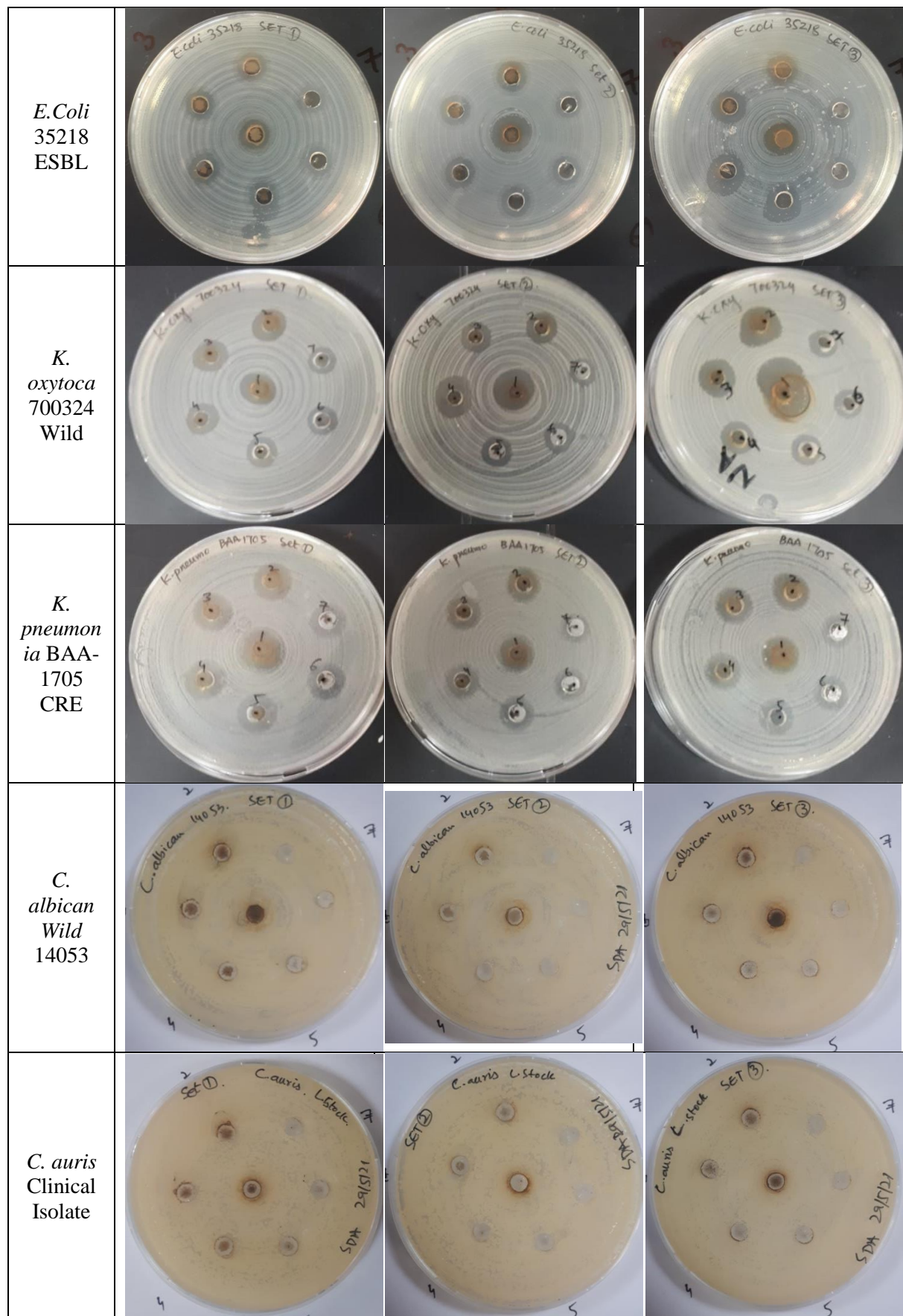


Figure 5-1: The halo zone of inhibition

Table 5-3: Antibacterial activity of green synthesized AgNPs using *Hypericum perforatum L.* aqueous extract at different times against tested bacterial strains.

Bacteria/ hole/set	Set 1 (after 4 months of synthesis)							Set 2 (after 7 months of synthesis)							Set 3 (after one year of synthesis)						
	1 mg/ ml	0.5 mg/ ml	0.25 mg/ ml	0.12 5 mg/ ml	0.06 25 mg/ ml	0.03 12 mg/ ml	0.01 56 mg/ ml	1 mg/ ml	0.5 mg/ ml	0.25 mg/ ml	0.12 5 mg/ ml	0.06 25 mg/ ml	0.03 12 mg/ ml	0.01 56 mg/ ml	1 mg/ ml	0.5 mg/ ml	0.25 mg/ ml	0.12 5 mg/ ml	0.06 25 mg/ ml	0.03 12 mg/ ml	0.01 56 mg/ ml
	1	2	3	4	5	6	7	1	2	3	4	5	6	7	1	2	3	4	5	6	7
<i>S. aureus</i> 29213	12	13	12	12	11	11	10	15	13	12	12	11	10	0	15	12	11.5	12	11	10	9
<i>MRSA</i> 43300	16	14	13	13	12	12	11	15	15	15	13	12	11	10	15	13.5	13	12.5	12	11	10
<i>E. coli</i> 25922	15	12	12	13	12	12	11	15	15	13	12	12	11	10	16	15	12	12	12	12	11
<i>K. pneumon iae</i> ESBL BAA- 1705	13	12	11	11	10	9	8	11	10	10	10	9	8	7	11	11	11	10	9	9	8
<i>K. oxytoca</i> W (700324)	12	12	11	11	10	10	9	15	15	11	11	10	9.5	9	21	13	13	10.5	10	9	9
<i>E. coli</i> CRE 35218	10	10	9	10	8	8	8	14	11	10.5	10	10	9	9	11	11	11	10	9	9	9
<i>C. albican</i> 14053	0	0	0	0	0	0	0	0	0	0	0	0	0	0	0	0	0	0	0	0	0
<i>C. auris</i> Lab strain	0	0	0	0	0	0	0	0	0	0	0	0	0	0	0	0	0	0	0	0	0

Chapter 5: Additional Experiments

5.2.1.8 Discussion

The results of Table 3 show the effect of nanoparticles stored for different periods of time on the growth of different bacteria strains. As expected the halo zone of growth inhibition is increased as the concentration is increased (direct proportion) for the bacteria strains *S. aureus* 29213, *MRSA* 43300, *E. coli* 25922, *K. pneumoniae* ESBL BAA-1705, *K. oxytoca* W (700324) and *E. coli* CRE 35218. Whereas, no effect was seen using different concentrations and sizes of nanoparticles on *C. albican* 14053 and *C. auris* Lab strain.

The results did not show any significant change in the effect of silver on bacteria when used after long periods of its synthesis, and this indicates that green synthesis of silver nanoparticles using our developed protocol did not lose its effectiveness as a result of storage for relatively long periods of time.

5.2.2 Microtiter plate method

5.2.2.1 Microorganism's strains

Multiple bacterial and Yeast colonies from the overnight Blood agar (SPML Riyadh, Saudi Arabia) cultures were inoculated in Muller Hinton Broth (2X) (Thermo Fisher Scientific Inc.) or Sabouraud Dextrose broth (2X) (Thermo Fisher Scientific Inc) respectively, and were incubated at 37°C in a shaker for 24 hrs.

Table 5-4: Bacteria and yeast strains used for the study

Plate No	Microorganism name	ATCC NO.
A	<i>S. aureus</i> (wild type)	29213
A	<i>S. aureus</i> (Methicillin resistant)	43300
A	<i>E. coli</i> (Wild type)	25922
A	<i>E. coli</i> (ESBL)	35218
B	<i>K. oxytoca</i> (Wild)	700324
B	<i>K. Pneumoniae</i> (CRE)	BAA-1705
B	<i>C. albican</i>	14053
B	<i>C. auris</i>	Lab isolate

5.2.2.2 Preparation of working Inoculum (5×10^6 CFU/ml density): (1ml/specie)

A density of 5×10^5 CFU/mL for each test microorganism is recommended by CLSI for MICs determination. The following steps were followed

A 0.5 McFarland turbidity Standard (Density= 1.5×10^8 CFU/mL) of MHB cultures were made either by inoculating the overnight plates culture in the sterilized MHB in Glass tubes or by diluting the broth Cultures using DensiCHEK™ Plus instrument (bioMérieux USA). A 3μL of the 0.5 McFarland in each well had a final density of 5×10^5 CFU/mL as required.

Chapter 5: Additional Experiments

5.2.2.3 Pouring in Microtiter plate

3 column per 1 microorganisms was assigned as shown in table 04. Out of three one column was assigned for each raw material and nanoparticles respectively. A total of 150 μL mixture according to table 4, was poured in each well following addition of 50 μL of testing compound. 100 μL sterile MHB or SDB was added in **NC** well instead of testing microorganism while 50 μL of sterile deionized water that was also used for compounds dilutions was added in **GC** wells instead of testing compounds (table 5). During pouring the micropipette tip was changed to prevent cross contamination.

Table 5-5:

Ingredient	Quantity per well
MHB (2X)/SDB (2X)	100 μL
0.5 McFarland testing MO	3 μL
Distill water	47 μL
Testing Compound	50 μL
Total volume	200 μL

Table 5-6: Micro-well plate testing arrangement scheme

Plate A	Conc.	<i>S. aureus</i> 29213			<i>S. aureus</i> (MRSA) 43300			<i>E. coli</i> 25922			<i>E. coli</i> (ESBL) 35218		
	Well	CA	T	CB	CA	T	CB	CA	T	CB	CA	T	CB
	Dilution	1	2	3	4	5	6	7	8	9	10	11	12
A	NC	NG	NG	NG	NG	NG	NG	NG	NG	NG	NG	NG	NG
B	1 220 $\mu\text{g/ml}$	G	NG	NG	G	NG	NG	G	NG	NG	G	NG	NG
C	2 110 $\mu\text{g/ml}$	G	NG	NG	G	NG	NG	G	NG	NG	G	NG	NG
D	3 55 $\mu\text{g/ml}$	G	NG	NG	G	NG	NG	G	NG	NG	G	NG	NG
E	4 27.5 $\mu\text{g/ml}$	G	NG	NG	G	NG	NG	G	NG	G	G	NG	NG
F	5 13.75 $\mu\text{g/ml}$	G	G	NG	G	G	NG	G	NG	NG	G	NG	NG
G	6 6.875 $\mu\text{g/ml}$	G	G	G	G	G	G	G	NG	NG	G	NG	NG
H	GC	G	G	G	G	G	G	G	G	G	G	G	G

CA: Brown powder, T: Nanoparticle/brown liquid, CB: AgNo3/crystals
G: viable colony growth observed, NG= no growth observed during viable test

Chapter 5: Additional Experiments

Plate B	Specie	<i>K. oxytoca</i> 700324			<i>K. pneumoniae</i> CRE (Lab)			<i>C. albican</i> 14053			<i>C. auris</i> Lab isolate		
	Well	CA	T	CB	CA	T	CB	CA	T	CB	CA	T	CB
	Dilution	1	2	3	4	5	6	7	8	9	10	11	12
A	NC	NG	NG	NG	NG	NG	NG	NG	NG	NG	NG	NG	NG
B	1 220 µg/ml	G	NG	NG	G	NG	NG	G	NG	NG	G	NG	NG
C	2 110 µg/ml	G	NG	NG	G	NG	NG	G	NG	NG	G	NG	NG
D	3 55 µg/ml	G	NG	NG	G	NG	NG	G	NG	NG	G	NG	G
E	4 27.5 µg/ml	G	NG	NG	G	NG	NG	G	G	G	G	G	G
F	5 13.75 µg/ml	G	NG	NG	G	NG	NG	G	G	G	G	G	G
G	6 6.875 µg/ml	G	NG	NG	G	G	NG	G	G	G	G	G	G
H	GC	G	G	G	G	G	G	G	G	G	G	G	G

CA: Brown powder, T: Nanoparticle/brown liquid, CB: AgNo3/crystals
G: viable colony growth observed, NG= no growth observed during viable test

5.2.2.4 Preparation of Antimicrobial dilutes

The testing stock compounds were serially diluted according to table No 6. A 50µL of each diluted compound working solution was poured in the specified Microplate well as shown in table 5. After pouring, the micro well plates were sealed with sterile tape and were incubated at 37°C for 24 hours.

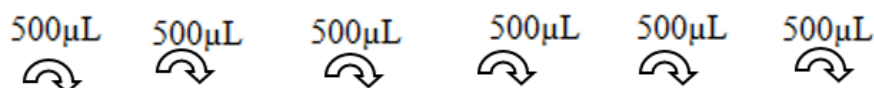


Table 5-7: Testing compound dilution factors

Final Quantity	500µL	500µL	500µL	500µL	500µL	500µL	1000µL
Final Concentration	440µg/ml	220 µg/ml	110 µg /ml	55 µg /ml	27.5µg /ml	13.75 µg /ml	6.875 µg/ml

5.2.2.5 Verification of final inoculum density:

To ensure that inoculum density of the MHB is within recommended range, a 10µL of inoculum from each GC well was diluted in 10ml of Sterile 0.85% Saline. Then 100 µL of the dilute was spread on MHA/SDA plate following 24hrs incubation. After incubation at least 50 colonies count indicated the recommended density of 5×10^5 CFU/ml.

Chapter 5: Additional Experiments

5.2.2.6 MIC reading

The turbidity of the micro well plates was observed using inverted mirror or Micro-well plate reader for turbidity check.

5.2.3 Viability test

Since some of the wells were very dark to read, A 10 μ L of the specimen from the well was inoculated on MHA/SDA following Incubation at 37C for 24hrs. No growth after incubation indicated correct MIC determination.

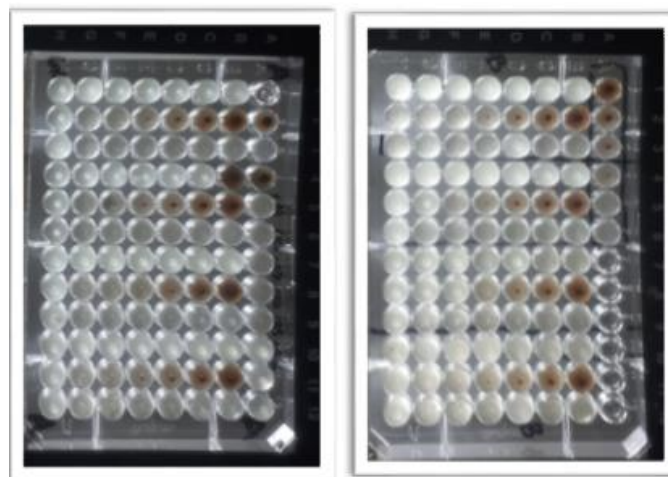


Figure 5-2: Microdilution plates

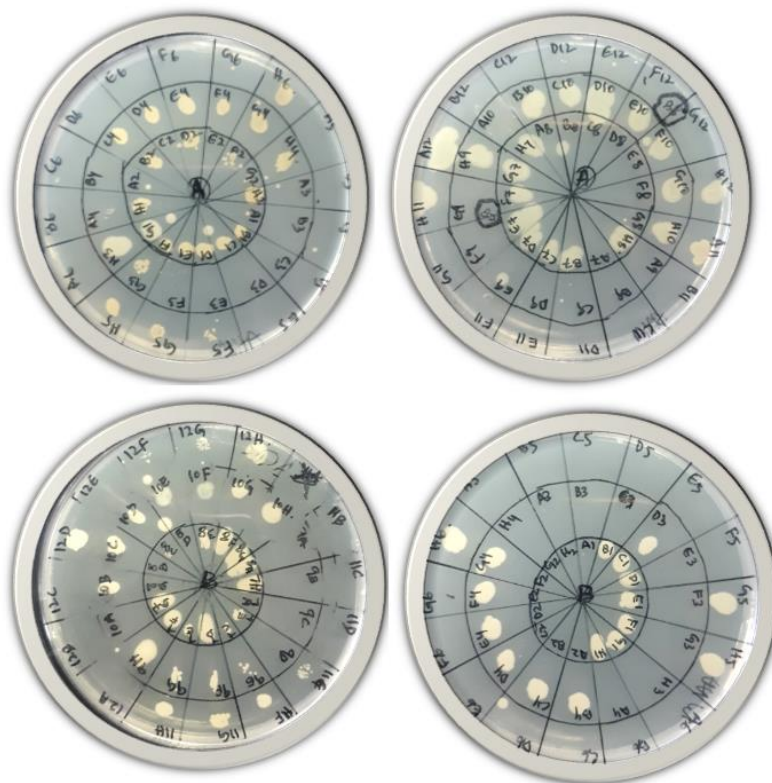


Figure 5-3: Viability test plate

Chapter 5: Additional Experiments

Table 5-8: The minimum inhibitory concentration of AgNPs, AgNO₃ and St. John's Wort aqueous extract against tested bacterial strains

Bacterial strain	MIC (µg/ml)		
	AgNPs	St. John's wort extract	AgNO ₃
<i>S. aureus</i> (wild type) 29213	27.5	X	13.75
<i>S. aureus</i> (Methicillin resistant) 43300	27.5	X	13.75
<i>E. coli</i> (Wild type) 25922	< 6.88	X	< 6.88
<i>E. coli</i> (ESBL) 35218	< 6.88	X	< 6.88
<i>K. oxytoca</i> (Wild) 700324	< 6.88	X	< 6.88
<i>K. Pneumoniae</i> (CRE) BAA-1705	13.75	X	< 6.88
<i>C. albican</i> 14053	55	X	55
<i>C. auris</i> Lab isolate	55	X	110

5.2.3.1 Discussion

Through the results presented in Table 4, we note that the aqueous extract of St. John's wort did not show any activity against the eight strains of bacteria studied, while the silver prepared by our method gave minimum inhibitory concentration values either identical to the values of silver nitrate as in *E. coli* (Wild type) 25922, *E. coli* (ESBL) 35218, *K. oxytoca* (Wild) 700324 and *C. albican* 14053 or higher than them as in *S. aureus* (wild type) 29213, *S. aureus* (Methicillin resistant) 43300 and *K. Pneumoniae* (CRE) BAA-1705 or lower than them as in *C. auris* Lab isolate. It is worth noting here that at the lowest concentrations at which bacteria did not grow, we took a sample from them and conducted a viability analysis, and after 24 hours we did not notice any growth of bacteria, and this indicates that silver is lethal and inhibiting growth at the same time.

Chapter 5: Additional Experiments

5.3 Comparison of the antimicrobial activities of *Hypericum perforatum L.*- Mediated green synthesis of AgNPs with antibiotics, silver nitrate, *Hypericum perforatum L.* aqueous extract and Citrate-capped AgNPs.

Methods for antimicrobial activity

Sample preparation

Different samples including silver nitrate, plant extract, and silver nanoparticles (prepared either chemically or plant extract) were prepared at the same concentrations in water as solvent.

Tested organisms

The microorganisms used in the in vitro antimicrobial study were as follows:

Gram-positive bacteria: *Bacillus subtilis* (ATCC 6633), *Bacillus cereus* (ATCC 6629) and *Staphylococcus aureus* (ATCC 6538).

Gram-negative bacteria: *Escherichia coli* (ATCC25922), *Proteus mirabillus* (ATCC9240) and *Salmonella enterica* (ATCC 25566).

Pathogenic yeast: *Candida albicans* (ATCC 10231).

5.3.1 Antimicrobial assay

Qualitative evaluations were executed in nutrient agar plates according to a previous published study^{2,3}. The inoculation of all microorganisms were prepared from fresh overnight broth cultures using Brain Heart infusion broth medium incubated at 37°C. The inoculum size of these pathogenic strains was prepared and adjusted to approximately 0.5 McFarland standard (1.5×10^8 CFU/ mL); 25.0 µL of both bacterial and yeast inocula were inoculated into each plate after the medium cooled and solidified, containing 20.0 mL of the sterile nutrient agar medium (NA). Several discs were punched out from these agar plates using 1.0 cm cork borer followed by pipetting 100.0 µL of the previously prepared samples on the 0.9 cm well and dispersed spontaneously with well diffusion method. Finally, These inoculated plates with samples were placed in the refrigerator for one hour, followed by incubation at 37°C for 24 hours, and zones of inhibition (ZI) were measured in mm^{2,3}. Different type of antibiotic standard were applied on the same test strains to compare with the tested samples of nano-silver, silver nitrate and plant extract.

5.3.2 TEM Images

A few drops of the bacteria cells suspension are placed on a carbon-coated Cu grid and then left on filter paper for about 5 minutes to dry. 3 drops of a 20% glutaraldehyde solution are added to the sample and then left for 5 minutes to dry. 3 drops of 1% phosphotungstic acid (negative stain for TEM) are added to the sample and then left for 5 minutes to dry. load on TEM device; Jeol-HR. TEM, model-JEM-2100 Japan. Examine under a microscope and obtain images.

Chapter 5: Additional Experiments

5.3.3 Results

Table 5-9: Antimicrobial activity of different concentrations of Silver nitrate Powder sample by measuring Inhibition zone diameter (millimeter) after 24 hours incubation period and at 37 °C applying the well diffusion technique

Samples	Code	Silver nitrate Powder						
	Concentration	0.0	10.0	25.0	50.0	100.0	150.0	200.0
Test bacteria	µg/ml							
1- <i>Bacillus subtilis</i>		NiL	NiL	12.0	15.0	17.0	20.0	22.0
2- <i>Bacillus cereus</i>		NiL	NiL	NiL	NiL	11.0	13.0	15.0
3- <i>Staphylococcus aureus</i>		NiL	NiL	11.0	15.0	16.0	17.0	19.0
4- <i>Escherichia coli</i>		NiL	NiL	11.0	14.0	16.0	17.0	17.0
5- <i>Proteus mirabilis</i>		NiL	NiL	NiL	10.0	14.0	15.0	17.0
6- <i>Salmonella enterica</i>		NiL	NiL	NiL	11.0	15.0	18.0	18.0
7- <i>Candida albicans</i>		NiL	NiL	20.0	27.0	30.0	34.0	40.0

*in this and other following tables: NiL: No antimicrobial activity.

Table 5-10: Antimicrobial activity of different concentrations of Silver nano particles reduced by plant extract sample by measuring Inhibition zone diameter (millimeter) after 24 hours incubation period and at 37 °C applying the well diffusion technique

Samples	Code	Silver nano particles						
	Concentration µg/ml	0.0	5.0	12.0	25.0	50.0	75.0	100.0
Test bacteria								
1- <i>Bacillus subtilis</i>		NiL	NiL	NiL	10	12.0	14.0	16.0
2- <i>Bacillus cereus</i>		NiL	NiL	NiL	11	12.0	13.0	16.0
3- <i>Staphylococcus aureus</i>		NiL	NiL	11.0	15.0	16.0	17.0	18.0
4- <i>Escherichia coli</i>		NiL	NiL	NiL	11.0	17.0	17.0	17.0
5- <i>Proteus mirabilis</i>		NiL	NiL	NiL	12	15.0	17.0	17.0
6- <i>Salmonella enterica</i>		NiL	NiL	NiL	11	15.0	17.0	17.0
7- <i>Candida albicans</i>		NiL	NiL	NiL	10	11.0	13.0	14.0

Chapter 5: Additional Experiments

Table 5-11: Antimicrobial activity of different concentrations of plant extract sample by measuring Inhibition zone diameter (millimeter) after 24 hours incubation period and at 37 °C applying the well diffusion technique

Samples	Code	plant extract sample						
		Concentration µg/ml	0.0	10.0	25.0	50.0	100.0	150.0
Test bacteria								
1-	<i>Bacillus subtilis</i>	NiL	NiL	NiL	NiL	NiL	NiL	NiL
2-	<i>Bacillus cereus</i>	NiL	NiL	NiL	NiL	NiL	NiL	NiL
3-	<i>Staphylococcus aureus</i>	NiL	NiL	NiL	NiL	NiL	NiL	NiL
4-	<i>Escherichia coli</i>	NiL	NiL	NiL	NiL	NiL	NiL	NiL
5-	<i>Proteus mirabilis</i>	NiL	NiL	NiL	NiL	NiL	NiL	NiL
6-	<i>Salmonella enterica</i>	NiL	NiL	NiL	NiL	NiL	NiL	NiL
7-	<i>Candida albicans</i>	NiL	NiL	NiL	NiL	NiL	NiL	NiL

Table 5-12: Antimicrobial activity of different concentrations of Silver nano particles produced chemically by measuring Inhibition zone diameter (millimeter) after 24 hours incubation period and at 37 °C applying the well diffusion technique

Samples	Code	Silver nano particles prepared chemically						
		Concentration µg/ml	0.0	10.0	25.0	50.0	100.0	150.0
Test bacteria								
1-	<i>Bacillus subtilis</i>	NiL	NiL	NiL	NiL	NiL	NiL	NiL
2-	<i>Bacillus cereus</i>	NiL	NiL	NiL	NiL	NiL	NiL	NiL
3-	<i>Staphylococcus aureus</i>	NiL	NiL	NiL	NiL	NiL	NiL	NiL
4-	<i>Escherichia coli</i>	NiL	NiL	NiL	NiL	NiL	NiL	NiL
5-	<i>Proteus mirabilis</i>	NiL	NiL	NiL	NiL	NiL	NiL	NiL
6-	<i>Salmonella enterica</i>	NiL	NiL	NiL	NiL	NiL	NiL	NiL
7-	<i>Candida albicans</i>	NiL	NiL	NiL	NiL	NiL	NiL	NiL

Chapter 5: Additional Experiments

Table 5-13: Antimicrobial activity of different antibiotics standard by measuring Inhibition zone diameter (millimeter) after 24 hours incubation period and at 37 °C applying the well diffusion technique

Samples	Code	antibiotics standard					
	Antibiotic name	CN	CTX	E	LEV	CIP	VA
Test bacteria							
1-	<i>Bacillus subtilis</i>	20.0	NiL	22.0	25.0	32.0	22.0
2-	<i>Bacillus cereus</i>	16.0	NiL	16.0	27.0	22.0	18.0
3-	<i>Staphylococcus aureus</i>	21.0	NiL	26.0	26.0	26.0	19.0
4-	<i>Escherichia coli</i>	15.0	NiL	NiL	25.0	25.0	NiL
5-	<i>Proteus mirabillus</i>	12.0	NiL	NiL	17.0	17.0	NiL
6-	<i>Salmonella enterica</i>	16.0	NiL	16.0	22.0	22.0	20.0
7-	<i>Candida albicans</i>	21.0	NiL	20.0	30.0	30.0	22.0

Chapter 5: Additional Experiments

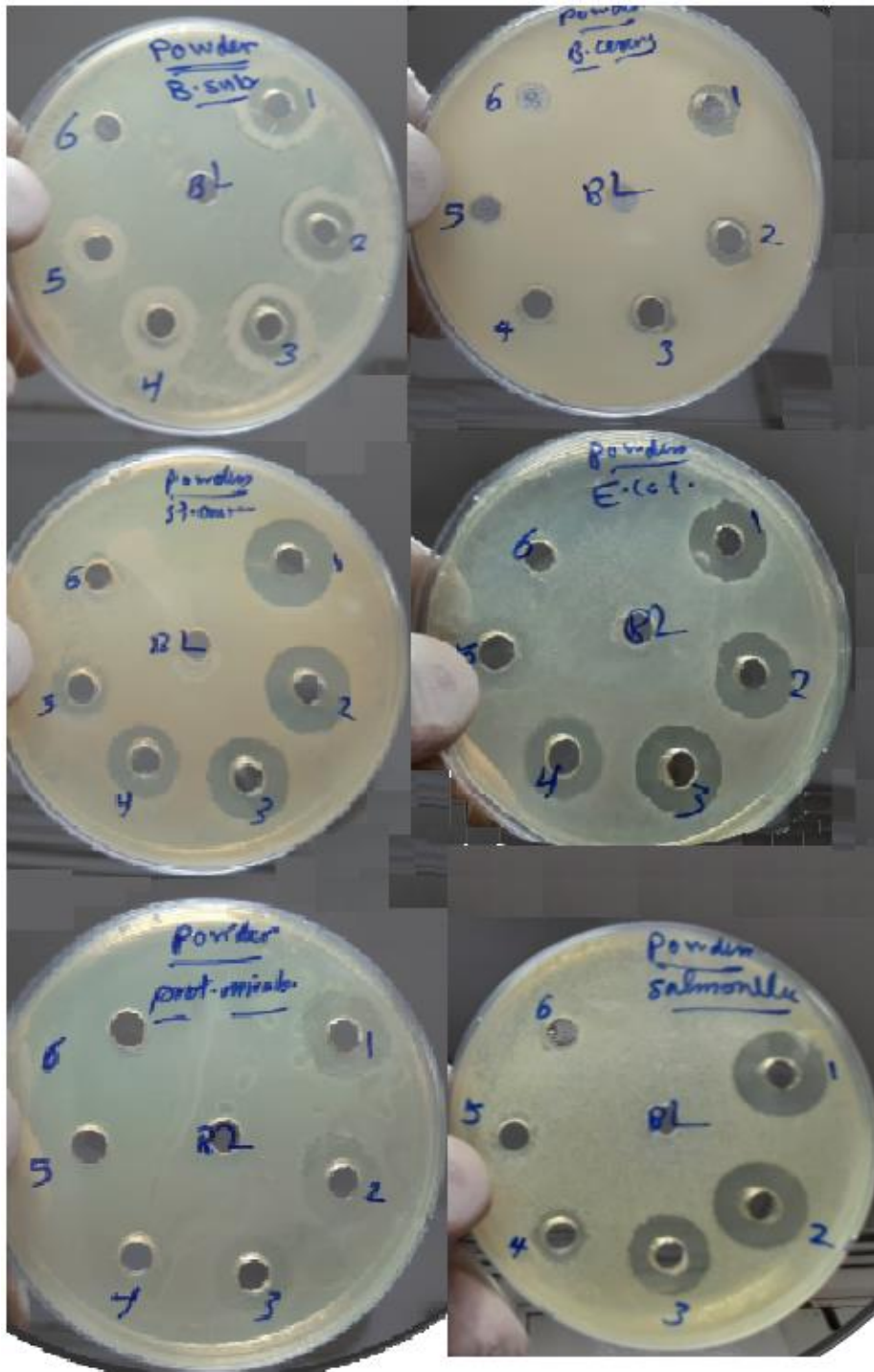


Figure 5-4: Antimicrobial effects of silver nitrate

Chapter 5: Additional Experiments

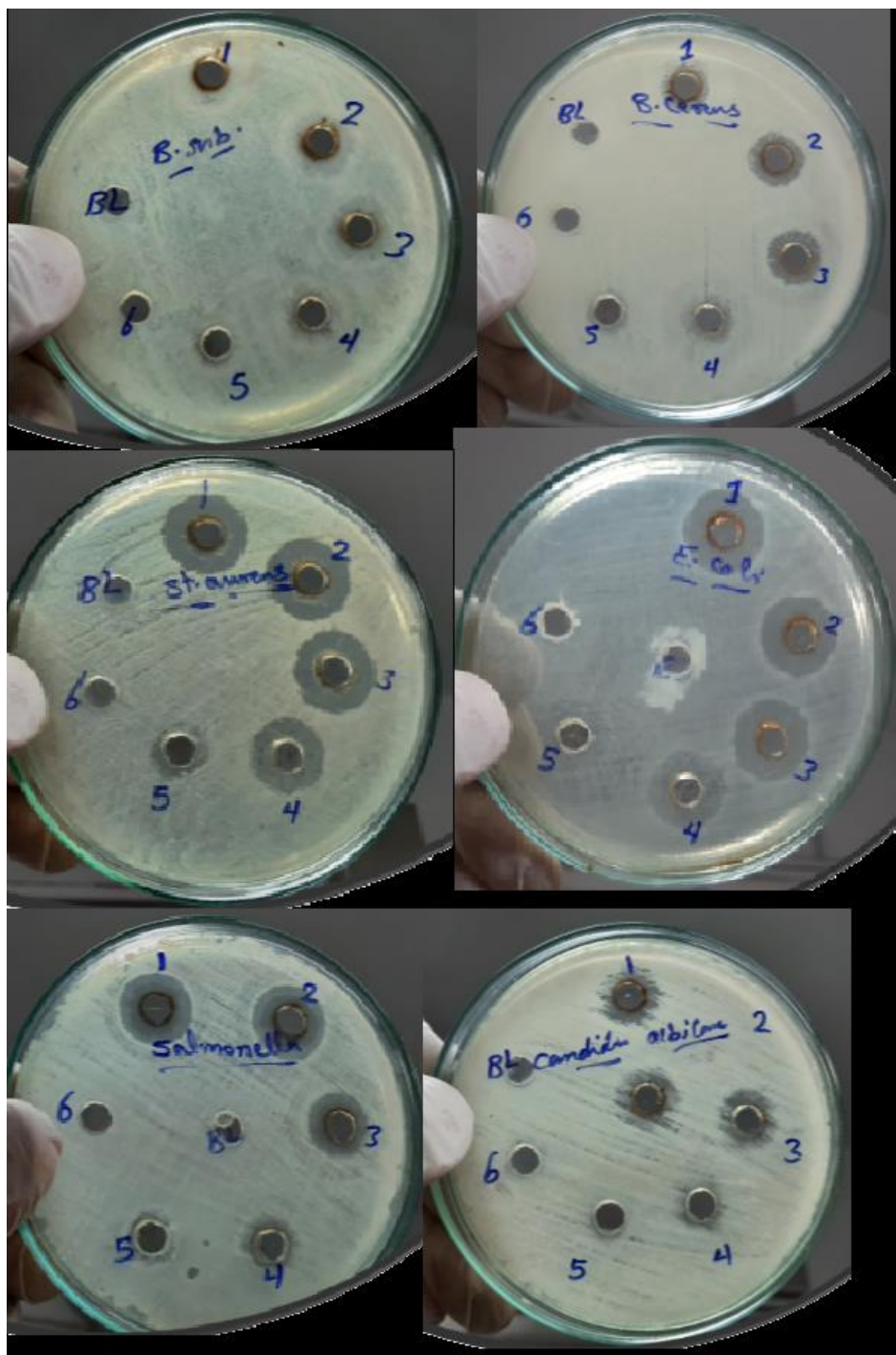


Figure 5-5: Antimicrobial effects of silver nitrate

5.3.4 Discussion

The previous analyzes were conducted to compare the effect of silver nanoparticles, which we prepared using an aqueous extract of St. John's wort, with silver nanoparticles prepared by a chemical method using citrate, silver nitrate, aqueous extract of St. John's wort and some antibiotics. Although half of the concentrations used of AgNPs synthesized using St. John's wort compared with other materials were used due to the little amount of silver nanoparticles at the time of analysis. However, the silver prepared in our way gave a very high efficacy

Chapter 5: Additional Experiments

comparable to silver nitrate alone, and perhaps better than it if we used the same concentrations. Silver nanoparticles prepared by a chemical method using citrate and aqueous extract of St. John's wort did not give any results at the concentrations used. This proves the effectiveness of silver prepared using the aqueous extract of the St. John's wort against a wide range of microbes, and therefore it is a promising material for industry to be used or combined with antibiotics against multiple pathogens.

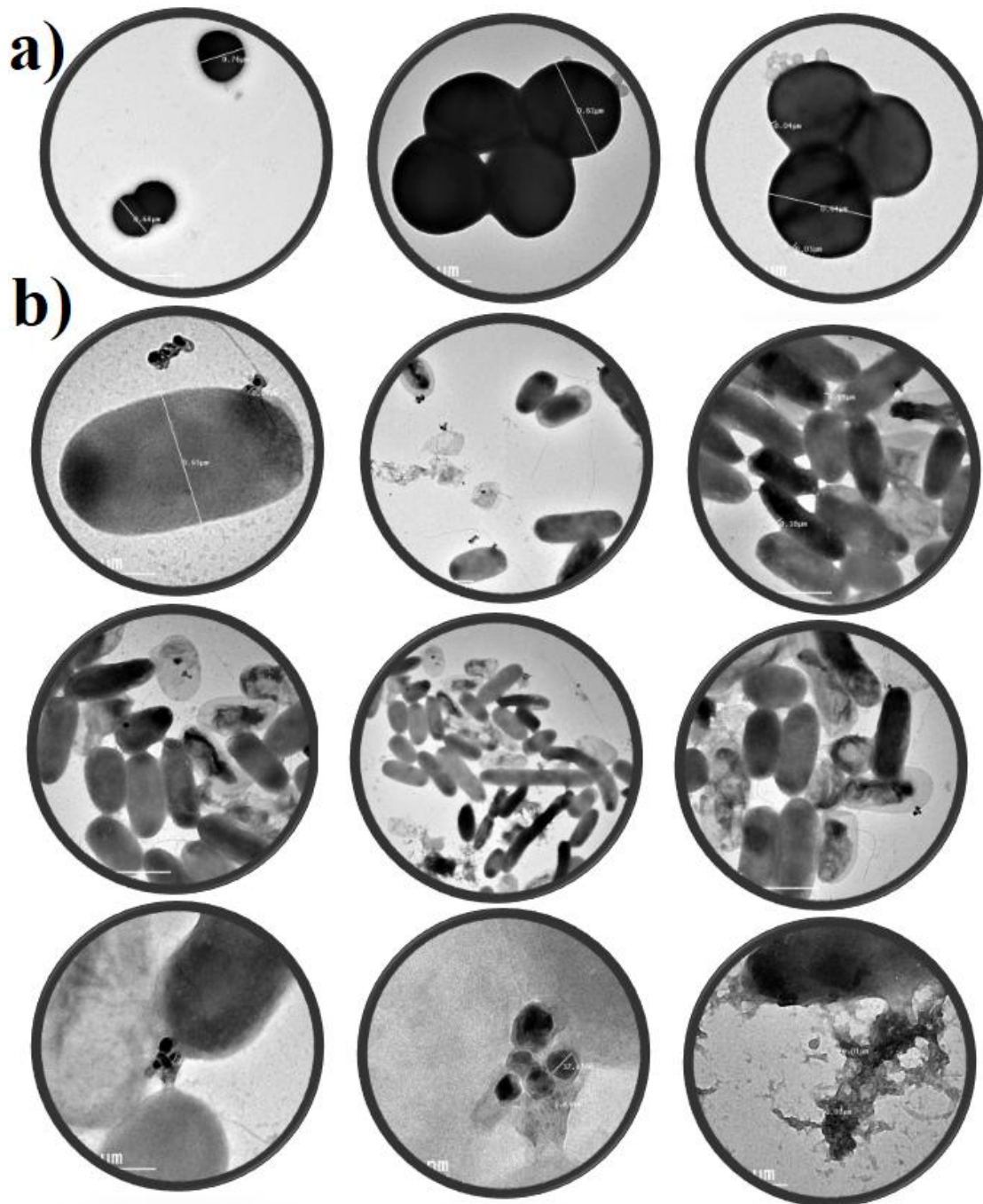


Figure 5-6: Transmission electron microscope (TEM) images of Candida albicans bacteria exposed to silver nanoparticles (AgNPs): A: bacteria only, B: several images of bacteria with AgNPs, where the different stages are illustrated which are nanoparticles attached on the cell wall, extrusion of cytoplasmic contents, AgNPs-loaded cells and a fully lysed cell.

Chapter 5: Additional Experiments

5.4 Effect of green synthesized AgNPs on leishmaniasis

5.4.1 Materials and Methods

5.4.1.1 Leishmania culture

In this work, *L. tropica* Syrian strain (LT_SYR_24) was isolated and typed by PCR at the Dermatology Hospital of Damascus University, Damascus, Syria ⁴. *Leishmania* cells were grown in RPMI-1640 culture medium containing L-glutamine (Sigma, Germany), penicillin/streptomycin 100 U/mL, and 10 % heat-inactivated fetal bovine serum FBS (Cytogen, Germany). A direct counting method by hemocytometer chamber (Neubauer chamber) was performed to estimate the number of *L. tropica* promastigotes. Stationary-phase promastigotes of *L. tropica* were incubated in 96-well microplates (50000 cell/well) with the different concentrations of Ag NPs ($\mu\text{g/mL} = \text{ppm}$) for 24 h at 26 °C.

5.4.1.2 Viability Assay by XTT

XTT is a colorimetric assay method based on the dye tetrazolium used to detect cell viability, where only living cells can metabolize this yellow soluble dye and convert it to orange colored formazan that can be measured at wavelength 450 nm. The viability test was performed for *leishmania* cells (50000 cell/well) treated with Ag NPs in the presence of control untreated cells. 20 μL of XTT mixture (Roche Diagnostics) was added to each well (96-well microplate) and the microplate was incubated for 4 hours at 37 °C, after which the absorbance was read using microplate reader device. Each treatment condition was performed in triplicate and the average values of the absorbance readings for replicates were correlated to the control untreated cells representing 100 % of cell viability.

5.4.1.3 Apoptosis Assay using Annexin V

Annexin V binding assay was performed using sfGFP-Annexin-V as previously described for cultured cell lines ^{5,6}. After treatment with the indicated concentrations of Ag NPs, the cells ($\sim 10^6$ cells) were harvested and centrifuged at 3000 rpm for 10 min. After discarding the supernatant liquid, 500 μL of binding buffer HBS (10 mM Hepes, 150 mM NaCl, 2.5 mM CaCl₂, pH 7.4) and 5 μL sfGFP-Annexin-V (1 mg/mL) were added to the pellets and incubated at 25°C under dark conditions for 5 min. Percentages of apoptotic cells, absorbing Annexin-V, after treatment conditions were identified by flow cytometry.

5.4.1.4 Cell Cycle Assay

Leishmania cells ($\sim 10^6$ cells) were harvested and centrifuged (3000 rpm) for 10 min. 500 μL PBS was added to resuspend the cells. Then 95 % ethanol was added to a final volume of 2 mL, and was stored at 4 °C overnight. The cell sample was centrifuged and washed twice with PBS, then was suspended and stained in 500 μL PBS containing 5 μL Propidium Iodide (PI, 1 mg/mL) for 30 min in the dark. Cell cycle analysis was performed by flow cytometer.

Chapter 5: Additional Experiments

5.4.1.5 Flow Cytometry

PI and/or sfGFP-Annexin-V stained leishmania promastigotes ($\sim 10^6$ cell/mL) were analysed by acquisition on a BD FACS Calibur™ flow cytometer (BD Biosciences) with a 488 nm argon ion laser and a 635 nm red diode laser. The light scatter and fluorescent parameters were set at logarithmic gain, and Leishmania cells were identified according to their characteristic forward and side scatter properties, with 10000 total events per sample acquired. Flow cytometric data acquisition and analysis were conducted by BD Cellquest™ Pro software. Graphs and statistical analysis were achieved using GraphPad Prism 7.0. A probability value less than 0.05 ($p < 0.05$) was considered as statistically significant difference.

5.4.2 Results

5.4.2.1 Cytotoxicity of Ag NPs to *L. tropica* promastigotes

In order to calculate the percentage of apoptotic and alive cells in *L. tropica* promastigotes, flow cytometry assay was employed after staining with Annexin-V. Here, this study showed that the percentages of apoptosis induced in promastigotes exposed to 0.5 $\mu\text{g/mL}$ and 1 $\mu\text{g/mL}$ concentrations of Ag NPs after 24 h incubation were estimated 46.8 % and 86.8 %, respectively. However, the percentage of alive cells in the control group (without treatment) was determined 98% (Fig. 7A). Percentage of apoptotic cells was found to increase in a dose-dependent manner by increasing the concentration of Ag NPs, where the top effect on apoptosis induction was achieved using the concentration of 1 $\mu\text{g/mL}$ after 24 h, whereas IC^{50} was at concentration of 0.43 $\mu\text{g/mL}$ of Ag NPs (Fig. 7B).

5.4.2.2 Effect of Ag NPs on the viability of *L. tropica* promastigotes

Cytotoxicity of Ag NPs against *L. tropica* promastigotes was investigated by optical density (OD) following XTT assay (Fig. 7B). Parasite viability was found to decrease in a dose-dependent manner by increasing the concentration of Ag NPs, where the top toxicity was achieved using the concentration of 0.62 $\mu\text{g/mL}$ after 24 h, whereas IC^{50} was at concentration of 0.29 $\mu\text{g/mL}$ of Ag NPs.

5.4.2.3 Effect of Ag NPs on the cell cycle of *L. tropica* promastigotes

In order to ascertain the effect of Ag NPs on the cell cycle of Leishmania promastigotes, the cells were incubated after treatment with the fluorescent DNA dye propidium iodide, and then the cells were analyzed for their content of genomic DNA by flow cytometry, where it was possible to distinguish between three phases of the cell cycle (G1, S and G2). The results showed that treatment with Ag NPs (0.5 or 1 $\mu\text{g/mL}$) had no effect on the percentage of cells in the G1 phase, while its effect was limited to decrease slightly the percentage of cells in the G2 phase (Fig. 8A). Accurate statistical comparison of the data demonstrated that the ratio of cells in the G1 phase is equal between the control and treated conditions, while showed a significant increase in the percentage of cells in the S phase in the condition treated with 0.5 $\mu\text{g/mL}$ compared to the untreated control cells, and the difference was about 3.3 %. On the other hand, the percentage of cells in the G2 phase decreased 5.4 % in this treated condition compared to the control (Fig. 8B).

Chapter 5: Additional Experiments

5.4.3 Discussion

Leishmaniasis is still widely recognized as one of the major health problems worldwide. The current treatment against leishmaniasis was not satisfactory, and the drugs used (glucantime and pentostam) were not complete options due to high cost, toxicity, painful treatment, many side effects, as well as emergence of drug resistance in some endemic areas. Therefore, researchers are constantly striving to develop and design effective anti-Leishmania agents that can fully achieve treatment goals. In several previous studies, the results showed that silver nanoparticles have anti-leishmanial effect⁷. Mahbali et al. found with 100 ppm (100 µg/mL) of nanosilver can damage 85% of infected macrophages with amastigotes of *L. major*^{8,9}. In this study, the efficacy of different concentrations of Ag NPs against *L. tropica* promastigotes was observed. Clear toxicity was observed for *L. tropica* in the presence of Ag NPs. The results showed that the presence of living parasites decreased significantly by increasing the Ag NPs concentration compared to the standard untreated cells. In other words, Ag NPs completely inhibited the proliferation of *L. tropica* promastigotes after 24 h of treatment. Such toxic effect was explained by apoptosis phenomena rather than clear cell cycle arrest. Many studies reported similar effects of Ag NPs with different microorganisms¹⁰. In this regard, cytotoxic effect of these nanomaterial against bacteria, viruses, fungi and different types of cancer has been examined, and results demonstrated that Ag NPs has satisfactory levels of cytotoxicity effect against these cancers and microorganisms¹¹⁻¹⁴.

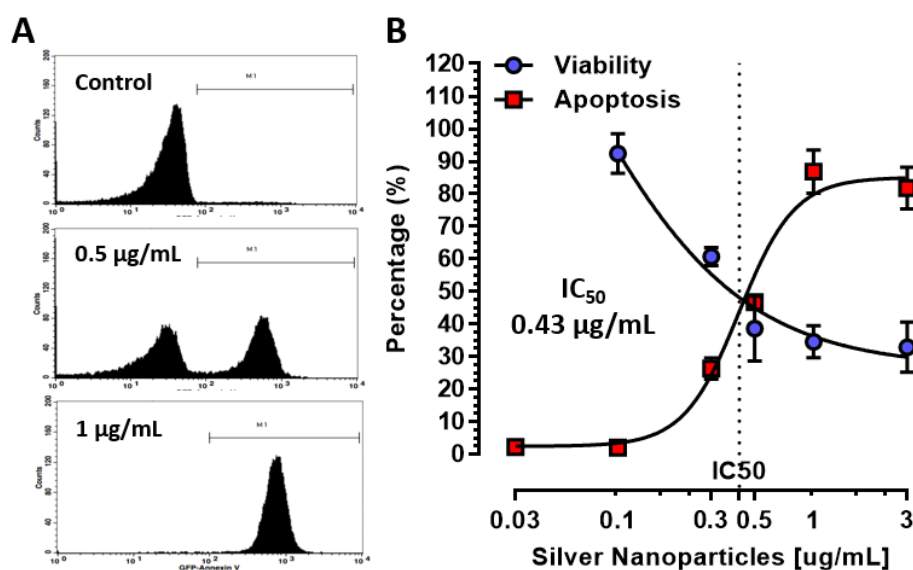


Figure 5-7: Effect of Ag NP on the viability and apoptosis of *L. tropica* cells. (A) *L. tropica* cells in 96-well plate (50000 cell/well) were treated for 24h with 0, 0.5 and 1 µg/mL of Ag NPs then incubated with Annexin V (10 µg/ml) and the increase of their green fluorescence signal was analyzed by flow cytometry. (B) After treatment with the indicated concentrations of Ag NPs (µg/mL), percentage of viable cells was determined using XTT method and values were normalized to control untreated cells. Percentage of apoptotic cells in the population was determined using Annexin V assay.

Chapter 5: Additional Experiments

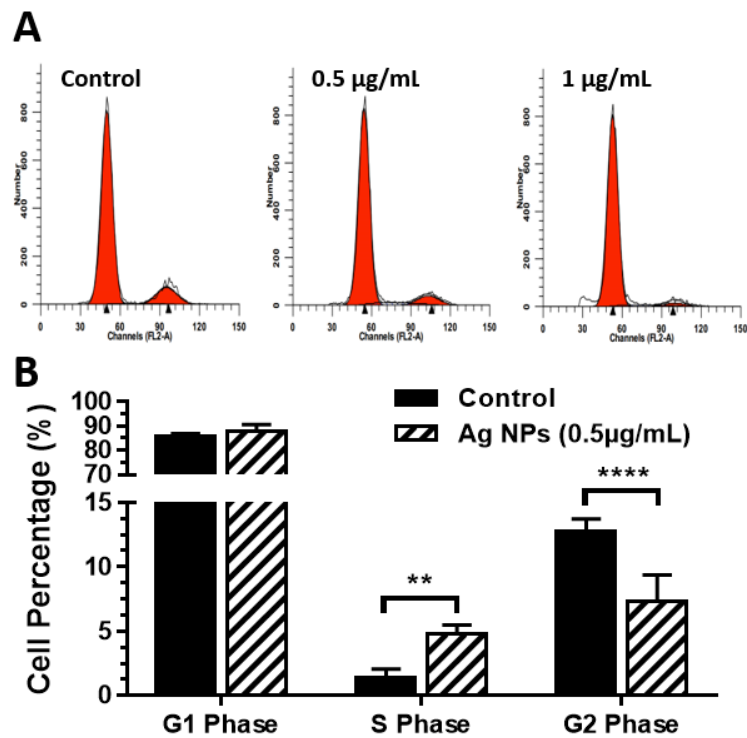


Figure 5-8: Effect of Ag NPs on the cell cycle of *L. tropica* cells. (A) Treated *L. tropica* cells with 0, 0.5 and 1 µg/mL of Ag NPs for 24 h were incubated with propidium iodide and their cell cycle was analyzed by flow cytometry. (B) Statistical comparison of cell populations values at different cell cycle phases between untreated and treated *Leishmania* (0.5 µg/mL of Ag NPs for 24 h), at least 3 experimental replicates were used. Two stars for statistical probability less than and four stars for statistical probability $p < 0.01$ and four stars was used for p values less than 0.0001.

Chapter 5: Additional Experiments

5.5 Development of a protocol to prepare selective thiolate Aptamer-conjugated silver nanoparticles and their effects on healthy and cancerous cells

The conjugation of Aptamers with silver nanoparticles in a controlled manner has been used for many biological purposes like biosensing, imaging and diagnostics and targeted treatment. In the context of cancer therapies aptamers have the ability to specifically bind to antigens expressed on the cancer cell surface-mediated by molecular recognition. But the appropriate surface conjugation strategies are often a prerequisite for every possible application as these interactions ultimately affect the colloidal stability and efficacy of the nanoparticles. Generally, the strategies for conjugation biomolecules or Aptamers to metal nanoparticles fall into four categories ¹⁵:

- Binding of the biomolecule to the surface of the inorganic particle core through ligand mediated binding, commonly by chemisorption, e.g. thiol groups.
- Electrostatic interactions between positively charged biomolecules and negatively charged nanoparticles or vice versa.
- Covalent binding by conjugation chemistry, exploiting functional groups on both particle and biomolecules.
- Non-covalent, affinity-based receptor–ligand systems.

AgNPs have a surface plasmon peak at 400 nm to display yellow color with even higher extinction coefficients. AgNPs are an excellent substrate for surface enhanced Raman spectroscopy (SERS), and possess strong anti-microbial activities. Therefore, DNA-functionalized AgNPs may expand the toolbox of nanotechnology. The lack of work on AgNPs can be attributed to difficulties associated with the preparation of their DNA conjugates ¹⁶. The surface modified silver nanoparticles exhibit improved biocompatibility and intracellular uptake required for drug delivery. The plasmonic nature of noble metal nanoparticles, such as silver, is useful for imaging of the surface of certain cell types or specific areas within individual cells for applications in imaging and cancer therapies. The photodynamic properties of silver nanoparticles may be considered useful in the case of targeted cancer cell or tumor destruction ^{15, 17}.

Because the functional group at the surface of silver nanoparticles are hydroxyl groups (most of the compounds in the St. John's wort are phenols), So silver nanoparticles cant conjugate with amine-modified aptamer through EDC/NHS carbodiimide chemistry (EDC/NHS coupling chemistry). EDC/NHS coupling chemistry is commonly used to alter the surface chemistry of NPs with biological molecules to reduce their toxicity. EDC is a water-soluble cross-linker agent, which activates carboxyl groups and forms an amine-reactive O-acylisourea intermediate that spontaneously reacts with primary amines to form an amide bond ^{18, 19}. One of the important strategies that have been developed to attach aptamer to metal surfaces is Sulfhydryl-Aptamer metal Coordination. The strength of the thiol–metal coordination interaction provides the basis to fabricate robust self-assembled monolayers for diverse applications. The attachment of thiolated nucleic acids to metal nanoparticles has enabled many milestone achievements in nanobiotechnology. But the immobilization of thiolated Aptamers (aptamer, after 5- thiol or 3-thiol modification) on the surface of metal nanoparticles such as

Chapter 5: Additional Experiments

gold and silver is not as easy as we think because both have a negative charge on their surface. Initially, the conjugation of gold with thiolated aptamer was studied, and to overcome the charge repulsion problem, salts such as sodium chloride were added. But adding high concentrations of salt causes the gold nanoparticles to agglomerate before the aptamer coupling with it. To solve this problem, salt was added gradually over several days and this method was called salt-aging. This protocol has not been successful with silver nanoparticles by other researchers. Other methods have been developed by other researchers to overcome this problem in silver, such as using modified DNA with more thiol groups to better achieve DNA attachment and coating AgNPs surface with a monolayer of gold or polymer, but it was expensive and ineffective¹⁹⁻²¹.

Used Aptamer

The aptamer (S15-Thiol) used in this thesis was purchased from Integrated DNA Technologies (IDT) with the following properties:

Sequence: 5'-5ThioMC6-D/ACG CTC GGA TGC CAC TAC AGG CTA TCT TAT GGA AAT TTC GTG TAG GGT TTG GTG TGG CGG GGC TAC TCA TGG ACG TGC TGG TGA C -3'

DNA Bases: 85 Molecular Weight: 26728.5 Extinction Coefficient: 805700 l/(mole.cm)

Thiol-modified oligos ordered from IDT are shipped in their oxidized form, with the sulfur atoms protected by an S=S bond. Thus, Thiol-modified oligos need to be reduced before use. Thiol-modified oligos require a reduction step to remove the protecting group from oligos before they are used. One of these ways is to use Tris (2-carboxyethyl) phosphine (TCEP). An excess concentration of TCEP.HCl (10 mM), dissolved in deionized water, was added to the aptamers (100 μ M). The mixture was stirred at a slow pace for two hours at room temperature. The aptamers could then be used without the need to remove the TCEP from the mixture.

5.5.1 Experimental

5.5.1.1 Preparation of DNA-AgNPs

1) 500 μ L of AgNPs (20-50 nm, 0.11 nM) and 2.5 μ L of Aptamers (100 μ M) were mixed and stirred vigorously for 16 hours in the dark. 5 μ l citrate buffer (500 mM, pH 3) was added and after 10 minutes, another 5 ml was added. After 30 minutes, HEPES buffer (500 mM, pH 7.6) is added in 3 successive batches, the time between them is 5 minutes. The sample is centrifuged as follows: 5 minutes at 3000 rpm, 5 minutes at 6000 rpm and 20 minutes at 13000 rpm. The filtrate is separated from the sediment, where 500 μ l of HEPES buffer (5 mM, pH 7.6) is added to the sediment, and the previous centrifugation process is repeated. The washing process is repeated at least 3 times to get rid of all the amount of unbound aptamers. Finally, the resulting Aptamer-AgNPs dissolved in deionized water or in HEPES buffer (5 mM, pH 7.6) and the supernatants resulting from the centrifugation for the first time and for all later washing operations are concentrated to a volume of 500 μ l or 1 ml using a rotary evaporator to measure the concentration of the free aptamer (unbound). Thus, through it, we can determine the amount of the attached Aptamer at the surface of AgNPs.

Chapter 5: Additional Experiments

The purpose of adding the citrate buffer (500 mM, pH 3) is to reduce the PH of the solution, as well as obtain a low concentration of salts (sodium ions), all in order to facilitate the binding of the aptamers on the surfaces of silver nanoparticles. Because at PH=3, the charge density of the AgNPs will be reduced and some of the DNA bases such as adenine and cytosine will be protonated, thus charge repulsion between DNA and AgNPs and among DNA strands will be significantly reduced. Because a little concentration of Na⁺ is still required since both AgNPs and DNA were still negatively charged even at pH 3. Reducing the pH by adding citrate buffer (500 mM, pH 3) was done in stages and not all at once because if the pH was lowered all at once, it would cause agglomeration of silver nanoparticles without binding with the aptamer. To determine the best pH value for the conjugation, different pH values (1, 3, 4, 5, 7 and 9) of citrate buffer were used. The purpose of adding the HEPES buffer (500 mM, pH 7.6) is to return the pH value of the solution to almost 7 after its binding with the aptamer.

- Other factors were also changed, such as the concentration of silver nanoparticles (0.11, 0.14, 0.3 and 0.5 nM) and incubation time (30 min, 60 min 16 hrs, 24 hrs and 48 hrs) to get the best conditions for attached thiolated Aptamer on the surface of AgNPs via the silver–sulfur bond (thiol–Ag linkage).

2) Thiolated Aptamer samples were used as received without further treatment (i.e. no TCEP or DTT treatment). In a typical experiment, Thiolated Aptamer (100 μM, 2.5 μL) was mixed with AgNPs (20-50 nm, 0.5 nM, 500μL) in a microcentrifuge tube (lower protein binding). The mixture was then placed in a laboratory freezer (set at -20 °C) for 2 h, followed by thawing at room temperature. Finally, the mixture was centrifuged and washed as described in the previous protocol.

- Different factors were studied such as concentration of AgNPs (0.11, 0.14 and 0.5 nM), Freezing degree (-20 and -80), Freezing time (2 h and 24 h).

5.5.1.2 Quantification of DNA loading density

1) To quantify the number of DNA strands attached to each AgNPs. Concentrated supernatants measured using UV-vis spectrometry, where calibration stock Aptamer solution was prepared by dissolving the DNA in a buffer or Milli-Q water. The DNA solution was then diluted to 1 and 0.5 μM in a used buffer or Milli-Q water to measure the actual DNA concentration using UV-vis spectrometry.

2) Using Quant-iT™ OliGreen® ssDNA Kit (Cat. no. 011492): supernatants containing free aptamers also contain phenols that have separated from the capping agent layer on the surfaces of AgNPs. These compounds absorb UV at 230-240 nm and this peak overlaps with the aptamer peak at 260 nm. Therefore, the previous method is considered unacceptable and does not give the correct reading for calculating the concentration of the aptamer. This is what prompted us to search for an accurate method for quantifying single-stranded DNA in supernatants. the Quant-iT™ OliGreen® ssDNA reagent is an ultrasensitive fluorescent nucleic acid stain for quantifying single-stranded DNA (ssDNA) in solution and enables quantifying as little as 100 pg/mL ssDNA with a standard spectrofluorometer and fluorescein excitation and emission wavelengths.

Chapter 5: Additional Experiments

- The Quant-iT™ OliGreen® reagent solution was prepared by diluting to a ratio of 1/1000 using HEPES buffer (5 mM, pH 7.6). For a standard curve, different concentrations of purely used aptamer were prepared in the same buffer. 3 samples from each supernatant were used. An equal volume from samples and the prepared standard with the reagent were mixed well and incubated for 2 to 5 minutes at room temperature, protected from light. Equal volumes of all previous samples plated in 96-well black microplates with Light Blocking Flat-Bottom and then fluorescence measured using a fluorescence microplate reader and standard fluorescein wavelengths (excitation ~480 nm, emission ~520 nm).

5.5.1.3 Characterization of DNA-AgNPs

5.5.1.3.1 DLS and Zeta potential

Dynamic Light Scattering (DLS) measures the Hydrodynamic Diameter of nanoparticles or the Brownian motion in a dispersion. Hydrodynamic diameter is the size of a hypothetical sphere that diffuses at the same rate as that of the particle being measured²². By measuring the hydrodynamic diameters of AgNPs and Aptamer-Conjugated AgNPs it can confirm the attaching of aptamers on the nanoparticle surfaces. Before measuring the hydrodynamic diameter, the concentrations of all samples were adjusted to be of the same absorbance value using a UV-VIS spectrophotometer (NanoDrop 2000), then the hydrodynamic diameter was measured using Litesizer™ 500 from Anton Paar and the conditions were Solvent: water, temperature: 27°C and refraction index: (Ag) 0.135.

5.5.1.3.2 Zeta potential

On the surfaces of nanoparticles in a colloidal solution there are two layers of opposite ions, one of which is called surface potential and the other is called Stern potential. The electric potential at the edge of the double layer is the zeta potential, whose value plays an important role in stabilizing the nanoparticles in the colloidal solution²³.

5.5.1.3.3 Fourier transform infrared spectroscopy – attenuated total reflectance (FTIR-ATR)

Infrared (IR) spectroscopy is an analytical instrument used to analyze samples in the form of liquid, gas and solid which measure absorbance or transmittance on the y-axis and wavelength or frequency on the x-axis. The electromagnetic spectrum of infrared radiation consists of three regions, near, medium and far-infrared. Near-IR (12820-4000 cm⁻¹) is suitable for quantitative analysis, mid-IR (400-4000 cm⁻¹) gives information about different functional groups, which is very helpful in organic chemistry and Far-IR (33-400 cm⁻¹), which is used to measure the vibrations of molecules with heavy atoms²⁴. Ag2S were used to compare and all samples were concentrated. The device used is Vertex 80V from BRUKER and the conditions were Pressure: under vacuum (~1 hPa), Spectrum range: 50-650 cm⁻¹, Method: ATR, Platinum, Diamond, Type: A 225/QHP, Resolution: 2 cm⁻¹ and Scans: 8.

5.5.1.3.4 Gel Electrophoresis

Gel electrophoresis is a method used to separate a mixed population of DNA or proteins in a polyacrylamide or agarose matrix. Agarose gel is used to separate larger macromolecules such as nucleic acids, while polyacrylamide is normally used for protein separation. The molecules

Chapter 5: Additional Experiments

are separated by their sizes and charges when an electric field is applied through the matrix²⁵. The most commonly used buffers for gel electrophoresis are TAE (TRIS-Acetate-EDTA) and TBE (TRIS-Borate-EDTA), which exhibit good conductivity. EDTA in the buffer works as a chelating agent that isolates divalent ions. In order to visualize the nucleic acids in the gel, dyes are used and the gel is illuminated with UV light.

1 g of Agarose standard was solved in 100 ml Tris Acetate EDTA (TAE) solution. The mixture was microwaved for 3 mins. Afterward, the solution was constantly stirred while cooling down. The gel was put into the tray used for the electrophoresis and then covered with around 700 ml of TAE solution. 15 μ l of samples mixed with 5 μ l of GreenGoTaq were then loaded into the wells in the gel. The electrophoresis was carried out for around 20-35 mins at 100 V.

5.5.1.4 Cell Culture and evaluation of In Vitro Cytotoxicity effects

Normal human bronchial epithelial BEAS2B cells and Human NSCLC A549 were purchased from (CLS Cell Lines Service GmbH, Eppelheim, Germany) and cultured in Dulbecco's modified Eagle medium (DMEM) (Merck KGaA, Darmstadt, Germany) supplemented with 10% fetal calf serum (FCS) (Merck KGaA, Darmstadt, Germany) and 1% penicillin-streptomycin (PS). Cells were incubated and maintained at 37° C in a 5% CO₂ humidified atmosphere. The cells were sub-cultivated, when the confluence reached almost 80%. The number of cells was calculated employing hemocytometer and suspended trypsinized cells. For Cell Titer Blue (CTB, Promega, Germany) cell viability test, cell suspension with concentration of 8×10^4 cell/mL was prepared and 100 μ L of suspension was added to every well of the 96-well plate (VWR, Hannover, Germany), corresponding to 8000 cells per well. Plates were incubated at cell culture conditions as stated above for 24 h, then the medium was removed from wells and 100 μ L of different concentrations (0, 1.13, 4.5, 18 and 80 μ g/mL for A549 cells and 0, 5, 10, 27 and 93 μ g/mL) of Aptamer-conjugated AgNPs dispersed in medium were added (three replicates per concentration). The control contained no AgNPs. Plates were incubated at the same conditions as stated above for cell culture for 0, 3, 6, and 24 h for both cells. After the incubation time specified for each sample, the medium was removed, then 100 μ L of prepared CTB solution (Promega, Cat. Number G8080, Walldorf, Germany) (1:10 (v/v) in basal medium) was added into every well, in order to evaluate cell viability (metabolic activity and relative cell number). As blank for the measurement, three completely empty wells were filled with Cell Titer Blue prepared solution, then the plates were incubated under the same conditions mentioned previously for one hour. Current fluorescence was measured in every well in the plates using a microplate fluorometer (544Ex/590Em) (Fluoroskan Ascent, Thermo Electron Corp, Waltham, MA, USA). The fluorescence of blank was subtracted from the fluorescence of every concentration then relative cell viability was expressed as a percentage to positive control. The relative cell viability for every sample was commensurate with values of fluorescence and was calculated according to the following formula: Relative cell viability (%) = [(Fluorescence of sample - Blank) / (Fluorescence of control - Blank)] \times 100

Origin (Version 2021) was used to calculate the half-maximal inhibitory value (IC₅₀).

5.5.1.5 Cell viability analysis using calcein-AM and Propidium Iodide (PI)

A549 and BEAS-2B cells were cultured in a 96-well plate (about 8000 cells in every well) and incubated overnight. the medium was removed and Aptamer-AgNPs with various

Chapter 5: Additional Experiments

concentrations (60, 30, 15, 7.5 and 3.7 $\mu\text{g/ml}$) was added (volume 100 μl every well, With not forgetting the control for healthy cells and cancer cells, where their medium was added in wells) and incubated for 8 hours. the solutions from the wells were removed and mixed dye (calcein-AM and Propidium Iodide) solution (2 $\mu\text{g/ml}$) was added. after 10 min incubation, stained cells were imaged using a fluorescence microscope (Olympus Ix50) equipped with an Olympus camera (SC30, Japan) was used to capture the images of cells with CellSens Standard (Olympus Co. Japan) software (Excitation filter: BPxxx–xxx, barrier filter: BAxxx) and Scale bar 50 μm .

5.5.1.6 Cell death: flow cytometric analysis

The cell death events and types of cell populations (normal or dying cells) were studied after treatment of A549 and BEAS-2B cells with Aptamer-conjugated silver nanoparticles. The assay uses Annexin V–fluorescein isothiocyanate (FITC) and PI to identify phosphatidyl serine sites on the membrane of apoptotic cells, as well as sites of membrane damage in necrotic cells, respectively. Therefore, this assay measured two parameters: whether the cells have affinity first to Annexin V-FITC and secondly whether the cells have an affinity to PI. The assay gave an overview of the cell population based on their respective affinities: apoptotic cells (Annexin V-FITC positive and PI negative or positive for both Annexin V-FITC and PI), necrotic cells (Annexin V-FITC negative and PI positive) and viable cells (Annexin V-FITC negative and PI negative). 24 well plate was used to culture A549 and BEAS-2B cells because analysis needs at least 30000 cells for every concentration. After incubation of A549 and BEAS-2B cells for 3h with Aptamer-conjugated silver nanoparticles (5 concentrations for each cell type: 60, 30, 15, 7.5 and 3.7 $\mu\text{g/ml}$ for A549 and 67, 38, 19, 12 and 6 $\mu\text{g/ml}$ for BEAS-2B cells in addition to the control), cells were trypsinized, sedimented and resuspended in binding buffer (every sample in 100 μL binding buffer). four microliters each of the Annexin V–FITC and PI reagents were added, and the tubes were thoroughly mixed and incubated for 10 minutes at room temperature in the dark. Within 1 hour, flow cytometric analysis was done. A 488 nm wavelength laser was used for excitation. early-stage apoptosis (Annexin V) was detected in FL-1 using a 525/30 BP filter while Late-stage apoptosis and necrosis (PI) was detected in FL-2 using a 575/30 BP filter. Using single-stained and unstained cells, standard compensation was done in the Quanta SC MPL Analysis software (Beckman Coulter).

5.5.1.7 Cellular uptake of aptamer-coated Ag NPs

A549 cells and BEAS-2B cells were separately incubated with serial concentrations of aptamer-coated AgNPs for 0, 3, 6 and 24 hours at 37 C. After the specified incubation period, the cells were washed two times with PBS, trypsinized and concentrated HNO₃ was added over the night at room temperature. finally, Analysis of cellular silver content for every well was performed using atomic absorption spectrometry (AAS). All analyses were performed in at least three replicates.

5.5.2 Result and Discussion

The aim of this work was to evaluate the conjugation of thiolated aptamer on the surface of green synthesized silver nanoparticles using *Hypericum perforatum L.* aqueous extract, then study the effect of the resulting conjugated AgNPs on cancer cells (A549 cells) and healthy cells (BEAS-2B cells), In order to prove that the aptamer did not lose its effectiveness during

Chapter 5: Additional Experiments

the conjugation process and at the same time study the toxicity effect of silver nanoparticles prepared by the green method using the aqueous extract of the *Hypericum perforatum L.* plant on cells, whether they were healthy or cancerous. This work will constitute an excellent qualitative leap in the field of targeted therapy because here we do not need additional processes to load the drug onto the nanoparticles, and at the same time we do not need many complications to know the percentage of drug liberation from these nanoparticles when placed on the surface or penetrating the cancer cells.

5.5.2.1 DLS and Zeta

The hydrodynamic diameters were measured for silver nanoparticles and all experimental samples in HEPES buffer. Through the results of hydrodynamic diameter and zeta potential, we note that the best conditions for conjugation in the first protocol used were the use of nanosilver with a concentration of 0.11 nM and the pH value of the medium is 3 or 4 (the results are close).

Table 5-14: the best samples were prepared by changing the different conditions

Sample Nr.	hydrodynamic diameter (nm)	Zeta (mV)	Apt/particle	Ratio %
1	110	-36	1727	36
2	113	-34	79	4
3	103	-36	1781	37
4	114	-38	1127	24
5	167	-25	546	7.8
6	103	-37	1930	40
7	107	-36	1726	36

The first protocol: (1- AgNPs: 0.11 nM, PH: 3 and mix all night. 2- AgNPs: 0.11 nM, PH: 3 and mixing just one hour. 3- AgNPs: 0.11 nM, PH: 4 and mix all night. 4- AgNPs: 0.11 nM, PH: 3 and mix all night with thermomixer). Second protocol: (5- AgNPs: 0.11 nM, freezing all night at -20 °C. 6- AgNPs: 0.5 nM, freezing all night at -20 °C and 7- AgNPs: 0.5 nM, freezing all night at -80 °C).

The hydrodynamic diameter of AgNPs in HEPES buffer was 101 nm and zeta potential -19.4 mV. We note that the value of the hydrodynamic diameter and the zeta potential of the nanoparticles increases when they are bonded with the aptamer, and this result is expected and logical as a result of the aptamer attachment on the surfaces of these nanoparticles. But by comparing the best results in the previous table, we find that sample No. 6 is the best for us because it gives a high conjugation rate and does not have aggregation and the resulting concentration is sufficient to prepare suitable quantities for subsequent analyzes (toxicity effects).

5.5.2.2 UV-VIS Spectroscopy

Through the figure 9, we notice that the peaks of the spectrum did not change much (slight shift of 1 to 5 nm) when they are attached with the aptamer, and this indicates that the conjugation was successful in most of the conditions followed and that the silver particles with

Chapter 5: Additional Experiments

the aptamer did not aggregate or precipitate in the solution, otherwise, we would have noticed this by shifting the tops significantly or the emergence of shoulders.

5.5.2.3 Infrared Spectroscopy

To prove the conjugation between the aptamer and AgNPs was achieved successfully, the FTIR-ATR spectra of Ag₂S, AgNPs and the aptamer-modified AgNPs conjugated for the different samples were carried out (Figure 10). As shown in the previous figure Ag₂S has 3 distinct peaks in the infrared spectrum at around 150, 350, and 600 cm⁻¹. Free AgNPs do not exhibit all of these peaks, specifically the two latter peaks. On the other hand, the spectra of the conjugates can be correlated to that of Ag₂S. The peak at 600 cm⁻¹ corresponds to the peak on the spectra from the report ²⁶, which states that this peak characterizes the vibration of Ag-S. This result implies that a silver-sulfide bond between the aptamers and silver nanoparticles was achieved during the conjugation. In comparison to this spectrum, that of However, on the spectra of the conjugates, the peak at 600 cm⁻¹ is slightly shifted and there is a second peak at around 530 cm⁻¹. It could be assumed that the peaks were the results of the interactions between AgNPs and aptamers.

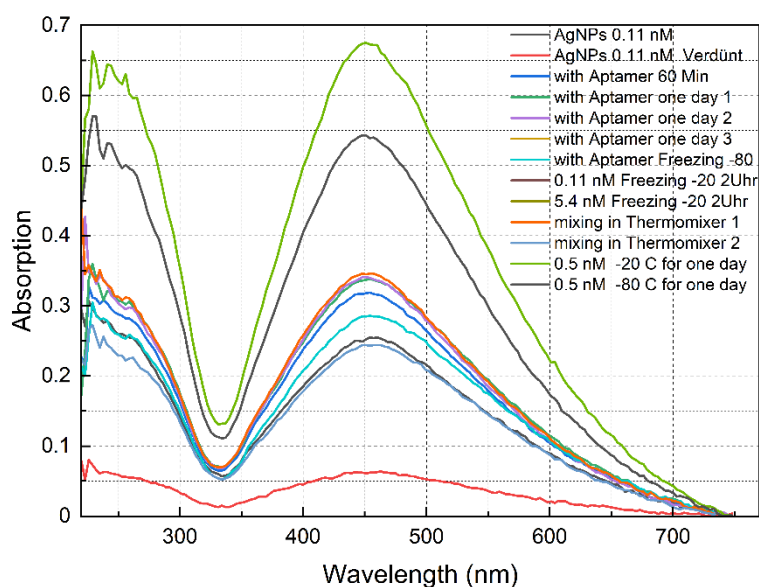


Figure 5-9: UV-vis spectra of just AgNPs, Aptamer attached AgNPs at different condition conjugation.

Chapter 5: Additional Experiments

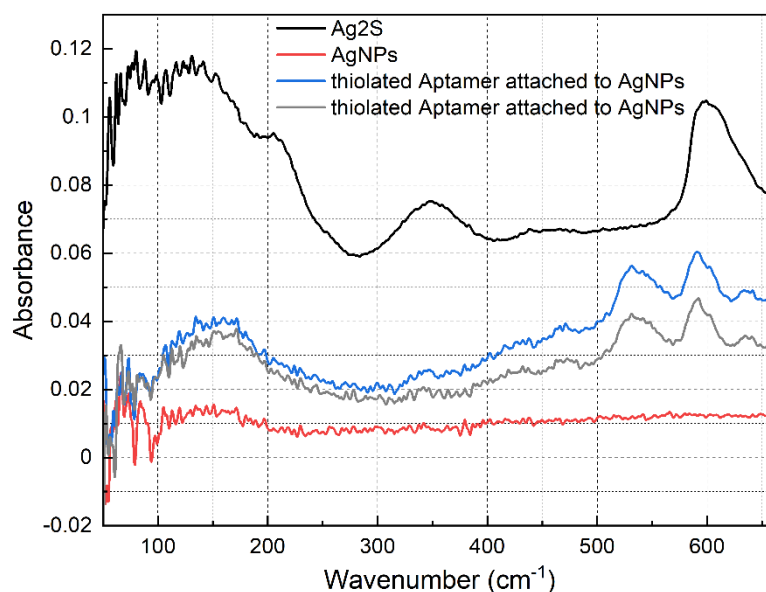


Figure 5-10: IR-spectra of AgNPs, Ag₂S and two examples of aptamer-modified AgNPs.

5.5.2.4 Gel Electrophoresis

Gel electrophoresis is a procedure for isolation and analyzing proteins, RNA and DNA according to their molecular weight and charge. The bigger or longer the particles are, the lower their ability to migrate through the gel. As shown in Figure 11, if the aptamers were attached on the surface of silver nanoparticles, they would be larger and travel shorter than pure aptamers, so exhibiting a shift in their band positions and less brightness than the pure Aptamer.

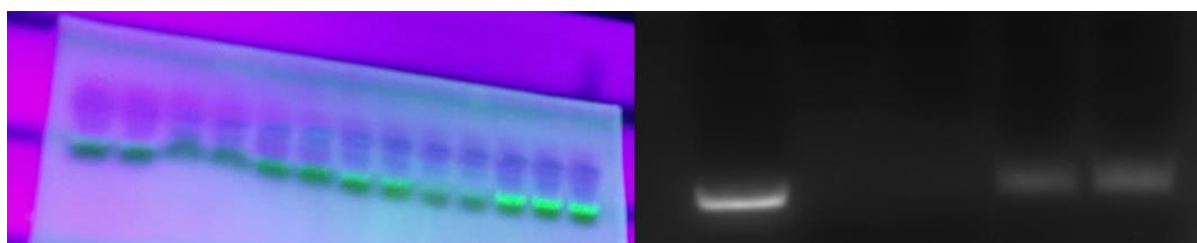


Figure 5-11: Agarose gel electrophoresis analysis of AgNPs-attached aptamer produced using various conditions in addition to a pure aptamer. It is clearly shown that pure aptamer gives high brightness compared to samples with silver.

5.5.2.5 Determination of Time- and Dose-Dependent Cytotoxicity of Aptamer-conjugated AgNPs

In CTB test for the evaluation of the cell viability, viable cells turn blue resazurin into pink resorufin generating a fluorescent signal, while nonviable cells cannot do that because they lost their metabolic activity. Both, the influence of exposure time, and Aptamer-conjugated AgNPs dose were studied. The time ranged between 0, 3, 6 and 24 h, and the dose range of Aptamer-conjugated AgNPs was between 1.13 μg and 90 $\mu\text{g}/\text{mL}$. The range of viability observed for A549 cells and BEAS2B cells are shown in Figure 12. In fact, as shown in Figure 12, due to the presence of aptamers on the surface of silver nanoparticles that have a high selectivity for A549 cancer cells, it notice that AgNPs, from the first moments of incubation, affected cancer

Chapter 5: Additional Experiments

cells significantly, as the value of half-maximal inhibitory concentration 6. As is known, the viability of cells decreases with increasing concentration and exposure time, as we note that the value of IC₅₀ decreased by half after only 24 hours. While for healthy cells at time 0, no difference was observed in cell viability, but with the increase in exposure time, the effect appeared, but it remained very low compared to the effect on cancer cells. These promising results could constitute the nucleus of a scientific leap in the field of selective medicine, because usually we need to load the drug with the aptamer on the surfaces of the nanoparticles, but in our case this silver alone is capable of killing cancer cells without resorting to additional complex processes to load the drug in addition to the aptamer on the surfaces of the nanoparticles, which their function is only to transport the drug.

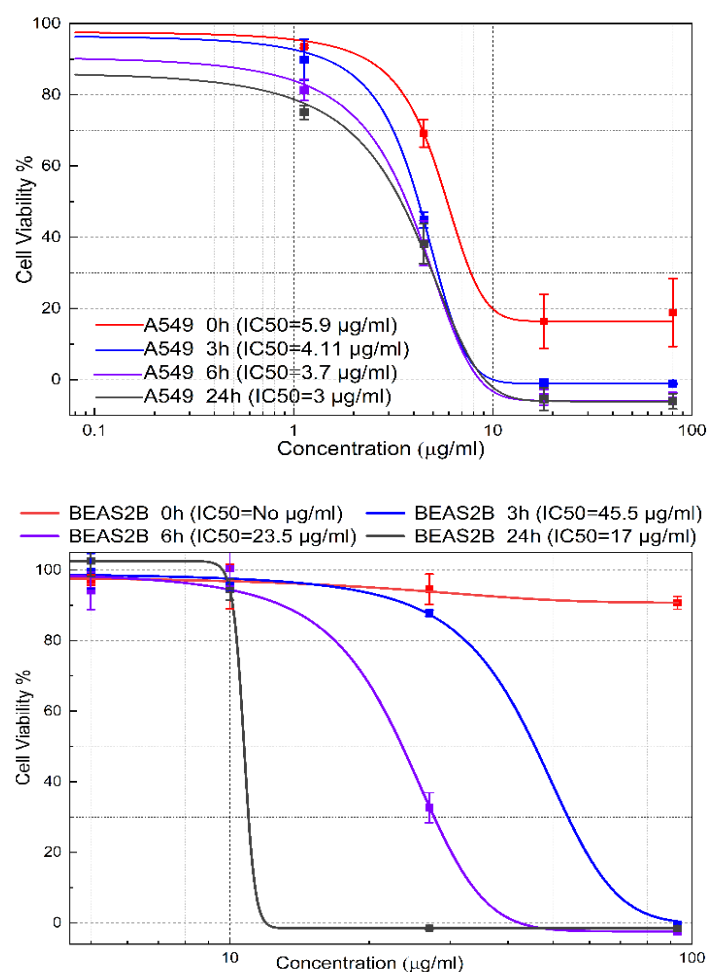


Figure 5-12: Relative cell viability (%) of A549 cells and BEAS-2B cells as a function of AgNPs concentration for 0, 3, 6, and 24 h determined by cell titer-blue cytotoxicity assay. The experiments were performed with three replicates and the standard deviation was calculated.

Chapter 5: Additional Experiments

5.5.2.6 Cell viability analysis using calcein-AM and Propidium Iodide (PI)

Calcein-AM is the acetomethoxy form of calcein, a highly lipophilic, cell membrane permeable dye. Intracellular esterase converts the non-fluorescent Calcein-AM to the highly fluorescent calcein, which is retained within live cells and produces an intense green fluorescence. The DNA-binding agent Propidium Iodide is cell membrane impermeable and only enters dead cells or those with damaged cell membranes. Intracellular PI binds DNA and undergoes an approximate 40-fold enhancement in fluorescence intensity. As a result, live cells will produce a strong green fluorescence resulting from the conversion of Calcein-AM to calcein, while dead cells produce a strong red fluorescence due to the presence of Propidium Iodide. As shown in fluorescence microscope images of A549 adenocarcinoma lung cancer cells and BEAS-2B cells treated with S15 aptamer–AgNPs conjugates after 8 h of incubation. Cells were stained with calcein-AM (green) which detects enzymatic activity in live cells and propidium iodide (red) which detects dead cells with compromised membranes. As shown in Figure 13, compared with BEAS-2B cells, Aptamer-AgNPs demonstrated high inhibition against tumor cells (A549). Besides, Aptamer-AgNPs exhibited enhanced therapeutic effects on cancer cells, suggesting a high cytotoxic effect at low concentrations. Moreover, Aptamer-AgNPs under the same conditions exhibited relatively low cytotoxicity against BEAS-2B. This result may be attributed to the high selectivity of the aptamer present on the surfaces of silver nanoparticles, which leads these particles immediately to the surfaces of cancer cells and then enters them and destroys them. Overall, Aptamer conjugated silver nanoparticles can be efficiently used as a targeting therapy for A549 tumors ²⁷.

Chapter 5: Additional Experiments

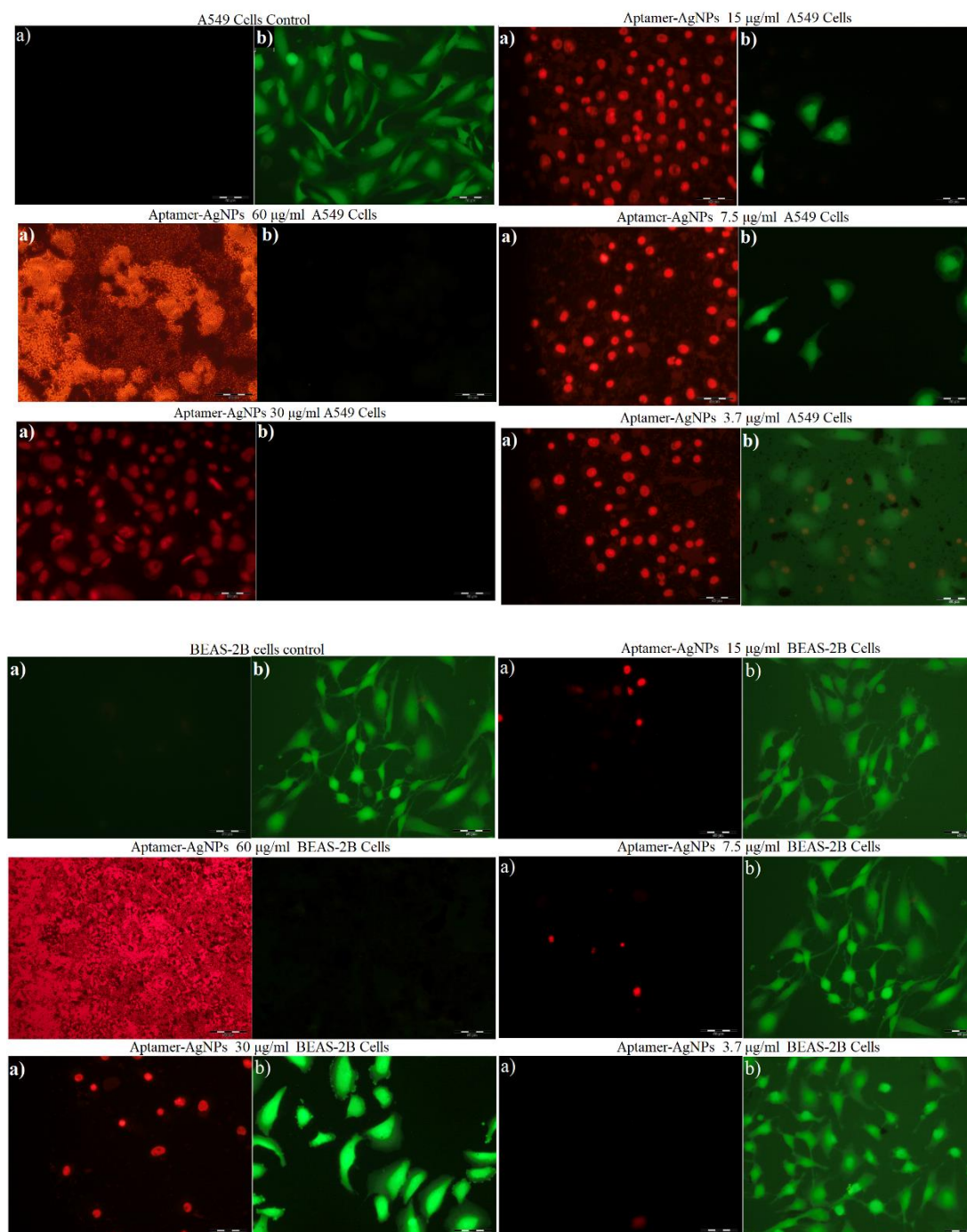


Figure 5-13: fluorescence images of calcein-AM (green) and propidium iodide (red) stained human A549 non-small cell lung carcinoma cells and normal human bronchial epithelial BEAS2B cells which served as normal non-target cells, before and after Aptamer-AgNPs treatment.

5.5.2.7 Percentages of cell populations (live, early apoptosis and late apoptosis (necrosis)) after treatment of A549 cells and BEAS-2B cells with Aptamer-conjugated silver nanoparticles

In order to further understand the mechanisms of cellular damage seen in both cell lines, a flow cytometry test was carried out. Treated and damaged cells for two used types were stained with PI for necrosis and Annexin V for apoptosis. A549 cells and BEAS-2B cells were treated for just 3h with Aptamer conjugated AgNPs and after that, late apoptotic, necrotic and live cells

Chapter 5: Additional Experiments

were then quantified using flow cytometry. Flow cytometric analysis revealed that the majority of both cells (A549 and BEAS-2B cells) in the untreated control were viable, as they stained negative for both Annexin V and PI (figure 14-18). In BEAS-2B cells, the dose-dependent effect of Ag NPs on cell viability (Fig 16-18) was similar to that detected by the CTB assay, and dose-dependent increase in necrosis/late apoptosis at high concentrations 67 and 38 $\mu\text{g/ml}$ Ag NPs (Fig. 14), whereas a slight increase in early apoptosis was detected at lower concentrations. there was a slight reduction in living cells at the concentrations 6 and 12 $\mu\text{g/ml}$ and a slight increase in early apoptotic cells compared to control, whereas a big reduction in living cells at the very high concentrations 67 and 38 and 19 mg/ml and a big increase in necrotic cell populations (positive for PI).

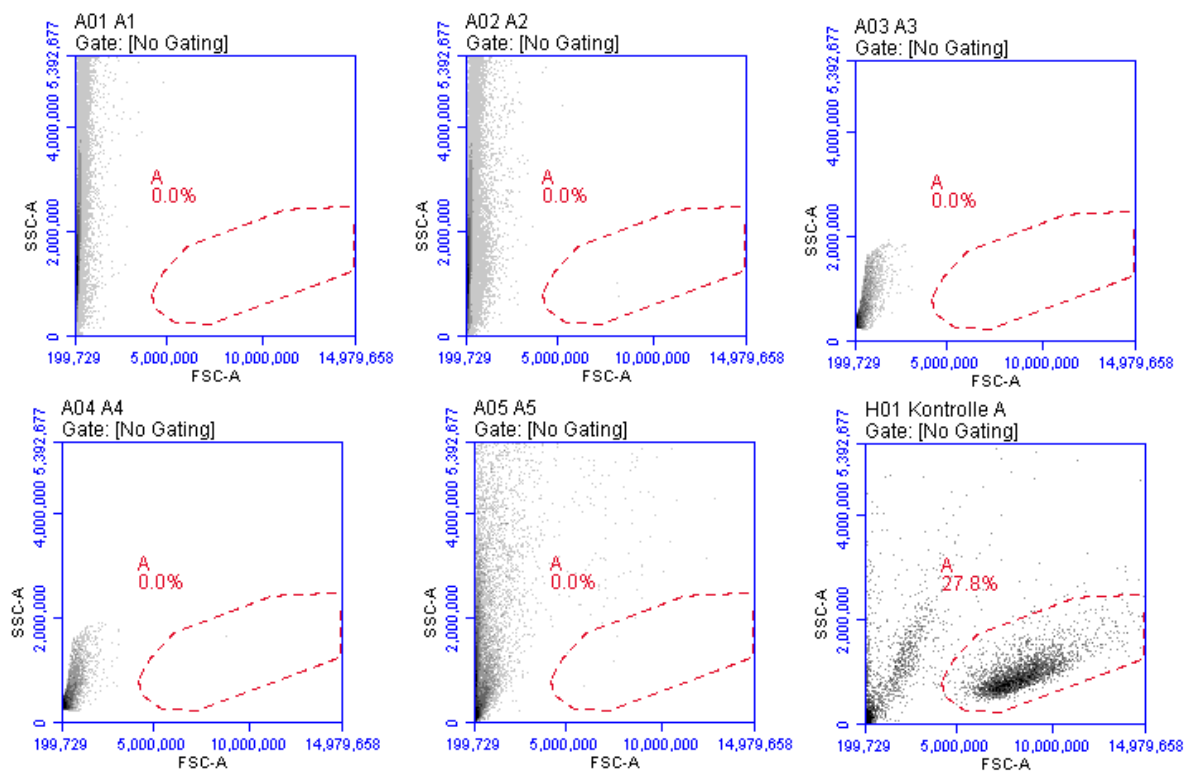


Figure 5-14: scatter for A549 cells

Chapter 5: Additional Experiments

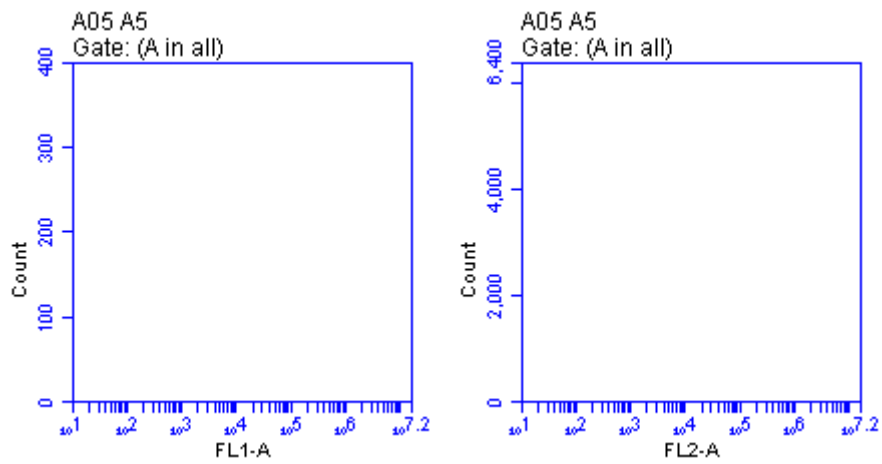


Figure 5-15: Annexin-PI for A549 cells

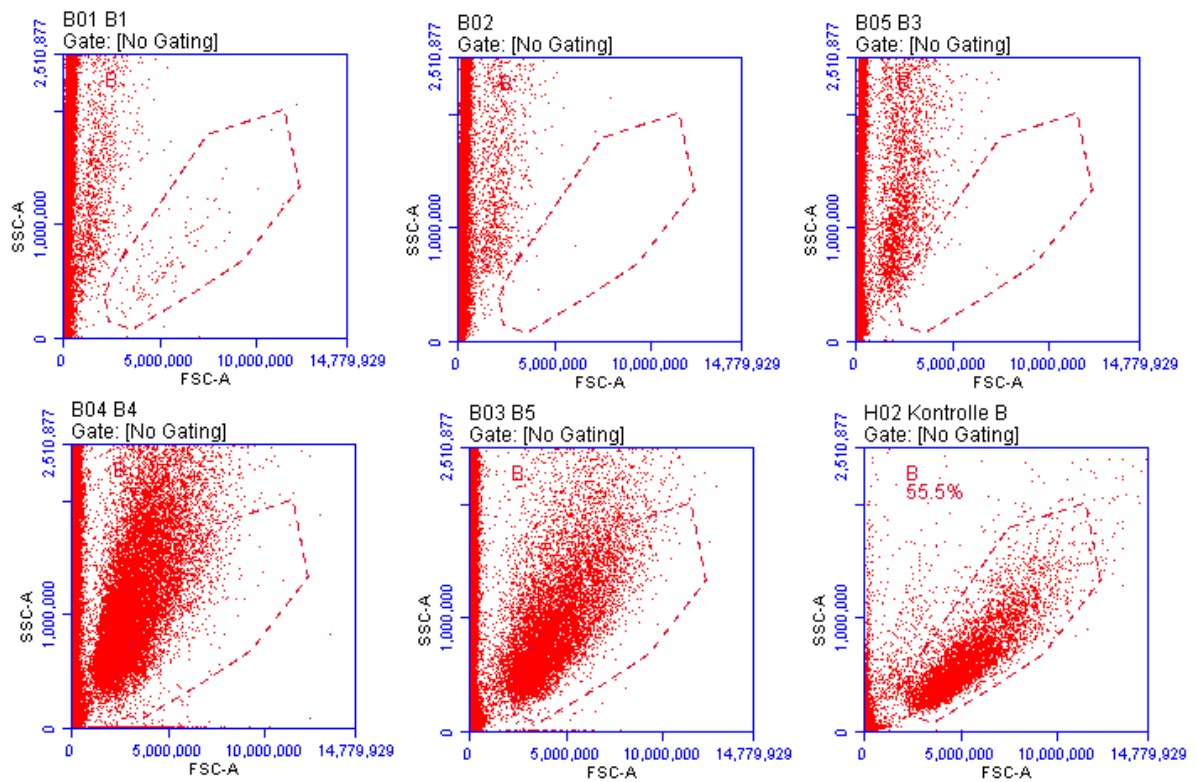


Figure 5-16: Scatter for BEAS-2B cells

Chapter 5: Additional Experiments

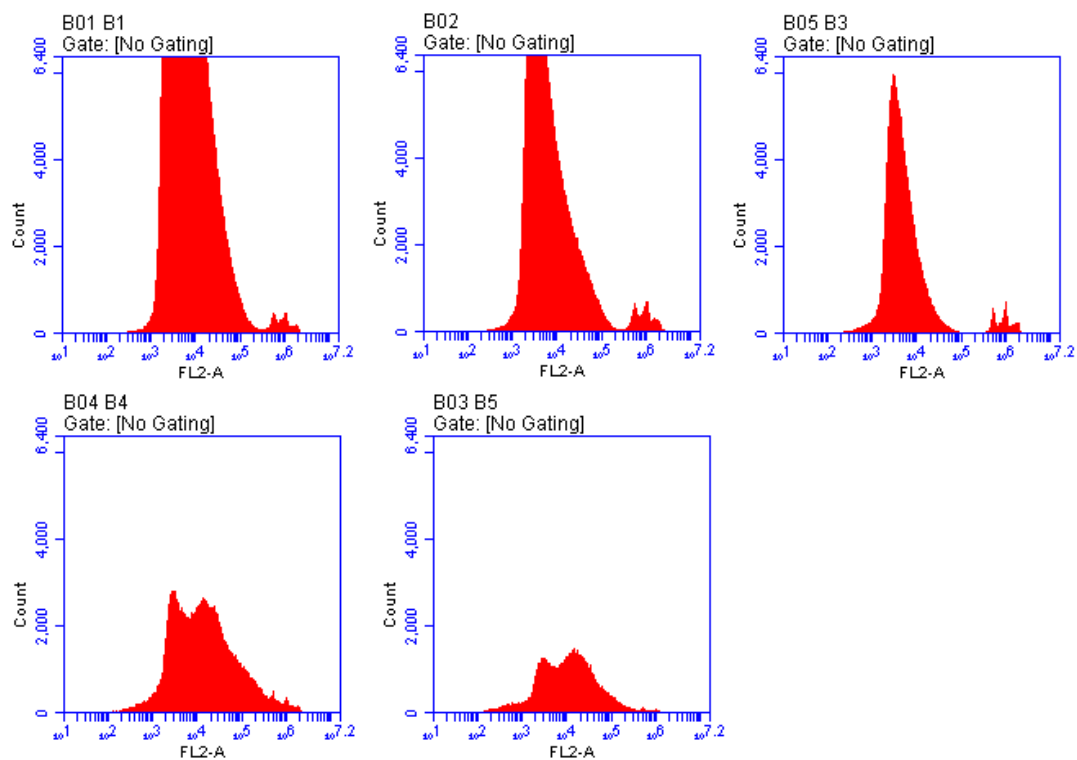


Figure 5-17: PI for BEAS-2B cells

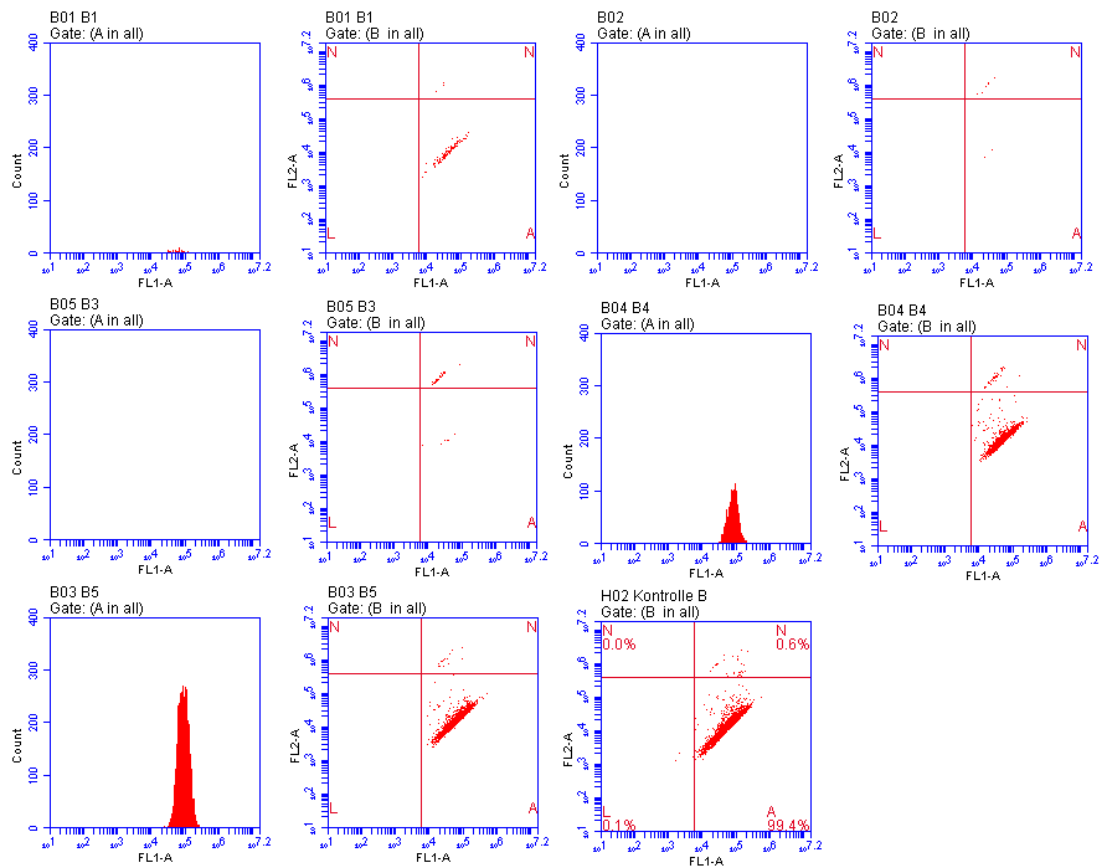


Figure 5-18: Annexin-apoptosis for BEAS-2B cells

Chapter 5: Additional Experiments

5.5.2.8 Cellular uptake of Ag NPs

The results of cellular uptake of aptamer-coated AgNPs are shown in Figure 19. This parameter was clearly dose-dependent, that is, there was a direct relationship between the uptake and concentration of aptamer-coated AgNPs. It was found that BEAS-2B cells had a very much lower uptake than A549 (cancer cells), especially at medium and low concentrations. The difference was very clear. Interestingly, these results are in complete agreement with the results of toxicity and other results to prove the very high selectivity of the aptamer towards cancer cells, and this is promising for development the targeting therapy using silver as a drug via knowing which concentrations are better, which will have a high effect only on cancer cells without having any effect on healthy cells.

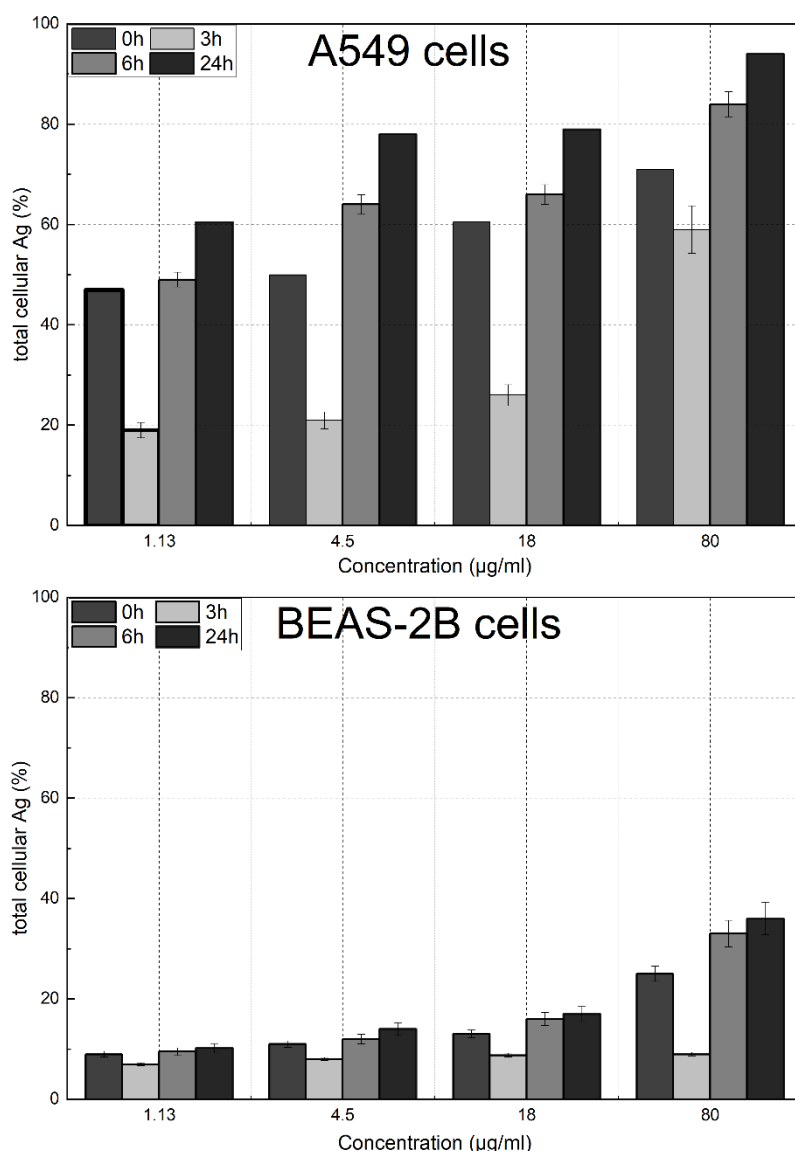


Figure 5-19: total silver concentrations in A549 cells and BEAS-2B cells after exposure to Apt-AgNPs for 3h.

Chapter 5: Additional Experiments

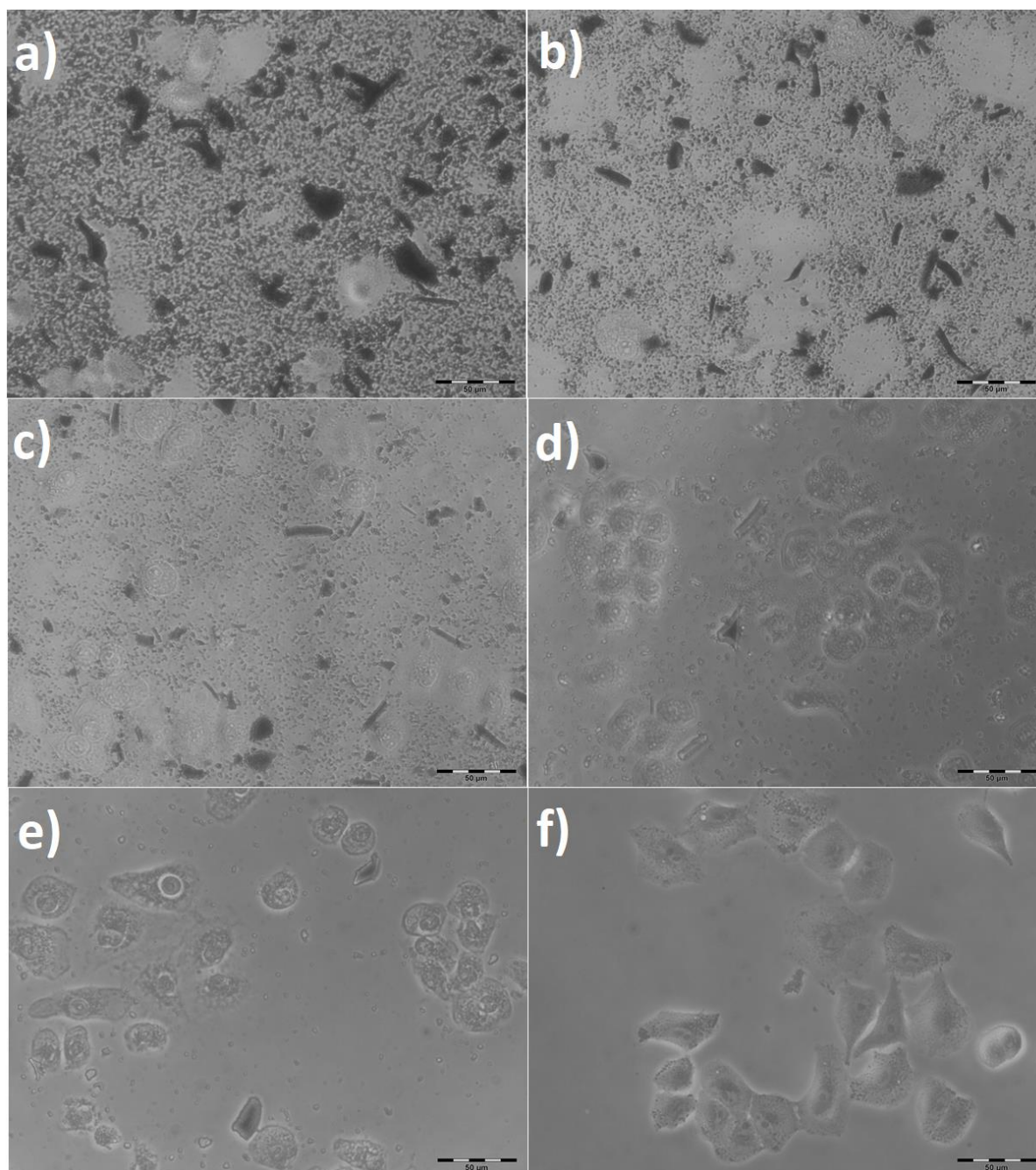


Figure 5-20: Optical microscope images of A549 cells showing the morphological changes induced by the treatment for 3 hours with aptamer-conjugated AgNPs a) 60 µg/ml, b) 30 µg/ml, c) 15 µg/ml, d) 7.5 µg/ml, e) 3.7 µg/ml and f) control. Scale bar 50 µm.

Chapter 5: Additional Experiments

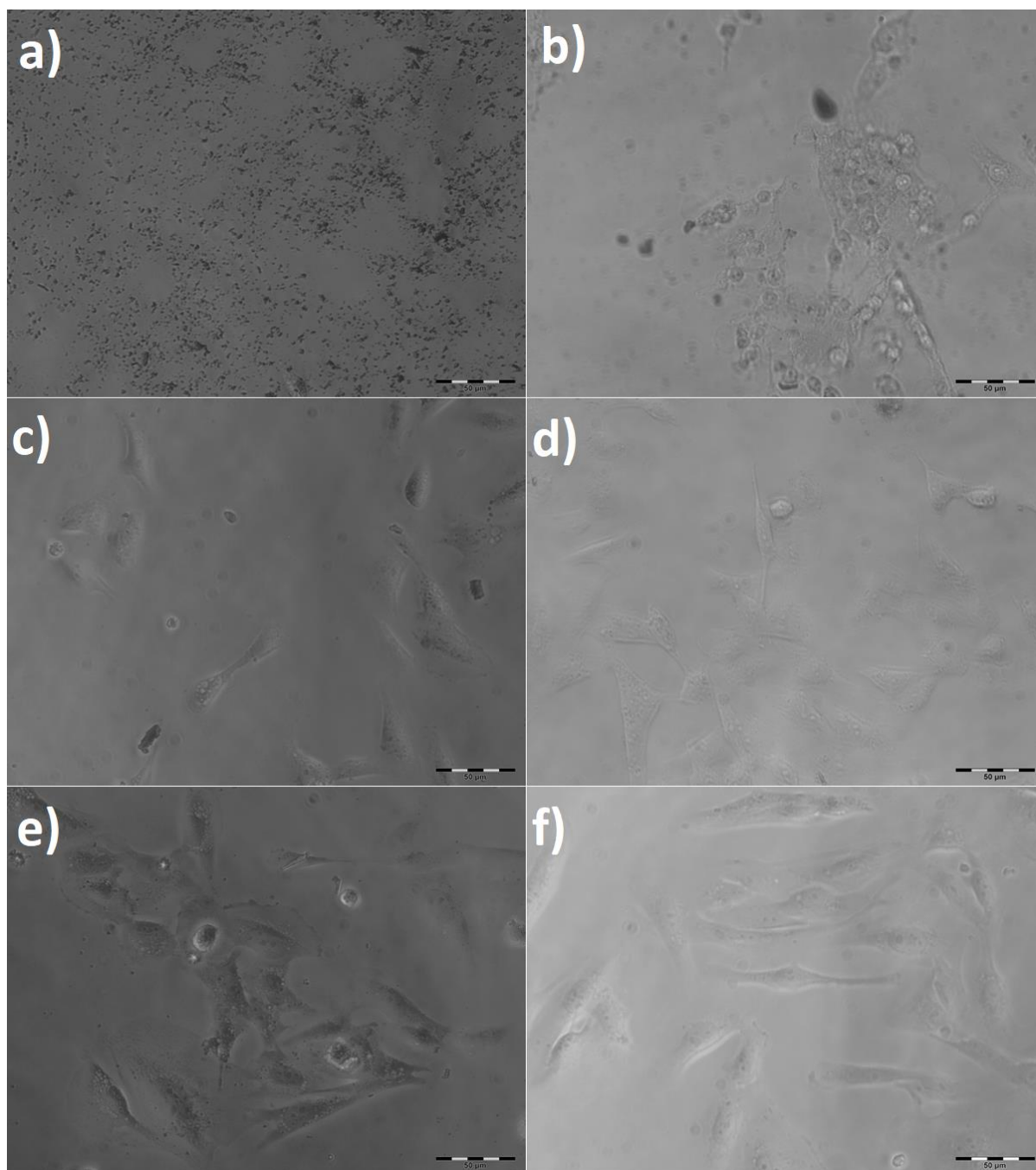


Figure 5-21: Optical microscope images of BEAS-2B cells showing the morphological changes induced by the treatment for 3 hours with aptamer-conjugated AgNPs a) 60 $\mu\text{g/ml}$, b) 30 $\mu\text{g/ml}$, c) 15 $\mu\text{g/ml}$, d) 7.5 $\mu\text{g/ml}$, e) 3.7 $\mu\text{g/ml}$ and f) control. Scale bar 50 μm .

Chapter 5: Additional Experiments

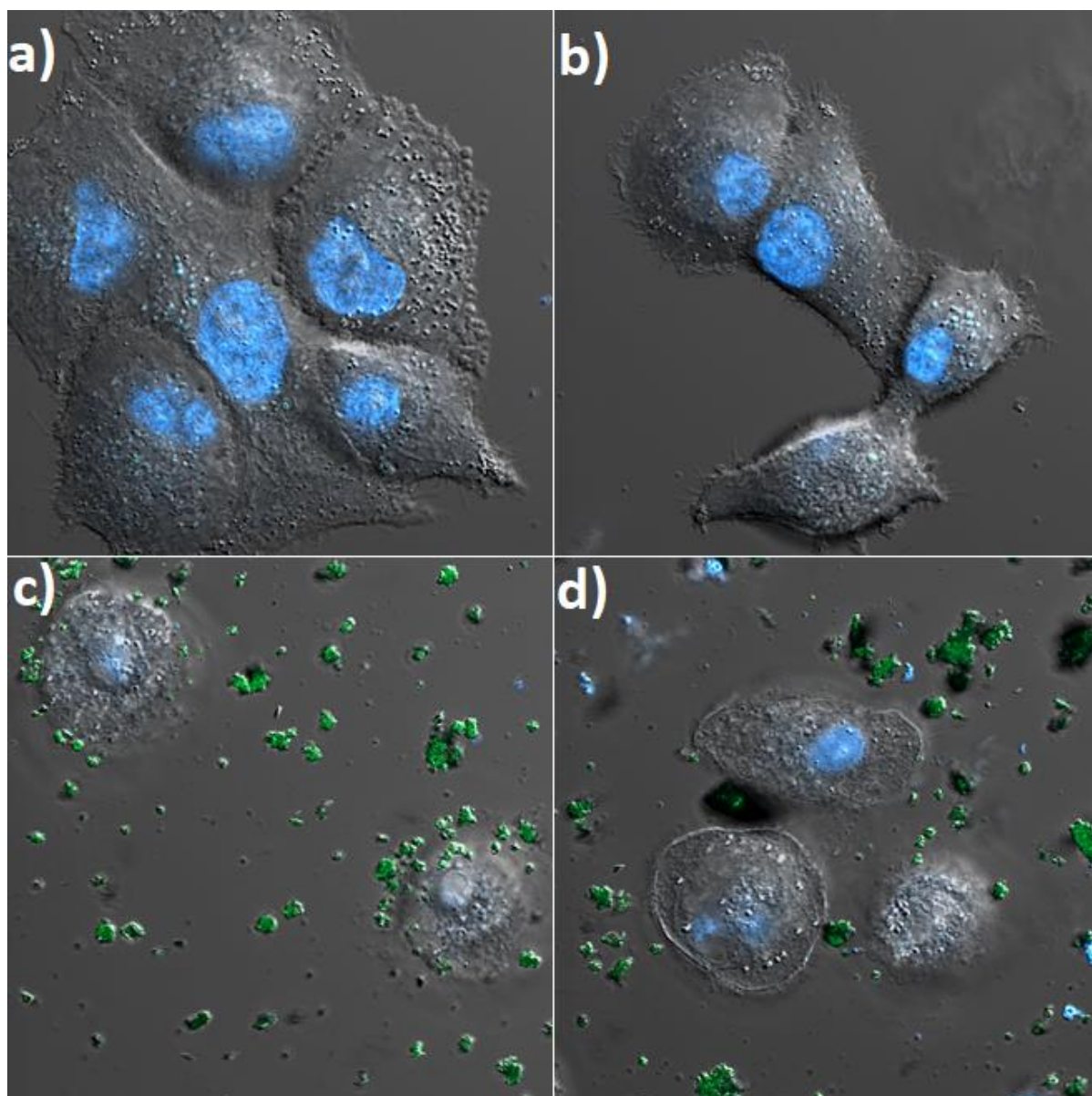


Figure 5-22: confocal microscope images of A549 cells Where a and b are the controls, and c and d are the cancer cells treated with AgNPs at a concentration of 16 $\mu\text{g/ml}$ for 3 hours. The nuclear region is shown in blue and stained with Hoechst 33342. The merging images of all the signals are also produced. Scale bar 10 μm .

Chapter 5: Additional Experiments

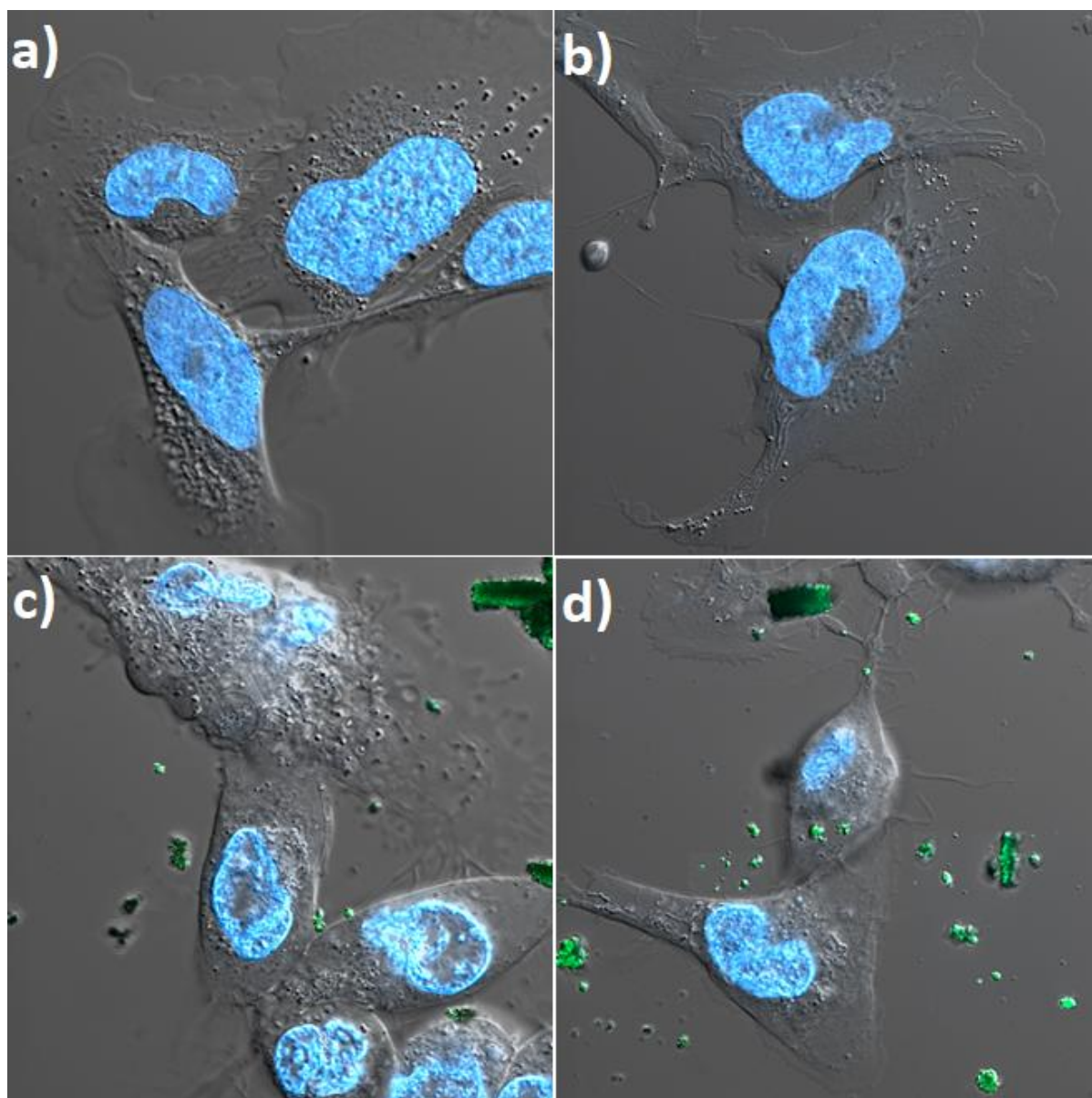


Figure 5-23: confocal microscope images of BEAS-2B cells Where a and b are the controls, and c and d are the cancer cells treated with AgNPs at a concentration of 16 $\mu\text{g/ml}$ for 3 hours. The nuclear region is shown in blue and stained with Hoechst 33342. The merging images of all the signals are also produced. Scale bar 10 μm .

Chapter 5: Additional Experiments

5.5.3 References

1. Instrument User Manual.
https://dmec.moh.gov.vn/documents/10182/13112657/upload_01390382_1575198820418.pdf?version=1.0&fileId=13113416.
2. Mostafa, F. A.; Abd El Aty, A. A.; Hamed, E. R.; Eid, B. M.; Ibrahim, N. A., Enzymatic, kinetic and anti-microbial studies on *Aspergillus terreus* culture filtrate and *Allium cepa* seeds extract and their potent applications. *Biocatal. Agric. Biotechnol.* **2016**, *5*, 116-122.
3. El-anssary, A. A.; Raoof, G. F. A.; Saleh, D. O.; El-Masry, H. M., Bioactivities, physicochemical parameters and GC/MS profiling of the fixed oil of *Cucumis melo* L seeds: A focus on anti-inflammatory, immunomodulatory, and antimicrobial activities. *Journal of Herbmmed Pharmacology* **2021**, *10* (4), 476-485.
4. Hammoudeh, N.; Kweider, M.; Abbady, A.-Q.; Soukkarieh, C., Sequencing and Gene Expression Analysis of *Leishmania tropica* LACK Gene. *Iran J Parasitol* **2014**, *9* (4), 574-583.
5. Twair, A.; Kassem, I.; Murad, H.; Abbady, A. Q., Secretion of Recombinant Human Annexin V in Fusion with the Super Folder GFP for Labelling Phosphatidylserine-Exposing Membranes. *The Journal of Membrane Biology* **2021**, *254* (2), 175-187.
6. Abbady, A. Q.; Twair, A.; Ali, B.; Murad, H., Characterization of Annexin V Fusion with the Superfolder GFP in Liposomes Binding and Apoptosis Detection. **2017**, *8*.
7. Dalimi, A.; Karimi, M.; Jameie, F.; Ghafarifar, F.; Dalimi, A., The killing in vitro effect of Half-Wave Rectified Sine electricity plus silver nanoparticle on *Leishmania major* promastigotes and BALB/C mice skin leishmanial lesion healing. *Trop. Biomed.* **2018**, *35* (1), 50-58.
8. Mohammadi, M.; Zaki, L.; KarimiPourSaryazdi, A.; Tavakoli, P.; Tavajjohi, A.; Poursalehi, R.; Delavari, H.; Ghaffarifar, F., Efficacy of green synthesized silver nanoparticles via ginger rhizome extract against *Leishmania major* in vitro. *PLoS One* **2021**, *16* (8), e0255571.
9. Mohebbali, M.; Rezayat, M.; Gilani, K.; Sarkar, S.; Akhoundi, B.; Esmaeili, J.; Satvat, T.; Elikae, S.; Charehdar, S.; Hooshyar, H., Nanosilver in the treatment of localized cutaneous leishmaniasis caused by *Leishmania major* (MRHO/IR/75/ER): an in vitro and in vivo study. *DARU Journal of Pharmaceutical Sciences* **2009**, *17* (4), 285-289.
10. Jebali, A.; Kazemi, B., Nano-based antileishmanial agents: A toxicological study on nanoparticles for future treatment of cutaneous leishmaniasis. *Toxicol. in Vitro* **2013**, *27* (6), 1896-1904.
11. Kovács, D.; Igaz, N.; Gopisetty, M. K.; Kiricsi, M., Cancer Therapy by Silver Nanoparticles: Fiction or Reality? *Int. J. Mol. Sci.* **2022**, *23* (2).
12. Abdalrahim, A.; Armin, F.; Nadja C., B.; Pascal, R.; Thomas, S.; Johanna-Gabriela, W., Hypericum perforatum L.-Mediated Green Synthesis of Silver Nanoparticles Exhibiting Antioxidant and Anticancer Activities. *Nanomaterials* **2021**, *11* (2), 487.
13. Medici, S.; Peana, M.; Nurchi, V. M.; Zoroddu, M. A., Medical Uses of Silver: History, Myths, and Scientific Evidence. *J. Med. Chem.* **2019**, *62* (13), 5923-5943.
14. Huy, T. Q.; Huyen, P. T. M.; Le, A. T.; Tonezzer, M., Recent Advances of Silver Nanoparticles in Cancer Diagnosis and Treatment. *Anti-Cancer Agents Med. Chem.* **2020**, *20* (11), 1276-1287.

Chapter 5: Additional Experiments

15. Ravindran, A.; Chandran, P.; Khan, S. S., Biofunctionalized silver nanoparticles: Advances and prospects. *Colloids Surf., B* **2013**, *105*, 342-352.
16. Divsar, F.; Habibzadeh, K.; Shariati, S.; Shahriarinnour, M., Aptamer conjugated silver nanoparticles for the colorimetric detection of arsenic ions using response surface methodology. *Anal. Methods* **2015**, *7* (11), 4568-4576.
17. Sperling, R. A.; Parak, W. J., Surface modification, functionalization and bioconjugation of colloidal inorganic nanoparticles. *Philosophical Transactions of the Royal Society A: Mathematical, Physical and Engineering Sciences* **2010**, *368* (1915), 1333-1383.
18. Keleştemur, S.; Altunbek, M.; Culha, M., Influence of EDC/NHS coupling chemistry on stability and cytotoxicity of ZnO nanoparticles modified with proteins. *Appl. Surf. Sci.* **2017**, *403*, 455-463.
19. Odeh, F.; Nsairat, H.; Alshaer, W.; Ismail, M. A.; Esawi, E.; Qaqish, B.; Bawab, A. A.; Ismail, S. I., Aptamers Chemistry: Chemical Modifications and Conjugation Strategies. *Molecules* **2020**, *25* (1).
20. Zhang, X.; Servos, M. R.; Liu, J., Fast pH-assisted functionalization of silver nanoparticles with monothiolated DNA. *Chem. Commun.* **2012**, *48* (81), 10114-10116.
21. Lee, J.-S.; Lytton-Jean, A. K. R.; Hurst, S. J.; Mirkin, C. A., Silver Nanoparticle–Oligonucleotide Conjugates Based on DNA with Triple Cyclic Disulfide Moieties. *Nano Lett.* **2007**, *7* (7), 2112-2115.
22. Stetefeld, J.; McKenna, S. A.; Patel, T. R., Dynamic light scattering: a practical guide and applications in biomedical sciences. *Biophys. Rev.* **2016**, *8* (4), 409-427.
23. Kumar, A.; Dixit, C. K., 3 - Methods for characterization of nanoparticles. In *Advances in Nanomedicine for the Delivery of Therapeutic Nucleic Acids*, Nimesh, S.; Chandra, R.; Gupta, N., Eds. Woodhead Publishing: 2017; pp 43-58.
24. Theophile, T., *Infrared spectroscopy: Materials science, engineering and technology*. BoD–Books on Demand: 2012.
25. Hames, B. D., *Gel electrophoresis of proteins : a practical approach*. 3rd ed. ed.; Oxford : Oxford university press: 1998.
26. Zamiri, R.; Abbastabar Ahangar, H.; Zakaria, A.; Zamiri, G.; Shabani, M.; Singh, B.; Ferreira, J. M. F., The structural and optical constants of Ag₂S semiconductor nanostructure in the Far-Infrared. *Chem. Cent. J.* **2015**, *9* (1), 28.
27. Sun, Y.; Sun, J.; Wu, X.; Li, Y.; Li, X.; Li, R.; Wang, T.; Bi, W.; Cui, W.; Yu, Y., Mechanism of zirconia microgroove surface structure for osseointegration. *Mater. Today Adv.* **2021**, *12*, 100159.

6 Chapter Six: Summarizing Discussion and Conclusions

6.1 Vorwort

In dieser Arbeit wurde ein Protokoll zur Biosynthese von Silber-Nanopartikeln unter Verwendung von wässrigen Extrakten des Johanniskrauts aus Syrien entwickelt. Die resultierenden Nanopartikel wurden mit vielen Techniken wie UV-VIS, DLS, Zetapotential, XRD, EDX, SEM, TEM, AAS, TGA, FTIR-ATR, AFM und NTA-Analyse charakterisiert. Dann die antioxidativen Aktivitäten unter Verwendung von DPPH-, ABTS- und SO-Assays, antimikrobielle Wirkungen gegen etwa 20 verschiedene Arten (grampositive, gramnegative Bakterien und pathogene Hefen), Anti-Leishmania-Aktivität gegen den syrischen *L. tropica*-Stamm (LT_SYR_24) und die Antikrebsaktivität gegen Hela-, HepG2- und A549-Zellen wurden untersucht. Alle Ergebnisse waren ausgezeichnet und sehr vielversprechend. Die Pflanze wurde mit verschiedenen Lösungsmitteln extrahiert und ein Protokoll entwickelt, um separate Peaks im HPLC-Diagramm zu erhalten. Eine UHPLC-ESI-Q-TOF-MS-Analyse im positiven Ionenmodus wurde durchgeführt. Durch den Vergleich mit den Standards mit Molekülionen konnten wir etwa 10 Verbindungen im Pflanzenextrakt identifizieren und mithilfe von MS/MS konnten wir die organischen Verbindungen aus dem Pflanzenextrakt identifizieren, die auf den Oberflächen von Silber-Nanopartikeln als Verkappungsmittel vorhanden sind. Außerdem wurde ein Protokoll entwickelt, um diese Nanopartikel zu modifizieren und sie mit dem Aptamer zu konjugieren, das eine hohe Selektivität für Lungenkrebszellen aufweist. Die Wirksamkeit dieser modifizierten Nanopartikel gegen gesunde (BEAS-2B-Zellen) und kanzeröse Lungenzellen (A549-Zellen) wurde untersucht, um herauszufinden, wie wichtig die Konjugation nur bei der Ausrichtung auf Tumorstellen ist. Mehrere Techniken und Analysen wurden verwendet, um diese Aktivität zu bestimmen, nämlich: CTB-Test, Zelllebensfähigkeit mit Calcein AM+PI, Apoptose und Nekrose unter Verwendung von Annexin+PI und Morphologie unter Verwendung von Licht- und konfokalem Mikroskop. Die Ergebnisse waren hervorragend und sehr vielversprechend und werden nach weiteren Studien *in vitro* und *in vivo* die Grundlage für die Entwicklung einer zielgerichteten Therapie bilden.

Dieses Kapitel enthält zunächst eine kleine theoretische Einführung dann erklären Sie die vollständigen Ergebnisse auf vereinfachte und prägnante Weise

Chapter 6: Summarizing Discussion and Conclusions

In ancient civilizations, such as the Greeks, Romans, and others, silverware or silver coins were inserted into barrels of water or milk to keep water and other drinks pure for long periods and to prevent ulceration and decomposition. In the early 1800s, doctors sewed surgical wounds with silver wire and placed silver paper over wounds sustained to soldiers during World War I to avoid infection and facilitate healing. Colloidal silver was used extensively in the early twentieth century in medicine, for example as a bactericide in hospitals. This treatment is both effective and safe, but its popularity declined during the age of antibiotics. But in the eighties, the problem of bacterial resistance to antibiotics arose, and this is what revived interest once again in silver, especially with the emergence of nanotechnology. Silver nanoparticles (AgNPs) have received distinctive interest, particularly in biomedicine. AgNPs have very high activity against most microbes and cancer cells. Interest in AgNPs has broadly increased in most other cutting-edge medical applications, including wound repair, bone healing, dental material filling, vaccine adjuvants, antidiabetic agents, and bioimaging.

The following are the most important uses of silver in the past and at present:

- Silver has the ability to murder more than 650 various fungi, germs, bacteria, viruses and just in 5-7 minutes.
- Silver inhibited about 657 isolates belonging to 22 types of bacteria.
- A large number of studies have proven that silver in its various forms and at very low concentrations was able to kill most of the different bacterial strains and species, including gram-positive and gram-negative.
- Other studies also showed the ability of silver to kill various fungi.
- Silver is an antiviral agent: recent studies show the effect of AgNPs on herpes simplex virus and influenza type 3 virus, in addition to its previously studied effect against a number of viruses such as influenza A/H1N1, murine norovirus (MNV)-1, monkeypox virus, HIV-1, Tacaribe virus (TCRV), recombinant respiratory syncytial virus (RSV) and hepatitis B virus (HBV).
- Silver nanoparticles are able to cure ulcerative colitis in mice and gastrointestinal diseases such as diarrhea, ulcers, colitis and gastric dysfunction.
- Since silver is effective against bacteria and infections, so it is able to treat various skin diseases such as warts, psoriasis, acne, lupus, dermatitis, hemorrhoids, eczema, rashes and seborrhea.
- Silver can treat eye infections: silver nitrate has a long history in the treatment of ophthalmic infections. However, AgNPs exhibited minimal toxicity against eye cells.
- Silver can treat cystitis: nanocrystalline silver has been reported to decrease bladder inflammation.
- Silver can relieve allergies: contact allergies in murine models.
- Silver arsphenamine was utilized to heal syphilis while silver proteinases like Argyrols and Protargol were used against gonorrhea.

Chapter 6: Summarizing Discussion and Conclusions

- Recent studies have proven the effectiveness of silver against diabetes by preparing it in green ways.
- Silver has shown great efficacy against malaria.
- Several studies have proven the effectiveness of silver against chronic arthritis.
- Silver has been used to treat cough, tetanus, nervous and motor problems, appendicitis, poliomyelitis, typhus, colds, ulcers, chronic fatigue syndrome, diphtheria, and scarlet fever.
- Colloidal silver produced by electrolysis of silver electrodes is still used in water and water filters to provide safe drinking water in developing countries.
- Silver nanoparticles of different sizes and compositions showed great activity against a wide range of cancer cells.

Cancer of its various types is one of the most common diseases that lead to many deaths in the world, as the incidence of it is constantly increasing, which affects the population structure and the economy of most countries of the world. Therefore, there is an urgent need to develop effective and advanced treatment methods to reduce the adverse effects of cancer incidence. The known treatments for cancer are radiotherapy, chemotherapy and surgery. In addition to the side effects of traditional treatments, different tumors were able to develop resistance to different drugs, so it was necessary to develop new drugs to treat these tumors. With the emergence of nanotechnology and nanomaterials, interest has increased in to use of these materials, which have unique chemical, physical and biological properties, in the treatment of multiple diseases, with cancer at the forefront. Nanoparticles were used to transfer treatment or as a treatment, as they reduced side effects by targeting only the affected areas. Among many nanoparticles, silver nanoparticles have received the most attention as a treatment for tumors and multiple cancer cells. AgNPs exhibited perfect activities against different cancer cells such as colon cancer, breast cancer, ovarian cancer, cervical cancer, pancreatic ductal adenocarcinoma, lung cancer, hepatocellular carcinoma, melanoma, osteosarcoma, etc. Several studies confirm that different factors influence the anticancer activity of AgNPs such as sizes, shapes, doses/concentrations in different tumor cells, pH, dose and exposure time, cell lines and tumor microenvironment, Surface Charge and Protein Corona.

The preparation of silver nanoparticles using plant extracts has been getting a lot of attention lately because of its easy availability, nontoxicity, simplicity, cost-effectiveness and high reducing potential. Silver nanoparticles of different shapes and sizes were prepared using different plant parts such as roots, fruit, stems, leaves, flower, peel, seed, leaves and others. The various organic components present in these extracts such as phenols, flavonoids, lipids, carbohydrates, proteins, amino acids and others where their functional groups reduce silver ions to silver metal. The preparation of silver nanoparticles using plant extracts is affected by several factors, including the concentration of silver nitrate and plant extract, temperature, PH value, time and speed of the reaction, and according to the change of these factors, particles of different sizes and shapes will be obtained. AgNPs synthesized by plant extracts or other biogenic preparation exhibited the most motivating advantages because they had a more effective and lower toxicity compared to nanoparticles prepared using chemical substances,

Chapter 6: Summarizing Discussion and Conclusions

perhaps due to the presence of an organic layer on its surface. according to the used part in the plant extracts, the reaction conditions and the cancer cell line tested, different effects leading to cell death have been reported, such as disruption of membrane integrity, decreased cell growth, cytoplasmic condensation, cell clumping, cell shrinkage, and nuclear condensation and fragmentation, DNA laddering, caspase-dependent and mitochondrial-dependent pathways. Interestingly, most of the silver nanoparticles prepared using plant extracts showed no toxicity or low toxicity with healthy cells compared to cancer cells. The reason for this behavior may be found in a pH-dependent mechanism of AgNPs dissolution. Silver does not dissolve in acids as a metal, but silver nanoparticles dissolve and release large amounts of silver ions in the acidic medium. Since tumors have an acidic medium, silver nanoparticles affect tumors significantly compared to their effect on healthy tissues. The estimation of the toxicity of metals is accurately correlated to its bioavailability and evaluated by its solubility, oxidation state, complexation ability towards biological targets (i.e. proteins or other coordinating species), excretion and detoxification routes. In fact, Silver nanoparticles are insoluble compounds, therefore they are non-reactive and less associated with toxic effects.

The currently increasing popular interest in silver as an alternative to standard antibiotics and as a systemic treatment prompted further research into this compound, especially as it is prepared in greenways. AgNPs among other metals is nowadays receiving the greatest interest worldwide in order to develop a new generation of diagnostic tools and effective treatment solutions for cancer cells. AgNPs in cancer diagnosis, their cytotoxicity, and their role as carrier systems for cancer treatment, where, AgNPs can be used either as a direct therapy or as a drug delivery system for cancer treatment.

6.2 Development of a protocol for green preparation of silver nanoparticles from aqueous extract of *Hypericum perforatum L.* (St. John's Wort)

St John's wort aqueous extract was used as a source of the biological reducing and capping agent in biosynthesis reaction of silver nanoparticles (AgNPs). A lot of parameters like the amount of plant extract and its concentration, the silver nitrate concentration and its volume, the reaction time and temperature, stirring speed were studied by conducting several experimental trials. To reach the optimal protocol for preparing silver nanoparticles utilizing aqueous extracts, several protocols have been tried. The final protocol can be summarized as follows:

Aerial parts of *Hypericum perforatum L.* (St. John's wort) were collected in July–August 2018 from the Ghab Plain in Syria (google maps: 35.586856, 36.355724 and 180-200 m above sea level), and harvested during the flowering season. The plant was washed several times to remove dust and possible sludge, dried at room temperature in the dark and ground in an electric grinder. The powder (350 mg) was added to 800 ml of distilled water in a 1000 ml Erlenmeyer flask. The mixture was heated to maintain a gentle boiling for 4 hours until the volume was reduced to approx. 250 ml. The mixture was cooled to room temperature and filtered with Whatman filter paper (Nr. 40). The supernatant was centrifuged at 23015 xg for 30 minutes and then filtered through a Sartolab Vakuumfilter 180C5, 0.22 µm Polyethersulfon, 500 ml. The supernatant was kept it in the refrigerator at 4 ° C. 40 ml of the prepared extract solution was heated to 80°C with stirring at 750 rpm. 10 mL of silver nitrate solution (0.05 M)

Chapter 6: Summarizing Discussion and Conclusions

was added drop by drop with continuous stirring at 750 rpm. When all the silver nitrate solution is finished, the solution was removed from heating and stirring and left to cool at the temperature of the laboratory and in the dark with coverage to prevent oxidation. The obtained silver nanoparticles were washed with deionized water by use of centrifugal concentrators (Vivaspin 10 kDa, PES) tubs 10 times or direct centrifugation at 15,000 rpm for one hour, and the process was repeated at least 4 times to remove residual organic compounds and the remaining nitrate ions. Finally, the resulting silver nanoparticles were stable with an average diameter between 20 and 50 nm.

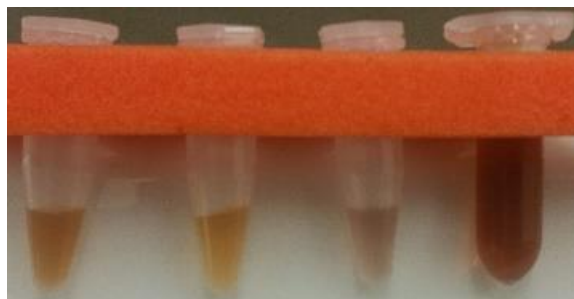


Figure 6-1: Images of some phytochemical-capped AgNPs

6.3 Characterization of Biosynthesized Silver nanoparticles

AgNPs were described using different apparatuses like ultraviolet light spectroscopy (UV-VIS), Dynamic Light Scattering (DLS) and Zeta Potential, Fourier Transform Infrared (FTIR) Spectroscopy, x-ray diffraction (XRD), Scanning Electron Microscopy (SEM), Transmission Electron Microscopy (TEM), Energy Disperse X-ray Spectroscopy (EDX), Atomic Force Microscopy (AFM) and Nanoparticle Tracking Analysis (NTA).

Chapter 6: Summarizing Discussion and Conclusions

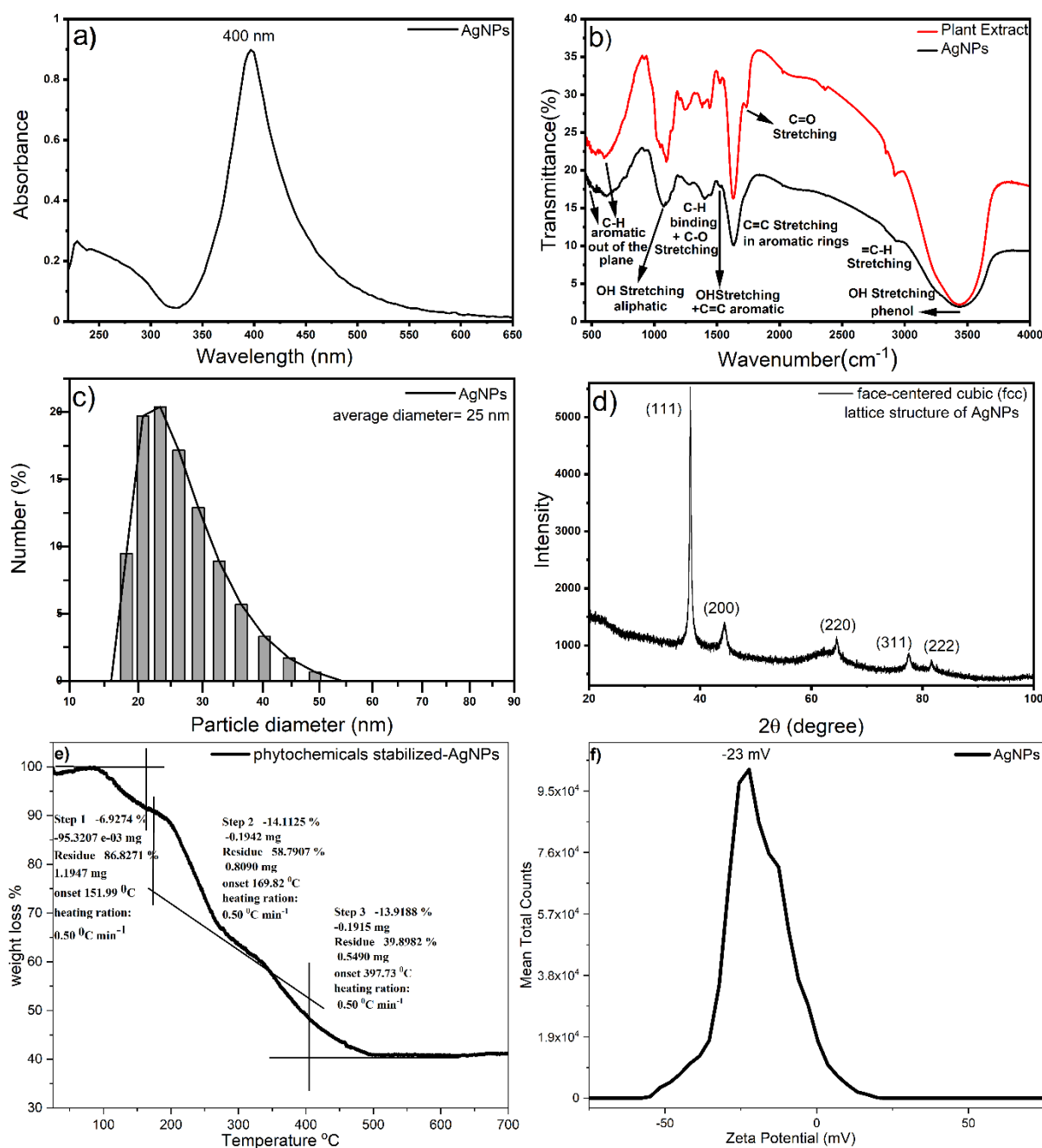


Figure 6-2: a) UV-Vis spectrum of biosynthesized AgNPs utilized *Hypericum perforatum L. aqueous Extract*; b) FTIR-ATR spectra of *St John's Wort Aqueous Extract* and *St John's Wort-AgNPs*; c) Dynamic light scattering data which characterize the hydrodynamic diameter for green synthesized-AgNPs in the range of 25 nm with a Polydispersity index range of 0.19; d) X-ray diffraction pattern of Biologically Synthesized Silver Nanoparticles using *St John's Wort Aqueous Extract*, the peaks in the XRD spectrum are due to X-ray diffraction from the (111), (200), (220), (311) and (222) planes; which can be called Miller indices; e) TGA curve of *Hypericum perforatum L.-stabilized silver nanoparticles* demonstrating the weight loss of organic compounds (Phytochemicals) adsorbed on the surfaces of nanoparticles as a protective layer when the temperature increases and f) Zeta Potential.

Chapter 6: Summarizing Discussion and Conclusions

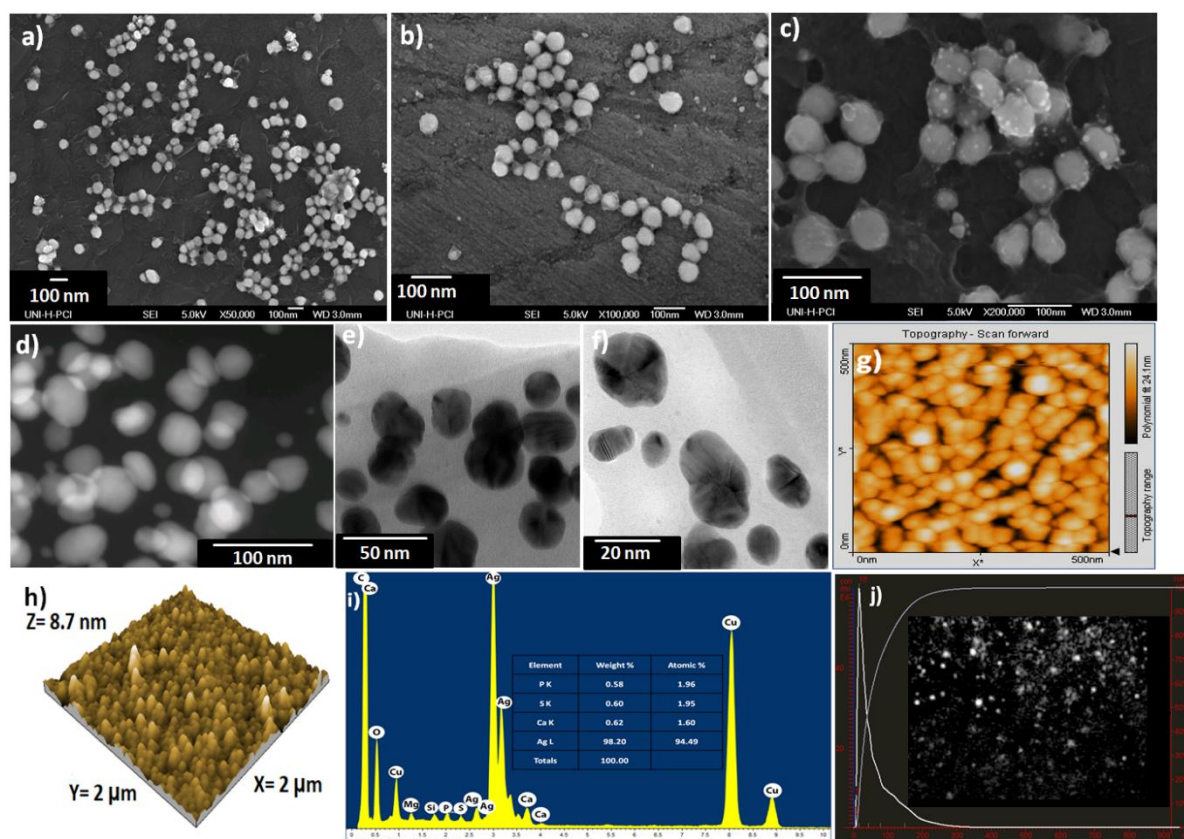


Figure 6-3: a, b and c) SEM images of Organically Coated *Hypericum Perforatum L Green Synthesized Silver Nanoparticles*; AgNPs with white color with an average diameter of 20-50 nm, While clearly visible the organic protective layer in dark gray surrounding these nanoparticles; d) scanning transmission electron microscopy dark-field (STEM-DF); e, f) high-resolution transmission electron microscopy (HRTEM) at different magnifications; g) AFM image of biogenic AgNPs synthesized using *Hypericum Perforatum L aqueous extract*, scan scale: 500 nm×500 nm; h) 2 μm x 2 μm AFM topography image of phenolic compounds-capped AgNPs displayed as a three-dimensional projection; i) EDX profile of biosynthesized silver nanoparticles and j) nanoparticle tracking analysis of AgNPs. Particle size vs. particle concentration and representative nanoparticle tracking analysis video frame.

Through the results presented in figure 2a, it noticed one intense peak in the UV-Vis spectrum with a maximum of about 400 nm, which refers to the idealistic surface plasmon resonance (SPR) of conducting electrons from the surface of silver nanoparticles. The surface plasma resonance indicates that the obtained silver is very small and spherical because its value is very sensitive to the size and shape of nanoparticles¹. FTIR, ATR spectrum (figure 2b) shows the functional groups at the surface of AgNPs, i.e. prove the presence of biomolecules from *St John's wort extract* which stay as a capping agent surrounding the silver nanoparticles. *St John's wort extract* includes hydroxyl groups, alkyl moiety and aromatic rings. The presence of the broad peak near 3400 cm⁻¹ indicates the existence of (O-H) stretching in phenols and the existence of bands in the range of 2900-2990 cm⁻¹ matching to C-H stretching, peaks in the range of 1923-2000 cm⁻¹ confirm the presence of an aromatic ring, the peak near 1617

Chapter 6: Summarizing Discussion and Conclusions

cm^{-1} refer to C=O stretching and C-C stretching in the aromatic ring, the band near 1734 cm^{-1} pointing to C=O stretching, the bands near 1385 & 1445 cm^{-1} matching to C-H bending and the peaks in the range of $670\text{-}770 \text{ cm}^{-1}$ refer to C-H aromatic out of the plane ²⁻⁵ and other peaks are mentioned in detail in Table S3 in the supplementary of the article ⁶. The hydrodynamic average diameter, Polydispersity index (PDI) and zeta potential values of biosynthesized AgNPs were 30-60 nm, 0.17-0.21 and -16 to -21 mV respectively (figure 2c and f). The size measured here is larger than what it gets using an SEM and TEM microscope and this is very normal because the DLS method calculates the hydrodynamic diameter of nanoparticles, that is, we measure their size with the organic coating layer on their surface as a protective and stabilizer agent. The X-ray diffraction spectrum (figure 2d) exhibited several of Bragg's reflections at 2 theta diffraction angles: 38.25° , 44.44° , 64.5° , 77.58° , 81.71° which refer to indices of (111), (200), (220), (311) and (222) planes respectively. These results prove that the formed spherical AgNPs are face-centered cubic (fcc) crystalline in shape. The broad of the peaks is due to AgNPs have a small size ⁷ which can measure using Debye-Scherrer's equation. The XRD data were in agreement with the reference NIST M&A collection code: N AL3281 Pattern: 03-065-2871. Figure 3e shows TGA analysis of green-synthesized AgNPs with stabilizer at the surface with heating rate 0.5°C min from 25°C to 1000°C in flowing N_2 . The decomposition takes place in 2 or 3 steps sometimes. The first phase of degradation happened between 92 and 164°C with a weight loss of 6.93% and this loss of weight may be due to surface adsorbed H_2O molecules and some molecules of hexose ring. The second and third phases of the weight loss occurred between $170\text{-}315$ and $324\text{-}492^\circ\text{C}$ consecutively, with a weight loss of 50%, this weight loss was due to the combustion of the protective layer which decomposition in two steps. The weight loss of the capped-AgNPs as a result of adsorption of bioorganic metabolites at the surface of AgNPs (capping agent) was almost between 40-60 %, this depends on the number of washing times with Vivaspin tubes and the conditions of centrifugation used. In summary, the results of TGA analysis correspond to the results of FTIR and prove that resulting silver nanoparticles from synthesis were mixed in nature with a strongly coordinated metal-organic framework. SEM images (figure 3a,b and c) indicated that biosynthesized AgNPs containing monodispersed spherical silver nanoparticles with sizes ranging from 20-50 nm, in addition to the organic layer (The protective layer consisting of phytochemicals from St. John's Wort aqueous extract that is adsorbed on the surfaces of these nanoparticles to protect their particles in the nanosize from growing and agglomeration and to make these nanoparticles stable in the colloidal solution) on its surface, which appear clearly in these images. Scanning transmission electron microscopy dark-field (STEM-DF) and high-resolution transmission electron microscopy (HRTEM) images at different magnifications (figure 3d, e and f) exhibited that the size of these nanoparticles is in the range of 20-50 nm and it is also spherical in shape. Atomic Force Microscope (AFM) images (figure 3g and h) showed that Green-synthesized AgNPs are similar in size (30 nm) and shape (spherical) and this indicates that they are spread uniformly. Energy-dispersive X-ray patterns (figure 3i) showed several signals at 2.8, 3.5 and 3.8 keV which refers to the existence of AgNPs because these values return to the binding energies of Ag-L, Ag-M ⁸⁻¹⁰. C and O peaks correspond to phytochemicals compounds in St John's wort aqueous extract which adsorbed at the surface of biosynthesized AgNPs as a protective layer. The presence of Cu and others is due to the TEM used grid and holder. Nanoparticle tracking analysis (NTA), is a more precise analytical

Chapter 6: Summarizing Discussion and Conclusions

instrument than the Dynamic light scattering method to evaluate particle size distribution¹¹⁻¹². So we carried out additional itemized size distribution measurements using this technique. Particle size distribution of the number calculated using the NTA technique revealed monodisperse silver nanoparticles with an average diameter of 18-50 nm and this agrees closely with the results of DLS. It concludes that phytochemicals-coated silver nanoparticles with an average diameter between 20 and 40 nm have resulted.

6.4 Identification of the organic compounds at the surface of silver nanoparticles

In order to identify the organic compounds present on the surface of nanoparticles, a special protocol was initially required to isolate the compounds in the plant extract using High-performance liquid chromatography. In this study, the same aerial parts of the St. John's wort (leaves, stem, petals, and flowers) that were used for the biosynthesis of silver nanoparticles were extracted using different solvents: water at 100 and 37 ° C, ethanol 100% and 70% at 37 ° C, methanol 100% and 70% at 37 ° C and acetone 100% and 70% at 37 ° C. The water I and water II extraction processes resulted in a yellow-brown solid with a yield of 21% for water I and 16% for water II. The organic solvents resulted in a black-gray solid with a yield of 25.5% for ethanol 70% (light gray), 7% for ethanol 100% (black gray), 22.9% for methanol 70% (light gray), 18% for methanol 100% (black gray), 23.2% for acetone 70% (light gray) and 7% for acetone 100% (black gray). The yields resulting from the mixture of water with organic solvents were much higher when compared with the yields of the pure organic solvents. Also, extracting with water using the tea method resulted in higher yields than boiling with water for a long time. By increasing the polarity of the solvent, higher yields were obtained, indicating that mainly hydrophobic compounds were extracted. Therefore, we conclude that extracting the plant with water using the tea method or using a mixture of water with organic solvents produces higher yields of the resulting extract when compared with pure organic solvents or continuous boiling with water for long periods. Many conditions have been changed such as; different types of HPLC used Columns (Normal Phase, Reverse Phase, Ion Exchange and Size Exclusion Columns), flow rate, pressure, composition, concentrations and mix ratios changing based on the time of the gradient in the mobile phase, Injected sample volumes and temperature. Other variables have also been studied like: Checking the stability of the extracts in the solvents, Introduction of a water pulse in a known gradient program, effects of an Isocratic Initial Area, slightly inverted gradient, hart inverse gradient, basic characterization of selected extracts with new extraction agents, effects of low temperature at 10 ° C, substance analysis of an extract by adding different standards and Comparing the UV spectra of the obtained peaks with the UV spectra of the expected compounds for these peaks to confirm that these peaks belong to the proposed compounds. Finally, an easy and inexpensive protocol was developed to obtain completely separate, non-overlapping peaks.

The extracts were analyzed by utilizing high-performance liquid chromatography- equipped with a diode array detector (HPLC-DAD) coupled with UV-visible spectrophotometry at a full spectrum (200–800 nm). Detection was carried out at 260 for phloroglucinols (Hyperforin and derivates), 590 nm for naphthodianthrones (Hypericins) and at 350 for other flavonols, flavones and caffeoylquinic acids. The extract compounds were identified by using column Kinetex C18 100 A (Phenomenex, Germany, dimensions: 100 mm × 4.6 mm, 5 µm particle size) and guard

Chapter 6: Summarizing Discussion and Conclusions

column C18 4 x 3.0 mm (Phenomenex, Germany) at room temperature ($25\pm 2^\circ\text{C}$). Solvent A was 0.1 % formic acid, and solvent B was 0.1 % formic acid, 95 % MeOH, 5 % H₂O. The mobile phase was freshly prepared daily, filtered through a 0.45 μm nylon filter and degassed after preparation for 15 min in an ultrasonic bath. The gradient mode was 0 min 95% A, 5% B; 82 min 0% A, 100% B; 92 min 0% A, 100% B; 93 min 95% A, 5% B; 100 min 95% A, 5% B and the flow rate was 1 mL/min.

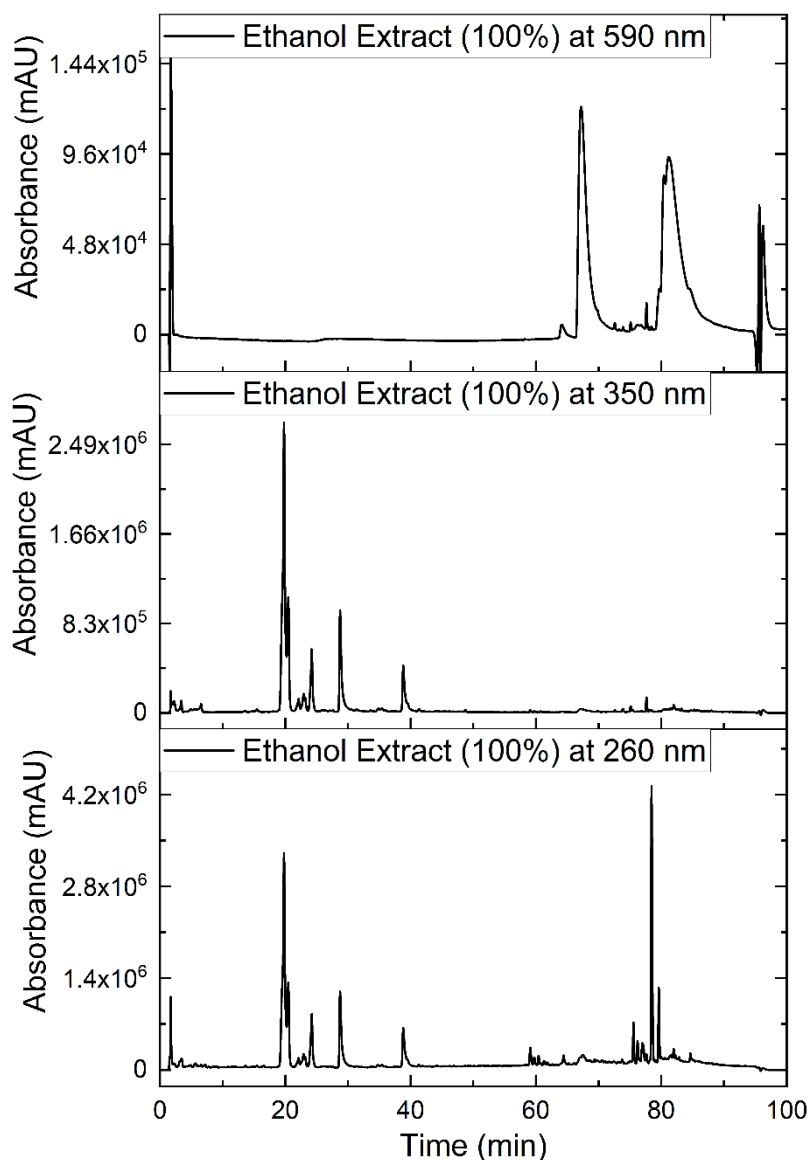


Figure 6-4: HPLC chromatograms of ethanolic extract of *Hypericum perforatum* L. (detection at 260, 350 and 590 nm) and it is almost the same for all extracts with other solvents, but the difference is only in the intensity of the peaks.

Five standards (chlorogenic acid, quercetin, quercitrin hydrate, hyperoside and hypericin) were used, and a comparison with their retention times was performed to identify these compounds in the extracts. UV diagrams for the previously identified compounds have been extracted from HPLC UV Detector and compared with what is in the literature to prove the presence of these compounds.

Chapter 6: Summarizing Discussion and Conclusions

Combined (HPLC-DAD) and electrospray ionization–mass spectrometry (LC-ESI-MS) in positive mode has therefore also been used to separate the bioactive molecules ions $[M+H]^+$ of the compounds in the extracts by their mass-to-charge ratio (m/z) and to detect them qualitatively and quantitatively by their respective m/z and abundance. For high-performance liquid chromatography with mass detection (HPLC-MS) analysis, a Waters Acquity ultra-performance UPLC with a Kinetex 5 μm C18-column (Phenomenex, 100x4.6 mm) was used with the same gradient for HPLC. A chromatogram was recorded in parallel to the mass spectrum. MS analysis was carried out on a Q-ToF Premier (Waters) using electrospray ionization (positive ions, 3 kV capillary voltage; 250 °C desolvation temperature; 650 L/h desolvation gas flow (nitrogen)). Finally, by matching the prominent protonated molecular ions $[M+1]^+$ or $[M+Na]^+$ of resulting compounds from MS analysis with the molecular weights of compounds known to be present in this plant and through the previous result, 10 compounds have been proven to be present in these extracts, namely hypericin, rutin, hyperoside, quercitrin, quercetin, biapigenin, hyperforin, quercitrin hydrate, adhyperforin and chlorogenic acid. In fact, about 60 compounds were known through correlating known masses with the protonated molecular ions through mass analysis and through characteristic fragmentation patterns. But since MS is not enough to say completely that it has been identified, it will be confirmed by a later MSMS analysis.

Isolation and identification of organic compounds of St. John's wort at the surface of AgNPs: In this research, a distinguished protocol was developed to remove about 80% of the compounds of St. John's wort plant adsorbed on the surface of silver nanoparticles as a capping agent, which can play an important role in their subsequent modification for use as a targeting drug against incurable diseases, and the protocol is as follows: A mixture of organic solvents prepared as follows: 20% EtOH, 20% MeOH, 30% acetone and 30% Ethyl acetate, was used to wash the previously dried silver nanoparticles several times. After several times of washing in the previous solution and then separating by centrifugation, all the filtrate is collected in one tube and the solvents are evaporated to obtain a solid that is dissolved only in ethanol HPLC Grade and an HPLC, HPLC/MS and MS/MS were performed for it to identify these phytochemical compounds and their percentage. Thermogravimetric analysis (TGA) and FTIR were used to prove the isolation of this capping agent from the silver nanoparticle's surface and their approximate proportion.

TGA and FTIR analysis (figure 5a and b) proved that the capping agent surrounding the silver nanoparticles was removed by 80% using the previous protocol, wherein the thermal decomposition analysis up to 1000 °C, the percentage of broken materials decreased from 60% to approximately 12% and in the FTIR spectrum, the intensity of the peaks decreased very significantly, or sometimes the peaks disappeared.

Chapter 6: Summarizing Discussion and Conclusions

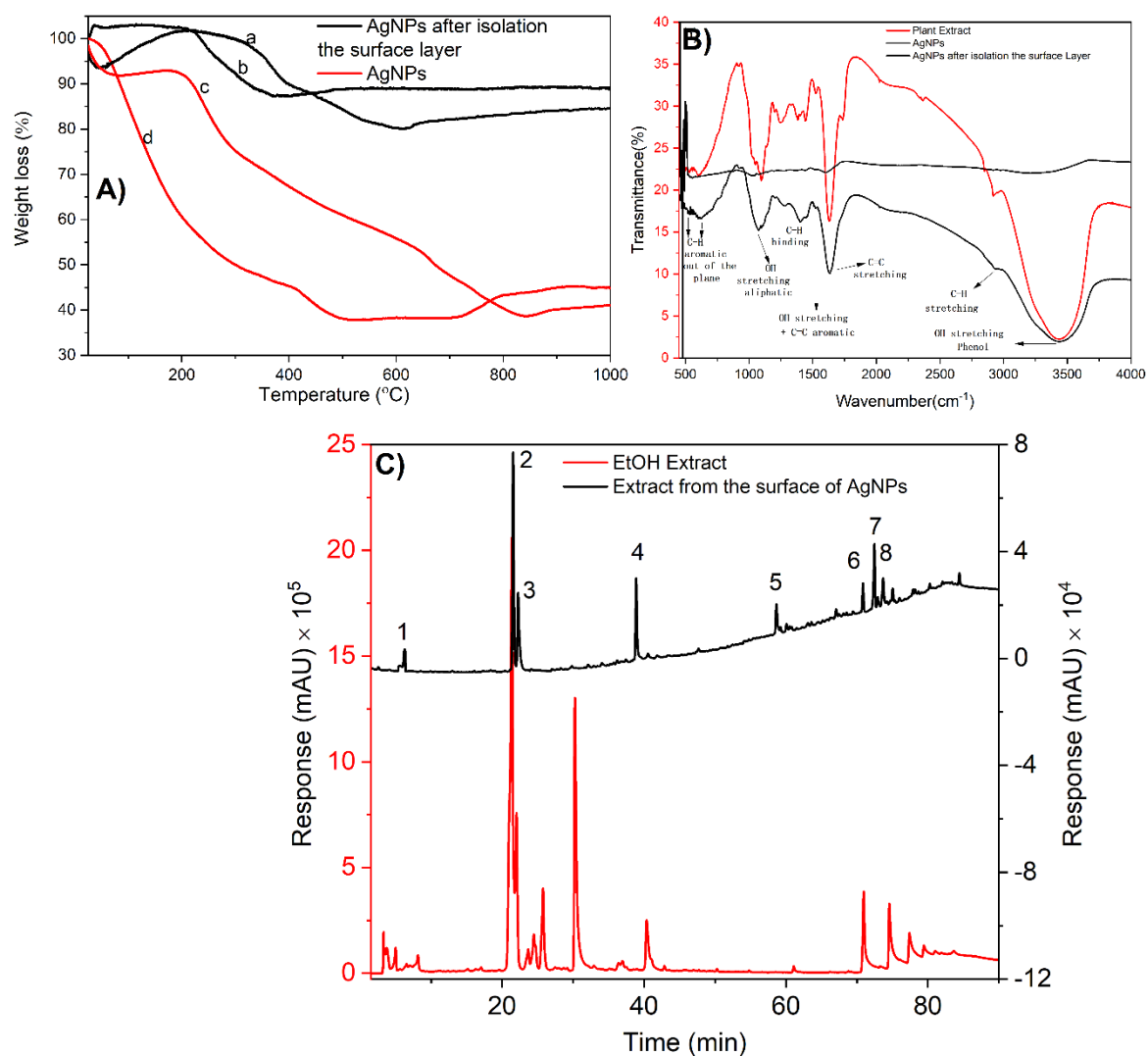


Figure 6-5: a) Thermogravimetric analysis diagram of AgNPs before and after isolation of the capping agent layer; b) ATR-FTIR spectra of *Hypericum perforatum L.* aqueous Extract, biosynthesized AgNPs before and after isolation of the capping agent layer and c) HPLC Chromatograms of St John's Wort extract and the supernatant obtained from the organic layer on the surface of silver nanoparticles.

By comparing the HPLC spectra of St. John's wort extract and the supernatant isolated from the surfaces of silver nanoparticles using the previous protocol (figure 5c), we note that there are 8 perfectly identical peaks in the plots and this confirms the presence of 8 compounds of the plant extract on the surfaces of the silver nanoparticles. By comparing the location of these peaks, which we had previously identified in the extract itself (i.e., by molecular ion identified via MS analysis), as well as by performing a filtrate-only HPLCESI-Q-TOF MS/MS analysis, we were able to demonstrate the presence of only these eight phytochemicals from the extract. The eight identified compounds present on the surfaces of AgNPs belong to different classes and they are Neochlorogenic acid (phenolic acids or phenyl propane), Hyperoside, Isoquercitrin (flavonoid glycosides or Flavonol glycosides), I3,II8 Biapigenin (Biflavonoids), Furohyperforin, Hyperforin, Furoadhyperforin and Adhyperforin (Phloroglucinols). These eight compounds are bioactive compounds of the St. John's Wort plant, which have unique

Chapter 6: Summarizing Discussion and Conclusions

properties, especially in the medical field. They have been used frequently in multiple treatments for different diseases.

6.5 Total phenol and Antioxidant activities of St John's Wort extracts

Total phenolic contents of St. John's wort extracts (water I or water II, ethanolic and methanolic) were estimated using Folin–Ciocalteu assay (figure 6b and d) and antioxidant activity were determined using 2,2-diphenyl-1-picrylhydrazyl (DPPH) and (2,2'-azino-bis(3-ethylbenzothiazoline-6-sulfonic acid) (ABTS) assays (figure 6a and c). The free radical-scavenging capacities for different extracts show that extraction by the tea method gave much greater phenols and activity against the free radicals than the extraction with pure organic solvents. Although it was not statistically proven that a direct relationship between the phenol content and the antioxidant activity, in our case the extracts with the higher phenolic content gave greater antioxidant activity.

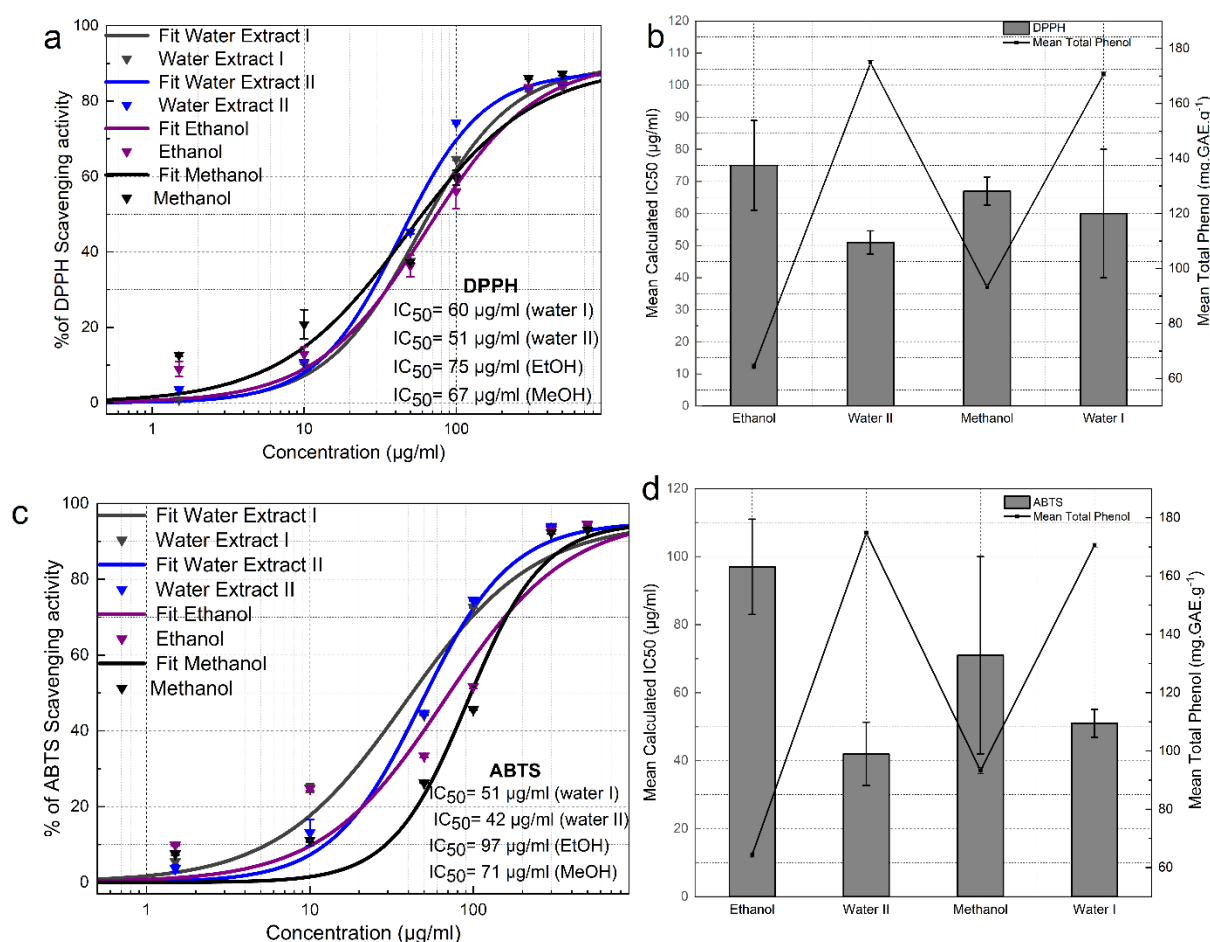


Figure 6-6: a,c) calculation of IC₅₀ of the *Hypericum perforatum* L. extracts using DPPH and ABTS scavenging assays and b, d) association between phenolic content and antioxidant activity for *Hypericum perforatum* L. extracts by DPPH and ABTS.

Chapter 6: Summarizing Discussion and Conclusions

6.6 Applications of biosynthesized AgNPs

6.6.1 Antioxidant activities

biosynthesized AgNPs using St. John's wort aqueous extract exhibited high scavenging activity against several free radicals such as 1,1-Diphenyl-2-picrylhydrazyl Free Radical (DPPH), 2, 2'-azino-bis-(3-ethylbenzothiazoline-6-sulfonic acid) radical cation (ABTS), and superoxide anion radical (SO).

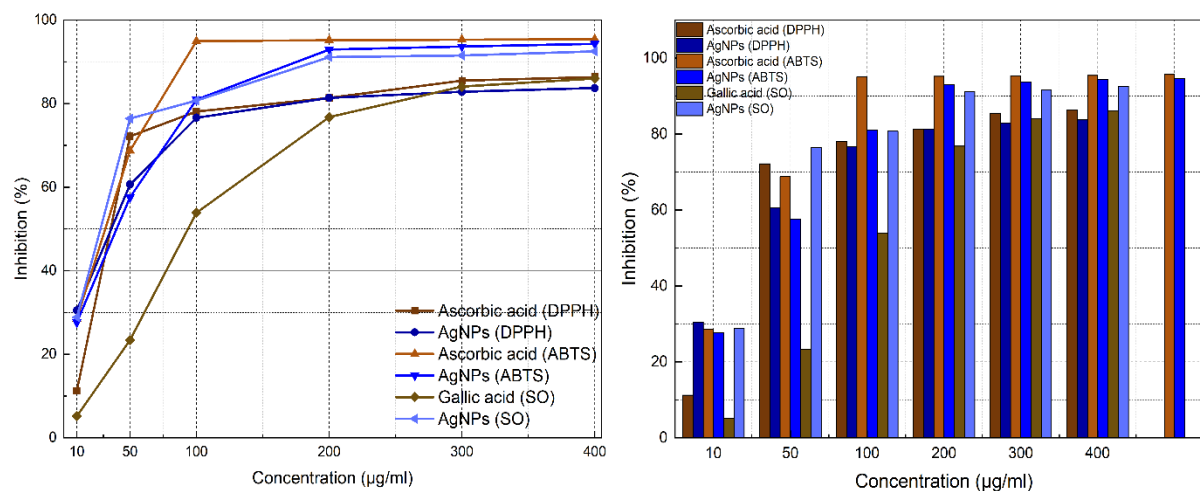


Figure 6-7: Antioxidant activity of AgNPs against DPPH free radical, ABTS radical and Superoxide anion radical with comparing with their standards.

In DPPH assay, silver showed great activity in scavenging free radicals, that is, it was able to reduce the radicals of purple color to yellow color. The IC₅₀ value of AgNPs was 35.88 µg/ml, which is very close to the value of the standard ascorbic acid (IC₅₀ = 35.44 µg/ml), and this indicates that the effectiveness of silver prepared by our method was very large and greater than others prepared by others in the literature¹³⁻¹⁷. In the ABTS assay, silver also exhibited big scavenging activity against cation radicals. The IC₅₀ value of AgNPs was 26.78 µg/ml, which is also very close to the value of the standard ascorbic acid (IC₅₀ = 23 µg/ml), and this value is also higher effectiveness compared to others described in the literature^{14, 16, 18-19}. In the SO assay, AgNPs exhibited very high scavenging activity against superoxide radicals. The IC₅₀ value of AgNPs was 27.77 µg/ml, which is much lower than the value of standard Gallic acid 94 µg/ml and also less than the effect of silver mentioned in the literature^{14, 16, 18, 20-25}.

6.6.2 Antimicrobial activities

Antimicrobial activity was carried out at 3 different times in different places.

6.6.2.1 First, in cooperation with the Faculty of Medicine and Department of Biological Sciences at Mutah University in Jordan.

AgNPs were tested against Gram-positive bacteria [*Staphylococcus aureus* (ATCC 43300), *Bacillus cereus* (ATCC 11778) and *B. subtilis* (ATCC 6633)] and against Gram-negative bacteria [*Pseudomonas aeruginosa* (ATCC 13048), β -lactamase *Klebsiella pneumoniae* (clinical isolate), extended-spectrum β -lactamase *E. coli* (ESBL, clinical isolate), and *Escherichia coli* (ATCC 25922)]. Two different experiments were performed to measure the antibacterial activity, namely the Well diffusion test and Micro-broth dilution assay, and both

Chapter 6: Summarizing Discussion and Conclusions

assays were performed according to Clinical and Laboratory Standards Institute guidelines, with some modifications.

6.6.2.1.1 Well diffusion test

Overnight bacterial culture was seeded in Muller Hinton agar plates (MHA) (Oxoid, UK) at cell density 10^6 cell/ml and in which 6 mm diameter wells were made using a sterile Cork borer. To each well in the bacterial agar plates, either 120 μ l aliquots (100 μ g/well), 60 μ l aliquots (50 μ g/well) from AgNPs preparation, or aqueous plant extract (2.5 mg/well) were applied. As a positive control, streptomycin (10 μ g/disc, Bio Basic Inc, Canada) was used and the results are presented as means of triplicate tests \pm SD.

6.6.2.1.2 Micro-broth dilution assay

This method is used to measure the lowest concentration needed to inhibit bacterial growth (MIC). AgNPs and the positive control were tested starting from 100 μ g/ml and 50 μ g/ml, respectively. Samples were serially diluted in 100 μ l Muller Hinton broth (MHB), to which 100 μ l of tested bacterial strain was added to each well in a cell density 2×10^6 cell/ml. The preparation was incubated for 24 hours at 37 °C. Aliquots from the preparations in micro-broth dilution assay, where there were no visible growths, were plated on agar plates with proper medium and incubation for 24-48 hours to determine if the nanoparticle has a bactericidal or bacteriostatic effect.

6.6.2.1.3 Effect of AgNPs on growth kinetics of *S. aureus*

To study the effect of AgNPs on the kinetics of bacterial growth. *S. aureus* was grown at a cell density of 10^6 cells/ml in sterile test tubes containing 10 ml of MHB. Various concentrations of AgNPs (1, 3, 6, 12, 24 μ g/ml) were added to bacterial culture test tubes with incubation for 24 h on an orbital shaker at 37 °C and 150 rpm. A 1 ml sample was withdrawn after 3-h and up to 24-h intervals to measure bacterial growth in terms of increase in the optical cell density at $\lambda 600$ nm (OD₆₀₀nm) using UV/Vis spectrophotometer.

6.6.2.1.4 Determination of the antibacterial activity of AgNPs in relation to colony-forming units (CFU)

Different concentrations of AgNPs (1, 3, 6, 12, and 24 μ g/ml) were utilized to determine their effect on *S. aureus* growth on Muller Hinton agar plates. The bacterium was grown overnight and then diluted to a cell density equivalent to 0.5 McFarland ($\approx 1.5 \times 10^8$ CFU/ml). They were diluted to 10⁵ fold and 100 μ l were spread on solid agar plates containing different AgNPs concentrations. The plates were incubated for 24 hours at 37°C and the grown colonies were photographed.

6.6.2.1.5 Time-kill kinetics assay

aliquots of 1 ml from the prepared suspension ($\approx 1.5 \times 10^8$ CFU/ml) of *S. aureus* were inoculated into test tubes containing 10 ml MHB with concentrations of the AgNPs equal to $\frac{1}{2}$ MIC, MIC, and 2 MIC. All tubes were incubated at 37°C and samples were taken at intervals of 30 minutes starting at the time of inoculation and up to 300 minutes. The number of surviving bacteria was determined by spreading 100 μ l of appropriate bacterial dilutions in sterile saline over the top of MHA plates with incubation at 37 °C for 24 h; The number of bacterial colonies was counted and expressed in CFU/ml. Time-kill curves were constructed by plotting the

Chapter 6: Summarizing Discussion and Conclusions

Log₁₀ (CFU/ml) against the exposure time (minutes). The assay was performed in triplicate and the results are presented as means of three independent tests \pm SD.

6.6.2.1.6 Wound migration assay

Normal human dermal fibroblast cell line (ATCC® PCS-201-012) were cultured in a 12-well microtiter plate as a monolayer; they were seeded at a cell density of 5×10^4 cell/ml. The cells were grown for 24 hours in Dulbecco's Modified Eagle Medium supplemented with 10% heat-inactivated fetal calf serum, L-glutamine, 65 μ g/mL of penicillin G, and 100 μ g/mL of streptomycin sulfate. They were incubated at 37°C in a humidified atmosphere containing 5.0% CO₂. Wound with uniform size was made in each well using sterile micro-tip; culture medium was aspirated from each well, well was washed with sterile phosphate buffer solution (pH 7.4), and fresh media with different concentrations of AgNPs (1, 3, 5, and 10 μ g/ml) were added to each well seeded with the cell line. Two wells containing a fresh medium without the test compounds were used as untreated controls. The culture was photographed at 0 time and after 24 hours using an inverted microscope. Wound migration (closure) was measured by the following equation:

% Wound migration = $1 - (\text{area of the wound at TS} / \text{area of the wound at T0}) \times 100$, where TS is 24 hours from wounding and T0 is 0 hour wounding.

6.6.2.1.7 Results

Based on inhibition zones results, Gram-positive bacterial were more affected by AgNPs than the Gram-negative in a concentration-dependent method with lower activity against *B. subtilis* from other Gram-positive strains. Inhibition zones in Gram-positive bacteria were 13.3-32 mm whereas 13-19.7 mm in *P. aeruginosa* and *K. pneumoniae* as Gram-negative bacteria. The Minimum concentration (MIC) required to cause no bacterial strains to grow was between 6.25 - 12.5 μ g/ml with activities against most bacteria (table 1).

Table 6-1: Antibacterial activities (inhibition zones and MIC) of AgNPs against tested bacterial strains

Bacterial strain	Inhibition zone (mm \pm SD)			MIC (μ g/ml)	
	(μ g/well)		S	AgNPs	S
	50	100	(10 μ g/disc)		
<u>Gram-positive</u>					
<i>B. subtilis</i>	11.7 \pm 0.6	13.3 \pm 0.6	23.3 \pm 1.6	12.5c	0.63s
<i>B. cereus</i>	19.0 \pm 1	24.3 \pm 2.1	29.7 \pm 1.3	6.25s	0.31s
<i>S. aureus</i>	27.7 \pm 1.5	32.0 \pm 1.3	31.3 \pm 0.7	12.5c	0.63c
<u>Gram-negative</u>					
<i>E. coli</i>	NA	NA	18.0 \pm 1.3	> 100	5c
<i>E. coli</i> (clinical)	NA	NA	12.3 \pm 0.7	> 100	> 10
<i>K. pneumonia</i> (clinical)	10.3 \pm 0.6	13 \pm 1	15.7 \pm 0.7	12.5c	10c
<i>P. aeruginosa</i>	16.7 \pm 1.5	19.7 \pm 1.1	17.1 \pm 0.3	6.25s	2.5s

Regarding the effect of silver nanoparticles on the kinetics of bacterial growth (the study was done on *S. aureus*) (figure 8), it noted that with increasing the concentrations of AgNPs (at a concentration of 6 μ g/ml and below), the OD value at 600 nm decreased in different time periods comparing the control culture. at a concentration of 6 μ g/ml ($\frac{1}{2}$ MIC), the maximum cell density reached was about 50%, while at concentrations higher than 6 μ g/ml, there was no

Chapter 6: Summarizing Discussion and Conclusions

growth at all throughout the entire cultivation period. The specific growth rate decreased from 0.21 h⁻¹ in the control culture to 0.04 h⁻¹ in the culture exposed to 6 µg/ml AgNPs (table 2). Previous results indicate that AgNPs have a significant toxic effect on the tested bacteria and that their toxicity increases with the increasing concentration of AgNPs.

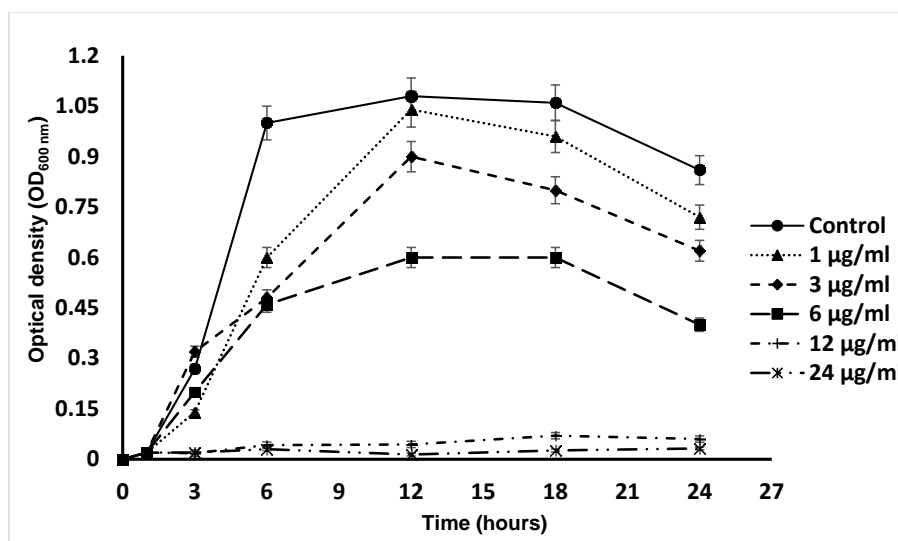


Figure 6-8: The growth curve of *S. aureus* in Muller Hinton broth contain various concentrations of AgNPs

Table 6-2: Specific growth rate and maximum growth intensity (OD_{600nm}) of *S. aureus* at different concentrations of AgNPs

Concentration (µg/ml)	Specific growth rate (h ⁻¹)	Maximum growth intensity (OD _{600nm})
control	0.21 ± 0.012	0.91 ± 0.17
1	0.09 ± 0.007	0.86 ± 0.15
3	0.06 ± 0.015	0.63 ± 0.11
6	0.04 ± 0.006	0.55 ± 0.05
12	-	0.065 ± 0.01
24	-	0.035 ± 0.004

For the colony-forming unit (CFU), the number of colonies decreases with the increase in the concentration of silver nanoparticles, and starting from 12 µg/ml, no colony remains, meaning they all disappear.

Chapter 6: Summarizing Discussion and Conclusions

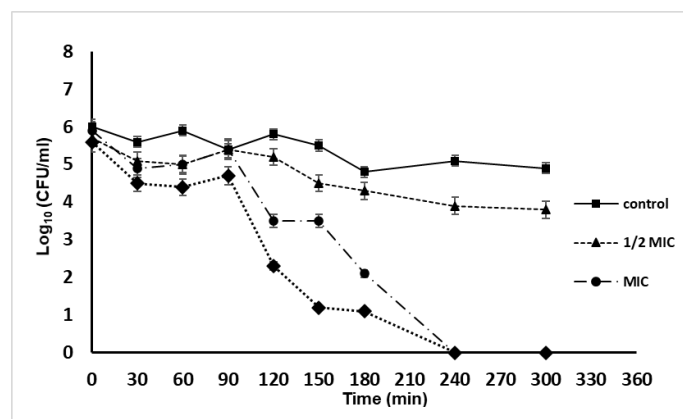


Figure 6-9: Time-kill curve of *S. aureus* in Mueller Hinton broth medium containing different concentrations of AgNPs

Time-kill test (Fig. 9) shows that the effect of silver nanoparticles at different concentrations begins after 90 minutes of incubation. At $\frac{1}{2}$ MIC concentration of AgNPs, the Log₁₀ (CFU/ml) was decreased by 10% compared to the control culture, while at MIC and 2 MIC concentrations of AgNPs, the Log₁₀ (CFU/ml) was decreased almost 103 fold after 120 min of cultivation. These results indicate that AgNPs killed bacteria after 240 minutes of cultivation.

Wound migration

The effect of the AgNPs on the fibroblast cell migration was studied. In fact, wound migration was non-significantly inhibited when fibroblast cells were treated with 1-5 μ g/ml AgNPs (inhibition 19%-23% compared to control), but it was significantly inhibited at 10 μ g/ml (inhibition 46.8%, $p < 0.5$). Fibroblast cells play a fundamental role in body homeostasis through the secretion of growth factors, the release of matrix metalloproteinases, collagen expression, and facilitating contraction of healing wounds²⁶. These results revealed that the ability of AgNPs in promoting wound healing depends on the test system employed, in vivo or in vitro, as well as the presence of bio-factors such as growth factors and cytokines.

6.6.2.2 Second, in cooperation with the Department of Microbiology, College of Medicine in Imam Abdulrahman bin Faisal University in Saudi Arabia.

6.6.2.2.1 Well diffusion test

The objective of conducting the analysis is to determine the effect of storing silver nanoparticles prepared using aqueous extract of St. John's wort in the refrigerator at a temperature of 4 °C on their effectiveness against microbes. In general, measuring the antimicrobial activity of silver nanoparticles after being stored for different periods. In this experiment, silver was stored for different periods of time, which are 4 months, 7 months and a whole year, then its activity against 8 different types of microbes was studied. As expected the halo zone of growth inhibition is increased as the concentration is increased (direct proportion) for six of the eight bacteria strains used. Whereas, no effect was seen using different concentrations and sizes of nanoparticles on *C. albican* 14053 and *C. auris* Lab strain. The results did not show any significant change in the effect of silver on bacteria when used after long periods of its synthesis, and this indicates that the green synthesis of silver nanoparticles

Chapter 6: Summarizing Discussion and Conclusions

using our developed protocol did not lose its effectiveness as a result of storage for relatively long periods of time.

Table 6-3: Bacteria and yeast strains used for the study

Microorganism name	ATCC NO.
<i>S. aureus</i> (wild type)	29213
<i>S. aureus</i> (Methicillin resistant)	43300
<i>E. coli</i> (Wild type)	25922
<i>E. coli</i> (ESBL)	35218
<i>K. oxytoca</i> (Wild)	700324
<i>K. Pneumoniae</i> (CRE)	BAA-1705
<i>C. albican</i>	14053
<i>C. auris</i>	Lab isolate

It is interesting to note in this analysis that there are 3 types of the same bacterial strains that were studied in Jordan. But two of them in the previous analyzes in Jordan did not give any activity, while here it gave a great result and great activity against these two strains. We can explain this for several reasons. The first reason is that when preparing the samples, it was not prepared well, or there was an error in preparing the required concentrations. The second explanation is the proportion of the layer of organic materials on the surfaces of silver nanoparticles, meaning that it was not washed well. This leads to the accumulation of a large number of layers of organic matter on the surfaces of silver nanoparticles, thus hindering its anti-bacterial activity.

6.6.2.2.2 Micro-broth dilution assay

This experiment was done for two main goals, the first is to measure the lowest concentration needed to inhibit bacterial growth (MIC), and the second and most important objective is to compare the antibacterial activity of silver prepared in our way with silver nitrate and aqueous extract of St. John's wort.

Table 6-4: The minimum inhibitory concentration of AgNPs, AgNO₃ and St. John's Wort aqueous extract against tested bacterial strains

Bacterial strain	MIC (µg/ml)		
	AgNPs	St. John's wort extract	AgNO ₃
<i>S. aureus</i> (wild type) 29213	27.5	X	13.75
<i>S. aureus</i> (Methicillin resistant) 43300	27.5	X	13.75
<i>E. coli</i> (Wild type) 25922	< 6.88	X	< 6.88
<i>E. coli</i> (ESBL) 35218	< 6.88	X	< 6.88
<i>K. oxytoca</i> (Wild) 700324	< 6.88	X	< 6.88
<i>K. Pneumoniae</i> (CRE) BAA-1705	13.75	X	< 6.88
<i>C. albican</i> 14053	55	X	55

Chapter 6: Summarizing Discussion and Conclusions

<i>C. auris</i> Lab isolate	55	X	110
--------------------------------	----	---	-----

Through the results presented in Table 4, we note that the aqueous extract of St. John's wort did not show any activity against the eight strains of bacteria studied, while the silver prepared by our method gave minimum inhibitory concentration values either identical to the values of silver nitrate as in *E. coli* (Wild type) 25922, *E. coli* (ESBL) 35218, *K. oxytoca* (Wild) 700324 and *C. albican* 14053 or higher than them as in *S. aureus* (wild type) 29213, *S. aureus* (Methicillin resistant) 43300 and *K. Pneumoniae* (CRE) BAA-1705 or lower than them as in *C. auris* Lab isolate.

6.6.2.3 Third, in cooperation with the Chemistry of Natural and Microbial Products Department, Pharmaceutical and Drug Industries Research Institute, National Research Centre, Egypt.

The purpose of these analyzes is to the comparison of the antimicrobial activities of *Hypericum perforatum L.*-Mediated green synthesis of AgNPs with antibiotics, silver nitrate, *Hypericum perforatum L.* aqueous extract and Citrate-capped AgNPs.

Table 6-5: Bacteria and yeast strains used for the study

Microorganism name	ATCC NO
<u>Gram-positive</u>	
<i>Bacillus subtilis</i>	6633
<i>Bacillus cereus</i>	6629
<i>Staphylococcus aureus</i>	6538
<u>Gram-negative</u>	
<i>Escherichia coli</i>	25922
<i>Proteus mirabilis</i>	9240
<i>Salmonella enterica</i>	25566
<u>Pathogenic yeast</u>	
<i>Candida albicans</i>	10231

The concentration of silver nanoparticles used was about half the value of the concentrations used from other materials and the results were comparable to the values of silver nitrate and the antibiotics used. It is also interesting that silver nanoparticles prepared using citrate, sodium hydroxide and aqueous extracts of St. John's wort did not give any antimicrobial activity. These and previous results all prove the efficacy of silver prepared by our method against a wide range of microbes, and therefore it can be promising for later application in products in the market. Through the transmission electron microscope images (figure 10) of bacteria treated with silver nanoparticles, we can monitor the different stages through which silver nanoparticles are positioned on the cell wall first and then penetrate the cell membrane and clump inside the cell and then affect it through the mechanisms that were previously proposed by a large number of researchers²⁷.

Chapter 6: Summarizing Discussion and Conclusions

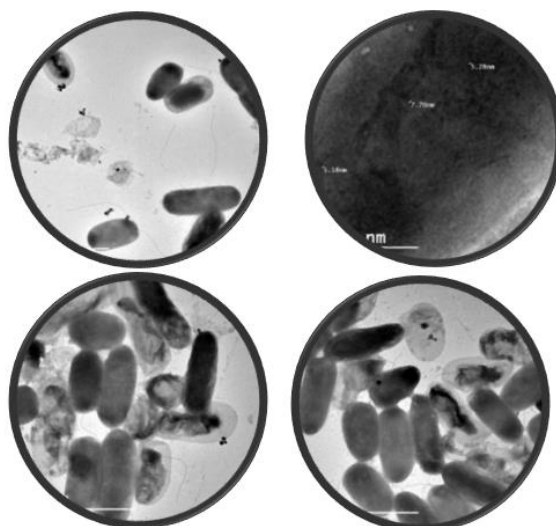


Figure 6-10: Transmission electron microscope (TEM) images of *Candida albicans* bacteria exposed to AgNPs.

6.6.2.4 Fourthly, in cooperation with Division of Molecular Biomedicine, Department of Molecular Biology and Biotechnology, Atomic Energy Commission of Syria (AECS), P. O. Box 6091, Damascus, Syria.

In this section, the effect of silver nanoparticles prepared using aqueous extract of St. John's wort on the *Leishmania Tropic* Syrian strain (LT_SYR_24) was studied.

6.6.2.4.1 Viability using XTT assay

L. tropica cells were incubated in 96-well microplates (50000 cells/well) for 24 h at 26 °C with different concentrations of AgNPs, in addition to the presence of control cells, each sample was replicated 3 times. Then 20 μ L of XTT mixture was added to each well and the microplate was incubated for 4 hours at 37 °C, after which the absorbance at wavelength 450 nm was measured using a microplate reader device. The resulted values were correlated to the control untreated cells representing 100 % of cell viability.

6.6.2.4.2 Apoptosis Assay using Annexin V

After incubating the cells with a series of silver concentrations, they were harvested using centrifugation and then redispersed using a binding buffer HBS. Subsequently, 5 μ L of sfGFP-Annexin-V (1 mg/mL) was added and incubated in the dark for 5 minutes. Finally, the percentage of apoptotic cells was calculated using flow cytometry.

6.6.2.4.3 Cell Cycle Assay

After incubating the cells with a series of silver concentrations, they were harvested using centrifugation and then redispersed using PBS and 95 % ethanol and stored at 4 °C overnight. Subsequently, the cells were centrifuged and washed with PBS, after that suspended and stained using PBS and 5 μ L of Propidium Iodide (PI, 1 mg/mL) for 30 min in the dark. Finally, the Cell cycle analysis was done using flow cytometry.

Chapter 6: Summarizing Discussion and Conclusions

6.6.2.4.4 Results

It showed (figure 11) that parasite viability decreases with increasing concentration of Ag NPs, the maximal toxicity was achieved using 0.62 $\mu\text{g/ml}$ concentration after 24 h, while IC₅₀ was at 0.29 $\mu\text{g/ml}$ Ag NPs concentration.

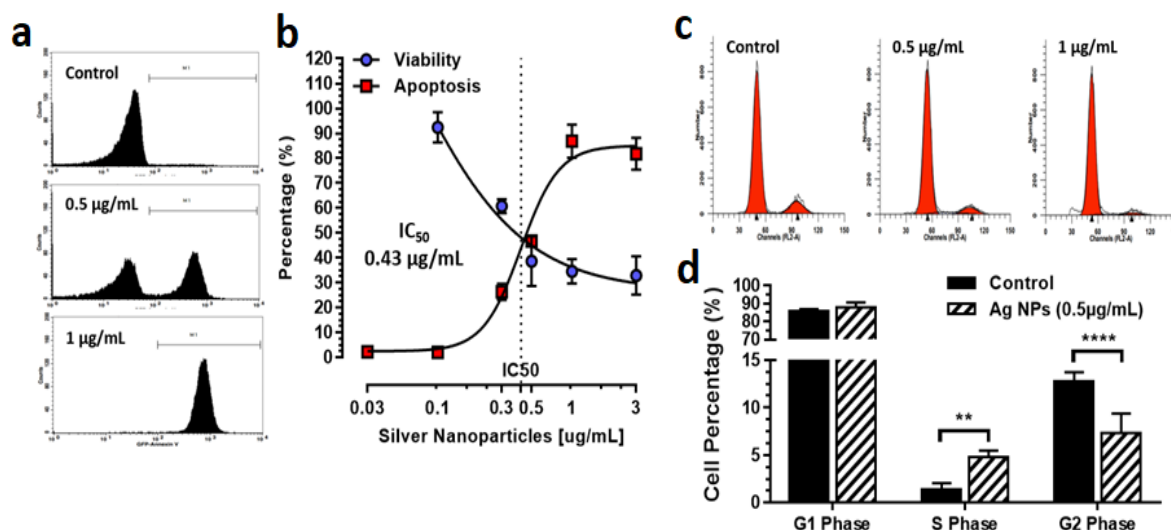


Figure 6-11: Effect of AgNPs on a) apoptosis; b) viability and c) cell cycle of *L. tropica* cells.

When AgNPs were incubated with cells at concentrations of 0.5 $\mu\text{g/ml}$ and 1 $\mu\text{g/ml}$ for 24 hours, the percentage of induced apoptosis was 46.8% and 86.8%, respectively, compared to control cells (figure 11 a and b). That is, the percentage of apoptotic cells increases with increasing concentration of AgNPs, where the highest concentration of apoptosis is 1 $\mu\text{g/ml}$ after 24 hours, and IC₅₀ was 0.43 $\mu\text{g/mL}$. After treatment with AgNPs, the cells were incubated with the fluorescent DNA dye propidium iodide, and then the cells were analyzed for their content of genomic DNA by flow cytometry, where it was possible to distinguish between three phases of the cell cycle (G1, S and G2) (Figure 11c). Statistical comparisons showed that the percentage of cells in the G1 phase was equal between the control and treated conditions, while it showed a significant increase of 3.3% of cells in the S phase at 0.5 $\mu\text{g/ml}$ compared to the control cells (Figure 11d), on the other hand, the percentage of cells in the G2 phase decreased of 5.4% at 0.5 $\mu\text{g/ml}$ compared to the control (Figure 11d).

6.6.3 Anticancer activities

Cell Titer-Blue or Cell Viability Assay has been performed for monitoring cell viability for three types of cancer cells are HeLa, HepG2 and A549 cells after treatment with a series of concentrations of silver nanoparticles prepared using aqueous extract of St. John's wort. This method is based on the principle that living cells have the ability to convert resazurin (redox dye) to resorufin (fluorescent product). The anti-cancer activity of silver nanoparticles was also measured during different incubation periods of 2, 5, 8 and 24 hours.

Chapter 6: Summarizing Discussion and Conclusions

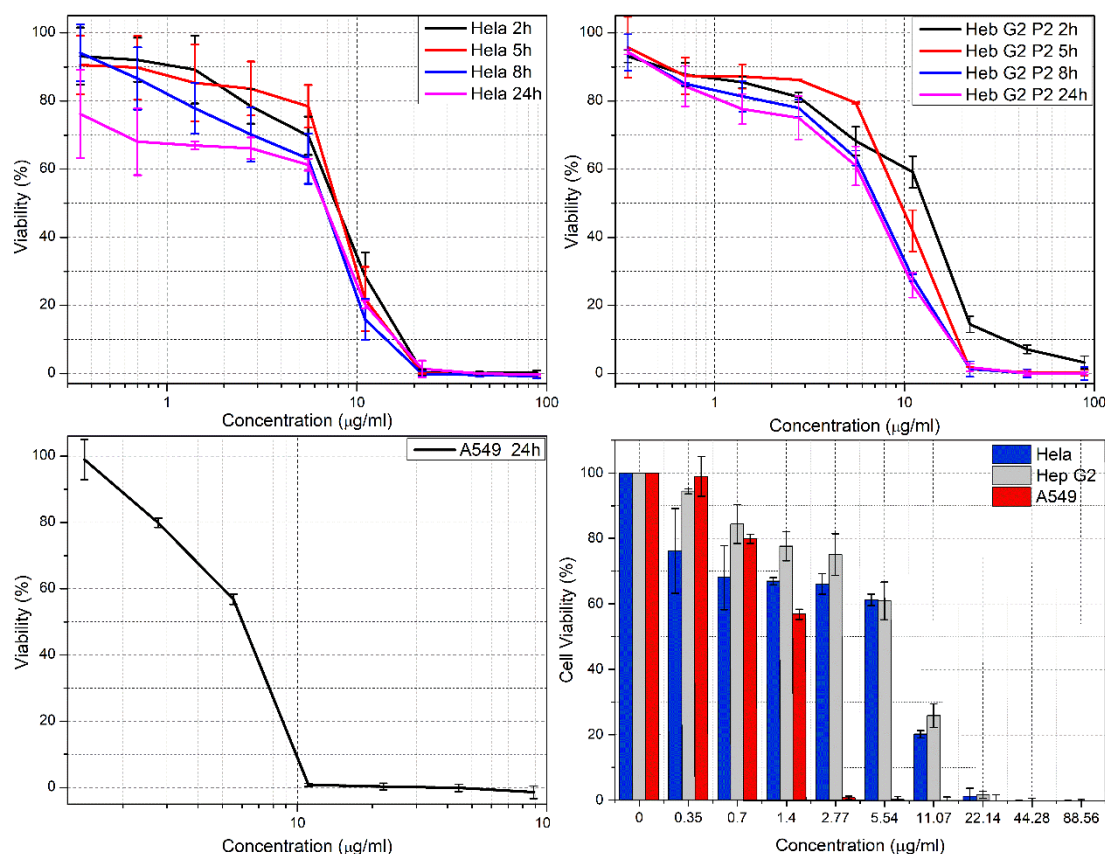


Figure 6-12: Relative cell viability (%) of HeLa, Hep G2 and A549 cells as a function of AgNPs concentration for 2, 5, 8 and 24 h determined by Cell titer-Blue cytotoxicity assay. The experiments were performed with four replicates and the standard deviation was calculated.

Figure 12 shows that with the increasing concentration of AgNPs, the viability of cells for the three types of cells studied in this research decreases significantly. This effect also varies according to the time of exposure to the nanoparticles. The effect of silver nanoparticles prepared by our method was clear and very significant on the types of cancer cells studied and at relatively low concentrations, where the values of IC₅₀ against HeLa cells were 7.71, 7.87, 6.75 and 6.72 $\mu\text{g/mL}$; against HepG2 12.44, 9.52, 7.19 and 6.88 $\mu\text{g/mL}$ and against A549 6.08 $\mu\text{g/mL}$ at 2, 5, 8 and 24 h respectively. These results are very promising for the application of silver prepared in this way in the fight against cancer, especially since there is an organic layer on its surfaces that prevents its toxic effect on healthy cells, and this must be proven in later studies, God willing.

6.7 Development of a protocol to prepare aptamer-Conjugated AgNPs

These experiments aim to conjugate single-stranded oligonucleotide-based aptamers (APTs), which are excellent ligands for tumor cell targeting with AgNPs prepared using an aqueous extract of St. John's wort. The process of coupling the aptamer with silver nanoparticles must be well studied because it may affect the effectiveness of these nanoparticles later when applied, or it may also affect the stability of these nanoparticles in the colloidal solution. Therefore, a very large protocol and multiple conditions have been tried, such as pH conjugation values, aptamer and silver nanoparticles used concentrations, using modified

Chapter 6: Summarizing Discussion and Conclusions

DNA, temperature, reaction time, stirring speed, adding salts at different reaction times to screen the negative charges of the DNA and increase the DNA loading on the AgNPs (salt aging), in addition to the buffer solution in which the coupling takes place and other conditions. All the previous conditions were carefully studied to achieve the desired goal.

An appropriate protocol has been reached: thiolated Aptamer samples were used as received without further treatment (i.e. no TCEP or DTT treatment) (100 μ M, 2.5 μ L) was mixed with AgNPs (20-50 nm, 0.5 nM, 500 μ L) in a microcentrifuge tube (lower protein binding). The mixture was then placed in a laboratory freezer (set at -20 °C) all night, followed by thawing at room temperature. Then, the mixture was centrifuged as follows: 5 minutes at 3000 rpm, 5 minutes at 6000 rpm and 20 minutes at 13000 rpm. The filtrate is separated from the sediment, where 500 μ l of HEPES buffer (5 mM, pH 7.6) is added to the sediment, and the previous centrifugation process is repeated. The washing process is repeated at least 3 times to get rid of all the amount of unbound aptamers. Finally, the resulting Aptamer-AgNPs dissolved in deionized water or in HEPES buffer (5 mM, pH 7.6) and the supernatants resulting from the centrifugation for the first time and for all later washing operations are concentrated to a volume of 500 μ l or 1 ml using a rotary evaporator to measure the concentration of the free aptamer (unbound). Thus, through it, we can determine the amount of the attached Aptamer at the surface of AgNPs. Through the previous protocol and using the methods mentioned, it was found that the percentage of aptamer functionalized silver nanoparticles is about 40% of the amount used and the number of aptamers on the surface of each nanoparticle is about 1930.

Using different characterization techniques for the resulting sample such as UV-VIS, DLS, Zeta potential, FTIR-ATR, agarose gel electrophoresis and Quant-iT™ OliGreen® reagent to prove the binding of aptamers on the surfaces of silver nanoparticles.

6.7.1 Study the anticancer effect of the selective ssDNA aptamer-modified AgNPs on human non-small cell lung cancer A549 and normal human bronchial epithelial BEAS2B cells; in Vitro study.

6.7.1.1 Cytotoxicity effects

The previously mentioned test, CTB analysis, was used to evaluate the cell viability. Aptamer-conjugated silver nanoparticles concentrations were 60, 30, 15, 7.5 and 3.7 μ g/ml for A549 cells and 67, 38, 19, 12 and 6 μ g/ml for BEAS-2B cells. The exposure times are 0, 3, 6, and 24 hours.

6.7.1.2 Cellular Viability--Calcein / Propidium Iodide

No fluorescent calcein-AM dye turns into the fluorescent calcein dye by intracellular esterase activity in live cells, while Propidium iodide (PI) does not enter viable cells, but in dead cells it manages to reach the nucleic acids and enters them and binding to DNA by intercalating between the bases, resulting in a significantly increased fluorescence and is thus used to identify dead cells. Calcein and propidium iodide (PI) were used to evaluate cellular viability and cell death.

6.7.1.3 Flow cytometry-based apoptosis and necrosis detection

Apoptosis is the body's way to eliminate cells in a systematic way and can be detected by measuring the externalization of phosphatidylserine on the plasma membrane using

Chapter 6: Summarizing Discussion and Conclusions

fluorescent-tagged annexin V. When a cell dies, the cell membrane loses its integrity, allowing anything to enter into the cell. Propidium iodide (PI) is a popular red-fluorescent nuclear and chromosome counterstain. Since propidium iodide is not permeant to live cells, it is also commonly used to detect dead cells in a population. PI binds to DNA by intercalating between the bases with little or no sequence preference.

6.7.1.4 Cellular uptake of Ag NPs

The physical and chemical properties, such as size, shape, surface charge, composition and the nature of the ligand on its surface, determine the mechanism (phagocytosis, micropinocytosis, endocytosis, direct diffusion, or adhesive interactions) by which nanoparticles internalized by cells. After exposing the cancer and normal cells to different concentrations of silver nanoparticles at different times, they are washed thoroughly, and then the amount of silver that entered the cells is determined through AAS.

6.7.2 Results

As shown in Figure 13, and from the IC₅₀ values, it is evident that the effect of silver nanoparticles loaded with aptamer on cancer cells is much greater than its effect on healthy cells at different concentrations and different times of exposure. The aptamer-modified AgNPs exhibited selective binding and internalization to target A549 cells, but not by normal human bronchial epithelial BEAS2B, thus exhibiting high specificity. These results are excellent and encouraging for later studies to use it as a targeting therapy, especially here that we do not need to load the drug on the nanoparticles as well, since silver alone is able to kill cells without the complications of loading the drug and the side effects that can result from loading the drug and aptamers on their surfaces.

It noted from figure 14 that at high concentrations of silver nanoparticles loaded with aptamer, most cells die in both types, but at medium and low concentrations of 30 and below, the effect of silver nanoparticles on cancer cells is very large compared to healthy cells.

Chapter 6: Summarizing Discussion and Conclusions

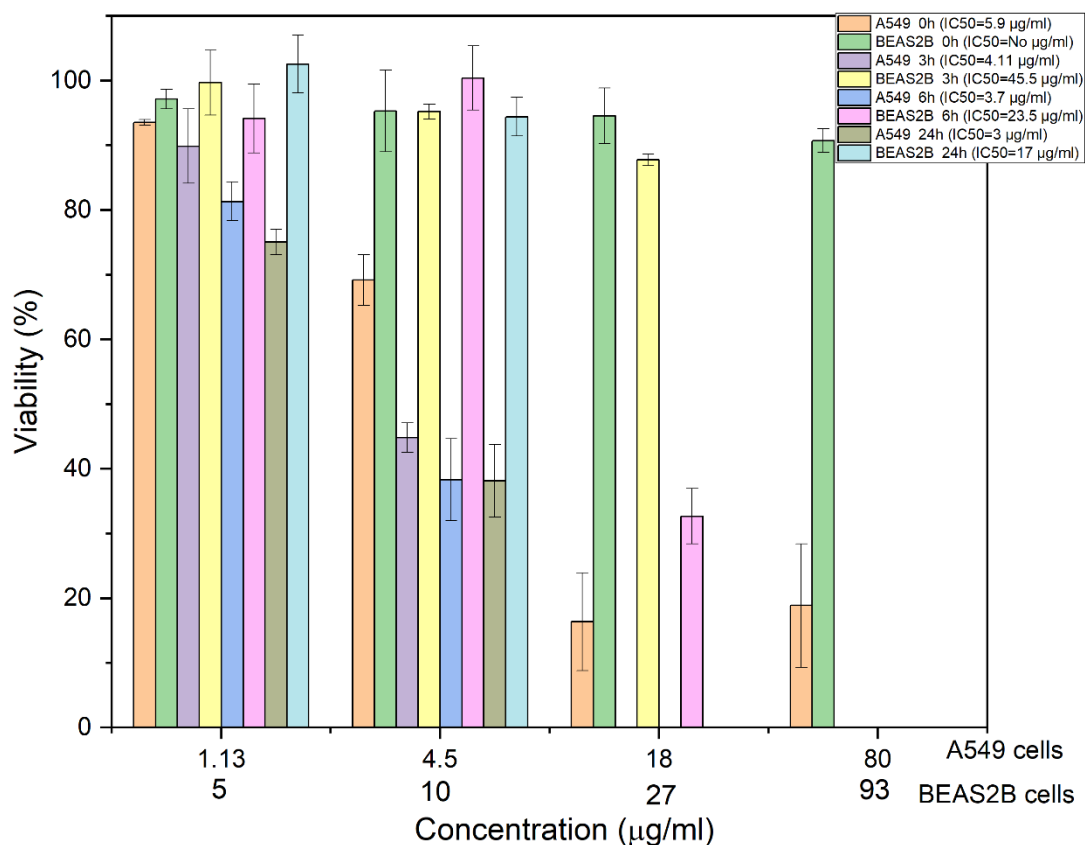


Figure 6-13: *in vitro* cytotoxicity of aptamer conjugated silver nanoparticles against A549 and BEAS2B cells at different concentrations and various exposure times

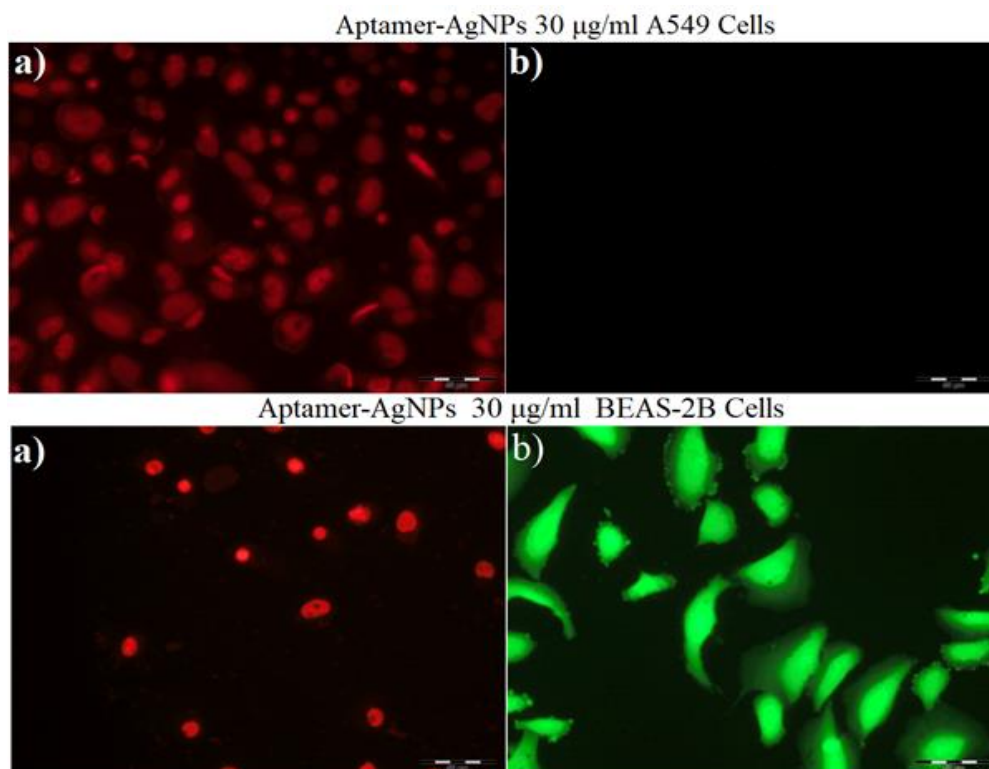


Figure 6-14: fluorescence images of live cells (green) and dead cells (red) for A549 and BEAS 2B cells before and after incubation with 30 µg/ml Aptamer-AgNPs.

Chapter 6: Summarizing Discussion and Conclusions

For flow cytometric analysis, after only 3 hours of incubation with aptamer-modified AgNPs, all cancer cells (A549) died completely, also at the lowest concentration of 3.7 $\mu\text{g/ml}$, while healthy cells (BEAS-2B) died at very high concentrations, and at medium and low concentrations, the effect of silver on them was limited (apoptosis more than necrosis) and also depends on the concentration. Regarding the analysis of the cellular uptake of silver in cancerous and healthy cells (figure 15), it was noted that the percentage of cellular uptake increases with the increase in the exposure time, and it also increases with the increase in the concentration of silver used for both cells, but what is interesting is that the percentage of cellular uptake of silver in cancer cells is much greater than in healthy cells, and this confirms the validity of previous results and at the same time proves the selective effectiveness of aptamer towards cancer cells.

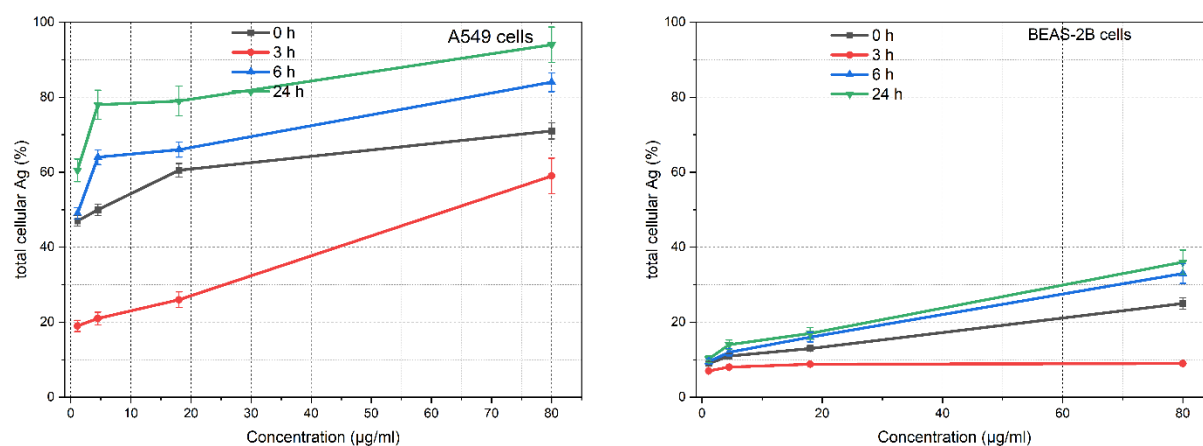


Figure 6-15: The percentage of cellular uptake of Ag NPs in A549 cells and BEAS-2B cells after exposure to Apt-AgNPs for 3h. The data are expressed as mean \pm SD of three independent experiments.

Chapter 6: Summarizing Discussion and Conclusions

6.8 Conclusions

In this work, an easy, fast, inexpensive, environmentally friendly and effective protocol was developed to prepare silver nanoparticles using an aqueous extract of St. John's wort. Different techniques were used to characterize the resulting silver nanoparticles such as UV-VIS, DLS, Zeta potential, FTIR-ATR, XRD, SEM, TEM, AFM, EDX, AAS and TGA and showed that this green method produced stable spherical nanoparticles in the colloidal solution with a size ranging from 20 to 50 nm and it has a crystalline structure as it is face-centered cubic and these particles are surrounded by a protective layer of a group of phenolic compounds, which maintains them in nanoscale dimensions and protects them from agglomeration and precipitation in the solution and thus also maintains its stability.

The biosynthesized AgNPs showed very high effects against a range of free radicals as the antioxidant concentrations against 2,2-diphenyl-1-picrylhydrazyl radical, superoxide anion radical and 2, 2'-azino-bis-(3-ethylbenzothiazoline-6-sulfonic acid) radical cation were very low. AgNPs showed also very high cytotoxicity against various cancer cells such as Hela, Hep G2 and A549 cells at low concentrations and short exposure times. Also, the effect of the prepared silver nanoparticles on a large number of microbes, about 20 species (gram-positive bacteria, gram-negative bacteria and Pathogenic yeast) at different storage times and in comparison with silver prepared in a chemical way, with antibiotics, with silver nitrates, and with the extract alone have been studied and was quite highly effective against almost all tested microbes. The activity of prepared AgNPs was also studied against leishmaniasis, and the results were very promising.

Since the toxicity and biological activity of obtained nanoparticles toward different pathogens are affected by several factors, namely shape, size, size distribution, particle morphology, particle content, surface area, surface charge, nature and components of the protective layer, solubility ratio, interaction of particles in the solution, the type of reducing agent used, and the efficiency of releasing ions from these particles. The main factor, unanimously by most researchers, is the nature and components of the protective layer. Therefore, St. John's wort was extracted using different solvents and the yield was determined, then a fast, simple, and reproducible high-performance liquid chromatography- equipped with a diode array detector (HPLC-DAD), coupled with UV-visible spectrophotometry at a full spectrum (200–800 nm) were development to get separate and not overlapping peaks in the HPLC spectra which were studied at three wavelengths (260 nm for phloroglucinols, 590 nm for naphthodianthrones and at 350 nm for other flavonols, flavones and caffeoylquinic acids. high-performance liquid chromatography combined with electrospray ionization–mass spectrometry (LC-ESI-MS) under positive ionization mode was conducted to separate the bioactive molecules ions $[M+H]^+$ of the compounds in the extracts by their mass-to-charge ratio (m/z) and to detect them qualitatively and quantitatively by their respective m/z and abundance. by Comparison with five reference substances (Chlorogenic acid, Quercetin, Hyperoside, Quercitrin hydrate and Hypericin), comparison of the retention times of peaks in HPLC diagrams with standards materials and what is reported in the literature, comparing the UV absorption spectra of peaks with the UV spectra of reference substances and what is mentioned in the literature and by matching the prominent protonated molecular ion $[M+1]^+$ of compounds with the molecular weights of these compounds which known previously in this plant, ten compounds: Hypericin,

Chapter 6: Summarizing Discussion and Conclusions

Rutin, Hyperoside, Quercitrin_hydrate, Quercetin, Biapigenin, Hyperforin, Quercitrin, Adhyperforin and Chlorogenic acid were identified, proven and confirmed in St John's Wort plant extract. An easy and simple protocol was developed to isolate the organic layer present on the surfaces of silver nanoparticles. Then, using the previously developed HPLC-MS protocols, in addition to conducting a subsequent MSMS analysis, the phenolic compounds existing on the surfaces of silver nanoparticles were finally determined, which are: Neochlorogenic acid, Hyperoside, Isoquercitrin, 13,II8-biapigenin, Furohyperforin, Hyperforin, Furoadhyperforin and Adhyperforin. The total phenolic substance in the different prepared extracts was quantified by Folin–Ciocalteu method and anti-radicals activity were calculated using DPPH and ABTS approaches. The results showed that the tea extraction method gave the highest percentage of phenols and the highest antioxidant activity, while the pure organic solvents gave lower phenols and lower antioxidant activity.

Lung cancer is the most common and deadly cancer in the world, as it is currently the number one killer among other types of cancer and the number of people who die from this disease is equivalent to those who die from breast, prostate and colon cancer combined. Since aptamers are better than antibodies due to the ease of preparation and the ability to target cancer cells, and after bitter attempts and many experiments, we have developed an easy, fast and simple protocol to bind silver nanoparticles prepared using the aqueous extract of St. John's wort with an aptamer that has high selectivity towards lung cancer cells. Several techniques have been performed to demonstrate aptamer conjugation on the surfaces of silver nanoparticles such as UV-VIS, DLS, Zeta potential, FTIR-ATR, gel electrophoresis and Quant-iT™ OliGreen® ssDNA Kit (Cat. no. 011492). CTB test, Cell viability analysis using calcein-AM and Propidium Iodide (PI), Cell death using flow cytometric analysis, Cellular uptake using AAS analysis, light and confocal microscopy images showed high cytotoxicity and cellular internalization through selective binding and targeting by aptamer in lung cancer cells (A549 cells) and not in other healthy cells (BEAS-2B cells).

Chapter 6: Summarizing Discussion and Conclusions

References

1. Mock, J. J.; Barbic, M.; Smith, D. R.; Schultz, D. A.; Schultz, S., Shape effects in plasmon resonance of individual colloidal silver nanoparticles. *J. Chem. Phys.* **2002**, *116* (15), 6755-6759.
2. Pavia, D. L.; Lampman, G. M.; Kriz, G. S.; Vyvyan, J. J. A. L. M., *Introduction to spectroscopy: cengage learning*. 2008; Vol. 153, p 752.
3. Nichita, C.; Giurginca, M.; Bazdoaca, C.; Parvu, L.; Meghea, A., Vegetal antioxidants obtained from *Hypericum perforatum* species. *Rev. Chim.* **2007**, *58* (9), 910-913.
4. R., A.; M., R., Phytochemical screening by FTIR spectroscopic analysis of leaf extracts of selected Indian Medicinal plants. *Int.J.Curr.Microbiol.App.Sci.* **2014**, *3* (1), 395-406.
5. Kozarski, M.; Klaus, A.; Vunduk, J.; Zizak, Z.; Niksic, M.; Jakovljevic, D.; Vrvic, M. M.; Van Griensven, L. J., Nutraceutical properties of the methanolic extract of edible mushroom *Cantharellus cibarius* (Fries): primary mechanisms. *Food Funct* **2015**, *6* (6), 1875-86.
6. Alahmad, A.; Feldhoff, A.; Bigall, N. C.; Rusch, P.; Scheper, T.; Walter, J. G., *Hypericum perforatum* L.-Mediated Green Synthesis of Silver Nanoparticles Exhibiting Antioxidant and Anticancer Activities. *Nanomaterials (Basel)* **2021**, *11* (2), 487.
7. Zia, F.; Ghafoor, N.; Iqbal, M.; Mehboob, S., Green synthesis and characterization of silver nanoparticles using *Cydonia oblong* seed extract. *Appl. Nanosci.* **2016**, *6* (7), 1023-1029.
8. Bharathi, D.; Diviya Josebin, M.; Vasantharaj, S.; Bhuvaneshwari, V., Biosynthesis of silver nanoparticles using stem bark extracts of *Diospyros montana* and their antioxidant and antibacterial activities. *J. Nanostruct. Chem.* **2018**, *8* (1), 83-92.
9. Mehmood, A.; Murtaza, G.; Bhatti, T. M.; Kausar, R., Phyto-mediated synthesis of silver nanoparticles from *Melia azedarach* L. leaf extract: Characterization and antibacterial activity. *Arabian J. Chem.* **2017**, *10*, S3048-S3053.
10. Mallikarjuna, K.; John Sushma, N.; Narasimha, G.; Manoj, L.; Deva Prasad Raju, B., Phytochemical fabrication and characterization of silver nanoparticles by using Pepper leaf broth. *Arabian J. Chem.* **2014**, *7* (6), 1099-1103.
11. Vasco, F.; Andrea, H.; Wim, J., Critical Evaluation of Nanoparticle Tracking Analysis (NTA) by NanoSight for the Measurement of Nanoparticles and Protein Aggregates. *Pharm. Res.* **2010**, *27* (5), 796-810.
12. Yuchen, F.; Preety, S.; Lukasz J., O.; Jonathan J., A.; James J., M., Cationic liposome-hyaluronic acid hybrid nanoparticles for intranasal vaccination with subunit antigens. *J. Controlled Release* **2015**, *208*, 121-129.
13. Kalaiselvi, M.; Subbaiya, R.; Selvam, M., Synthesis and characterization of silver nanoparticles from leaf extract of *Parthenium hysterophorus* and its anti-bacterial and antioxidant activity. *Int J Curr Microbiol Appl Sci* **2013**, *2* (6), 220-227.
14. Moteriya, P.; Chanda, S., Biosynthesis of silver nanoparticles formation from *Caesalpinia pulcherrima* stem metabolites and their broad spectrum biological activities. *J. Genet. Eng. Biotechnol.* **2018**, *16* (1), 105-113.
15. Seralathan, J.; Stevenson, P.; Subramaniam, S.; Raghavan, R.; Pemaiah, B.; Sivasubramanian, A.; Veerappan, A., Spectroscopy investigation on chemo-catalytic, free radical scavenging and bactericidal properties of biogenic silver nanoparticles synthesized using *Salicornia brachiata* aqueous extract. *Spectrochim. Acta, Part A* **2014**, *118*, 349-355.
16. Moteriya, P.; Chanda, S., Synthesis and characterization of silver nanoparticles using *Caesalpinia pulcherrima* flower extract and assessment of their in vitro antimicrobial, antioxidant, cytotoxic, and genotoxic activities. *Artif. Cells Nanomed. Biotechnol.* **2017**, *45* (8), 1556-1567.
17. Ramachandran, L.; Nair, C. K. K., Therapeutic potentials of silver nanoparticle complex of α -lipoic acid. *Nanomater. Nanotechnol.* **2011**, *1*, 14.

Chapter 6: Summarizing Discussion and Conclusions

18. Mittal, A. K.; Bhaumik, J.; Kumar, S.; Banerjee, U. C., Biosynthesis of silver nanoparticles: elucidation of prospective mechanism and therapeutic potential. *J. Colloid Interface Sci.* **2014**, *415*, 39-47.
19. Ajayi, E.; Afolayan, A., Green synthesis, characterization and biological activities of silver nanoparticles from alkalized *Cymbopogon citratus* Stapf. *Adv. Nat. Sci.: Nanosci. Nanotechnol.* **2017**, *8* (1), 015017.
20. Sudha, A.; Jeyakanthan, J.; Srinivasan, P., Green synthesis of silver nanoparticles using *Lippia nodiflora* aerial extract and evaluation of their antioxidant, antibacterial and cytotoxic effects. *Resour.-Effic. Technol.* **2017**, *3* (4), 506-515.
21. Keshari, A. K.; Srivastava, R.; Singh, P.; Yadav, V. B.; Nath, G., Antioxidant and antibacterial activity of silver nanoparticles synthesized by *Cestrum nocturnum*. *J. Ayurveda Integr. Med.* **2018**.
22. Inbathamizh, L.; Ponnu, T. M.; Mary, E. J., In vitro evaluation of antioxidant and anticancer potential of *Morinda pubescens* synthesized silver nanoparticles. *J. Pharm. Res.* **2013**, *6* (1), 32-38.
23. Guntur, S. R.; Kumar, N. S.; Hegde, M. M.; Dirisala, V. R., In Vitro Studies of the Antimicrobial and Free-Radical Scavenging Potentials of Silver Nanoparticles Biosynthesized From the Extract of *Desmostachya bipinnata*. *Anal. Chem. Insights* **2018**, *13*, 1177390118782877.
24. Mata, R.; Nakkala, J. R.; Sadras, S. R., Biogenic silver nanoparticles from *Abutilon indicum*: Their antioxidant, antibacterial and cytotoxic effects in vitro. *Colloids Surf., B* **2015**, *128*, 276-286.
25. Mata, R.; Nakkala, J. R.; Sadras, S. R., Catalytic and biological activities of green silver nanoparticles synthesized from *Plumeria alba* (frangipani) flower extract. *Materials Science and Engineering: C* **2015**, *51*, 216-225.
26. Vieira, L. F. d. A.; Lins, M. P.; Viana, I. M. M. N.; dos Santos, J. E.; Smaniotto, S.; Reis, M. D. d. S., Metallic nanoparticles reduce the migration of human fibroblasts in vitro. *Nanoscale Research Letters* **2017**, *12* (1), 200.
27. Medici, S.; Peana, M.; Nurchi, V. M.; Zoroddu, M. A., Medical Uses of Silver: History, Myths, and Scientific Evidence. *J. Med. Chem.* **2019**, *62* (13), 5923-5943.

Chapter 6: Summarizing Discussion and Conclusions

7 Curriculum Vitae and Publications

Curriculum Vitae

Persönliche Daten	
Name	Abdalahim Alahmad
Geburtsdatum/ -or	24.04.1984, Al-Mayadin, Deir Ez Zur/ Syrien
Akademischer Werdegang	
01/2017 – 03/2022	Promotion im Fach Chemie: Institut für Technische Chemie, LUH, Hannover, Deutschland
10/2010 – 03/2014	Master in Materialwissenschaft und -technik, Institut für Naturwissenschaften und Polymertechnologie, Höheres Institut für angewandte Wissenschaft und Technologie in Damaskus, Syrien Thema der Masterarbeit: Herstellung und Charakterisierung von Silber-Nanostrukturen
09/2005 – 10/2009	Bachelor of Science Fachbereich Angewandte Chemie, Naturwissenschaft Fakultät, Damaskus Universität, Syrien.
09/2004 – 06/2005	Gymnasium, Oberschule für Jungen in der Stadt Al-Mayadin, Syrien
Beruflicher Werdegang	
07/2017 – 12/2021	wissenschaftlich Hilfskraft, Institut für Technische Chemie LUH, Hannover, Deutschland
09.2016 – 12.2016	Praktikum, Institut für Technische Chemie LUH, Hannover, Deutschland
22.06.2018	Zertifikat Deutsch C1 - Sprachstand Bescheinigung Universität Vechta, Vechta (Deutschland)
08.2016 – 11.2016	Zertifikat Deutsch B2 Universität Osnabrück - International Office, Osnabrück (Deutschland)
11.2015 – 05.2016	Zertifikat Deutsch B1 VHS Cloppenburg, Cloppenburg (Deutschland)
04.2017 – 05.2022	Stipendium der Avicenna Studienwerk e.V Osnabrück (Deutschland)
11.2021 – 12.2021	Stipendium der Graduiertenakademie - LUH, Hannover, Deutschland
06. 2021	Zertifikat HTC: Agiles Projektmanagement, Medizinische Hochschule Hannover, Deutschland
03. 2020	Zertifikat Von der Idee zum Patent, Workshop LUH, Hannover, Deutschland

Curriculum Vitae and Publications

02. 2020	Zertifikat Qualitätsmanagement in der biopharmazeutischen Industrie, Institut für Technische Chemie, LUH, Hannover, Deutschland
10.2019	Zertifikat Bildverarbeitung und -analyse für wissenschaftliche Veröffentlichungen Graduate School of Natural Sciences (GRANAT), Naturwissenschaftlichen Fakultät, LUH, Hannover, Deutschland
12.2016 – 04.2017	Stipendium der Deutsche Bundesstiftung Umwelt, Osnabrück (Deutschland)
10.2010 – 06.2013	Wissenschaftlich Mitarbeiter, Laboratorien Naturwissenschaftliche Fakultät, Institut für Chemie und Physik, Damaskus Universität, Syrien
09.2010 – 04.2014	Chemielehrer an der Aref Al-Nakdi Gymnasium Schule, Damaskus, Syrien

Betreute Abschlussarbeiten im Rahmen der Promotion

Masterarbeit von Sergej Kraft

Titel: Analyse der Zusammensetzung von *Hypericum perforatum* Extrakten

Jahr: 2019

Masterarbeit von Samuel Edward Hakim

Titel: Biokonjugation von biosynthetisierten Silbernanopartikeln mit Aptameren

Jahr: 2019 - 2020

Bachelorarbeit

Titel: Grüne Synthese von Silbernanopartikeln mit Mono- und Polysacchariden als Reduktions- und Schutzmittel

Jahr: 2018

Curriculum Vitae and Publications

Publications

1. **Alahmad, A.**; Eleoui, M.; Falah, A.; Alghoraibi, I.J. Preparation of colloidal silver nanoparticles and structural characterization. *Physical Sciences Research International* 2013, 1, 89-96, <http://www.netjournals.org/pdf/PSRI/2013/4/13-023.pdf>.
2. **Alahmad, A.** Preparation and Characterization of Silver Nanoparticles. *Int. J. Chemtech Res.* 2014, 6, 450-459, [https://sphinxesai.com/2014/ChemTech/JM14CT51_100/CT=53\(450-459\)JM14.pdf](https://sphinxesai.com/2014/ChemTech/JM14CT51_100/CT=53(450-459)JM14.pdf).
3. Alghoraibi, I.; **Alahmad, A.** Colloidal synthesis and structural characterizations of silver nanoparticles by using wet chemistry. *Int. J. Chemtech Res.* 2014, 6, 871-880, [https://sphinxesai.com/2014/ChemTech/JM14CT51_100/CT=99\(871-880\)JM14.pdf](https://sphinxesai.com/2014/ChemTech/JM14CT51_100/CT=99(871-880)JM14.pdf).
4. Alghoraibi, I.; Soukkarieh, C.; Zein, R.; **Alahmad, A.**; Walter, J.G.; Daghestani, M. Aqueous extract of Eucalyptus camaldulensis leaves as reducing and capping agent in biosynthesis of silver nanoparticles. *Inorg. Nano-Metal Chem.* 2020, 50, 895-902, [doi:10.1080/24701556.2020.1728315](https://doi.org/10.1080/24701556.2020.1728315).
5. Zein, R.; Alghoraibi, I.; Soukkarieh, C.; Salman, A.; **Alahmad, A.** In-vitro anticancer activity against Caco-2 cell line of colloidal nano silver synthesized using aqueous extract of Eucalyptus Camaldulensis leaves. *Heliyon* 2020, 6, [doi:10.1016/j.heliyon.2020.e04594](https://doi.org/10.1016/j.heliyon.2020.e04594).
6. He, C.; Qiu, K.; **Alahmad, A.**; Pott, R. Particulate matter capturing capacity of roadside evergreen vegetation during the winter season. *Urban For. Urban Greening* 2020, 48, 126510, [doi:10.1016/j.ufug.2019.126510](https://doi.org/10.1016/j.ufug.2019.126510).
7. **Abdallah, A.**; Armin, F.; Nadja C., B.; Pascal, R.; Thomas, S.; Johanna-Gabriela, W. Hypericum perforatum L.-Mediated Green Synthesis of Silver Nanoparticles Exhibiting Antioxidant and Anticancer Activities. *Nanomaterials* 2021, 11, 487, [doi:10.3390/nano11020487](https://doi.org/10.3390/nano11020487).
8. **Alahmad, A.**; Alghoraibi, I.; Zein, R.; Kraft, S.; Dräger, G.; Walter, J.-G.; Scheper, T. Identification of Major Constituents of Hypericum perforatum L. Extracts in Syria by Development of a Rapid, Simple, and Reproducible HPLC-ESI-Q-TOF MS Analysis and Their Antioxidant Activities. *ACS Omega* 2022, 10.1021/acsomega.1c06335, [doi:10.1021/acsomega.1c06335](https://doi.org/10.1021/acsomega.1c06335).
9. **Alahmad, A.**; Al-Zereini, WA.; Tahani; Al-Madanat, O.; Alghoraibi, I.; Al-Qaralleh, O.; Al-Qaraleh, S.; Walter, J.-G.; Scheper, T. Green synthesis of silver nanoparticles using Hypericum perforatum L. aqueous extract with the evaluation of its antibacterial activity against clinical and food pathogens. *Pharmaceutics* 2022, 14(5), 1104 [doi:10.3390/pharmaceutics14051104](https://doi.org/10.3390/pharmaceutics14051104).
10. Zein, R.; Alghoraibi, I.; Soukkarieh, C.; **Alahmad, A.** Investigation of Cytotoxicity of Bio-synthesized Colloidal Nano Silver Against Locally Leishmania Tropica: In Vitro Study. *Materials* 2022, 15(14), 4880; [doi: 10.3390/ma15144880](https://doi.org/10.3390/ma15144880).

Curriculum Vitae and Publications

11. Zein, R.; Alghoraibi, I.; Soukkarieh, C.; M. T. Ismail; **Alahmad, A.** Influence of Polyvinylpyrrolidone concentration on properties and anti-bacterial activity of green synthesized silver nanoparticles. *Micromachines* 2022, 13(5), 777; doi: [10.3390/mi13050777](https://doi.org/10.3390/mi13050777).
12. samer Y. Al-Qaraleh; Sawsan A. Oran; Wael A. Al-Zereini; Aiman I. Al-Qtaitat and **Abdalahim alahmad**. Improved anti-breast cancer activity of green synthesized selenium nanoparticles and induction of apoptosis by conjugation the nanoparticles with polyethylene glycol (PEG). *Nanotechnology Reviews*. Submitted

Poster Presentations

- **Abdalahim, A.**; Johanna-Gabriela, W.; Thomas, S. Green biosynthesis of Silver Nanoparticles (AgNPs) by using aqueous extracts of *Hypericum perforatum L* (St John's wort) for cancer targeting. 24th World Nano Conference in May 2018 Rome, Italy.
- **Abdalahim, A.**; Johanna-Gabriela, W.; Thomas, S. Silver Nanoparticles (AgNPs) synthesized with *Hypericum perforatum L* (St John's wort) extracts. Nanoday Conference in Laboratorium für Nano- und Quantenengineering 2019 Hannover, Germany.